UC Santa Barbara

UC Santa Barbara Electronic Theses and Dissertations

Title

Tales of Taming Cyclopentadiene: A Highly Reactive Diene for Materials Synthesis, Photopatterning and Property Enhancement via Diels—Alder Click Chemistry

Permalink

https://escholarship.org/uc/item/2f53h5fm

Author

Bailey, Sophia Jamie

Publication Date

2022

Peer reviewed|Thesis/dissertation

eScholarship.org Powered by the California Digital Library
University of California

UNIVERSITY OF CALIFORNIA

Santa Barbara

Tales of Taming Cyclopentadiene: A Highly Reactive Diene for Materials Synthesis, Photopatterning and Property Enhancement via Diels–Alder Click Chemistry

A dissertation submitted in partial satisfaction of the

requirements for the degree Doctor of Philosophy

in Chemistry

by

Sophia J. Bailey

Committee in charge:

Professor Javier Read de Alaniz, Chair

Professor Craig J. Hawker

Professor Christopher M. Bates

Professor Alison Butler

December 2022

The dissertation of Sophia J. Bailey is approved.

_____
Alison Butler

_____
Christopher M. Bates

_____
Craig J. Hawker

_____
Javier Read de Alaniz, Committee Chair

December 2022

Tales of Taming Cyclopentadiene: A Highly Reactive Diene for Materials Synthesis, Photopatterning and Property Enhancement via Diels–Alder Click Chemistry

Copyright © 2022

by

Sophia J. Bailey

This dissertation is dedicated to my mom, Sonia Bailey. Your unconditional love and support have made me the woman that I am today. I love you.

ACKNOWLEDGEMENTS

To start, I would like to thank Javier for being the most incredible PhD advisor one could ask for. You've supported and encouraged me to pursue any crazy idea that I brought to you, many of which failed to make it into this dissertation… or even a complete lab notebook page for that matter. But the few ideas that actually worked out fueled my excitement and curiosity for research and lead me down a wandering yet incredibly rewarding path. Thank you for everything. You make me believe that there are truly good people in academia and inspire me to be one of them.

I would also like to thank my undergraduate research mentor, Bill. I never would have started research, let alone apply to graduate school, if you hadn't tracked me down and invited me to join your lab while I was a student in your organic lecture. I am forever grateful for your mentorship, guidance, and friendship. To all of my other scientific mentors – Erika, Uttar, Emre, Andre – thank you for everything you've taught me and the insights you've shared.

I have been so incredibly grateful for the collaborative environment fostered at UCSB, and I would like to thank all the wonderful professors that have helped and supported me throughout my PhD, even if I wasn't a formal advisee – Craig, Max, Angela, Megan, Matt – thank you! I would also like to thank the amazing staff scientists that keep our shared instrument facilities running smoothly – Rachel, Amanda, Juan Manuel, Hongjun, Dmitriy – thank you for everything you do and your eagerness to provide advice and assistance throughout my research. Additionally, all the staff that keep the department and research running deserve a huge thank you, and a special thanks to Adrian, Trevor, Cabe and Phil who made purchasing chemicals and supplies, keeping the lab from falling apart, and disposing of hazardous waste as pleasant of experiences as they could possibly be. Also, a huge thank you

to all the researchers that I have gotten to learn from, work alongside, and share ideas with. To my number one collaborator, Erik, thank you so much. You have been such a great person to work with and I am so grateful to have had such a wonderful colleague to share so many challenges and triumphs. I would also like to thank the amazing undergraduate researchers that I have had the pleasure to work with – Michelle, Arsalan and Kiara – thank you all for your willingness to learn, nod at my confusing analogies, and, most importantly, laugh at my bad jokes.

One of the best parts of graduate school has been the community I have built here. Thank you to all the lab mates who became friends: Kyle and Jamie, duuudes do I miss you guys! Thanks for all the laughs and novelty playlists. Fritz, thank you for always being down for a hike, a vent session or a "Sophia needs a distraction" conversation. Even though you ditched me by graduating a year early, I am thankful to have gone through our PhDs together. Serena, thank you for reminding me that there is more to life than lab and creating the most inclusive and fun spaces. Also, thanks for all the tasty hangs, #piebois4life. Dr. Julie, thank you for always being willing to proofread a draft, nitpick a figure or bounce an *exciting* idea off of. You have been a huge inspiration to me, thank you so much for the guidance, mentorship, and great puns. Main-main – Thi, Cassidy and Guillén – you guys have really served as a family to me, and I am so incredibly appreciative of each of you. You have made the last year of graduate school so bittersweet and I am going to miss you all so much. Except for Thi's "Watcha doin'?" – I will not miss that. To the cohort friends I somehow managed to make outside of lab: Vani, thank you for always being there for me. You da best. And a huge thanks to Shannon, Greta, Christina, Max, Arun, Jacob who made holidays spent in Santa Barbara feel more like home.

Having a community outside of the university has also played such an important part in my time here and reminded me that there is more to being a person than graduate school. I would like to thank every member of Mission City Roller Derby, playing a full-contact sport does wonders for one's mental health, but doing it with such a supportive and fun group of people has been an absolute pleasure. To my Santa Barbara Familia –Lupe, Rafael, Steph, Kevin, Cyn and Rafa – thank you for taking me in as one of our own. I am so lucky to have you all.

I'd also like to thank the people who have been in my life long before graduate school. Allie and Marco, thank you for being unapologetically yourselves. Spending time with you over the last several years has been so refreshing. I am so grateful to have you as my friends. Kathy, thank you so much for your unconditional love and support. You have no idea how much you have shaped who I am in life. To my very best friend, Angelique, thank you for truly getting me. We are both terrible at keeping in touch, but I am glad that we have managed to do it. You are the best listener and so incredibly supportive, I am so lucky to have you in my life. To my family, Aimee, Evan, Dad and Sandra, thank you for always supporting me and shaping me into the goofy person I am. And finally, the very biggest thanks to my Mom, my biggest hype man and number one supporter. Thank you for everything.

VITA OF SOPHIA J. BAILEY

DECEMBER 2022

EDUCATION

Bachelor of Science in Chemistry, New Mexico State University, May 2018 (GPA 4.0/4.0)
Doctor of Philosophy in Chemistry, University of California, Santa Barbara, December 2022 (expected)

RESEARCH EXPERIENCE

Intern, Sapphire Energy, Inc. (Summer 2015)

- Experience in microalgae care (adjustment of nutrients, pH and CO_2), health monitoring (microscopy) and pond scale up (media preparation 10^3 liters) for industrial biofuel applications.

Undergraduate Researcher, New Mexico State University (2016–2018)

- Conducted research in synthetic organic chemistry under the advisement of Professor William A. Maio.
- Developed synthetic methods for the preparation of non-natural cannabidiol derivatives.
- Experience in synthesis, purification (column chromatography, distillation, crystallization) and characterization (^{1}H NMR, ^{13}C NMR, polarimetry, MS, IR) of organic compounds.

Research Assistant, University of California, Santa Barbara (2018–2022)

- Research focus at the interface of synthetic organic and polymer chemistry under the advisement of Professor Javier Read de Alaniz.
- Development of Diels–Alder click platforms for application in polymer chemistry involving organic synthesis and polymer characterization (^{1}H NMR, ^{13}C NMR, MS, IR, MALDI, SEC).
- Computational (DFT) and synthetic design of a novel photo-protecting group for reactive dienes for on-demand Diels–Alder cycloadditions.
- Development and application of a biocompatible Diels–Alder-based photopatterning platform for the patterning of hydrogels for cell culture.
- Implementation of rational mechanochemical design principles in Diels–Alder-based hydrogel systems.

TEACHING AND MENTORSHIP EXPERIENCE

Peer Learning Assistant, Department of Chemistry and Biochemistry, Department of Biology and Department of Mathematical Science, New Mexico State University (2015–2018)
Volunteer Instructor, SciTrek Elementary Outreach, University of California, Santa Barbara (2018–2022)

Teaching Assistant, Organic Chemistry Laboratory, Department of Chemistry and Biochemistry, University of California, Santa Barbara (Winter and Spring 2020)
Intern Mentor, Center for Science and Engineering Partnerships EUREKA! Program, University of California, Santa Barbara (2020–2021)
Volunteer Instructor, Elementary Biopolymer Workshop, California NanoSystems Institute, University of California, Los Angeles (Fall 2021)
Undergraduate Mentor, Women in STEM, University of California, Santa Barbara (2021–2022)
Instructor, School for Scientific Thought, University of California, Santa Barbara (Winter 2022)
Intern Mentor, Partnership for Research and Education in Materials, University of California, Santa Barbara (Summer 2022)
Facilitator, Family Ultimate Science Exploration, University of California, Santa Barbara (Fall 2022)

PUBLICATIONS

1. Truong, T. P; **Bailey, S. J.**; Golliher, A. E.; Monroy, E. Y.; Shrestha, U. K.; Maio, W. A. Exploiting Carvone to Demonstrate Both Stereocontrol and Regiocontrol: 1,2- vs 1,4-Addition of Grignard Reagents and Organocuprates. *J. Chem. Educ.* **2018**, *95*(3), 438–444. DOI: 10.1021/acs.jchemed.7b00892.
2. **Bailey, S. J.**; Sapkota, R. R.; Golliher, A. E.; Dungan, B.; Talipov, M.; Holguin, F. O.; Maio, W. A. Lewis–Acid-Mediated Union of Epoxy-Carvone Diastereomers with Anisole Derivatives: Mechanistic Insight and Application to the Synthesis of Non-natural CBD Analogues. *Org. Lett.* **2018**, *20*(15), 4618–4621. DOI: 10.1021/acs.orglett.8b01909.
3. St. Amant, A. H.;* Discekici, E. H* **Bailey, S. J.**; Zayas, M. S.; Song, J.; Shankel, S. L.; Nguyen, S. N.; Bates, M. W.; Anastasaki, A.; Hawker, C. J.; Read de Alaniz, J. Norbornadienes: Robust and Scalable Building Blocks for Cascade "Click" Coupling of High Molecular Weight Polymers. *J. Am. Chem. Soc.* **2019**, *141*(34), 13619–13624. DOI: 10.1021/jacs.9b06328.
4. **Bailey, S. J.**; Discekici, E. H.; Barbon, S. M.; Nguyen, S. N.; Hawker, C. J.; Read de Alaniz, J. Norbornadiene Chain-End Functional Polymers as Stable, Readily Available Precursors to Cyclopentadiene Derivatives. *Macromolecules* **2020**, *53*(12), 4917–4924. DOI: 10.1021/acs.macromol.0c00967.
5. Seshadri, S.; **Bailey, S. J.**; Zhao, L.; Fisher, J.; Sroda, M.; Chiu, M.; Stricker, F.; Valentine, M. T.; Read de Alaniz, J.; Helgeson, M. E. Influence of Polarity Change and Photophysical Effects on Photosurfactant-Driven Wetting. *Langmuir* **2021**, *37*(33), 9939–9951. DOI: 10.1021/acs.langmuir.1c00769.
6. **Bailey, S. J.**; Stricker, F.; Hopkins, E.; Wilson, M. Z.; Read de Alaniz, J. Shining Light on Cyclopentadienone–Norbornadiene Diels–Alder Adducts to Enable Photoinduced Click Chemistry with Cyclopentadiene. *ACS Appl. Mater. Interfaces* **2021**, *13*(30), 35422–35430. DOI: 10.1021/acsami.1c08670.
7. Zhao, L.; Seshadri, S.; Liang, X.; **Bailey, S. J.**; Haggmark, M.; Gordon, M.; Helgeson, M. E.; Read de Alaniz, J.; Luzzatto-Fegiz, P.; Zhu, Y. Depinning of Multiphase Fluid

Using Light and Photo-Responsive Surfactants. *ACS Cent. Sci.* **2022**, *8*(2), 235–245. DOI: 10.1021/acscentsci.1c01127

8. **Bailey, S. J.**; Barney, C. W.; Sinha, N.; Pangali, S. V.; Hawker, C. J.; Helgeson, M.; Valentine, M. T.; Read de Alaniz, J. Rational Mechanochemical Design of Diels–Alder Crosslinked Biocompatible Hydrogels with Enhanced Properties. *Mater. Horiz.* **2022**, *9*, 1947–1953. DOI: 10.1039/D2MH00338D.
9. Guillen Campos, J. J.; Stricker, F.; Clark, K.D.; Park, M.; **Bailey, S. J.**; Kuenstler, A.; Hayward, R.; Read de Alaniz, J. Controlled Diels–Alder "Click" Strategy to Access Mechanically Aligned Main-chain Liquid Crystal Networks. *Angew. Chem. Int. Ed.* **2022**, e202214339. DOI: 10.1002/anie.202214339.
10. **Bailey, S. J.**; Hopkins, E.; Rael, K. D.; Hashmi, A.; Urueña, J. M.; Wilson, M. Z.; Read de Alaniz, J. Design, Synthesis, and Application of a Water-Soluble Photocage for Aqueous Cyclopentadiene-based Diels–Alder Photoclick Chemistry in Hydrogels. *Submitted.*
11. **Bailey, S. J.**;* Hopkins, E.;* Wilson, M. Z.; Read de Alaniz, J. Diels–Alder-based Patterning of Natural Hydrogels for Cell Culture. *In progress.*

AWARDS AND HONORS

AP Scholar Award (2014)

Crimson Scholar, New Mexico State University (2014–2018)

High Achiever Leadership Scholarship, New Mexico State University (2014–2018)

First Place Paideia Documented Argument Contest, New Mexico State University English Department (2015)

Latimer R. Evans Scholarship Award in Organic Chemistry, New Mexico State University Department of Chemistry and Biochemistry (2016)

Atmar & Davis Memorial Award in Chemistry, New Mexico State University Department of Chemistry and Biochemistry (2016)

Ralph Wilkins Award in Chemistry, New Mexico State University Department of Chemistry and Biochemistry (2017)

Marie Heaton Endowed Award in Physical Chemistry, New Mexico State University Department of Chemistry and Biochemistry (2017)

G.R. Hamiel Memorial Award in Chemistry, New Mexico State University Department of Chemistry and Biochemistry (2017)

Alycia & Hans Fuchs Memorial Award in Chemistry, New Mexico State University Department of Chemistry and Biochemistry (2017)

ACS Undergraduate Award in Physical Chemistry (2017)

Darleane Hoffman Chemistry and Biochemistry Award, New Mexico State University Department of Chemistry and Biochemistry (2018)

ACS Division of Organic Chemistry Outstanding, Senior Organic Chemistry Student Chemistry (2018)

Chancellors Fellowship, University of California, Santa Barbara (2018–2022)

BioPACIFIC Fellow, BioPacific Materials Innovation Platform, University of California, Santa Barbara (2021–2022)

Runner-up, Grad Slam Competition, University of California, Santa Barbara (2022)

PRISM Cohort 9, Postdoctoral Recruitment in Science and Medicine, Stanford University (2022)

PRISM Baker Postdoctoral Fellowship, Stanford University (2022)

FIELDS OF STUDY

Major Field: Organic and Polymer Chemistry with Javier Read de Alaniz

Studies in Organic Methodology with William A. Maio.

ABSTRACT

Tales of Taming Cyclopentadiene: A Highly Reactive Diene for Materials Synthesis, Photopatterning and Property Enhancement via Diels–Alder Click Chemistry

by

Sophia J. Bailey

The application of highly efficient “click” reactions to the synthesis and modification of soft materials has been a fruitful endeavor enabling chemists, material scientists, and engineers to efficiently prepare materials with optimized performance and utility. Diels–Alder (DA) cycloadditions are a particularly attractive class of click reaction for use in polymer and biomaterials as they are highly modular and can proceed rapidly in the absence of a catalyst given the appropriate diene–dienophile pairing. However, traditional diene choice for normal electron demand DA cycloadditions has been dominated by dienes that provide building block stability at the price of efficient reactivity (i.e., furan and anthracene). Cyclopentadiene (Cp) is an incredibly promising diene for rapid DA click chemistry; however, Cp is inherently unstable and readily dimerizes at room temperature. This instability prohibits the inclusion of Cp units in molecular and polymer building blocks, thus, limiting the utility of Cp-based DA cycloadditions in polymer materials.

Herein, several “tales” of taming the reactivity of this unruly diene are presented which enable the rapid synthesis, spatiotemporal functionalization, and property enhancement of

polymer materials. In the first story, the use of norbornadiene (NBD) as a Cp precursor is described which enables the synthesis of complex polymer architectures. By incorporating NBD onto the chain end of macromolecular building blocks, a library of block copolymers was accessed from modular click reactions upon treatment of stable Cp precursors with a deprotecting agent, highlighting the utility of rapid DA cycloadditions in polymer click chemistry. Building upon the theme of on-demand Cp production, the second story presents the design and application of a novel Cp photocage. We demonstrate that access to photoprotected Cp affords spatiotemporal control over rapid DA click reactions, enabling the implementation of a DA-based photopatterning platform within polymer networks. To facilitate implementation in biological systems, an aqueous, photocaged Cp derivative was developed and implemented in a variety of PEG based hydrogels for subsequent patterning with dienophiles. Notably, because of the radical-free nature of this DA pattering platform, we demonstrate that this strategy can be used to pattern radical-sensitive, protein-based matrices for cell culture. Through patterned administration of biochemical cues within these bioactive hydrogels, we demonstrate spatial control over cellular growth and signaling. Finally, the last tale describes the use of a sterically tamed cyclopentadiene to access biocompatible materials with improved bulk properties. Through rational consideration of the mechanochemical activity of traditional furan–maleimide cycloadducts, we present a Cp derivative that increases the mechanical strength of the resulting cycloadduct and demonstrate the enhanced fracture resistance in corresponding hydrogel materials. With access to these three tamed Cp derivatives, practical uses of normal electron demand DA cycloadditions can be realized for the rapid synthesis and selective modification of polymer architectures to provide enhanced properties with novel biological and therapeutic applications.

TABLE OF CONTENTS

1 Chapter 1: *Introduction* 1

1.1 Click Chemistry: Synthesis Made Easy 1

1.2 Polymer Click Chemistry: A modular approach to macromolecule synthesis 3

1.3 Bioorthogonal Chemistry: Clicking in the presence of life 5

1.4 Photoclick Chemistry: An exciting route to spatiotemporal control 7

1.5 Normal Electron Demand Diels–Alder Cycloadditions: Not so Clickable 9

1.6 Thesis Scope 12

1.7 References 12

2 Chapter 2: *Norbornadiene as a Stable Precursor to Cyclopentadiene for Rapid Block Copolymer Synthesis* 19

2.1 Abstract 19

2.2 Introduction 20

2.3 Results and Discussion 23

2.4 Conclusion 40

2.5 Acknowledgements 40

2.6 Supporting Information 41

2.7 References 132

3 Chapter 3: *Shining Light on Cyclopentadienone–Norbornadiene Diels–Alder Adducts to Enable Photoinduced Click Chemistry with Cyclopentadiene* 138

3.1 Abstract 138

3.2 Introduction 139

3.3 Results and Discussion 144

3.4 Conclusion 155
3.5 Acknowledgments 156
3.6 Supporting Information 157
3.7 References 218
4 Chapter 4: *Design, Synthesis, and Application of a Water-soluble Photocage for Aqueous Cyclopentadiene-based Diels–Alder Photoclick Chemistry in Hydrogels* 225
4.1 Abstract 225
4.2 Introduction 226
4.3 Results and Discussion 230
4.4 Conclusion 241
4.5 Acknowledgments 241
4.6 Supporting Information 242
4.7 References 326
5 Chapter 5: *Diels–Alder-based Patterning of Natural Hydrogels for Cell Culture* 332
5.1 Abstract 332
5.2 Introduction 333
5.3 Results and Discussion 335
5.4 Conclusion 345
5.5 Acknowledgments 346
5.6 Supporting Information 346
5.7 References 362
6 Chapter 6: *Rational Mechanochemical Design of Diels–Alder Crosslinked Biocompatible Hydrogels with Enhanced Properties* 365

6.1 Abstract 365
6.2 Introduction 367
6.3 Results and Discussion 369
6.4 Conclusion 378
6.5 Acknowledgments 379
6.6 Supporting Information 380
6.7 References 428
7 Chapter 7: Future Directions and Outlook 434
7.1 Concluding remarks 437
7.2 References 437

ABBREVIATIONS

DA	Diels–Alder
rDA	retro Diels–Alder
NEDDA	normal electron demand Diels–Alder
IEDDA	inverse electron demand Diels–Alder
Cp	cyclopentadiene
Mal	maleimide
CuAAC	copper catalyzed azide–alkyne cycloaddition
SPAAC	strain promoted azide–alkyne cycloaddition
ECM	extracellular matrix
NBD	norbornadiene
DpTz	3,6-Di-2-pyridyl-1,2,4,5-tetrazine
ROP	ring opening polymerization
ATRP	atom transfer radical polymerization
RAFT	reversible addition/fragmentation chain transfer
PLA	polylactide
SEC	size exclusion chromatography
DBU	1,8-diazabicyclo[5.4.0]undec-7-ene
DCC	*N,N′*-dicyclohexylcarbodiimide
DMAP	4-dimethylaminopyridine
PEG	poly(ethylene glycol)
PMMA	poly(methyl methacrylate)
DCM	dichloromethane
THF	tetrahydrofuran
TLC	thin layer chromatography
NMR	nuclear magnetic resonance
CPD	cyclopentadienone
CPD–NBD	cyclopentadienone–norbornadiene
UV	ultraviolet
LED	light emitting diode
BAPO	trimethylbenzoyl)phosphine oxide
PBA	poly(butyl acrylate)
Cy5	Cyanine 5 dye
Cy3	Cyanine 3 dye
PBS	phosphate buffered saline
DMSO	dimethyl sulfoxide
PEGDA	poly(ethylene glycol) diacrylate
NHS	*N*-hydroxysuccinimide
DFT	density functional theory
LAP	lithium phenyl-2,4,6-trimethylbenzoylphosphinate
DLP	digital light processing
DMD	digital micromirror device
EGF	epidermal growth factor
KTR	kinase translocation reporter
hESC	human embryonic stem cell

CoGEF	constrained geometries simulate external force
SpCp	spiro[2.4]hepta-4,6-diene
dFA	distal furan
pFA	proximal furan
SANS	small angle neutron scattering

1 Chapter 1: *Introduction*

1.1 Click Chemistry: Synthesis Made Easy

The ability to rapidly piece together molecular building blocks can accelerate discoveries from new therapeutics to high-performance materials. However, efficient, and easy-to-use conjugation methods are needed to facilitate these new discoveries in the hands of chemists and non-chemists alike. Coincidently, at the time of writing this dissertation, the 2022 Nobel Prize in Chemistry was awarded to K. Barry Sharpless, Morten Meldal and Carolyn R. Bertozzi for their work developing methods to do just that: establishing the field of click chemistry.[1] The "click chemistry" concept was introduced in 2001 by Sharpless and colleagues who argued that the rapid preparation of novel molecules via "click" reactions would provide more rapid drug discovery than traditional natural product total synthesis and derivatization.[2] This seminal report also outlined specific criteria a reaction must meet to be deemed clickable:

That is, the reaction must be

- *modular*
- *wide in scope*
- *high yielding*
- *stereospecific*

and have

- *readily available starting materials*
- *simple conditions*
- *benign or easily removed solvents*
- *no or safe byproducts*

- *simple purification*.[2]

Several reaction types were originally identified which fulfilled these criteria and possessed a "spring-loaded" thermodynamic drive (> 20 kcal/mol) for the formation of a single product: 1,3-dipolar cycloadditions, Diels–Alder cycloadditions, nucleophilic ring opening reactions, non-aldol carbonyl chemistries (hydrazone/oxime formation), and additions to carbon–carbon double bonds (**Figure 1.1**).[2] To date, the most predominantly employed click reaction is a highly efficient 1,3-dipolar cycloaddition that was reported independently by the groups of Sharpless and Meldal in 2002: the copper catalyzed azide–alkyne cycloaddition (CuAAC).[3,4] CuAAC has prevailed as the gold (or rather *copper*) standard of click chemistries; however, other reactions have also found a distinguished place under the "click chemistry" umbrella (**Figure 1.1**). Notably, the strain promoted azide–alkyne cycloaddition (SPAAC), which was established in 2004 by Bertozzi and coworkers, has been the workhorse click reaction in biological systems and is discussed in depth in **Section 1.1.2.**.[5] Additionally, the tetrazine ligation/inverse electron demand Diels–Alder (IEDDA) cycloaddition,[6–8] oxime ligation,[9,10] sulfur(VI) fluoride exchange (SuFEx) reaction,[11] thiol–Michael addition (thiol–MA)[12] and thiol–ene reaction[13] have found great utility as click reactions (**Figure 1.1**).

Although originally presented as a tool for synthetic chemists to accelerate the discovery of novel molecules with useful properties, the accessibility of click reactions has enabled advancements to be made across numerous fields from chemical biology[14] to materials science.[15] This rapid adoption of click chemistry principles by new research communities has relied upon the establishment of additional click criteria (i.e. bioorthogonality, rapid kinetics, scalability, spatiotemporal control) depending on the intended use. The remainder of this chapter discusses three click subfields (polymer click chemistry, bioorthogonal chemistry and

photoclick chemistry) relevant to the advancement of soft materials discussed throughout this dissertation followed by an introduction to the specific click reaction that is the subject of investigation: the normal electron demand Diels–Alder cycloaddition.

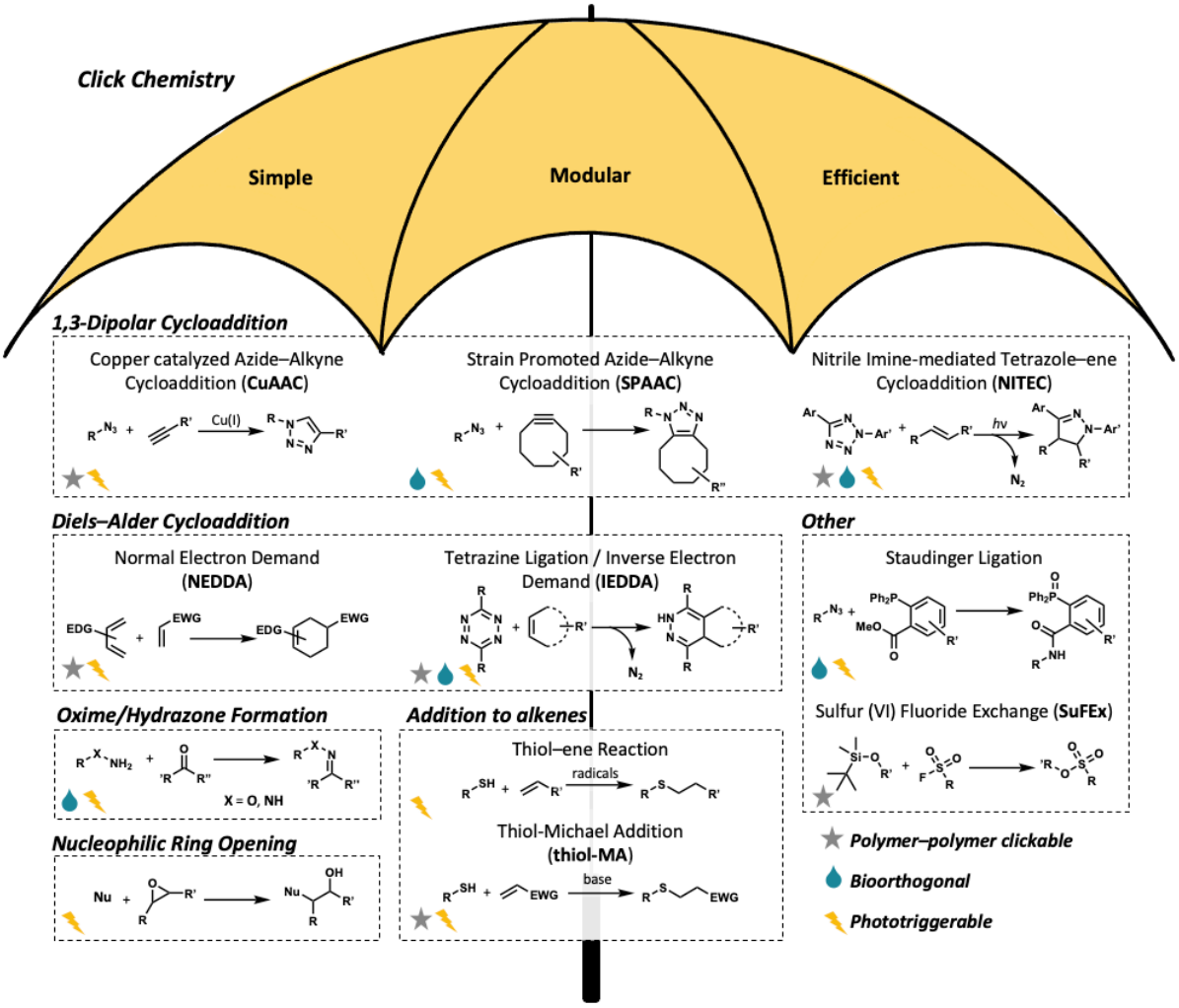

Figure 1.1. Graphic depiction of common reactions falling under the "Click Chemistry Umbrella."

1.2 Polymer Click Chemistry: A modular approach to macromolecule synthesis

The universality of click chemistry principles was quickly recognized by polymer chemists who echoed the need for modular, efficient, and simple reactions to accelerate the synthesis and modification of macromolecules. The debut of click chemistry in macromolecular

synthesis came in 2004, just a few years after the establishment of click chemistry principles for drug discovery, where CuAAC was employed in the elegant preparation of dendritic materials.[16] Following this seminal report in the polymer community, the modularity of the click approach was quickly exploited in the preparation of block copolymers,[17] and to-date click chemistry has become a go-to route for polymer modification and architecture construction (star, cyclic, grafted and network, **Figure 1.2a**).[18] In fact, by 2009 the click philosophy was recognized to have led to a notable shift in polymer chemists' approach to material synthesis and was attributed to considerable innovation within the field.[19]

The unique challenges associated with the removal of excess macromolecular click partners, limited purification techniques (precipitation), and need for industrial scale applications have led the polymer community to define their own guidelines for selecting polymer click reactions. In addition to the originally outlined criteria, polymer click reactions, particularly those involving polymer–polymer conjugation, must also proceed on a *fast timescale* using *equimolar click partners* and be *purified on large-scale*.[20] To date, CuAAC,[21] DA cycloadditions,[22] thiol–MA[12] and thiol–ene reactions[23] have dominated the polymer click space due to their *ease-of-use* for large scale macromolecular synthesis and *scalability* of macromolecular click building blocks. However, emerging click reactions like SuFEx[24] and triazolinedione (TAD) click/trans-click[25] are also gaining popularity within the polymer community. The application of click chemistries to macromolecular synthesis has fueled innovation over the last twenty years and the growing toolbox of polymer click reactions promises access to novel architectures and improved function in next-generation polymer materials.

1.3 Bioorthogonal Chemistry: Clicking in the presence of life

Accomplishing controlled chemical conjugation within living systems poses a unique set of challenges: aqueous environment with fixed pH (7.4) and temperature (37 °C), extremely low concentrations of biomolecules (nanomolar to micromolar), numerous native functionalities from proteins, glycans, lipids and nucleic acids, and a general sensitivity to metals, radicals, chemical reagents and other foreign additives.[14] Thus, establishing orthogonality in this demanding environment becomes of utmost importance in the application of click reactions to biological systems. Thus, bioorthogonal reactions must possess *rapid kinetics* to overcome the incredibly low concentrations of biomolecules and *exceptional selectivity* in the presence of biological functionalities. Logistically, these reactions must proceed under physiological conditions, requiring *aqueous solubility, water insensitivity* and *absence of toxicity* at the concentrations required for efficient clicking.[26]

Although CuAAC has demonstrated its utility in bioconjugation,[27] the toxicity of copper(I) has limited its use in living systems. Inspired by the efficient 1,3-dipolar cycloaddition by alkyne activation with copper(I), Bertozzi and coworkers presented the strain-promoted azide–alkyne cycloaddition (SPAAC) by taking advantage of the inherent strain in cyclooctyne units (18 kcal/mol) to accelerate the rate of reaction.[5] Although bioorthogonal, the relatively slow reaction ($k = 10^{-3}$ M^{-1} s^{-1}) has warranted the development of more destabilized cyclooctyne derivatives by introducing electron withdrawing groups (i.e. fluorine atoms) or additional ring strain.[28] The bioorthogonal click predecessor to SPAAC, the Staudinger ligation, was introduced by Bertozzi and Saxon before the establishment of click chemistry, yet with the similar goal of enabling highly selective and efficient conjugation between azides and triarylphosphine derivatives.[29,30] Like SPAAC, the Staudinger ligation takes advantage of

azides as small, bioinert functionalities that can be introduced into biological systems with minimal perturbation. Although it has been utilized extensively for bioconjugation,[31,32] the Staudinger ligation also suffers from slow rates ($k = 10^{-3}$ M^{-1} s^{-1}) and derivatization of azide derivatives has been required to increase the reactivity.[32]

Two other click reaction types have also proven themselves as distinguished bioorthogonal reactions: oxime/hydrazone formation[9] and IEDDA tetrazine ligation.[6] As was key for SPAAC and Staudinger ligations, the success of these two reactions stems from bioorthogonal functionalities. The alkoxyamines, hydrazines, tetrazines and strained alkenes used in these click reactions do not have native biological functions, thus enabling high selectivity for click reactions. Notably, the IEDDA between tetrazine and strained alkenes has prevailed as one of the fastest conjugation methods available (up to $k = 10^{6}$ M^{-1} s^{-1}).[7] These unmatched kinetics and biorthogonality have fueled the development of IEDDA for cellular imaging, drug delivery and biomaterials synthesis.[7]

A major challenge facing bioorthogonal click reactions, however, is the commercial availability and synthetic challenge of tetrazines and strained cyclic ring systems. For the labeling of cells, having expensive or difficult to scale precursors[33] does not pose a significant problem, as small amounts of materials (nanograms to micrograms) are needed. However, in the case of using click chemistry for biomaterials synthesis, the combination of the seemingly mutually exclusive principles of polymer and bioorthogonal click reactions is needed. Elegant examples of biomaterials synthesis in the presence of living cells have been demonstrated with SPAAC[34] and IEDDA[35] which exhibit great promise in tissue engineering applications. Thus, the translation of bioorthogonal click chemistries to large scale (grams to kilograms)

biomaterials systems is needed to expand the utility of bioorthogonal click chemistry past chemical biology applications.

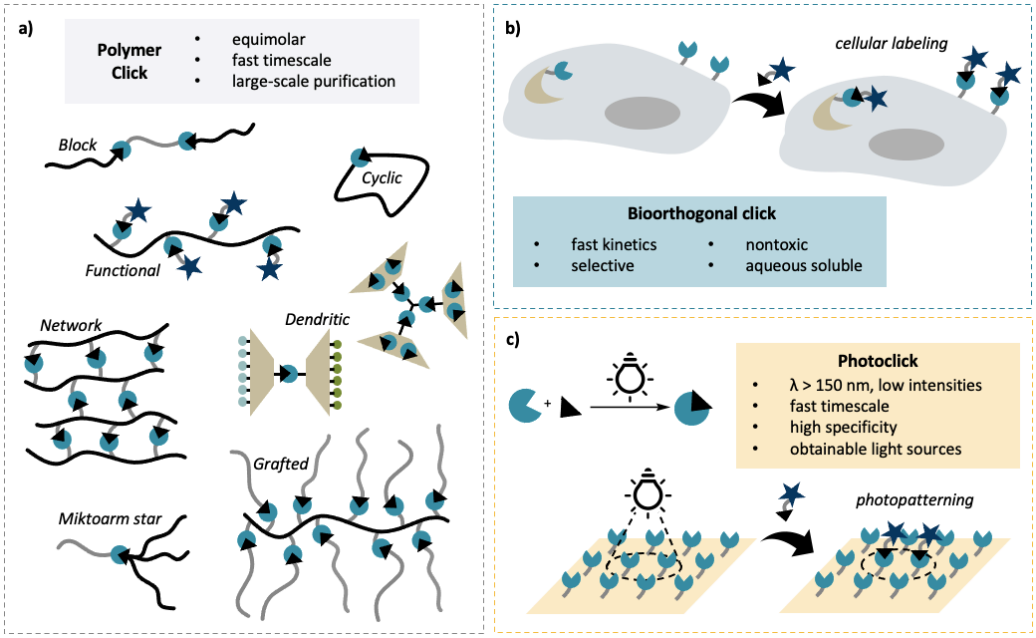

Figure 1.2. Requirements for and graphic depiction of click examples for a) polymer clicks,[20] b) bioorthogonal clicks[26] and c) photoclicks.[35]

1.4 Photoclick Chemistry: An exciting route to spatiotemporal control

The term "photoclick chemistry" was first coined in 2008 by Lin and coworkers to describe a bioorthogonal, photoinduced, nitrile imine-mediated tetrazole–ene 1,3-dipolar cycloaddition (NITEC) that had been used to selectively functionalize a protein in bacterial cells.[37] Since this illuminating report, researchers have found numerous ways to trigger many of the previously established click chemistries with light.[38] Thiol–ene chemistry can use a photoinitiator to induce the radical-based mechanism, granting it automatic "photoclick" status. CuAAC has been induced by photoreduction of Cu(II) to Cu(I);[39,40] whereas, IEDDA has been induced by photooxidation of dihydrotetrazine to tetrazine.[41] Furthermore, base-catalyzed nucleophilic

addition click reactions can be rendered photo-induced by the use of photolatent bases.[42] The installation of photoremovable protecting groups on clickable moieties provides another route to light triggered click chemistry. This strategy has been demonstrated via the photouncaging a number of clickable functionalities including thiols,[43] cyclooctynes,[44] tetrazines,[45] and alkoxyamines.[46,47] Additionally, a well-established photoenolization of *ortho*-methyl phenyl ketones and aldehydes has enabled a variety of photo-DA cycloadditions upon reactions of the transiently formed enol-based dienes with appropriate dienophiles.[48,49] Given the growing interest in photo-induced click reactions, Bowman and colleagues recently proposed an additional set of criteria for photoclick chemistry: these reactions must *avoid high energy wavelengths (<150 nm)* and be *triggered at low light intensity* while proceeding on *fast timescales* and with *high specificity*.[36] Additionally, to promote accessibility the *equipment for irradiation must be easily obtainable*.[36]

The spatiotemporal control afforded by photoclick reactions has enabled numerous applications including localized cellular labeling, surface modification and patterning, and on-demand polymer network formation.[36] A particularly exciting application of photoclick chemistry is in the preparation and patterning of hydrogels for tissue engineering.[50] Hydrogels are water-swollen polymer networks that are often employed as extracellular matrix (ECM) mimics due to their high water content and comparable mechanical properties to natural tissues.[51] Impressively, photoclick reactions have enabled on-demand hydrogel formation in the presence of cells as well as 3D hydrogel patterning with biomolecules to enable spatial control over cellular processes.[50] However, establishing photoclick chemistries with bioorthogonality for the preparation of ECM mimics remains a challenge. Typically, thiol–ene is the go-to photoclick reaction for patterning hydrogels for its ease of use;[50] however, the

reliance on photoinitiators and a radical propagating mechanism can be deleterious to certain cell lines[52] and proteins.[53] Furthermore, the possibility for off-target reactivity with native cysteine residues prohibits this reaction from true bioorthogonality. Thus, tissue engineering technologies based on thiol–ene photoclick chemistry are limited to radical insensitive biomolecules, matrices and cell cultures. To address these issues, the Deforest group has worked towards developing photo-click strategies that avoid radical propagation through the use of photocaged alkoxyamine moieties, which enable bioorthogonal photoclick-based hydrogel formation in the presence of cells[47] and photopatterning in radical-sensitive protein-based matrices.[54] This work highlights the need to establish novel photopatterning strategies from non-radical propagating photoclick chemistries to advance tissue engineering technologies.

1.5 Normal Electron Demand Diels–Alder Cycloadditions: Not so Clickable

As highlighted throughout **Sections 1.1–1.4.**, the Diels–Alder (DA) cycloaddition has proven itself to be an esteemed click reaction with exceptional utility throughout total synthesis,[55] polymer construction,[22] and bioconjugation.[7] This reaction was first *correctly* described in 1928 by Otto Diels and Kurt Alder[56] and comprises a [4+2]-cycloaddition between a 4π electron containing diene with a 2π electron containing dienophile to form a 6-membered ring. The widespread utility of this reaction originates from it being metal, additive and byproduct free, synthetically accessible, and highly efficient when the correct choice of diene and dienophile are employed. In the normal electron demand system, reactivity is achieved by introducing electron donating groups on the diene, effectively raising the energy of the highest occupied molecular orbital (HOMO), or conversely, lowering the lowest unoccupied molecular orbital (LUMO) of the dienophile through electron withdrawing groups. By reducing the

HOMO–LUMO gap, improved orbital overlap leads to facile electrocyclization of the electronically matched diene/dienophile pairs.[57] In contrast, IEDDA reactions occur between electron rich dienophiles and electron poor dienes.

Although NEDDA reactions have found utility in the construction of materials, the "clickability" of commonly employed diene/dienophile pairs (furan/maleimide and anthracene/maleimide) in polymer synthesis is arguable. With modest second order rate constants of 10^{-5} and 10^{-3} M^{-1} s^{-1} for the non-aqueous cycloaddition between maleimide dienophiles with furan[58] or anthracene,[59] respectively, these cycloadditions hardly fulfill the "*fast timescale"* requirement of polymer click chemistry. As depicted in **Figure 1.3.** even with hydrophobic acceleration by 100–1000 times,[58,59] these rate constants are comparable to SPAAC at best, remaining orders of magnitude slower than their inverse electron demand analogs[7] and other omnipresent click reactions like CuAAC[28] and thiol–MA.[60] Subsequently, NEDDA polymer click reactions often require long reaction times and high temperatures for efficient clicking.[61] Incidentally, it is the facile reversibility at low temperatures (approximately 100 °C) of the furan/maleimide system that is more commonly exploited in NEDDA "click" polymers for the developing remendable, self-healing materials.[62–64] For robust DA click reactions, IEDDA has instead dominated as the go-to click reaction due to its superior kinetics and bioorthogonality, as NEDDA dienophiles (i.e. maleimides) often possess reactivity towards native biological functionalities (i.e. thiols).[26] However, the synthetic and commercial accessibility of NEDDA dienes and dienophiles, as well as the metal-free, aqueous accelerated and orthogonal features of electrocyclizations warrant the development of more reactive NEDDA diene/dienophile pairings to add to the click toolbox.

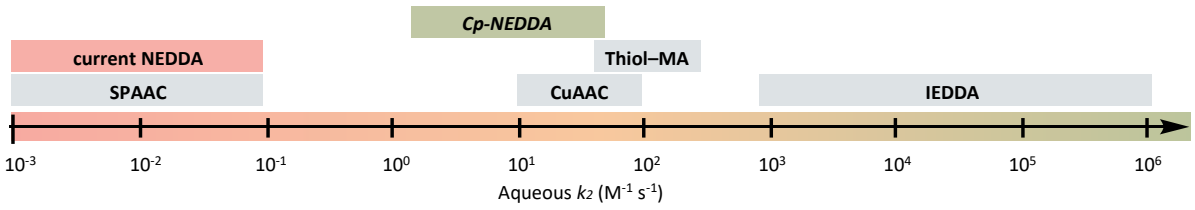

Figure 1.3. Scale depicting aqueous second order rate constants of common click reactions in comparison to reactivity currently utilized NEDDA reactions and Cp-based NEDDA reactions.

Work towards the development of highly reactive dienophiles has been successful;[25] however, the maleimide dienophile is not to blame for the aforementioned lack of reactivity in NEDDA cycloadditions. In fact, this electron-poor dienophile will react rapidly when coupled to more activated dienes: *cyclopentadiene* (Cp) derivatives provide rapid cycloadditions with maleimide with rate constants comparable to CuAAC (**Figure 1.3.**)![58] In addition to possessing an electron-rich and cyclic structure which locks Cp into the *cis* diene geometry needed for electrocyclization, the pronounced reactivity of Cp is attributed to the proximity of the C1 and C4 diene carbons which reduces the required distortion needed to access the cycloaddition transition state geometry.[65] This ultrafast diene has been utilized in polymer–polymer coupling reactions[66] and shows great promise in promoting NEDDA to an indisputable click reaction.[67] Furthermore, Cp has recently been reported for use in IEDDA bioconjugation with tetrazines, highlighting its potential for use in bioorthogonal click chemistry.[60] However, this promising reactivity for click chemistry comes with the tradeoff of stability. The Cp unit is susceptible to dimerization with a half-life of approximately 28 hours at room temperature.[67] Thus, materials functionalized with cyclopentadiene units must be stored at low temperatures (<20 °C) and are not compatible with long-term storage. This inherent instability has prohibited its widespread adoption in NEDDA click reactions, and largely limited the research community to much slower NEDDA dienes.

1.6 Thesis Scope

Given the promise of cyclopentadiene for rapid NEDDA click chemistry, the ability to harness the reactivity of this diene would greatly advance its utility in soft materials synthesis and applications. The subsequent chapters of this dissertation present several strategies that we have developed to tame this unruly diene. First, Chapter 2 introduces norbornadiene as a stable cyclopentadiene precursor that enables rapid, on-demand click reactions with dienophiles upon treatment with a chemical agent to form cyclopentadiene in situ. This strategy was used to prepare block copolymers from norbornadiene and maleimide bearing building blocks via rapid NEDDA click reactions at room temperature. Building upon the employment of cyclopentadiene precursors for on demand click chemistry, Chapter 3 presents cyclopentadienone–norbornadiene (CPD–NBD) adducts as a photocaged cyclopentadienes for photoclick-based patterning. To expand this photopatterning strategy to biological systems, Chapter 4, outlines the computational and synthetic design of a water soluble CPD–NBD adduct for use in aqueous systems and Chapter 5 demonstrates the use of CPD–NBD adducts to pattern protein-based hydrogels for cell culture. After covering various strategies to prepare materials from Cp-based NEDDA cycloadditions, Chapter 6 takes a step back to consider the effects of cycloadducts on final material properties. Specifically, mechanochemical design principles are employed to prepare cyclopentadiene-based hydrogels with enhanced properties. Finally, Chapter 7 provides an outlook on cyclopentadiene–based DA strategies for biological materials applications.

1.7 References

(1) *The Nobel Prize in Chemistry 2022*. NobelPrize.org. https://www.nobelprize.org/prizes/chemistry/2022/press-release/ (accessed 2022-10-05).

(2) Kolb, H. C.; Finn, M. G.; Sharpless, K. B. Click Chemistry: Diverse Chemical Function from a Few Good Reactions. *Angew. Chem. Int. Ed.* **2001**, *40* (11), 2004–2021. DOI: 10.1002/1521-3773(20010601)40:11<2004::AID-ANIE2004>3.0.CO;2-5.

(3) Rostovtsev, V. V.; Green, L. G.; Fokin, V. V.; Sharpless, K. B. A Stepwise Huisgen Cycloaddition Process: Copper(I)-Catalyzed Regioselective "Ligation" of Azides and Terminal Alkynes. *Angew. Chem. Int. Ed. Engl.* **2002**, *41* (14), 2596–2599. DOI: 10.1002/1521-3773(20020715)41:14<2596::AID-ANIE2596>3.0.CO;2-4.

(4) Tornøe, C. W.; Christensen, C.; Meldal, M. Peptidotriazoles on Solid Phase: [1,2,3]-Triazoles by Regiospecific Copper(I)-Catalyzed 1,3-Dipolar Cycloadditions of Terminal Alkynes to Azides. *J. Org. Chem.* **2002**, *67* (9), 3057–3064. DOI: 10.1021/jo011148j.

(5) Agard, N. J.; Prescher, J. A.; Bertozzi, C. R. A Strain-Promoted [3 + 2] Azide−Alkyne Cycloaddition for Covalent Modification of Biomolecules in Living Systems. *J. Am. Chem. Soc.* **2004**, *126* (46), 15046–15047. DOI: 10.1021/ja044996f.

(6) Blackman, M. L.; Royzen, M.; Fox, J. M. Tetrazine Ligation: Fast Bioconjugation Based on Inverse-Electron-Demand Diels−Alder Reactivity. *J. Am. Chem. Soc.* **2008**, *130* (41), 13518–13519. DOI: 10.1021/ja8053805.

(7) Oliveira, B. L.; Guo, Z.; Bernardes, G. J. L. Inverse Electron Demand Diels–Alder Reactions in Chemical Biology. *Chem. Soc. Rev.* **2017**, *46* (16), 4895–4950. DOI: 10.1039/C7CS00184C.

(8) Knall, A.-C.; Slugovc, C. Inverse Electron Demand Diels–Alder (IEDDA)-Initiated Conjugation: A (High) Potential Click Chemistry Scheme. *Chem. Soc. Rev.* **2013**, *42* (12), 5131. DOI: 10.1039/c3cs60049a.

(9) Kölmel, D. K.; Kool, E. T. Oximes and Hydrazones in Bioconjugation: Mechanism and Catalysis. *Chem. Rev.* **2017**, *117* (15), 10358–10376. DOI: 10.1021/acs.chemrev.7b00090.

(10) Collins, J.; Xiao, Z.; Müllner, M.; Connal, L. A. The Emergence of Oxime Click Chemistry and Its Utility in Polymer Science. *Polym. Chem.* **2016**, *7* (23), 3812–3826. DOI: 10.1039/C6PY00635C.

(11) Dong, J.; Krasnova, L.; Finn, M. G.; Sharpless, K. B. Sulfur(VI) Fluoride Exchange (SuFEx): Another Good Reaction for Click Chemistry. *Angew. Chem. Int. Ed.* **2014**, *53* (36), 9430–9448. DOI: 10.1002/anie.201309399.

(12) Nair, D. P.; Podgórski, M.; Chatani, S.; Gong, T.; Xi, W.; Fenoli, C. R.; Bowman, C. N. The Thiol-Michael Addition Click Reaction: A Powerful and Widely Used Tool in Materials Chemistry. *Chem. Mater.* **2014**, *26* (1), 724–744. DOI: 10.1021/cm402180t.

(13) Hoyle, C. E.; Bowman, C. N. Thiol-Ene Click Chemistry. *Angew. Chem. Int. Ed.* **2010**, *49* (9), 1540–1573. DOI: 10.1002/anie.200903924.

(14) Jewett, J. C.; Bertozzi, C. R. Cu-Free Click Cycloaddition Reactions in Chemical Biology. *Chem. Soc. Rev.* **2010**, *39* (4), 1272. DOI: 10.1039/b901970g.

(15) Xi, W.; Scott, T. F.; Kloxin, C. J.; Bowman, C. N. Click Chemistry in Materials Science. *Adv. Funct. Mater.* **2014**, *24* (18), 2572–2590. DOI: 10.1002/adfm.201302847.

(16) Wu, P.; Feldman, A. K.; Nugent, A. K.; Hawker, C. J.; Scheel, A.; Voit, B.; Pyun, J.; Fréchet, J. M. J.; Sharpless, K. B.; Fokin, V. V. Efficiency and Fidelity in a Click-Chemistry Route to Triazole Dendrimers by the Copper(I)-Catalyzed Ligation of Azides and Alkynes. *Angew. Chem. Int. Ed.* **2004**, *43* (30), 3928–3932. DOI: 10.1002/anie.200454078.

(17) Opsteen, J. A.; van Hest, J. C. M. Modular Synthesis of Block Copolymers via Cycloaddition of Terminal Azide and Alkyne Functionalized Polymers. *Chem. Commun.* **2005**, No. 1, 57. DOI: 10.1039/b412930j.

(18) Geng, Z.; Shin, J. J.; Xi, Y.; Hawker, C. J. Click Chemistry Strategies for the Accelerated Synthesis of Functional Macromolecules. *J. Polym. Sci.* **2021**, *59* (11), 963–1042. DOI: 10.1002/pol.20210126.

(19) Barner-Kowollik, C.; Inglis, A. J. Has *Click Chemistry* Lead to a Paradigm Shift in Polymer Material Design? *Macromol. Chem. Phys.* **2009**, *210* (12), 987–992. DOI: 10.1002/macp.200900139.

(20) Barner-Kowollik, C.; Du Prez, F. E.; Espeel, P.; Hawker, C. J.; Junkers, T.; Schlaad, H.; Van Camp, W. "Clicking" Polymers or Just Efficient Linking: What Is the Difference? *Angew. Chem. Int. Ed.* **2011**, *50* (1), 60–62. DOI: 10.1002/anie.201003707.

(21) Meldal, M. Polymer "Clicking" by CuAAC Reactions. *Macromol. Rapid Commun.* **2008**, *29* (12–13), 1016–1051. DOI: 10.1002/marc.200800159.

(22) Tasdelen, M. A. Diels–Alder "Click" Reactions: Recent Applications in Polymer and Material Science. *Polym. Chem.* **2011**, *2* (10), 2133. DOI: 10.1039/c1py00041a.

(23) Lowe, A. B. Thiol-Ene "Click" Reactions and Recent Applications in Polymer and Materials Synthesis. *Polym. Chem.* **2010**, *1* (1), 17–36. DOI: 10.1039/B9PY00216B.

(24) Brendel, J. C.; Martin, L.; Zhang, J.; Perrier, S. SuFEx – a Selectively Triggered Chemistry for Fast, Efficient and Equimolar Polymer–Polymer Coupling Reactions. *Polym. Chem.* **2017**, *8* (48), 7475–7485. DOI: 10.1039/C7PY01636K.

(25) Billiet, S.; De Bruycker, K.; Driessen, F.; Goossens, H.; Van Speybroeck, V.; Winne, J. M.; Du Prez, F. E. Triazolinediones Enable Ultrafast and Reversible Click Chemistry for the Design of Dynamic Polymer Systems. *Nat. Chem.* **2014**, *6* (9), 815–821. DOI: 10.1038/nchem.2023.

(26) Sletten, E. M.; Bertozzi, C. R. Bioorthogonal Chemistry: Fishing for Selectivity in a Sea of Functionality. *Angew. Chem. Int. Ed.* **2009**, *48* (38), 6974–6998. DOI: 10.1002/anie.200900942.

(27) Hong, V.; Presolski, S. I.; Ma, C.; Finn, M. G. Analysis and Optimization of Copper-Catalyzed Azide-Alkyne Cycloaddition for Bioconjugation. *Angewandte Chemie* **2009**, *121* (52), 10063–10067. DOI: 10.1002/ange.200905087.

(28) McKay, C. S.; Finn, M. G. Click Chemistry in Complex Mixtures: Bioorthogonal Bioconjugation. *Chemistry & Biology* **2014**, *21* (9), 1075–1101. DOI: 10.1016/j.chembiol.2014.09.002.

(29) Saxon, E.; Bertozzi, C. R. Cell Surface Engineering by a Modified Staudinger Reaction. *Science* **2000**, *287* (5460), 2007–2010. DOI: 10.1126/science.287.5460.2007.

(30) Sletten, E. M.; Bertozzi, C. R. From Mechanism to Mouse: A Tale of Two Bioorthogonal Reactions. *Acc. Chem. Res.* **2011**, *44* (9), 666–676. DOI: 10.1021/ar200148z.

(31) Bednarek, C.; Wehl, I.; Jung, N.; Schepers, U.; Bräse, S. The Staudinger Ligation. *Chem. Rev.* **2020**, *120* (10), 4301–4354. DOI: 10.1021/acs.chemrev.9b00665.

(32) Heiss, T. K.; Dorn, R. S.; Prescher, J. A. Bioorthogonal Reactions of Triarylphosphines and Related Analogues. *Chem. Rev.* **2021**, *121* (12), 6802–6849. DOI: 10.1021/acs.chemrev.1c00014.

(33) Chadwick, R.; Van Gyzen, S.; Liogier, S.; Adronov, A. Scalable Synthesis of Strained Cyclooctyne Derivatives. *Synthesis* **2014**, *46* (05), 669–677. DOI: 10.1055/s-0033-1340509.

(34) DeForest, C. A.; Polizzotti, B. D.; Anseth, K. S. Sequential Click Reactions for Synthesizing and Patterning Three-Dimensional Cell Microenvironments. *Nat. Mater.* **2009**, *8* (8), 659–664. DOI: 10.1038/nmat2473.

(35) Alge, D. L.; Azagarsamy, M. A.; Donohue, D. F.; Anseth, K. S. Synthetically Tractable Click Hydrogels for Three-Dimensional Cell Culture Formed Using Tetrazine–Norbornene Chemistry. *Biomacromolecules* **2013**, *14* (4), 949–953. DOI: 10.1021/bm4000508.

(36) Fairbanks, B. D.; Macdougall, L. J.; Mavila, S.; Sinha, J.; Kirkpatrick, B. E.; Anseth, K. S.; Bowman, C. N. Photoclick Chemistry: A Bright Idea. *Chem. Rev.* **2021**, *121* (12), 6915–6990. DOI: 10.1021/acs.chemrev.0c01212.

(37) Song, W.; Wang, Y.; Qu, J.; Lin, Q. Selective Functionalization of a Genetically Encoded Alkene-Containing Protein via "Photoclick Chemistry" in Bacterial Cells. *J. Am. Chem. Soc.* **2008**, *130* (30), 9654–9655. DOI: 10.1021/ja803598e.

(38) Kumar, G. S.; Lin, Q. Light-Triggered Click Chemistry. *Chem. Rev.* **2020**, *121* (12), 6991–7031. DOI: 10.1021/acs.chemrev.0c00799.

(39) Adzima, B. J.; Tao, Y.; Kloxin, C. J.; DeForest, C. A.; Anseth, K. S.; Bowman, C. N. Spatial and Temporal Control of the Alkyne–Azide Cycloaddition by Photoinitiated Cu(II) Reduction. *Nat. Chem.* **2011**, *3* (3), 256–259. DOI: 10.1038/nchem.980.

(40) Tasdelen, M. A.; Yagci, Y. Light-Induced Copper(I)-Catalyzed Click Chemistry. *Tetrahedron Lett.* **2010**, *51* (52), 6945–6947. DOI: 10.1016/j.tetlet.2010.10.166.

(41) Zhang, H.; Trout, W. S.; Liu, S.; Andrade, G. A.; Hudson, D. A.; Scinto, S. L.; Dicker, K. T.; Li, Y.; Lazouski, N.; Rosenthal, J.; Thorpe, C.; Jia, X.; Fox, J. M. Rapid

Bioorthogonal Chemistry Turn-on through Enzymatic or Long Wavelength Photocatalytic Activation of Tetrazine Ligation. *J. Am. Chem. Soc.* **2016**, *138* (18), 5978–5983. DOI: 10.1021/jacs.6b02168.

(42) Zhang, X.; Xi, W.; Wang, C.; Podgórski, M.; Bowman, C. N. Visible-Light-Initiated Thiol-Michael Addition Polymerizations with Coumarin-Based Photobase Generators: Another Photoclick Reaction Strategy. *ACS Macro Lett.* **2016**, *5* (2), 229–233. DOI: 10.1021/acsmacrolett.5b00923.

(43) Wylie, R. G.; Shoichet, M. S. Three-Dimensional Spatial Patterning of Proteins in Hydrogels. *Biomacromolecules* **2011**, *12* (10), 3789–3796. DOI: 10.1021/bm201037j.

(44) Poloukhtine, A. A.; Mbua, N. E.; Wolfert, M. A.; Boons, G.-J.; Popik, V. V. Selective Labeling of Living Cells by a Photo-Triggered Click Reaction. *J. Am. Chem. Soc.* **2009**, *131* (43), 15769–15776. DOI: 10.1021/ja9054096.

(45) Liu, L.; Zhang, D.; Johnson, M.; Devaraj, N. K. Light-Activated Tetrazines Enable Precision Live-Cell Bioorthogonal Chemistry. *Nat. Chem.* **2022**, *14* (9), 1078–1085. DOI: 10.1038/s41557-022-00963-8.

(46) DeForest, C. A.; Tirrell, D. A. A Photoreversible Protein-Patterning Approach for Guiding Stem Cell Fate in Three-Dimensional Gels. *Nat. Mater.* **2015**, *14* (5), 523–531. DOI: 10.1038/nmat4219.

(47) Farahani, P. E.; Adelmund, S. M.; Shadish, J. A.; DeForest, C. A. Photomediated Oxime Ligation as a Bioorthogonal Tool for Spatiotemporally-Controlled Hydrogel Formation and Modification. *J. Mater. Chem. B* **2017**, *5* (23), 4435–4442. DOI: 10.1039/C6TB03400D.

(48) Gruendling, T.; Oehlenschlaeger, K. K.; Frick, E.; Glassner, M.; Schmid, C.; Barner-Kowollik, C. Rapid UV Light-Triggered Macromolecular *Click* Conjugations via the Use of *o* -Quinodimethanes. *Macromol. Rapid Commun.* **2011**, *32* (11), 807–812. DOI: 10.1002/marc.201100159.

(49) Pauloehrl, T.; Delaittre, G.; Winkler, V.; Welle, A.; Bruns, M.; Börner, H. G.; Greiner, A. M.; Bastmeyer, M.; Barner-Kowollik, C. Adding Spatial Control to Click Chemistry: Phototriggered Diels-Alder Surface (Bio)Functionalization at Ambient Temperature. *Angew. Chem. Int. Ed.* **2012**, *51* (4), 1071–1074. DOI: 10.1002/anie.201107095.

(50) Grim, J. C.; Marozas, I. A.; Anseth, K. S. Thiol-Ene and Photo-Cleavage Chemistry for Controlled Presentation of Biomolecules in Hydrogels. *J. Control. Release* **2015**, *219*, 95–106. DOI: 10.1016/j.jconrel.2015.08.040.

(51) Drury, J. L.; Mooney, D. J. Hydrogels for Tissue Engineering: Scaffold Design Variables and Applications. *Biomaterials* **2003**, *24* (24), 4337–4351. DOI: 10.1016/S0142-9612(03)00340-5.

(52) Williams, C. G.; Malik, A. N.; Kim, T. K.; Manson, P. N.; Elisseeff, J. H. Variable Cytocompatibility of Six Cell Lines with Photoinitiators Used for Polymerizing

Hydrogels and Cell Encapsulation. *Biomaterials* **2005**, *26* (11), 1211–1218. DOI: 10.1016/j.biomaterials.2004.04.024.

(53) Dean, R. T.; Fu, S.; Stocker, R.; Davies, M. J. Biochemistry and Pathology of Radical-Mediated Protein Oxidation. *Biochem. J.* **1997**, *324* (1), 1–18. DOI: 10.1042/bj3240001.

(54) Batalov, I.; Stevens, K. R.; DeForest, C. A. Photopatterned Biomolecule Immobilization to Guide Three-Dimensional Cell Fate in Natural Protein-Based Hydrogels. *Proc. Natl. Acad. Sci. USA* **2021**, *118* (4), e2014194118. DOI: 10.1073/pnas.2014194118.

(55) Nicolaou, K. C.; Snyder, S. A.; Montagnon, T.; Vassilikogiannakis, G. The Diels-Alder Reaction in Total Synthesis. *Angew. Chem. Int. Ed.* **2002**, *41* (10), 1668–1698. DOI: 10.1002/1521-3773(20020517)41:10<1668::AID-ANIE1668>3.0.CO;2-Z.

(56) Diels, O.; Alder, K. Synthesen in der hydroaromatischen Reihe. *Justus Liebigs Ann. Chem.* **1928**, *460* (1), 98–122. DOI: 10.1002/jlac.19284600106.

(57) Sauer, J.; Sustmann, R. Mechanistic Aspects of Diels-Alder Reactions: A Critical Survey. *Angew. Chem. Int. Ed. Engl.* **1980**, *19* (10), 779–807. DOI: 10.1002/anie.198007791.

(58) St. Amant, A. H.; Lemen, D.; Florinas, S.; Mao, S.; Fazenbaker, C.; Zhong, H.; Wu, H.; Gao, C.; Christie, R. J.; Read de Alaniz, J. Tuning the Diels–Alder Reaction for Bioconjugation to Maleimide Drug-Linkers. *Bioconjugate Chem.* **2018**, *29* (7), 2406–2414. DOI: 10.1021/acs.bioconjchem.8b00320.

(59) Rideout, D. C.; Breslow, R. Hydrophobic Acceleration of Diels-Alder Reactions. *J. Am. Chem. Soc.* **1980**, *102* (26), 7816–7817. DOI: 10.1021/ja00546a048.

(60) Ting, C.-Y.; Kolbeck, P. T.; Colombo, R.; Chakiath, C.; Rice, M.; Marelli, M.; Christie, R. J. Cyclopentadiene as a Multifunctional Reagent for Normal- and Inverse-Electron Demand Diels–Alder Bioconjugation. *Bioconjugate Chem.* **2022**, *33* (9), 1609–1619. DOI: 10.1021/acs.bioconjchem.2c00222.

(61) Durmaz, H.; Colakoglu, B.; Tunca, U.; Hizal, G. Preparation of Block Copolymers via Diels Alder Reaction of Maleimide- and Anthracene-End Functionalized Polymers: Preparation of Block Copolymers. *J. Polym. Sci. A Polym. Chem.* **2006**, *44* (5), 1667–1675. DOI: 10.1002/pola.21275.

(62) Chen, X.; Dam, M. A.; Ono, K.; Mal, A.; Shen, H.; Nutt, S. R.; Sheran, K.; Wudl, F. A Thermally Re-Mendable Cross-Linked Polymeric Material. *Science* **2002**, *295* (5560), 1698–1702. DOI: 10.1126/science.1065879.

(63) Liu, Y.-L.; Chuo, T.-W. Self-Healing Polymers Based on Thermally Reversible Diels–Alder Chemistry. *Polym. Chem.* **2013**, *4* (7), 2194. DOI: 10.1039/c2py20957h.

(64) Gandini, A. The Furan/Maleimide Diels–Alder Reaction: A Versatile Click–Unclick Tool in Macromolecular Synthesis. *Prog. Polym. Sci.* **2013**, *38* (1), 1–29. DOI: 10.1016/j.progpolymsci.2012.04.002.

(65) Levandowski, B. J.; Houk, K. N. Theoretical Analysis of Reactivity Patterns in Diels–Alder Reactions of Cyclopentadiene, Cyclohexadiene, and Cycloheptadiene with Symmetrical and Unsymmetrical Dienophiles. *J. Org. Chem.* **2015**, *80* (7), 3530–3537. DOI: 10.1021/acs.joc.5b00174.

(66) Inglis, A. J.; Sinnwell, S.; Stenzel, M. H.; Barner-Kowollik, C. Ultrafast Click Conjugation of Macromolecular Building Blocks at Ambient Temperature. *Angew. Chem. Int. Ed.* **2009**, *48* (13), 2411–2414. DOI: 10.1002/anie.200805993.

(67) Levandowski, B. J.; Raines, R. T. Click Chemistry with Cyclopentadiene. *Chem. Rev.* **2021**, *121* (12), 6777–6801. DOI: 10.1021/acs.chemrev.0c01055.

2 Chapter 2: *Norbornadiene as a Stable Precursor to Cyclopentadiene for Rapid Block Copolymer Synthesis*

The project presented in this chapter originated from a desire to harness the reactivity of cyclopentadiene (Cp) for rapid normal electron demand Diels–Alder (NEDDA) cycloadditions. To overcome the challenges associated with Cp-functionalized polymer building blocks, we envisioned that the employment of a precursor that could readily provide Cp on demand would provide building block stability for long term storage, while greatly expanding the utility of NEEDA cycloadditions for click chemistry. This chapter describes the fruits of this concept: initial work demonstrated the viability of a Cp precursor for on demand polymer click chemistry (originally published in the *Journal of the American Chemical Society* and reprinted with permission from *J. Am. Chem. Soc.* **2019**, *141*(34), 13619–13624. DOI: 10.1021/jacs.9b06328. Copyright 2019 American Chemical Society.). Additionally, this chapter outlines my work to diversify the polymer types and architectures that could be accessed through the platform (originally published in *Macromolecules* and reprinted with permission from *Macromolecules* **2020**, *53*(12), 4917–4924. DOI: 10.1021/acs.macromol.0c00967. Copyright 2020 American Chemical Society.).

2.1 Abstract

Herein, we report the development of a scalable and synthetically robust building block based on norbornadiene (NBD) that can be broadly incorporated into a variety of macromolecular architectures using traditional living polymerization and post-polymerization functionalization techniques. By taking advantage of a selective and rapid deprotection with tetrazine, highly reactive “masked” cyclopentadiene (Cp) functionalities can be introduced into

synthetic polymers as chain-end groups in a quantitative and efficient manner. The orthogonality of this platform further enables a cascade click process where the "unmasked" Cp can rapidly react with dienophiles, such as maleimides, through a conventional Diels–Alder reaction. Coupling proceeds with quantitative conversions allowing high molecular weight block copolymers to be prepared in a single step under ambient conditions.

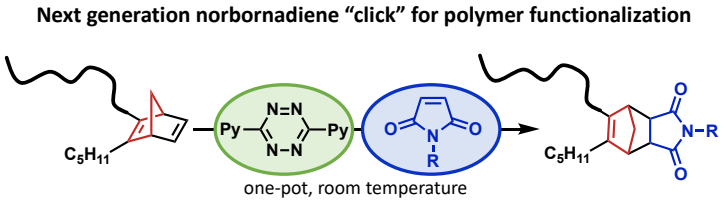

Figure 2.1. Graphical Abstract. Norbornadiene for one-pot cyclopentadiene-based click chemistry.

2.2 Introduction

The concept of "click" chemistry, is based on the philosophy that chemical reactions should be modular, simple, high yielding and orthogonal.[1] These essential characteristics have had a profound impact across the broader chemical sciences, transforming scientific disciplines ranging from bioconjugation to functional polymer synthesis.[2,3] A range of post-polymerization modification strategies have emerged from the concept of "click" chemistry, enabling the synthesis of polymers with a diverse array of functionalities and architectures.[4,5] Among these strategies, the copper catalyzed azide–alkyne click (CuACC) represents one of the most highly utilized "click" platforms in polymer synthesis, driven by the synthetic availability of alkyne and azide building blocks.[6] Notably, direct incorporation of azide units through simple post-polymerization processes has enabled this strategy to be widely adopted.[7] Although this method offers efficient functionalization and subsequent click chemistry, a

longstanding drawback for traditional CuAAC-based systems is the presence of metal catalysts and the potential hazards associated with azides which specific safety precautions be exercised. The challenges associated with copper toxicity have been mitigated by the development of copper-free or strain-promoted azide–alkyne click (SPACC) chemistry; based on cyclooctyne derivatives,[8] the inherent strain in the cyclooctyne ring dramatically increases the rate of the uncatalyzed reaction,[9] enabling rapid room temperature coupling to azides. However the long-term instability of dibenzoazacyclooctyne systems (DIBAC) (storage at –20 °C),[10] the difficulties in scalability and prohibitively high cost[11,12] renders general use in functional polymer synthesis challenging. As such, SPAAC has been mostly limited to small-scale systems such as dendritic[13] or biological applications.[14]

A more cost-effective and scalable metal-free "click" platform for polymer synthesis is the Diels–Alder (DA) cycloaddition reaction. DA systems have been utilized across numerous applications ranging from surface functionalization,[15] constructing complex polymer architectures,[16–18] forming dynamic networks,[19,20] and the preparation of antibody–drug conjugates.[21] Typically, a trade-off between stability and efficiency is encountered when choosing dienes and dienophiles for polymer functionalization. Furan or anthracene-based dienes, in combination with maleimide dienophiles, are arguably the most commonly utilized building blocks for DA cycloaddition couplings in polymer synthesis (**Figure 2.2a**).[22] However, despite their orthogonality, scalability, and wide spread availability, these derivatives suffer from long reaction times and high temperatures for efficient coupling.[16] Furthermore, the propensity for furan-maleimide DA adducts to undergo retro Diels-Alder (rDA) reactions renders them unsuitable for applications requiring elevated temperatures.[19]

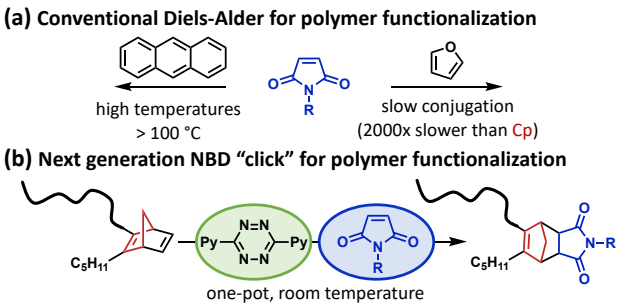

Figure 2.2. (a) Current methods for maleimide-polymer conjugation using anthracene or furan (b) Strategy reported herein introducing masked Cp into polymers, highlighted by red bonds.

To overcome these challenges, an attractive strategy is to simply increase the reactivity of the diene or dienophile. Du Prez and co-workers have reported the use of triazolinedione (TAD) compounds as 'spring-loaded' dienophiles which react with dienes at room temperature within minutes.[23] The high reactivity of TAD compounds offers an elegant method for functionalizing polymers when less reactive dienes are required. In contrast, the reactivity of the diene can be increased through the use of cyclopentadiene (Cp) derivatives.[24,25] Recognizing the potential of Cp as a polymer "click" platform, Barner-Kowollik and coworkers have developed synthetic routes to access Cp-functionalized polymers for conjugation with maleimides,[26] electron-deficient dithioesters,[27–29] and carbon nanoparticles.[30,31] For stable backbones such as polystyrene or poly(ethylene glycol), nucleophilic substitution using ionic cyclopentadienyl salts (NaCp,[27] LiCp,[32] or Me_2AlCp[33]) allows for the efficient synthesis of Cp functionalized chain end derivatives. In the case of reactive backbones, such as polyesters, an alternative substitution strategy using nickelocene ($NiCp_2$) has been developed.[28,34,35] Despite the success of these strategies, the ability to incorporate Cp has been limited to chain-ends via post-polymerization strategies followed by immediate use due to the general instability[25] of Cp and its high reactivity towards electron-

deficient vinyl monomers.[36] Identifying the limitations of traditional click strategies and the associated promise of cyclopentadiene (Cp) derivatives as a highly efficient coupling platform, we report the utilization of norbornadiene (NBD) as a stable Cp precursor that can be incorporated into a variety of polymers and stored under ambient conditions for months (12+) with no observable degradation or unwanted reactivity. A key insight in this study is the use of a cascade sequence of DA reactions to quantitatively couple the NBD units with dienophiles such as functional maleimides.[37] This "unmasking" of the NBD group is mediated by small-molecule tetrazine derivatives through an initial inverse-DA reaction, leading to the in situ generation of Cp functionalities that can then undergo efficient conjugation with maleimide-functionalized materials (**Figure 2.2b**). This novel cascade platform is metal free, air tolerant, and quantitative for even demanding systems such as the coupling of high molecular weight, chain-end-functionalized linear polymers. This allows well-defined block copolymers to be prepared on multigram scale that are difficult to synthesize using traditional polymerization strategies.

2.3 Results and Discussion

2.3.1 Norbornadiene derivatives as functional initiators for cascade "click" coupling of high molecular weight polymers

Drawing inspiration from small molecule reports[38,39] and the pioneering development of additive-free polymer functionalization based on norbornene-tetrazine coupling chemistry by Dove, Du Prez, and O'Reilly,[18] we identified norbornadiene (NBD), as a potential "masked" Cp precursor that would be amenable to a wide verity of polymerization techniques and long-term storage. Upon treatment with tetrazine, the high ring strain (32.2 kcal/mol)[42-45] enables a

cascade of selective cycloaddition reactions.[41–43] This highly efficient process proceeds through an initial inverse electron-demand DA (IEDDA) reaction that releases N_2, followed by a retro-DA (rDA), to yield pyridazine[44] and Cp as products.[38,39] Thus, we envisioned that through the use of NBD-functionalized initiators, chain-end functionalized polymers could be prepared and utilized in a tetrazine-trigged DA click with maleimide-functionalized materials.

2.3.1.1 Preparation of a scalable NBD functional initiators

Initial studies on the scalable synthesis of an NBD functionalized initiators employed the commodity chemical dicyclopentadiene (**1**) and methyl 2-octynoate (**2**), an inexpensive and innocuous flavoring agent ($30 per kg). When **1** and **2** are heated neat in a pressure vessel at 200 °C, the resulting methyl ester (**3**) can be isolated via distillation and subsequently reduced with DIBAL to furnish the NBD alcohol **4**[45] on a 50 g scale in a typical laboratory setting (**Figure 2.3**). The simplicity of this process coupled with the availability of alkyne derivatives allows a range of other NBD derivatives to be prepared. A notable example includes the reaction of **1** with propargyl alcohol which affords the unsubstituted NBD alcohol directly.[46] Significantly it was observed that the NBD derivatives were stable and could be stored at room temperature under ambient conditions with no observable degradation or instability over 6+ months. In addition, a variety of functionalization reactions can be performed on the NBD building block to give functional initiator units for subsequent polymerization reactions (**Figure S2.13–2.20**). For example, the alcohol **4** can be esterified to give the RAFT chain transfer agent, **5** or the ATRP initiator, **6**, in high yields.

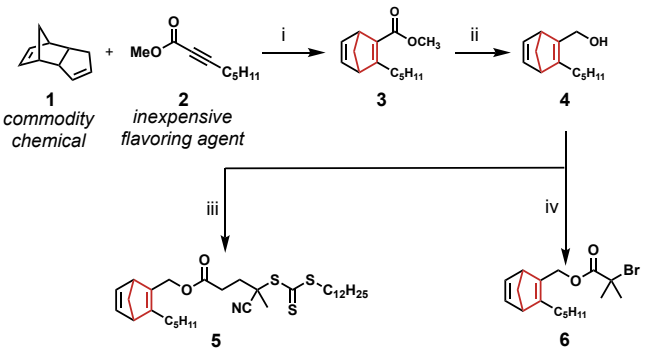

Figure 2.3. Synthesis of norbornadiene polymer building blocks. i) neat, pressure vessel, 200 °C, 5 h, 50% ii) DIBAL, THF, 0 °C, 30 min, 71% iii) CDTPA, EDC·HCl, DMAP, DCM, rt, 16 h, 92% iv) α-Bromoisobutryl bromide, pyridine, THF, 0 °C, 2 h, 72%.

2.3.1.2 NBD as a precursor to Cp-functionalized polymers

To demonstrate the versatility of **4** as a stable, "masked" Cp unit, end-functionalized polylactide (PLA) **P1** (**Figure 2.4a**) was prepared using the base-catalyzed ROP of D,L-lactide and **4** as an initiator. Significantly, the resulting polymer was determined to have a degree of polymerization of ~500 (M_n = 42,000 g/mol and $Đ$ = 1.04), which compares favorably with the theoretical DP of 440 and illustrates the compatibility of the NBD unit under basic conditions. Additionally, ^{1}H NMR spectroscopy shows the unique signals for the alkene present in the NBD units and confirms the efficient introduction of NBD at the end of the high molecular weight PLA chain.

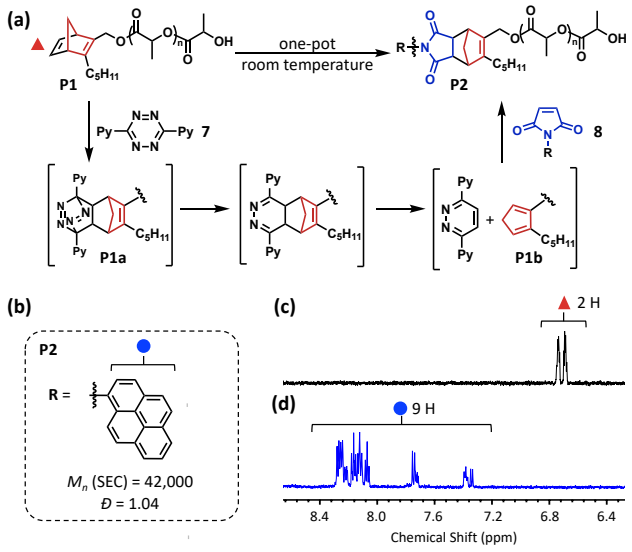

Figure 2.4. (a) One-pot deprotection of NBD and conjugation with maleimide. Note: quenched with norbornene after 4 h. (b) Pyrene chain end functionality introduced to PLA. ^{1}H NMR of (c) NBD-functionalized PLA, **P1** and (d) PyrM-functionalized PLA, **P2** in dichloromethane-d_2.

To validate the efficient conjugation via a "cascade click" sequence, a solution of **P1** in $CDCl_3$ was treated with the commercially available tetrazine (DpTz, 2.4 equiv) and *N*-(1-pyrenyl)maleimide (PyrM, 1.2 equiv) at room temperature with no precaution to exclude water or oxygen. As highlighted by **Figure 2.4a**, the cascade process proceeds through an initial inverse electron-demand DA (IEDDA) reaction with DpTz (**7**) at the unsubstituted olefin of NBD (**P1** to **P1a**). Upon release of N_2 from **P1a** a subsequent retro-DA occurs to yield an in situ generated terminal Cp unit (**P1b**) which undergoes a DA reaction with the functionalized maleimide (**8**) to give the desired pyrene-functionalized **P2**. Following purification by precipitation, **P2** was obtained in quantitative yield with SEC characterization before and after functionalization confirming no change in molar mass distribution. Significantly, incorporation of pyrene was determined to be >95% by both ^{1}H NMR and UV-Vis spectroscopy calibrating against known concentrations of PyrM (**Figure 2.4d**, **S2.21**−**2.24**).

2.3.1.3 One-pot block copolymer synthesis

The facile introduction of reactive Cp units to the chain ends of polymeric systems now opens up the intriguing possibility of coupling stable, end functionalized polymers to give high molecular weight block copolymers and other complex macromolecular architectures. To showcase the potential of this new strategy, a PLA-*b*-PEG-*b*-[G-4 dendron] triblock copolymer (**P5**) was prepared in a single step by coupling of a chain end functionalized PLA-NBD ((**P3**), M_n = 21,800) derivative with a maleimide-terminated PEG-*b*-[G-4 dendron] (**P4**). Significantly, only a minor excess of **P4** (1.5 equivalents) was required to drive the reaction to completion with SEC showing the expected increase in molecular weight for the desired triblock copolymer and no detectable **P3** (**Figure S2.33–2.34**). The ability to quickly and efficiently link polymer precursors promotes a "mix and match" approach, that we envision will enable easy access to a range of polymeric architectures.

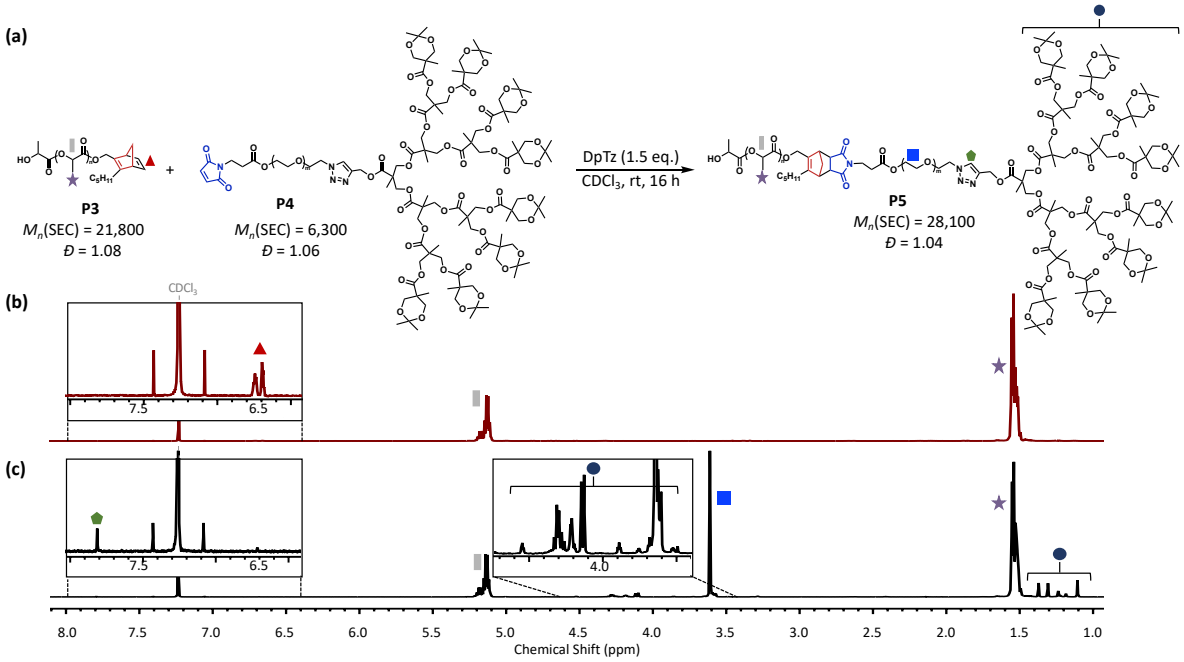

Figure 2.5. (a) Chemical schematic for synthesis of triblock copolymer, **P5**, using a sequential deprotection-conjugation strategy between NBD-functionalized PLA (**P3**) and maleimide-terminated PEG-*b*-[G-4 dendron] (**P4**); ^{1}H NMR of (b) NBD-functionalized PLA, **P3** and (c) triblock **P5** in chloroform-d.

2.3.2 Post-polymerization functionalization with norbornadiene to access stable, readily available precursors to cyclopentadiene derivatives

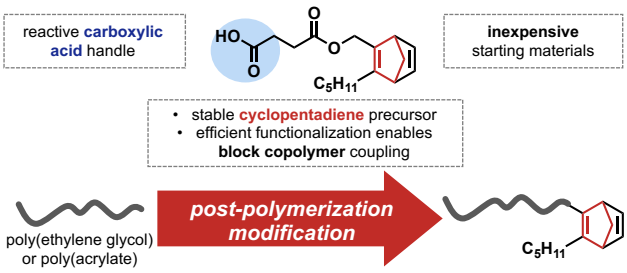

Figure 2.6. Graphical Abstract. Post-polymerization functionalization with norbornadiene.

Although NBD-functional initiators enabled access to polymers derived from ring opening polymerization (ROP), reversible addition/fragmentation chain transfer (RAFT) polymerization, and atom transfer radical polymerization (ATRP), only ROP techniques could reliably afford high molecular weight polymers for our NBD click platform. Polymers prepared by ATRP were limited to low conversions and molecular weights (**Figure S2.15–2.20**). At higher conversions, loss of control was observed likely due to undesired reactivity of the NBD unit with free radicals.[47] We hypothesized that the use of a post-polymerization functionalization strategy would allow for the introduction of NBD functionality into polymer systems prepared by radical polymerization methods and expand the utility of this approach to commercially available polymers such as poly(ethylene glycol) (PEG) (**Figure 2.7**).

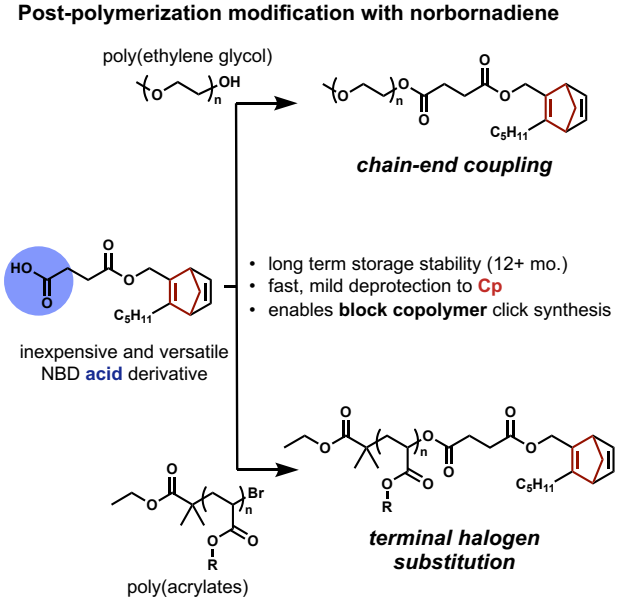

Figure 2.7. Postpolymerization functionalization using a carboxylic acid bearing norbornadiene (NBD) derivative allows for preparation of stable poly(ethylene glycol) (PEG) and poly(acrylate) click building blocks.

2.3.2.1 Preparation of NBD derivatives for post-polymerization modification

To demonstrate that NBD-based building blocks with an appropriate functional group handle can serve as a general strategy for post-polymerization processes, we first developed a robust and scalable synthesis of two carboxylic acid NBD derivatives, **9** and **10** (**Figure 2.8a**). NBD **9** was accessed in one step via hydrolysis of methyl ester NBD (**3**); whereas, **10** can be prepared in one step from the base catalyzed ring opening of succinic anhydride with alcohol (**4**) to produce **10** in near quantitative yield. To evaluate the ability to liberate the desired Cp reactive unit, NBD **9** and **10** were treated with 1.5 equivalents of dipyridyl-tetrazine in deuterated chloroform at room temperature and monitored by ^{1}H NMR (**Figure 2.8b-d**). Of note, in situ formation of the Cp unit was observed for derivative **10** within 10 minutes, and complete conversion to **10a** was achieved in just over 2 hours (**Figure 2.8d**). The proximity of the electron withdrawing group on compound **9** inhibited the efficiency the Diels–Alder cascade with tetrazine and the rate of deprotection to **9a** was reduced. After 6 hours, unreacted **9** was still observed by ^{1}H NMR (**Figure 2.8c**). This highlights the importance of increasing the electron density of the NBD unit to enable an efficient inverse demand Diels–Alder with tetrazine which is critical for the in situ formation of the Cp unit and the general deprotection strategy.

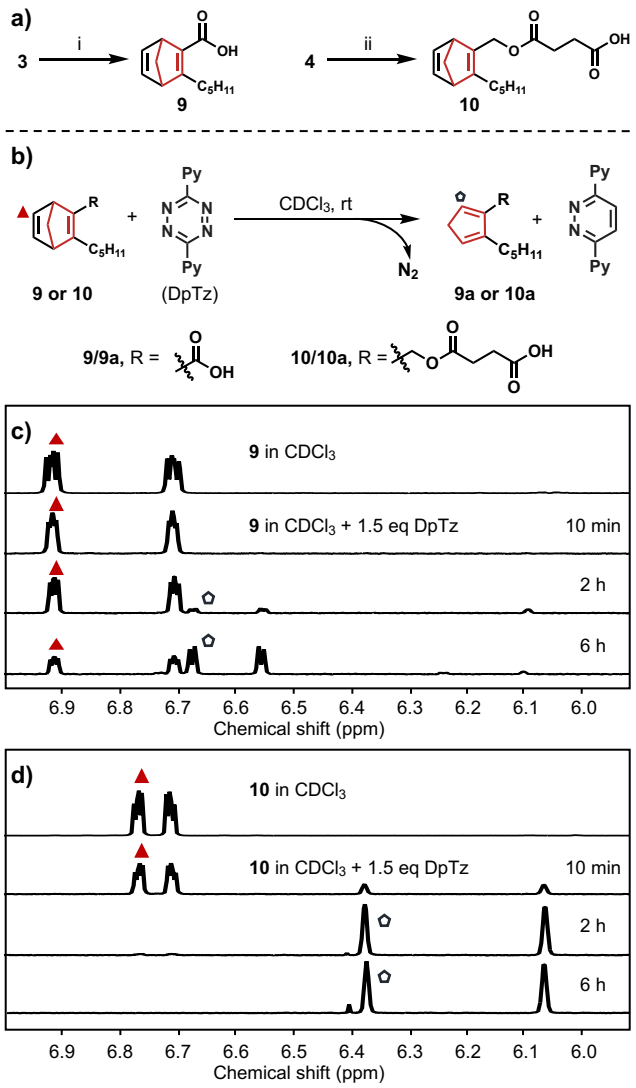

Figure 2.8. a) Synthesis of norbornadiene acids for polymer modification. i) neat, pressure vessel, 200 °C, 5 h, 50% ii) NaOH, MeOH, H_2O, reflux, 15 h, then HCl, 66% iii) DIBAL, THF, 0 °C, 30 min, 71% iv) succinic anhydride, Et_3N, DMAP, DCM, rt, 1 h, 97%. b) Scheme of norbornadiene deprotection to cyclopentadiene. c) ^{1}H NMR overlays monitoring the deprotection of **9** to **9a**. d) ^{1}H NMR overlays monitoring the deprotection of **10** to **10a**.

2.3.2.2 NBD functionalization of poly(acrylates)

The development of a robust synthetic route to **10**, allowed exploration of direct nucleophilic substitution of bromine terminated poly(acrylates) (**Figure 2.9a**). For incorporation of NBD functionality onto poly(acrylates), we chose to initially study the base

catalyzed nucleophilic substitution of the terminal bromine as a viable approach. The use of 1,8-diazabicyclo[5.4.0]undec-7-ene (DBU) as a catalyst in the direct substitution of terminal bromine with carboxylic acids is well established, having been used with (meth)acrylic acids, to produce well-defined macromonomers.[48,49] Using this strategy, we envisioned that NBD units might be easily incorporated at the chain-end of a variety of poly(acrylate) backbones. Treatment of **P6a**, poly(cyclohexyl acrylate), with a pre-mixed solution of acid **10** (4 eq) and DBU (4.1 eq) in ethyl acetate (EtOAc) provided near quantitative NBD functionalization after stirring for 60 h at room temperature (**Figure 2.9a-c**). Significantly, no precautions were taken to exclude water or oxygen which further increases the utility of the strategy. As highlighted in **Figure 2.9b**, following treatment of poly(cyclohexyl acrylate) (**P6a**) with the DBU/**10** solution and precipitation in methanol, resonances corresponding to the alkene protons of NBD are observed at 6.75 ppm. Integration of these resonances indicate >95% incorporation of NBD. To further confirm successful substitution of bromine for NBD, matrix assisted laser desorption/ionization time of flight (MALDI-TOF) mass spectroscopy was used. Comparison of the MALDI-TOF spectra of **P6a** and **P7a** show a shift in molecular weight corresponding to the loss of bromine and gain of the terminal NBD unit with the observed molecular weights in agreement with calculated values (**Figure 2.9c**).

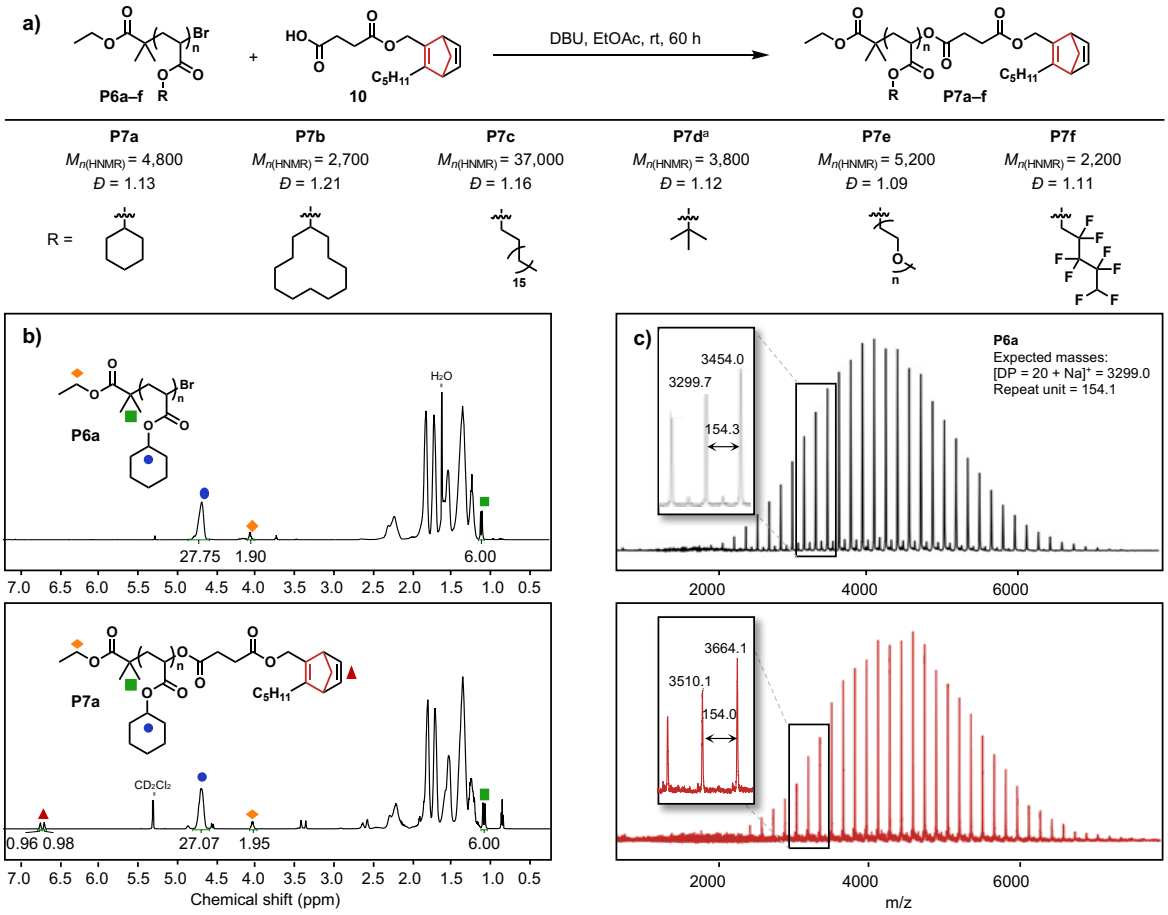

Figure 2.9. a) General reaction for substitution of NBD unit onto polymers prepared by ATRP. [a]functionalization performed in acetonitrile. b) ^{1}H NMR of **P6a** and **P7a** in deuterated dichloromethane. c) MALDI-TOF spectra of **P6a** and **P7a** agree with expected masses corresponding to functionalization of the ω-chain-end with NBD.

With optimized conditions in hand, we next explored the generality of this approach on a library of poly(acrylate) polymers possessing different pendant groups – cyclic, hydrophobic, hydrophilic, and fluorinated – prepared by photoinduced atom-transfer radical polymerization (ATRP) (**P6a–f**).[50–53] Full synthetic details for the synthesis of poly(cyclohexyl acrylate) (**P6a**), poly(cyclodecyl acrylate) (**P6b**), poly(octadecyl acrylate) (**P6c**), poly(tert-butyl acrylate) (**P6d**), poly(poly(ethylene glycol) acrylate) (**P6e**), and poly(octafluoropentyl acrylate) (**P6f**) are provided in the Supporting Information. The **P6a–f** library of polymers was successfully functionalized with **10** using the optimized DBU catalyzed conditions to afford **P7a–f** (**Figure**

2.9a). Of note, the rate of substitution could also be increased by heating the solution at 50 °C, which reduced the reaction time to 48 h for substitution onto **P6a**. Furthermore, the limitations previously encountered using NBD functional initiators are easily overcome with this post-polymerization approach, allowing for the preparation of high molecular weight (35 kDa+) NBD-functionalized poly(acrylates) (**P7c**). After functionalization, these monofunctional derivatives could be easily purified from excess starting materials and small molecule by-products by precipitation or dialysis. Successful functionalization of the poly(acrylates) was confirmed by ^{1}H NMR spectroscopy with the appearance and integration of unique resonances corresponding to the NBD unit indicating high chain-end fidelity (see supporting information for full details).

2.3.2.3 NBD functionalization of poly(ethylene glycol)

To further illustrate the power of this post-functionalization approach, we sought to broaden the process to quantitative functionalization of terminal hydroxy groups for commodity polymers. Driven by the utility of PEG based polymers in biomaterials, as well as the availability of maleimide derived functional materials such as antibody–drug conjugate payload,[21,54,55] dyes, and bioactive small molecules, we initially focused on PEG based systems. Using *N,N′*-dicyclohexylcarbodiimide (DCC) as the coupling agent, NBD-functionalized PEG was prepared from commercially available poly(ethylene glycol) monomethyl ether (**P8**, M_n = 5,000 gmol^{-1}). Coupling could be accomplished within 24 h upon treatment with excess **5** (2 equiv), DCC and catalytic 4-dimethylaminopyridine (DMAP) (**Figure 2.10a**). ^{1}H NMR spectroscopy following precipitation of **P9** in cold ethanol showed the expected resonances corresponding to successful NBD incorporation with integration values confirming >95% functionalization (**Figure 2.10b**).

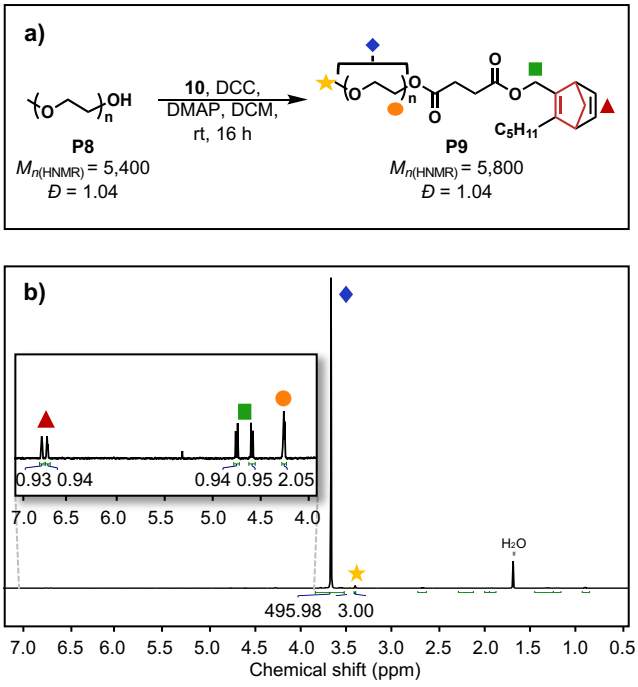

Figure 2.10. a) Functionalization of poly(ethylene glycol) chain-end with NBD. b) ^{1}H NMR of **P9** showing expected resonances corresponding to the NBD unit.

2.3.2.4 Block copolymer library prepared by "NBD Click"

To demonstrate the versatility of these functionalized polymeric building blocks, we sought to prepare block copolymers via the NBD click platform. It is worth noting that these cyclopentadiene precursor materials could be stored under ambient conditions for extended periods (12+ months) with no observable degradation, allowing large quantities to be prepared and fully characterized, followed by storage and later use in NBD click reactions. With these NBD-functionalized materials in hand, several maleimide bearing counterparts were prepared. The utility of the maleimide unit in Michael additions and DA cycloadditions has driven the establishment of a range of synthetic approaches for the preparation of functional maleimide derivatives.[56–58] As an illustrative example, a protected maleimide initiator was used in the polymerization of methyl methacrylate under metal free ATRP conditions[56,59] then

subsequently heated at 110 °C to deprotect the maleimide and afford an α-functionalized poly(methyl methacrylate) (mal-PMMA, **P10**, **Figures 2.11 and S2.66–2.68**). To perform NBD-based click coupling, **P7a** and **P10** were dissolved in deuterated chloroform with **P7a** in slight excess (1.14 equiv) (**Figure 2.11a**). Following dissolution, DpTz (2.28 equiv) was added and the reaction was allowed to proceed at room temperature while monitoring reaction completion by ^{1}H NMR. After 24 h the disappearance of the maleimide resonances of **P10** indicated quantitative clicking to **P7a** (**Figure S2.76**). The excess DpTz was quenched with norbornene before the block copolymer (PCHA-*b*-PMMA, **P11**) was precipitated in methanol, then hexanes, to remove excess small molecules and **P7a**. Analysis by size exclusion chromatography (SEC) confirmed a shift to higher molecular weight material which indicates successful diblock formation (**Figure 2.11b**). Furthermore, analysis by SEC and ^{1}H NMR corroborates that any unreacted **P7a** was successfully removed by precipitation (**Figures 2.11b** and **S2.77**).

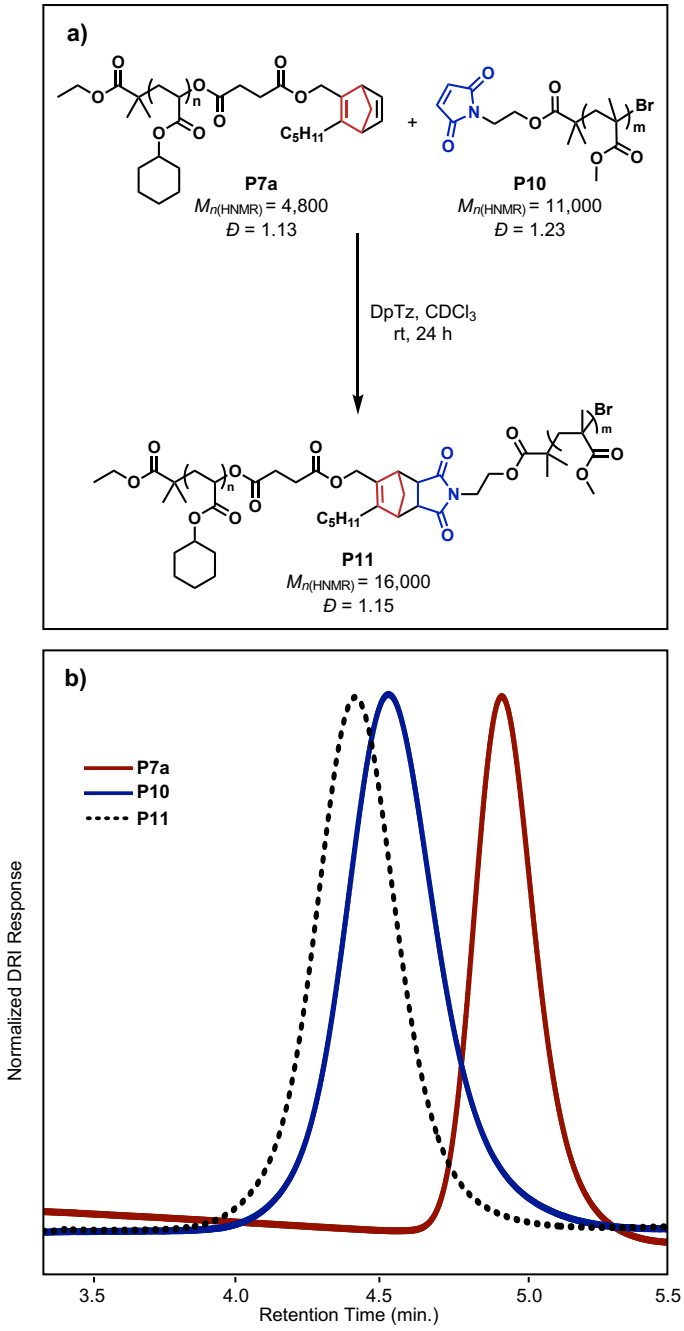

Figure 2.11. a) Synthesis of PCHA-b-PMMA diblock copolymer. b) SEC traces showing expected shift to higher molecular weight after NBD click.

Using the previously established metal-free ATRP conditions, a library of block polymers was prepared by combining maleimide and NBD-functionalized polymers in the presence of DpTz (**Figure 2.12**). To further expand the polymer coupling partners, a second maleimide-functionalized polymer (mal-PEG, **SP8**) was prepared in a similar fashion to the NBD-functionalized analog, using **P8**, DCC and DMAP (**Figure S2.74-2.75**). From this material, poly(acrylate)-*b*-poly(ethylene glycol) copolymers were prepared (**P13–P14**, **Figure 2.12**). Likewise, the NBD-functionalized PEG (**P9**) was used to prepare a poly(ethylene glycol)-*b*-poly(methacrylate) copolymer (**P18**) by clicking with a maleimide-functionalized poly(hexyl methacrylate) (**SP6**, **Figure 2.12**). In all cases examined, the NBD click method provides efficient and practical access to block copolymers bearing hydrophobic, hydrophilic, and fluorinated groups.

Finally, to demonstrate that this strategy can also be extended to triblock formation, a bifunctional poly(dodecyl acrylate) (**SP9**) was prepared by light induced ATRP of the protected maleimide initiator followed by substitution of the terminal bromine with **10** (**Figure S2.93–2.95**). From this bifunctional material, a triblock terpolymer, was prepared in two sequential clicks. In the first click, previously prepared NBD-PLA (**P3**) was treated with DpTz and the appearance of the Cp was monitored by ^{1}H NMR (**Figure S2.96**). Upon complete deprotection to the desired Cp-PLA (**SP10**), the excess DpTz was quenched to prevent undesired deprotection of the NBD unit upon addition of **SP9**. The intermediate diblock, **P19**, was purified and characterized (**Figures 2.12** and **S2.97–2.98**) before subjecting the material to a subsequent deprotection followed by click reaction with **SP8** to afford the triblock PLA-*b*-PDA-*b*-PEG with a final M_n of 33,000 gmol^{-1} and dispersity of 1.14 (**P20**, **Figures 2.12** and **S2.99–2.100**).

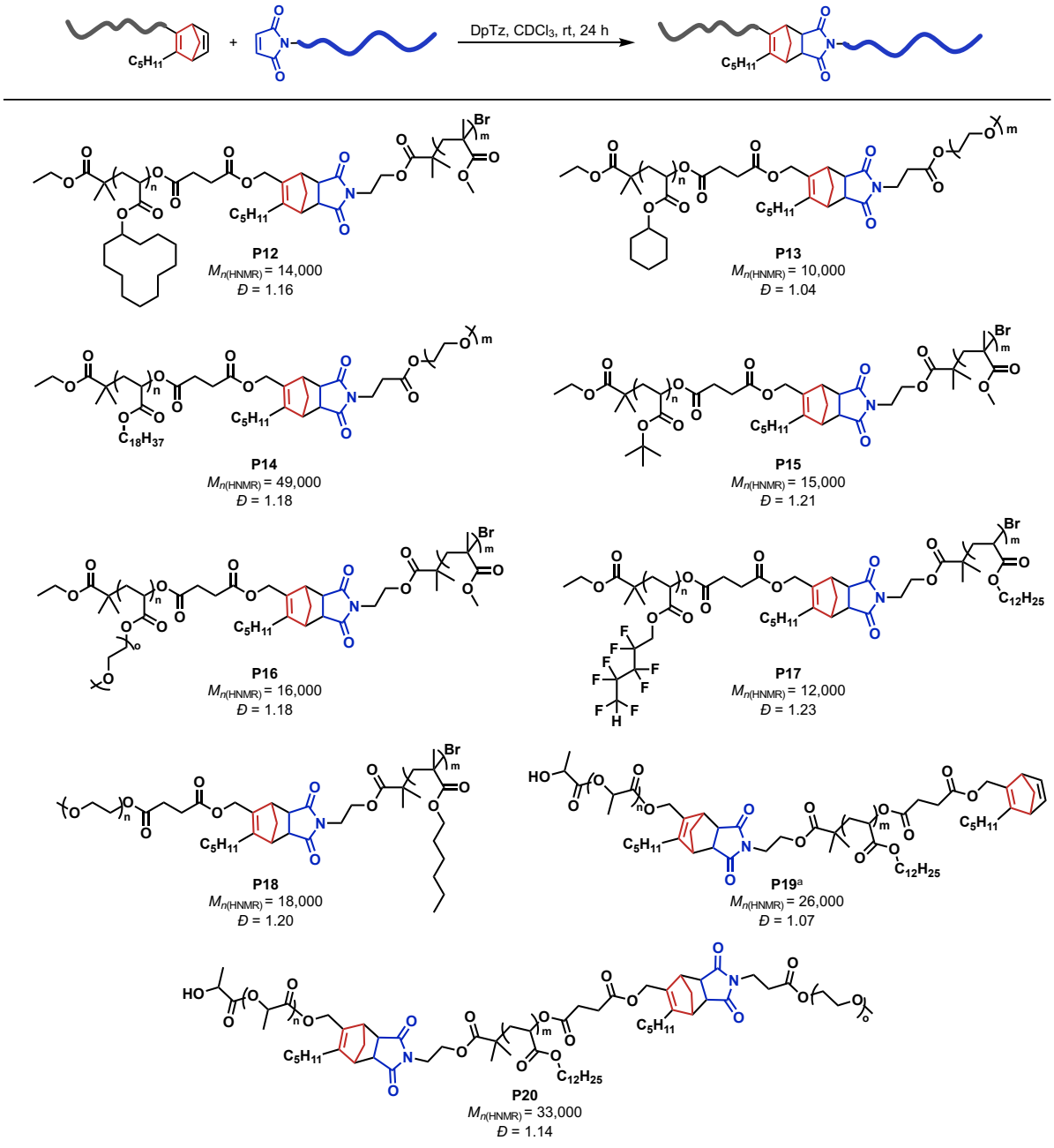

Figure 2.12. Scope of the NBD click platform to produce mix-and-match block copolymers. All reactions were performed in deuterated chloroform to allow for monitoring by ^{1}H NMR and confirmation of quantitative clicking before precipitation.

[a]Maleimide-poly(dodecyl acrylate)-NBD was added to solution after complete deprotection of poly(lactic acid)-NBD to Cp was observed by ^{1}H NMR and unreacted DpTz was quenched with norbornene.

2.4 Conclusion

In conclusion, we have developed a cascade click strategy for the facile preparation of high molecular weight macromolecular architectures. Based on synthetically accessible and chemically robust norbornadiene (NBD) building blocks, "masked" Cp units can be introduced into a range of polymeric systems. The general compatibility of NBD derivatives to access chain-end functionalized polymers from functional initiators and post-polymerization functionalization was demonstrated, highlighting the versatility and orthogonality of the NBD unit. Importantly, upon addition of DpTz, quantitative deprotection of NBD to form Cp is observed via a rapid cascade of DA reactions, and in the presence of a variety of functional maleimide derivatives, in situ coupling then occurs via a traditional DA cycloaddition. We demonstrate that this straightforward NBD functionalization of synthetic and commercially available polymers offers a streamlined route to create a library of diverse block copolymers from stable precursors in a highly efficient, metal-free process that requires no heating or precaution for an air- or moisture-free environment. Importantly, it is amenable across an array of functional maleimides, making this strategy accessible to the broader scientific community.

2.5 Acknowledgements

I would like to acknowledge Dr. Emre Discekici and Dr. Andre St. Amant for their ingenious conception of the "NBD Click" strategy, and sincerely thank them for their kindness, mentorship, and guidance throughout this work which served as a springboard for the subsequent projects outlined in this thesis. I would also like to thank the UCSB Graduate Division for financial support through a Chancellor's Fellowship and acknowledge the research reported here was partial support by the Office of Naval Research through the MURI of Photomechanical Materials Systems (ONR N00014-18-1-2624) and partial support the

National Science Foundation (NSF) Materials Research Science and Engineering Center at UC Santa Barbara, DMR-1720256 (IRG-2).

2.6 Supporting Information

Materials and Methods

Unless stated otherwise, reactions were conducted under an atmosphere of N_2 using reagent grade solvents. Dichloromethane (DCM) and methanol (MeOH) were stored over 3Å molecular sieves. Tetrahydrofuran (THF) was passed over a column of activated alumina. All commercially obtained reagents were used as received. All commercial vinyl monomers were purified by passing through a plug of basic alumina unless otherwise noted. Phen-CF_3 photocatalyst,[59] exo-furan maleimide ATRP initiator,[57] and cyclododecyl acrylate[52] were prepared following literature procedures. Thin-layer chromatography (TLC) was conducted with E. Merck silica gel 60 F254 pre-coated plates (0.25 mm) and visualized by exposure to UV light (254 nm) or stained with *p*-anisaldehyde, potassium permanganate, or bromocresol green. Flash column chromatography was performed using normal phase silica gel (60 Å, 0.040 – 0.063 mm, Geduran). ^{1}H NMR spectra were recorded on Varian spectrometers (400, 500, or 600 MHz) and are reported relative to the residual protio-signal in deuterated solvents. Data for ^{1}H NMR spectra are reported as follows: chemical shift (δ ppm), multiplicity, coupling constant (Hz) and integration. ^{13}C NMR spectra were recorded on Varian Spectrometers (100, 125, or 150 MHz). Data for ^{13}C NMR spectra are reported in terms of chemical shift (δ ppm). Mass spectra were obtained from the UC Santa Barbara Mass Spectrometry Facility on a (Waters Corp.) GCT Premier high resolution Time-of-flight mass spectrometer with an ESI or EI source. Matrix-Assisted Laser Desorption Ionization time of flight mass spectrometry (MALDI-ToF-MS) was conducted using a Bruker Microflex LRF MALDI TOF mass

spectrometer equipped with a 60 Hz nitrogen laser at 337 nm. Solutions in THF of dithranol as a matrix (saturated solution, 10 µL), sodium bromide as cationization agent (1.0 mg/ml, 2 µL) were mixed with the sample (1.0 mg/ml, 10 µL) and 1.0 µL of the mixture was applied to the target plate. Size exclusion chromatography (SEC) eluting with chloroform ($CHCl_3$) or THF and calibrated relative to polystyrene standards was performed on a Waters Alliance HPLC System, 2695 separation module with Wyatt DAWN HELEOS-II light scattering and Wyatt Optilab rEX refractive index detectors and/or a Waters Acquity Advanced Polymer Characterization (APC) System equipped with an Acquity UPLC refractive index detector.

Synthesis of Small Molecule Building Blocks

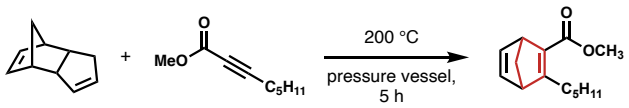

Methyl 3-pentylbicyclo[2.2.1]hepta-2,5-diene-2-carboxylate (3):

Methyl 2-octynoate (6.7 mL, 40 mmol, 1.0 eq.), dicyclopentadiene (3.2 mL, 24 mmol, 1.2 eq. of cyclopentadiene), and hydroquinone (100 mg) were added to a pressure vessel and sealed under an atmosphere of N_2. The vessel was heated to 200 °C for 5 h (63% conversion by NMR). The crude product was distilled twice (100–120 °C, ~200 mTorr) to afford racemic **3** (4.4 g, 20 mmol, 50%) as a clear and colorless liquid.

Large-scale modification:

Methyl 2-octynoate (59.0 mL, 350 mmol, 1 eq.), dicyclopentadiene (28.3 mL, 210 mmol, 0.6 eq.), and hydroquinone (0.87 g) were added to a 150 mL pressure vessel and sealed under an atmosphere of argon. The vessel was heated in a silicone oil bath to 200 °C for 6 h (84% conversion by NMR). The crude product was distilled once (110-115 °C, ~275 mTorr) to afford racemic **3** as a clear and colorless liquid (40.8 g, 185 mmol, 53%).

3: ^{1}H NMR (400 MHz, $CDCl_3$) δ 6.88 (dd, *J* = 3.1, 4.7 Hz, 1 H), 6.70 (dd, *J* = 3.3, 4.5 Hz, 1 H), 3.88 (br. s., 1 H), 3.72 (s, 3 H), 3.51 (br. s., 1 H), 2.75 - 2.60 (m, 2 H), 2.00 (tdd, *J* = 1.6, 6.3, 25.4 Hz, 2 H), 1.55 - 1.21 (m, 6 H), 0.89 (t, *J* = 7.0 Hz, 3 H) ppm; ^{13}C NMR (100 MHz, $CDCl_3$) δ 173.9, 166.3, 143.7, 140.7, 138.0, 71.0, 56.0, 51.0, 50.8, 31.5, 30.2, 26.4, 22.4, 13.9 ppm; IR (ATR) 2957, 2931, 2863, 1705, 1625, 1433, 1338, 1294, 1235, 1100, 1079, 714 cm^{-1}; HRMS (EI+) Exact mass cald. for $C_{14}H_{20}O_2^+$ $[M]^+$: 220.1458, found: 220.1466.

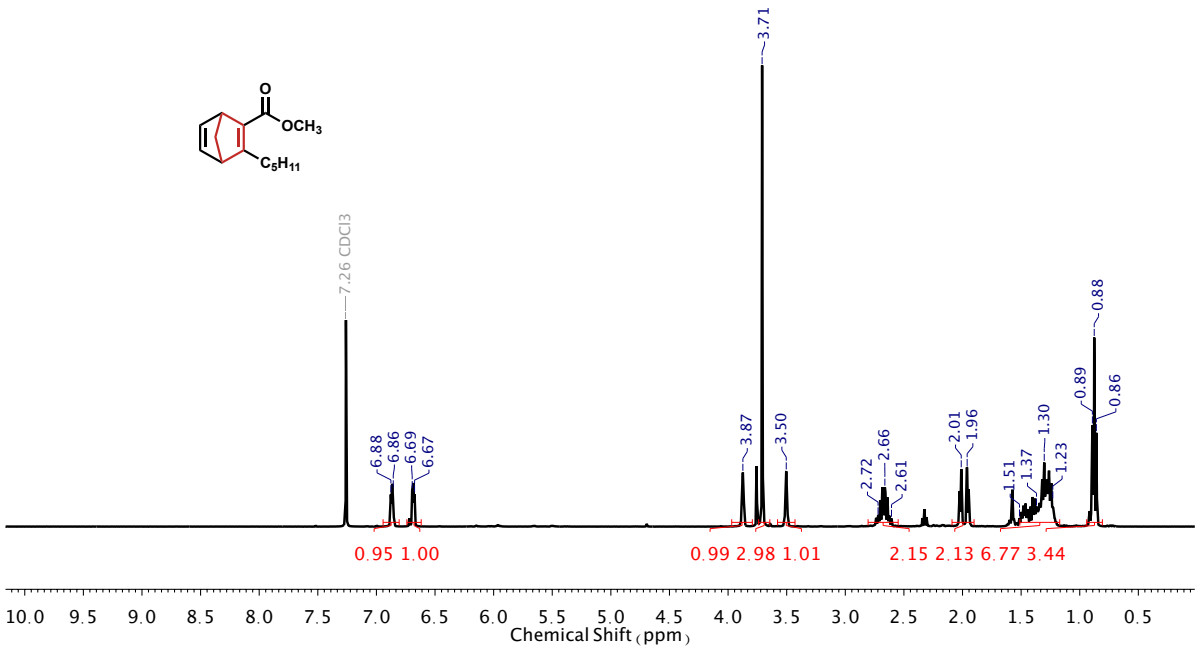

Figure S 2.1. ^{1}H NMR (400 MHz, $CDCl_3$) **3**

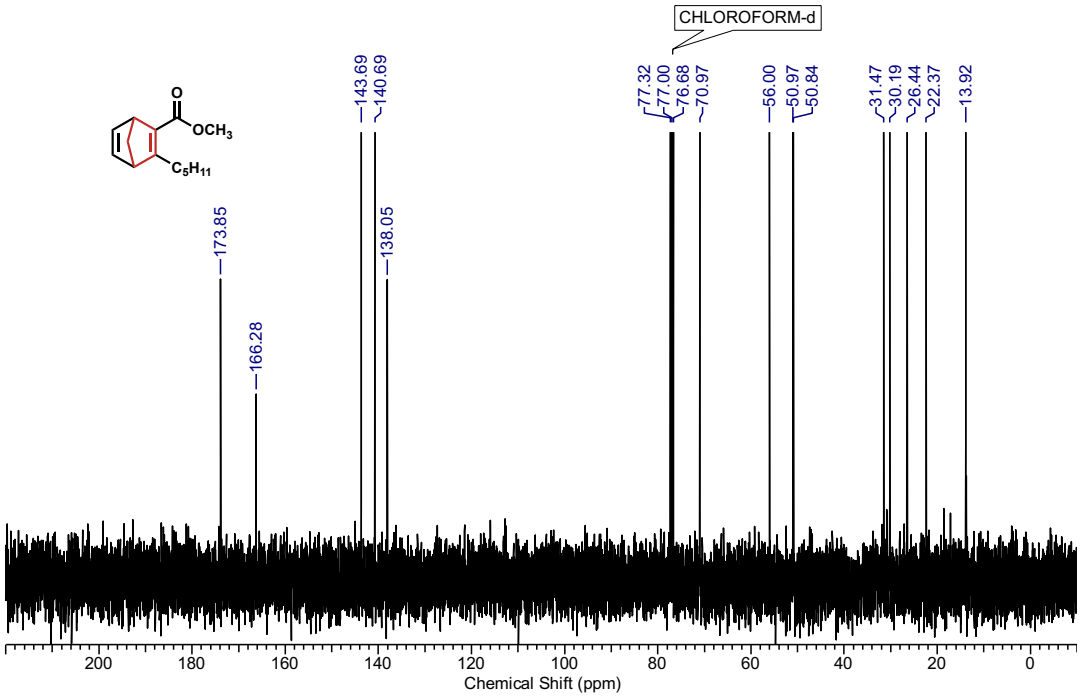

Figure S 2.2 ^{13}C NMR (100 MHz, $CDCl_3$) **3**

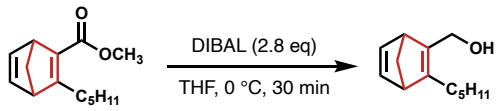

(3-Pentylbicyclo[2.2.1]hepta-2,5-dien-2-yl)methanol (4):

A solution of **3** (1.76 g, 8.01 mmol, 1.0 eq.) in THF (100 mL) was cooled to 0 °C. A solution of diisobutylaluminium hydride (DIBAL) in hexanes (1 M, 22.4 mL, 22.4 mmol, 2.8 eq.) was added dropwise over 10 min. The solution was maintained at 0 °C until complete consumption of the starting material (TLC, 30 min). The reaction was carefully quenched at 0 °C sequentially with water (0.8 mL), an aqueous solution of sodium hydroxide (NaOH) (1 M, 1.6 mL), and water (0.8 mL). The reaction mixture was removed from the ice bath and stirred a further 30 min. The reaction mixture was dried with $MgSO_4$, stirred a further 10 min, then filtered and rinsed with diethyl ether (Et_2O) (150 mL). The solvent was removed and the

residue subjected to flash column chromatography hexanes and ethyl acetate (EtOAc) as eluent (hexanes:EtOAc, 6:1) to yield racemic **4** (1.09 g, 5.67 mmol, 71%) as a clear and colorless oil. Spectral data matched that of literature reported data.[45]

Large-scale modification:

A 3 L three-neck round bottom flask equipped with stir bar, drop funnel and internal temperature probe was charged with THF (1.2 L) and **3** (40.8 g, 185 mmol, 1.0 eq.). The solution was cooled to 0 °C and a solution of DIBAL in hexanes (1 M, 518 mL, 518 mmol, 2.8 eq.) was added *via* drop funnel over 1.25 h while keeping the internal flask temperature between 0 and 5 °C. The solution was maintained at 0 °C until complete consumption of the starting material (TLC, 10 min). The reaction was carefully quenched at 0 °C with water (19 mL) over 30 min, an aqueous solution of NaOH (1 M, 37.5 mL) over 10 min, and water (19 mL) over 10 min. The reaction mixture was removed from the ice bath, stirred an additional 1 h and dried with $MgSO_4$ (100 g). The slurry was stirred a further 10 min, then filtered and rinsed with Et_2O (750 mL). The solvent was removed and the residue subjected to a silica plug (hexanes:EtOAc, 1:1) to yield racemic **4** (21.7 g, 113 mmol, 61%) as a clear and light yellow oil.

4: R_f (hexanes:EtOAc, 6:1): 0.29; ^{1}H NMR (400 MHz, $CDCl_3$) δ 6.81 (dd, J = 2.7, 5.1 Hz, 1 H), 6.73 (dd, J = 3.1, 5.1 Hz, 1 H), 4.26 (dd, J = 5.5, 12.1 Hz, 1 H), 4.14 (dd, J = 4.7, 12.1 Hz, 1 H), 3.55 (br. s., 1 H), 3.38 (br. s., 1 H), 2.27 - 2.17 (m, 1 H), 2.17 - 2.07 (m, 1 H), 1.92 (dd, J = 5.9, 15.7 Hz, 2 H), 1.47 - 1.24 (m, 4 H), 1.24 - 1.12 (m, 2 H), 0.98 (t, J = 5.5 Hz, 1 H), 0.88 (t, J = 7.2 Hz, 3 H) ppm; ^{13}C NMR (100 MHz, $CDCl_3$) δ 152.9, 145.1, 143.0, 142.2, 71.4, 58.9,

53.7, 51.8, 31.4, 28.2, 27.0, 22.5, 14.0 ppm; IR (ATR) 3324, 2959, 2928, 2860, 1457, 1378, 1304, 1230, 1209, 1016, 987 cm^{-1}; HRMS (EI+) Exact mass cald. for $C_{13}H_{18}^{+}$ $[M\text{-}H_2O]^{+}$: 174.1403, found: 174.1408.

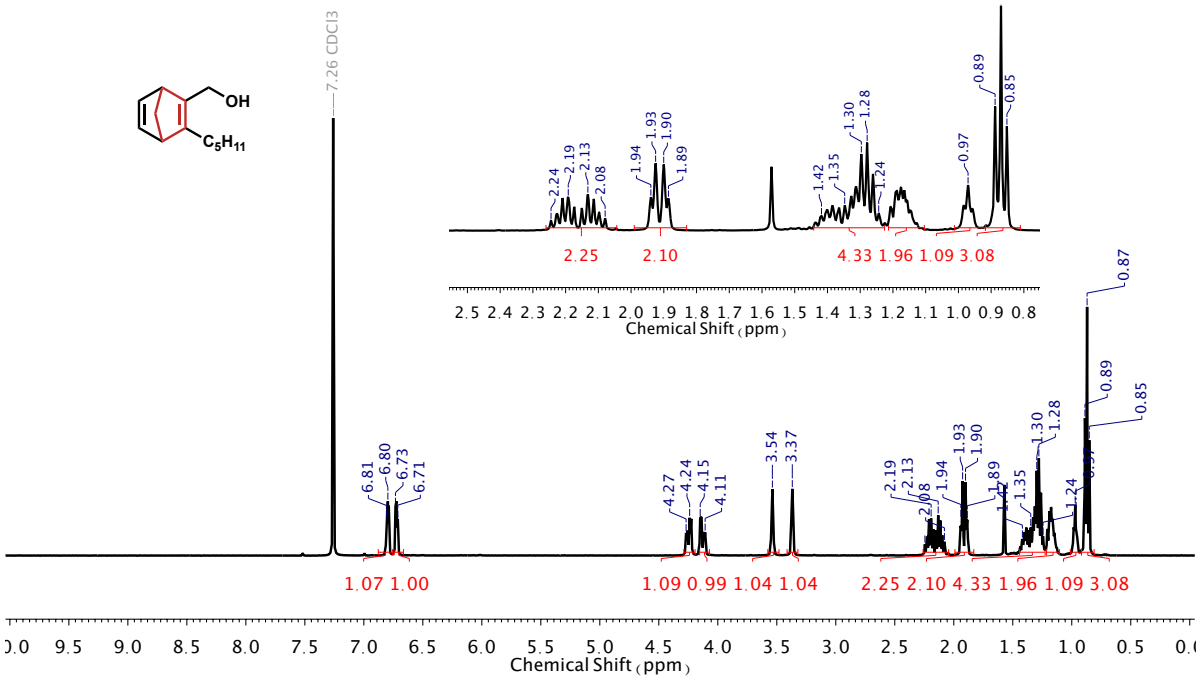

Figure S 2.3 ^{1}H NMR (400 MHz, $CDCl_3$) **4**

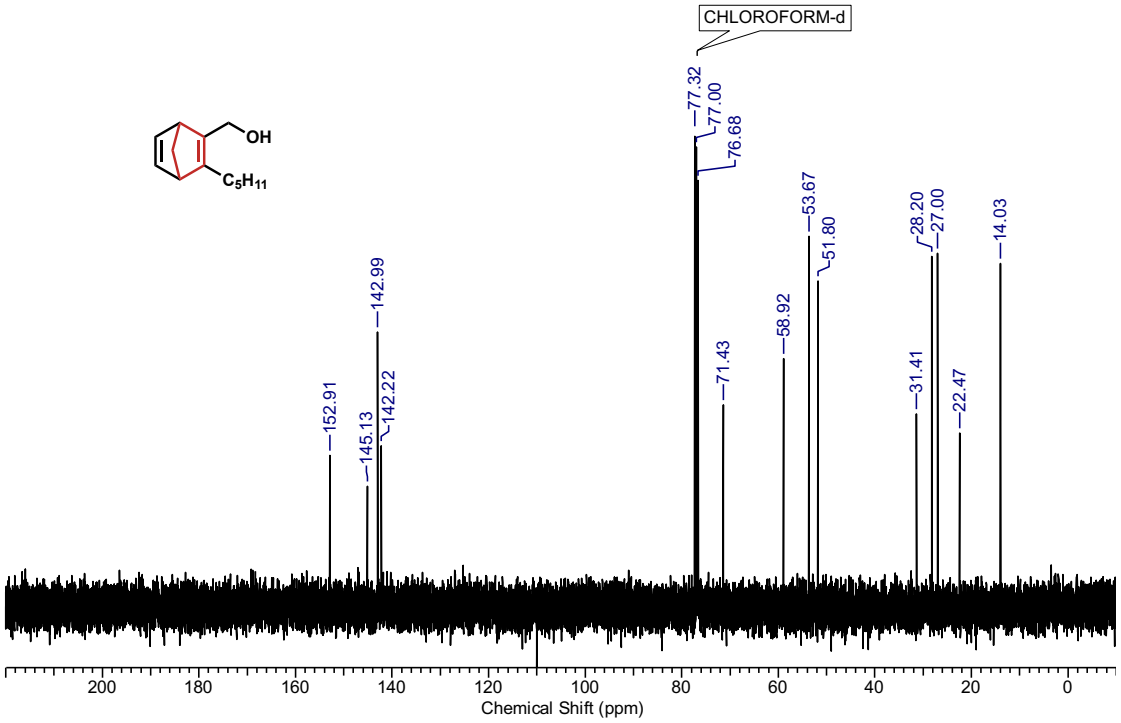

Figure S 2.4. ^{13}C NMR (100 MHz, $CDCl_3$) **4**

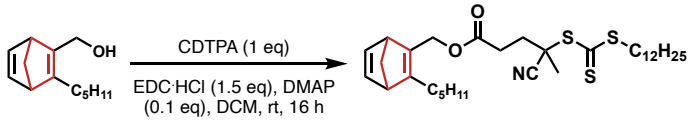

(3-pentylbicyclo[2.2.1]hepta-2,5-dien-2-yl)methyl 4-cyano-4-(((dodecylthio)carbonothioyl)thio)pentanoate (5):

Compound **4** (144 mg, 0.75 mmol, 1.5 eq.), EDC·HCl (14 mg, 0.75 mmol, 1.5 eq.), and dimethylaminopyridine (DMAP, 6 mg, 0.050 mmol, 0.10 eq.) were added to a solution of 4-cyano-4-[(dodecylsulfanylthiocarbonyl)sulfanyl]pentanoic acid (202 mg, 0.50 mmol, 1.0 eq.) in DCM (1 mL) in a vial. The reaction was capped under an atmosphere of air and stirred at rt for 16 h (the starting material was consumed by NMR). The reaction mixture was adsorbed to silica gel (2 g) and subjected to flash column chromatography (hexanes:EtOAc, 15:1) to yield diastereomeric **5** (266 mg, 0.46 mmol, 92%) as a yellow oil.

5: R_f (Hexanes:EtOAc, 15:1): 0.21; ^{1}H NMR (400 MHz, $CDCl_3$) δ 6.77 (dd, *J* = 3.0, 5.1 Hz, 1 H), 6.72 (dd, *J* = 2.9, 4.7 Hz, 1 H), 4.75 (dd, *J* = 1.0, 12.2 Hz, 1 H), 4.61 (d, *J* = 11.9 Hz, 1 H), 3.45 (br. s., 1 H), 3.39 (br. s., 1 H), 3.34 (t, *J* = 7.4 Hz, 2 H), 2.68 - 2.57 (m, 2 H), 2.57 - 2.48 (m, 1 H), 2.42 - 2.34 (m, 1 H), 2.24 (ddd, *J* = 6.5, 8.0, 14.1 Hz, 1 H), 2.15 (ddd, *J* = 6.5, 8.0, 14.1 Hz, 1 H), 1.96 (td, *J* = 1.6, 6.0 Hz, 1 H), 1.91 (td, *J* = 1.6, 6.0 Hz, 1 H), 1.88 (s, 3 H), 1.70 (quin, *J* = 7.5 Hz, 2 H), 1.45 - 1.14 (m, 24 H), 0.89 (dt, *J* = 3.1, 7.1 Hz, 6 H) ppm; ^{13}C NMR (125 MHz, $CDCl_3$) δ 216.9, 171.5, 156.1, 142.8, 142.0, 140.6, 119.0, 71.4, 61.3, 53.8, 52.2, 46.4, 37.0, 33.9, 31.9, 31.4, 29.8, 29.6, 29.5, 29.4, 29.3, 29.0, 28.9, 28.4, 27.7, 26.8, 24.8, 22.7, 22.5, 14.1, 14.0 ppm; IR (ATR) 2954, 2923, 2853, 1737, 1645, 1456, 1378, 1291, 1176, 1068, 861, 806 cm^{-1}; HRMS (ES+) Exact mass cald. for $C_{32}H_{51}NNaO_2S_3^+$ $[M+Na]^+$: 600.2974, found: 600.3001.

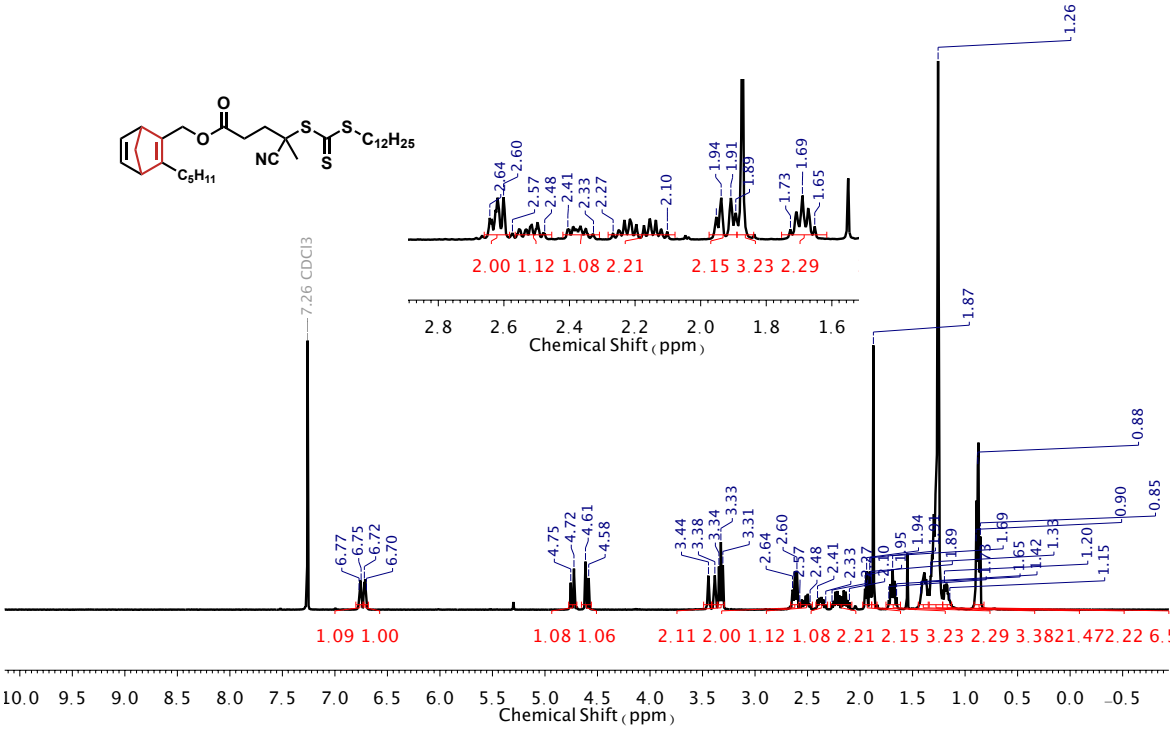

Figure S 2.5. ^{1}H NMR (400 MHz, $CDCl_3$) **5**

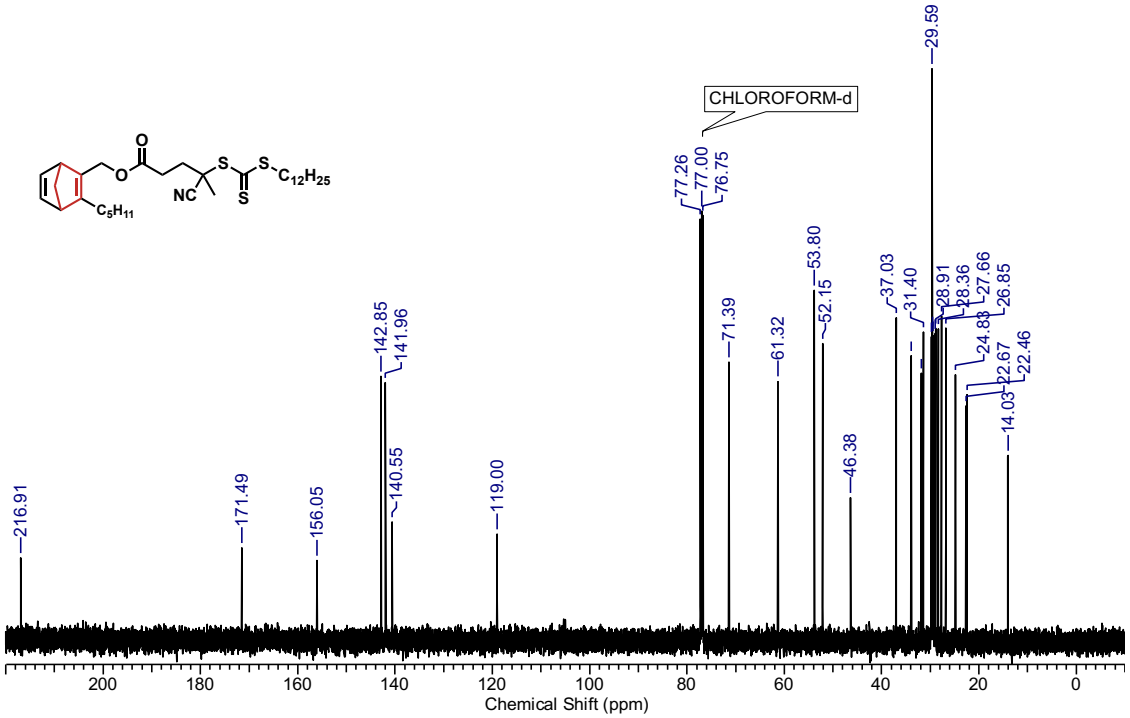

Figure S 2.6. ^{13}C NMR (125 MHz, $CDCl_3$) **5**

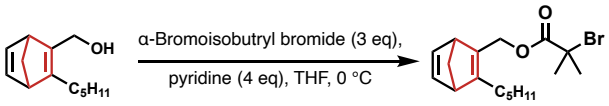

3-pentylbicyclo[2.2.1]hepta-2,5-dien-2-yl)methyl 2-bromo-2-methylpropanoate (6):

Compound **4** (0.380 g, 1.98 mmol, 1.0 eq.) and pyridine (0.64 mL, 7.90 mmol, 4.0 eq.) were added to THF (13 mL) and cooled to 0 ˚C. α-Bromoisobutyryl bromide (0.37 mL, 2.96 mmol, 1.5 eq.), was added drop-wise and the reaction solution was stirred at 0℃ for 2 h. The solvent removed and the residue was subjected to flash column chromatography (Hexanes:EtOAc, 20:1 and 2% triethylamine (Et_3N)) to yield **6** (0.485 g, 1.42 mmol, 72%) as a clear and colorless oil. The purified product was kept in a solution of hexane/EtOAc/Et_3N for stability.

6: R_f (Hexanes:EtOAc, 10:1) 0.35; ^1H NMR (600 MHz, $CDCl_3$) δ 6.75 (m, 1H), 6.69 (m, 1H), 4.81 (d, 1H), 4.66 (d, 1H), 3.48 (t, 1H), 3.36 (t, 1H), 2.23 (m, 1H), 2.18 (m, 1H), 1.94 (m, 1H),

1.91 (s, 6H), 1.89 (m, 1H), 1.38 (m, 2H), 1.27 (m, 2H), 1.17 (m, 2H), 0.85 (t, 3H) ppm. ^{13}C NMR (126 MHz, $CDCl_3$) δ 171.80, 156.44, 143.15, 141.99, 140.68, 71.60, 62.32, 56.29, 54.02, 52.32, 31.52, 31.03, 28.57, 26.98, 22.65, 14.20 ppm. IR (ATR): 2937, 2929, 2860, 1732, 1462, 1270, 1159, 1107 cm^{-1}; HRMS (ES+) Exact mass cald. for $C_{17}H_{25}BrO_2Na^+$ $[M+Na]^+$: 363.1, found: 363.1.

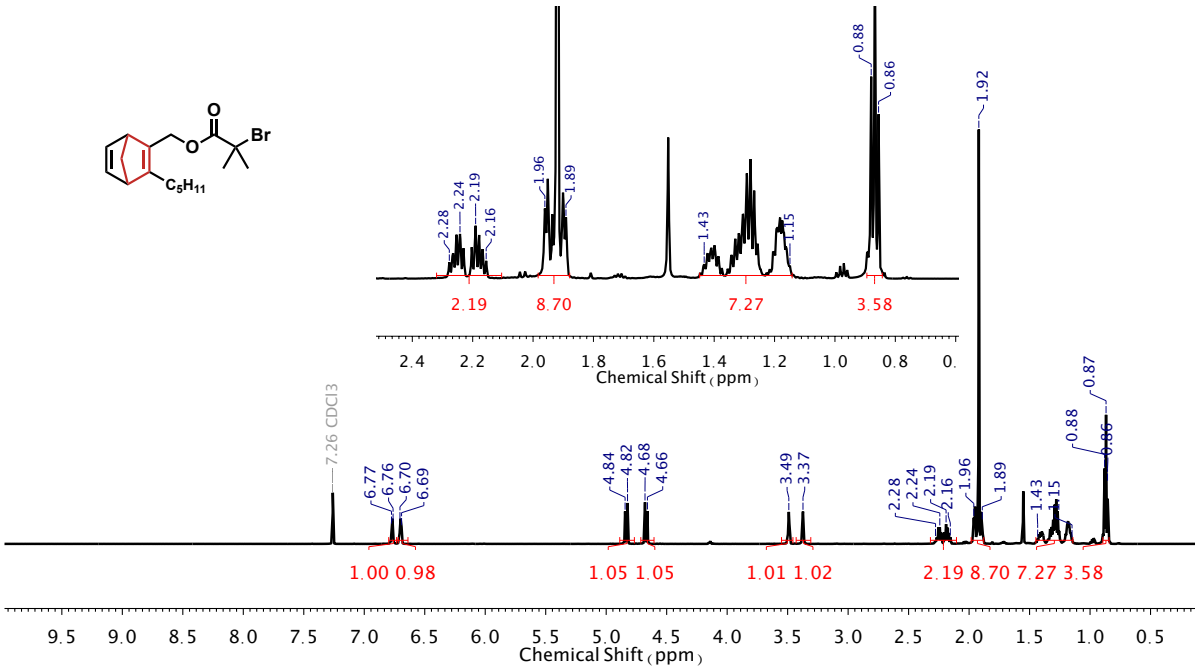

Figure S 2.7 ^{1}H NMR (400 MHz, $CDCl_3$) **6**

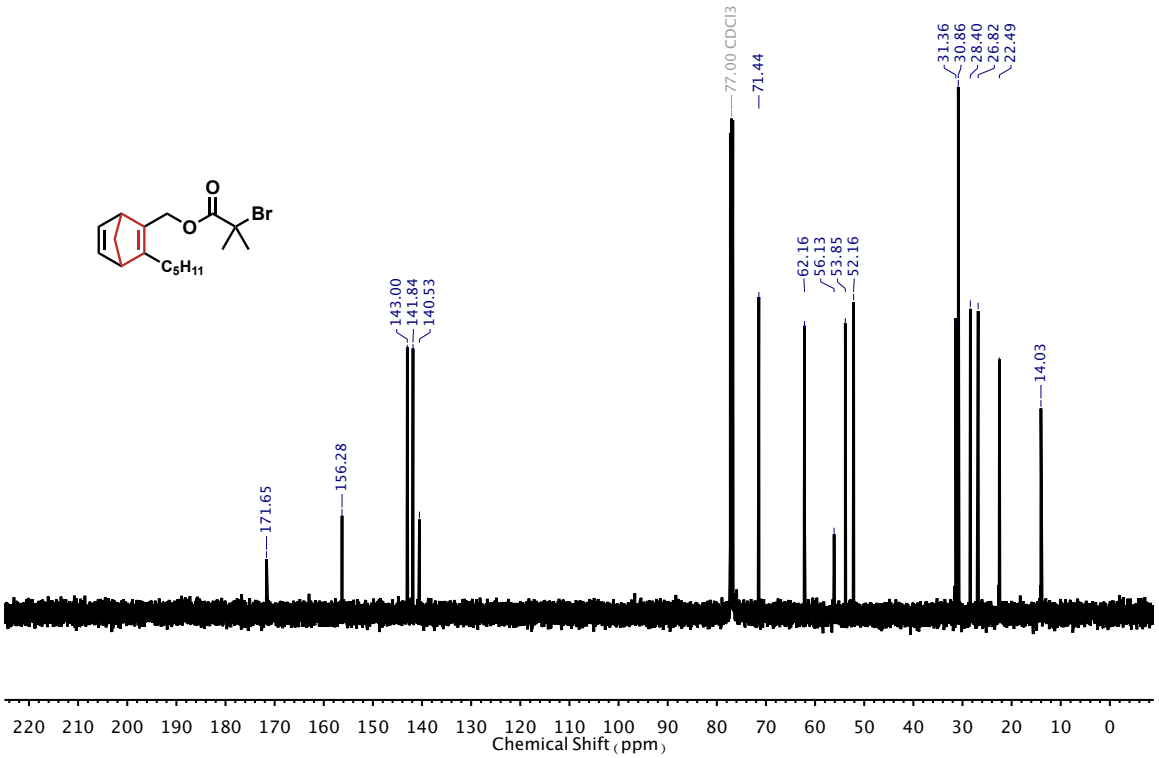

Figure S 2.8. ^{13}C NMR (100 MHz, $CDCl_3$) **6**

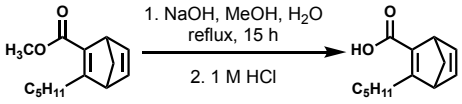

3-pentylbicyclo[2.2.1]hepta-2,5-diene-2-carboxylic acid (9):

Compound **3** (0.50 g, 2.3 mmol, 1 eq) was dissolved in methanol (MeOH) (5.0 mL) and added dropwise an aqueous solution of sodium hydroxide (NaOH) (2.5 M, 15. mL). The solution was refluxed for 15 h, at which point complete consumption of starting material was confirmed by TLC. The solution was cooled to 0 °C before acidifying with an aqueous solution of hydrochloric acid (HCl) (1 M, 50 mL) then extracting with diethyl ether (3 x 75 mL). The combined organic layers were washed with brine (1 x 100 mL), dried over $MgSO_4$ and the solvent removed. The residue was subjected to flash column chromatography (hexanes:EtOAc, 5:1) to yield **9** (320 mg, 1.6 mmol, 70%) as a clear oil.

9: R_f (Hexanes:EtOAc, 5:1): 0.39; ^{1}H NMR (400 MHz, $CDCl_3$) δ 6.89 (dd, *J* = 3.0, 5.0 Hz, 1 H), 6.68 (dd, *J* = 3.4, 4.6 Hz, 1 H), 3.89 (br. s., 1 H), 3.54 (br. s., 1 H), 2.79 - 2.65 (m, 2 H), 2.00 (dd, *J* = 6.5, 27.9 Hz, 2 H), 1.55 - 1.21 (m, 6 H), 0.88 (t, *J* = 7.1 Hz, 3 H) ppm; ^{13}C NMR (100 MHz, $CDCl_3$) δ 177.3, 171.3, 143.9, 140.5, 137.7, 71.0, 56.5, 50.8, 31.6, 30.6, 26.5, 22.5, 14.0 ppm; IR (ATR) 2957, 2927, 2858, 2643, 1659, 1615, 1558, 1416, 1292, 1254, 936, 710 cm^{-1}; HRMS (ES-) Exact mass cald. for $C_{13}H_{17}O_2^-$ [M-H]$^-$: 205.1228, found: 205.1228.

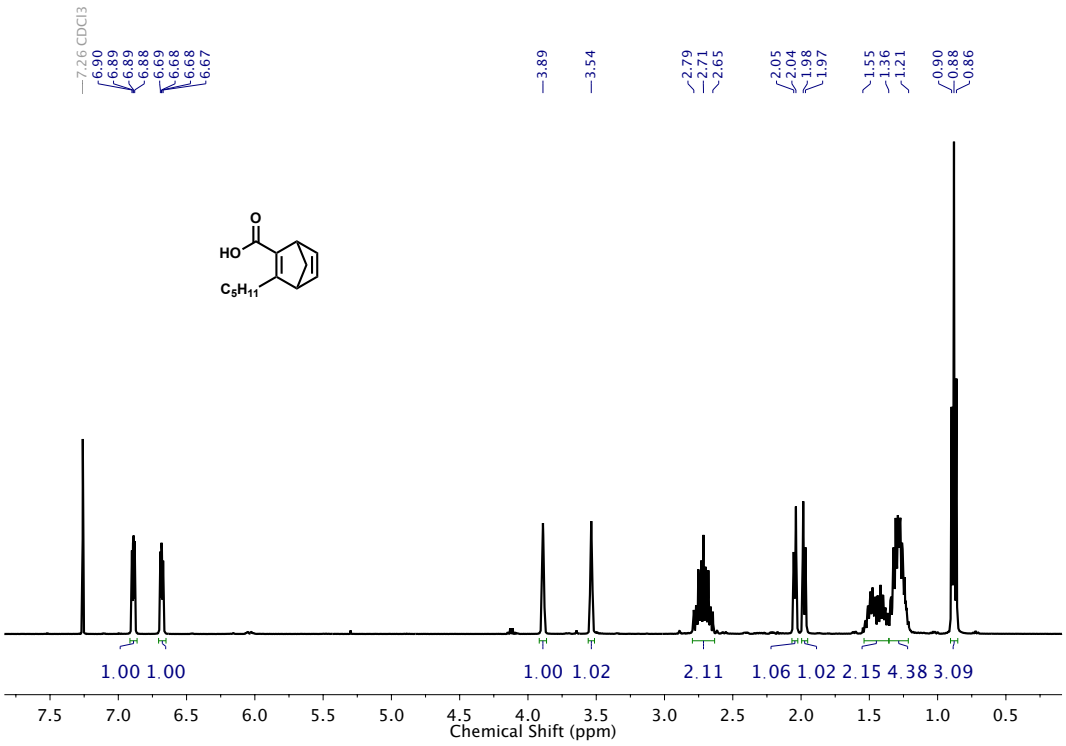

Figure S 2.9. ^{1}H NMR (400 MHz, $CDCl_3$) **9**

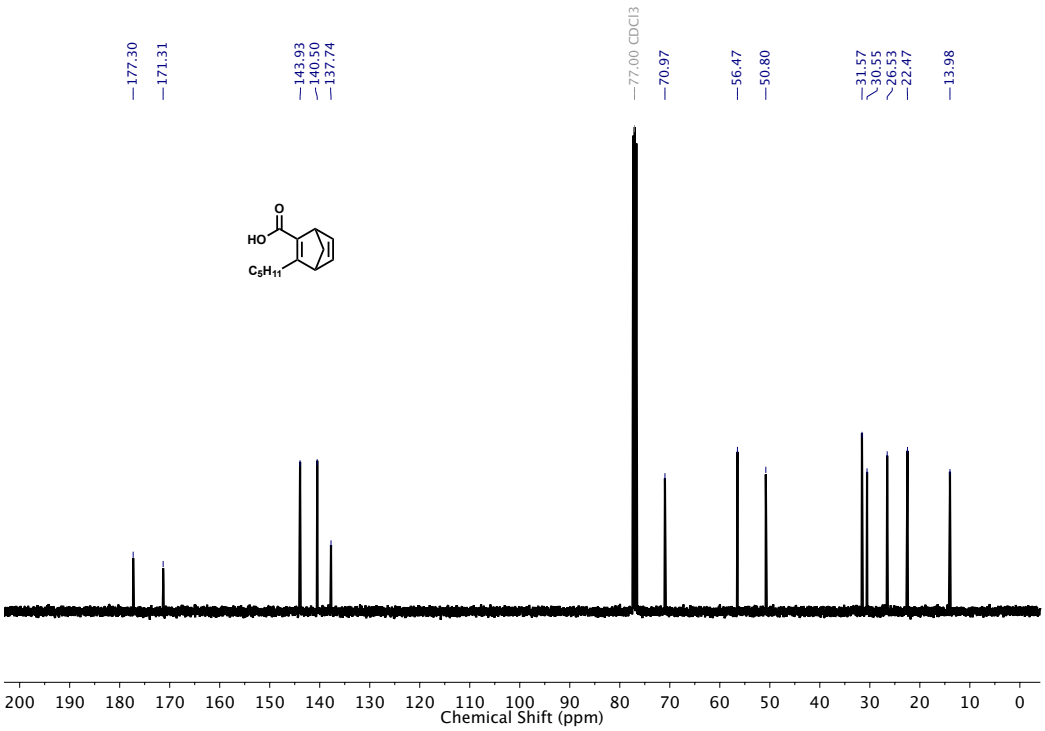

Figure S 2.10. ^{13}C NMR (100 MHz, $CDCl_3$) **9**

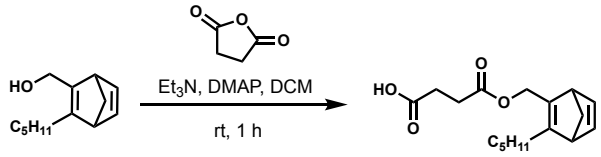

4-oxo-4-((3-pentylbicyclo[2.2.1]hepta-2,5-dien-2-yl)methoxy)butanoic acid (10):

Compound **4** (4.81 g, 25.0 mmol, 1 eq) and dichloromethane (DCM) (12 mL) were added to a 50 mL round bottom equipped with a magnetic stir bar. To the solution was added triethyl amine (2.53 mL, 25.0 mmol, 1 eq), 4-dimethylaminopyridine (305 mg, 2.50 mmol, 0.1 eq), and succinic anhydride (3.25 g, 32.5 mmol, 1.3 eq). The reaction was stirred at rt under an atmosphere of air until complete consumption of the starting material (TLC, 1 h). The solution was transferred to a separatory funnel along with additional DCM (350 mL). The organic layer was washed with aqueous HCl (1 M, 2 X 350 mL) then water (1 X 350 mL), dried over $MgSO_4$,

and the solvent removed to afford **10**, (7.23 g, 24.7 mmol, 99%) of viscous oil that solidifies upon refrigeration.

10: R_f (Hexanes:EtOAc, 6:1): 0.25; ^{1}H NMR (600 MHz, $CDCl_3$) δ 6.75 (dd, *J* = 3.1, 4.9 Hz, 1 H), 6.70 (dd, *J* = 3.1, 4.9 Hz, 1 H), 4.75 (d, *J* = 12.2, 1 H), 4.60 (d, *J* = 12.2, 1 H), 3.44 (br. s., 1 H), 3.37 (br. s., 1 H), 2.70 - 2.62 (m, 4 H), 2.25 - 2.12 (m, 2H), 1.91 (dd, *J* = 5.9, 29.1 Hz, 2 H), 1.43 - 1.14 (m, 6 H), 0.87 (t, *J* = 7.2 Hz, 3 H) ppm; ^{13}C NMR (100 MHz, $CDCl_3$) δ 177.4, 172.2, 155.8, 142.9, 141.9, 140.7, 71.3, 61.1, 53.8, 52.1, 31.4, 28.9, 28.8, 28.3, 26.8, 22.5, 14.0 ppm; IR (ATR) 2957, 2929, 2858, 1725, 1708, 1437, 1399, 1385, 1342, 1256, 1209, 1165, 1058, 955, 722, 701 cm^{-1}; HRMS (ES-) Exact mass cald. for $C_{17}H_{23}O_4^-$ [M-H]$^-$: 291.1596, found: 291.1581.

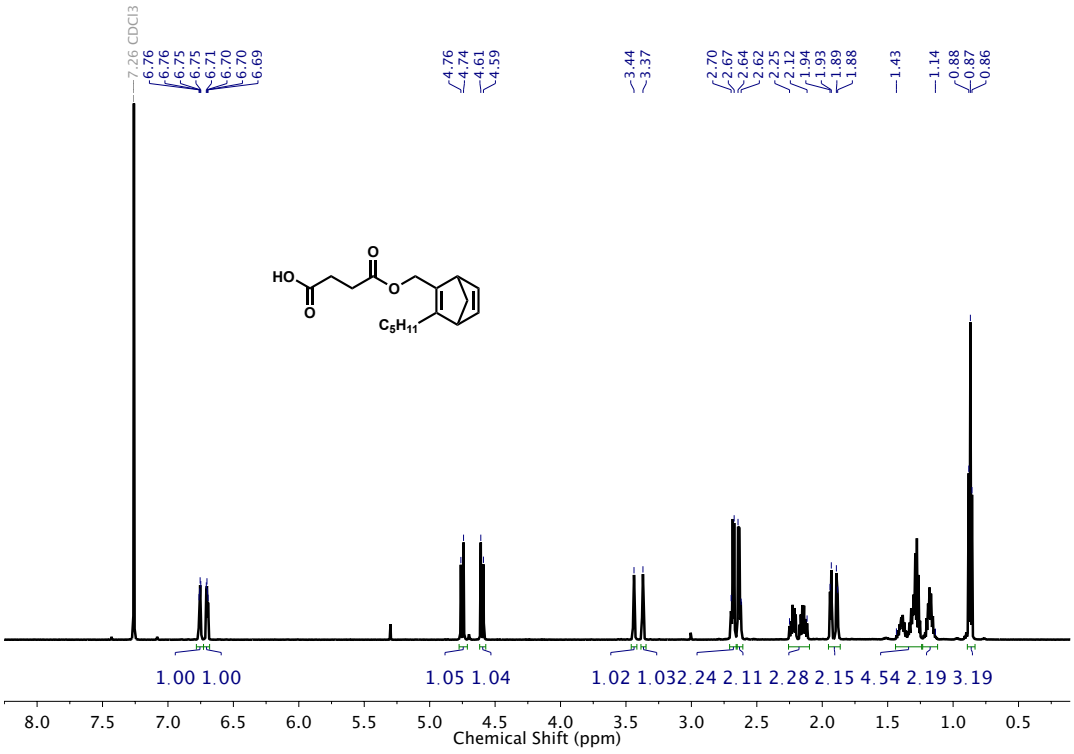

Figure S 2.11. ^{1}H NMR (600 MHz, $CDCl_3$) **10**

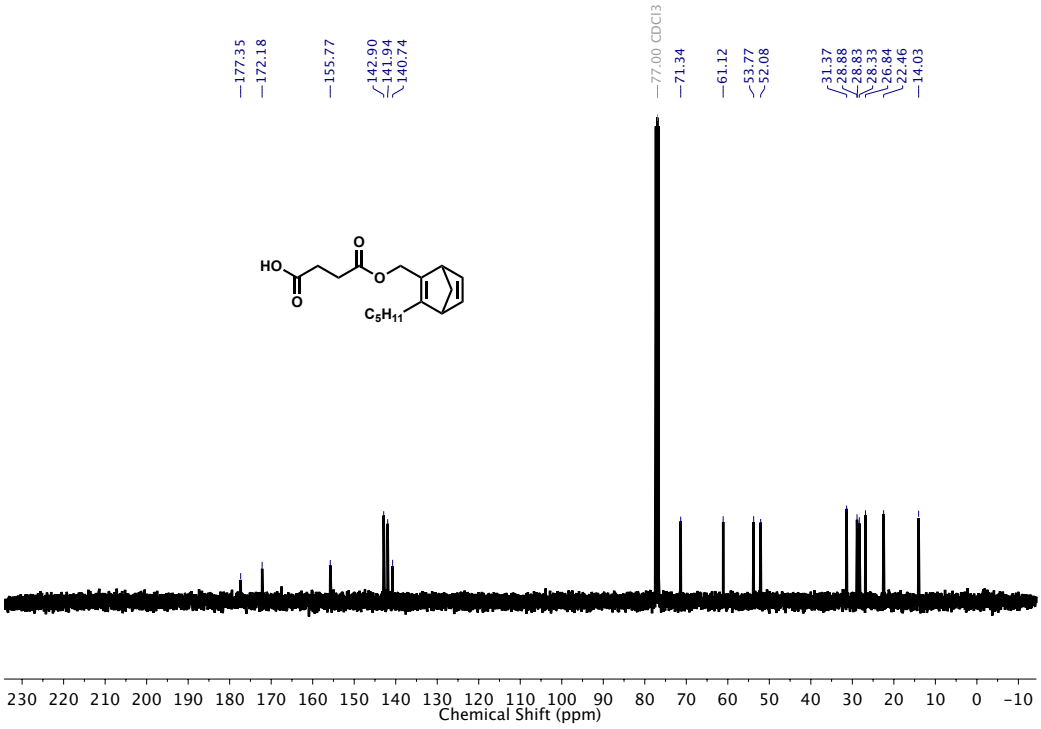

Figure S 2.12. ^{13}C NMR (100 MHz, $CDCl_3$) **10**

Synthesis of Functionalized Polymers

General Synthesis of NBD-PLA:

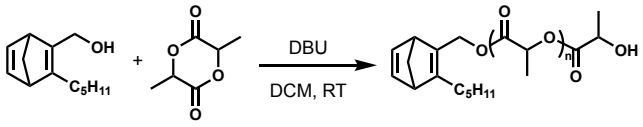

A 20-mL scintillation vial equipped with a magnetic stir bar was flame dried under three argon and evacuation cycles before transfer into a glovebox. *D,L*-lactide (205–360 eq.) was added and dissolved in anhydrous DCM (5 mL/g *D,L*-lactide). **4** (1 eq.) was added to the vial along with a 1.5 M THF solution of 1,8-biazabicyclo[5.4.0]undec-7-ene (DBU) (1 eq.). The polymerization was allowed to stir at rt until desired conversion (4–12 min) and quenched with benzoic acid (5 eq.). Monomer conversion was estimated by ^{1}H NMR in deuterated chloroform. The DCM was removed under reduced pressure and the crude mixture was re-

dissolved in a minimal amount of DCM. The mixture was subsequently precipitated into cold methanol before collecting the solid via vacuum filtration. The solid was re-dissolved in DCM, and the precipitation process was repeated twice. The obtained white solid was dried under reduced pressure.

Synthesis of P1:

Followed general synthesis of NBD-PLA using 360 eq. *D,L*-lactide and 1.7 eq. DBU. Conversion 61%, $M_{n(theoretical)}$ = 32,000 g/mol, $M_{n(NMR)}$ = 36,000 g/mol, $M_{n(SEC)}$ = 42,000 g/mol, $Đ$ = 1.04.

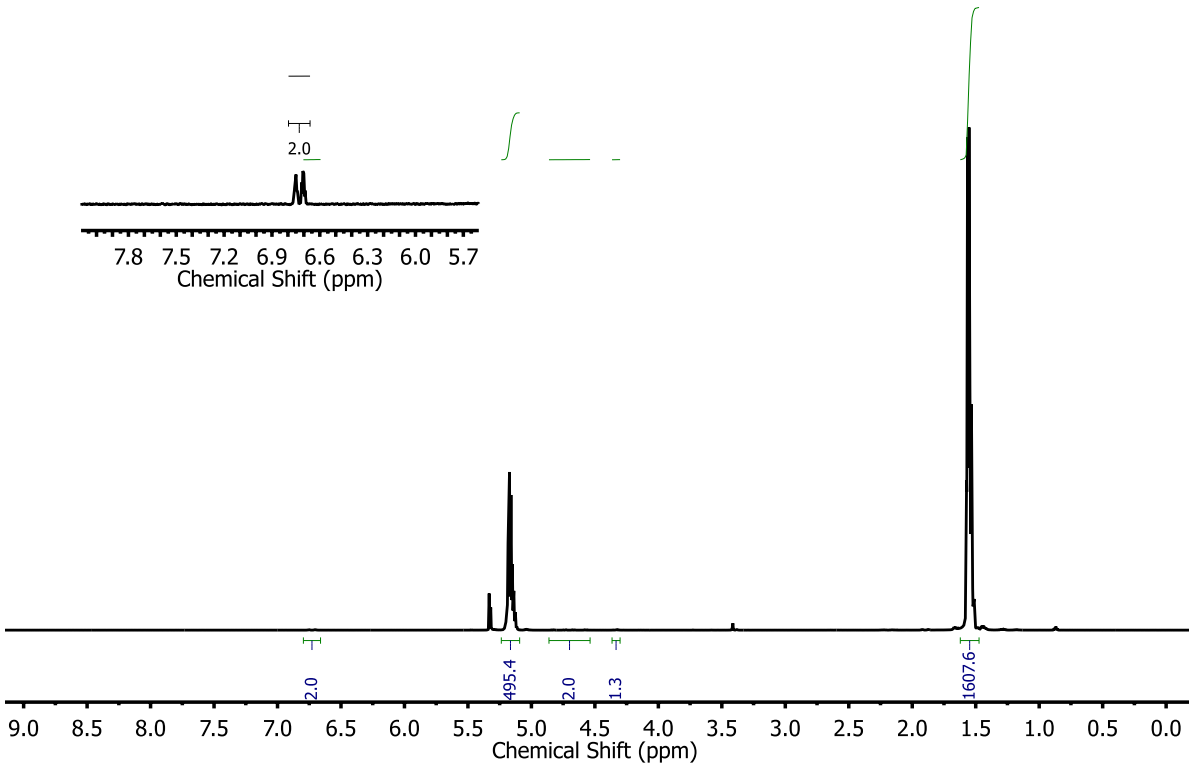

Figure S 2.13. ^{1}H NMR of spectrum of **P1** in CD_2Cl_2 showing the presence of expected chain-end resonances.

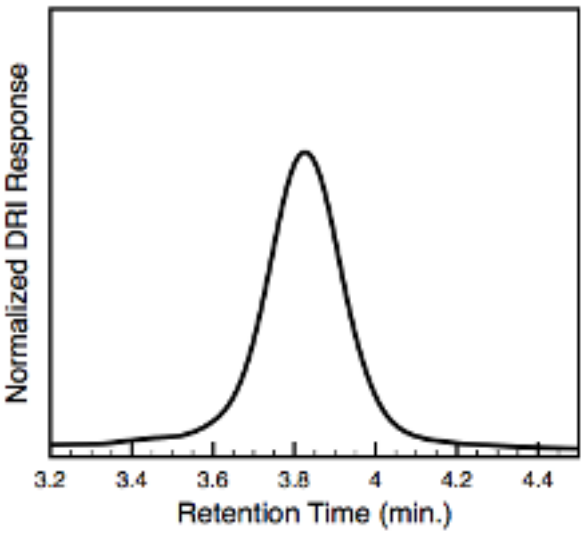

Figure S 2.14. SEC-RI trace of **P1**

Synthesis of S-P1:

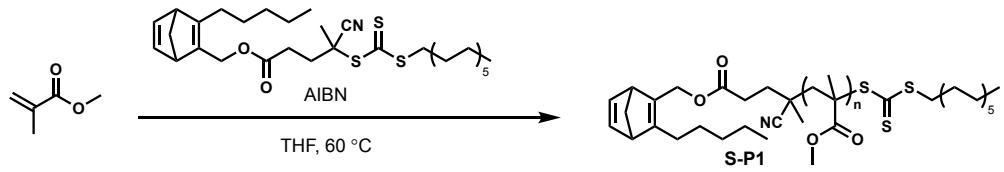

Methyl methacrylate (MMA, 825 µL, 7.75 mmol, 125 eq.) was dissolved in 0.825 mL of THF in a 1-dram vial equipped with a magnetic stir bar and septum cap. Following this, azobisisobutyronitrile (AIBN, 2 mg, 0.012 mmol, 0.2 eq.) and **5** (36 mg, 0.062 mmol, 1 eq.) were added and the resulting reaction mixture was degassed by argon bubbling for 10 min. The polymerization proceeded at 60 °C for 7 h. Monomer conversion was estimated by ^{1}H NMR in deuterated chloroform and determined to be 50%. THF was removed under reduced pressure, and the crude mixture was re-dissolved in a minimal amount of DCM. The mixture was precipitated into cold methanol before collecting the solid via vacuum filtration. The solid was re-dissolved in DCM, and the precipitation process was repeated a total of 3 times. ^{1}H

NMR analysis indicated successful incorporation of the NBD chain-end functionality. Conversion 50%, $M_{n(theoretical)}$ = 6,900 g/mol, $M_{n(NMR)}$ = 8,700 g/mol, $M_{n(SEC)}$ = 7,700 g/mol, $Đ$ = 1.14.

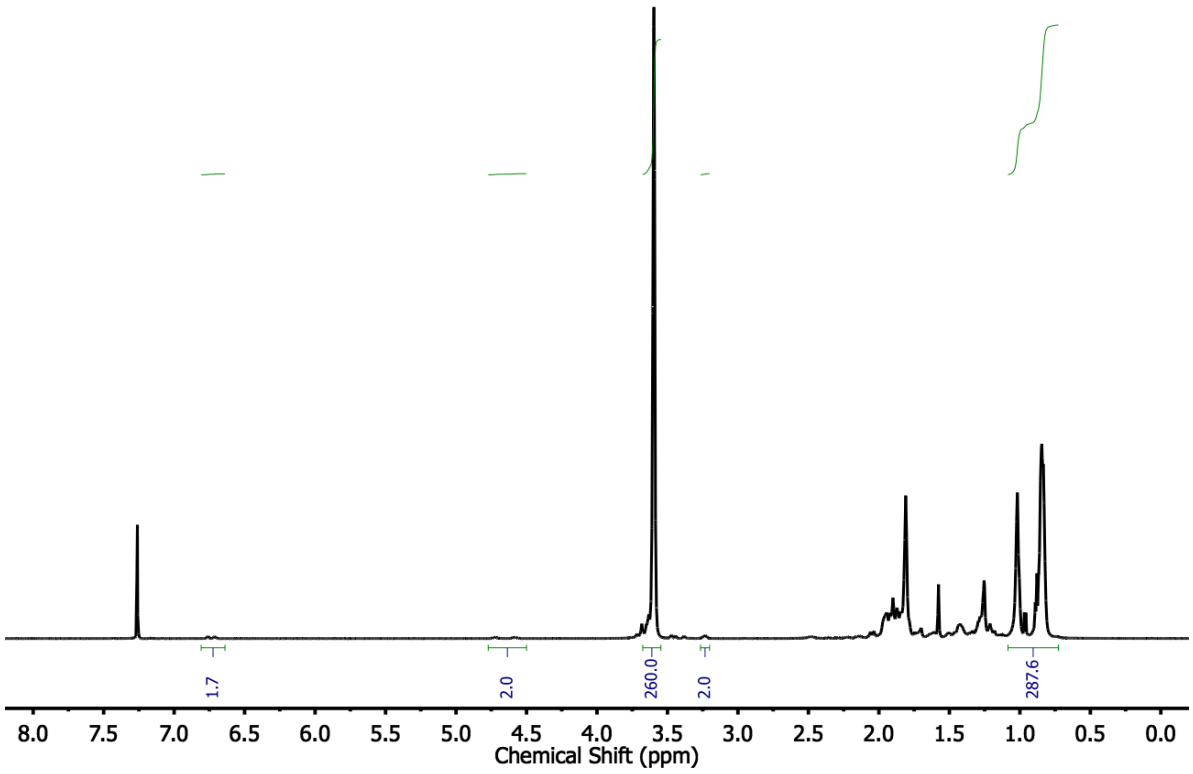

Figure S 2.15. ^{1}H NMR of spectrum of **S-P1** in $CDCl_3$ showing the presence of expected chain-end resonances.

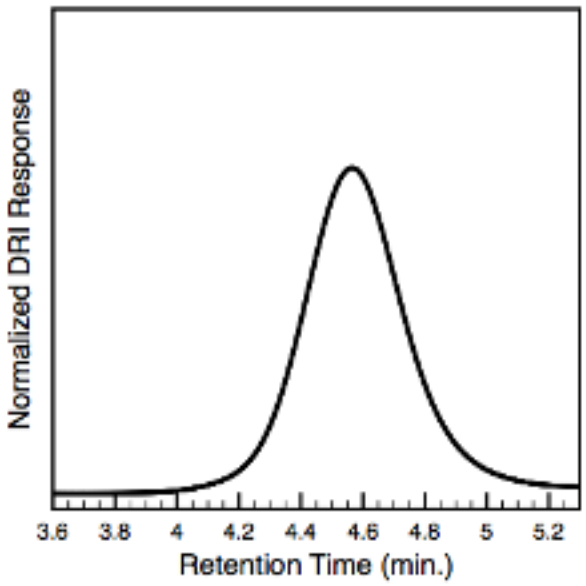

Figure S 2.16. SEC-RI trace of **S-P1**

Synthesis of S-P2

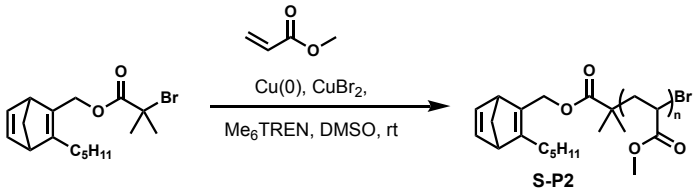

Copper(II) bromide ($CuBr_2$, 1.1 mg, 0.05 mmol, 0.50 eq.) and tris[2-(dimethylamino)ethyl]amine (Me_6TREN) (4.8 μL, 0.018 mmol, 0.18 eq.) were added to a 1-dram vial equipped with a septum sealed cap then dissolved in DMSO (0.50 mL) with sonication for 10 min. Methyl acrylate (0.45 mL, 5.0 mmol, 50 eq.) was added to the catalyst mixture. Compound **6** (34.1 mg, 0.1 mmol, 1.0 eq.) was added subsequently. Copper wire (3 cm, 22 AWG) was activated by soaking in concentrated HCl for 7 min, then wrapped around a magnetic stir bar and placed in the vial. The solution was degassed by argon bubbling for 10 min while keeping the stir bar suspended above the solution using a magnet. The polymerization was stirred at rt for 10 min. The crude polymer was precipitated once in cold

hexanes. The precipitated solid was collected, re-dissolved in dichloromethane and precipitated once in cold methanol MeOH. The precipitated solid was collected by vacuum filtration and dried under reduced pressure. Conversion 60%, $M_{n(\text{theoretical})}$ = 2,900 g/mol, $M_{n(\text{NMR})}$ = 2,100 g/mol, $M_{n(\text{SEC})}$ = 2,100 g/mol, $Đ$ = 1.31.

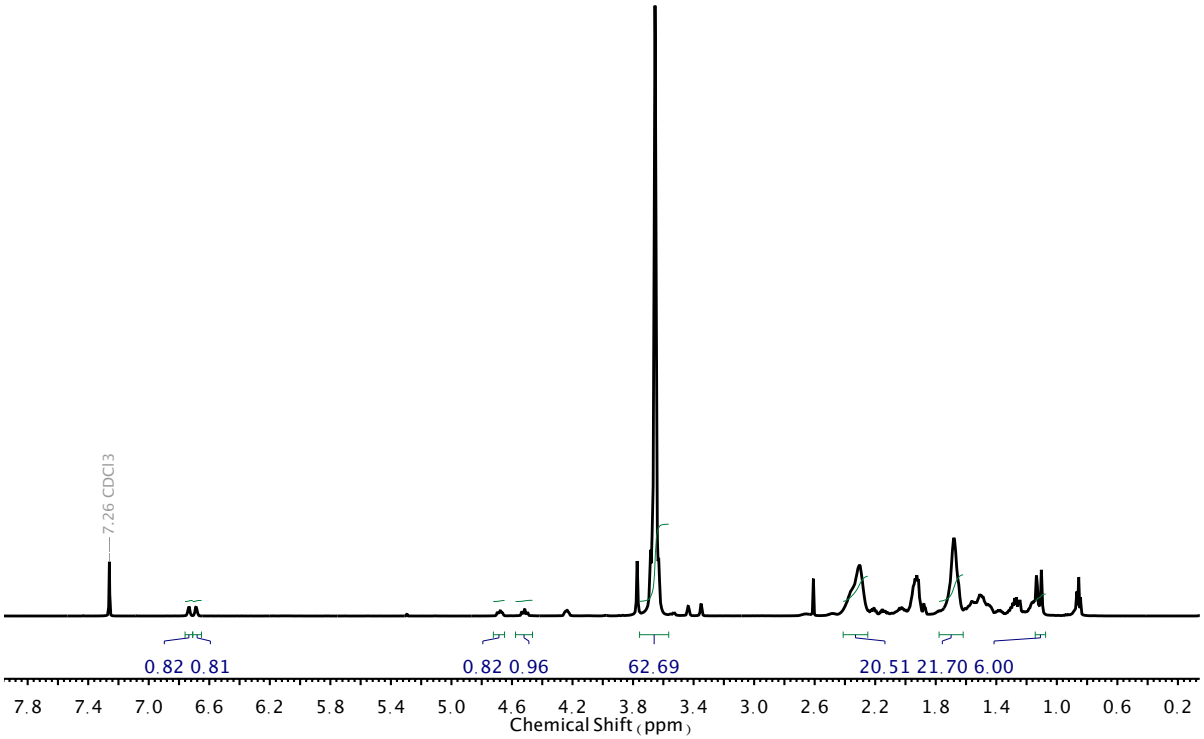

Figure S 2.17. ^{1}H NMR of spectrum of **S-P2** in $CDCl_3$ showing presence of expected chain-end resonances.

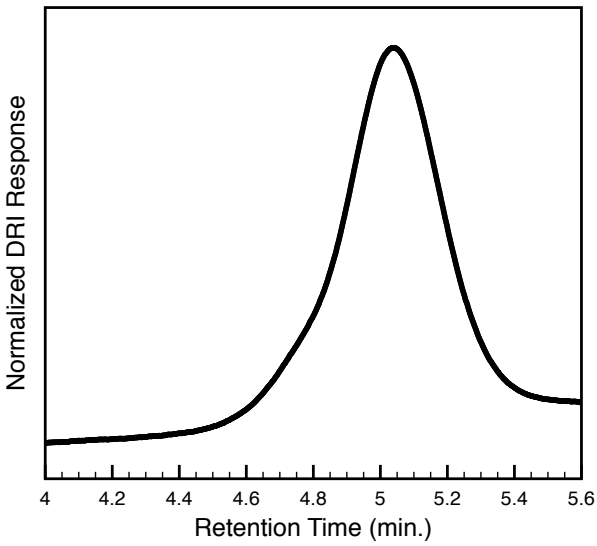

Figure S 2.18. SEC-RI trace of **S-P2.**

Synthesis of S-P3

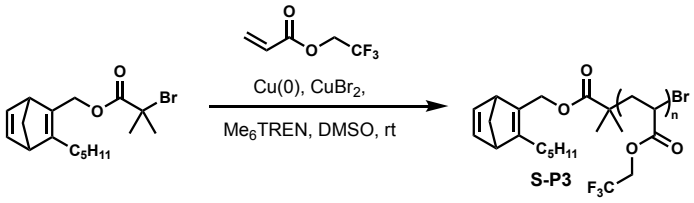

$CuBr_2$ (1.1 mg, 0.005 mmol, 0.5 eq.) and Me_6-Tren (4.8 μL, 0.018 mmol, 0.18 eq.) were added to a 20-mL vial equipped with a septum sealed cap and dissolved in DMSO (2.50 mL) via sonication for 10 min. Trifluoroethyl acrylate (2.54 mL, 10.0 mmol, 100 eq.) was added to the catalyst mixture. Compound **6** (34.1 mg, 0.1 mmol, 1 eq.) was added subsequently. Copper wire (3 cm, 22 AWG) was activated by soaking in concentrated HCl for 7 min then wrapped around a magnetic stir bar and placed in the vial. The solution was degassed by argon bubbling for 10 min while keeping the stir bar suspended above the solution with a magnet. The polymerization was stirred at rt for 20 min. The crude polymer was passed through basic alumina to remove copper before dialysis in DCM for 2 days. The dialyzed polymer solution

was collected by vacuum filtration and dried under reduced pressure. Conversion 20%, $M_{n(\text{theoretical})}$ = 3,400 g/mol, $M_{n(\text{NMR})}$ = 3,100 g/mol, $M_{n(\text{SEC})}$ = 1,800 g/mol, $Đ$ = 1.32.

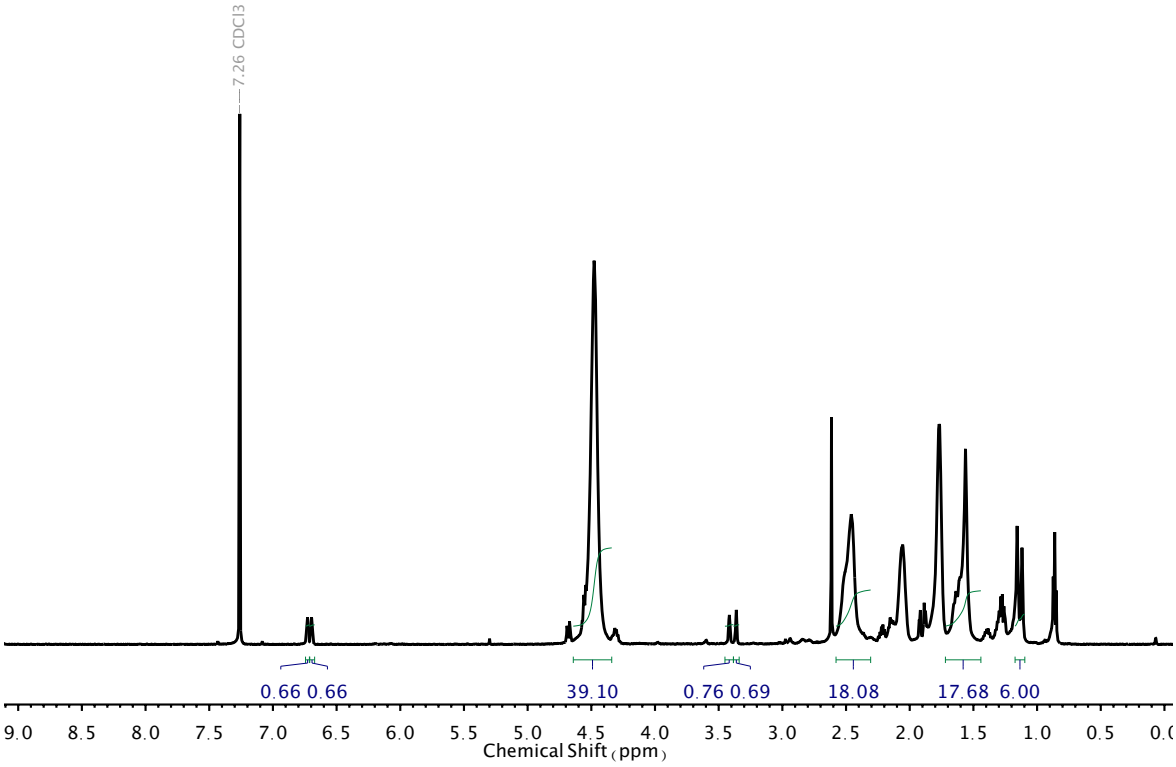

Figure S 2.19. ^{1}H NMR of spectrum of **S-P3** in $CDCl_3$ showing presence of expected chain-end resonances.

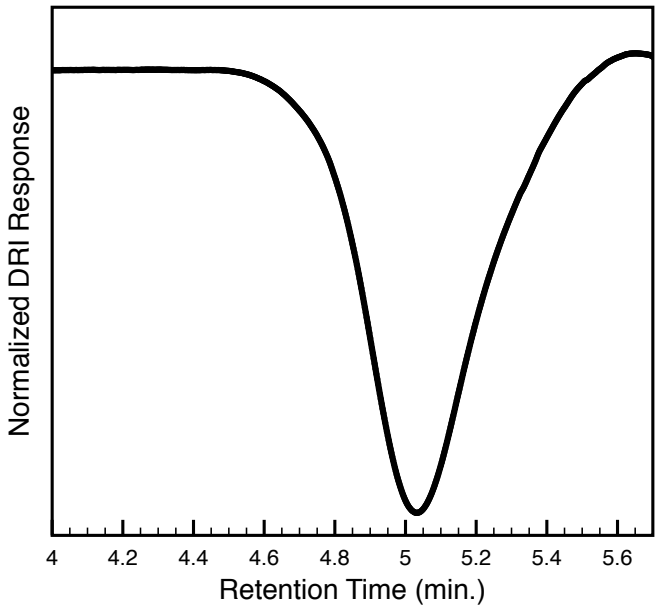

Figure S 2.20. SEC-RI trace of **S-P3.**

Synthesis of P2:

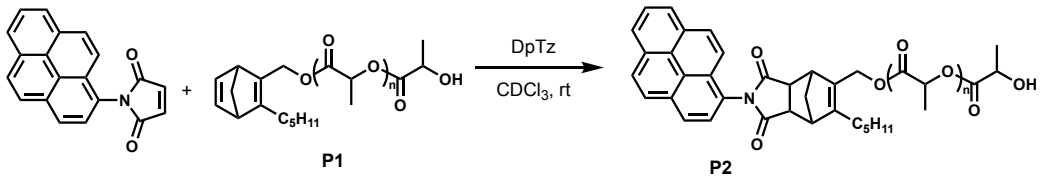

P1 (79 mg, 0.002 mmol, 1 eq.), 3,6-di-2-pyridyl-1,2,4,5-tetrazine (DpTz) (1.3 mg, 0.005 mmol, 2.4 eq.) and a solution of *N*-(1-pyrenyl)maleimide (**8**) in $CDCl_3$ (4 mg/mL, 0.2 mL, 0.003 mmol, 1.2 eq.)) were added to a 1-dram vial equipped with a septum cap. The vial was placed on a shaker at rt for 4 h, before adding approximately 1 mg of norbornene to quench the excess DpTz. The reaction was left to shake at rt for an additional 20 h. The crude reaction mixture was precipitated into cold methanol and centrifuged to collect the desired product. The supernatant was discarded, and the resulting solid was collected and re-dissolved in a minimal amount of DCM . The precipitation process was repeated 3 times before drying the obtained

polymer under reduced pressure. ^{1}H NMR of the purified polymer suggests near quantitative conversion to **P2**. $M_{n(NMR)}$ = 36,000 g/mol, $M_{n(SEC)}$ = 42,000 g/mol, $Đ$ = 1.04.

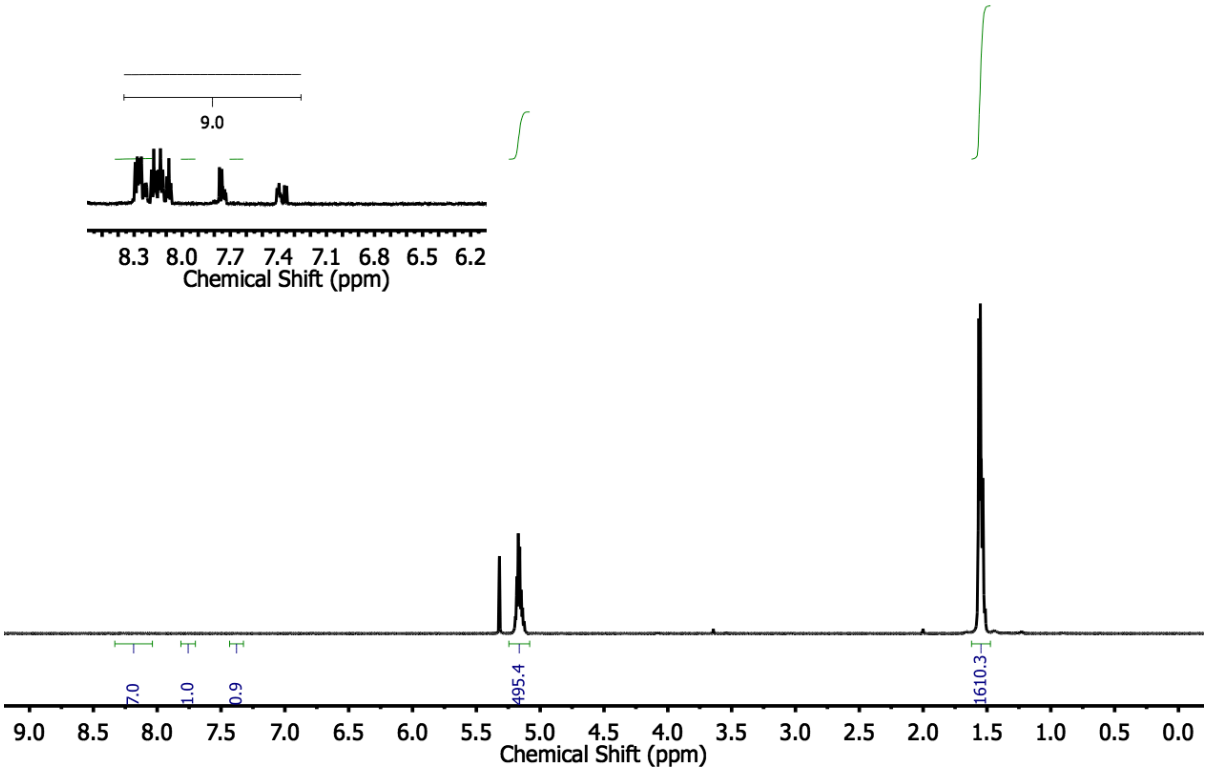

Figure S 2.21. ^{1}H NMR of spectrum of **P2** in $CDCl_3$ showing presence of expected chain-end resonances corresponding to pyrene following functionalization.

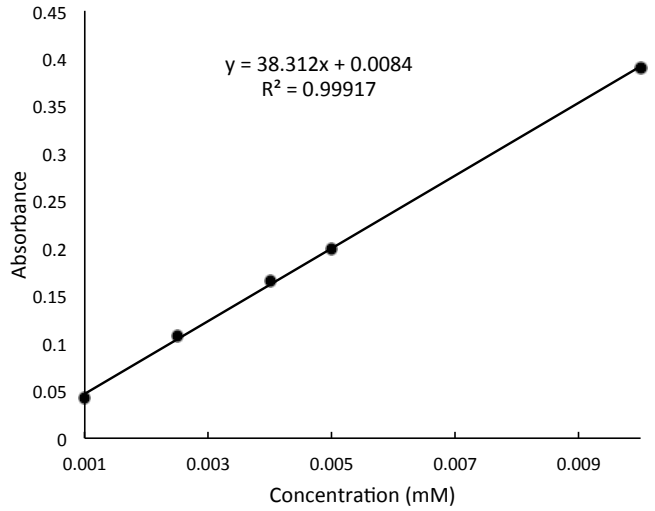

Figure S 2.22. Calibration curve prepared using serial dilutions of *N*-(1-pyrenyl)maleimide in DCM based on local maximum at 276 nm.

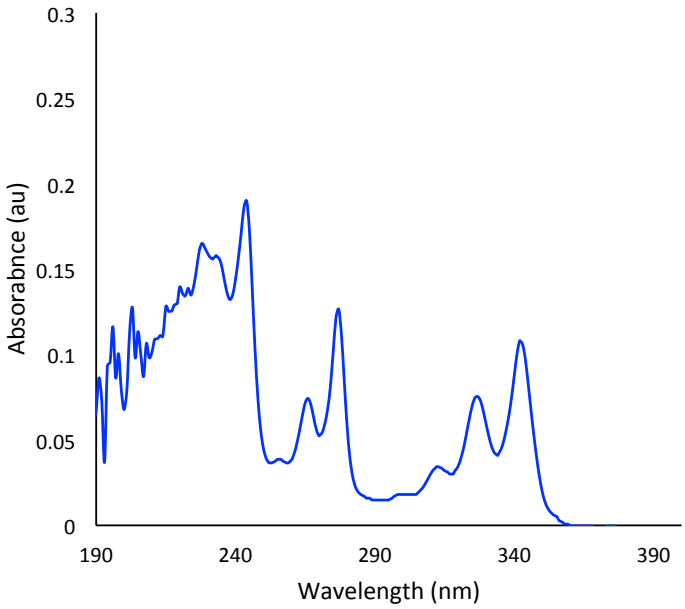

Figure S 2.23. Absorbance spectrum of a 0.003 mM solution of **P2** ($M_{n(NMR)}$ = 36,000 g/mol) in DCM shows incorporation of pyrene functionality. Using the absorbance value for the local 276 nm maximum and the linear regression equation obtained from the calibration curve, the incorporation of pyrene is estimated to be 0.98 pyrenes/per chain. These results support the quantitative incorporation calculated by ^{1}H NMR.

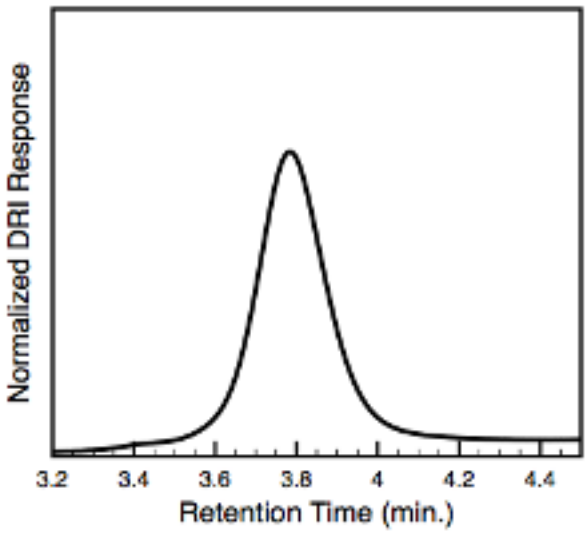

Figure S 2.24. SEC-RI trace of **P2** after functionalization showing no observable change in molar mass distribution.

Synthesis of P3:

Followed general synthesis of NBD-PLA using 210 eq. *D,L*-lactide. Conversion 51%, $M_{n(theoretical)}$= 15,700 g/mol, $M_{n(NMR)}$ = 19,700 g/mol, $M_{n(SEC)}$ = 21,800 g/mol, $Đ$ = 1.08.

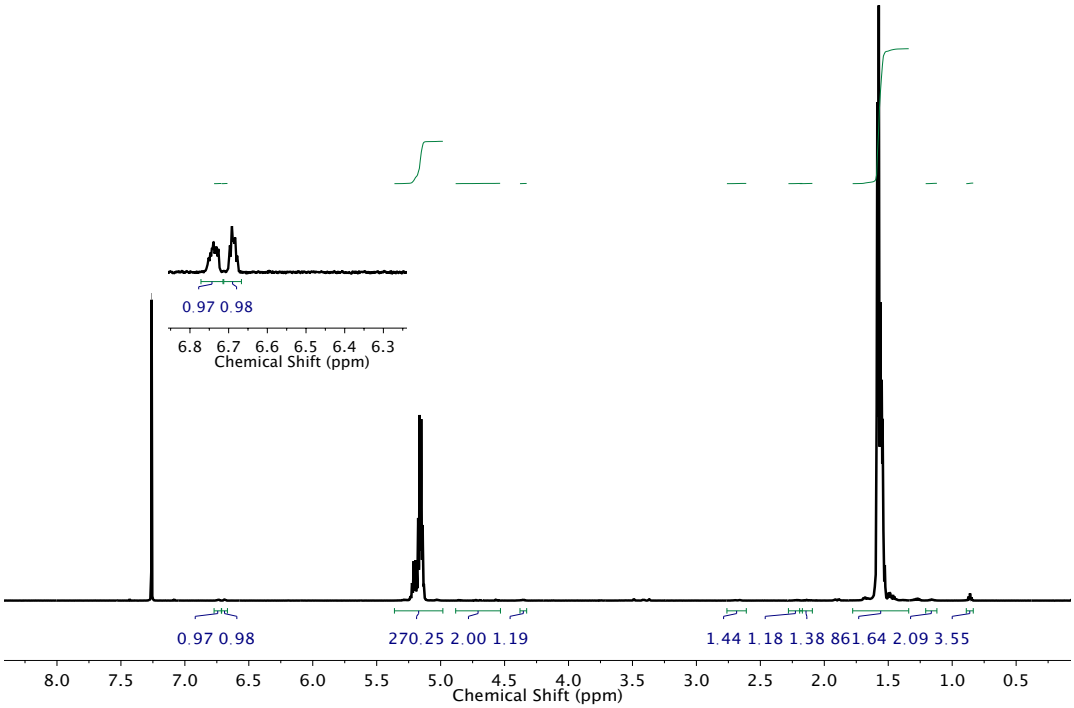

Figure S 2.25. ^{1}H NMR of spectrum of **P3** in $CDCl_3$ showing presence of expected chain-end resonances

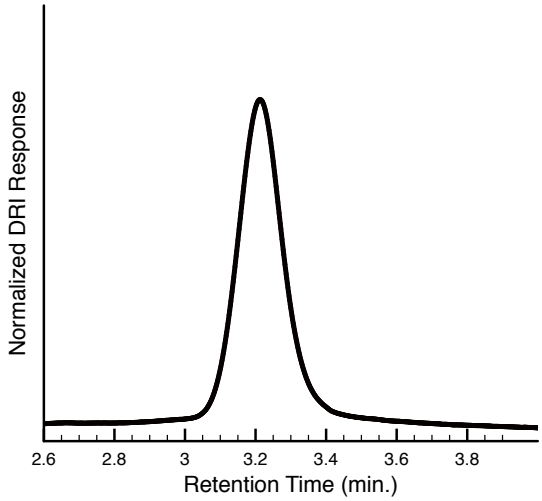

Figure S 2.26. SEC-RI trace of **P3.**

Synthesis of SP-5:

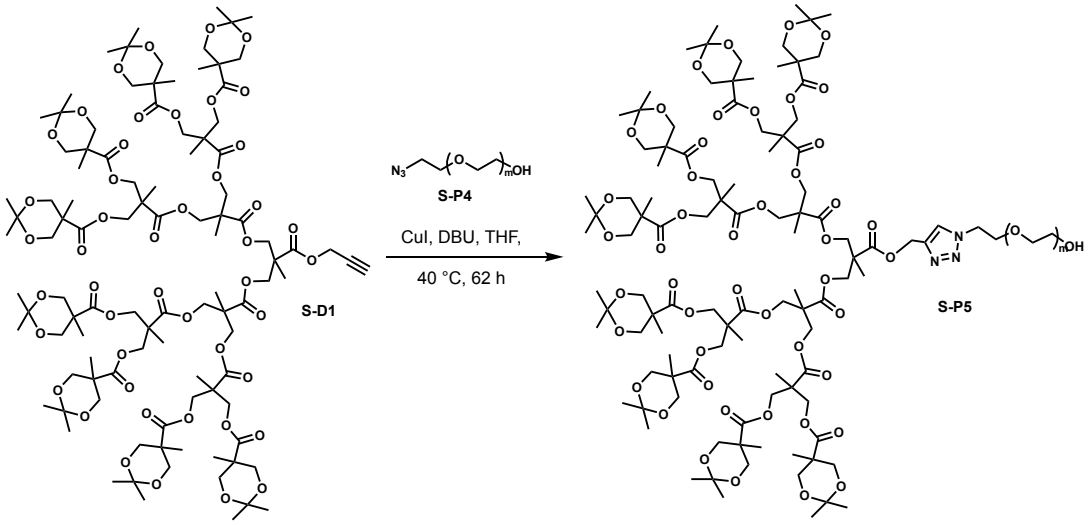

S-P4 (86 mg, 0.039 mmol, 1 eq., provided by Intezyne Technologies, $M_{n(NMR)}$ = 2,200 g/mol, $M_{n(SEC)}$ = 3,400 g/mol, $Đ$ = 1.13), **S-D1** (91 mg, 0.043 mmol, 1.1 eq., purchased from Polymer Factory) and CuI (1.5 mg, 0.008 mmol, 0.2 eq.) was added to a flame-dried, 1-dram vial under nitrogen and equipped with a stir bar. A solution of DBU (117 μL, 0.78 mmol, 20 eq.) and dry THF (2 mL) was transferred into the vial. The vial was sealed under nitrogen and heated at 40°C for 62 h. The solution was brought to rt before passing through a silica plug and rinsing with 20 mL of MeOH:DCM (1:9). The solvent was removed, and the crude polymer was precipitated three times in 10 mL cold EtOH (-78 °C) to afford 84 mg (0.019 mmol, 48%) of **S-P5**. $M_{n(NMR)}$ = 4,500 g/mol, $M_{n(SEC)}$ = 4,600 g/mol, $Đ$ = 1.12.

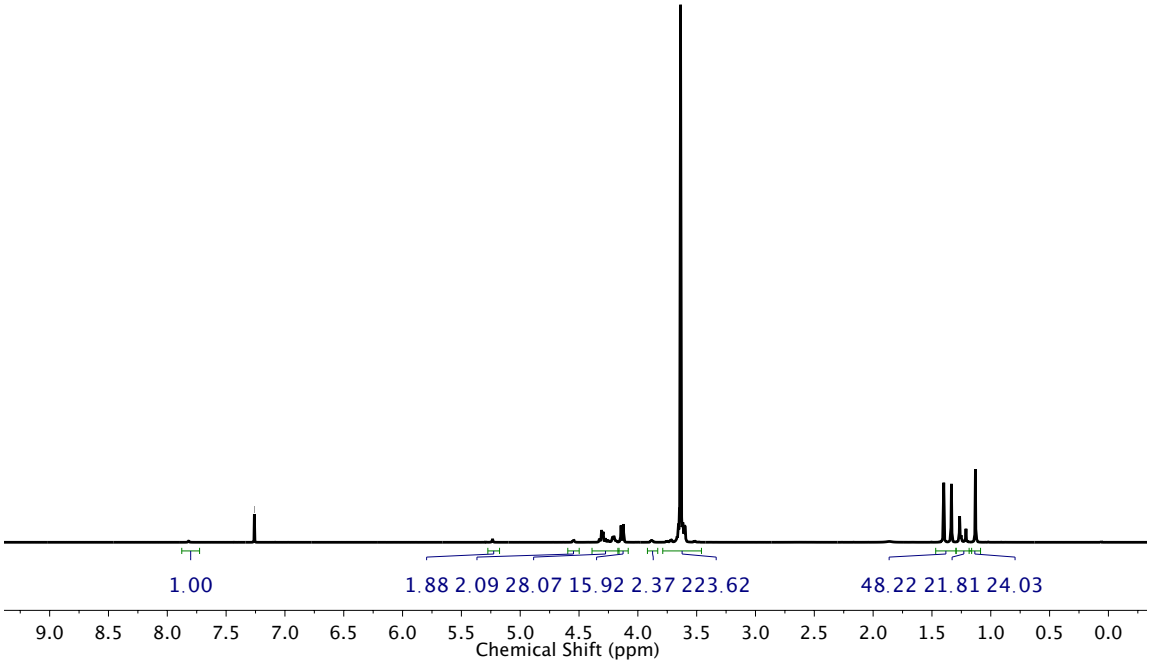

Figure S 2.27. ^{1}H NMR of spectrum of **S-P5** in $CDCl_3$ showing presence of expected triazole and dendron resonances.

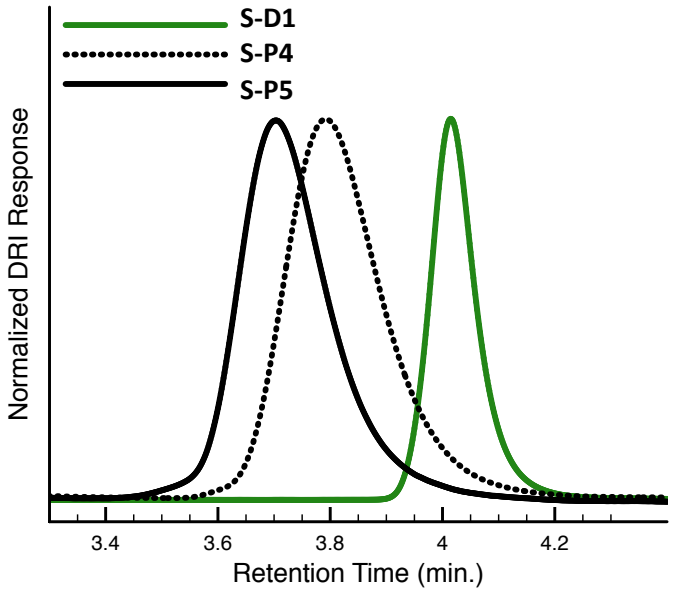

Figure S 2.28. Overlay of SEC-RI traces of **S-D1, S-P4** and **S-P5** showing expected shift to higher molecular weight after CuAAC.

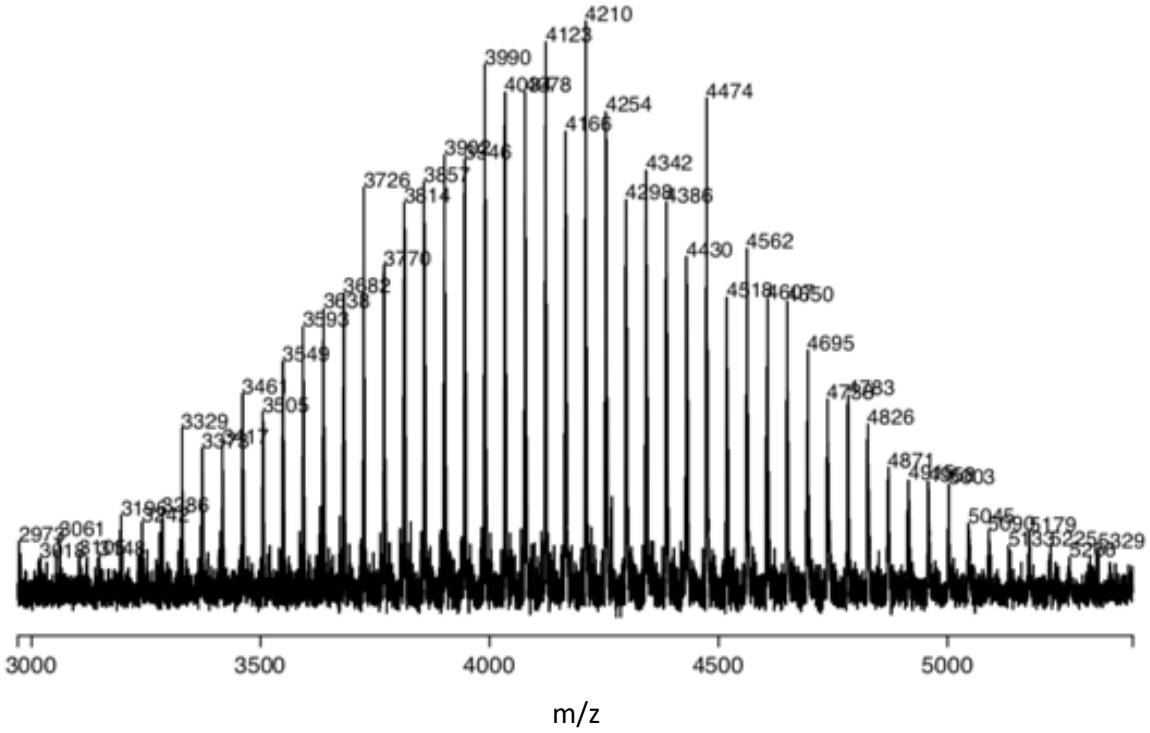

Figure S 2.29. MALDI shows expected distribution of masses for **S-P5**. Calculated [DP = 28 + Na]$^{+}$= 3504, observed 3505.

Synthesis of P4:

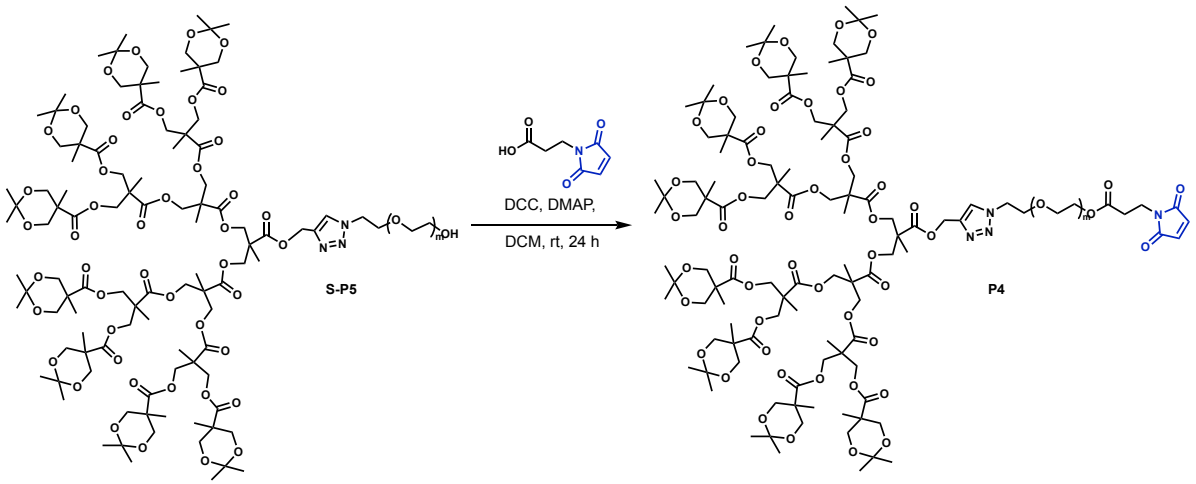

S-P5 (52.5 mg, 0.012 mmol, 1 eq.), 3-maleimidopropionic acid (8.1 mg, 0.048 mmol, 4 eq.), DCC (7.4 mg, 0.036 mmol, 3 eq.), DMAP (146 µL of 1mg/mL stock solution in DCM, 0.001

mmol, 0.1 eq.) and 0.2 mL DCM was added to a 2-mL vial equipped with stir bar. The vial was capped under air and allowed to stir for 24 h. The solvent was removed, and the crude material was dialyzed against 650 mL MeOH (1 kDa MWCO RC tubing) for 16 h to afford 23 mg (0.005 mmol, 43%) of **P4**. $M_{n(NMR)}$ = 4,500 g/mol, $M_{n(SEC)}$ = 6,300 g/mol, $Đ$ = 1.06.

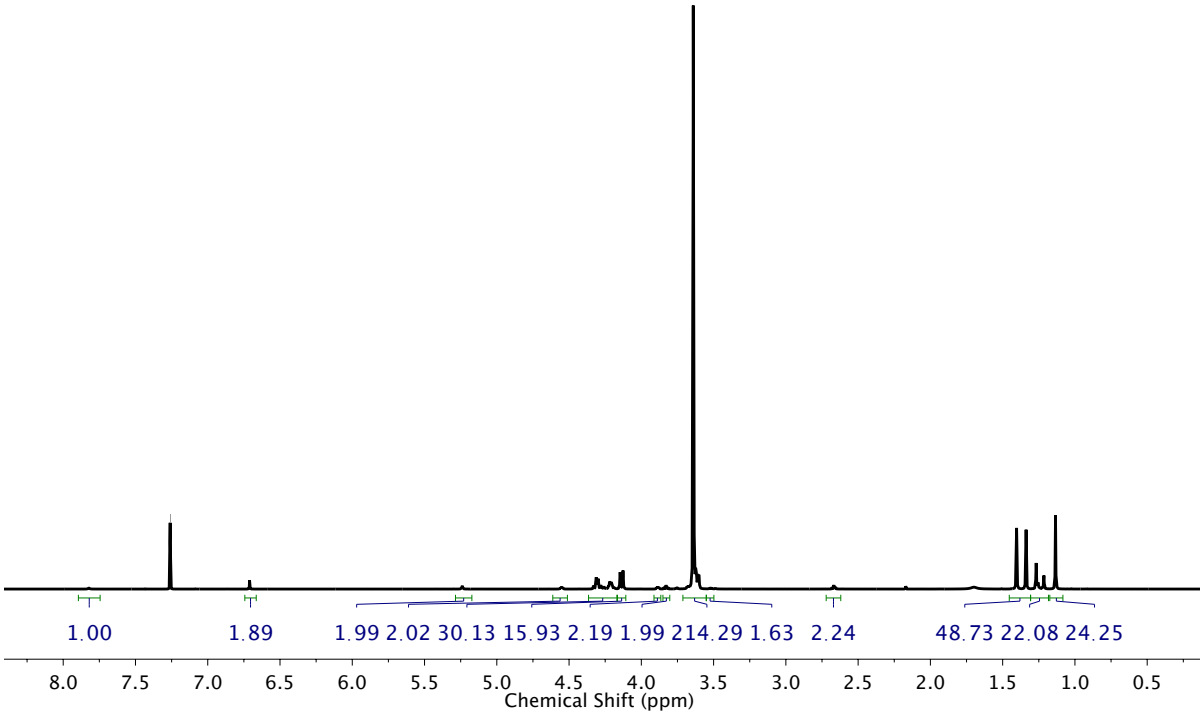

Figure S 2.30. ^{1}H NMR of spectrum of **P4** in $CDCl_3$ showing presence of expected chain end resonance corresponding to maleimide after functionalization.

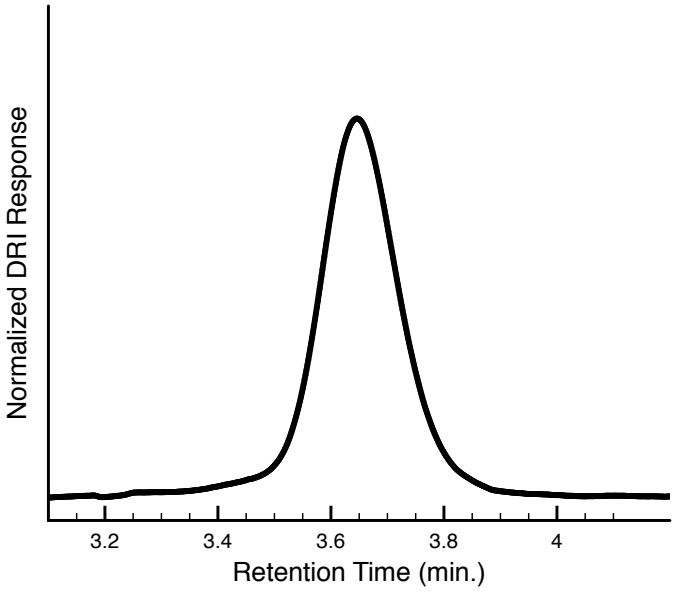

Figure S 2.31. SEC-RI trace of **P4**

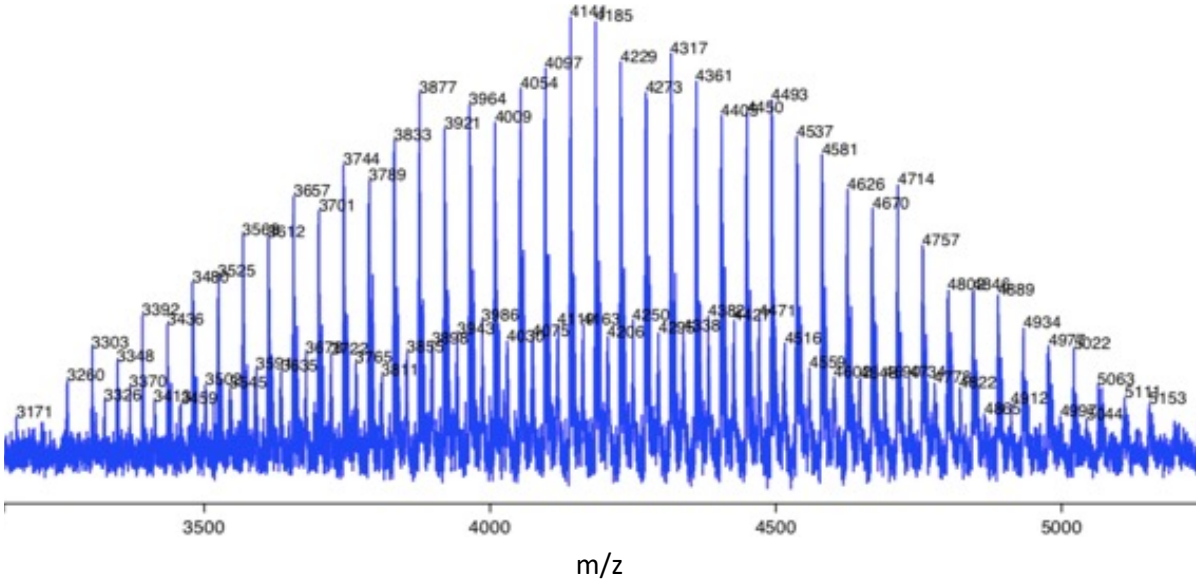

Figure S 2.32. MALDI shows expected distribution of masses for **P4**. Calculated [DP = 30 + Na]$^{+}$= 3743, observed = 3744. A second distribution is observed corresponding to additional coupling of second maleimide to unprotected dendron: Calculated [DP = 28 + Na] $^{+}$ = 3766, observed 3765.

Synthesis of P5:

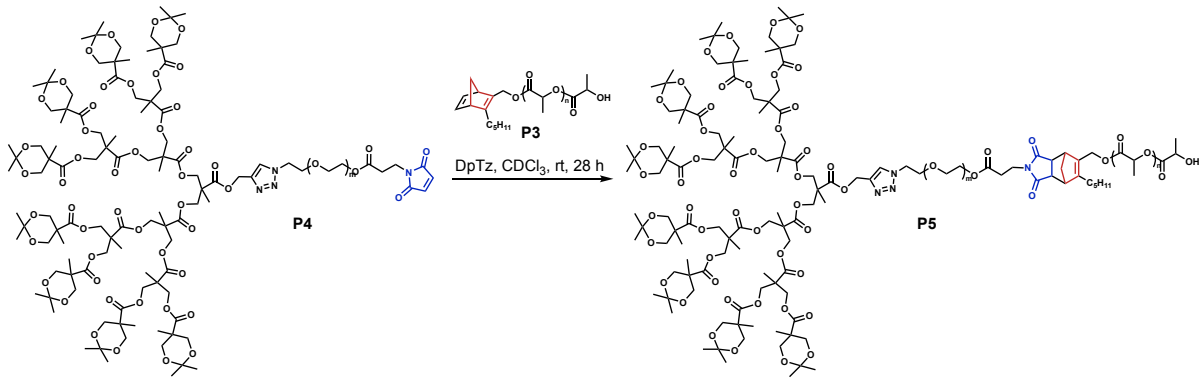

P3 (22.3 mg, 0.0011 mmol, 1 eq.), 3,6-di-2-pyridyl-1,2,4,5-tetrazine (DpTz) (0.5 mg, 0.0021 mmol, 1.9 eq.), and **P4** (7.8 mg, 0.0017 mmol, 1.5 eq.) were added to a 2 mL vial, and dissolved in 0.3 mL of $CDCl_3$. The vial was capped under air and stirred at rt for 28 h. The excess DpTz was quenched with approximately 0.2 mg norbornene and stirred an additional 30 min. The solvent was removed, and the crude polymer precipitated twice in 10 mL cold MeOH (-78 °C) to afford 8 mg (29%) of **P5**. $M_{n(SEC)}$ = 28,100 g/mol, $Đ$ = 1.04.

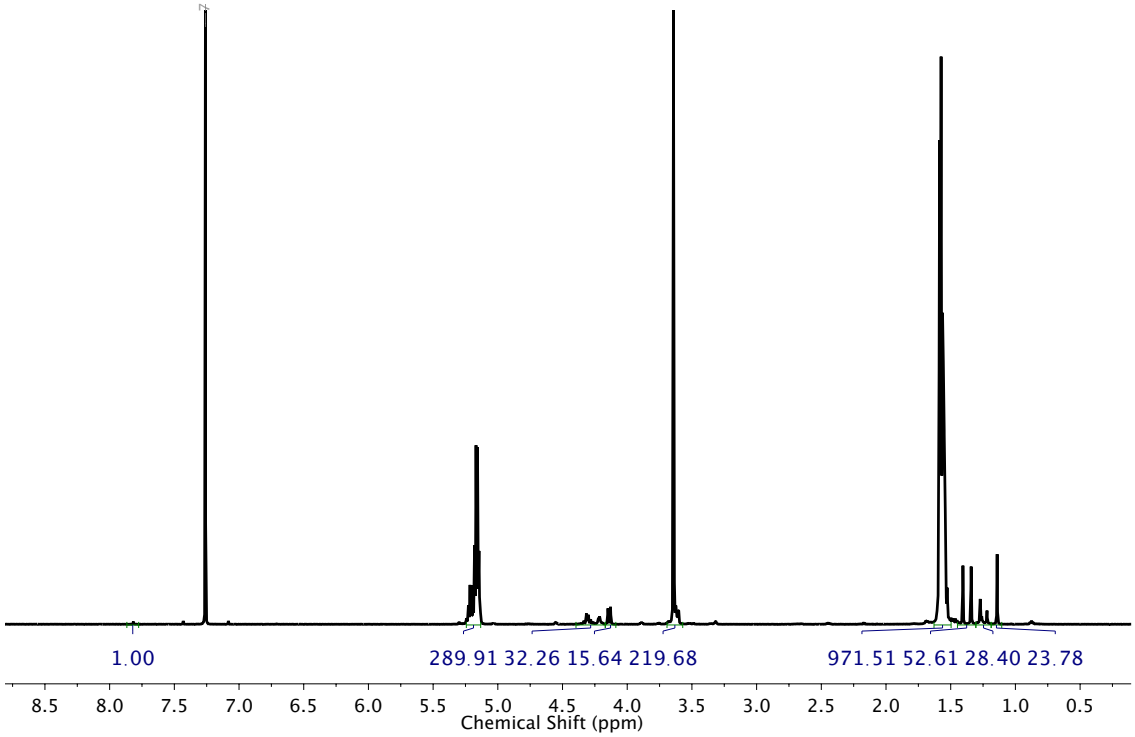

Figure S 2.33. ^{1}H NMR of spectrum of **P5** in $CDCl_3$ showing presence of triazole, dendron, PEG and PLA resonances.

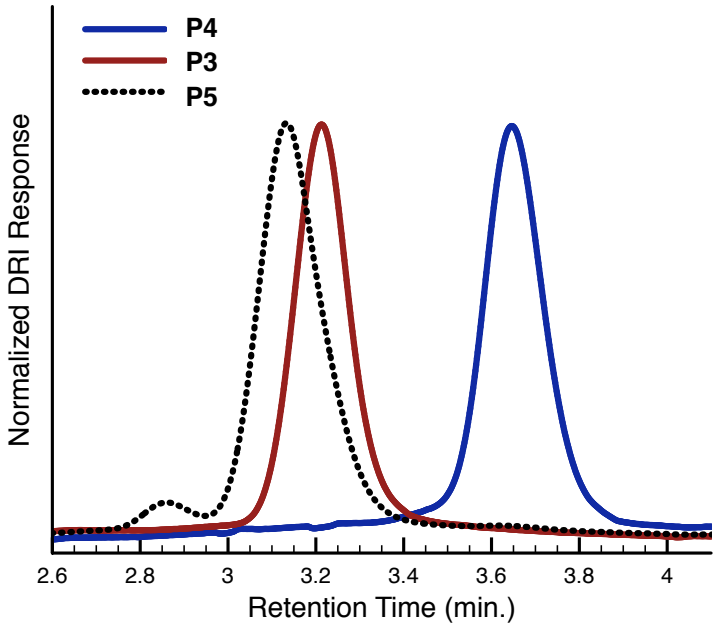

Figure S 2.34. Overlay of SEC-RI traces of **P3, P4** and **P5** showing expected shift to higher molecular weight after NBD click. Higher molecular weight peak attributed to double click of **P3** to bifunctional material observed in MALDI of **P4** (see **Figure S2.32**).

General procedure for polymerization of acrylates (P6a–f):

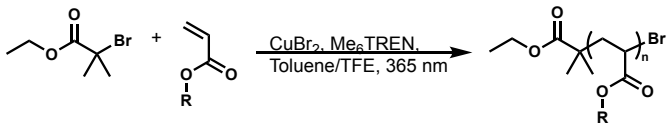

Light induced ATRP polymerization conditions were adapted from literature procedures.[50,52,53] A solution of copper(II) bromide (0.55 mg, 0.0024 mmol, 0.02 eq) and tris[2-(dimethylamino)ethyl]amine (Me_6TREN) (3.4 mg, 3.9 µL, 0.015 mmol, 0.12 eq) was prepared in 0.8 mL of trifluoroethanol. The mixture was allowed to sonicate for at least 30 minutes to completely dissolve the catalyst complex. In a 20 mL scintillation vial, acrylate (4.0 g, 12 mmol, 100 eq) was dissolved in 3.2 mL of toluene. The Cu(II)/ trifluoroethanol solution was transferred into the acrylate solution, followed by ethyl α-bromoisobutyrate (EBiB) (24 mg, 0.12 mmol, 1 eq). Final solution concentration obtained is 1 g acrylate/1 mL solvent (1:4 trifluoroethanol, toluene). The vial was capped with a septum and the solution was degassed with nitrogen for 10 min. With stirring, the polymerization mixture was then irradiated ($\lambda \approx$ 365 nm) in a commercial UV nail lamp system (2 – 13 h). The resulting polymer was purified by passing the crude reaction solution through a column of basic alumina followed by precipitation in methanol three times.

Synthesis of P6a:

The general polymerization procedure was performed using 5.0 g cyclohexyl acrylate (32 mmol, 37 eq) and 210 mg EBiB (0.86 mmol, 1 eq). Conversion = 70%. $M_{n(theor)}$ = 4,200 g/mol, $M_{n(NMR)}$ = 4,500 g/mol, $M_{n(SEC)}$ = 2,900 g/mol, $Đ$ = 1.16.

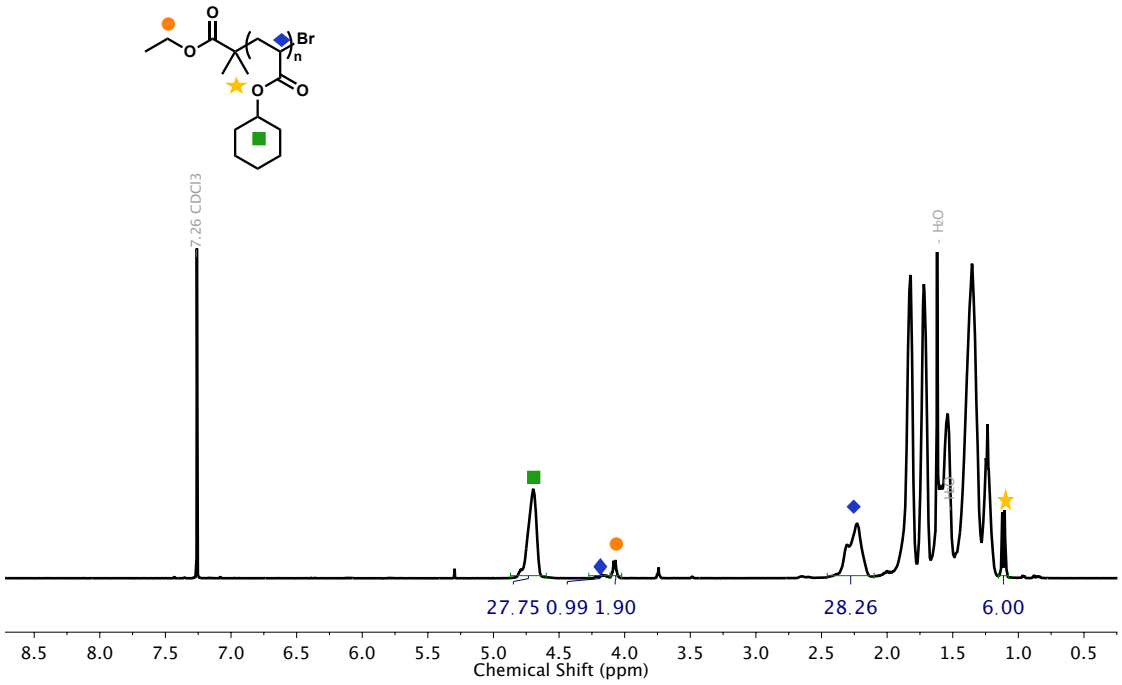

Figure S 2.35. ^{1}H NMR of spectrum of **P6a** in $CDCl_3$

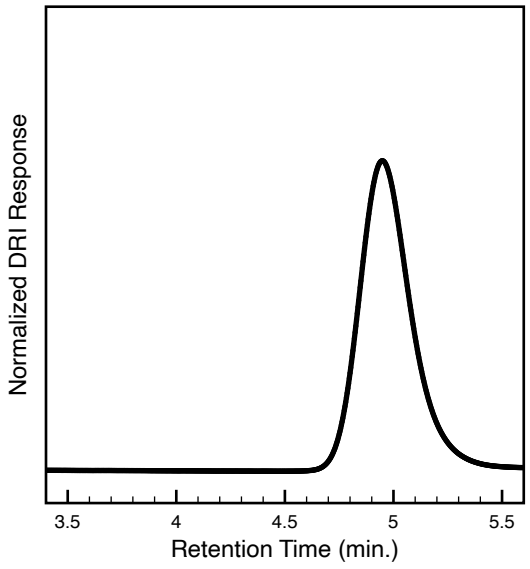

Figure S 2.36. SEC-RI trace of **P6a**

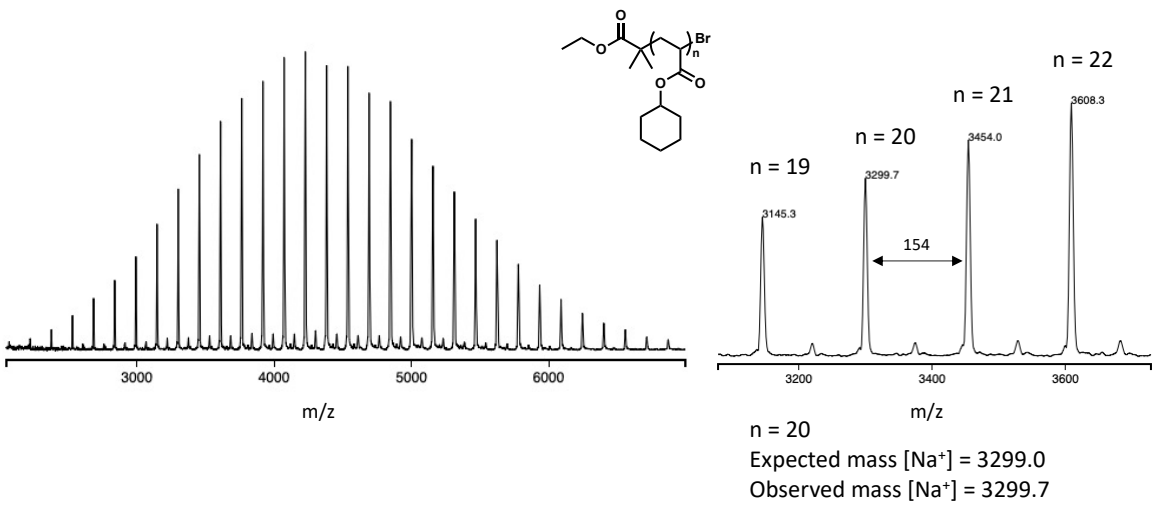

Figure S 2.37. MALDI-ToF-MS analysis of **P6a**

Synthesis of P6b:

The general polymerization procedure was performed using 0.30 g cyclododecyl acrylate[4] (1.3 mmol, 8 eq) and 31 mg EBiB (0.16 mmol, 1 eq). Conversion = 76%. $M_{n(theor)}$ = 1,600 g/mol, $M_{n(NMR)}$ = 2,100 g/mol, $M_{n(SEC)}$ = 1,000 g/mol, $Đ$ = 1.25.

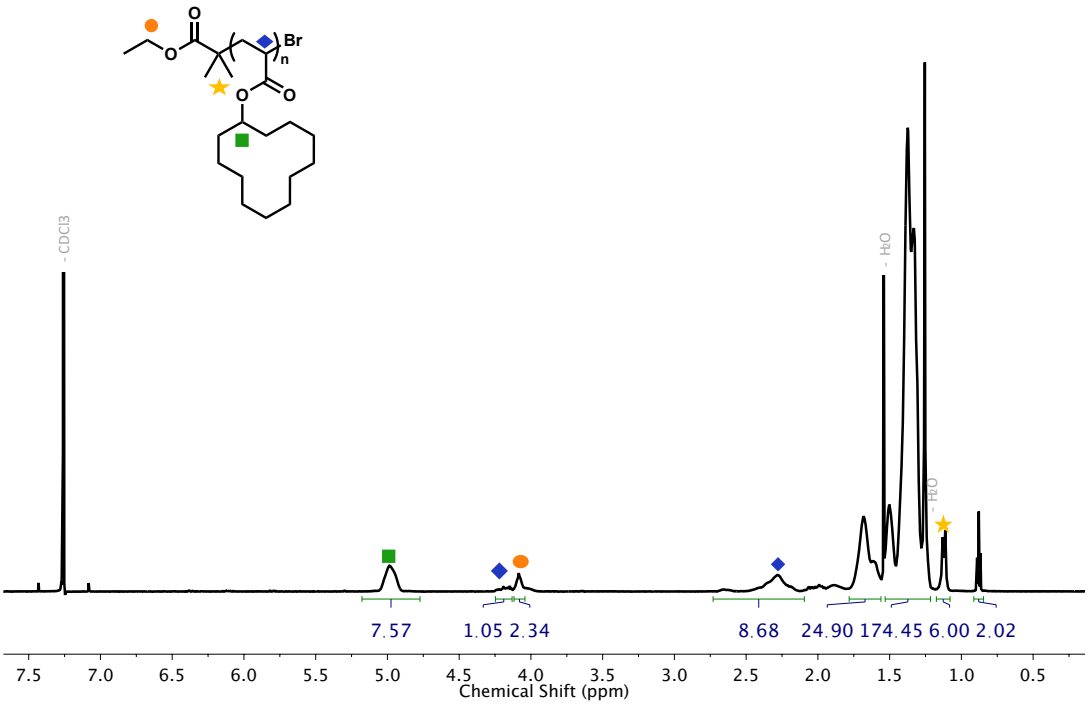

Figure S 2.38. ^{1}H NMR of spectrum of **P6b** in $CDCl_3$.

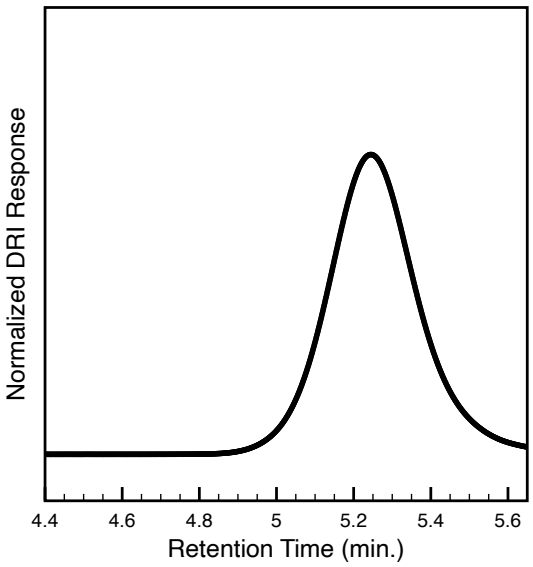

Figure S 2.39. SEC-RI trace of **P6b**

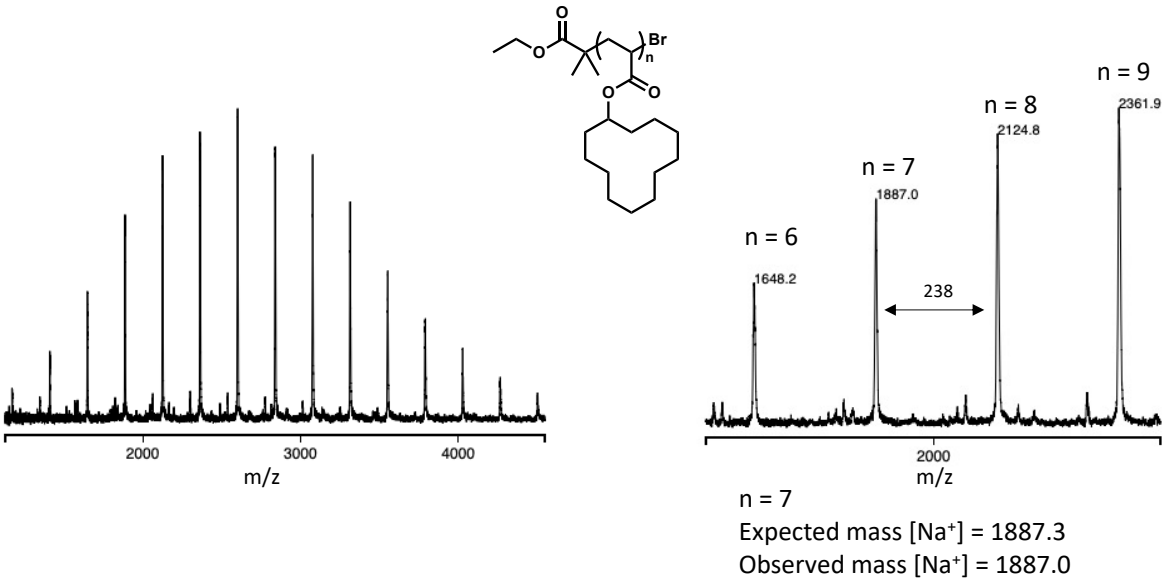

Figure S 2.40. MALDI-Tof-MS analysis of **P6b**.

Synthesis of P6c

The general polymerization procedure was performed using 4.0 g octadecyl acrylate (12 mmol, 100 eq) and 24 mg EBiB (0.12 mmol, 1 eq). Conversion = 85 %. $M_{n(theor)}$ = 28,000 g/mol $M_{n(NMR)}$ = 37,000 g/mol, $M_{n(SEC)}$ = 19,000 g/mol, $Đ$ = 1.17.

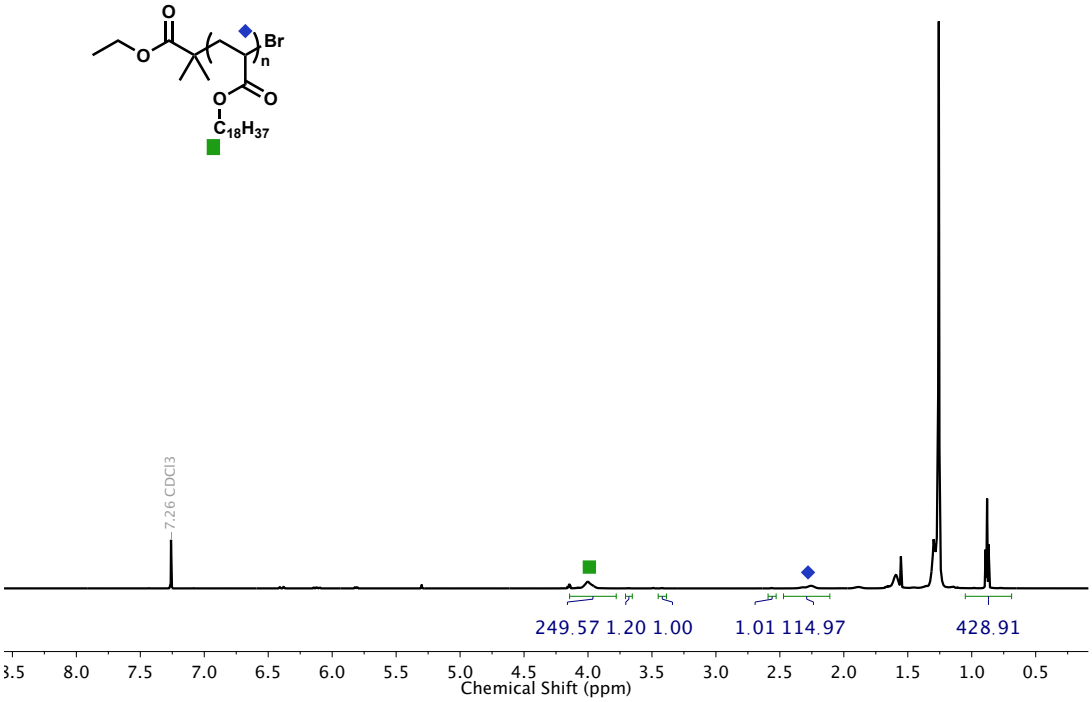

Figure S 2.41. ^{1}H NMR of spectrum of **P6c** in $CDCl_3$.

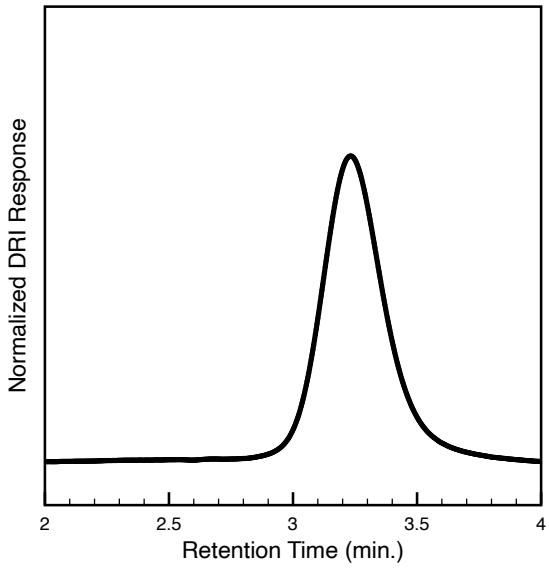

Figure S 2.42.SEC-RI trace of **P6c**.

Synthesis of P6d

The general polymerization procedure was performed using 2.5 g tertbutyl acrylate (19 mmol, 30 eq) and 120 mg EBiB (0.64 mmol, 1 eq). Conversion = 92%. $M_{n(theor)}$ = 3,700 g/mol, $M_{n(NMR)}$ = 3,500 g/mol, $M_{n(SEC)}$ = 4,100 g/mol, $Đ$ = 1.07.

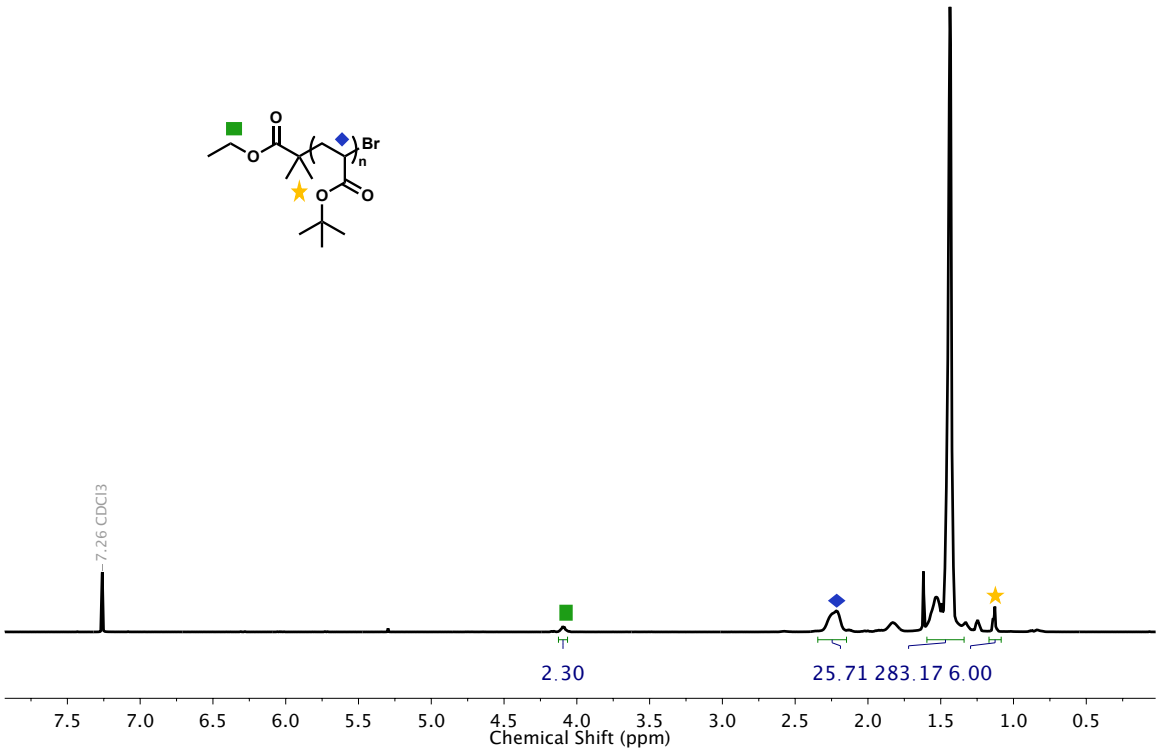

Figure S 2.43. ^{1}H NMR of spectrum of **P6d** in $CDCl_3$.

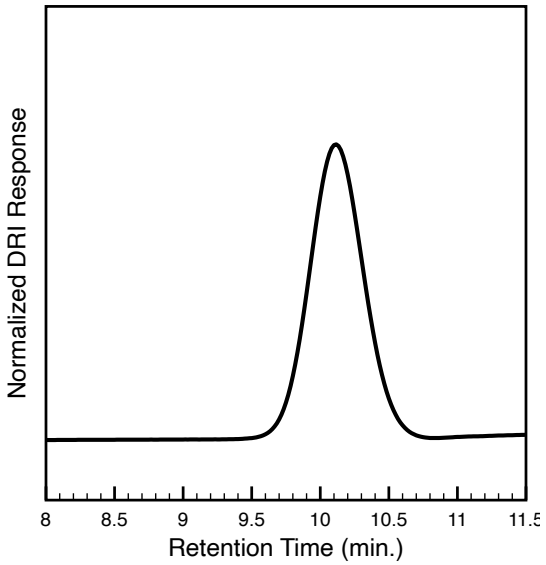

Figure S 2.44. SEC-RI trace of **P6d**

Synthesis of P6e

The general polymerization procedure was performed using 0.50 g poly(ethylene glycol) methyl ether acrylate (M_n = 480 g/mol, 1.0 mmol, 10 eq) and 20 mg EBiB (0.10 mmol, 1 eq). Precipitation was performed in cold diethyl ether. Conversion = 65%. $M_{n(theor)}$ = 3,300 g/mol, $M_{n(NMR)}$ = 3,600 g/mol, $M_{n(SEC)}$ = 5,000 g/mol, $Đ$ = 1.12.

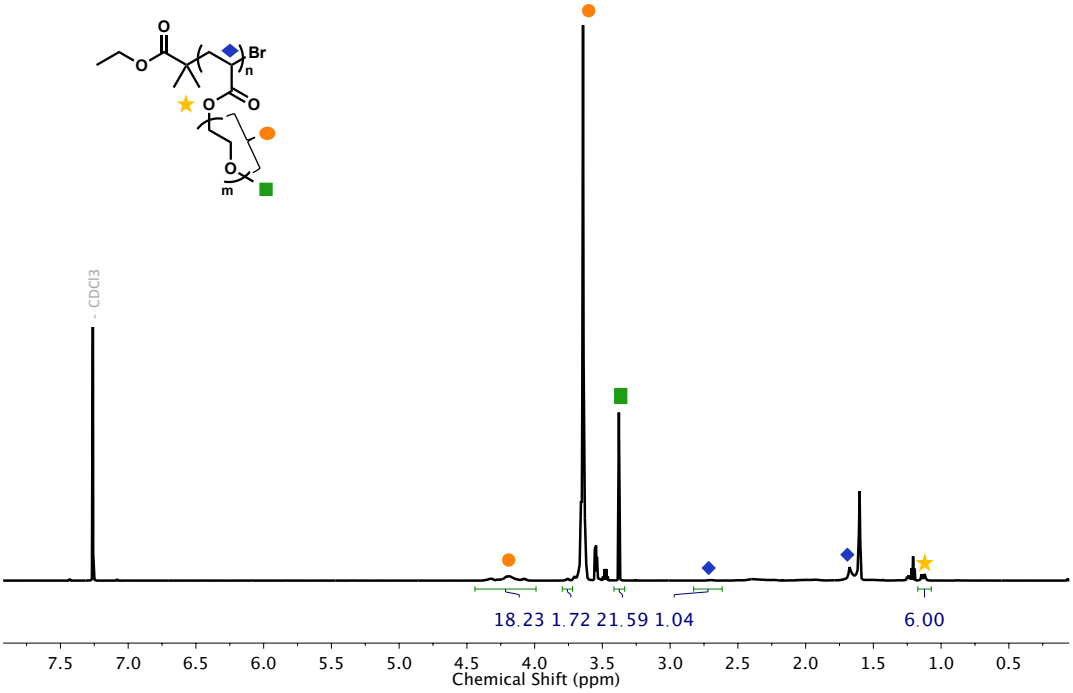

Figure S 2.45. ^{1}H NMR of spectrum of **P6e** in $CDCl_3$.

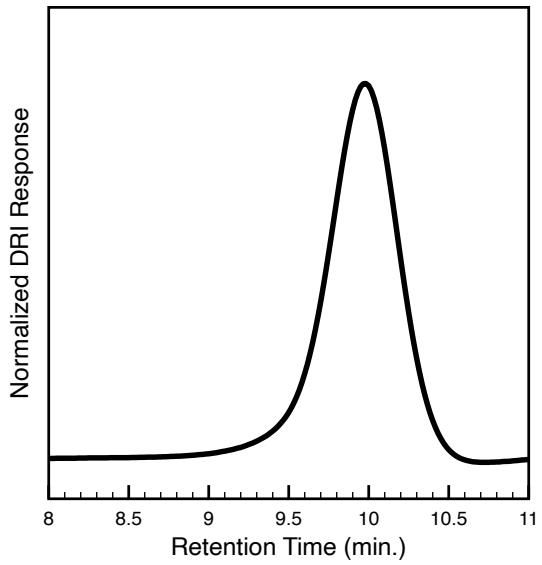

Figure S 2.46.SEC-RI trace of **P6e**.

Synthesis of P6f

The general polymerization procedure was modified for preparation of fluorinated polymer.[53] A solution of $CuBr_2$ (3.7 mg, 0.017 mmol, 0.01 eq) and Me_6TREN (23 mg, 26 μL, 0.099 mmo, 0.06 eq) was prepared in 1.71 mL of octafluoropropanol and 0.19 mL of dimethyl sulfoxide. The mixture was allowed to sonicate for at least 30 minutes to completely dissolve the catalyst complex. Once dissolved, octafluoropentyl acrylate (1.9 mL, 9.9 mmol, 6 eq) was added to the mixture followed by EBIB (242 μL, 1.65 mmol, 1 eq). The vial was capped with a septum and the solution was degassed with argon for 10 min. With stirring, the polymerization mixture was then irradiated ($\lambda \approx 365$ nm) for 13.5 h in a commercial UV nail lamp system. The resulting polymer was purified by passing the crude reaction solution through a column of basic alumina, then dialyzed against acetone using 1k cut-off RC dialysis tubing for 24 hours, switching out acetone three times. Conversion = 90%. $M_{n(theor)}$ = 1,700 g/mol, $M_{n(NMR)}$ = 2,000 g/mol, $M_{n(SEC)}$ = 1,100 g/mol, $Đ$ = 1.11.

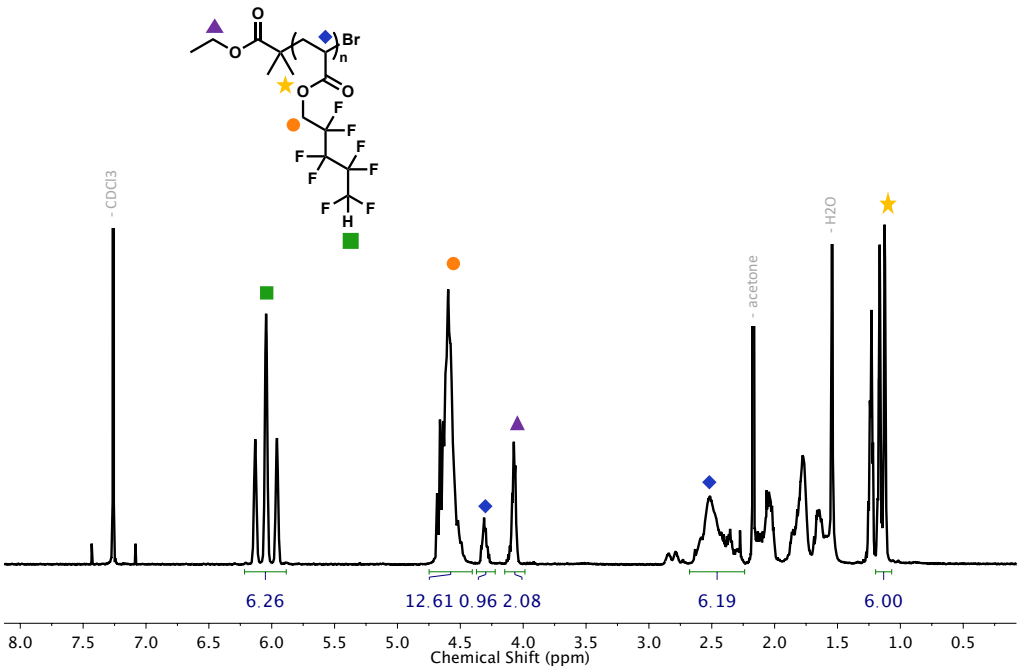

Figure S 2.47. ^{1}H NMR of spectrum of **P6f** in $CDCl_3$.

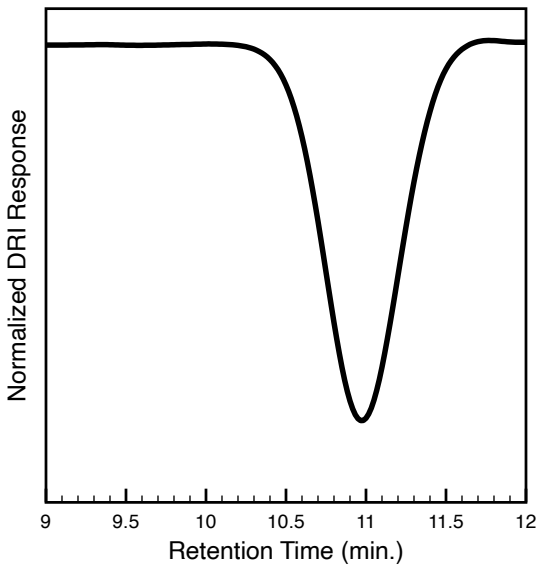

Figure S 2.48. SEC-RI trace of **P6f**.

General procedure for poly(acrylate) NBD functionalization (P7a–f):

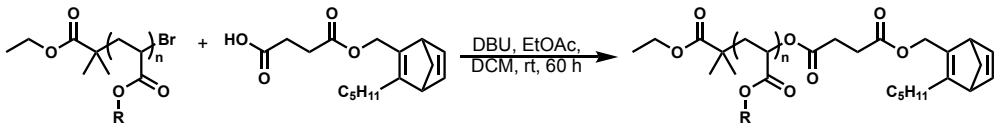

In a 1-dram vial equipped with stir bar, the desired bromide-terminated polyacrylate (0.125 mmol) was dissolved in minimal ethyl acetate (EtOAc) (0.75 mL). In a separate vial, 1,8-Diazabicyclo[5.4.0]undec-7-ene (DBU) (78.0 μL, 0.513 mmol, 4.1 eq) was added to a solution of compound **5** (146 mg, 0.500 mmol, 4 eq) in EtOAc (0.75 mL). Once dissolved, the acid-DBU solution was transferred to the polymer solution and the vial was capped under air. The solution was allowed to stir at rt for 60 h (at which complete formation of the ω-ester was confirmed by crude ^{1}H NMR). The crude reaction mixture was precipitated into MeOH (10 mL) and centrifuged to collect the desired product. The supernatant was discarded, and the resulting solid was re-dissolved in minimal DCM. The precipitation process was repeated twice before drying the material under reduced pressure to afford the desired NBD-terminated polyacrylate.

Synthesis of P7a:

The general procedure for functionalization was performed on poly(cyclohexyl acrylate), **P6a** (500 mg, 0.111 mmol). Yield = 295 mg (55%). $M_{n(NMR)}$ = 4,800 g/mol, $M_{n(SEC)}$ = 3,300 g/mol, $Đ$ = 1.13.

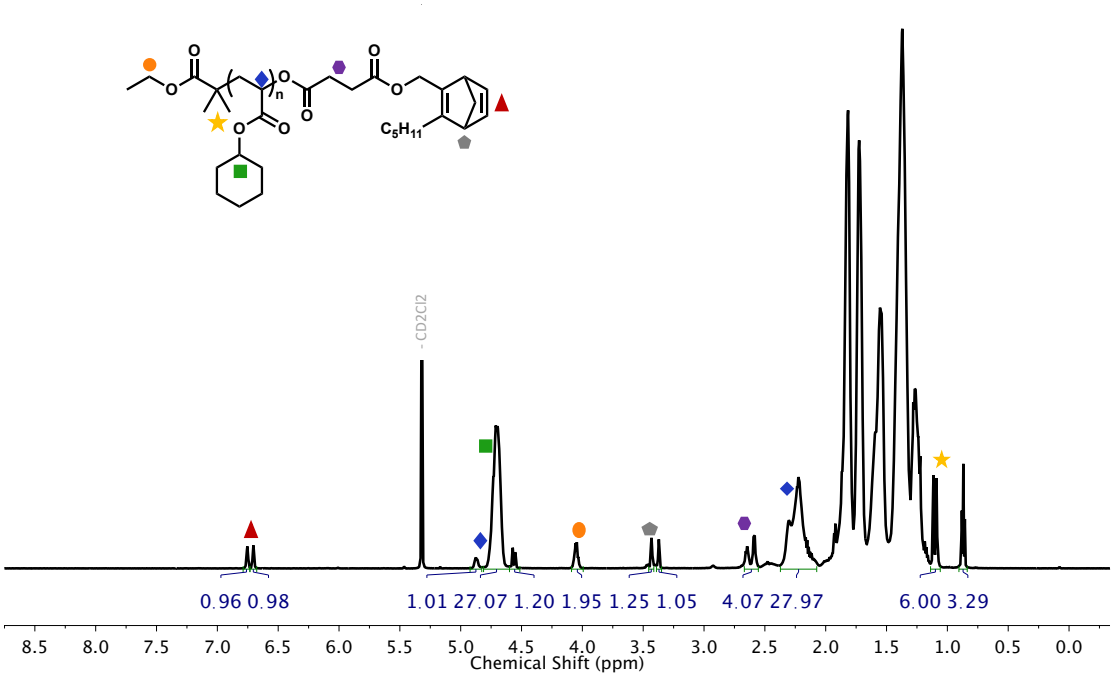

Figure S 2.49. ^{1}H NMR of spectrum of **P7a** in CD_2Cl_2 showing the presence of expected chain-end resonances indicating >96% incorporation of the NBD unit.

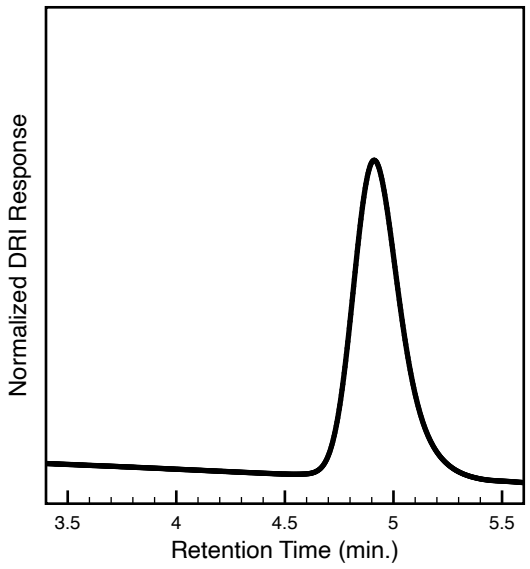

Figure S 2.50. SEC-RI trace of **P7a**

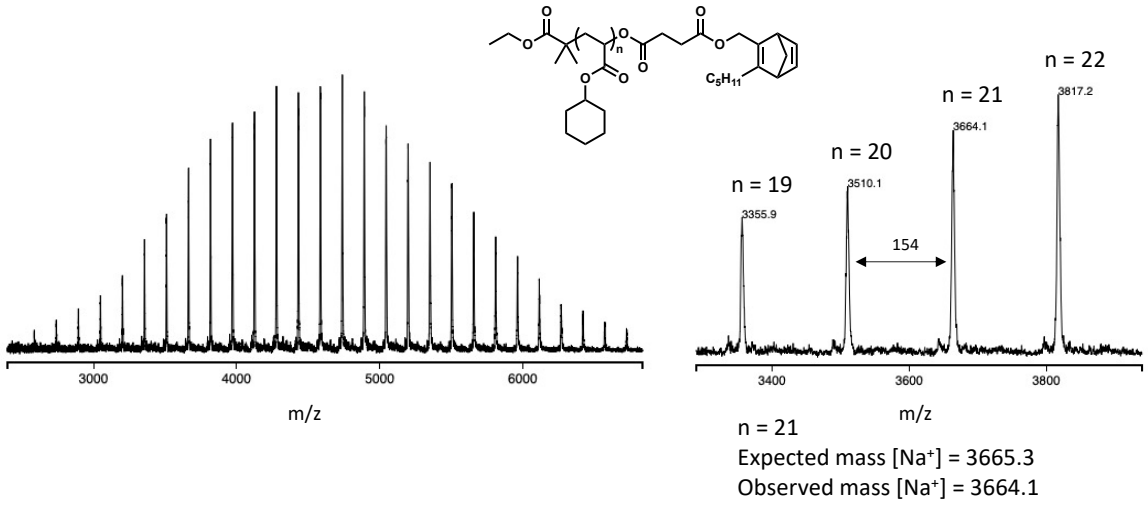

Figure S 2.51. MALDI-ToF-MS analysis of **P7a**.

Synthesis of P7b

The general procedure for functionalization was performed on poly(cyclododecyl acrylate), **P6b** (260 mg, 0.125 mmol). Yield = 179 mg (60%). $M_{n(NMR)}$ = 2,700 g/mol, $M_{n(SEC)}$ = 1,300 g/mol, $Đ$ = 1.21.

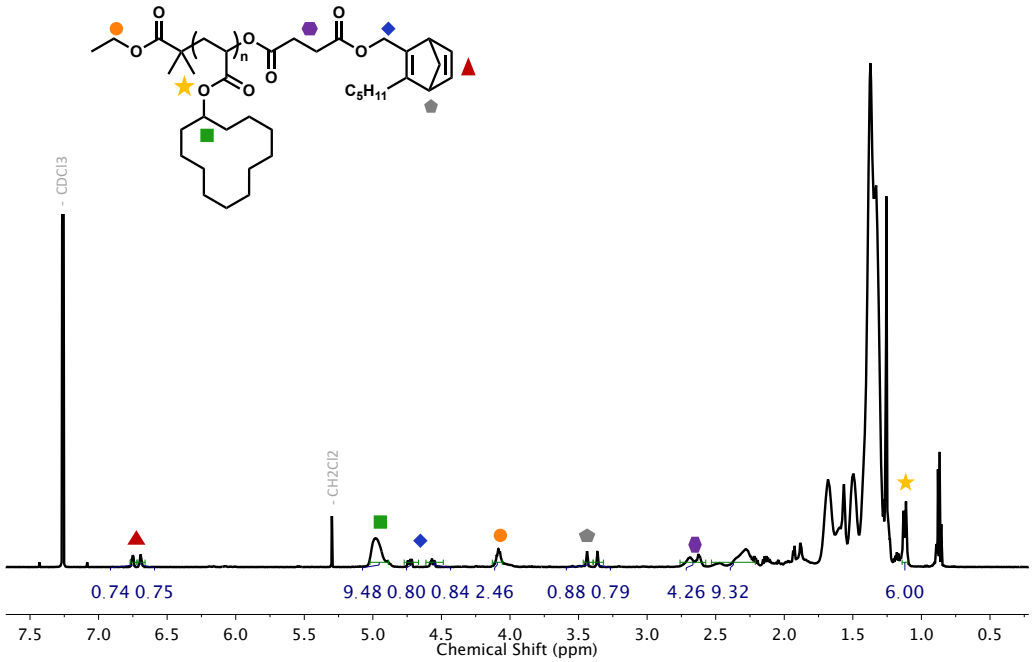

Figure S 2.52. ^{1}H NMR of spectrum of **P7b** in $CDCl_3$ showing the presence of expected chain-end resonances indicating >75% incorporation of the NBD unit.

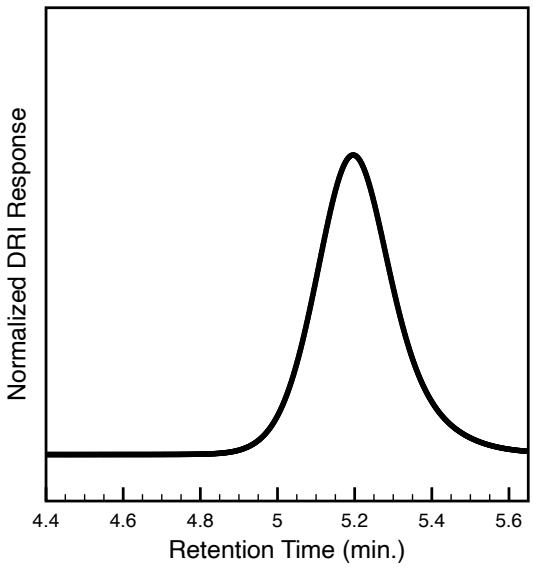

Figure S 2.53. SEC-RI trace of **P7b**.

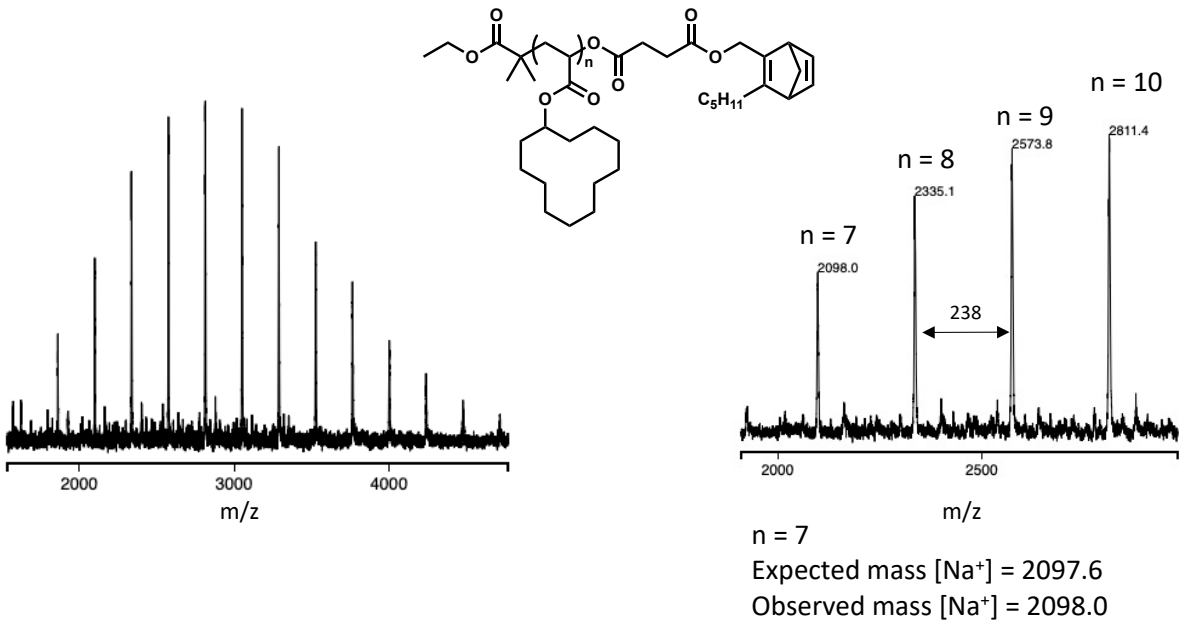

Figure S 2.54. MALDI-ToF-MS analysis of **P7b**.

Synthesis of P7c

The general procedure for functionalization was performed on poly(octadecyl acrylate), **P6c** (500 mg, 0.017 mmol). Reaction was maintained at 30 °C to prevent reaction mixture from solidifying and allowed to stir for 5 d to obtain good chain end incorporation. Yield = 328 mg (65%). $M_{n(NMR)}$ = 37,000 g/mol, $M_{n(SEC)}$ = 19,000 g/mol, $Đ$ = 1.16.

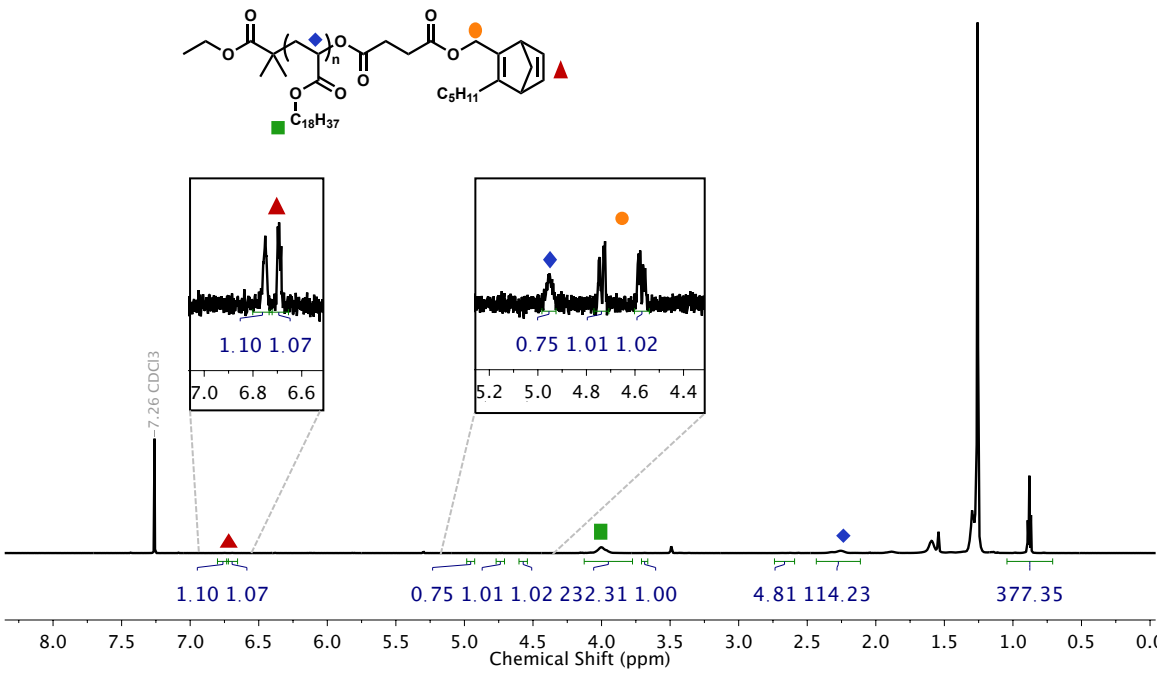

Figure S 2.55. ^{1}H NMR of spectrum of **P7c** in $CDCl_3$ showing the presence of expected chain-end resonances.

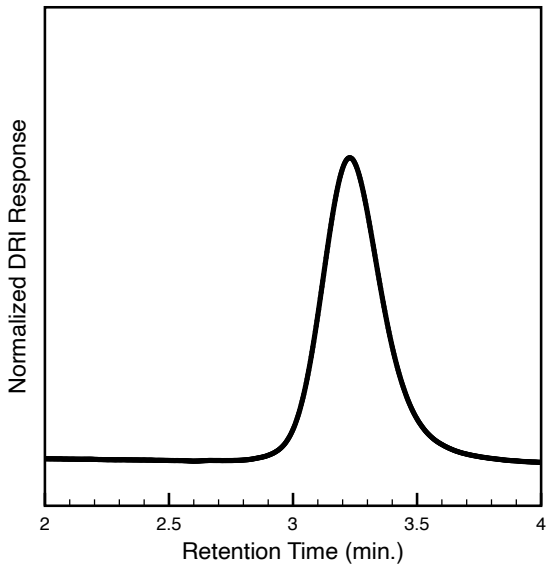

Figure S 2.56. SEC-RI trace of **P7c**

Synthesis of P7d

The general procedure for functionalization was performed on poly(tertbutyl acrylate), **P6d** (200 mg, 0.057 mmol) with acetonitrile (MeCN) as the reaction solvent. The polymer was precipitated twice in 25 mL MeOH/water mixture (1:1). Yield = 118 mg (55%). $M_{n(NMR)}$ = 3,800 g/mol, $M_{n(SEC)}$ = 2,900 g/mol, $Đ$ = 1.12.

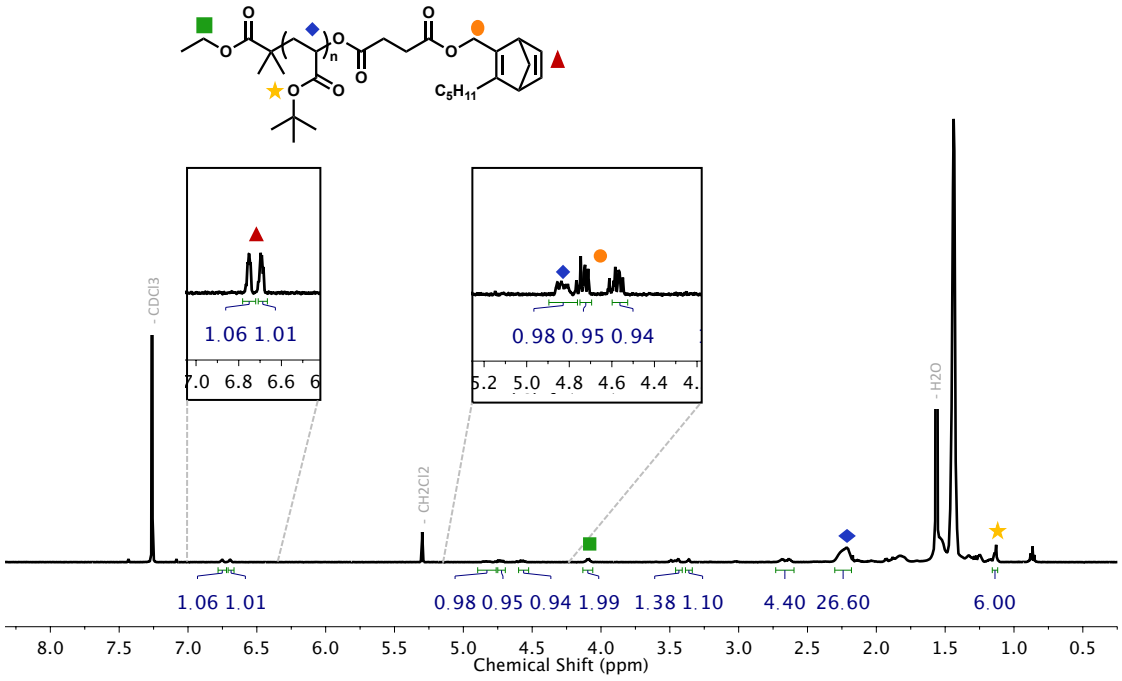

Figure S 2.57. ^{1}H NMR of spectrum of **P7d** in $CDCl_3$ showing the presence of expected chain-end resonances.

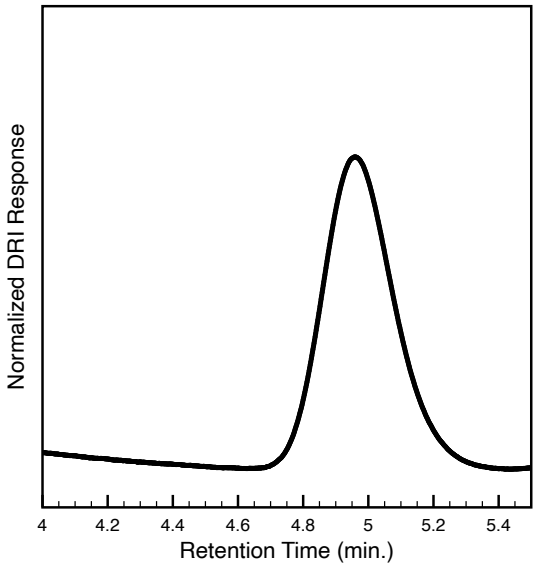

Figure S 2.58. SEC-RI trace of **P7d**

Figure S28.

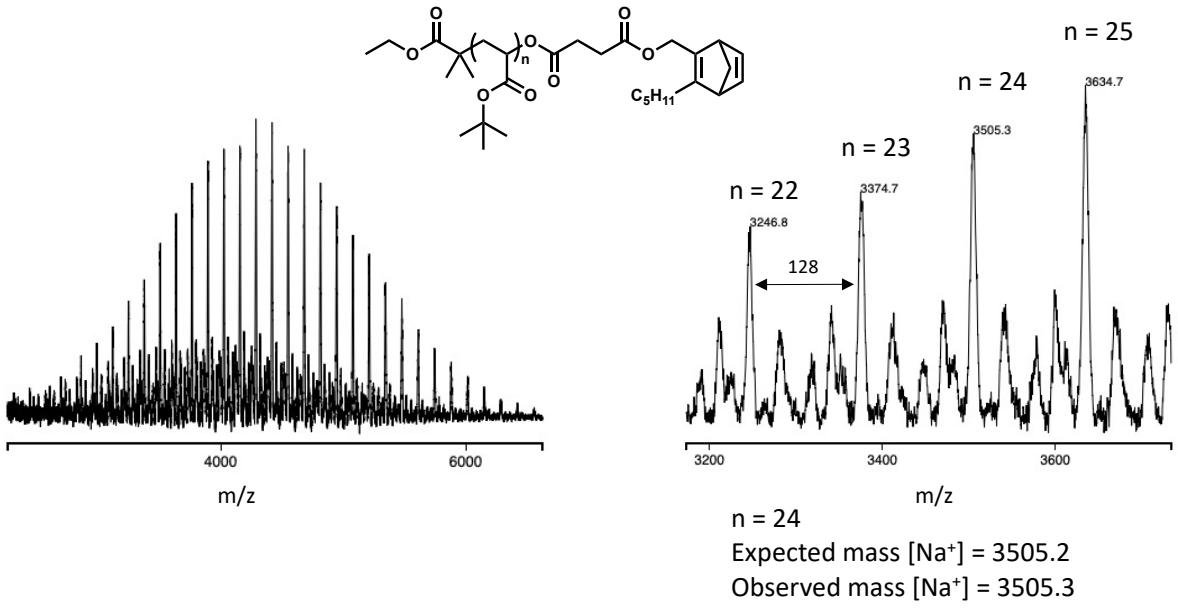

Figure S 2.59. MALDI-ToF-MS analysis of **P7d**.

Synthesis of P7e

The general procedure for functionalization was performed on poly(PEG acrylate), **P6e** (263 mg, 0.016 mmol). The polymer was precipitated six times in cold diethyl ether (3 mL). Yield = 30 mg (44%). $M_{n(NMR)}$ = 4,500 g/mol, $M_{n(SEC)}$ = 5,100 g/mol, $Đ$ = 1.11.

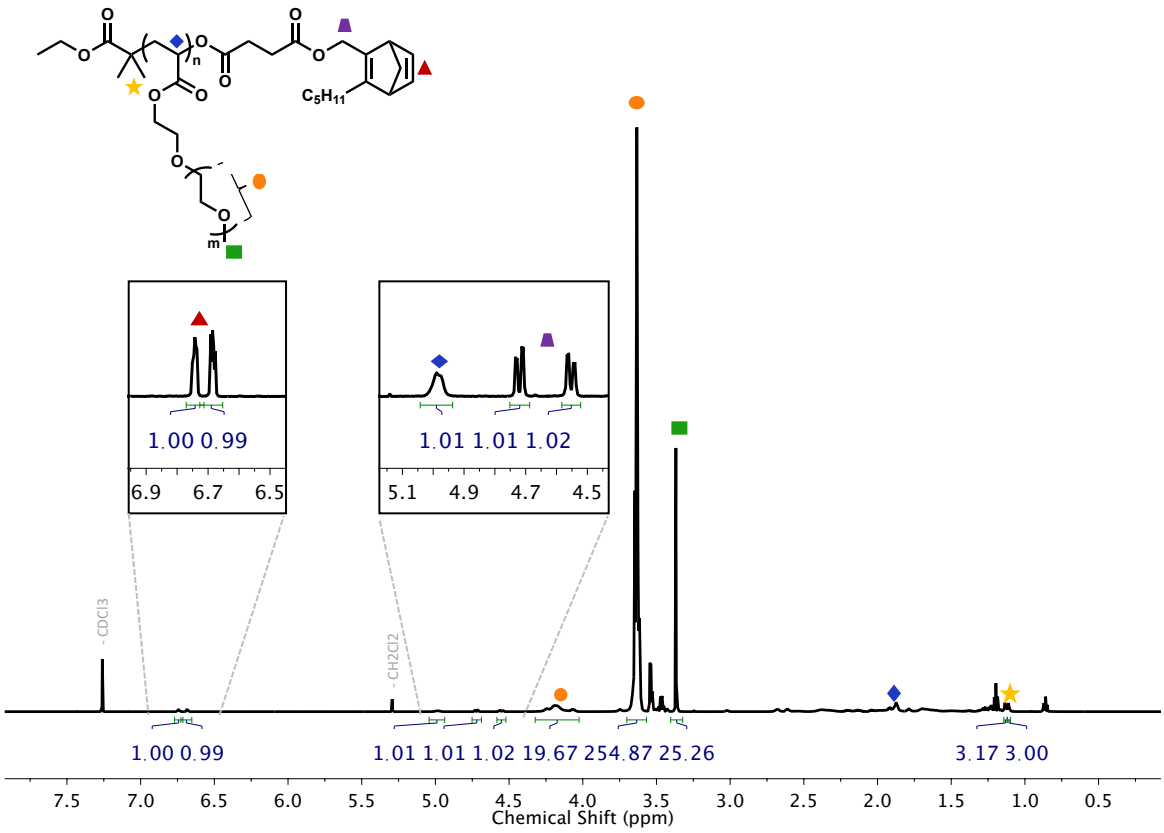

Figure S 2.60. ^{1}H NMR of spectrum of **P2e** in $CDCl_3$ showing the presence of expected chain-end resonances.

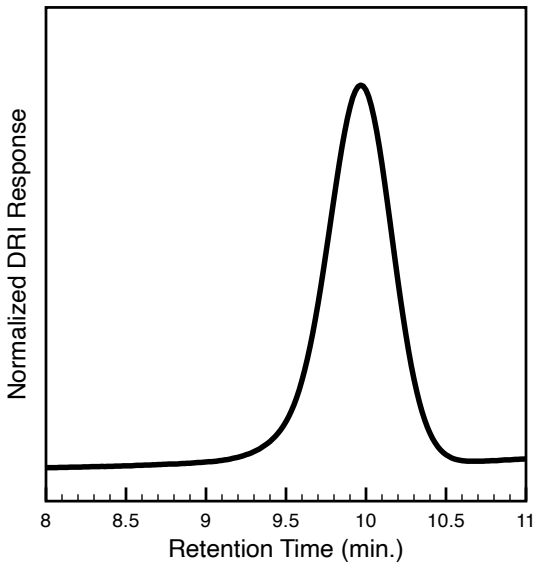

Figure S 2.61. SEC-RI trace of **P7e**

Synthesis of P7f

The general procedure for functionalization was performed on poly(octafluoropentyl acrylate), **P6f** (200 mg, 0.10 mmol). The polymer was purified by dialysis against acetone using 1k cut-off RC dialysis tubing for 24 hours, switching out acetone three times. Yield = 75 mg (32%). $M_{n(NMR)}$ = 2,200 g/mol, $M_{n(SEC)}$ = 1,300 g/mol, $Đ$ = 1.11.

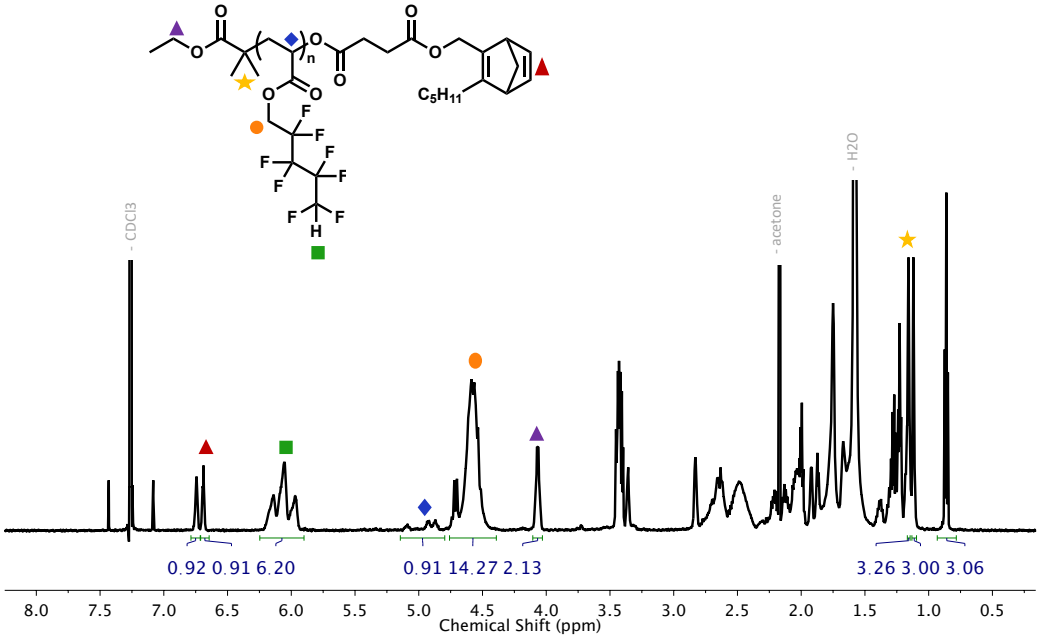

Figure S 2.62. ^{1}H NMR of spectrum of **P7f** in $CDCl_3$ showing the presence of expected chain-end resonances.

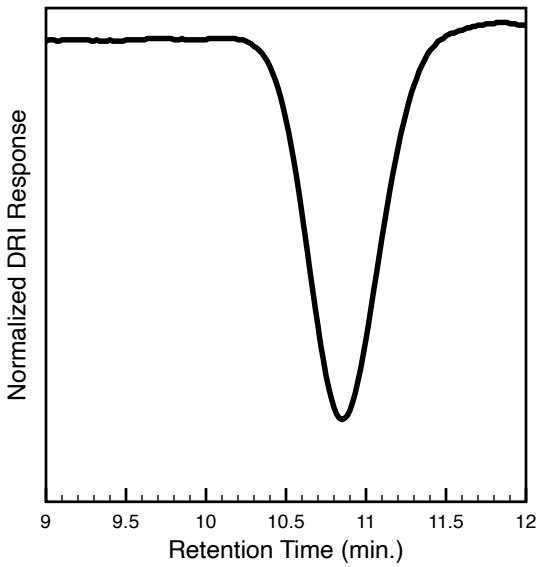

Figure S 2.63. SEC-RI trace of **P7f**

Synthesis of P9

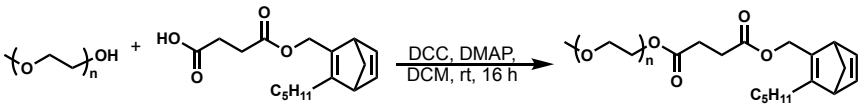

To a 20 mL vial equipped with stir bar was added **P8** (purchased from Sigma-Aldrich, $M_{n(NMR)}$ = 5,400 g/mol, $Đ$ = 1.04, 1.00 g, 0.185 mmol, 1 eq), compound **10** (108 mg, 0.370 mmol, 2 eq), N, N′-Dicyclohexylcarbodiimide (DCC) (57.3 mg, 0.278 mmol, 1.5 eq), 4-Dimethylaminopyridine (DMAP) (2.26 mg, 0.0185 mmol, 0.1 eq) and 4 mL DCM. The vial was capped under air starting and allowed to stir at rt for 16 h (at which complete formation of the ω-ester was confirmed by crude HNMR). The solvent was removed under reduced pressure and the residue taken up in ethanol (EtOH) (100 mL). The solution was cooled to 0 °C and left unagitated for 30 minutes to allow **P9** to precipitate. The solid was filtered, rinsed with cold EtOH (50 mL), then ether (50 mL) and dried under reduced pressure to afford the desired NBD-PEG, **P9** (762 mg, 0.136 mmol, 74%). $M_{n(NMR)}$ = 5,800 g/mol, $M_{n(SEC)}$ = 12,000 g/mol, $Đ$ = 1.04.

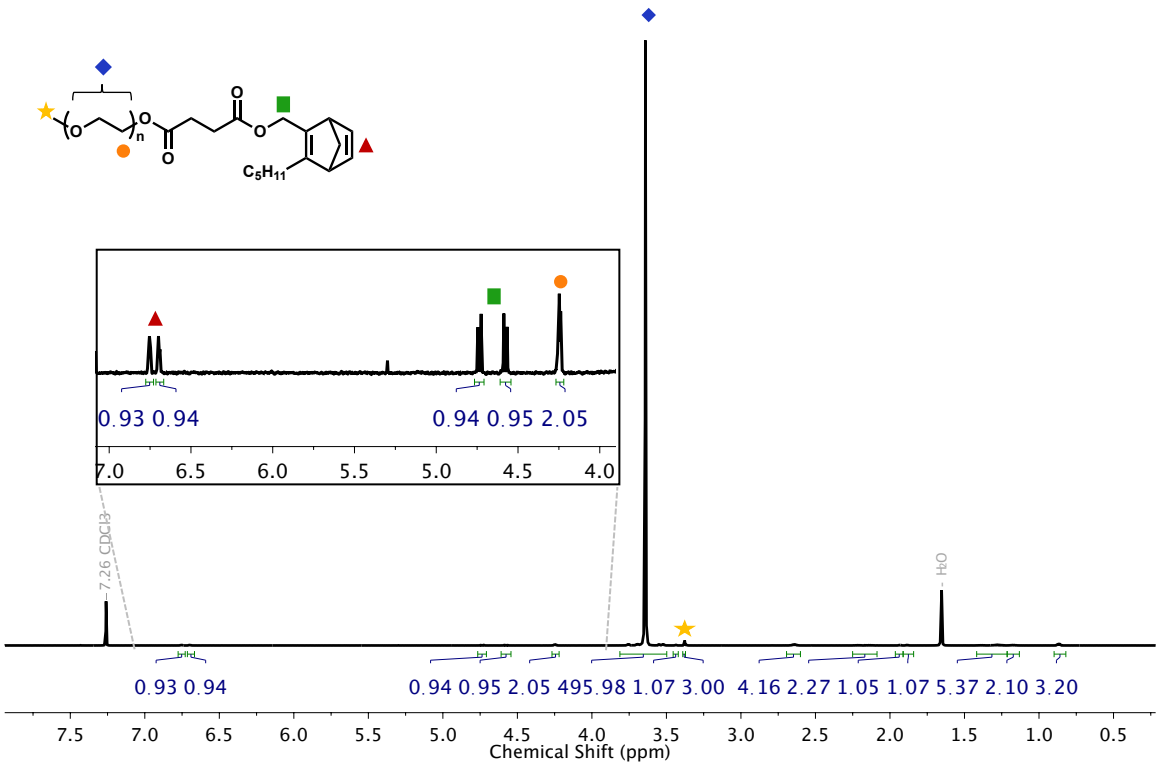

Figure S 2.64. ^{1}H NMR of spectrum of **P9** in $CDCl_3$ showing the presence of expected chain-end resonances.

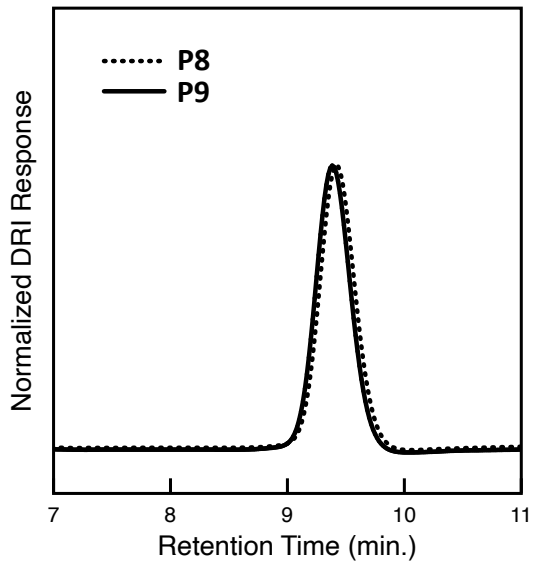

Figure S 2.65. Overlay of SEC-RI traces of **P8** and **P9** shows no observable change in molar mass distribution after NBD functionalization.

Synthesis of maleimide functionalized poly(methyl methacrylate) (P10)

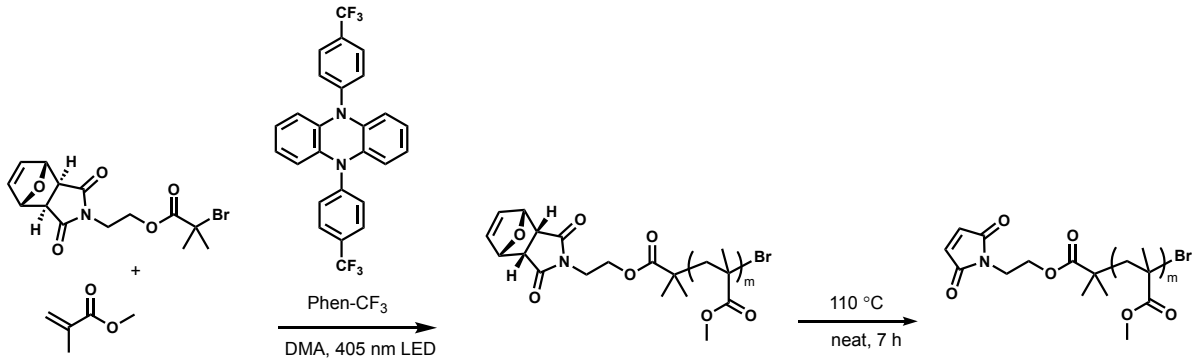

Adapted from literature procedure.[56] To a 20 mL scintillation vial equipped with magnetic stir bar was added Phen-CF3 photocatalyst (4.4 mg, 0.009 mmol, 0.05 eq) and *N,N*-dimethylacetamide (DMA) (2.1 mL). The solution was allowed to stir in the dark for at least 15 min to completely dissolve the catalyst. Once dissolved, methyl methacrylate (2.0 mL, 19 mmol, 100 eq) was added along with *exo* furan protected-maleimide ATRP initiator (67 mg, 0.19 mmol, 1 eq). The reaction mixture was degassed with nitrogen for 10 min before wrapping the cap with parafilm. The vial was irradiated under a 405 nm collimated LED for 4 h. Monomer conversion was estimated to be 73% based on analysis of the crude mixture by ^{1}H NMR. The polymer was purified by precipitation into hexanes (75 mL) followed by precipitation into methanol (2 x 75 mL). The resulting polymer was subsequently heated neat under vacuum at 110 °C for 7 h to yield **P10**. $M_{n(theor)}$ = 7,700 g/mol, $M_{n(HNMR)}$ = 11,000 $M_{n(SEC)}$ = 8,800 g/mol, $Đ$ = 1.23.

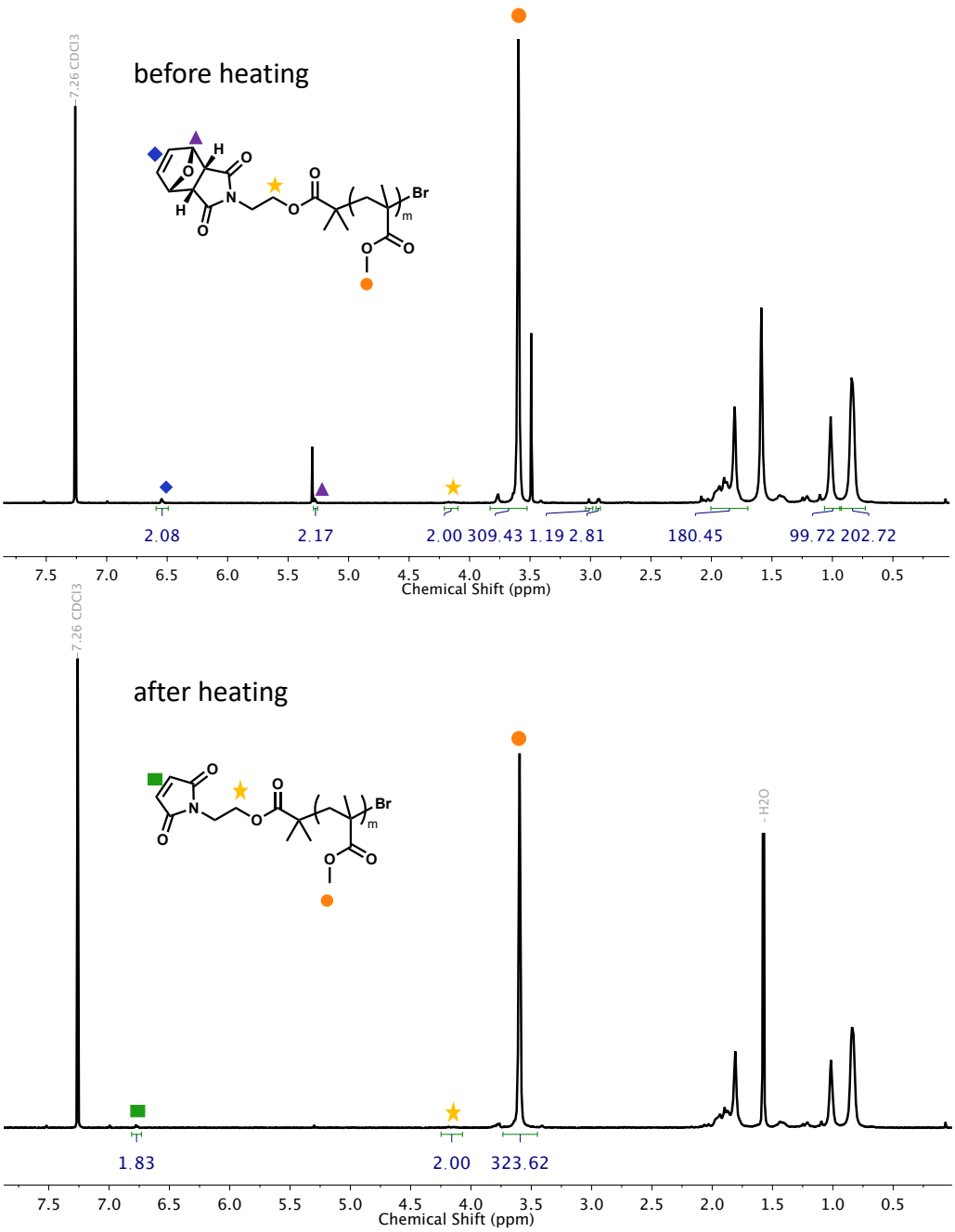

Figure S 2.66. ^{1}H NMR of spectrum of **P10** in $CDCl_3$ before and after heating to deprotect maleimide chain-end.

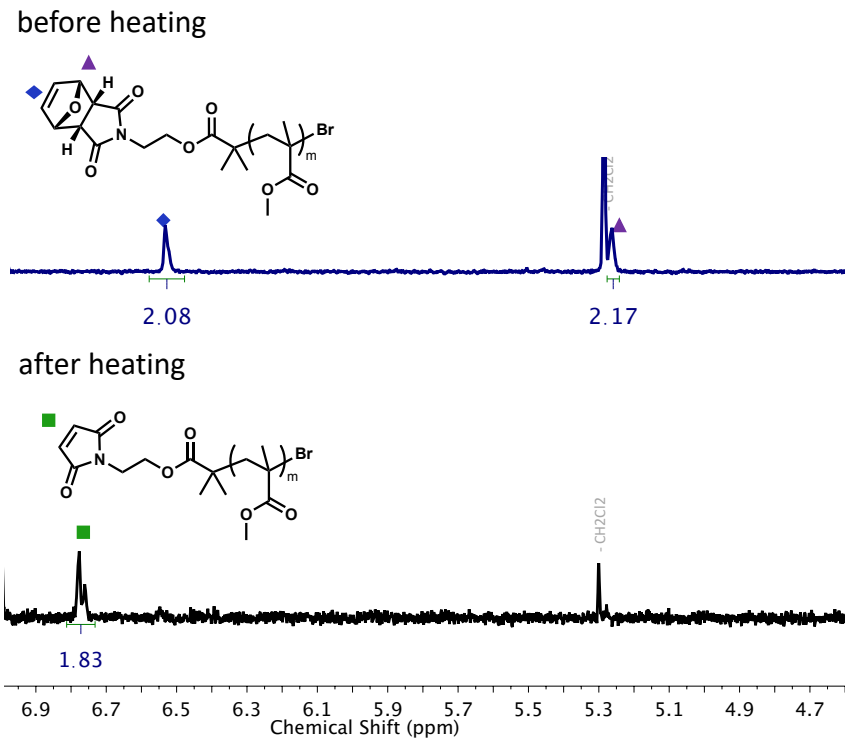

Figure S 2.67. Magnification of ^{1}H NMR of spectrum of **P10** in $CDCl_3$ before and after heating to deprotect maleimide chain-end.

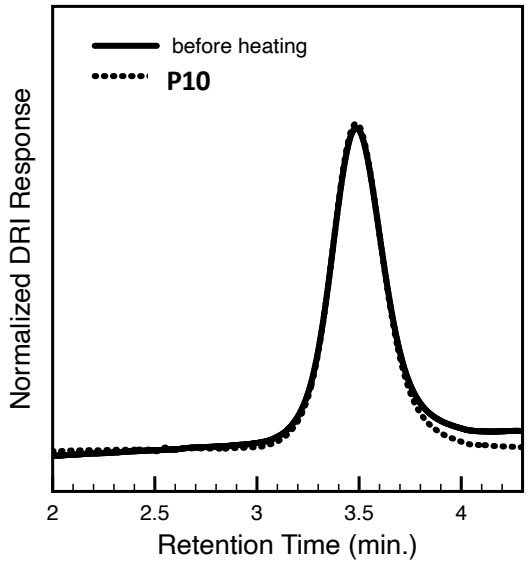

Figure S 2.68. SEC-RI trace of **P10**. Overlay of SEC-RI traces of before and after heating shows no observable change in molar mass distribution.

Synthesis of SP6

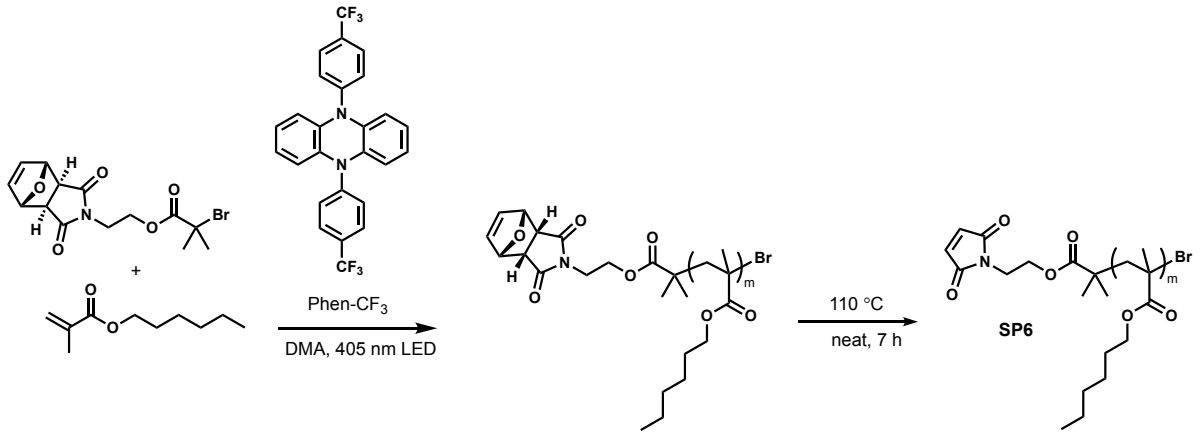

Adapted from literature procedure.[56] To a 20 mL scintillation vial equipped with magnetic stir bar was added Phen-CF3 photocatalyst (2.4 mg, 0.005 mmol, 0.05 eq) and *N,N*-dimethylacetamide (DMA) (2.0 mL). The solution was allowed to stir in the dark for at least 15 min to completely dissolve the catalyst. Once dissolved, hexyl methacrylate (2.0 mL, 10 mmol, 100 eq) was added along with *exo* furan protected-maleimide ATRP initiator (36 mg, 0.10 mmol, 1 eq). The reaction mixture was degassed with nitrogen for 10 min before wrapping the cap with parafilm. The vial was irradiated under a 405 nm collimated LED for 6 h. Monomer conversion was estimated to be 50% based on analysis of the crude mixture by ^{1}H NMR. The polymer was purified by precipitation into methanol (4 x 50 mL). The resulting polymer was subsequently heated neat under vacuum at 110 °C for 7 h to yield **SP6**. $M_{n(theor)}$ = 8,500 g/mol, $M_{n(HNMR)}$ = 14,000 $M_{n(SEC)}$ = 7,200 g/mol, $Đ$ = 1.29.

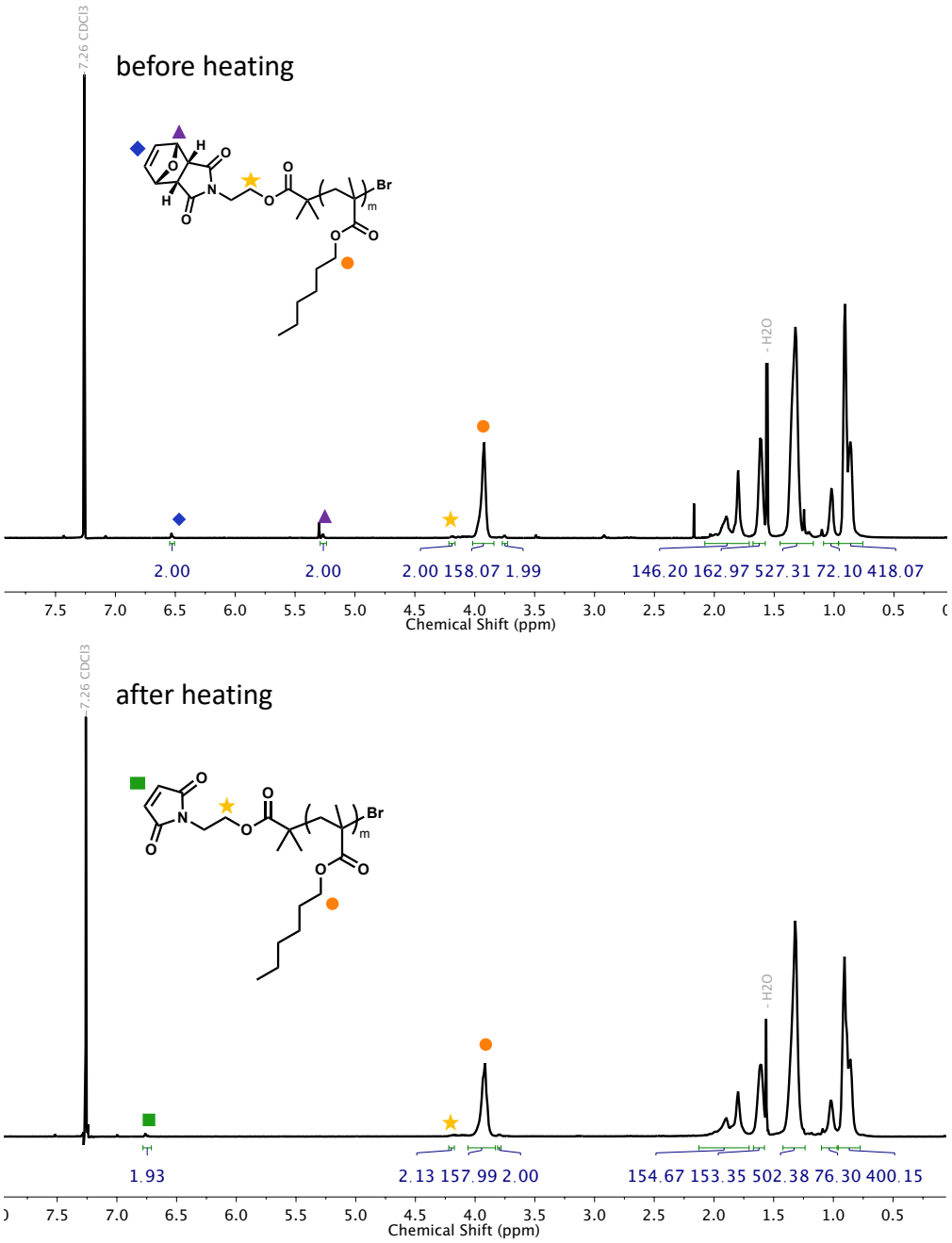

Figure S 2.69. ^{1}H NMR of spectrum of **SP6** in $CDCl_3$ before and after heating to deprotect maleimide chain-end.

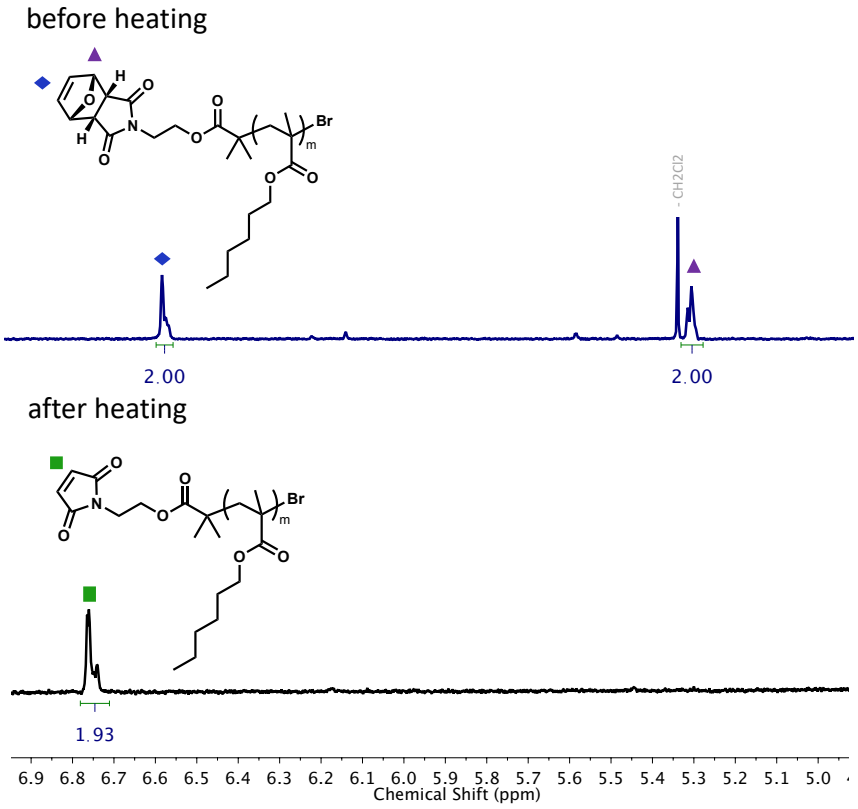

Figure S 2.70. Magnification of ^{1}H NMR of spectrum of **SP6** in $CDCl_3$ before and after heating to deprotect maleimide chain-end.

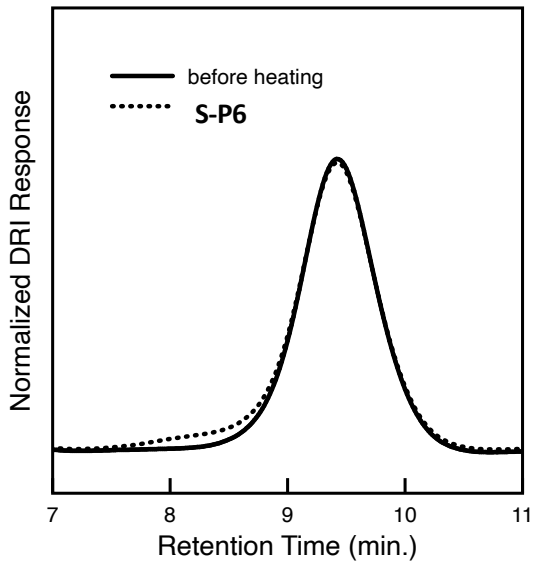

Figure S 2.71. SEC-RI trace of **SP6**. Overlay of SEC-RI traces of before and after heating shows no observable change in molar mass distribution.

Synthesis of SP7

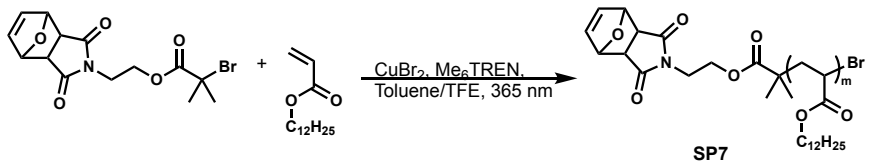

Light induced ATRP polymerization conditions were adapted from literature procedures.[50,52] A solution of copper(II) bromide (0.94 mg, 0.0042 mmol, 0.02 eq) and Me_6TREN (5.8 mg, 6.7 µL, 0.025 mmol, 0.12 eq) was prepared in 0.8 mL of trifluoroethanol. The mixture was allowed to sonicate for at least 30 minutes to completely dissolve the catalyst complex. In a 20 mL scintillation vial, dodecyl acrylate (3.5 g, 15 mmol, 70 eq) was dissolved in 2.8 mL of toluene. The Cu(II)/ trifluoroethanol solution was transferred into the acrylate solution, followed by *exo* furan protected-maleimide ATRP initiator (75 mg, 0.21 mmol, 1 eq). The vial was capped with a septum and the solution was degassed with nitrogen for 10 min. With stirring, the polymerization mixture was then irradiated ($\lambda \approx 365$ nm) for 1.75 h in a commercial UV nail lamp system. Monomer conversion was estimated to be 40% based on analysis of the crude mixture by ^{1}H NMR. The resulting polymer was purified by passing the crude reaction solution through a column of basic alumina followed by precipitation in methanol (100 mL) twice. $M_{n(theor)} = 7{,}100$ g/mol, $M_{n(HNMR)} = 7{,}100$ $M_{n(SEC)} = 6{,}000$ g/mol, $Đ = 1.15$.

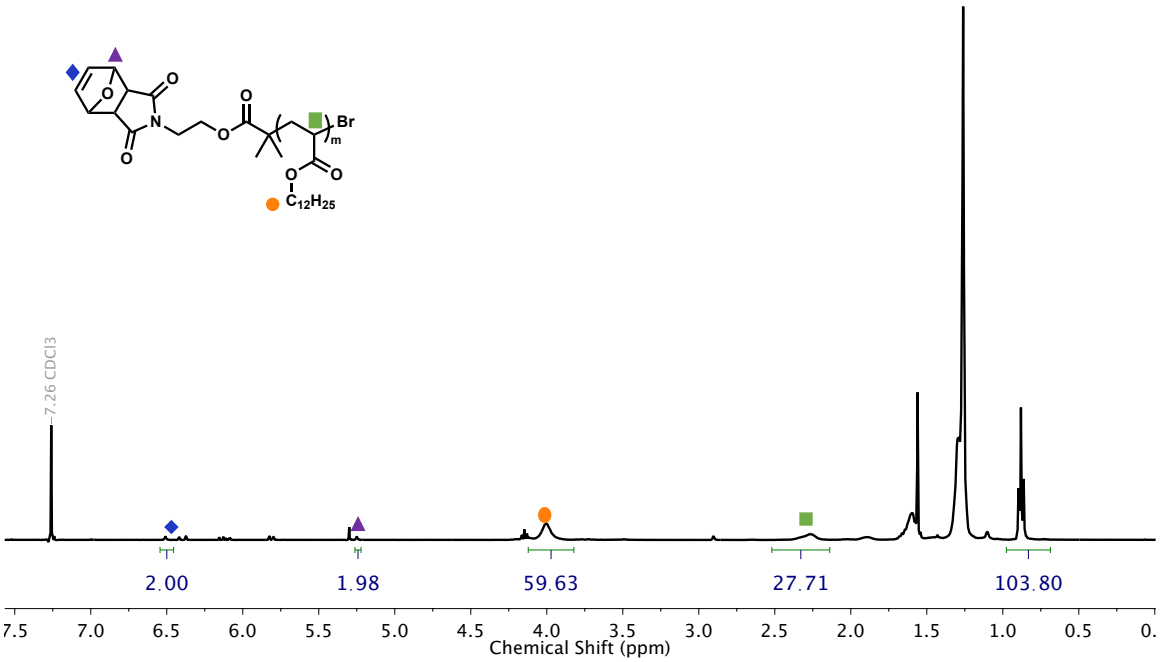

Figure S 2.72. ^{1}H NMR of spectrum of **SP7** in $CDCl_3$.

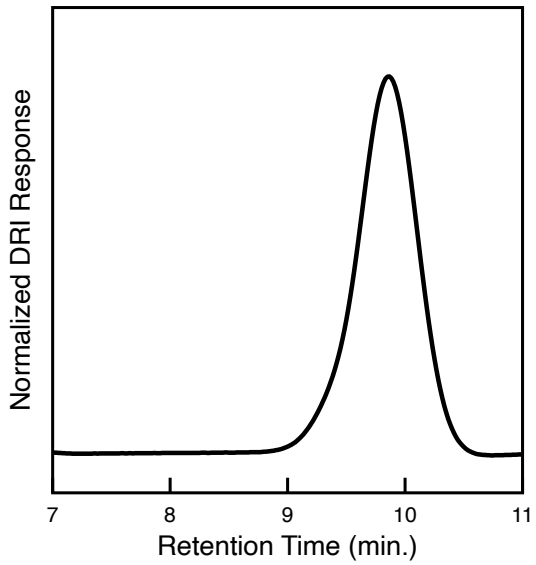

Figure S 2.73. SEC-RI trace of **SP7**.

Synthesis of SP8

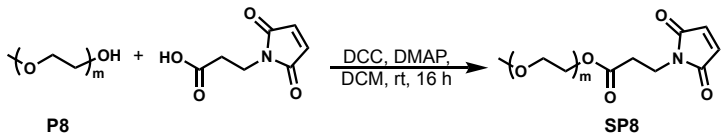

P8 SP8

To a 20 mL vial equipped with stir bar was added **P8** (purchased from Sigma-Aldrich, $M_{n(NMR)}$ = 5,400 g/mol, $Đ$ = 1.04, 1.00 g, 0.185 mmol, 1 eq), 3-maleimidopropionic acid (62.6 mg, 0.370 mmol, 2 eq), DCC (57.3 mg, 0.278 mmol, 1.5 eq), DMAP (1.13 mg, 0.00925 mmol, 0.05 eq) and 4 mL DCM. The vial was capped under air starting and allowed to stir at rt for 16 h (at which complete formation of the ω-ester was confirmed by crude HNMR). The solvent was removed under reduced pressure and the residue taken up in ethanol (EtOH) (60 mL). The solution was cooled to 0 °C and left unagitated for 30 minutes to allow P9 to precipitate. The solid was filtered, rinsed with cold EtOH (40 mL), then ether (100 mL) and dried under reduced pressure to afford the desired NBD-PEG, **SP8** (924 mg, 0.164 mmol, 89%). $M_{n(NMR)}$ = 5,600 g/mol, $M_{n(SEC)}$ = 11,000 g/mol, $Đ$ = 1.04.

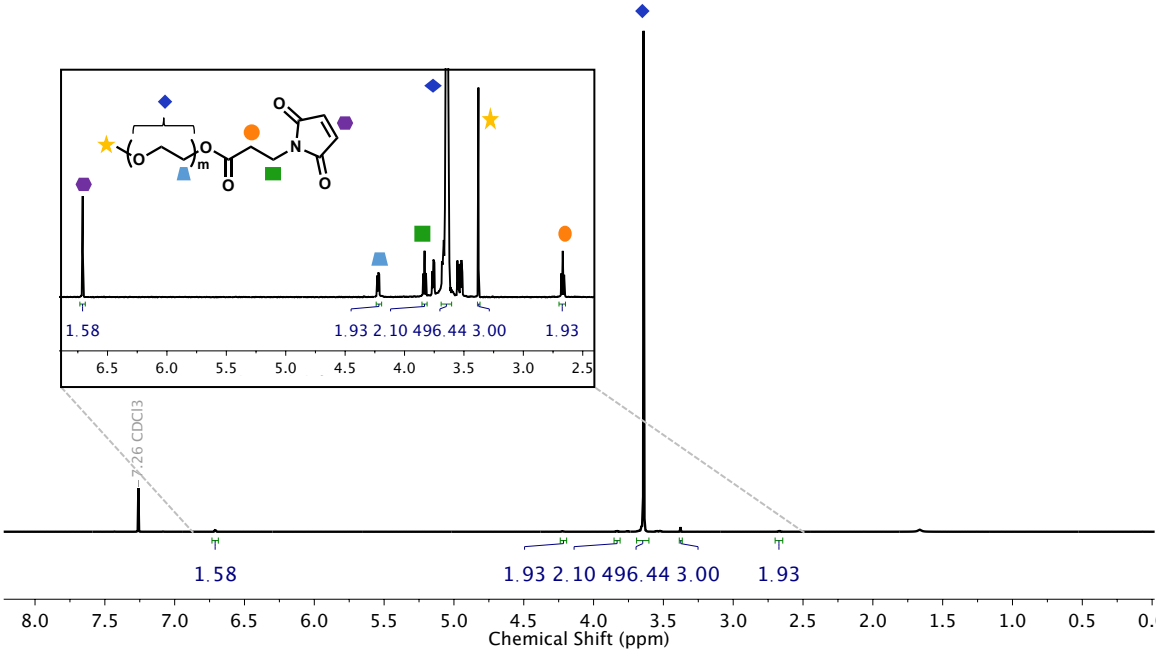

Figure S 2.74. ^{1}H NMR of spectrum of **SP8** in $CDCl_3$ showing the expected chain end resonances corresponding to functionalization with maleimide.

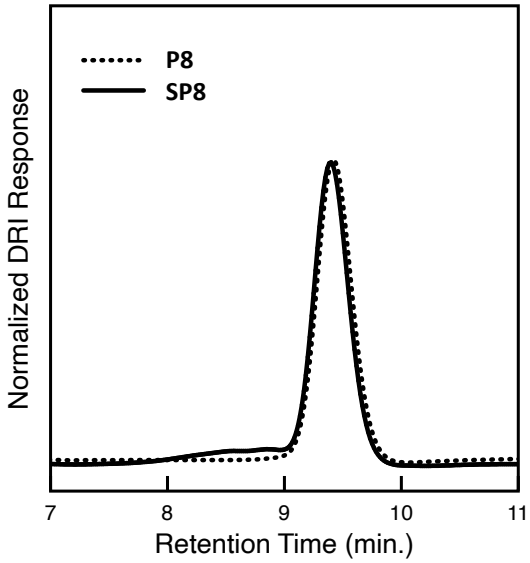

Figure S 2.75. Overlay of SEC-RI traces of **P8** and **SP8** shows no observable change in molar mass distribution after maleimide functionalization.

General NBD deprotection and DA click procedure (P11–P20):

The desired NBD functionalized polymer (1–1.2 eq) and maleimide functionalized polymer (1–1.4 eq) were dissolved in chloroform-d ($CDCl_3$) (1 mL/100 mg total polymer) in a 20 mL scintillation vial equipped with magnetic stir bar. The polymer with higher solubility in MeOH was chosen to be in excess (0.2 eq) for ease of purification of the homopolymer from the product block copolymer. 3,6-di-2-pyridyl-1,2,4,5-tetrazine (DpTz) (2 eq/NBD) was added to solution and the vial was capped under an atmosphere of air. A vent needle was placed in the cap and the solution was allowed to stir 9-24 h. Reaction completion was confirmed by crude ^{1}H NMR before norbornylene (2 eq/NBD) was added to solution and stirred for at least 15 minutes (pink DpTz color disappeared and solution became yellow, indicating complete quench of excess DpTz). The solvent was removed and the residue re-dissolved in minimal DCM. The block copolymer was precipitated into MeOH (chilled to -78 °C if necessary) and centrifuged to collect the desired product. The supernatant was discarded, and the resulting material was re-dissolved in minimal DCM. The precipitation process was repeated 1-2 times before drying the material under reduced pressure to afford the desired block copolymer.

Synthesis of P11

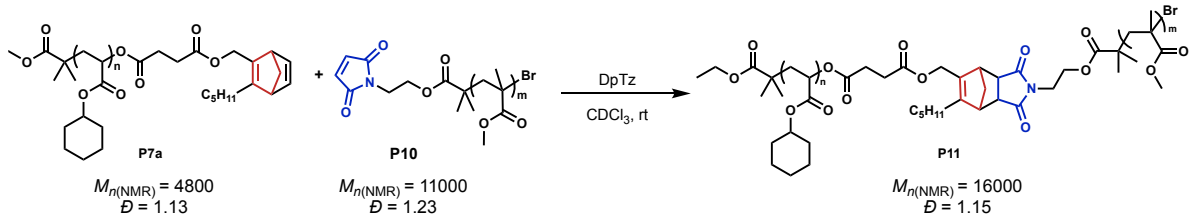

The general click procedure was performed using **P7a** (50 mg, 0.0104 mmol, 1.14 eq) and **P10** (100 mg, 0.00909 mmol, 1 eq). After precipitating twice into MeOH (25 mL), the copolymer was precipitated twice more into hexanes to afford the pure block copolymer **P11**. $M_{n(NMR)}$ = 16,000 g/mol, $M_{n(SEC)}$ = 12,000 g/mol, $Đ$ = 1.15.

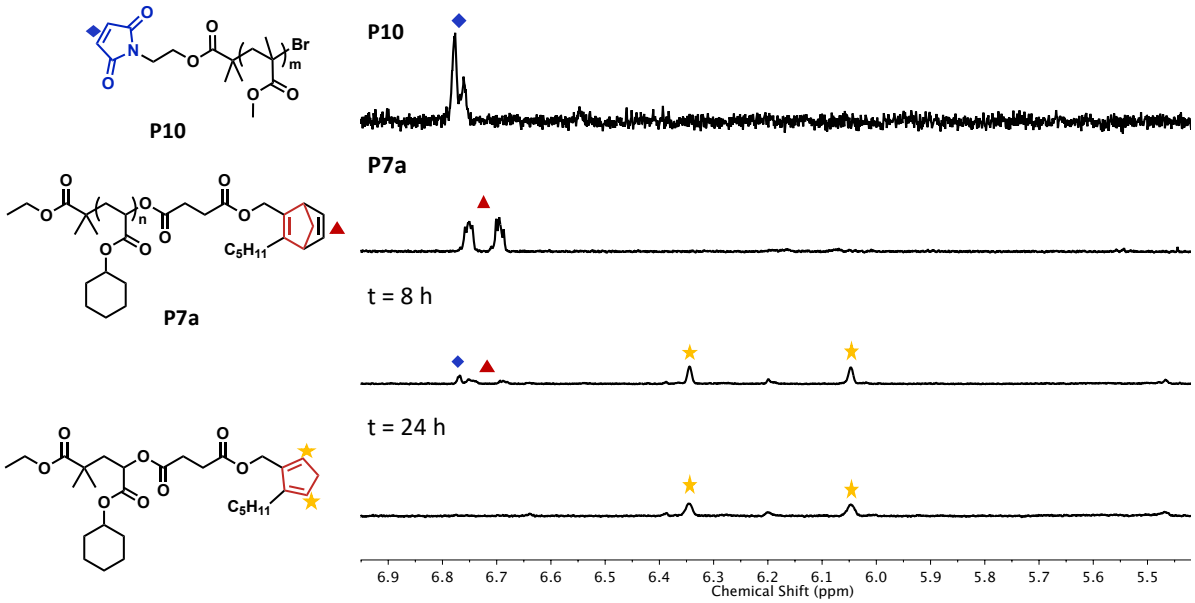

Figure S 2.76. Monitoring of reaction progress by crude ^{1}H NMR in $CDCl_3$. Reduction of maleimide peak of **P10** (blue diamond) and appearance of deprotected Cp peaks on **P7a** (yellow star) observed after 8 h. Complete disappearance of maleimide observed after 24 h indicating reaction completion.

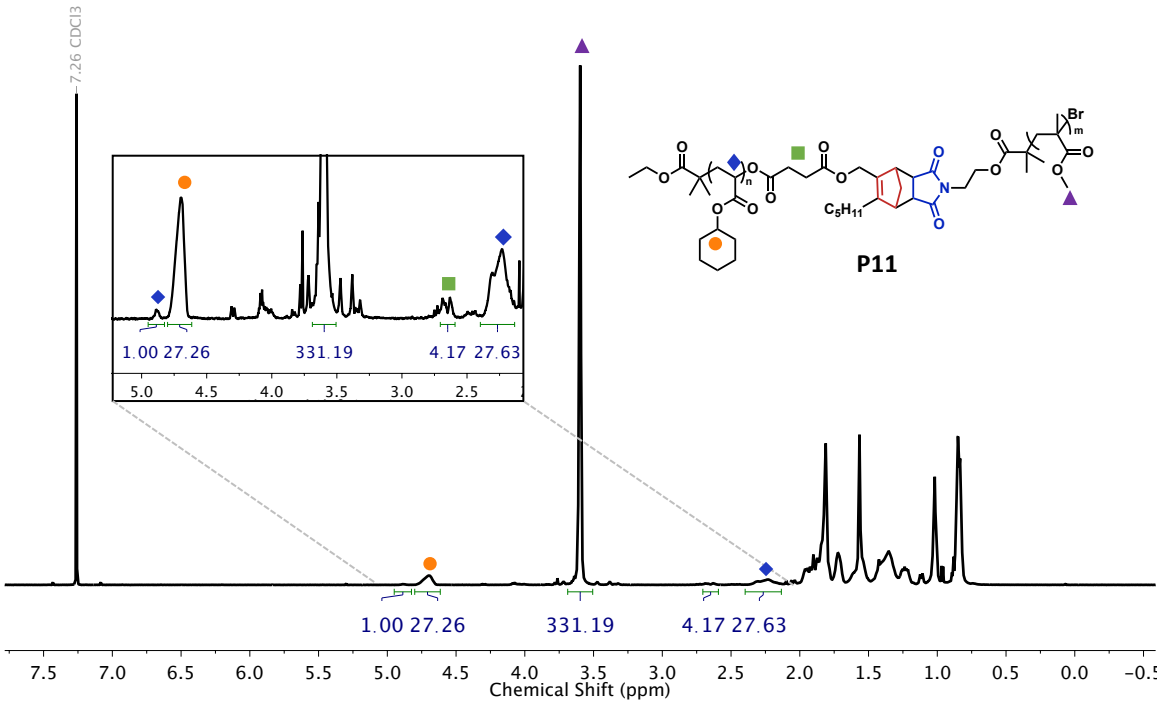

Figure S 2.77. ^{1}H NMR of spectrum of purified P11 confirming presence of both blocks.

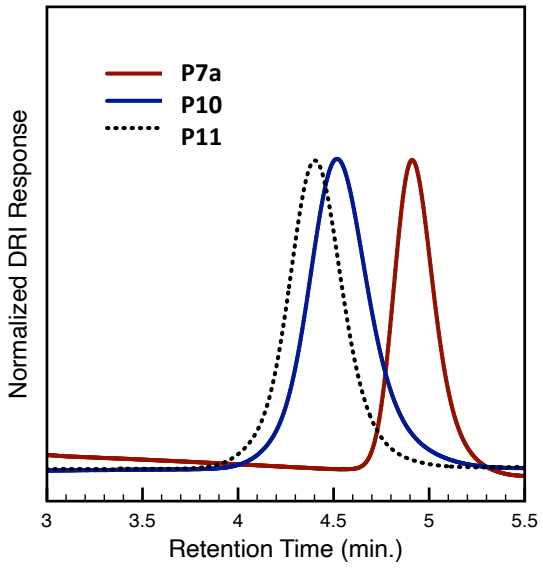

Figure S 2.78. Overlay of SEC-RI traces of **P7a**, **P10** and **P11** showing expected shift to higher molecular weight after NBD click.

Synthesis of P12

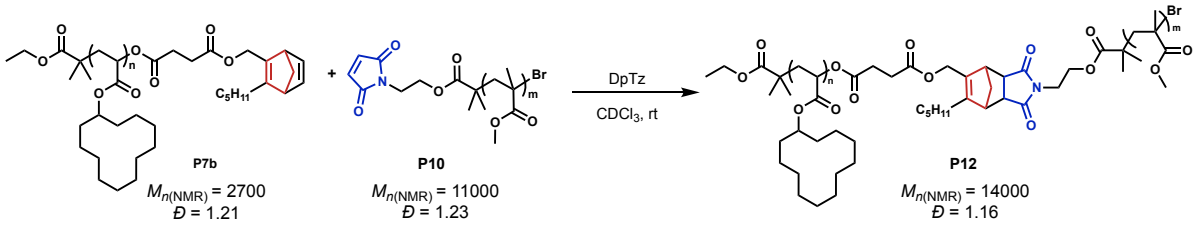

The general click procedure was performed using **P7b** (30 mg, 0.0111 mmol, 1.22 eq) and **P10** (100 mg, 0.00909 mmol, 1 eq). After precipitating twice into MeOH (25 mL), the polymer was precipitated twice more into hexanes to afford the pure block copolymer **P12**. $M_{n(NMR)}$ = 14,000 g/mol, $M_{n(SEC)}$ = 11,000 g/mol, $Đ$ = 1.16.

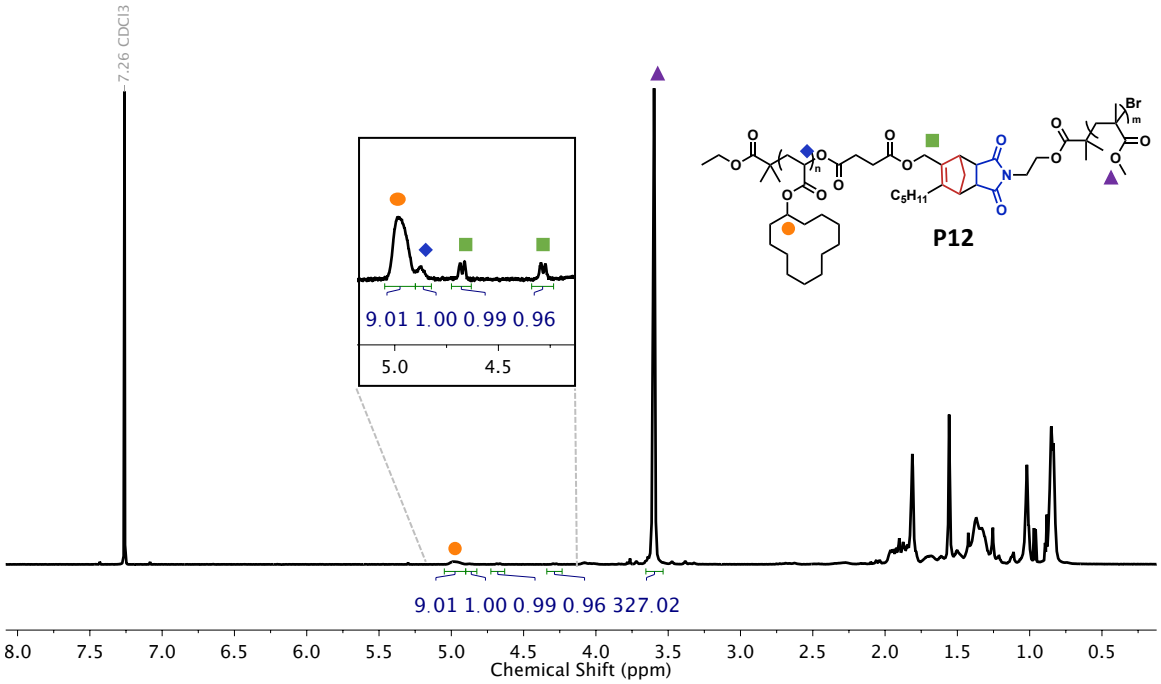

Figure S 2.79. ^{1}H NMR of spectrum of purified **P12** confirming presence of both blocks.

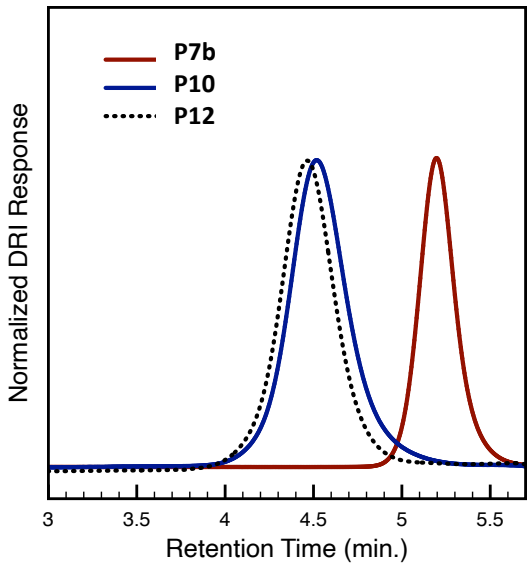

Figure S 2.80. Overlay of SEC-RI traces of **P7b**, **P10** and **P12** showing expected shift to higher molecular weight after NBD click.

Synthesis of P13

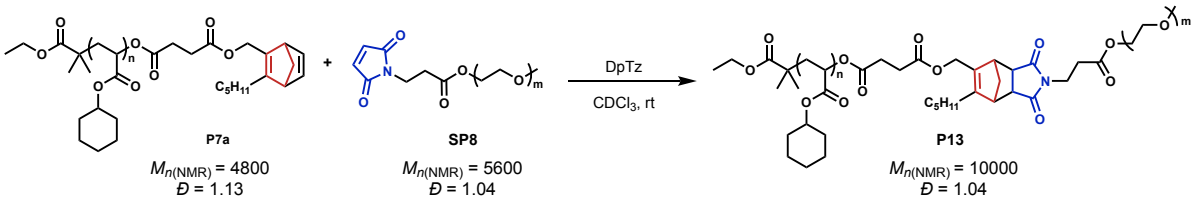

The general click procedure was performed using **P7a** (80 mg, 0.0167 mmol, 1 eq) and **SP8** (110 mg, 0.0196 mmol, 1.18 eq). The polymer was precipitated three times in MeOH (10 mL,- 78 °C) to afford the pure block copolymer **P13**. $M_{n(NMR)}$ = 10,000 g/mol, $M_{n(SEC)}$ = 15,000 g/mol, $Đ$ = 1.04.

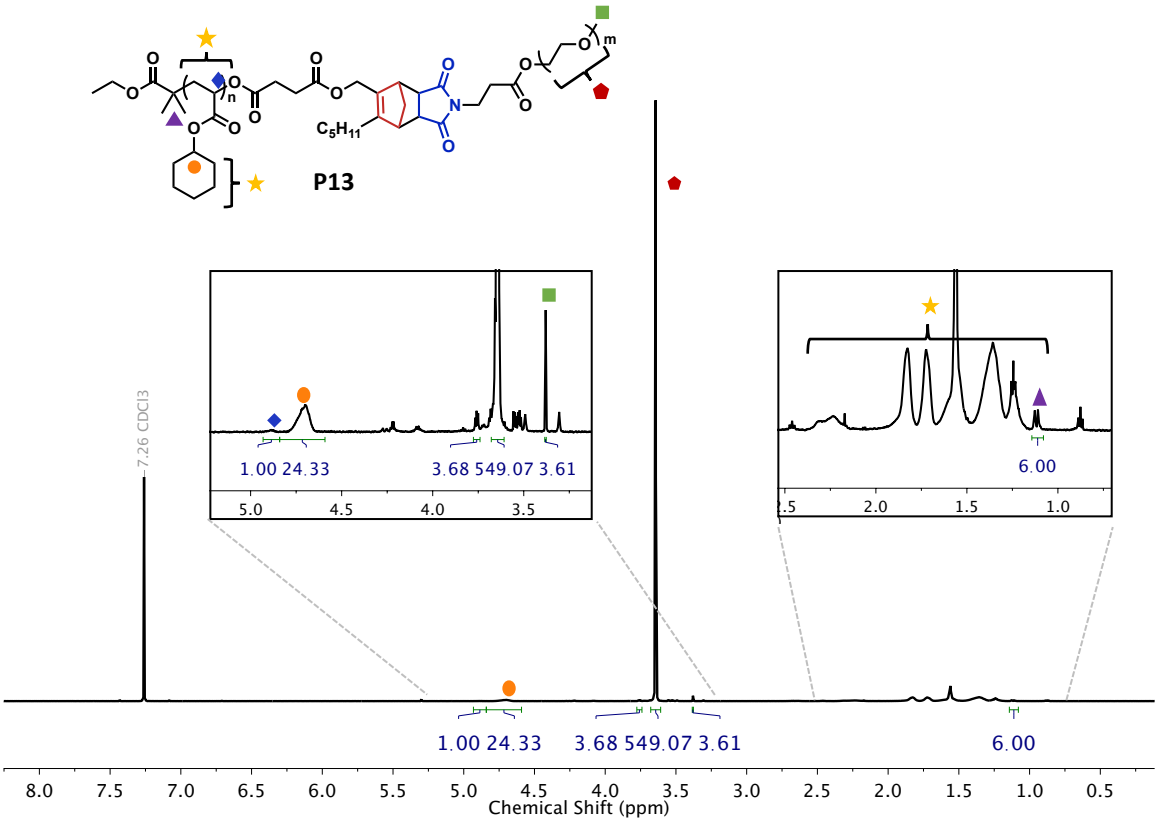

Figure S 2.81. [1]H NMR of spectrum of purified **P13** confirming presence of both blocks.

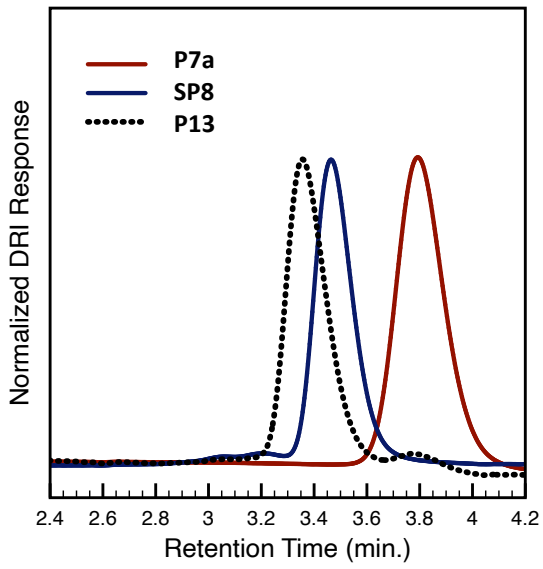

Figure S 2.82. Overlay of SEC-RI traces of **P7a**, **SP8** and **P13** showing expected shift to higher molecular weight after NBD click.

Synthesis of P14

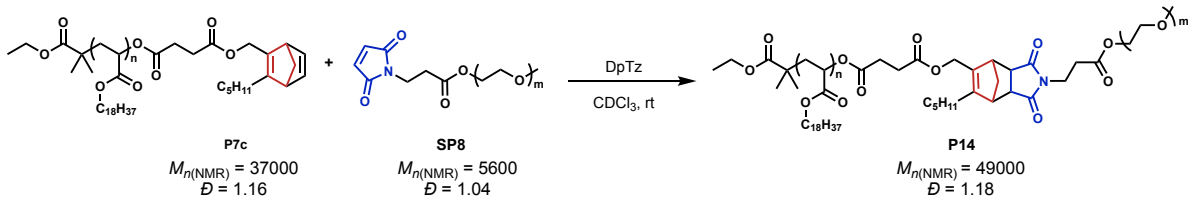

The general click procedure was performed using **P7c** (150 mg, 0.00405 mmol, 1 eq) and **SP8** (31.9 mg, 0.00569 mmol, 1.4 eq). The polymer was precipitated three times in MeOH (10 mL, -78 °C) to afford the pure block copolymer **P14**. $M_{n(NMR)}$ = 49,000 g/mol, $M_{n(SEC)}$ = 25,000 g/mol, $Đ$ = 1.18.

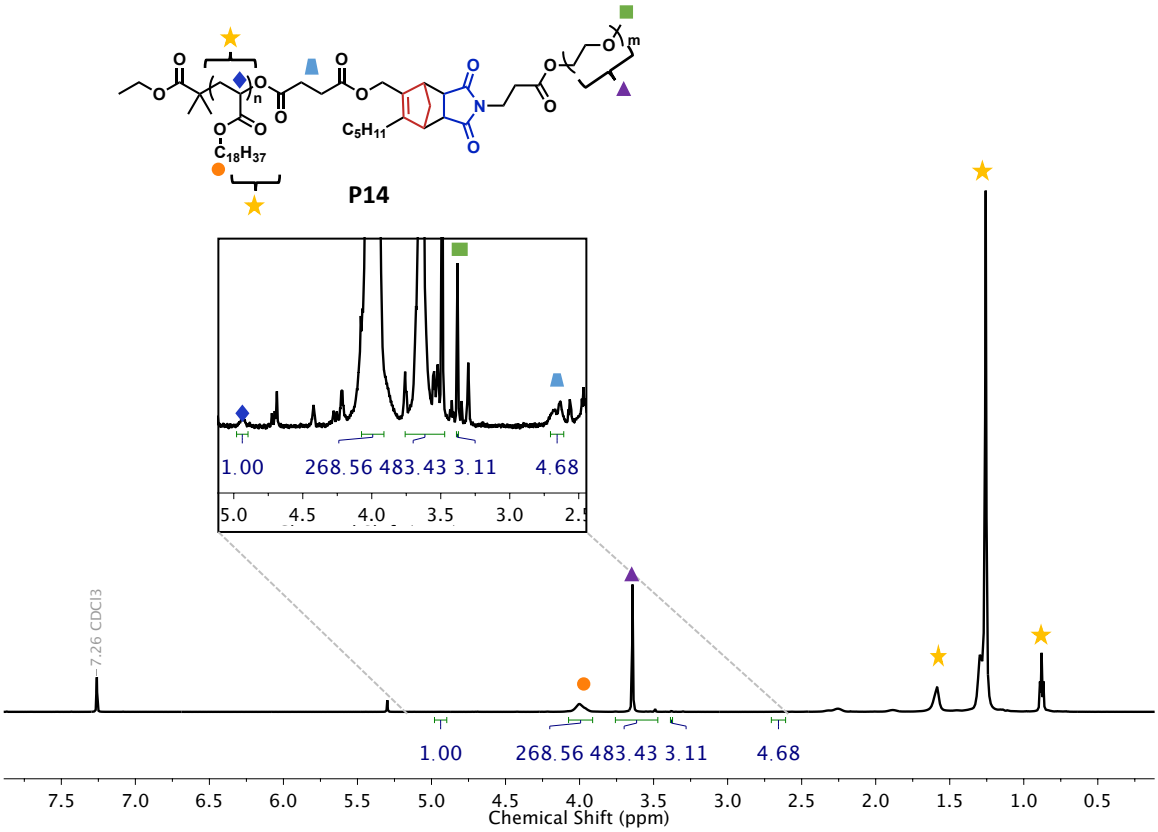

Figure S 2.83. ^{1}H NMR of spectrum of purified **P14** confirming presence of both blocks.

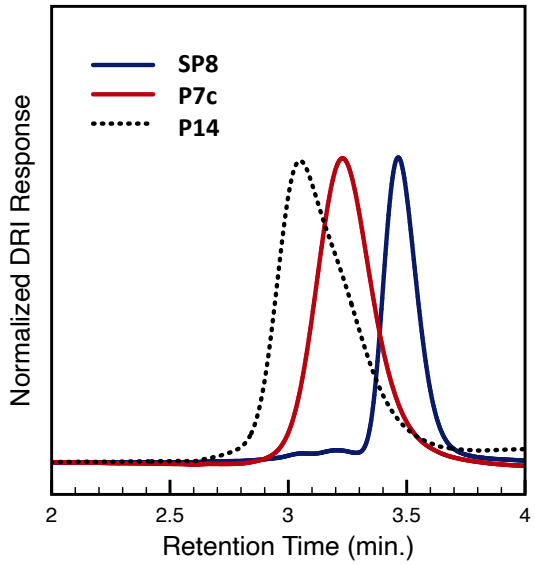

Figure S 2.84. Overlay of SEC-RI traces of **SP8**, **P7c** and **P14** showing expected shift to higher molecular weight after NBD click. Shoulder indicates some homopolymer **P7c** is present after precipitation.

Synthesis of P15

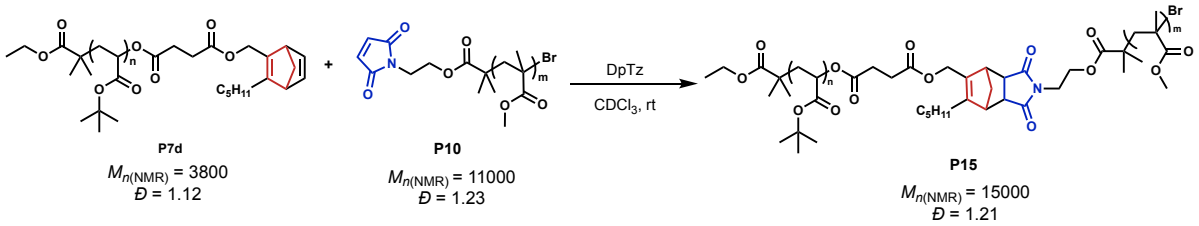

The general click procedure was performed using **P7d** (38 mg, 0.01 mmol, 2.3 eq) and **P10** (48 mg, 0.0044 mmol, 1 eq). The polymer was precipitated twice in MeOH (5 mL, -78 °C) to afford the pure block copolymer **P15**. $M_{n(NMR)}$ = 15,000 g/mol, $M_{n(SEC)}$ = 14,000 g/mol, $Đ$ = 1.21.

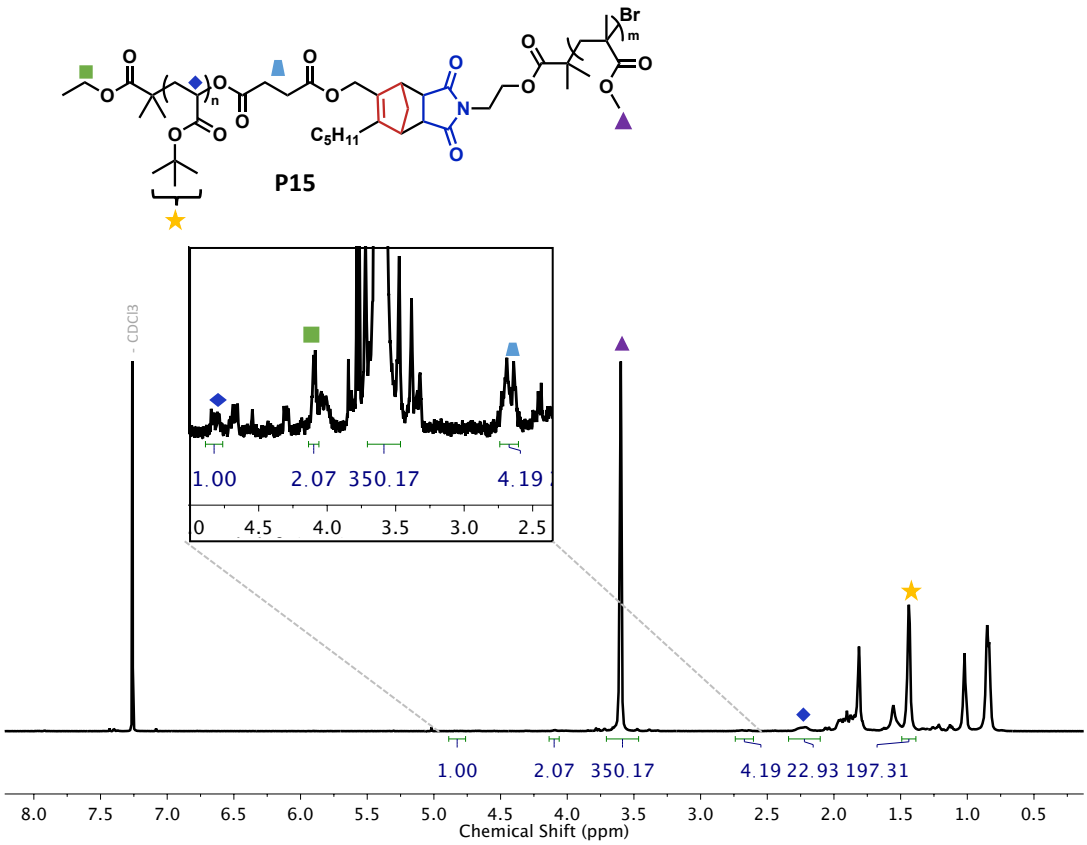

Figure S 2.85. ^{1}H NMR of spectrum of purified **P15** confirming presence of both blocks.

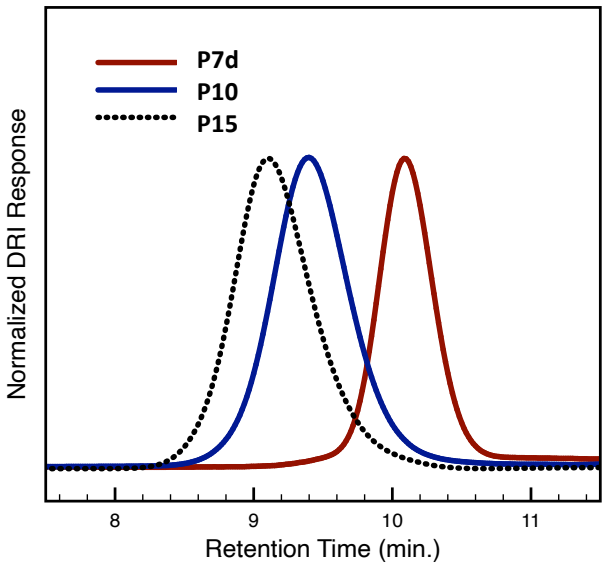

Figure S 2.86. Overlay of SEC-RI traces of **P7d**, **P10** and **P15** showing expected shift to higher molecular weight after NBD click.

Synthesis of P16

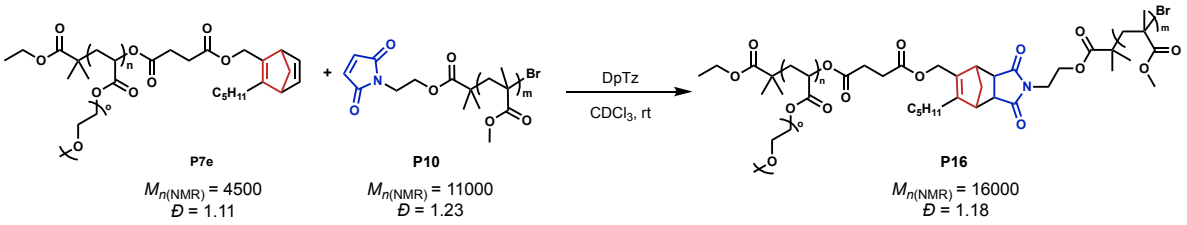

The general click procedure was performed using **P7e** (30 mg, 0.0067 mmol, 1.4 eq) and **P10** (51 mg, 0.0046 mmol, 1 eq). The polymer was precipitated twice in MeOH (5 mL, -78 °C) to afford the pure block copolymer **P16**. $M_{n(NMR)}$ = 16,000 g/mol, $M_{n(SEC)}$ = 14,000 g/mol, $Đ$ = 1.18.

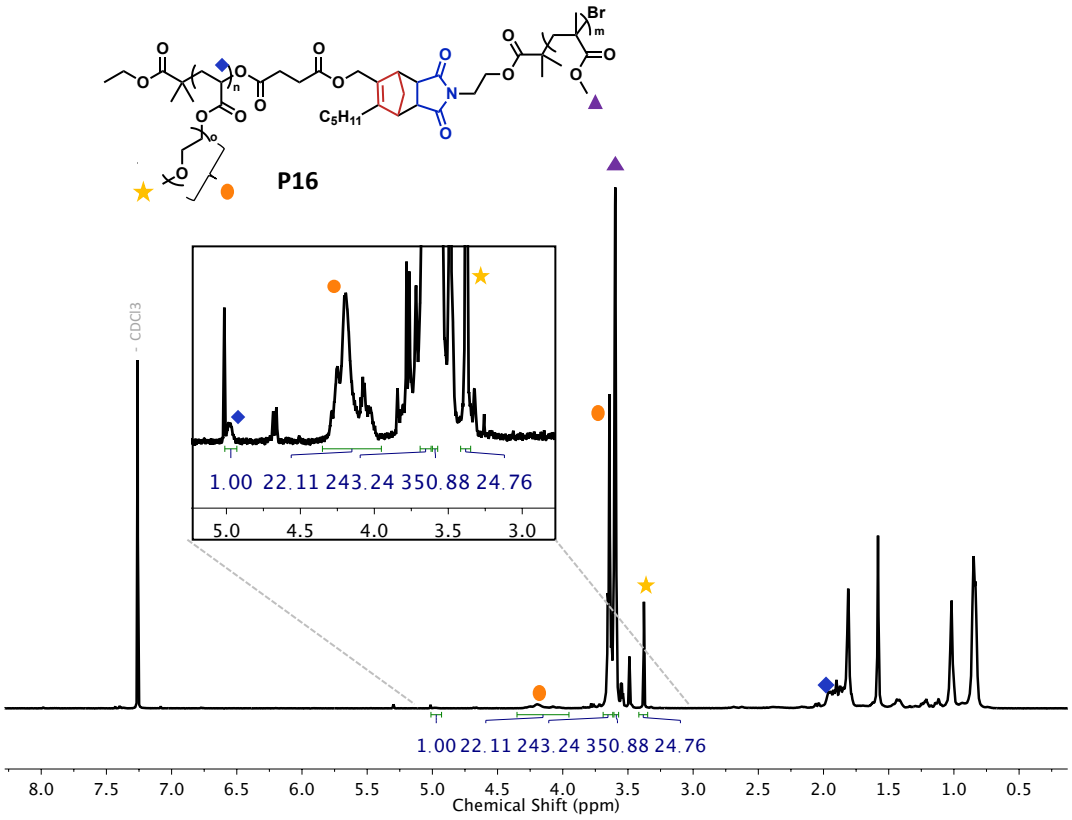

Figure S 2.87. [1]H NMR of spectrum of purified **P16** confirming presence of both blocks.

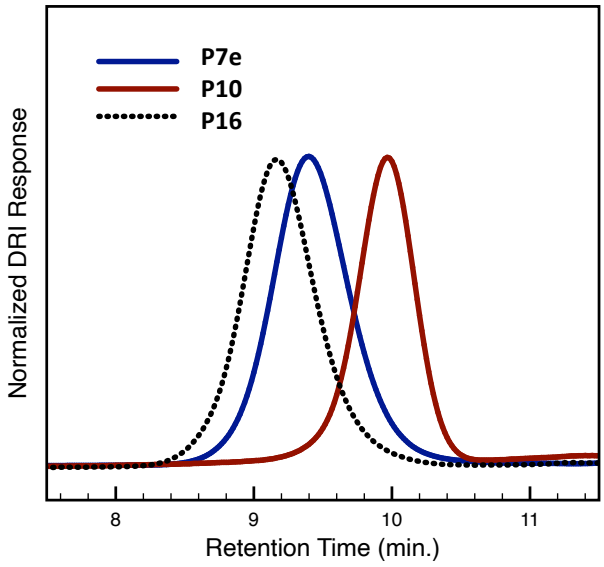

Figure S 2.88. Overlay of SEC-RI traces of **P7e**, **P10** and **P16** showing expected shift to higher molecular weight after NBD click. **Synthesis of P17**

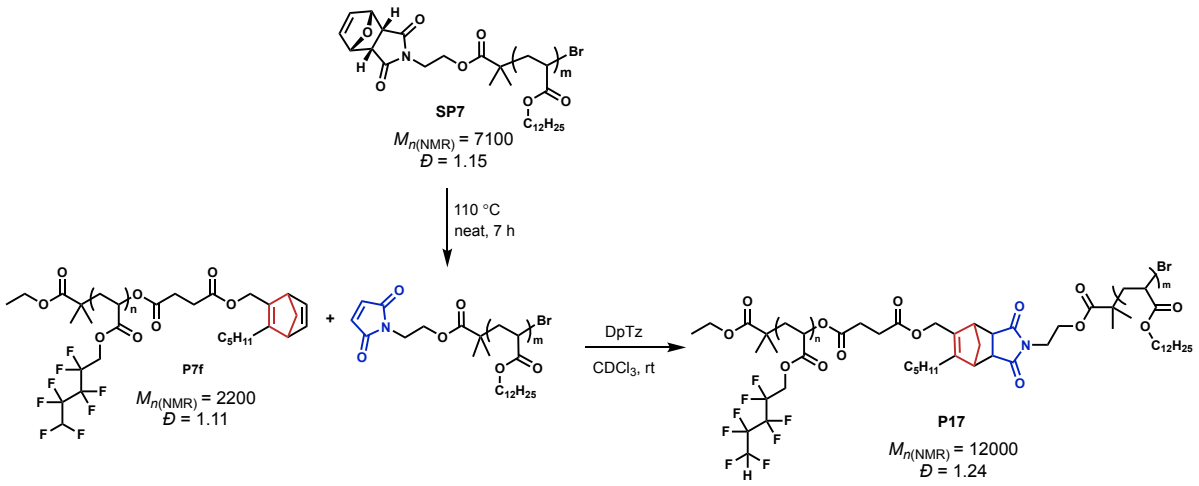

SP7 was heated neat under vacuum at 110 °C for 15 h to afford the maleimide functionalized poly(dodecyl acrylate) (mal-PDA). The general click procedure was performed using **P7f** (9.1 mg, 0.0041 mmol, 1.4 eq) and mal-PDA (21 mg, 0.0030 mmol, 1 eq). The polymer was precipitated twice in MeOH (3 mL) to afford the block copolymer **P17**. $M_{n(NMR)}$ = 12,000 g/mol, $M_{n(SEC)}$ = 5,700 g/mol, $Đ$ = 1.24.

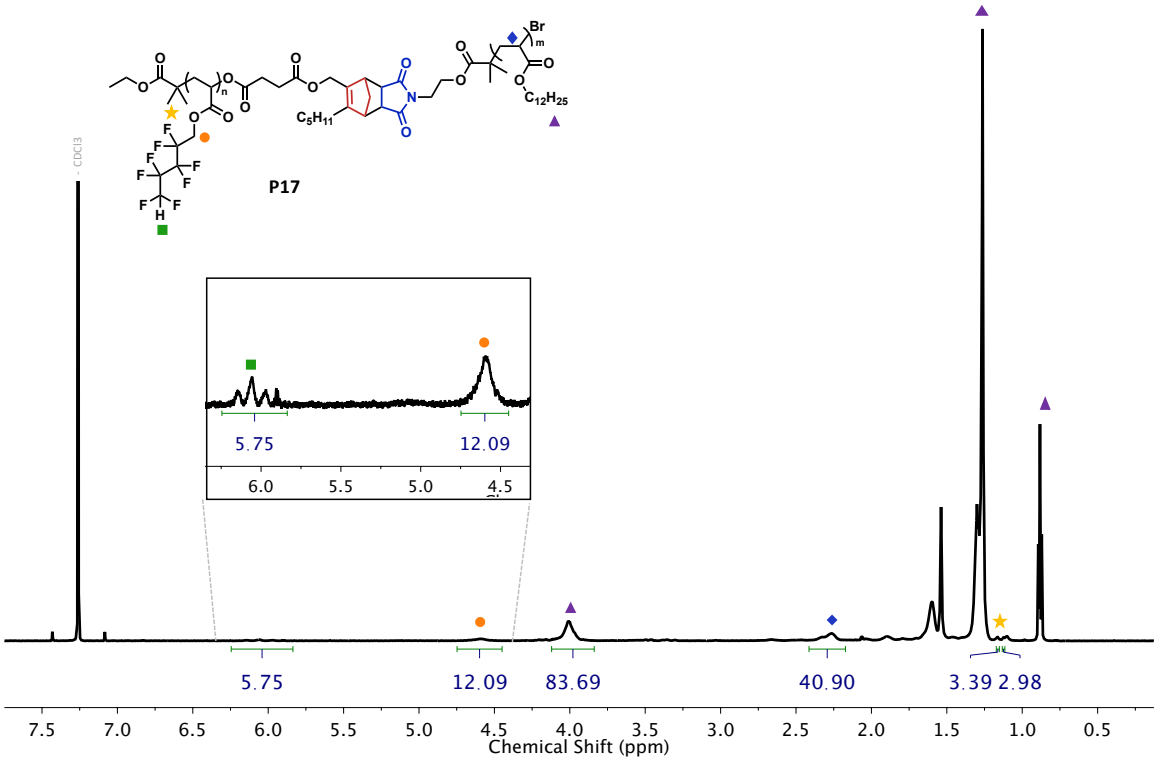

Figure S 2.89. [1]H NMR of spectrum of purified **P17** confirming presence of both blocks.

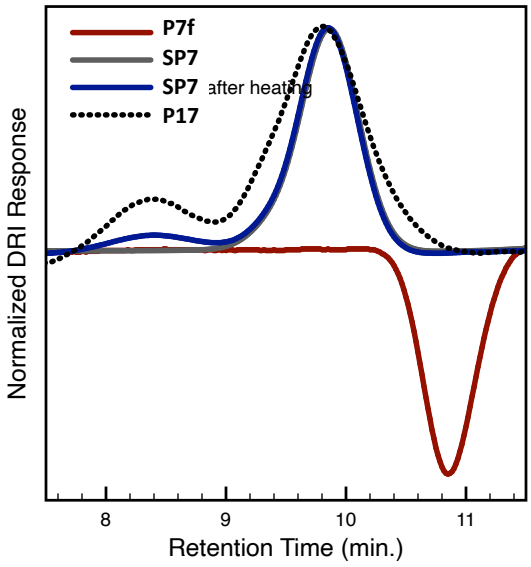

Figure S 2.90. Overlay of SEC-RI traces of **P7f**, **SP7** before and after heating, and **P17** . The formation of a higher molecular weight peak after deprotection of **SP7**, which is preferentially isolated by precipitation, leads to a bimodal distribution in the final product corresponding to the desired diblock **P17** and the higher molecular weight byproduct of **SP7** deprotection.

Synthesis of P18

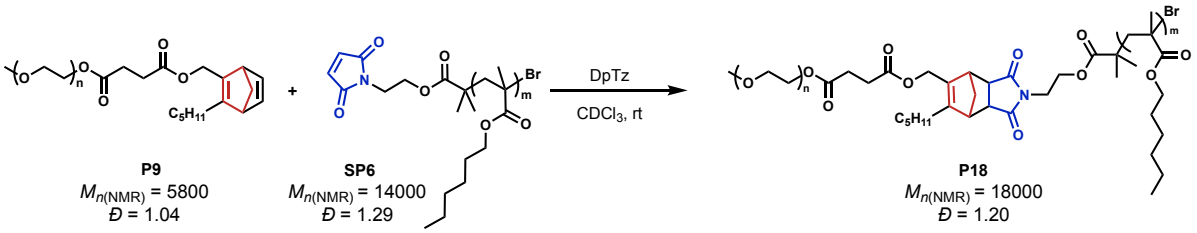

The general click procedure was performed using **P9** (75 mg, 0.0129 mmol, 1.18 eq) and **SP6** (152 mg, 0.0109 mmol, 1 eq). The polymer was precipitated three times in MeOH (10 mL, -78 °C) to afford the pure block copolymer **P18**. $M_{n(NMR)}$ = 18,000 g/mol, $M_{n(SEC)}$ = 20,000 g/mol, $Đ$ = 1.20.

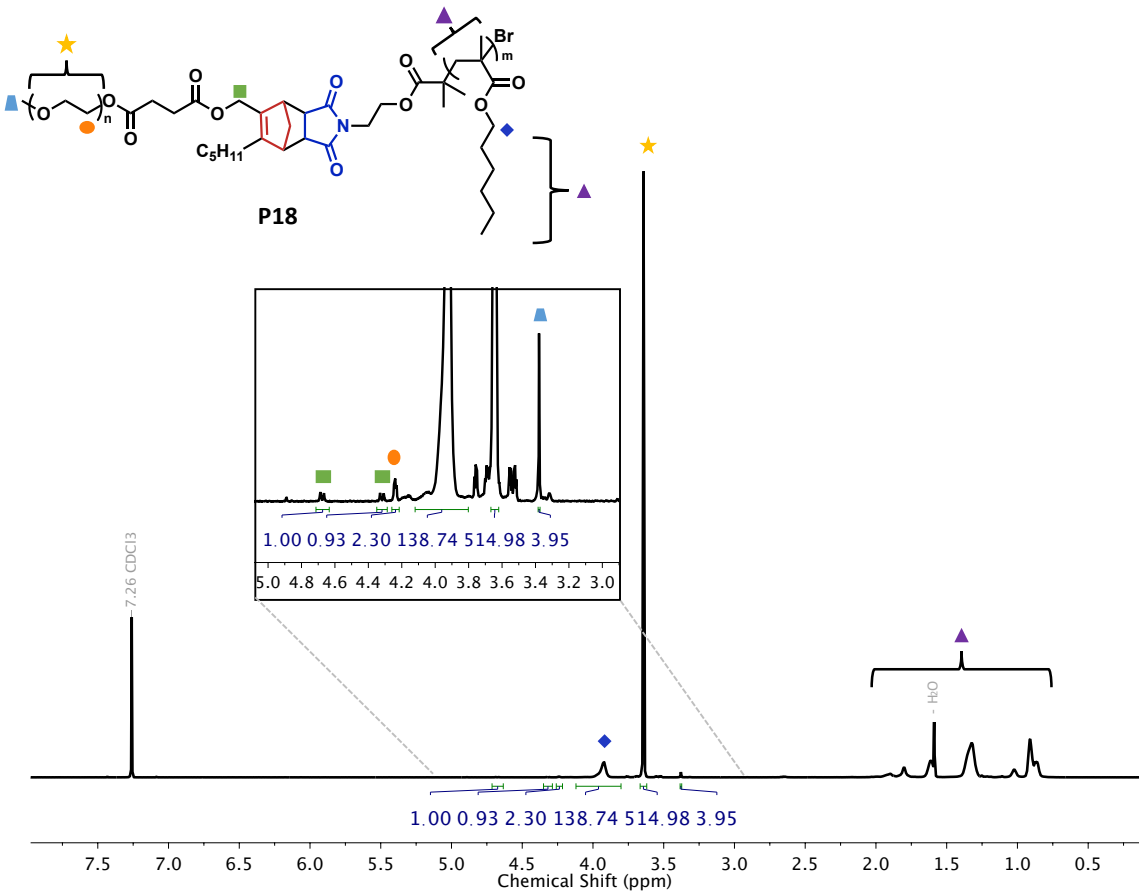

Figure S 2.91. [1]H NMR of spectrum of purified **P18** confirming presence of both blocks.

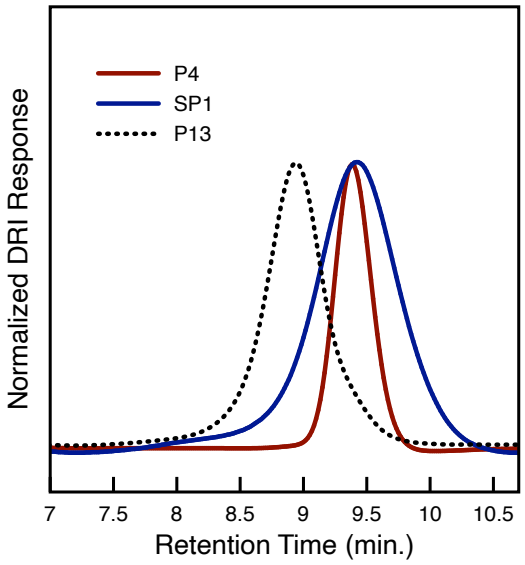

Figure S 2.92. Overlay of SEC-RI traces of **P9**, **SP6** and **P18** showing expected shift to higher molecular weight after NBD click.

Synthesis of SP9

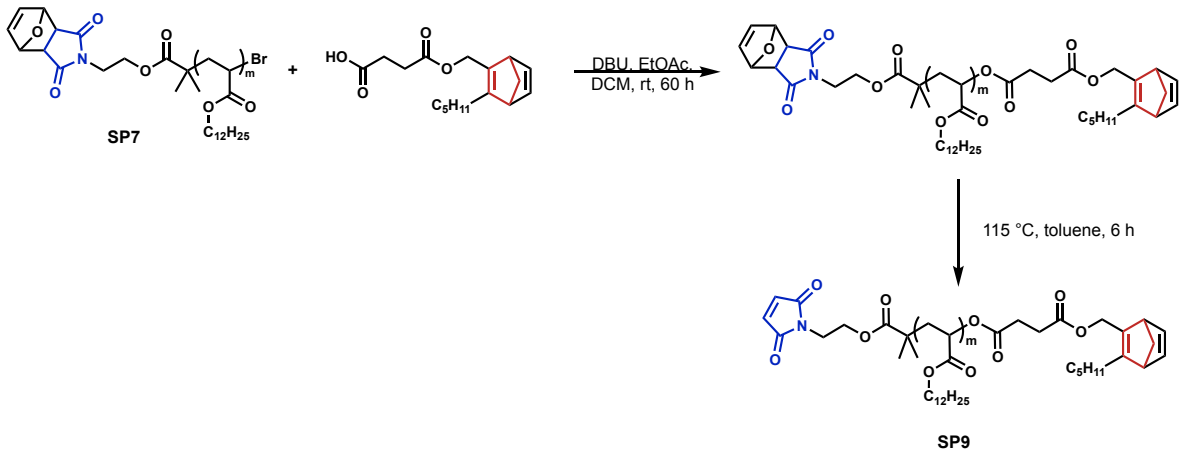

In a 20-mL vial equipped with stir bar, **SP7** (645 mg, 0.0908 mmol) was dissolved in minimal ethyl acetate (EtOAc) (1.0 mL). In a separate vial, DBU (55.7 µL, 0.372 mmol, 4.1 eq) was added to a solution of compound **10** (106 mg, 0.363 mmol, 4 eq) in EtOAc (0.40 mL). Once dissolved, the acid-DBU solution was transferred to the polymer solution with an additional 0.2 mL EtOAc. The vial was capped under air. The solution was allowed to stir at rt for 60 h

(at which complete formation of the ω-ester was confirmed by crude ^{1}H NMR). The crude reaction mixture was precipitated into MeOH (50 mL) and the resulting solid was re-dissolved in minimal DCM. The precipitation process was repeated twice before drying the material under reduced pressure. The polymer was then dissolved in toluene (5 mg/mL) and heated at 115 °C for 6 h to deprotect the maleimide and afford **SP9**. $M_{n(NMR)}$ = 7,700 g/mol, $M_{n(SEC)}$ = 6,300 g/mol, $Đ$ = 1.17.

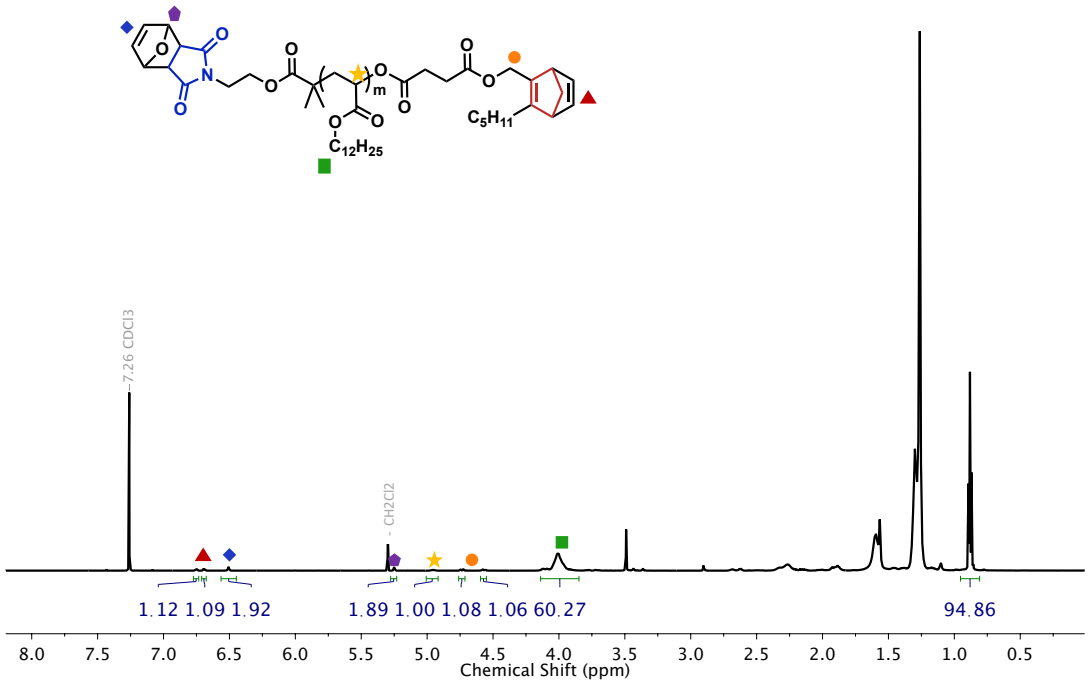

Figure S 2.93. ^{1}H NMR of spectrum of polymer in $CDCl_3$ before heating to deprotect maleimide chain-end.

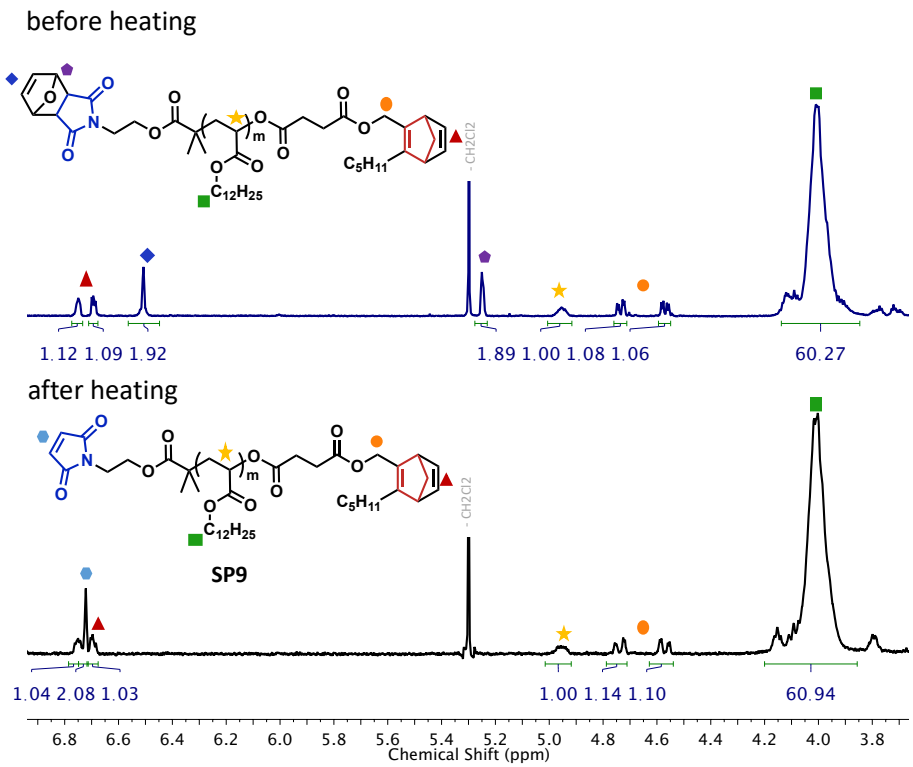

Figure S 2.94. Magnification of ^{1}H NMR of spectrum of **SP9** in $CDCl_3$ before and after heating to deprotect maleimide chain-end.

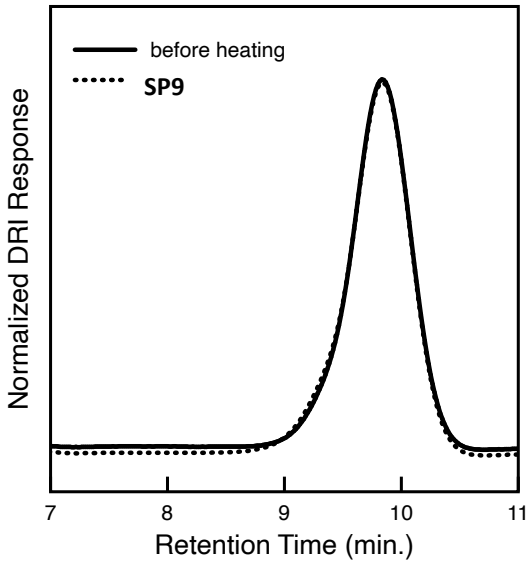

Figure S 2.95. SEC-RI trace of **SP9**. Overlay of SEC-RI traces of before and after heating shows no observable change in molar mass distribution.

Synthesis of P19

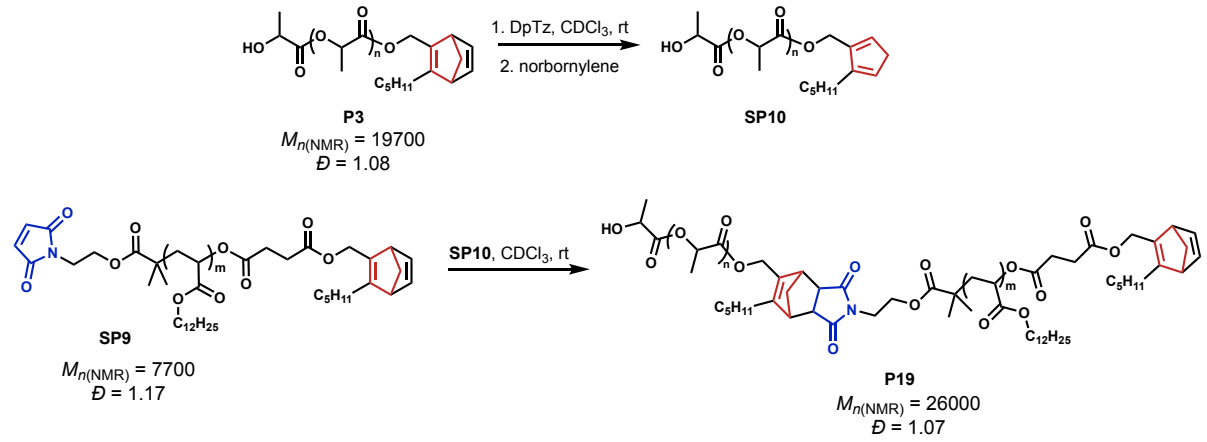

In a 1-dram vial equipped with magnetic stir bar, **P3** (200 mg, 0.010 mmol, 1.1 eq) was dissolved in $CDCl_3$ (2.0 mL). To the solution was added DpTz (9 mg, 0.038 mmol, 4.2 eq) and the vial was capped under an atmosphere of air. A vent needle was placed in the cap and the solution was allowed to stir 9 h. Reaction completion was confirmed by crude ^{1}H NMR before norbornene (8 mg, 0.085 mmol, 9.3 eq) was added to solution and stirred for 30 minutes. Upon complete disappearance of pink DpTz color (indicating complete quench of excess DpTz), **SP9** (70 mg, 0.0091 mmol, 1 eq) was added to solution. The vial was once again capped under an atmosphere of air and allowed to stir for 24 h. The solvent was removed and the residue re-dissolved in minimal DCM. The block copolymer was precipitated into rt MeOH (25 mL) and centrifuged to collect the desired product. The supernatant was discarded, and the resulting material was re-dissolved in minimal DCM. The precipitation process was repeated twice before drying the material under reduced pressure to afford **P19**. $M_{n(NMR)}$ = 26,000 g/mol, $M_{n(SEC)}$ = 28,000 g/mol, $Đ$ = 1.07.

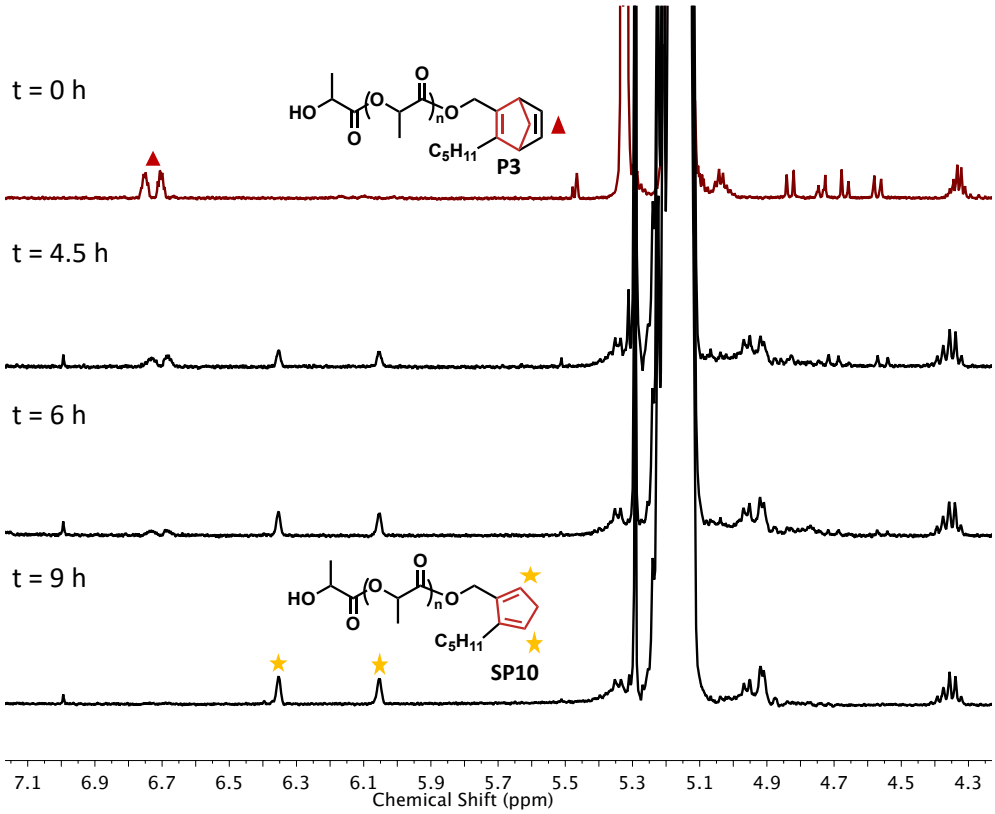

Figure S 2.96. Deprotection of **P3** to **SP10** by DpTz monitored by crude ^{1}H NMR in $CDCl_3$. Complete disappearance of NBD peaks (red triangle) and appearance of Cp peaks (yellow star) observed after 9 h.

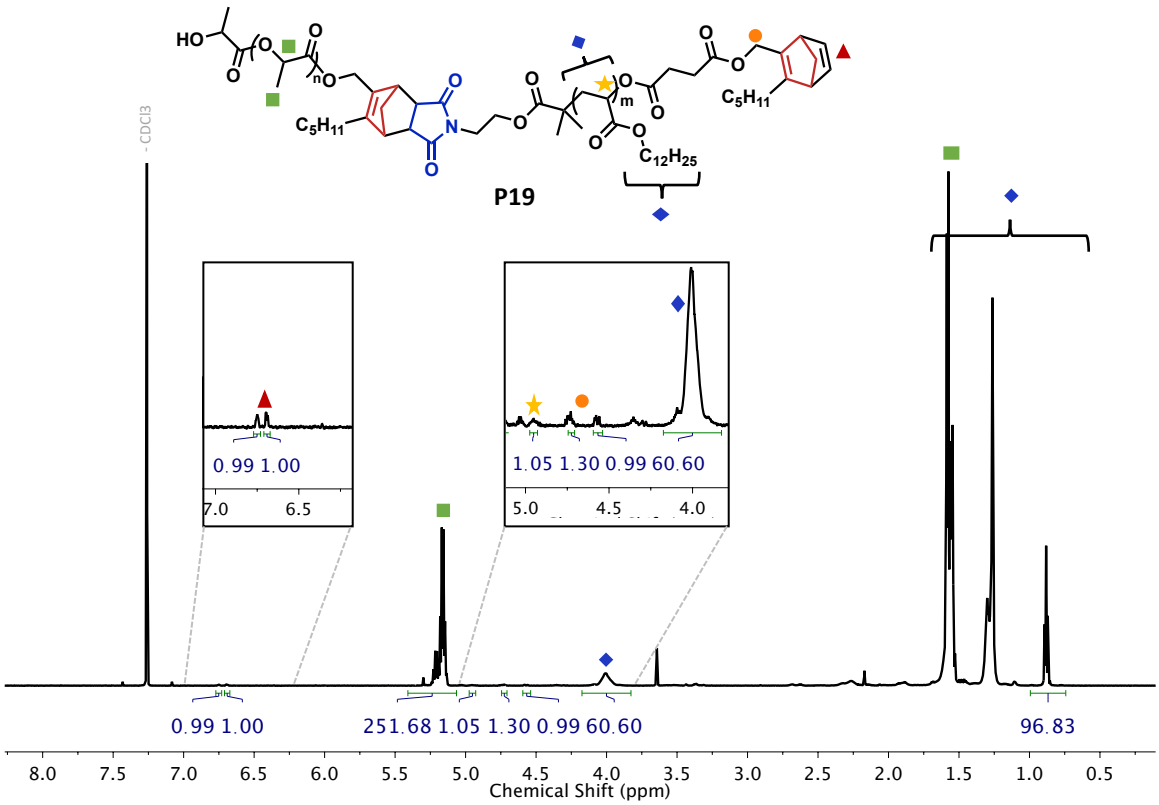

Figure S 2.97. ^{1}H NMR of spectrum of purified P19 confirming presence of both blocks.

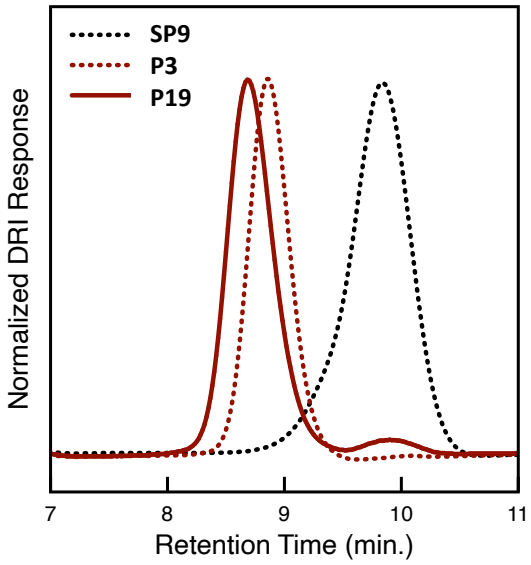

Figure S 2.98. Overlay of SEC-RI traces of **SP9**, **P3** and **P19** showing expected shift to higher molecular weight after NBD click.

Synthesis of P20

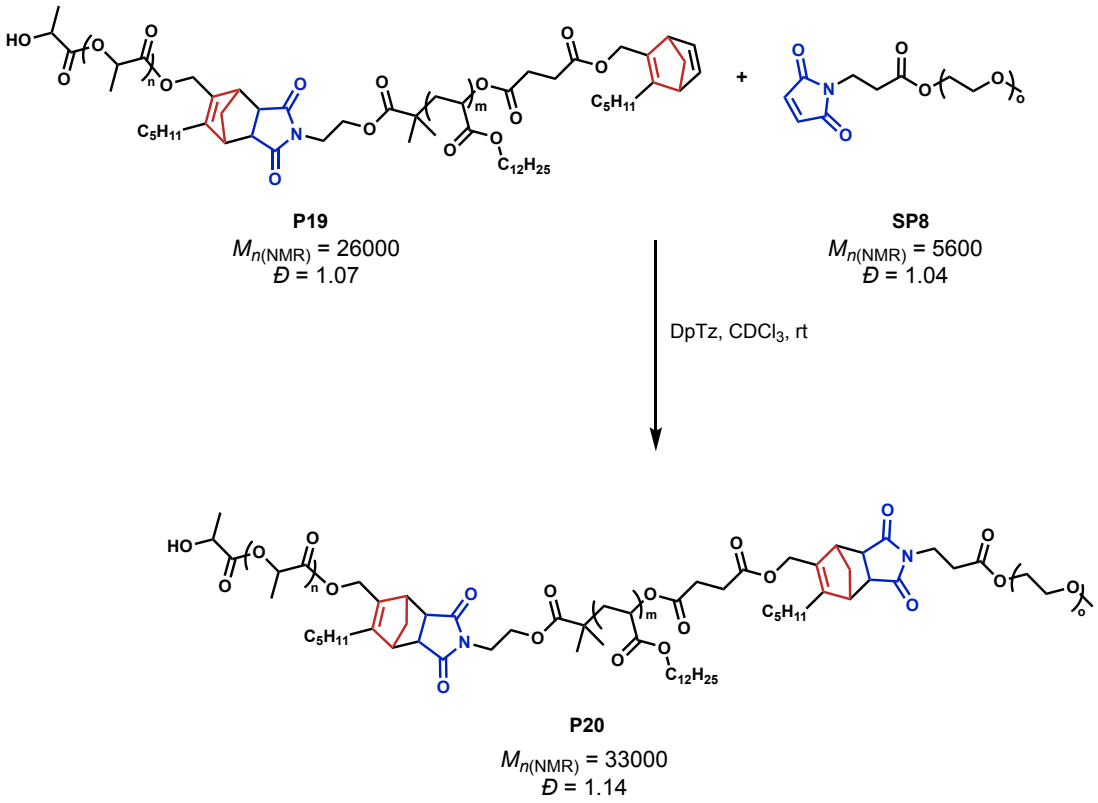

The general click procedure was performed using **P19** (75 mg, 0.0029 mmol, 1 eq) and **SP8** (21 mg, 0.0038 mmol, 1.3 eq). The polymer was precipitated three times in MeOH (10 mL, -78 °C) to afford the pure block copolymer **P20**. $M_{n(NMR)}$ = 33,000 g/mol, $M_{n(SEC)}$ = 33,000 g/mol, $Đ$ = 1.14.

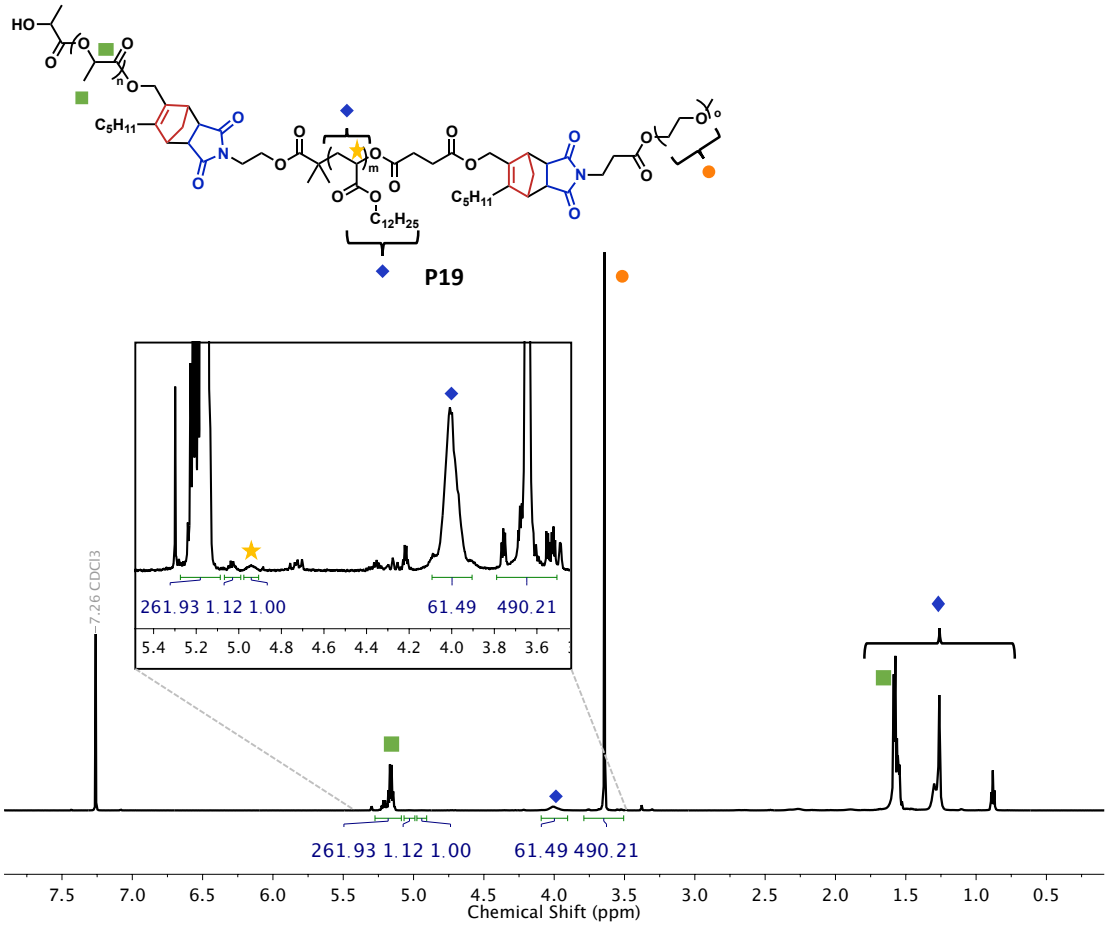

Figure S 2.99. ^{1}H NMR of spectrum of purified **P20** confirming presence of three blocks.

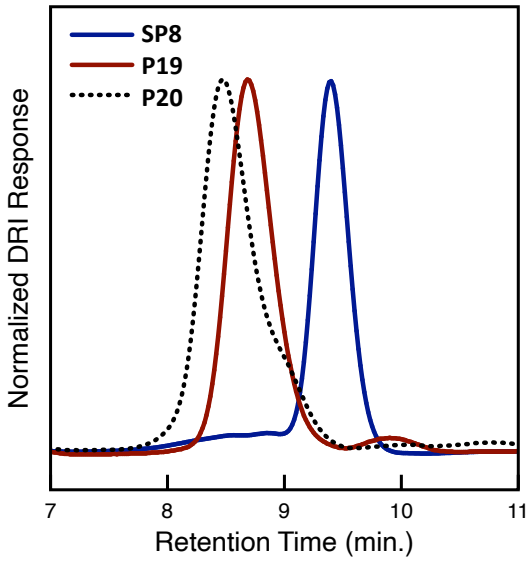

Figure S 2.100. Overlay of SEC-RI traces of **SP3**, **P14** and **P15** showing expected shift to higher molecular weight after NBD click.

2.7 References

(1) Kolb, H. C.; Finn, M. G.; Sharpless, K. B. Click Chemistry: Diverse Chemical Function from a Few Good Reactions. *Angew. Chem. Int. Ed.* **2001**, *40* (11), 2004–2021. DOI: 10.1002/1521-3773(20010601)40:11<2004::AID-ANIE2004>3.0.CO;2-5.

(2) Günay, K. A.; Theato, P.; Klok, H.-A. Standing on the Shoulders of Hermann Staudinger: Post-Polymerization Modification from Past to Present. *J. Polym. Sci. A Polym. Chem.* **2013**, *51* (1), 1–28. DOI: 10.1002/pola.26333.

(3) Lunn, D. J.; Discekici, E. H.; Read de Alaniz, J.; Gutekunst, W. R.; Hawker, C. J. Established and Emerging Strategies for Polymer Chain-End Modification. *J. Polym. Sci. Part A: Polym. Chem.* **2017**, *55* (18), 2903–2914. DOI: 10.1002/pola.28575.

(4) Blasco, E.; Sims, M. B.; Goldmann, A. S.; Sumerlin, B. S.; Barner-Kowollik, C. *50th Anniversary Perspective* : Polymer Functionalization. *Macromolecules* **2017**, *50* (14), 5215–5252. DOI: 10.1021/acs.macromol.7b00465.

(5) Brendel, J. C.; Martin, L.; Zhang, J.; Perrier, S. SuFEx – a Selectively Triggered Chemistry for Fast, Efficient and Equimolar Polymer–Polymer Coupling Reactions. *Polym. Chem.* **2017**, *8* (48), 7475–7485. DOI: 10.1039/C7PY01636K.

(6) Leophairatana, P.; De Silva, C. C.; Koberstein, J. T. How Good Is CuAAC "Click" Chemistry for Polymer Coupling Reactions? *J. Polym. Sci. Part A: Polym. Chem.* **2018**, *56* (1), 75–84. DOI: 10.1002/pola.28872.

(7) Lutz, J.-F.; Börner, H. G.; Weichenhan, K. Combining Atom Transfer Radical Polymerization and Click Chemistry: A Versatile Method for the Preparation of End-Functional Polymers: Combining Atom Transfer Radical Polymerization and Click Chemistry: *Macromol. Rapid Commun.* **2005**, *26* (7), 514–518. DOI: 10.1002/marc.200500002.

(8) Agard, N. J.; Prescher, J. A.; Bertozzi, C. R. A Strain-Promoted [3 + 2] Azide−Alkyne Cycloaddition for Covalent Modification of Biomolecules in Living Systems. *J. Am. Chem. Soc.* **2004**, *126* (46), 15046–15047. DOI: 10.1021/ja044996f.

(9) Tang, W.; Becker, M. L. "Click" Reactions: A Versatile Toolbox for the Synthesis of Peptide-Conjugates. *Chem. Soc. Rev.* **2014**, *43* (20), 7013–7039. DOI: 10.1039/C4CS00139G.

(10) Chadwick, R.; Van Gyzen, S.; Liogier, S.; Adronov, A. Scalable Synthesis of Strained Cyclooctyne Derivatives. *Synthesis* **2014**, *46* (05), 669–677. DOI: 10.1055/s-0033-1340509.

(11) Based on MilliporeSigma Price on September 20, 2022.

(12) Dommerholt, J.; Rutjes, F. P. J. T.; van Delft, F. L. Strain-Promoted 1,3-Dipolar Cycloaddition of Cycloalkynes and Organic Azides. *Top. Curr. Chem. (Z)* **2016**, *374* (2), 16. DOI: 10.1007/s41061-016-0016-4.

(13) McNelles, S. A.; Adronov, A. Rapid Synthesis of Functionalized High-Generation Polyester Dendrimers via Strain-Promoted Alkyne–Azide Cycloaddition. *Macromolecules* **2017**, *50* (20), 7993–8001. DOI: 10.1021/acs.macromol.7b01765.

(14) Pickens, C. J.; Johnson, S. N.; Pressnall, M. M.; Leon, M. A.; Berkland, C. J. Practical Considerations, Challenges, and Limitations of Bioconjugation via Azide–Alkyne Cycloaddition. *Bioconjugate Chem.* **2018**, *29* (3), 686–701. DOI: 10.1021/acs.bioconjchem.7b00633.

(15) Nebhani, L.; Barner-Kowollik, C. Orthogonal Transformations on Solid Substrates: Efficient Avenues to Surface Modification. *Adv. Mater.* **2009**, *21* (34), 3442–3468. DOI: 10.1002/adma.200900238.

(16) Durmaz, H.; Colakoglu, B.; Tunca, U.; Hizal, G. Preparation of Block Copolymers via Diels Alder Reaction of Maleimide- and Anthracene-End Functionalized Polymers: Preparation of Block Copolymers. *J. Polym. Sci. A Polym. Chem.* **2006**, *44* (5), 1667–1675. DOI: 10.1002/pola.21275.

(17) Gacal, B.; Durmaz, H.; Tasdelen, M. A.; Hizal, G.; Tunca, U.; Yagci, Y.; Demirel, A. L. Anthracene−Maleimide-Based Diels−Alder "Click Chemistry" as a Novel Route to Graft Copolymers. *Macromolecules* **2006**, *39* (16), 5330–5336. DOI: 10.1021/ma060690c.

(18) Hansell, C. F.; Espeel, P.; Stamenović, M. M.; Barker, I. A.; Dove, A. P.; Du Prez, F. E.; O'Reilly, R. K. Additive-Free Clicking for Polymer Functionalization and Coupling by Tetrazine–Norbornene Chemistry. *J. Am. Chem. Soc.* **2011**, *133* (35), 13828–13831. DOI: 10.1021/ja203957h.

(19) Liu, Y.-L.; Chuo, T.-W. Self-Healing Polymers Based on Thermally Reversible Diels–Alder Chemistry. *Polym. Chem.* **2013**, *4* (7), 2194. DOI: 10.1039/c2py20957h.

(20) Murphy, E. B.; Bolanos, E.; Schaffner-Hamann, C.; Wudl, F.; Nutt, S. R.; Auad, M. L. Synthesis and Characterization of a Single-Component Thermally Remendable Polymer Network: Staudinger and Stille Revisited. *Macromolecules* **2008**, *41* (14), 5203–5209. DOI: 10.1021/ma800432g.

(21) St. Amant, A. H.; Huang, F.; Lin, J.; Rickert, K.; Oganesyan, V.; Lemen, D.; Mao, S.; Harper, J.; Marelli, M.; Wu, H.; Gao, C.; Read de Alaniz, J.; Christie, R. J. A Diene-Containing Noncanonical Amino Acid Enables Dual Functionality in Proteins: Rapid Diels–Alder Reaction with Maleimide or Proximity-Based Dimerization. *Angew. Chem. Int. Ed.* **2019**, *58* (25), 8489–8493. DOI: 10.1002/anie.201903494.

(22) Tasdelen, M. A. Diels–Alder "Click" Reactions: Recent Applications in Polymer and Material Science. *Polym. Chem.* **2011**, *2* (10), 2133. DOI: 10.1039/c1py00041a.

(23) Billiet, S.; De Bruycker, K.; Driessen, F.; Goossens, H.; Van Speybroeck, V.; Winne, J. M.; Du Prez, F. E. Triazolinediones Enable Ultrafast and Reversible Click Chemistry for the Design of Dynamic Polymer Systems. *Nat. Chem.* **2014**, *6* (9), 815–821. DOI: 10.1038/nchem.2023.

(24) Sauer, J.; Lang, D.; Mielert, A. The Order of Reactivity of Dienes towards Maleic Anhydride in the Diels-Alder Reaction. *Angew. Chem. Int. Ed. Engl.* **1962**, *1* (5), 268–269. DOI: 10.1002/anie.196202683.

(25) Wilson, P. J.; Wells, J. H. The Chemistry and Utilization of Cyclopentadiene. *Chem. Rev.* **1944**, *34* (1), 1–50. DOI: 10.1021/cr60107a001.

(26) Yameen, B.; Rodriguez-Emmenegger, C.; Preuss, C. M.; Pop-Georgievski, O.; Verveniotis, E.; Trouillet, V.; Rezek, B.; Barner-Kowollik, C. A Facile Avenue to Conductive Polymer Brushes via Cyclopentadiene–Maleimide Diels–Alder Ligation. *Chem. Commun.* **2013**, *49* (77), 8623. DOI: 10.1039/c3cc44683b.

(27) Inglis, A. J.; Sinnwell, S.; Stenzel, M. H.; Barner-Kowollik, C. Ultrafast Click Conjugation of Macromolecular Building Blocks at Ambient Temperature. *Angew. Chem. Int. Ed.* **2009**, *48* (13), 2411–2414. DOI: 10.1002/anie.200805993.

(28) Yameen, B.; Zydziak, N.; Weidner, S. M.; Bruns, M.; Barner-Kowollik, C. Conducting Polymer/SWCNTs Modular Hybrid Materials via Diels–Alder Ligation. *Macromolecules* **2013**, *46* (7), 2606–2615. DOI: 10.1021/ma4004055.

(29) Schenzel, A. M.; Moszner, N.; Barner-Kowollik, C. Self-Reporting Dynamic Covalent Polycarbonate Networks. *Polym. Chem.* **2017**, *8* (2), 414–420. DOI: 10.1039/C6PY01840H.

(30) Nebhani, L.; Barner-Kowollik, C. Functionalization of Fullerenes with Cyclopentadienyl and Anthracenyl Capped Polymeric Building Blocks via Diels-Alder Chemistry. *Macromol. Rapid Commun.* **2010**, *31* (14), 1298–1305. DOI: 10.1002/marc.201000142.

(31) Zydziak, N.; Hübner, C.; Bruns, M.; Barner-Kowollik, C. One-Step Functionalization of Single-Walled Carbon Nanotubes (SWCNTs) with Cyclopentadienyl-Capped Macromolecules via Diels−Alder Chemistry. *Macromolecules* **2011**, *44* (9), 3374–3380. DOI: 10.1021/ma200107z.

(32) Toncelli, C.; Bouwhuis, S.; Broekhuis, A. A.; Picchioni, F. Cyclopentadiene-Functionalized Polyketone as Self-Cross-Linking Thermo-Reversible Thermoset with Increased Softening Temperature. *J. Appl. Polym. Sci.* **2016**, *133* (4), n/a-n/a. DOI: 10.1002/app.42924.

(33) Kennedy, J. P.; Castner, K. F. Synthesis of Substituted Cyclopentadienes and Cyclopentadiene-Functionalized Polymers. US4138441A, February 6, 1979.

(34) Hughes, R. P.; Trujillo, H. A. Selective Solubility of Organometallic Complexes in Saturated Fluorocarbons. Synthesis of Cyclopentadienyl Ligands with Fluorinated Ponytails. *Organometallics* **1996**, *15* (1), 286–294. DOI: 10.1021/om9507540.

(35) Inglis, A. J.; Paulöhrl, T.; Barner-Kowollik, C. Ambient Temperature Synthesis of a Versatile Macromolecular Building Block: Cyclopentadienyl-Capped Polymers. *Macromolecules* **2010**, *43* (1), 33–36. DOI: 10.1021/ma902464a.

(36) Gonzalez, A.; Holt, S. L. Effect of Microemulsions on the Diels-Alder Reaction: Endo/Exo Ratios in the Reaction of Cyclopentadiene and Methyl Methacrylate. *J. Org. Chem.* **1982**, *47* (16), 3186–3188. DOI: 10.1021/jo00137a037.

(37) Pilgrim, B. S.; Roberts, D. A.; Lohr, T. G.; Ronson, T. K.; Nitschke, J. R. Signal Transduction in a Covalent Post-Assembly Modification Cascade. *Nat. Chem.* **2017**, *9* (12), 1276–1281. DOI: 10.1038/nchem.2839.

(38) Dalkılıç, E.; Daştan, A. Synthesis of Cyclopentadiene Derivatives by Retro-Diels–Alder Reaction of Norbornadiene Derivatives. *Tetrahedron* **2015**, *71* (13), 1966–1970. DOI: 10.1016/j.tet.2015.02.023.

(39) Dalkılıç, E.; Güney, M.; Daştan, A.; Saracoglu, N.; Lucchi, O. D.; Fabris, F. Novel and Versatile Protocol for the Preparation of Functionalized Benzocyclotrimers. *Tetrahedron Lett.* **2009**, *50* (17), 1989–1991. DOI: 10.1016/j.tetlet.2009.02.070.

(40) Khoury, P. R.; Goddard, J. D.; Tam, W. Ring Strain Energies: Substituted Rings, Norbornanes, Norbornenes and Norbornadienes. *Tetrahedron* **2004**, *60* (37), 8103–8112. DOI: 10.1016/j.tet.2004.06.100.

(41) Sauer, J.; Heinrichs, G. Kinetik und umsetzungen von 1.2.4.5-tetrazinen mit winkelgespannten und elektronenreichen doppelbindungen. *Tetrahedron Lett.* **1966**, *7* (41), 4979–4984. DOI: 10.1016/S0040-4039(00)90312-5.

(42) Wilson, W. S.; Warrener, R. N. A Mild Retro-[Π4s+π2s] Cleavage Route to Furans and Fulvenes. *J. Chem. Soc., Chem. Commun.* **1972**, No. 4, 211–212. DOI: 10.1039/C39720000211.

(43) Barlow, M. G.; Haszeldine, R. N.; Pickett, J. A. Heterocyclic Polyfluoro-Compounds. Part 26. Synthesis of 3,6-Bis-Trifluoromethyl-Pyridazines and -Dihydropyridazines. *J. Chem. Soc., Perkin Trans. 1* **1978**, No. 4, 378. DOI: 10.1039/p19780000378.

(44) Oxtoby, N. S.; Blake, A. J.; Champness, N. R.; Wilson, C. Structural Influence of Cis and Trans Coordination Modes of Multi-Modal Ligands upon Coordination Polymer Dimensionality. *Dalton Trans.* **2003**, No. 20, 3838. DOI: 10.1039/b310754j.

(45) Tuktarov, A. R.; Akhmetov, A. R.; Khuzin, A. A.; Dzhemilev, U. M. Synthesis and Properties of Energy-Rich Methanofullerenes Containing Norbornadiene and Quadricyclane Moieties. *J. Org. Chem.* **2018**, *83* (7), 4160–4166. DOI: 10.1021/acs.joc.8b00119.

(46) Tanyeli, C.; Çelikel, G.; Akhmedov, İ. M. Resolution of (±)-2-Substituted Norbornadiene and Hexachloronorbornadiene Derivatives Using CCL and PLE. *Tetrahedron: Asymmetry* **2001**, *12* (16), 2305–2308. DOI: 10.1016/S0957-4166(01)00413-X.

(47) Alupei, V.; Choi, S. W.; Alupei, I. C.; Ritter, H. Forgotten Monomers: Free Radical Polymerization Behavior of Norbornadiene Derivatives in Comparison with Methyl Methacrylate. *Polymer* **2004**, *45* (7), 2111–2117. DOI: 10.1016/j.polymer.2004.01.056.

(48) Muehlebach, A.; Rime, F. Synthesis of Well-Defined Macromonomers and Comb Copolymers from Polymers Made by Atom Transfer Radical Polymerization. *J. Polym. Sci. A Polym. Chem.* **2003**, *41* (21), 3425–3439. DOI: 10.1002/pola.10940.

(49) Yang, W.; Kaneko, T.; Liu, X.-Y.; Chen, M.-Q.; Akashi, M. Bulk Synthesis of Poly(*Tert* -Butyl Methacrylate) Long Macromonomer with Narrow Distribution by Atom Transfer Radical Polymerization and Nucleophilic Substitution. *Chem. Lett.* **2006**, *35* (2), 222–223. DOI: 10.1246/cl.2006.222.

(50) Anastasaki, A.; Nikolaou, V.; Zhang, Q.; Burns, J.; Samanta, S. R.; Waldron, C.; Haddleton, A. J.; McHale, R.; Fox, D.; Percec, V.; Wilson, P.; Haddleton, D. M. Copper(II)/Tertiary Amine Synergy in Photoinduced Living Radical Polymerization: Accelerated Synthesis of ω-Functional and α,ω-Heterofunctional Poly(Acrylates). *J. Am. Chem. Soc.* **2014**, *136* (3), 1141–1149. DOI: 10.1021/ja411780m.

(51) Discekici, E. H.; Anastasaki, A.; Read de Alaniz, J.; Hawker, C. J. Evolution and Future Directions of Metal-Free Atom Transfer Radical Polymerization. *Macromolecules* **2018**, *51* (19), 7421–7434. DOI: 10.1021/acs.macromol.8b01401.

(52) Barbon, S. M.; Rolland, M.; Anastasaki, A.; Truong, N. P.; Schulze, M. W.; Bates, C. M.; Hawker, C. J. Macrocyclic Side-Chain Monomers for Photoinduced ATRP: Synthesis and Properties versus Long-Chain Linear Isomers. *Macromolecules* **2018**, *51* (17), 6901–6910. DOI: 10.1021/acs.macromol.8b01509.

(53) Discekici, E. H.; Anastasaki, A.; Kaminker, R.; Willenbacher, J.; Truong, N. P.; Fleischmann, C.; Oschmann, B.; Lunn, D. J.; Read de Alaniz, J.; Davis, T. P.; Bates, C. M.; Hawker, C. J. Light-Mediated Atom Transfer Radical Polymerization of Semi-Fluorinated (Meth)Acrylates: Facile Access to Functional Materials. *J. Am. Chem. Soc.* **2017**, *139* (16), 5939–5945. DOI: 10.1021/jacs.7b01694.

(54) St. Amant, A. H.; Huang, F.; Lin, J.; Lemen, D.; Chakiath, C.; Mao, S.; Fazenbaker, C.; Zhong, H.; Harper, J.; Xu, W.; Patel, N.; Adams, L.; Vijayakrishnan, B.; Howard, P. W.; Marelli, M.; Wu, H.; Gao, C.; Read de Alaniz, J.; Christie, R. J. A Reactive Antibody Platform for One-Step Production of Antibody–Drug Conjugates through a Diels–Alder Reaction with Maleimide. *Bioconjugate Chem.* **2019**, *30* (9), 2340–2348. DOI: 10.1021/acs.bioconjchem.9b00436.

(55) St. Amant, A. H.; Lemen, D.; Florinas, S.; Mao, S.; Fazenbaker, C.; Zhong, H.; Wu, H.; Gao, C.; Christie, R. J.; Read de Alaniz, J. Tuning the Diels–Alder Reaction for Bioconjugation to Maleimide Drug-Linkers. *Bioconjugate Chem.* **2018**, *29* (7), 2406–2414. DOI: 10.1021/acs.bioconjchem.8b00320.

(56) Discekici, E. H.; St. Amant, A. H.; Nguyen, S. N.; Lee, I.-H.; Hawker, C. J.; Read de Alaniz, J. *Endo* and *Exo* Diels–Alder Adducts: Temperature-Tunable Building Blocks for Selective Chemical Functionalization. *J. Am. Chem. Soc.* **2018**, *140* (15), 5009–5013. DOI: 10.1021/jacs.8b01544.

(57) Mantovani, G.; Lecolley, F.; Tao, L.; Haddleton, D. M.; Clerx, J.; Cornelissen, J. J. L. M.; Velonia, K. Design and Synthesis of *N* -Maleimido-Functionalized Hydrophilic Polymers via Copper-Mediated Living Radical Polymerization: A Suitable Alternative to PEGylation Chemistry. *J. Am. Chem. Soc.* **2005**, *127* (9), 2966–2973. DOI: 10.1021/ja0430999.

(58) Houseman, B. T.; Gawalt, E. S.; Mrksich, M. Maleimide-Functionalized Self-Assembled Monolayers for the Preparation of Peptide and Carbohydrate Biochips. *Langmuir* **2003**, *19* (5), 1522–1531. DOI: 10.1021/la0262304.

(59) Theriot, J. C.; Lim, C.-H.; Yang, H.; Ryan, M. D.; Musgrave, C. B.; Miyake, G. M. Organocatalyzed Atom Transfer Radical Polymerization Driven by Visible Light. *Science* **2016**, *352* (6289), 1082–1086. DOI: 10.1126/science.aaf3935.

3 Chapter 3: *Shining Light on Cyclopentadienone–Norbornadiene Diels–Alder Adducts to Enable Photoinduced Click Chemistry with Cyclopentadiene*

Building upon the success of on-demand click chemistry presented in Chapter 2, this chapter introduces a new Cp precursor that is, *excitingly*, photo-triggered. Encouraged by the facile access to Cp through the chemically triggered norbornadiene–tetrazine cascade utilized in my first project, I identified cyclopentadienone–norbornadiene (CPD–NBD) adducts as potential Cp precursors which could undergo a similar cascade to unveil Cp in response to an external trigger. In contrast to our first strategy which relies on the rapid, thermally induced DA cascade from norbornadiene–tetrazine adducts to afford Cp based building blocks – the selectivity and efficiency of the photo-induced cascade from CPD–NBD enables spatiotemporally controlled unmasking of Cp for in situ or post-irradiation click chemistry with dienophiles. Sections of this chapter were originally published in *ACS Applied Materials & Interfaces*. Reprinted with permission from *ACS Appl. Mater. Interfaces* **2021**, *13*(30), 35422–35430. DOI: 10.1021/acsami.1c08670. Copyright 2021 American Chemical Society.

3.1 Abstract

A new Diels–Alder (DA)-based photopatterning platform is presented, which exploits the irreversible, light-induced decarbonylation and subsequent cleavage of cyclopentadienone–norbornadiene (CPD–NBD) adducts. A series of CPD–NBD adducts have been prepared and systematically studied toward the use in a polymeric material photopatterning platform. By incorporating an optimized CPD–NBD adduct into polymer networks, it is demonstrated that cyclopentadiene may be unveiled upon 365 nm irradiation and subsequently clicked to a variety of maleimides with spatial control under mild reaction conditions and with fast kinetics. Unlike currently available photoinduced Diels–Alder reactions that rely on trapping transient,

photocaged dienes, this platform introduces a persistent, yet highly reactive diene after irradiation, enabling the use of photosensitive species such as cyanine dyes to be patterned. To highlight the potential use of this platform in a variety of material applications, we demonstrate two proof-of-concepts: patterned conjugation of multiple dyes into a polyacrylate network and preprogrammed ligation of streptavidin into poly(ethylene glycol) hydrogels.

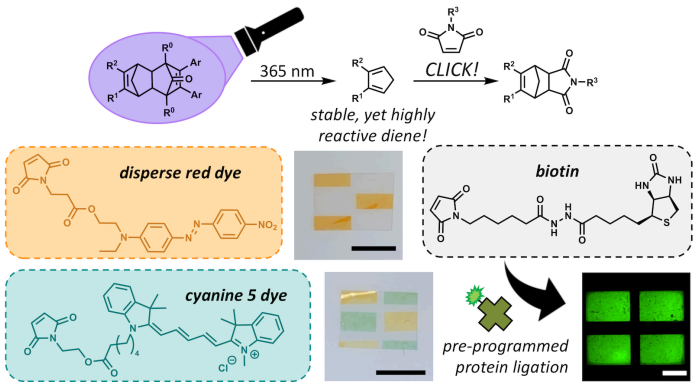

Figure 3.1. Graphical Abstract. The light-induced deprotection of a stable, yet highly reactive diene for Diels–Alder chemistry enables spatially controlled click reactions in polymer networks.

3.2 Introduction

The well-defined incorporation of functional molecules into polymer networks is an attractive endeavor with promise throughout materials science. In regard to bio-materials, the introduction of biologically relevant small molecules and proteins within synthetic hydrogels has numerous applications including adhesion,[1] drug delivery,[2] and tissue engineering.[3] Whereas, in the field of smart materials, a multitude of stimuli responsive molecules have been exploited within polymer networks such as liquid crystals,[4] photo-thermal agents,[5] and photoswitches.[6,7] Introducing these agents into polymer networks typically relies on non-covalent blending or the use of functionalized monomers; both resulting in bulk incorporation throughout the network. Of particular interest, however, is high resolution spatial control over

chemical functionalization, offering significant advantages in the microfabrication of materials varying from sequentially responsive actuators[8–10] to patterned cell microenvironments.[11–13] Successful preparation of these materials is dependent on identifying chemistries that offer spatial control while remaining highly efficient, mild and compatible with numerous functionalities and biological systems.

Diels–Alder (DA) cycloadditions are a distinguished click chemistry[14] that have been extensively employed throughout organic synthesis, materials science and bioconjugation. Unlike other common click chemistries, such as the copper(I)-catalyzed alkyne–azide cycloaddition,[15] thiol–Michael[16] or thiol–ene[17] which rely on toxic copper catalysis, additives, or radicals, DA cycloadditions offer a mild, additive-free approach while maintaining high efficiency, tunable kinetics, functional group tolerance and bio-orthogonality. In polymer chemistry, DA cycloadditions have served as the basis of a number of block co-polymer "click" reactions,[18–23] and the reversibility of the DA reaction has served as a platform for the preparation of thermally re-mendable polymer networks.[24–26] Within bio-materials, the fast and bio-orthogonal nature of the inverse electron demand Diels–Alder (IEDDA) cycloaddition has led to the development of a new bioconjugation platform[27] and numerous approaches to protein modification through IEDDA.[28] Normal-demand DA cycloadditions have also been successfully demonstrated in biological systems by developing strategies to enable the use of more reactive diene and dienophile partners for the preparation of antibody–drug conjugates,[29,30] and rapid 3D cell encapsulation.[31]

Given the highly efficient, mild and additive free nature of DA cycloadditions, efforts have been made to further extend the utility of these reactions through temporal and spatial control. The development of photo-caged dienes has offered significant advances in obtaining such

control in materials systems. The photo-enolization of *o*-substituted benzophenones was first presented in 1961,[32] and the use of such photocaged dienes was introduced to polymer chemistry by Meador et al. in 1996 (**Figure 3.2a**).[33] More recently, photo-enolization of *o*-methylbenzaldehydes (*o*-MBAs) to *o*-quinodimethanes (*o*-QDMs) has been employed in a number of DA systems by Barner-Kowollik and coworkers, including the click coupling of block copolymers[34,35] and the functionalization of (bio)surfaces.[36–38] In addition, the photochemical dehydration of 3-hydroxy-2-naphthalenemethanol derivatives has offered an alternative route to highly reactive diene intermediates.[39] Additionally, photogenerated dienophiles have also been investigated for block copolymer synthesis[40] and surface functionalization by photolysis of phenacyl sulfides followed by hetero-DA reactions.[41] Light has also been used to "gate" the reversibility of the DA reaction through the use of dithienylethene and dithienylfuran photoswitching systems.[42,43] The disadvantage to the currently available photogenerated diene systems, however, is the short lifetimes of the diene intermediates, requiring the in situ trapping with a dienophile. Because UV light is required for the photodeprotection in these systems,[34–39,41] in situ trapping is not compatible with photosensitive moieties or absorbing species required for many stimuli-responsive and biologically relevant applications. We therefore anticipate that developing an effective and efficient synthetic protocol to access highly reactive yet persistent dienes within materials will be vital to expand the potential applications of photo-induced DA cycloadditions. Importantly, the success of this goal will add to the tool-box of so called "photoclick" reactions[44] and will provide a complementary approach to existing methods for enabling functionalization of advanced materials with temporal and spatial control.

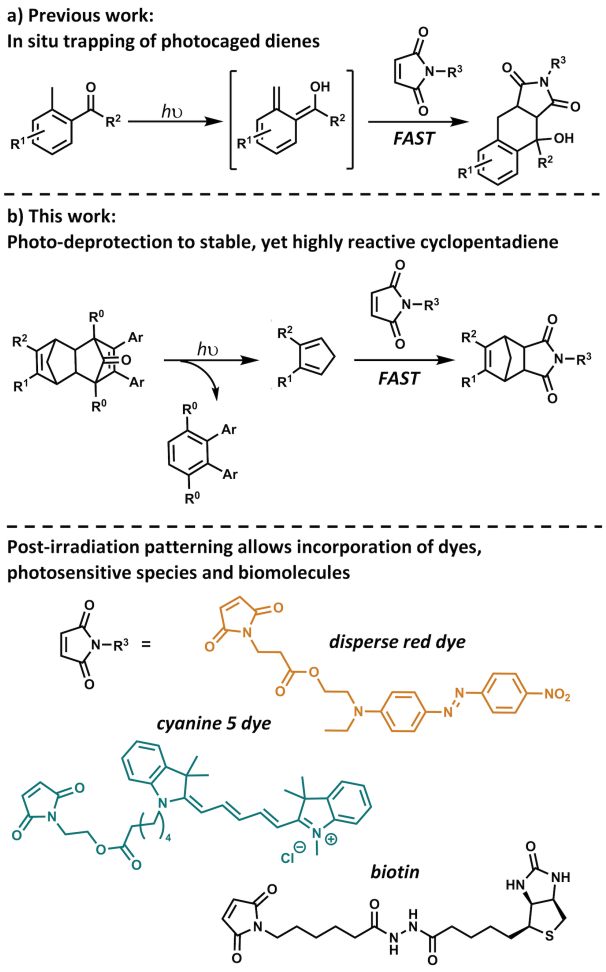

Figure 3.2. a) Traditional photocaged dienes can be photo-activated and undergo an in situ DA click reaction. b) The photo-triggered cleavage of norbornadiene-cyclopentadienone adducts to cyclopentadiene allows for either in situ or post irradiation DA click reaction with a variety of functional maleimides.

Over the recent years our group has become interested in cyclopentadiene for its reported high reactivity[45] and exploitation in polymer click reactions.[25,19,46,47] To expand the utility of this diene, we have sought to develop methods to harness the high reactivity to enable efficient bioconjugation[29] and controlled polymer click reactions.[22,48] Prompted by our recent utilization of norbornadiene functionalized polymers as a chemically triggered precursor to Cp;[22,48] we targeted the development of a photo-triggered platform which would offer spatiotemporal

control over the introduction of these highly reactive units. Inspired by reports of the photo- or thermally induced loss of carbon monoxide from bridged cyclopentadienone—norbornadiene (CPD–NBD) Diels–Alder adducts,[49–52] we envisioned that the resulting retro–DA cleavage could be exploited to obtain cyclopentadiene on demand. CPD–alkene adducts have been utilized extensively for the preparation substituted benzenes,[53,54] and have recently been employed in the preparation of CO releasing pro-drugs.[55,56] Notably, the photo-decarbonylation of CPD–maleimide adducts has been utilized to pattern surfaces with nonmodified peptides by utilizing a photo-activated triphenylene imide that is susceptible to ring opening by amines.[37] The disadvantage of this clever approach, however, is the necessity for significant excess of amine groups to achieve the imide ring opening and subsequent patterning. Irradiation of CPD–NBD adducts, on the other hand, would produce a highly reactive Cp species which readily reacts with dienophiles.[45] Furthermore, in contrast to current photo-induced Diels–Alder reactions which produce a transient diene, the loss of CO and formation of thermodynamically stable aromatic byproduct results in an irreversible reaction, allowing for the persistence of stable Cp units in the material until treatment with the dienophile of choice. A similar approach is taken in the irreversible photochemical activation of tetrazole for nitrile imine mediated tetrazole–ene cycloaddition (NITEC), which readily reacts with dipolarophiles.[57,58] The irreversible nature of NITEC has been demonstrated to provide much higher surface graft densities than the more transient *o*-MBA photoactivation to *o*-QDM.[59] In addition, although Cp is a highly reactive diene that can dimerize over extended storage,[22,60] it is inherently more stable than nitrile imines,[61] offering a persistent species after the cessation of irradiation. This unique feature would enable functionalization with a number of photosensitive species, as the spatially controlled Diels–Alder reaction could take place post-irradiation. Moreover, this

approach would also be amenable to in situ functionalization with maleimides that are stable to 365 nm irradiation, thus complementing existing approaches.

Herein, we report the use of such CPD–NBD adducts within polymer networks as photo-labile Cp precursors (**Figure 3.2b**) for subsequent DA-based patterning of dyes and biomolecules. We first present a comparative study investigating the synthesis, thermal stability, and photo induced Cp production from a series of CPD–NBD adducts; the results of this study provide an optimal candidate for utilization in patterning a variety of materials. We then outline two proof-of-concept photo-click demonstrations with maleimide bearing molecules – biotin and two common dyes – that highlight the potential use of this platform in bio- or stimuli- responsive materials.

3.3 Results and Discussion

3.3.1 Identification of the Optimal CPD–NBD Adduct

3.3.1.1 Efficiency of DA with Cyclopentadienone

For utilization in various polymeric materials systems, we sought to design a CPD–NBD adduct that could be prepared easily and in high yields from either commercially available or highly scalable starting materials. For this reason we chose to explore the Diels–Alder reaction with our previously reported, highly scalable NBD derivative Pe-NBD-OH[22,48] and three commercially available cyclopentadienones (CPD): tetraphenylcyclopentadienone (Ph-CPD), 2,5-dimethyl-3,4-diphenylcyclopentadienone (Me-CPD), and the fused analog to Ph-CPD, 1,3-diphenylcyclopenta[l]phenanthren-2-one (B-CPD). To investigate the efficiency of the initial DA reaction, each of the CPD derivatives (1.3 eq) were heated with Pe-NBD-OH (1.0 eq, 0.5 M in toluene) at 70 °C. After 21 h ^{1}H NMR of the crude reaction mixtures indicated

the formation of Ph-NBD–CPD, Me-CPD–NBD and B-CPD–NBD to be 7%, 16% and >98%; respectively. From this series, B-CPD proved to be an excellent candidate as the DA is observed to be near quantitative. Presumably, the increase in aromaticity upon formation of a phenanthrene subunit within the fused ring system of B-CPD–NBD helped improve the efficiency of this reaction. Furthermore, we believe sterics might also play a role; Me-CPD and B-CPD, which both have reduced steric hinderance in comparison to the Ph-CPD analog, were expected to undergo a more efficient cycloaddition with NBD. Of note, Me-CPD – which exists as a dimer[53] – required increased temperatures to promote the initial rDA between monomers and could be responsible for the lower yield of this derivative.

In an effort to improve yields of all adducts so comparative studies could be conducted, separate optimized reaction conditions were identified for each CPD derivative. Heating Pe-NBD-OH at 75 °C with Ph-CPD (2.0 eq) in chloroform for 5 days, followed by removal of excess Ph-CPD through a plug of silica followed by crystallization from hexane afforded the product Ph-CPD–NBD in a modest 33% yield. In an attempt to further increase conversion and reduce reaction time, the reaction temperature was increased to 85 °C. Thin-layer chromatography (TLC) of this reaction, however, indicated the formation of a non-polar byproduct indicative of an unwanted thermal decarbonylation and cleavage to the substituted benzene. Similar challenges were observed for the preparation of Me-CPD–NBD when the reaction temperature was increased in an effort to promote the retro-DA between Me-CPD dimers. Again, as observed with the Ph-CPD–NBD adduct, increased reaction temperature resulted in a non-polar byproduct, indicating thermal decomposition of Me-CPD–NBD. Thermal decomposition of these adducts was further confirmed by ^{1}H NMR spectroscopy of the isolated non-polar byproducts, indicating the production of Ph-benzene and Me-benzene.

Despite these challenges, optimized conditions – heating Pe-NBD-OH at 85 °C with Me-CPD (1.5 eq) in toluene for 24 h – improved the overall yield of Me-CPD-NBD from 17% to 42%. Additionally, the purposeful thermal decomposition of Ph-CPD–NBD and Me-CPD–NBD by refluxing in toluene as described in the Supplementary Information provided an efficient route to the substituted benzenes for subsequent UV-vis studies. Finally, it was found that the equivalents of B-CPD and reaction time could be reduced to 1.1 and 18 h, respectively. This optimized procedure afforded B-CPD–NBD in 81% yield and only required filtration of the reaction mixture to obtain purified material. Optimized reaction conditions and isolated yields for the three adducts are reported in **Figure 3.3a** and full synthetic details for each compound can be found in the Supplementary Information.

3.3.1.2 Thermal Stability of CPD–NBD Adducts

For the desired application of these adducts in photo-patterning, the competing thermal decarbonylation of CPD–NBD adducts[49,52] must be avoided as it could result in non-selective, off target DA reactions with maleimides. Furthermore, adduct stability would directly impact the long-term storage of these materials before patterning or the ability to invoke additional processing steps. Our initial investigation into the synthesis of these three adducts indicated that for Ph-CPD–NBD and Me-CPD–NBD, the thermal stabilities were relatively low as byproducts were observed upon prolonged heating in solution at 85 °C. To systematically compare the thermal stability of the three adducts thermo-gravimetric analysis (TGA) coupled with evolved gas analysis (EGA) by mass spectrometry was used. For Ph-CPD–NBD and Me-CPD–NBD, the adducts are shown to undergo thermal decomposition around 170 °C (**Figure 3.3b**); however, CO detection is observed starting at 156 °C and 152 °C for the two adducts,

respectively (**Figure S3.27–3.28**). Notably, B-CPD–NBD shows significantly improved thermal stability requiring an additional 50 °C for CO release (**Figure 3.3b**). This is in good agreement with literary reports of heating such fused adducts,[49,62] although thorough thermal analysis have not been reported.

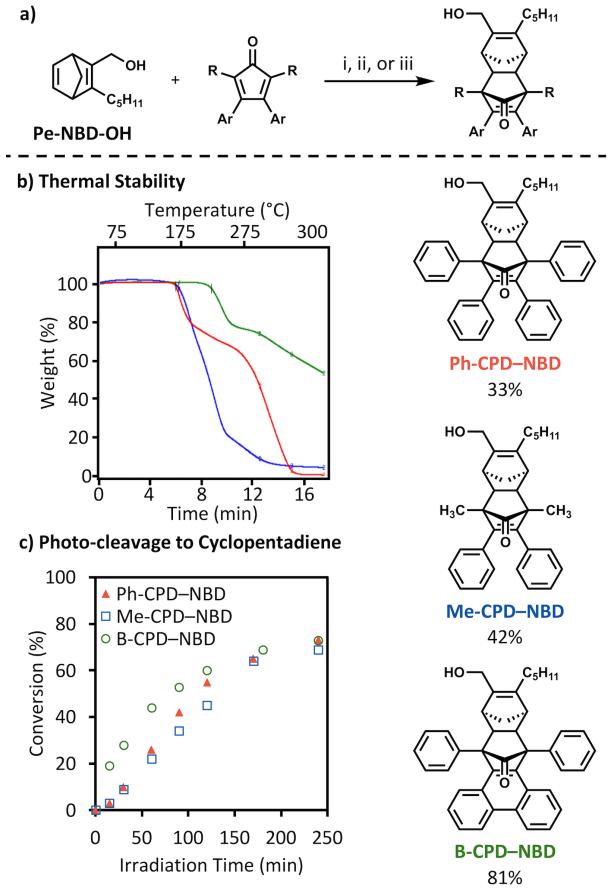

Figure 3.3. a) i) Ph-CPD (2.0 eq), chloroform, 75 °C, 5 d, 33% yield of Ph-CPD–NBD ii) Me-CPD (1.5 eq), toluene, 85 °C, 24 h, 42% yield of Me-CPD–NBD iii) B-CPD (1.1 eq), toluene, 70 °C, 18 h, 81% yield of B-CPD–NBD b) Thermo-gravimetric analysis of Ph-CPD–NBD (red trace), B-CPD–NBD (green trace), and Me-CPD–NBD (blue trace) at ramp of 20 °C/min from room temperature to 300 °C. c) Conversion to Cp upon irradiation of 25 mM solution of each adduct at 300 nm determined by ^{1}H NMR over 240 min.

3.3.1.3 Photo-Decarbonylation Studies

To probe the viability of each CPD–NBD adduct as a photo-labile Cp precursor, 25 μM solutions of each adduct were prepared and monitored by ^{1}H NMR while irradiated in a Rayonet RPR-200 chamber (300 nm). Irradiation was performed directly in sealed, nitrogen-sparged NMR tubes to avoid the formation of oxidized byproducts.[51,52] The initial rate of Cp production was highest for B-CPD–NBD, although a notable reduction in rate is observed over the course of the reaction (**Figure 3.3c**). This was attributed to the increase in absorbance of the fused ring system of the liberated B-benzene byproduct leading to product inhibition. This was confirmed by UV Vis spectroscopy which revealed an increase in molar absorptivity at 300 nm from 9100 $M^{-1}cm^{-1}$ of B-CPD–NBD to 27000 $M^{-1}cm^{-1}$ of B benzene (**Table 3.1**, **Figure S3.40–S3.42**). Additionally, irradiation of 25 μM B-CPD-NBD solutions doped with either 0.2 eq or 0.5 eq of B-benzene slowed the rate of photo-decarbonylation (**Figure S3.33**) further corroborating our assumption. It is possible that shorter wavelengths might offer a solution to the observed product inhibition, but the increased likelihood of degradation and the desire to present a mild patterning platform motivated us to move forward with long-wave UV irradiation.

To quantify the efficiency of the photo-induced production of cyclopentadiene from the three CPD–NBD adducts, quantum yields were determined at low conversions (<15%). In agreement with the initial monitoring study, the quantum yield of B-CPD-NBD was twice that of the two non-fused derivatives (**Table 3.1,** entry 3). In spite of the minor product inhibition observed at 300 nm for B-CPD–NBD, we were pleased to see significant liberation of Cp upon irradiation and encouraged by its facile synthesis and superior thermal stability. This adduct

was taken forward in two polymer networks to demonstrate its potential as a photopatterning platform via spatially controlled diene liberation and subsequent DA reactions.

Table 3.1. Photophysical properties of adducts and substituted benzene byproducts

	$\varepsilon_{max,\ 212\ nm}$ ($M^{-1}\ cm^{-1}$)	$\varepsilon_{300\ nm}$ ($M^{-1}\ cm^{-1}$)	Φ (%)
Ph-CPD–NBD	120000	7800	2.8 ± 0.4
Me-CPD–NBD	19000	2200	2.5 ± 0.3
B-CPD–NBD	39000	9100	5.3 ± 0.8
Ph-benzene	100000	1900	–
Me-benzene	20000	180	–
B-benzene	59000	27000	–

3.3.2 Preparation and Patterning of Polymer Networks

3.3.2.1 Preparation of Polyacrylate Networks

To highlight the potential of this photo-induced cleavage as a patterning platform, we first sought to incorporate the adduct using a traditional acrylate free radical polymerization. An acrylate monomer was prepared from B-CPD–NBD in one step (**Figure 3.4a**). Drawing from photopolymerization methods used to construct thin networks, glass cells were prepared of 50 μm thickness and infiltrated with a neat monomer mixture of B-CPD–NBD acrylate, butyl acrylate and 1,4-butanediol diacrylate. The visible light photoinitator, phenylbis(2,4,6-trimethylbenzoyl)phosphine oxide (BAPO), was employed to allow for photopolymerization at 405 nm and avoid unwanted decarbonylation of the incorporated CPD-NBD adducts during network formation. After photo-polymerization, the poly(butyl acrylate) (PBA) films were removed from the glass cells and taken forward in patterning studies. A second type of PBA

network was also prepared using Diels–Alder chemistry to crosslink tetra-PBA polymers, which also exhibited successful patterning (**Figure S3.49**).

3.3.2.2 Decarbonylation within Polymer Networks

We reasoned that the detection of carbon monoxide during irradiation of polymer thin films would offer a facile approximation of conversion. Numerous methods exist for the efficient detection of CO, particularly from the field of therapeutic CO-releasing systems.[55,63–65] Inspired by the use of commercially available CO detectors by several groups,[64,65] a small closed system equipped with a CO sensor purchased from SPEC sensors was prepared (Product No. 110-102, **Figure S3.50**). This simple CO detector allowed for the monitoring CO production in neat samples of B-CPD–NBD (**Figure S3.51**), or within polymer networks (**Figure 3.4b**). Similar to the ^{1}H NMR study demonstrated in Figure 1c, the initial rate slows due to product inhibition by B-benzene, and after 240 minutes of irradiation the concentration of CO remains constant. With this in mind, subsequent patterning studies were irradiated between 30–240 min before treatment with the desired maleimide and assumed to result in 50–70% conversion followed by near quantitative clicking to the maleimide of choice. These irradiation times are comparable to the 3 h irradiation reported for the photo-decarbonylation of CPD–maleimide adducts,[37] and presumably could be shortened to cytocompatible light doses (<10 min)[66] if complete photo-deprotection is not necessary.

3.3.2.3 Poly(butyl acrylate) Network Patterning with Dyes

Selective photo-induced liberation of Cp was visually confirmed by irradiating the networks with a collimated LED (Thorlabs, 365 nm, 6.1 mW/cm^2) through a simple quartz photomask (**Figure 3.4d**), then swelling in solutions of dichloromethane (DCM) containing

maleimide-dyes. Of note, efficient patterning is observed using long-range UV light (365 nm) and irradiation of films performed in air provided qualitatively similar results in dye pattern compared to irradiation of films in a vessel purged nitrogen (**Figure S3.53**). Although quantification of possible oxidized byproducts[51,52] could not be performed in the thin film, successful patterning without the exclusion of oxygen indicated minimal interference of these byproducts and prompted subsequent patterning studies to be performed using 365 nm irradiation and open to air to highlight the synthetic ease and mild nature of this patterning platform. Additionally, due to the incorporation of a persistent diene into the resulting polymer network, patterning did not require in situ trapping or immediate post-treatment with a maleimide; in fact, successful dye conjugation could be achieved by treating the materials with maleimides several hours post-irradiation. We predict patterning could be achieved with longer gaps between irradiation and maleimide treatment but did not investigate longer time scales as to avoid the potential of cyclopentadiene dimerization within the network.

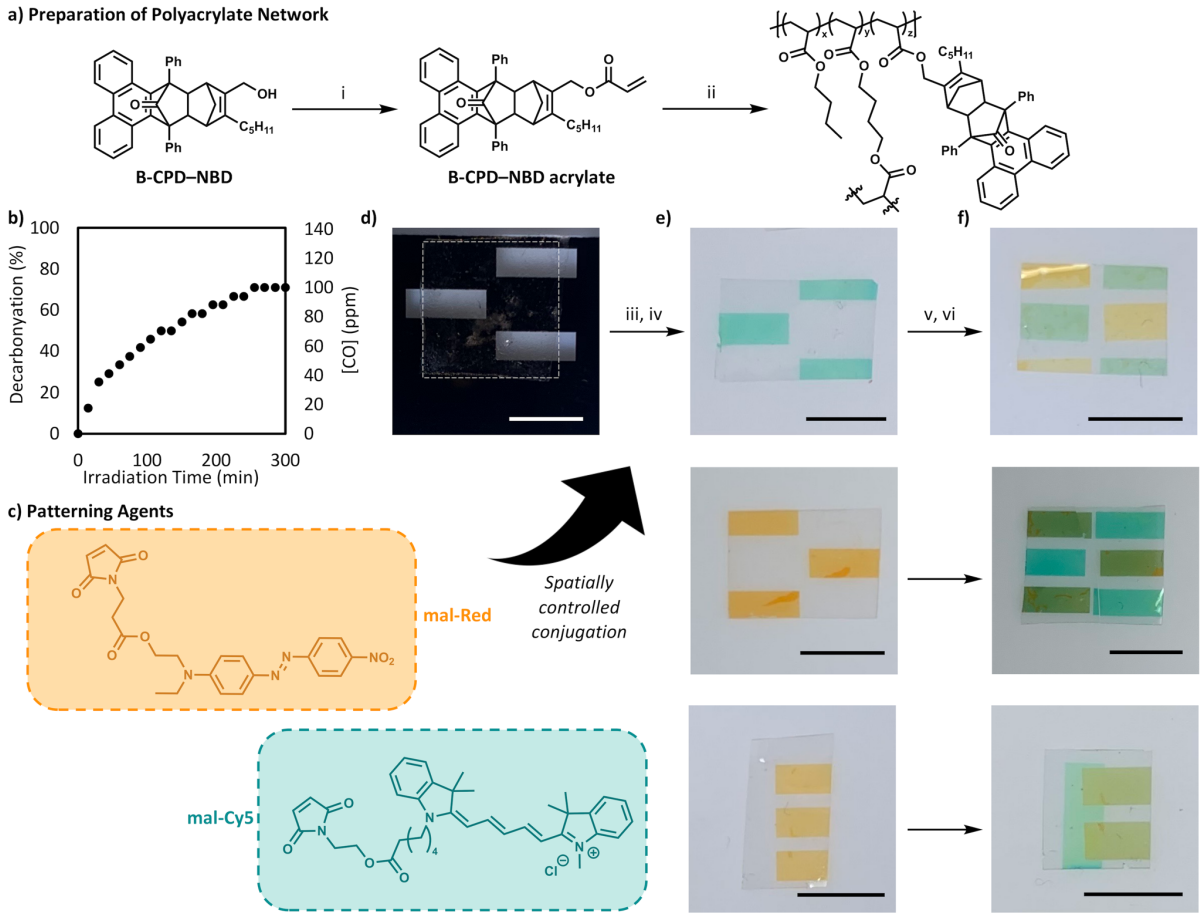

Figure 3.4. a) i) acryloyl chloride (1.5 eq), Et_3N (1.5 eq), DCM, 0 °C, 4 h, 80%. ii) butyl acrylate (74 mol%), 1,4-butanediol diacrylate (20 mol%), B-CPD–NBD acrylate (5 mol%), BAPO (1 mol%), 405 nm, 30 min, rt. b) Monitoring by CO sensor upon irradiation with 365 nm LED, plotted against ppm CO and calculated reaction completion. c) Structures of maleimide functionalized dyes. d) Photograph of quartz photomask used for patterning films with non-patterned film outlined in white. iii) 365 nm, 6.1 mW/cm^2. 30 min. iv) mal-Cy5 (10 mM in DCM), 1 h. e) Photographs of films after initial patterning. v) 365 nm, 6.1 mW/cm^2. 30 min. vi) mal-Red (10 mM in DCM), 1 h. f) Photographs of films after second patterning step. Scale bars = 5 mm.

Here, we demonstrate the ability to pattern two highly absorbing dyes, maleimide-Disperse Red 1 (mal-Red) and maleimide-Cyanine 5 (mal-Cy5), in pre-determined locations within a single polymer network. To prepare the multi-patterned material, films were irradiated under a quartz photomask for 30 min before swelling in a solution of either mal-Red or mal-Cy5. The material was rinsed with DCM to remove non-conjugated dye, affording the patterned thin

films depicted in **Figure 3.4e**. A second pattern could be programmed into the films by irradiation with a second, inverted quartz photomask for 30 min, followed by treatment with 10 mM solution of the alternative dye in DCM for 2 h. Rinsing to remove residual dye afforded multi-species patterned thin films (**Figure 3.4f**). It is worth noting that after the second patterning step, both dyes were consistently observed in locations of the first pattern, resulting in a green tint. This could be due to an interaction between the two dyes or clicking to Cp not consumed during the first dye treatment. A control experiment was performed by treating a Cy5 patterned film with commercially available Disperse Red 1 which did not contain the maleimide "click" functional group. Again, the staining was observed (**Figure S3.54**) indicating the cause of this is most likely an interaction of the two dyes rather than incomplete conversion of the initially exposed Cp units. That being said, we were quite pleased with the resolution achieved and simplicity of the patterning and believe this procedure will be compatible with a variety of diene functionalized species.

3.3.2.4 Hydrogel Patterning with Biotin and Streptavidin

To test the versatility of this platform, we next sought to apply the patterning technique to achieve pre-programmed protein immobilization in biocompatible PEG hydrogels. A functional linker was designed to incorporate B-CPD–NBD units into tetra-PEG based hydrogels, and as an additional testament to the utility of DA click chemistry, we chose to prepare the hydrogels themselves via DA cycloadditions. Commercially available tetra-PEG (M_n = 20000 g/mol) was functionalized with maleimide by modifying a reported carbodiimide coupling[48] (PEG-mal$_4$, $M_{n(HNMR)}$ = 21700 g/mol, **Figure 3.5a, S3.21–3.22**). Spiro[2.4]hepta-4,6-diene was chosen as the diene partner for initial network formation due to its efficient DA reactivity[29] while the inhibition of the dimerization leads to improved monomer stability.[67] A

diene-functionalized linker (B-CPD–NBD linker) was prepared in three steps from B-CPD–NBD (**Figure 3.5a**). Due to the insolubility of the B-CPD–NBD linker in water, the polymer network was prepared by combining PEG-mal$_4$ and B-CPD–NBD linker in DMSO (10wt% polymer), then drop-casting 100 μL into a glass dish with a 10 mm diameter well (1 mm depth). Upon network formation, the network was washed and incubated in PBS before irradiation and patterning.

The well-containing glass dish allowed for bottom-up irradiation of the hydrogel while swollen in PBS (**Figure 3.5d**). After irradiation, the hydrogel was incubated in a PBS/DMSO solution containing mal-biotin. The resulting functionalized hydrogel was then rinsed with methanol and PBS to remove non-conjugated mal-biotin. To offer a visual demonstration, the spatially biotinylated hydrogel was incubated with a solution containing Streptavidin–Alexa Fluor 514 conjugate for 1 h in the dark (**Figure 3.5b**). The hydrogel was rinsed thoroughly with PBS to remove non-ligated protein before examination by fluorescence microscopy. Detection of Alexa Fluor 514 revealed selective protein immobilization onto the hydrogel corresponding to the pre-determined photo-pattern (**Figure 3.5e, S3.56**). Furthermore, Z-stacks through the thickness of the sample reveal strong Alexa Fluor 514 fluorescence signal throughout the sample thickness (**Figure S3.55 and S3.57**), highlighting effective penetration and high efficiency of this hydrogel functionalization strategy.

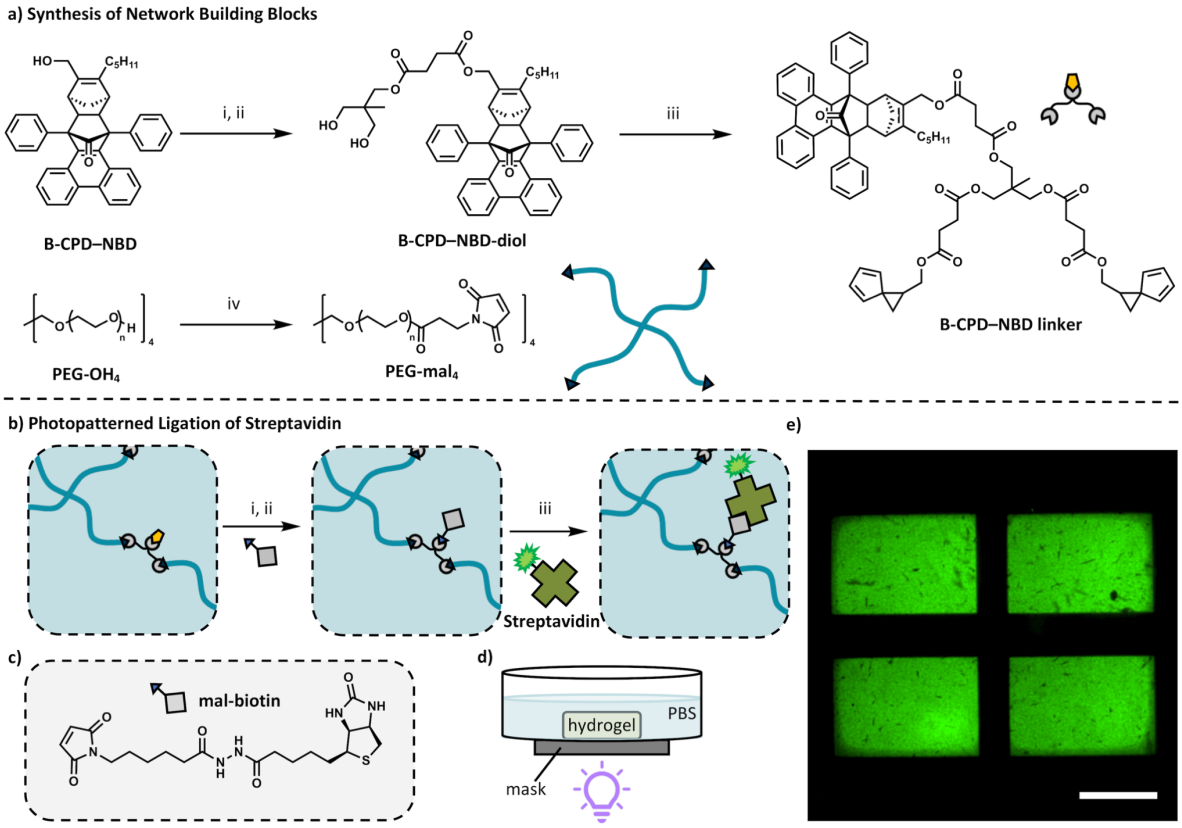

Figure 3.5. a) i) Succinic anhydride (1.3 eq), triethylamine (1.0 eq), 4-dimethylaminopyridine (DMAP, 0.1 eq), dichloromethane (DCM), 1 h, 81%, ii) trimethylolethane (4.0 eq), *N*-(3-Dimethylaminopropyl)-*N*′-ethylcarbodiimide hydrochloride (EDC, 1.5 eq), DMAP (0.1 eq), *N,N*-Dimethylformamide, rt, 3 h, 58%. iii) spiro[2.4]hepta-4,6-diene-COOH (3.0 eq), EDC (3.0 eq), DMAP (0.2 eq), DCM, rt, 1.5 h, 92%. iv) 3-maleimidopropanoic acid (10.0 eq), N,N′-Dicyclohexylcarbodiimide (11.0 eq), DMAP (0.1 eq), DCM, rt, 24 h. b) Schematic representation of maleimide-biotin photo-click, followed by streptavidin ligation i) 365 nm, PBS, 6.1 mW/cm^2. 30 min. ii) mal-biotin (1 mg/mL in 9:1 PBS, DMSO), 2 h. iii) Streptavidin–Alexa Fluor 514 conjugate (100 µL of 0.5 mg/mL in PBS dropped onto hydrogel), dark, 1 h. c) Structure of maleimide functionalized biotin. d) Schematic representation of hydrogel photopatterning set-up. e) Fluorescence image of resulting hydrogel with patterned ligation of Streptavidin–Alexa Fluor 514 conjugate. Multiple images were stitched due to the limited field of view. Scale bar = 1.5 mm.

3.4 Conclusion

A new Diels–Alder photo-click platform has been developed utilizing spatially controlled, on-demand unveiling of Cp in pre-formed polymer networks. Notably, due to the formation of

a stable diene that does not require in situ trapping, maleimides can be clicked post-irradiation. This allows access to functionalization with the cyanine dye utilized here, which is highly susceptible to bleaching by photooxidation.[68,69] We envision this patterning procedure could be used directly for the multi-species patterning of a multitude of materials, and particularly useful in patterning photo-thermal and photo-responsive units which are incompatible with the traditional in situ photo-clicking reactions currently available. Furthermore, the ability to conjugate multiple absorbing species, as we have demonstrated with Cyanine 5 and Disperse Red 1, offers exciting potential in sequential, wavelength-controlled responses in smart materials. Mild, efficient, bio-orthogonal chemistry also provides promise for use in biomaterials. The simple biotin–streptavidin protein ligation presented serves as a proof-of-concept, but the success of this platform within a biocompatible system and the use of a cytocompatible light source[66] validates the promise of this system within biological systems. Specifically, the spatially controlled functionalization of synthetic and naturally derived hydrogels could offer a means of studying the effect of heterogeneous physical or biochemical cues on cell behavior. Given the success of the two patterning applications debuted here and the promise within a range of next-generation materials including sequentially stimuli responsive polymers and spatially controlled cellular microenvironments, we believe this platform will offer a convenient and ubiquitous patterning method with numerous advantages over current systems.

3.5 Acknowledgments

I would like to thank Dr. Julie Peterson for her illuminating insights and exciting conversations throughout the development of this new photoprotecting strategy. I am also incredibly grateful for the staff of the UC Santa Barbara Mass Spectrometry Facility and TEMPO Facility within

the Materials Research Laboratory (MRL) for assisting data acquisition during shutdowns related to the COVID-19 pandemic. I would also like to thank the UCSB Graduate Division for financial support through a Chancellor's Fellowship and acknowledge the research reported here was partial support by the Office of Naval Research through the MURI of Photomechanical Materials Systems (ONR N00014-18-1-2624) and partial support from the BioPACIFIC Materials Innovation Platform of the National Science Foundation under award No. DMR-1933487.

3.6 Supporting Information

Synthesis

Materials and Methods

All chemicals were obtained from Sigma Aldrich, TCI Europe or Fisher Scientific. Dichloromethane (DCM), toluene and methanol (MeOH) were stored over 3 Å molecular sieves. Unless otherwise noted, all reagents were used as received without further purification and additional precautions to dry solvents or exclude oxygen from reactions were not taken. Pe-NBD-OH[22], B-CPD,[70] spiro[2.4]hepta-4,6-diene-COOH,[29] 4f-Bib,[71] 3-maleimidopropanoic acid,[72] Cy5-COOH,[73] exo-mal-OH,[74] and exo-mal-COOH[75] were prepared following literature procedures. Thin-layer chromatography (TLC) was conducted with E. Merck silica gel 60 F254 pre-coated plates (0.25 mm) and visualized by exposure to UV light (254 nm) or stained with *p*-anisaldehyde. Flash column chromatography was performed using normal phase silica gel (60 Å, 0.040 – 0.063 mm, Geduran) with hexanes, ethyl acetate (EtOAc), DCM and/or MeOH as eluents. ^{1}H and ^{13}C NMR spectra were recorded on Varian spectrometers (100, 400 or 600 MHz) and are reported relative to $CDCl_3$ (δ =

7.26 ppm for ^{1}H and 77.00 ppm for ^{13}C), DMSO-D6 (δ = 2.50 ppm for ^{1}H and 39.70 ppm for ^{13}C) or CD_2Cl_2 (δ = 5.32 ppm for ^{1}H). Data for ^{1}H NMR spectra are reported as follows: chemical shift (δ ppm), multiplicity, coupling constant (Hz) and integration. Data for ^{13}C NMR spectra are reported in terms of chemical shift (δ ppm). Mass spectra were obtained from the UC Santa Barbara Mass Spectrometry Facility on a (Waters Corp.) GCT Premier high-resolution Time-of-Flight mass spectrometer with an ESI or ESCI source. FTIR spectra were collected on a Thermo Nicolet iS10 FTIR Spectrometer equipped with a Smart Diamond attenuated total reflectance (ATR) accessory. Size exclusion chromatography (SEC) eluting with chloroform ($CHCl_3$) and calibrated relative to polystyrene standards was performed on a Waters Alliance HPLC System, 2695 separation module with Wyatt DAWN HELEOS-II light scattering and Wyatt Optilab rEX refractive index detectors. No unexpected or unusually high safety hazards were encountered in conducting the reported work.

Small Molecule Building Blocks

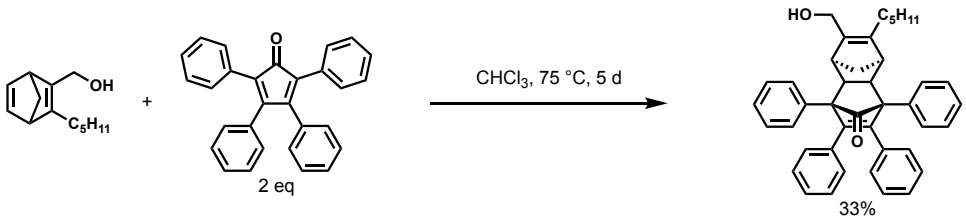

2-(hydroxymethyl)-3-pentyl-5,6,7,8-tetraphenyl-1,4,4a,5,8,8a-hexahydro-1,4:5,8-dimethanonaphthalen-9-one (Ph-CPD–NBD):

In a round bottom flask equipped with magnetic stir bar, Pe-NBD-OH[22] (2.00 g, 10.4 mmol, 1.00 eq) was dissolved in 100 mL chloroform. To this solution was added tetraphenylcyclopentadienone (Ph-CPD, 8.00 g, 20.8 mmol, 2.00 eq). The flask was fitted with a waterless reflux condenser and the solution refluxed at 75 °C under nitrogen and monitored

by TLC (hexanes:ethyl acetate, 6:1). Additional chloroform was added to maintain solvent level. After 5 d, complete consumption of NBD-OH had not been observed, but the reaction was allowed to cool to room temperature then passed through a silica plug to remove excess tetraphenylcyclopentadienone. The solvent was removed under reduced pressure, then the residue was dissolved in minimal ethyl acetate (EtOAc). 250 mL hexanes was added and the solution was left unagitated until crystal formation was observed. The solution was transferred to a freezer for 24 h before the solid was isolated by vacuum filtration to afford **Ph-CPD–NBD** as an off-white powder (residual pink from Ph-CPD, 1.99 g, 3.45 mmol, 33%).

Ph-CPD–NBD: R_f (Hexanes:EtOAc, 6:1): 0.25; ^{1}H NMR (600 MHz, $CDCl_3$) δ 7.41 (t, *J* = 7.8 Hz, 4H), 7.31 – 7.26 (m, 4H), 7.22 – 7.18 (m, 2H), 7.01 – 6.97 (m, 6H), 6.90 – 6.87 (m, 4H), 4.44 – 4.41 (m, 1H), 4.34 – 4.31 (m, 1H), 3.58 (s, 1H), 3.36 (s, 1H), 3.00 (d, *J* = 8.5 Hz, 1H), 2.89 (d, *J* = 8.5 Hz, 1H), 2.60 (d, *J* = 9.3 Hz, 1H), 2.35 – 2.20 (m, 2H), 1.65 – 1.57 (m, 2H), 1.43 (d, *J* = 9.2 Hz, 1H), 1.39 – 1.28 (m, 5H), 0.92 (t, *J* = 6.9 Hz, 3H) ppm; ^{13}C NMR (100 MHz, $CDCl_3$) δ 197.1, 150.5, 145.3, 140.2, 139.8, 136.3, 136.0, 134.9, 134.8, 129.7, 129.6, 129.3, 129.3, 128.0, 127.5, 127.5, 126.9, 126.9, 126.9, 65.9, 65.8, 57.8, 49.6, 47.6, 47.1, 46.7, 40.2, 31.8, 28.2, 27.2, 22.4, 14.0 ppm; FTIR (ATR) 3540, 3024, 2957, 2930, 2855, 1956, 1764, 1604, 1498, 1444, 1371, 1023, 773, 750, 694 cm^{-1}; HRMS (ES+) Exact mass calcd. for $C_{42}H_{40}O_2$ $[M+Na]^+$: 599.2926, found: 599.2933.

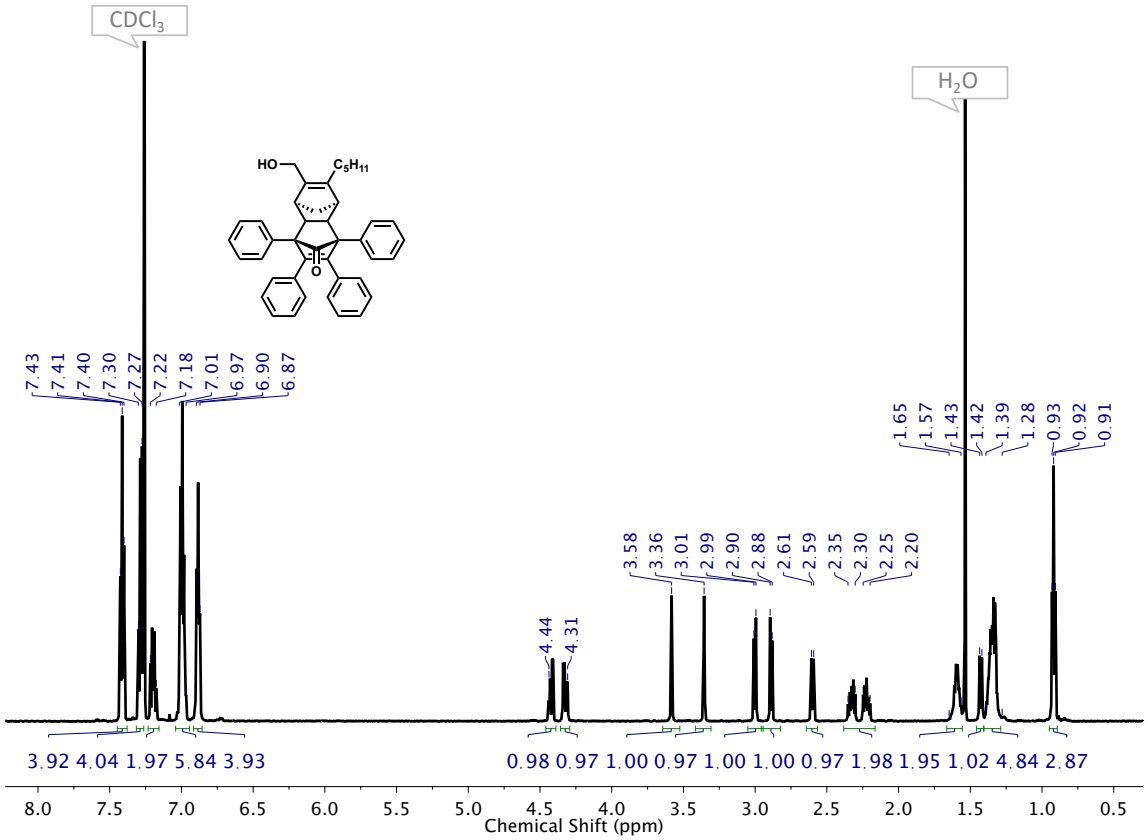

Figure S 3.1. ^{1}H NMR (600 MHz, $CDCl_3$) **Ph-CPD–NBD**

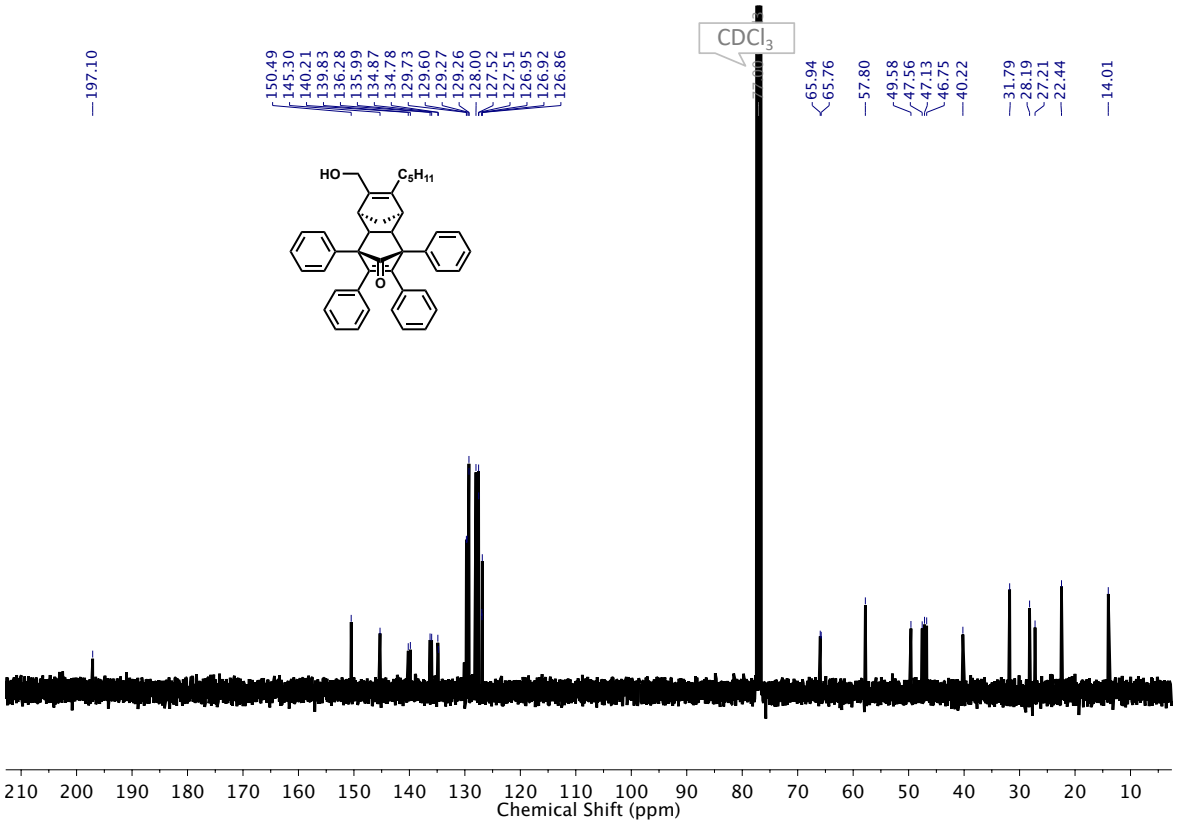

Figure S 3.2. ^{13}C NMR (100 MHz, $CDCl_3$) **Ph-CPD–NBD**

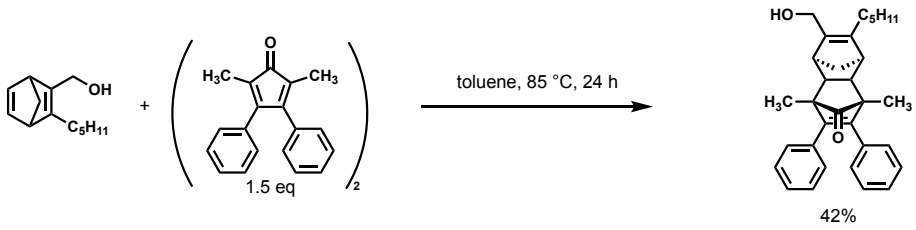

2-(hydroxymethyl)-5,8-dimethyl-3-pentyl-6,7-diphenyl-1,4,4a,5,8,8a-hexahydro-1,4:5,8-dimethanonaphthalen-9-one (Me-CPD–NBD):

In a round bottom flask equipped with magnetic stir bar, Pe-NBD-OH[22] (385 mg, 2.00 mmol, 1.00 eq) was dissolved in 10 mL toluene. To this solution was added 2,5-Dimethyl-3,4-diphenylcyclopentadienone, dimer (Me-CPD, 781 mg, 1.50 mmol, 0.750 eq). The flask was fitted with a waterless reflux condenser and the solution refluxed at 85 °C under nitrogen for 24 h while monitored by TLC (hexanes:ethyl acetate, 6:1). The solvent was removed under

reduced pressure and the residue subjected to column chromatography (hexanes:ethyl acetate, 6:1) to afford a **Me-CPD–NBD** (383 mg, 0.846 mmol, 42%) as a yellow foam.

Me-CPD–NBD: R_f (Hexanes:EtOAc, 6:1): 0.25; ^{1}H NMR (400 MHz, $CDCl_3$) δ 7.25 – 7.16 (m, 6H), 7.06 – 7.03 (m, 4H), 4.29 (d, *J* = 12.5 Hz, 1H), 4.09 (d, *J* = 12.6 Hz, 1H), 3.17 (s, 1H), 2.92 (s, 1H), 2.49 (d, *J* = 9.1 Hz, 1H), 2.22 – 2.14 (m, 1H), 2.07 – 1.97 (m, 3H), 1.48 – 1.21 (m, 7H), 1.28 (s, 3H), 1.27 (s, 3H), 0.89 (t, *J* = 7.0 Hz, 3H) ppm; ^{13}C NMR (100 MHz, $CDCl_3$) δ 202.0, 150.5, 144.8, 139.8, 139.3, 135.2, 135.1, 128.7, 128.7, 128.0, 127.9, 127.1, 57.5, 56.7, 56.6, 50.4, 50.1, 47.7, 45.8, 39.7, 31.8, 28.0, 26.8, 22.5, 14.0, 13.0, 12.9 ppm; FTIR (ATR) 3478, 3054, 2959, 2927, 2858, 1967, 1763, 1449, 1265, 999, 609, 597 cm^{-1}; HRMS (ES+) Exact mass calcd. for $C_{32}H_{36}O_2$ $[M+Na]^+$: 475.2613, found: 475.2620.

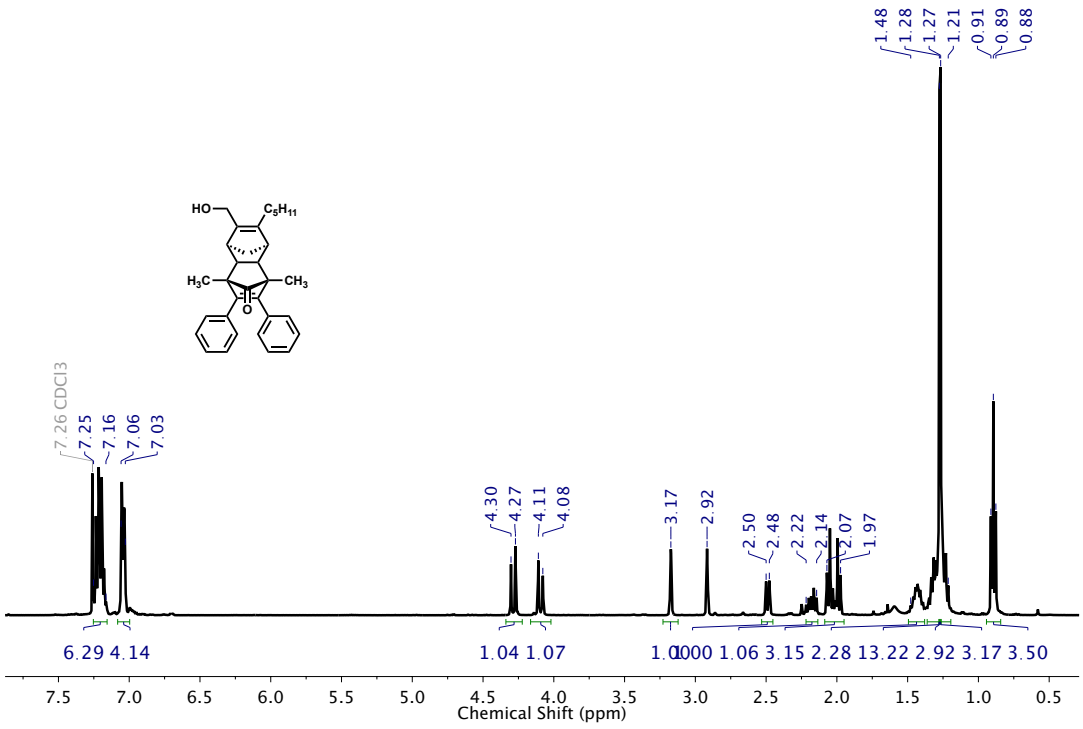

Figure S 3.3. ^{1}H NMR (400 MHz, $CDCl_3$) **Me-CPD–NBD**

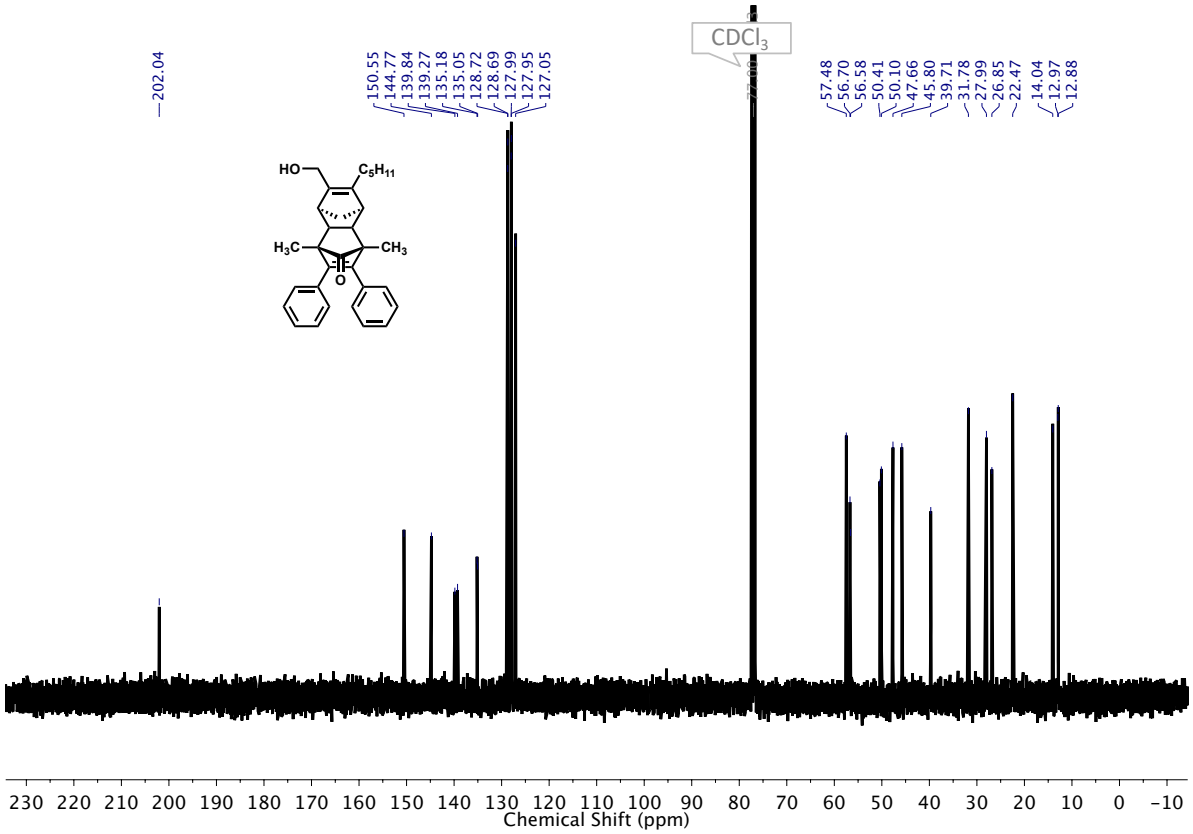

Figure S 3.4. ^{13}C NMR (100 MHz, $CDCl_3$) **Me-CPD–NBD**

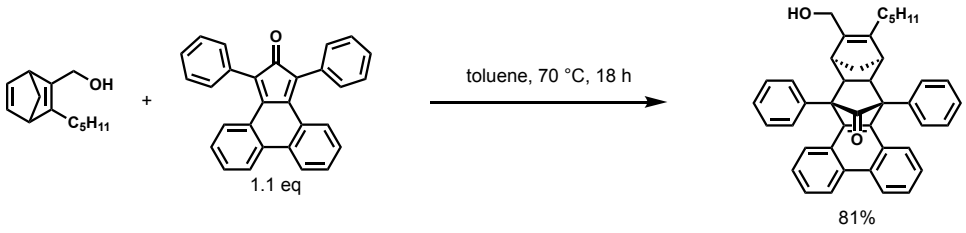

11-(hydroxymethyl)-12-pentyl-9,14-diphenyl-9,9a,10,13,13a,14-hexahydro-9,14:10,13-dimethanobenzo[*f*]tetraphen-15-one (B-CPD–NBD)

In a round bottom flask equipped with magnetic stir bar, Pe-NBD-OH[22] (1.50 g, 7.80 mmol, 1.00 eq) was dissolved in 15 mL toluene. To this solution was added 1,3-diphenylcyclopenta[l]phenanthren-2-one[10] (B-CPD, 3.28 g, 8.58 mmol, 1.10 eq). The solution was heated to 70 °C under nitrogen and monitored by TLC (hexanes:EtOAc, 7:1). Complete

consumption of NBD-OH was onfirmed after 18 h, and white precipitate was observed to crash out of solution. The solid was collected by vacuum filtration and rinsed with toluene (5 mL) to afford **B-CPD–NBD** as an off-white powder (B-CPD, 3.65 g, 6.35 mmol, 81%).

B-CPD–NBD: R_f (Hexanes:EtOAc, 7:1): 0.13; ^{1}H NMR (600 MHz, $CDCl_3$) δ 8.71 (dd, *J* = 8.2, 5.1 Hz, 2H), 7.93 (d, *J* = 7.7 Hz, 1H), 7.82 (d, *J* = 7.7 Hz, 1H), 7.65 (t, *J* = 7.4 Hz, 2H), 7.54 – 7.51 (m, 2H), 7.47 (q, *J* = 7.3 Hz, 2H), 7.40 (q, *J* = 8.1 Hz, 2H), 7.25 – 7.16 (m, 4H), 7.10 (t, *J* = 8.2 Hz, 2H), 4.32 (d, *J* = 5.2 Hz, 2H), 3.16 (d, *J* = 8.4 Hz, 1H), 3.13 (s, 1H), 3.04 (d, *J* = 8.4 Hz, 1H), 2.94 (s, 1H), 2.28 – 2.17 (m, 2H), 1.58 – 1.49 (m, 2H), 1.37 – 1.23 (m, 5H), 0.89 (t, *J* = 7.2 Hz, 3H), 0.42 (d, *J* = 9.6 Hz, 1H), -0.48 (d, *J* = 9.7 Hz, 1H) ppm; ^{13}C NMR (100 MHz, $CDCl_3$) δ 199.1, 150.1, 145.1, 137.3, 137.1, 135.1, 134.8, 131.6, 131.4, 130.9, 130.8, 129.2, 129.0, 128.8, 128.6, 127.9, 127.7, 127.7, 127.5, 126.3, 126.2, 125.4, 125.2, 123.4, 123.3, 63.6, 63.6, 57.8, 48.4, 46.6, 46.1, 45.2, 39.9, 31.7, 28.2, 27.1, 22.4, 14.0 ppm. FTIR (ATR) 3575, 3057, 3028, 2953, 2919, 2853, 1988, 1771, 1604, 1498, 1446, 1030, 896, 758, 699 cm^{-1}; HRMS (ES+) Exact mass calcd. for $C_{42}H_{38}O_2$ $[M+Na]^+$: 597.2770, found: 597.2776.

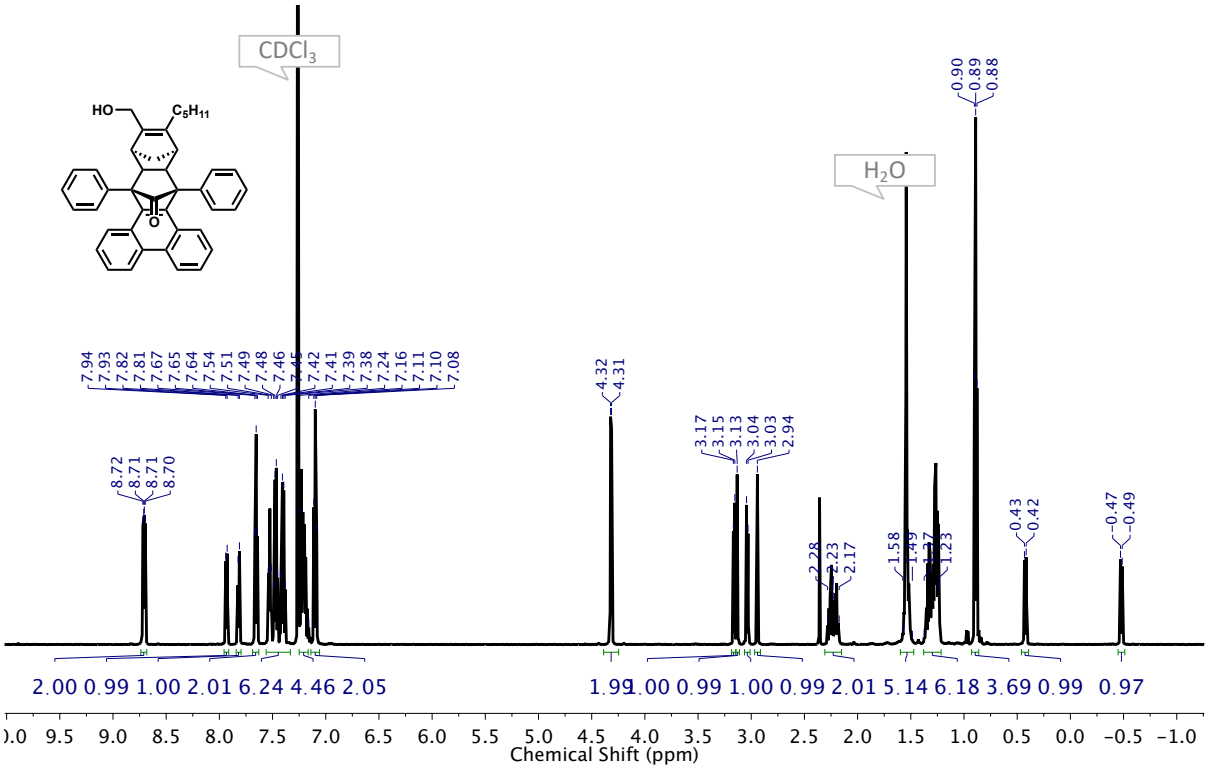

Figure S 3.5. ^{1}H NMR (600 MHz, $CDCl_3$) **B-CPD–NBD**

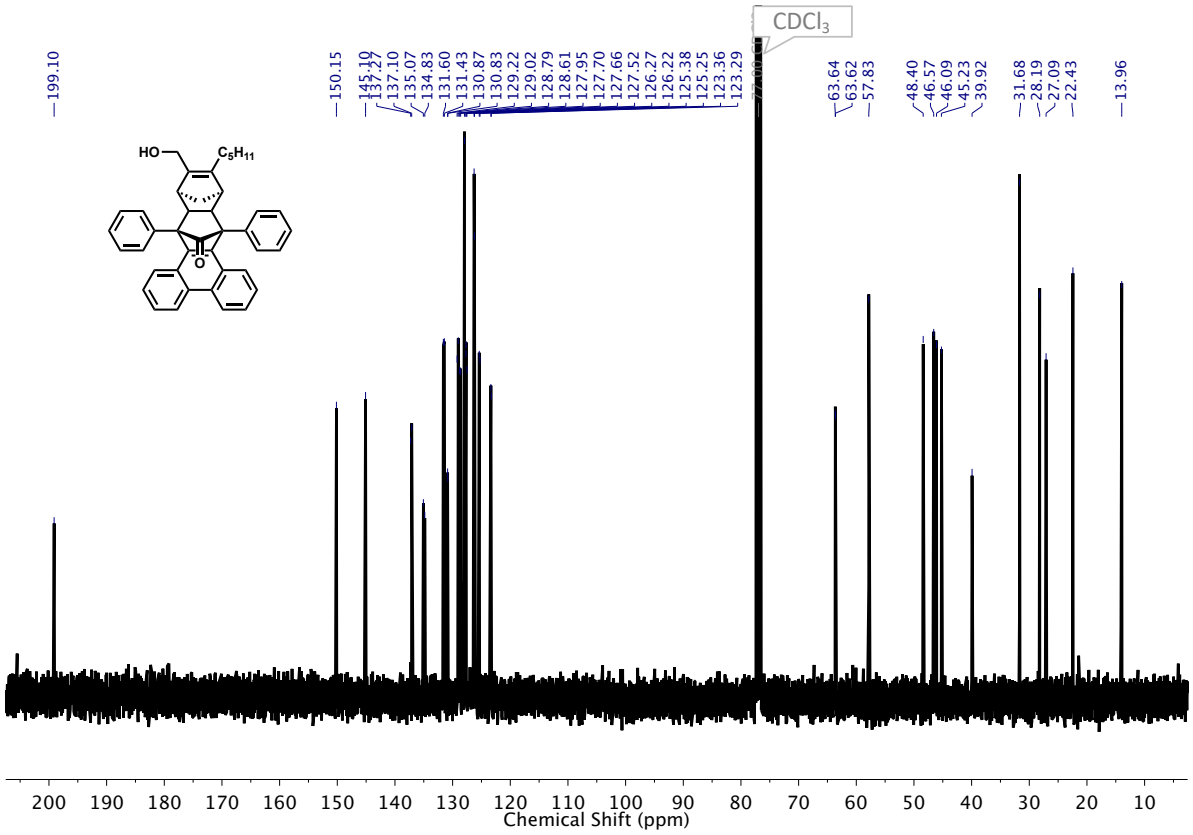

Figure S 3.6. ^{13}C NMR (100 MHz, $CDCl_3$) **B-CPD–NBD**

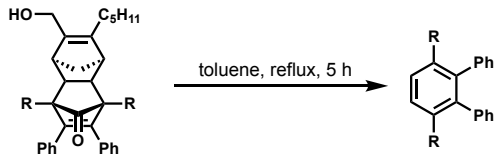

R = Me or Ph

1,2,3,4-tetraphenyl benzene (Ph-benzene) and 1,4-dimethyl-2,3-diphenyl benzene (Me-benzene)

A solution of CPD–NBD (0.100 mmol) in toluene (5 mL) was refluxed for 5 h. The solvent was removed under reduced pressure and the residue was subjected to a silica plug with hexanes as eluent. The solvent was removed and the solid triturated with hexanes to afford the substituted benzenes, Ph-benzene (49%) or Me-benzene (39%), used for UV Vis spectroscopy (Section 2.4). Spectral data matches reported literature for **Ph-benzene**[76] and **Me-benzene**.[77]

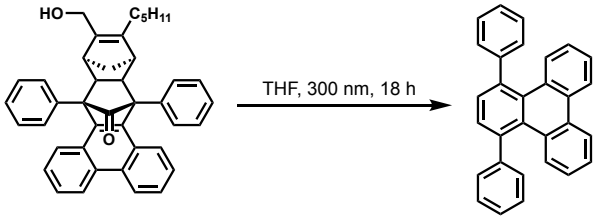

1,4-diphenyl triphenylene (B-benzene)

A solution of B-CPD–NBD alcohol (57.4 mg, 0.100 mmol) in tetrahydrofuran (2 mL) was sparged with nitrogen and transferred to an NMR tube. The tube was irradiated in a Rayonet RPR-200 chamber (300 nm) for 18 h. The solvent was removed, and the residue was subjected to a silica plug with hexanes as eluent. The solution was left unagitated allowing the product to crystallize out of solution. The material was collected by vacuum filtration and rinsed with cold hexanes to afford **B-benzene** as light yellow crystals (23.2 mg, 0.0612 mmol, 61%).

B-benzene: ^{1}H NMR (600 MHz, CD_2Cl_2) δ 8.46 (d, J = 8.0 Hz, 2H), 7.69 (d, J = 8.4 Hz, 2H), 7.54 (s, 2H), 7.47 – 7.37 (m, 12H), 7.08 (t, J = 8.2 Hz, 2H) ppm; ^{13}C NMR (100 MHz, $CDCl_3$) δ 144.6, 138.9, 131.2, 131.0, 130.2, 130.0, 129.9, 129.6, 129.0, 127.1, 126.6, 125.4, 123.2 ppm. FTIR (ATR) 3047, 3017, 2338, 1886, 1596, 1486, 1440, 1425, 754, 728, 697 cm^{-1}; HRMS (AP+) Exact mass calcd. for $C_{30}H_{20}$ $[M+H]^+$: 381.1643, found: 381.1649.

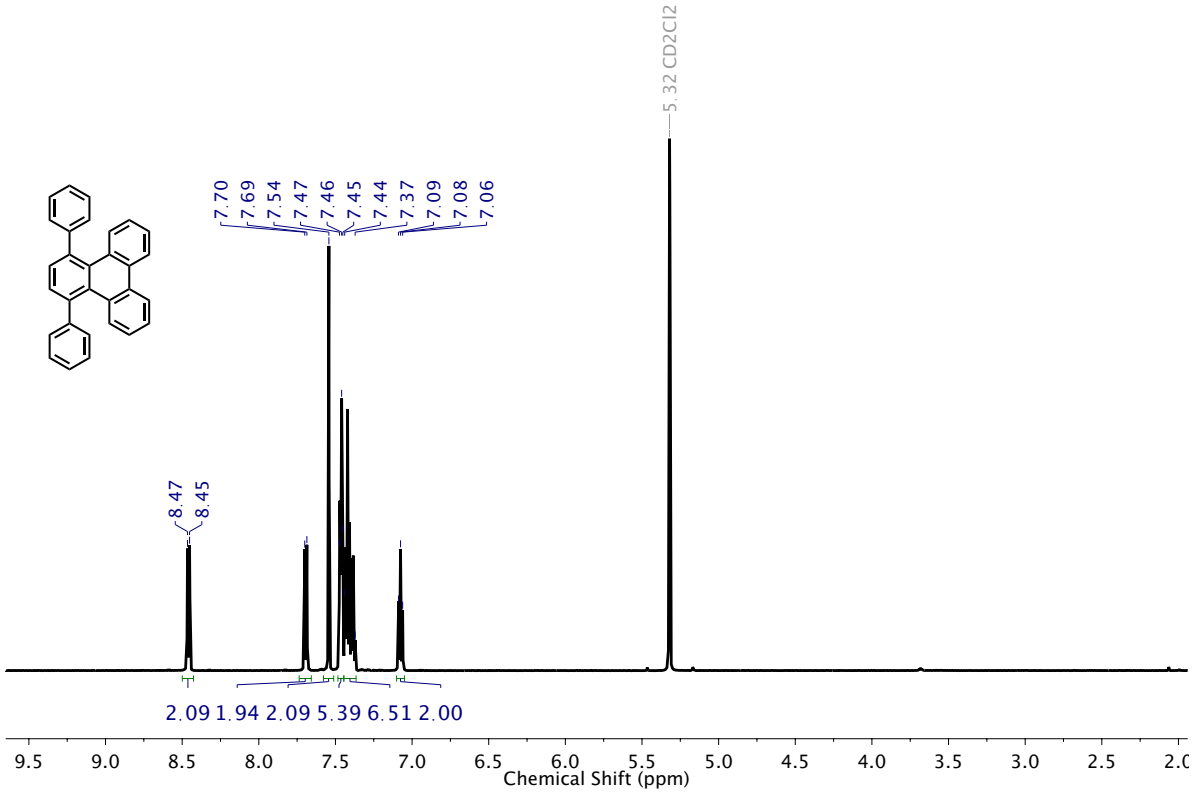

Figure S 3.7. ^{1}H NMR (600 MHz, CD_2Cl_2) **B-benzene**

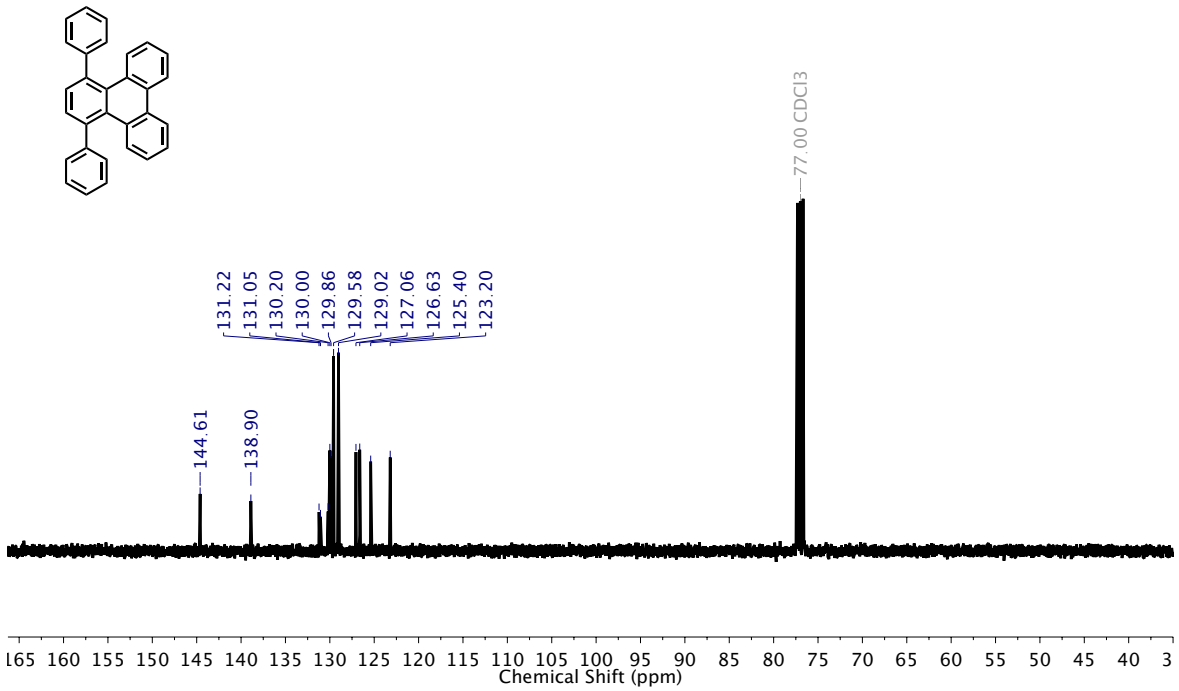

Figure S 3.8. ^{13}C NMR (100 MHz, $CDCl_3$) **B-benzene**

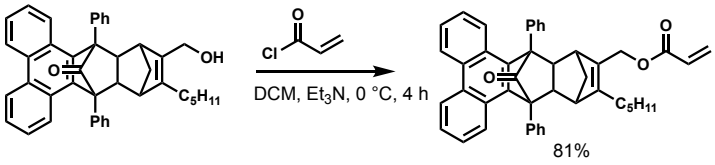

(15-oxo-12-pentyl-9,14-diphenyl-9,9a,10,13,13a,14-hexahydro-9,14:10,13-dimethanobenzo[*f*]tetraphen-11-yl)methyl acrylate (B-CPD–NBD acrylate)

A solution of B-CPD–NBD alcohol (1.15 g, 2.00 mmol, 1.00 eq) and Et_3N (0.418 mL, 3.00 mmol, 1.50 eq) in DCM (6.25 mL) was cooled to 0 °C under nitrogen. Acryloyl chloride (0.283 mL, 3.48 mmol, 2.00 eq) was added dropwise and the solution maintained at 0 °C for 4 h while monitored by TLC (hexanes:EtOAc, 5:1) complete consumption had occurred. The reaction mixture was transferred to a separatory funnel and washed with 1 M NaOH (12.5 mL), 1 M HCl (12.5 mL), then brine (12.5 mL), dried over $MgSO_4$, filtered, and the solvent removed. The residue subjected to column chromatography (hexanes:ethyl acetate, 9:1) and several drops of MEHQ (1 mg/ mL in DCM) were added to the combined fractions before the solvent was removed under reduced pressure to afford a light yellow foam (1.01 g, 1.61 mmol, 81%).

B-CPD–NBD acrylate: R_f (Hexanes:EtOAc, 5:1): 0.40; ^{1}H NMR (400 MHz, $CDCl_3$) δ 8.71 (d, *J* = 8.4, 2H), 7.91 (d, *J* = 7.7 Hz, 1H), 7.82 (d, *J* = 7.7 Hz, 1H), 7.66 (t, *J* = 7.6 Hz, 1H), 7.62 (t, *J* = 7.5 Hz, 1H), 7.57 – 7.36 (m, 6H), 7.25 – 7.17 (m, 4H), 7.10 (t, *J* = 7.3 Hz, 2H), 6.49 (d, *J* = 17.3 Hz, 1H), 6.23 (dd, *J* = 17.3, 10.5 Hz, 1H),), 5.89 (d, *J* = 10.5 Hz, 1H), 4.89 (d, *J* = 12.5 Hz, 1H),), 4.79 (d, *J* = 12.5 Hz, 1H), 3.22 (d, *J* = 8.4, 1H), 3.08 (d, *J* = 8.5, 1H), 3.01 (s, 1H), 2.96 (s, 1H), 2.38 – 2.21 (m, 2H), 1.63 – 1.48 (m, 2H), 1.40 – 1.22 (m, 4H), 0.89 (t, *J* = 7.0 Hz, 3H), 0.48 (d, *J* = 9.8 Hz, 1H), -0.46 (d, *J* = 9.8 Hz, 1H) ppm; ^{13}C NMR (100 MHz, $CDCl_3$) δ 198.8, 166.3, 153.5, 140.3, 137.2, 135.0, 134.8, 131.6, 131.5, 131.3, 130.9, 130.9, 129.1, 129.0, 128.8, 128.7, 128.2, 127.9, 127.9, 127.7, 127.7, 127.5, 126.3, 126.3,

125.3, 125.3, 123.4, 123.3, 63.7, 63.6, 59.8, 48.5, 47.5, 46.1, 45.0, 40.4, 31.7, 28.1, 27.3, 22.4, 14.0 ppm. FTIR (ATR) 3030, 2954, 2927, 2856, 2166, 2019, 1776, 1719, 1605, 1499, 1446, 1404, 1178, 759, 698 cm^{-1}; HRMS (ES+) Exact mass calcd. for $C_{45}H_{40}O_3$ $[M+Na]^+$: 651.2875, found: 651.2883.

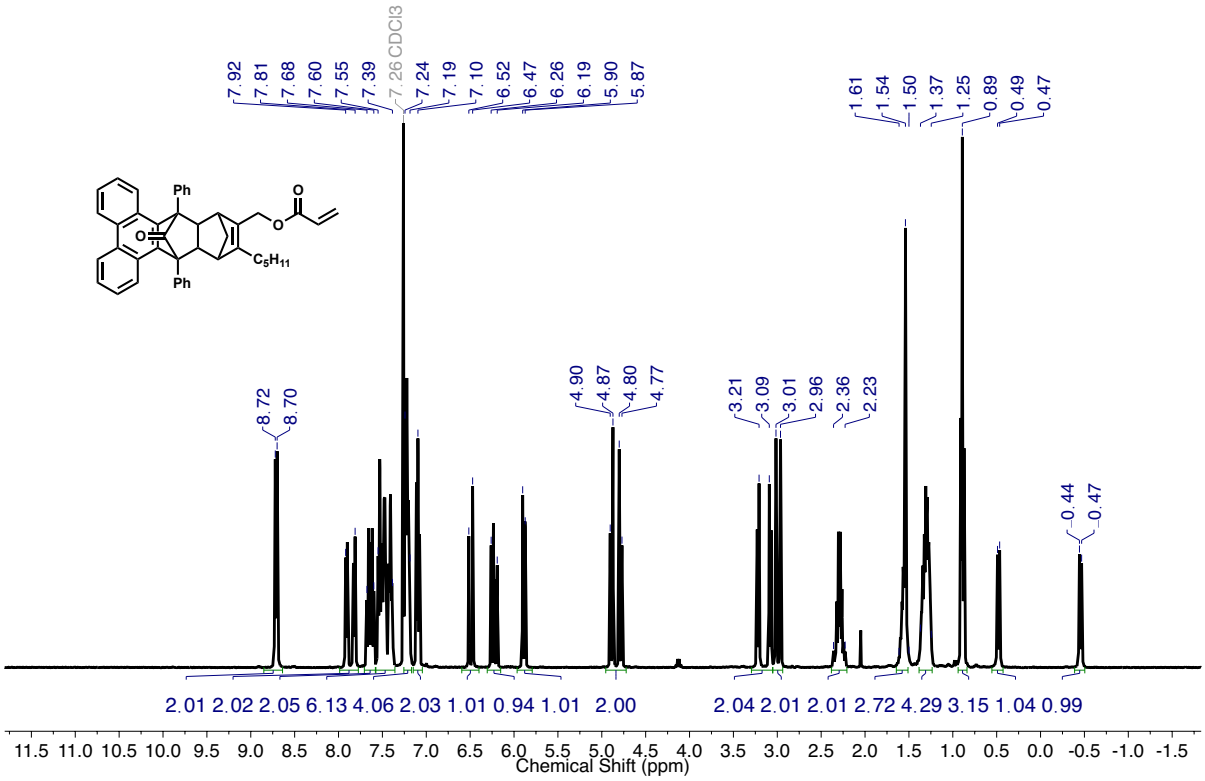

Figure S 3.9. ^1H NMR (400 MHz, $CDCl_3$) **B-CPD–NBD acrylate**

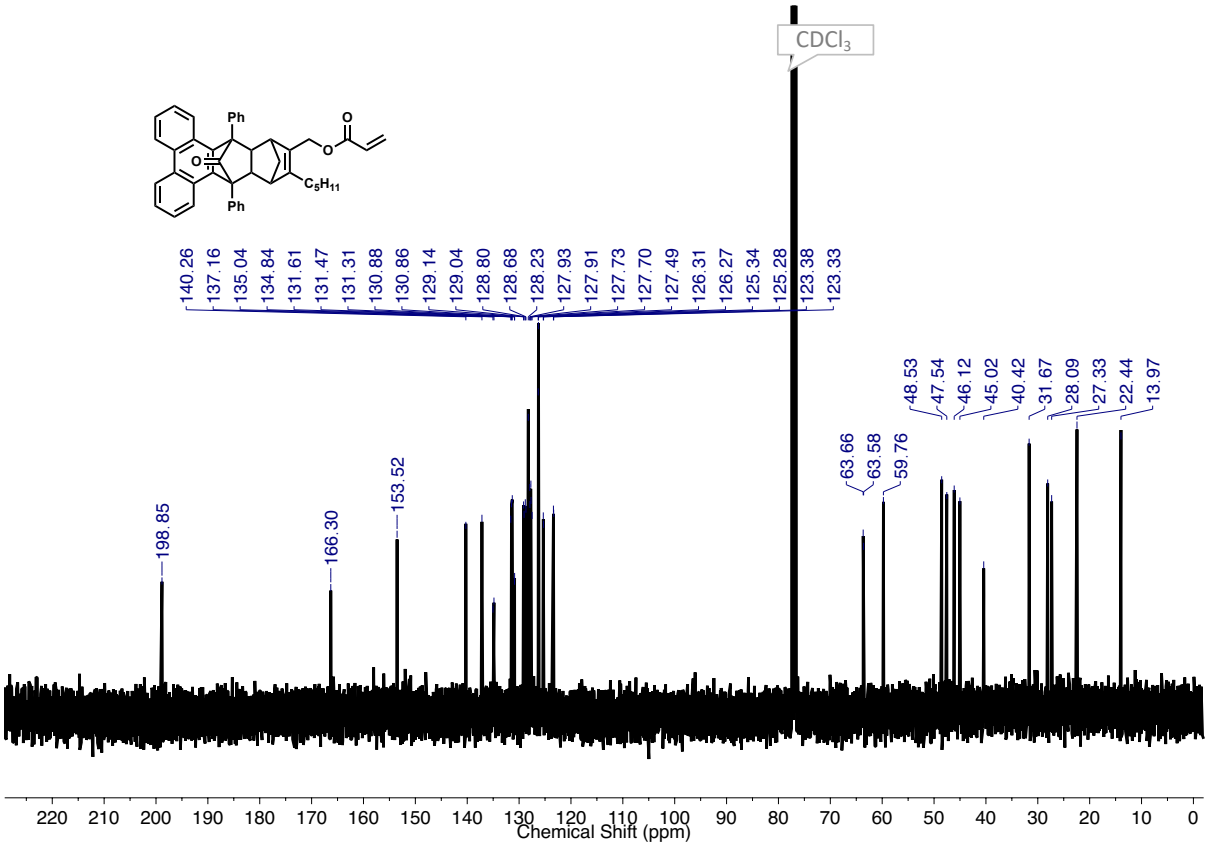

Figure S 3.10. ^{13}C NMR (100 MHz, $CDCl_3$) **B-CPD–NBD acrylate**

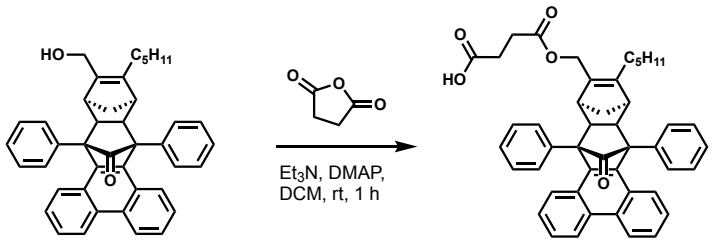

81%

4-oxo-4-((15-oxo-12-pentyl-9,14-diphenyl-9,9a,10,13,13a,14-hexahydro-9,14:10,13-dimethanobenzo[*f*]tetraphen-11-yl)methoxy)butanoic acid (B-CPD–NBD-COOH)

To a solution of B-CPD–NBD alcohol (2.00 g, 3.48 mmol, 1.00 eq) and dichloromethane (DCM, 5.00 mL) in a 25 mL flask equipped with a magnetic stir bar was added triethylamine (0.485 mL, 3.48 mmol, 1.00 eq), 4-dimethylaminopyridine (DMAP, 42.5 mg, 0.348 mmol, 0.100 eq), and succinic anhydride (453 mg, 4.52 mmol, 1.30 eq). The reaction was allowed to stir under an atmosphere of air and monitored by TLC (hexanes:ethyl acetate, 5:1). Complete consumption of B-CPD–NBD alcohol occurred after 1 h, and the solution was transferred to a separatory funnel with DCM (50 mL). The organic layer was washed with 1 M HCl (1 X 50 mL, 1 x 25 mL) then brine (1 X 50 mL), dried over MgSO4, filtered, and the solvent removed. The green, gooey residue was triturated in a solution of hexanes:ethyl acetate (95:5) and filtered to afford **B-CPD–NBD-COOH** as a white powder (1.89 g, 2.81 mmol, 81%).

B-CPD–NBD-COOH: ^{1}H NMR (400 MHz, $CDCl_3$) δ 8.71 (d, *J* = 10.0 Hz, 2H), 7.94 (d, *J* = 7.8 Hz, 1H), 7.81 (d, *J* = 7.8 Hz, 1H), 7.66 (q, *J* = 7.2 Hz, 2H), 7.55 – 7.46 (m, 4H), 7.42 – 7.38 (m, 2H), 7.24 – 7.19 (m, 4H), 7.09 (d, *J* = 8.4 Hz, 2H), 4.88 (d, *J* = 12.4 Hz, 1H), 4.68 (d, *J* = 12.4 Hz, 1H), 3.18 (d, *J* = 8.5 Hz, 1H), 3.05 (d, *J* = 8.5 Hz, 1H), 3.00 (s, 1H), 2.95 (s, 1H), 2.77 – 2.65 (m, 4H), 2.34 – 2.18 (m, 2H), 1.62 – 1.46 (m, 2H), 1.38 – 1.22 (m, 5H), 0.89 (t, *J* = 7.0 Hz, 3H), 0.46 (d, *J* = 9.8 Hz, 1H), -0.47 (d, *J* = 9.8 Hz, 1H) ppm; ^{13}C NMR (100 MHz,

$CDCl_3$) δ 198.9, 172.2, 153.5, 140.1, 137.1, 135.0, 134.8, 131.6, 131.5, 130.9, 130.8, 129.1, 129.0, 128.8, 128.7, 127.9, 127.9, 127.7, 127.7, 127.5, 126.3, 126.3, 126.3, 125.3, 125.3, 123.4, 123.3, 63.6, 63.6, 60.1, 48.5, 47.4, 46.0, 45.0, 40.3, 31.7, 28.8, 28.6, 28.1, 27.3, 22.4, 14.0 ppm; FTIR (ATR) 3059, 3027, 2924, 2860, 2569, 1980, 1774, 1727, 1706, 1437, 1170, 955, 747, 696 cm^{-1}; HRMS (ES+) Exact mass calcd. for $C_{46}H_{42}O_5$ $[M+Na]^+$: 697.2930, found: 697.2934.

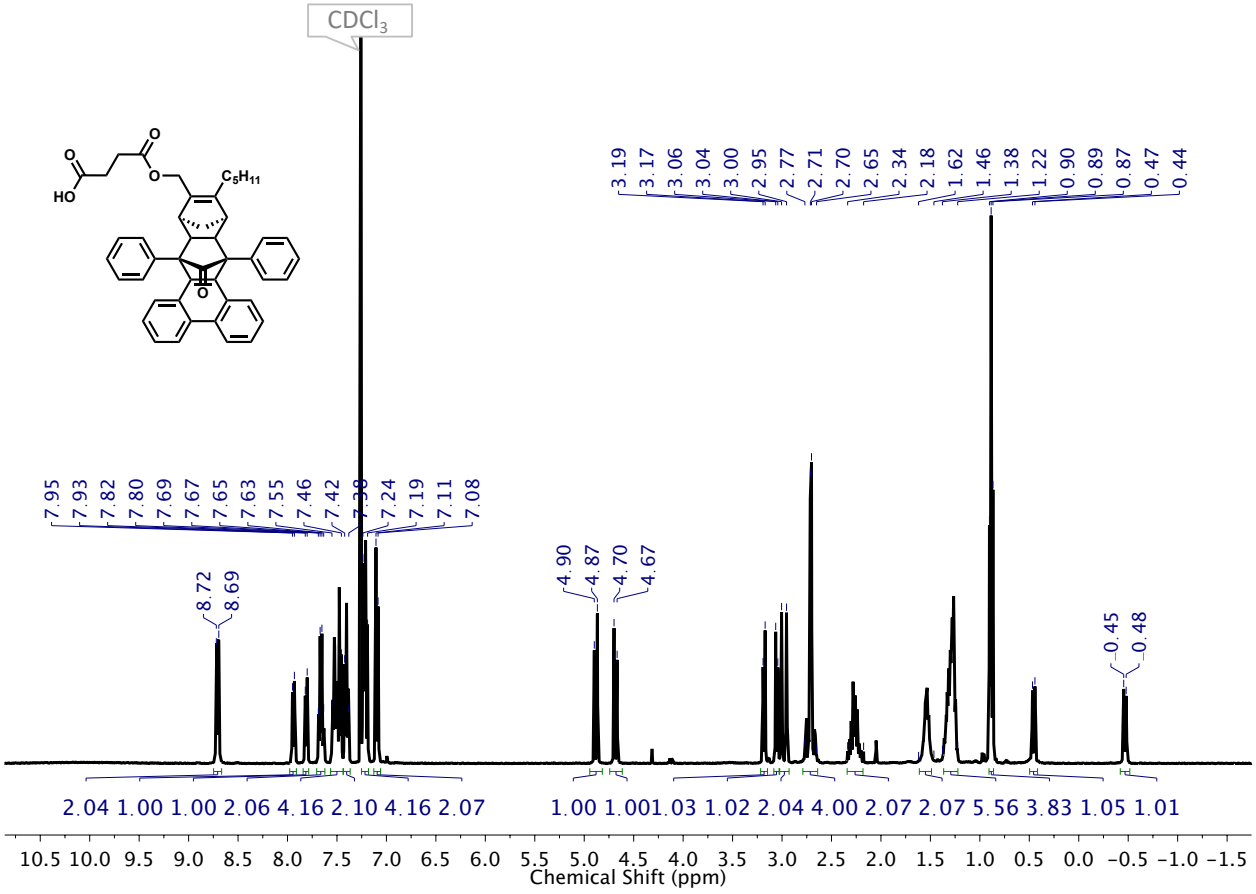

Figure S 3.11. ^1H NMR (400 MHz, $CDCl_3$) **B-CPD–NBD-COOH**

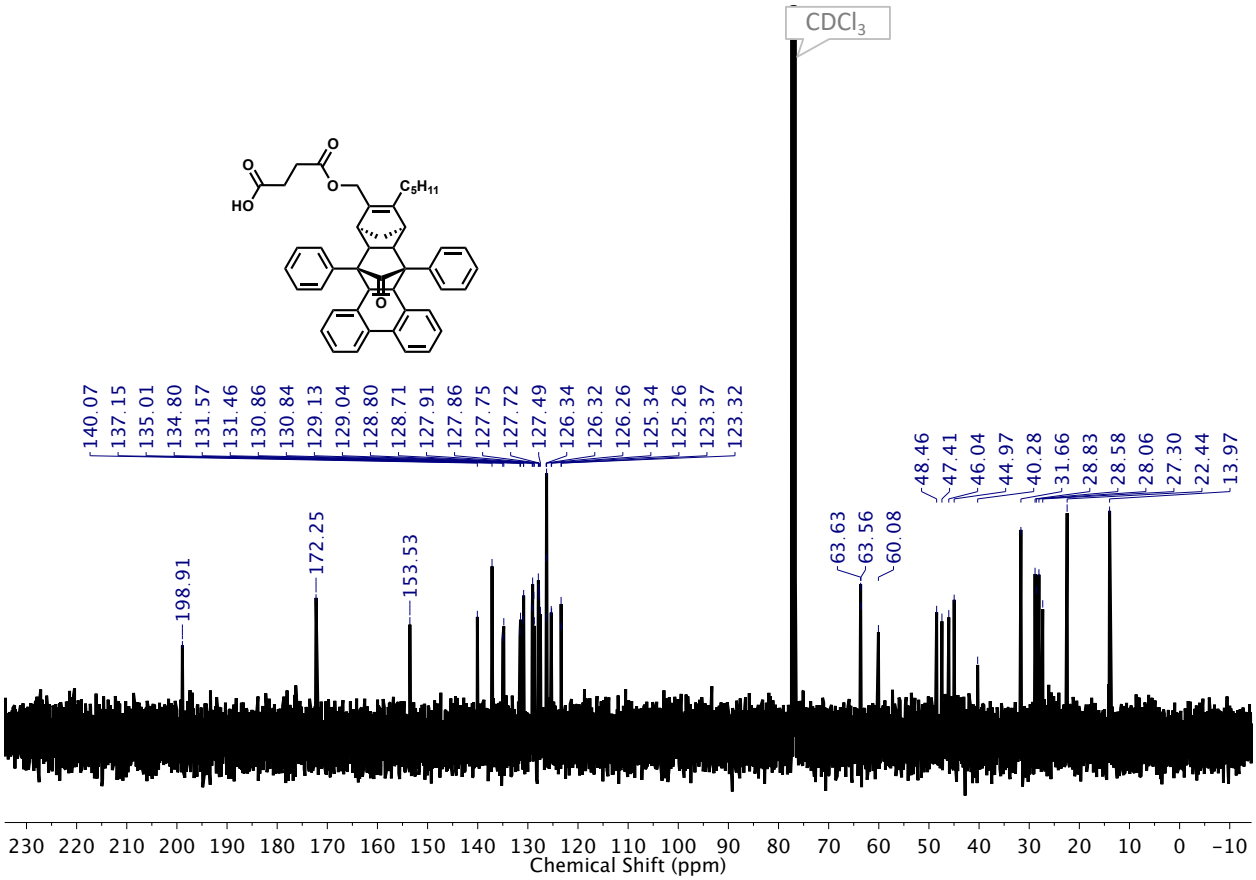

Figure S 3.12. ^{13}C NMR (100 MHz, $CDCl_3$) **B-CPD–NBD-COOH**

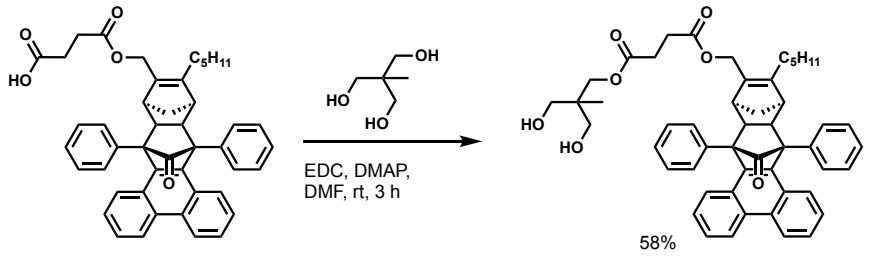

3-hydroxy-2-(hydroxymethyl)-2-methylpropyl ((15-oxo-12-pentyl-9,14-diphenyl-9,9a,10,13,13a,14-hexahydro-9,14:10,13-dimethanobenzo[*f*]tetraphen-11-yl)methyl) succinate (B-CPD–NBD diol)

Trimethylolethane (1.20 g, 10.0 mmol, 4.00 eq), *N*-(3-Dimethylaminopropyl)-*N*′-ethylcarbodiimide hydrochloride (EDC, 719 mg, 3.75 mmol, 1.50 eq) and DMAP (30.5 mg, 0.250 mmol, 0.100 eq) were dissolved in *N,N*-Dimethylformamide (DMF, 20 mL). A solution of B-CPD–NBD-COOH (1.69 g, 2.50 mmol, 1.00 eq) in 5 mL DMF was added dropwise over 30 min and allowed to stir while monitoring by TLC (hexanes:EtOAc, 1:1). Complete consumption of CPD–NBD-COOH was observed after 3 h and the solvent was removed under reduced pressure. The residue was taken up in 50 mL EtOAc, washed with water (2 X 50 mL), then brine (1 X 50 mL), dried over $MgSO_4$, filtered, and the solvent removed. The residue subjected to column chromatography TLC (hexanes:EtOAc, 2:1 — 100% EtOAc) to afford **B-CPD–NBD diol** (1.12 g, 1.44 mmol, 58%) as a white powder.

B-CPD–NBD diol: R_f (Hexanes:EtOAc, 2:1): 0.21; ^{1}H NMR (400 MHz, $CDCl_3$) δ 8.71 (d, *J* = 8.5 Hz, 2H), 7.94 (d, *J* = 7.7 Hz, 1H), 7.81 (d, *J* = 7.8 Hz, 1H), 7.66 (q, *J* = 7.0 Hz, 2H), 7.53 (t, *J* = 7.6 Hz, 2H), 7.48 (t, *J* = 7.2 Hz, 2H), 7.41 (t, *J* = 7.4 Hz, 2H), 7.23 – 7.19 (m, 4H), 7.09 (d, *J* = 8.5 Hz, 2H), 4.86 (d, *J* = 12.4 Hz, 1H), 4.67 (d, *J* = 12.4 Hz, 1H), 4.23 – 4.16 (m, 2H), 3.58 – 3.47 (m, 4H), 3.19 (d, *J* = 8.4 Hz, 1H), 3.06 (d, *J* = 8.5 Hz, 1H), 3.01 (s, 1H), 2.95 (s,

1H), 2.83 – 2.58 (m, 6H), 2.33 – 2.20 (m, 2H), 1.60 – 1.46 (m, 2H), 1.38 – 1.21 (m, 4H), 0.89 (t, J = 7.1 Hz, 3H), 0.81 (s, 3H), 0.46 (d, J = 9.8 Hz, 1H), -0.47 (d, J = 9.8 Hz, 1H) ppm; ^{13}C NMR (100 MHz, $CDCl_3$) δ 199.0, 173.2, 172.4, 153.7, 139.9, 137.2, 137.1, 135.0, 134.8, 131.6, 131.5, 130.9, 130.8, 129.1, 129.0, 128.8, 128.8, 127.9, 127.8, 127.8, 127.7, 127.5, 126.3, 126.3, 125.3, 125.3, 123.4, 123.3, 67.8, 67.7, 66.8, 63.6, 63.6, 60.2, 48.5, 47.5, 46.1, 44.9, 40.7, 40.3, 31.7, 29.1, 29.1, 28.0, 27.3, 22.4, 16.8, 14.0 ppm; FTIR (ATR) 3399, 3031, 2928, 2051, 1775, 1728, 1447, 1150, 1043, 753, 723, 698 cm^{-1}; HRMS (ES+) Exact mass calcd. for $C_{51}H_{52}O_7$ $[M+Na]^+$: 799.3611, found: 799.3619.

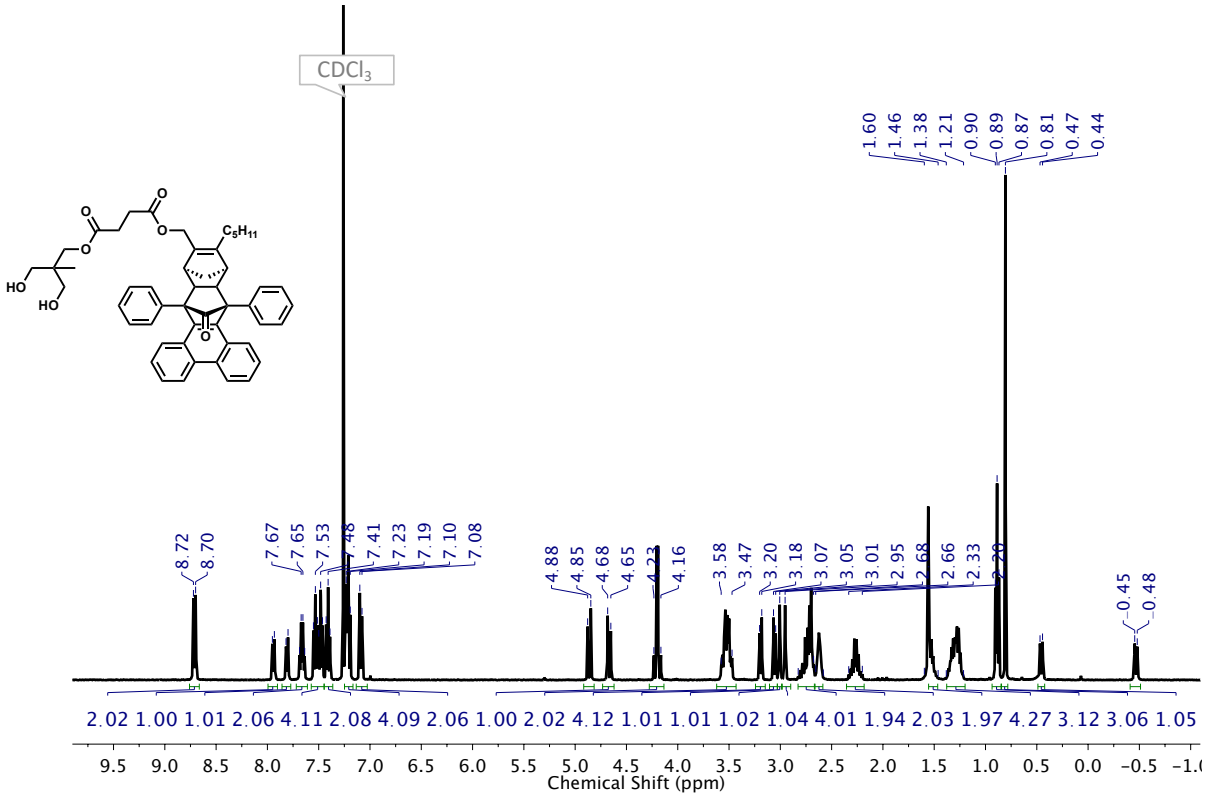

Figure S 3.13. ^{1}H NMR (400 MHz, $CDCl_3$) **B-CPD–NBD diol**

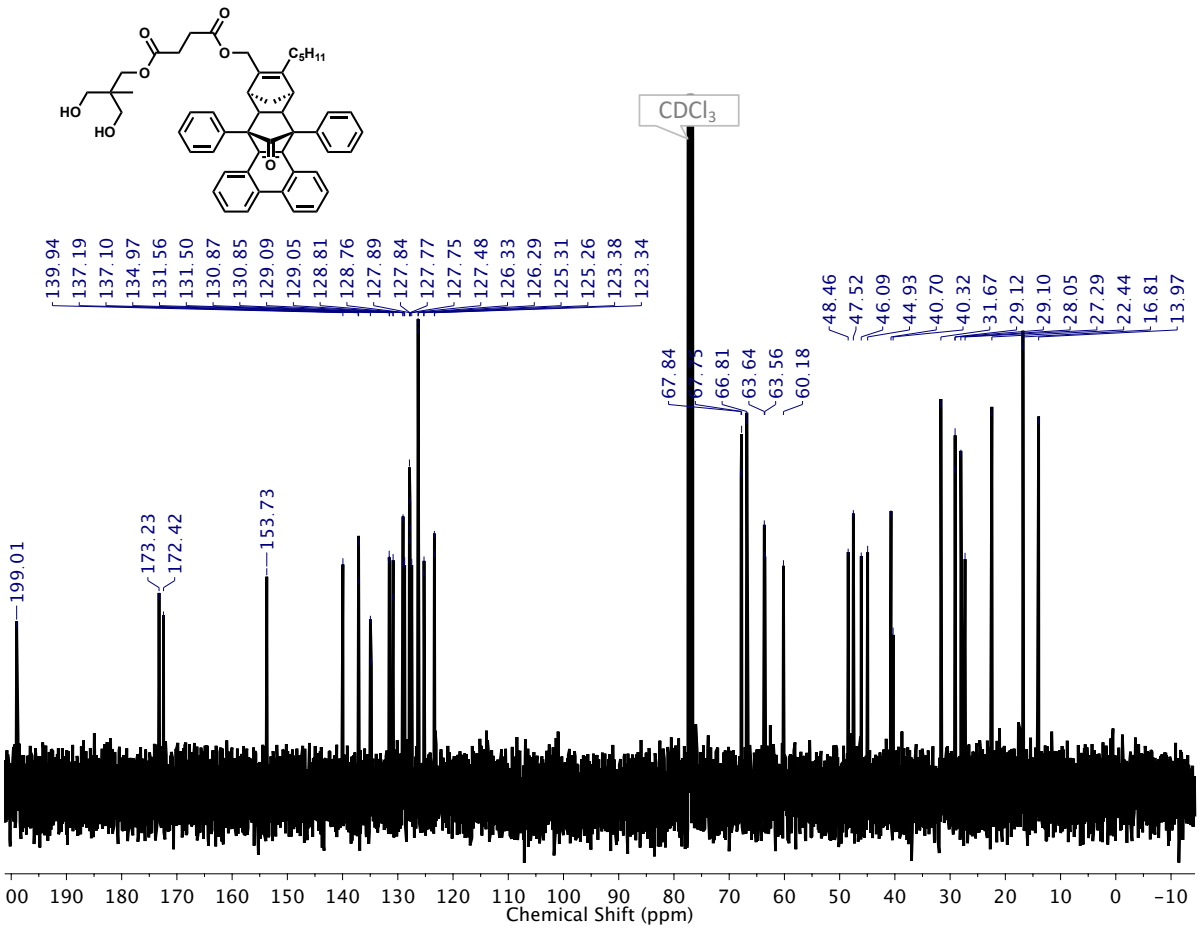

Figure S 3.14. ^{13}C NMR (100 MHz, $CDCl_3$) **B-CPD–NBD diol**

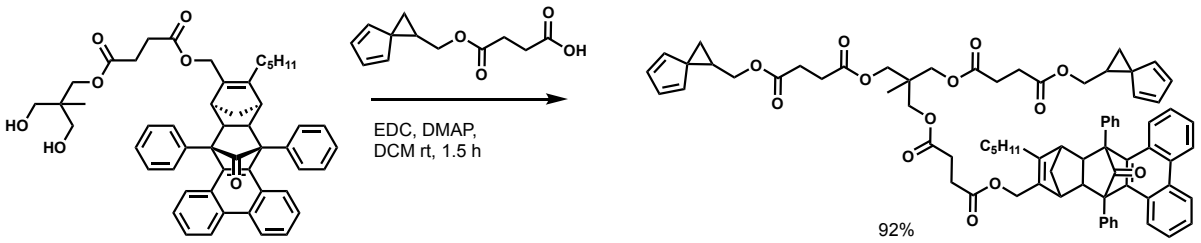

***O*,*O*'-(2-methyl-2-(((4-oxo-4-((15-oxo-12-pentyl-9,14-diphenyl-9,9a,10,13,13a,14-hexahydro-9,14:10,13-dimethanobenzo[*f*]tetraphen-11-yl)methoxy)butanoyl)oxy)methyl)propane-1,3-diyl) bis(spiro[2.4]hepta-4,6-dien-1-ylmethyl) disuccinate (B-CPD–NBD linker)**

B-CPD–NBD diol (572 mg, 0.736 mmol, 1.00 eq), spiro[2.4]hepta-4,6-diene-COOH[29] (491 mg, 2.21 mmol, 3.00 eq), EDC (424 mg, 2.21 mmol, 3.00 eq) and DMAP (18.0 mg, 0.147 mmol, 0.200 eq) were dissolved in DCM (4.9 mL). The solution was allowed to stir while monitoring by TLC (hexanes:EtOAc, 1:1). Complete consumption of B-CPD–NBD diol was observed after 1.5 h. The reaction mixture was transferred to a separatory funnel with an additional 20 mL DCM, washed with water (2 X 25 mL), then brine (1 X 25 mL), dried over $MgSO_4$, filtered, and the solvent removed. The residue subjected to loaded onto a plug of silica and eluted with 1:1, hexanes:EtOAc, to afford a **B-CPD–NBD linker** (801 mg, 0.676 mmol, 92%) as a white powder.

B-CPD–NBD linker: R_f (Hexanes:EtOAc, 1:1) = 0.64; ^{1}H NMR (400 MHz, $CDCl_3$) δ 8.71 (d, *J* = 8.5 Hz, 2H), 7.95 (d, *J* = 7.8 Hz, 1H), 7.81 (d, *J* = 7.8 Hz, 1H), 7.66 (q, *J* = 7.5 Hz, 2H), 7.53 (t, *J* = 7.7 Hz, 2H), 7.48 (t, *J* = 7.2 Hz, 2H), 7.40 (t, *J* = 7.6 Hz, 2H), 7.24 – 7.18 (m, 4H), 7.10 (d, *J* = 8.3 Hz, 2H), 6.55 (dt, *J* = 5.2, 1.8 Hz, 2H), 6.47 (dt, *J* = 5.0, 1.7 Hz, 2H), 6.20 (dt, *J* = 5.2, 1.7 Hz, 2H), 6.05 (dt, *J* = 5.0, 1.7 Hz, 2H), 4.85 (d, *J* = 12.4 Hz, 1H), 4.68 (d, *J* =

12.4 Hz, 1H), 4.33 (d, *J* = 7.6 Hz, 1H), 4.30 (d, *J* = 7.6 Hz, 1H), 4.19 (d, *J* = 7.1 Hz, 1H), 4.16 (d, *J* = 7.1 Hz, 1H), 4.03 – 3.97 (m, 6H), 3.19 (d, *J* = 8.5 Hz, 1H), 3.06 (d, *J* = 8.5 Hz, 1H), 3.01 (s, 1H), 2.95 (s, 1H), 2.80 – 2.64 (m, 4H), 2.61 (s, 8H), 2.39 (quint., *J* = 7.5 Hz, 2H), 2.35 – 2.20 (m, 2H), 1.82 (dd, *J* = 8.6, 4.4 Hz, 2H), 1.67 (dd, *J* = 7.0, 4.5 Hz, 2H), 1.60 – 1.48 (m, 2H), 1.38 – 1.23 (m, 4H), 1.00 (s, 3H), 0.89 (t, *J* = 7.1 Hz, 3H), 0.45 (d, *J* = 9.7 Hz, 1H), -0.47 (d, *J* = 9.8 Hz, 1H) ppm; ^{13}C NMR (100 MHz, $CDCl_3$) δ 198.8, 172.3, 172.1, 171.9, 171.9, 153.4, 140.1, 138.9, 137.2, 137.2, 135.0, 134.8, 134.4, 131.6, 131.5, 131.2, 130.9, 130.8, 129.1, 129.0, 128.8, 128.7, 127.9, 127.7, 127.7, 127.5, 126.3, 126.3, 125.3, 125.3, 123.4, 123.3, 66.3, 65.9, 65.9, 63.6, 63.5, 60.0, 48.4, 47.4, 46.0, 45.0, 41.6, 40.3, 38.4, 31.7, 29.0, 28.9, 28.9, 28.9, 28.1, 27.3, 25.3, 22.4, 17.3, 17.0, 14.0 ppm; FTIR (ATR) 3065, 3030, 2929, 2324, 2050, 1777, 1728, 1447, 1385, 1145, 981, 752, 699 cm^{-1}; HRMS (ES+) Exact mass calcd. for $C_{75}H_{76}O_{13}$ $[M+Na]^+$: 1207.5184, found: 1207.5184.

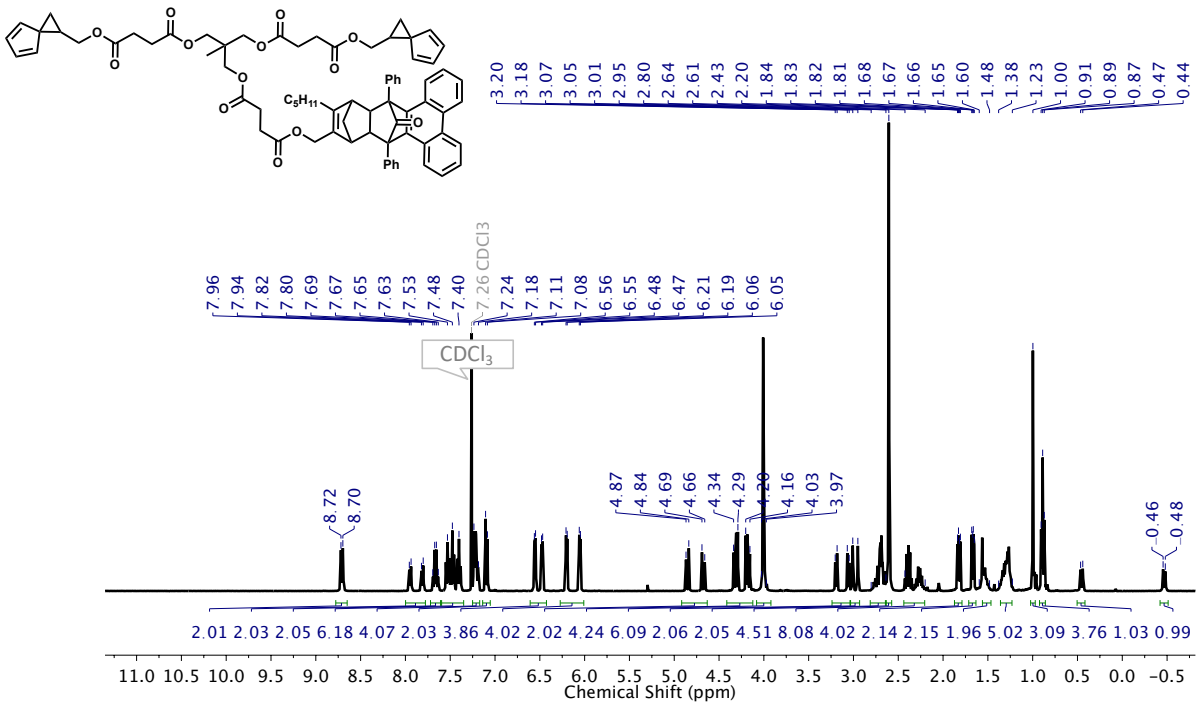

Figure S 3.15. ^{1}H NMR (400 MHz, $CDCl_3$) **B-CPD–NBD linker**

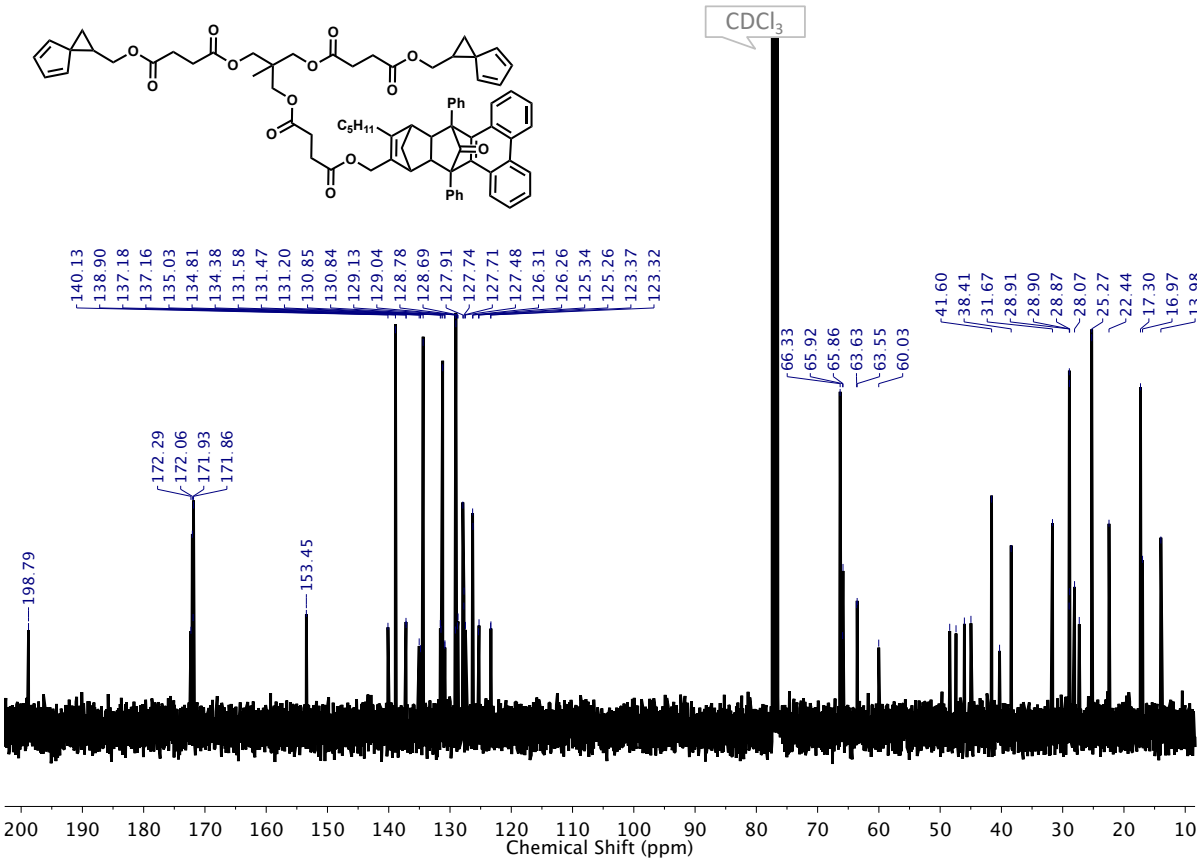

Figure S 3.16. ^{13}C NMR (100 MHz, $CDCl_3$) **B-CPD–NBD linker**

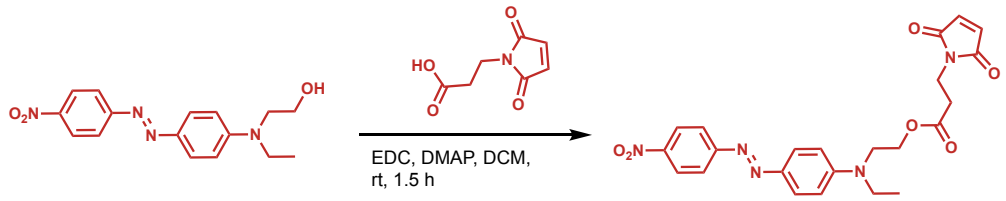

Maleimide-Disperse Red 1 (mal-Red)

3-maleimidopropanoic acid[72] (254 mg, 1.50 mmol, 1.50 eq), EDC (288 mg, 1.50 mmol, 1.50 eq) and DMAP (12.2 mg, 0.100 mmol, 0.100 eq) were dissolved in DCM (5 mL). To this solution was added Disperse Red 1 (314 mg, 1.00 mmol, 1.00 eq). The solution was allowed to stir while monitoring by TLC (hexanes:EtOAc, 1:1). Complete consumption of Disperse Red 1 was observed after 1.5 h. 10 mL DCM was added and they organic layer was washed with water (2 x 10 mL). The organic layer was concentrated under reduced pressure, then the residue was dissolved in DCM (1 mL). The product was precipitated out of solution by adding MeOH (10 mL) and cooling on ice. The red powder was collected by vacuum filtration and rinsed with cold MeOH (10 mL) to afford **mal-Red** as a red powder (415 mg, 0.892 mmol, 89%).

Mal-Red: R_f (Hexanes:EtOAc, 1:1) = 0.62; ^{1}H NMR (400 MHz, $CDCl_3$) δ 8.33 (d, J = 9.1 Hz, 2H), 7.93 (d, J = 9.1 Hz, 2H), 7.90 (d, J = 9.2 Hz, 2H), 6.80 (d, J = 9.3 Hz, 2H), 6.69 (s, 2H), 4.30 (t, J = 6.4 Hz, 2H), 3.83 (t, J = 7.0 Hz, 2H), 3.68 (t, J = 6.4 Hz, 2H), 3.53 (q, J = 7.1 Hz, 2H), 2.64 (t, J = 7.0 Hz, 2H), 1.26 (t, J = 7.1 Hz, 3H) ppm; ^{13}C NMR (100 MHz, $CDCl_3$) δ 170.6, 170.3, 156.7, 151.2, 147.4, 143.8, 134.2, 126.2, 124.7, 122.6, 111.4, 61.6, 48.6, 45.6, 33.5, 32.9, 12.3 ppm; FTIR (ATR) 3102, 2970, 2935, 2907, 1735, 1701, 1599, 1586, 1510, 1448, 1388, 1339, 1132, 830, 694 cm^{-1}; HRMS (ES+) Exact mass calcd. for $C_{23}H_{23}N_5O_6$ $[M+Na]^+$: 488.1546, found: 488.1554.

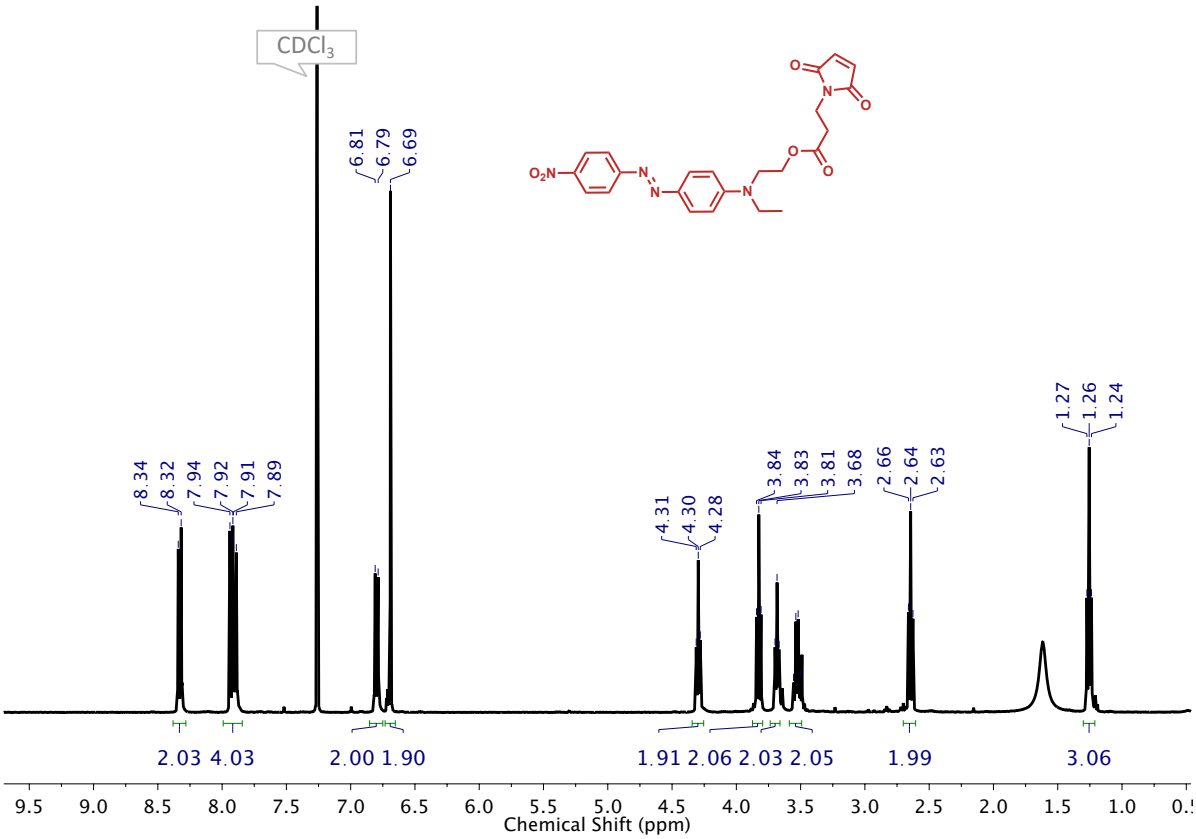

Figure S 3.17. ^{1}H NMR (400 MHz, $CDCl_3$) **mal-Red**

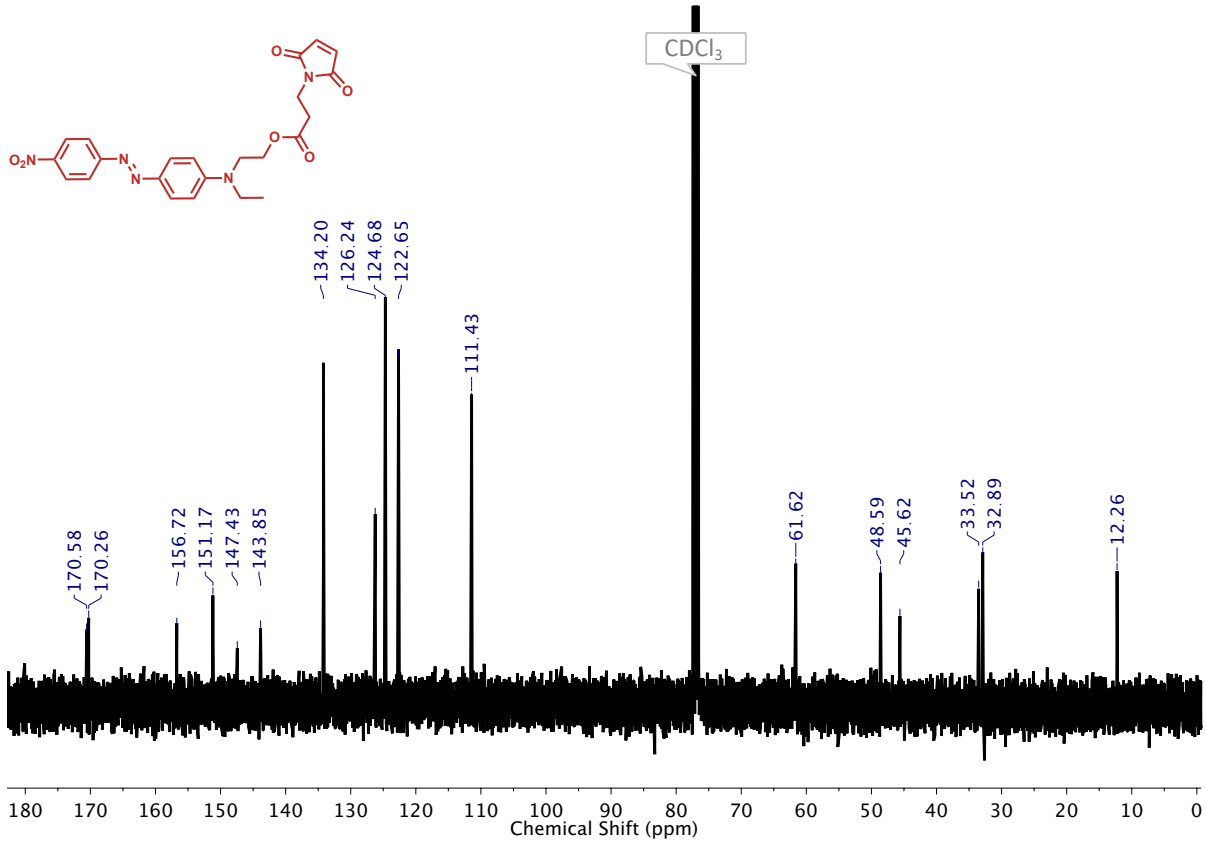

Figure S 3.18. ^{13}C NMR (100 MHz, $CDCl_3$) **mal-Red**

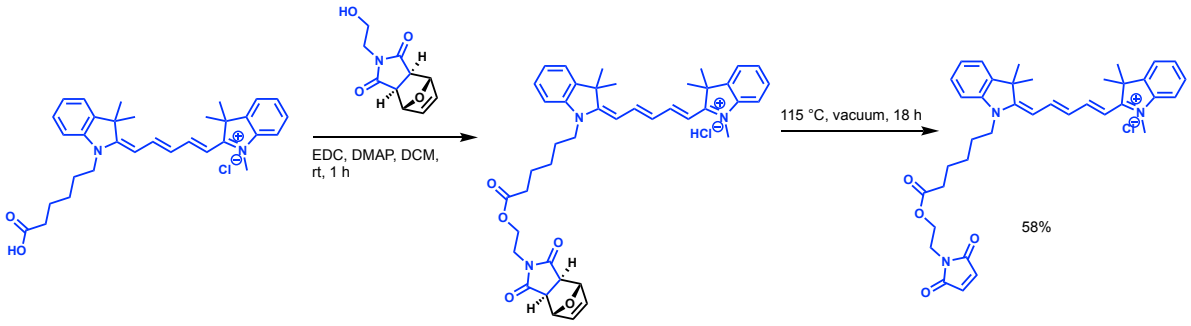

Maleimide-Cyanine 5 (mal-Cy5)

Exo-mal-OH[77] (191 mg, 0.867 mmol, 1.50 eq), EDC (166 mg, 0.867 mmol, 1.50 eq) DMAP (7.06 mg, 0.0578 mmol, 0.100 eq), and Cy5-COOH[73] (300 mg, 0.578 mmol, 1.00 eq) were dissolved in DCM (3 mL). The solution was allowed to stir while monitoring by TLC (MeOH:EtOAc, 5:95). Complete consumption of Cy5-COOH was observed after 1 h. 10 mL DCM was added and they organic layer was washed with water (2 x 10 mL). The organic layer was concentrated under reduced pressure, then the residue was residue loaded onto a plug of silica. Excess exo-mal-OH was removed by rinsing with EtOAc (50 mL), then the protected mal-Cy5 was eluted in a mixture of MeOH:EtOAc, 5:95 (100 mL). The solvent was removed under reduced pressure, then the neat residue was heated at 115°C under high vacuum for 18 h to afford **mal-Cy5** (215 mg, 0.335 mmol, 58%) as an iridescent dark violet foam.

Mal-Cy5: R_f (MeOH:EtOAc, 5:95) = 0.25; ^{1}H NMR (400 MHz, DMSO-d_6) δ 8.33 (t, J = 13.1 Hz, 2H), 7.62 (d, J = 7.4 Hz, 2H), 7.41 –7.37 (m, 4H), 7.27 – 7.22 (m, 2H), 7.03 (s, 2H), 6.55 (t, J = 12.3 Hz, 1H), 6.30 (d, J = 13.9 Hz, 1H), 6.26 (d, J = 13.9 Hz, 1H), 4.12 (t, J = 5.3 Hz, 2H), 4.07 (t, J = 6.9 Hz, 2H), 3.63 (t, J = 5.3 Hz, 2H), 3.60 (s, 3H), 2.22 (t, J = 7.2 Hz, 2H), 1.73 – 1.61 (m, 2 H), 1.68 (s, 12H), 1.56 – 1.49 (m, 2H), 1.39 – 1.31 (m, 2H) ppm; ^{13}C NMR (100 MHz, DMSO- d_6) δ 173.4, 172.8, 172.7, 171.0, 154.2, 154.2, 143.0, 142.2, 141.3, 141.2, 134.8, 128.6, 128.5, 125.5, 124.9, 124.8, 122.6, 122.5, 111.3, 111.2, 103.5, 103.2, 61.1,

49.0, 36.7, 33.3, 31.3, 27.4, 27.3, 27.2, 26.8, 25.6, 24.1 ppm; FTIR (ATR) 3099, 2958, 2924, 2859, 2164, 1978, 1702, 1599, 1478, 1442, 1366, 1328, 1132, 1071, 917, 693 cm^{-1}; HRMS (ES+) Exact mass calcd. for $C_{38}H_{44}N_3O_4$ $[M]^+$: 606.3332, found: 606.3345.

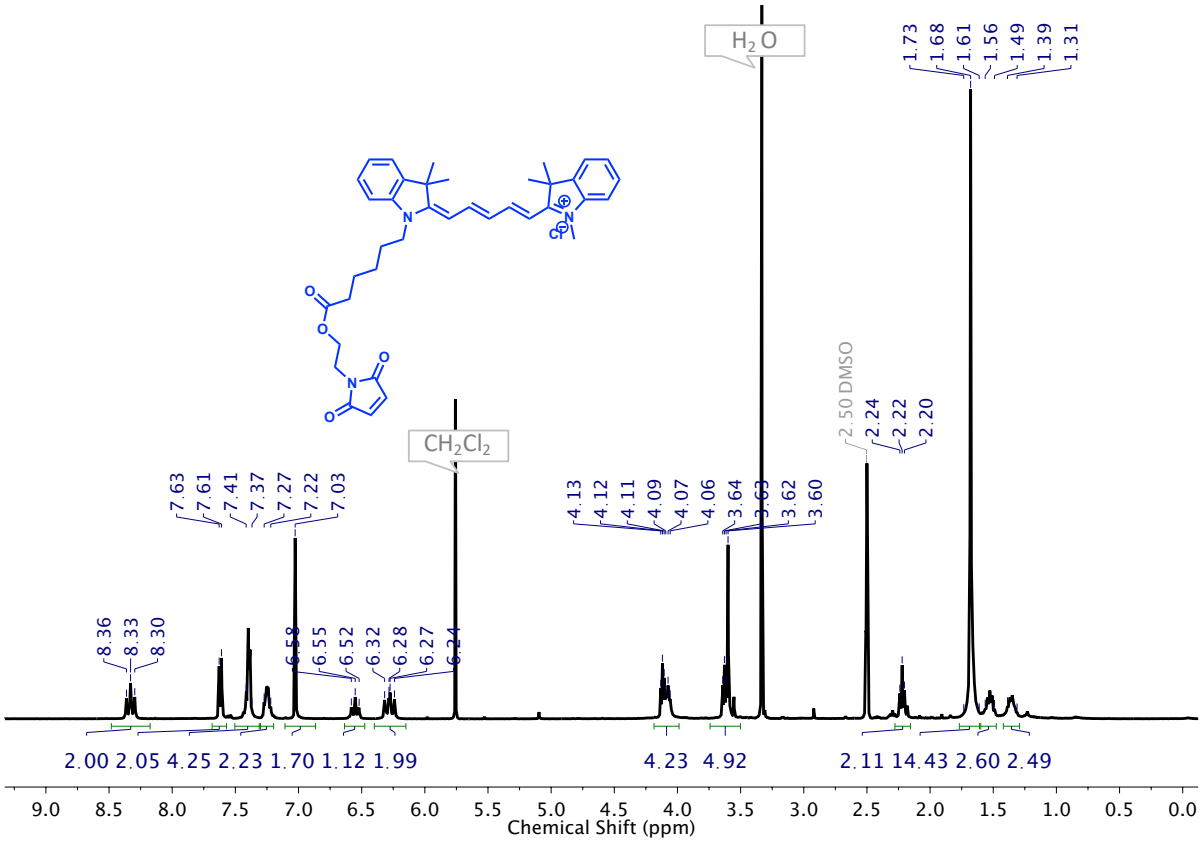

Figure S 3.19. ^{1}H NMR (400 MHz, DMSO-D6) **mal-Cy5**

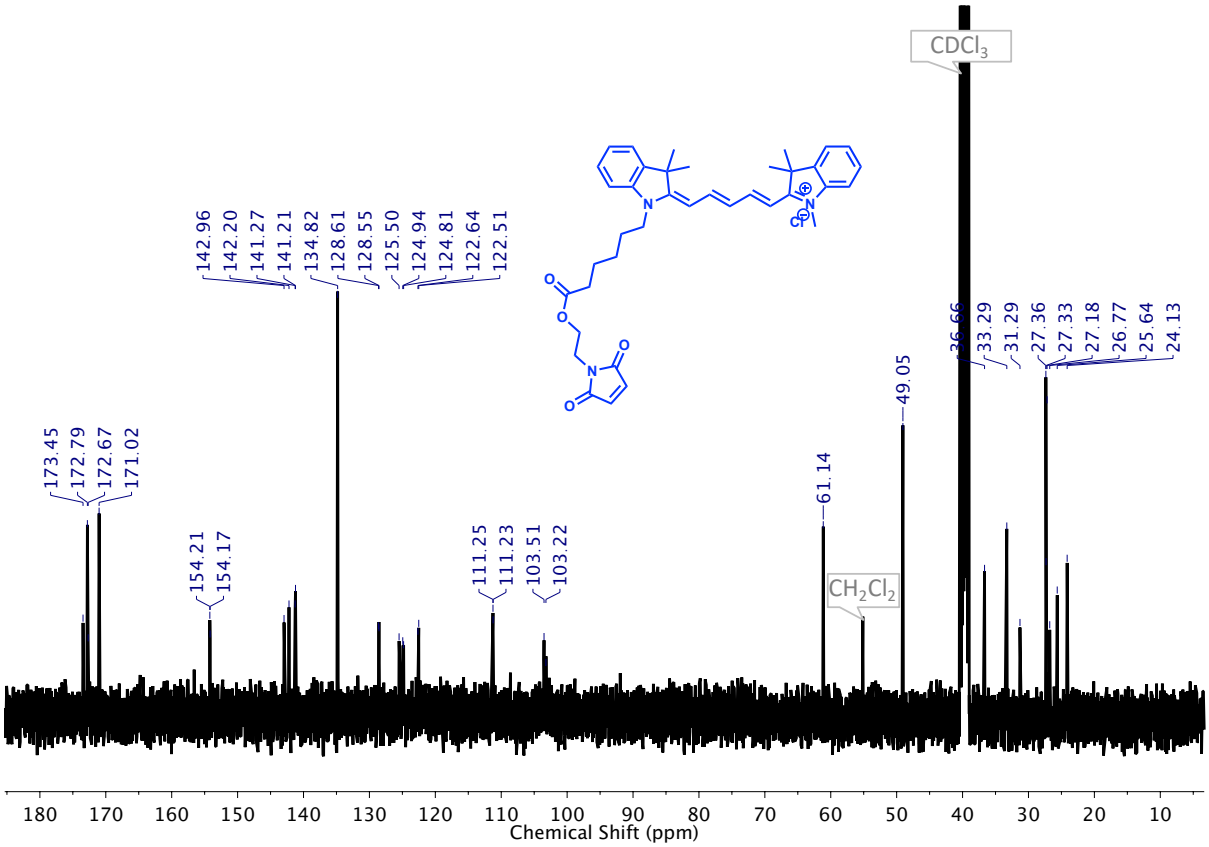

Figure S 3.20. ^{13}C NMR (100 MHz, DMSO-D6) **mal-Cy5**

Synthesis of Polymer Building Blocks

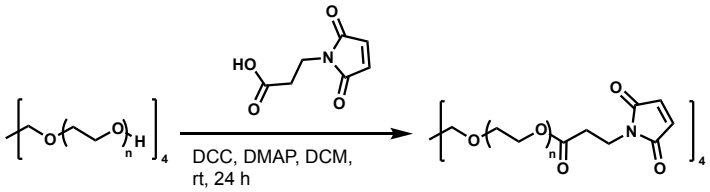

Maleimide functionalization of tetra-PEG:

To a 20 mL vial equipped with stir bar was added tetra-PEG (purchased from JenKem Technology, M_n = 20,000 g/mol, 1.00 g, 0.0500 mmol, 1.00 eq), 3-maleimidopropanoic acid[72] (84.6 mg, 0.500 mmol, 10.0 eq), *N,N′*-Dicyclohexylcarbodiimide (DCC) (113 mg, 0.550 mmol, 11.0 eq), DMAP (0.500 mL of 10 mM stock solution in DCM, 0.00500 mmol, 0.100 eq) and 3.5 mL DCM. The vial was capped under air starting and allowed to stir at rt for 24 h (at which complete formation of the ester was confirmed by crude ^{1}H NMR). Ethanol (EtOH, 20 mL) was added to the reaction mixture, then the solution was cooled to 0 °C and left unagitated for 30 min to allow the material to precipitate. The solid was filtered and rinsed with cold EtOH. The material was dissolved in minimal DCM and the precipitation was repeated once more, then dried under reduced pressure to afford the corresponding maleimide functionalized tetra-PEG, **PEG-mal$_4$** (769 mg, 0.0354 mmol, 71% recovered yield). $M_{n(NMR)}$ (DP = 119/arm) = 21,700 g/mol, $M_{n(SEC)}$ = 37,600 g/mol, $Đ$ = 1.14.

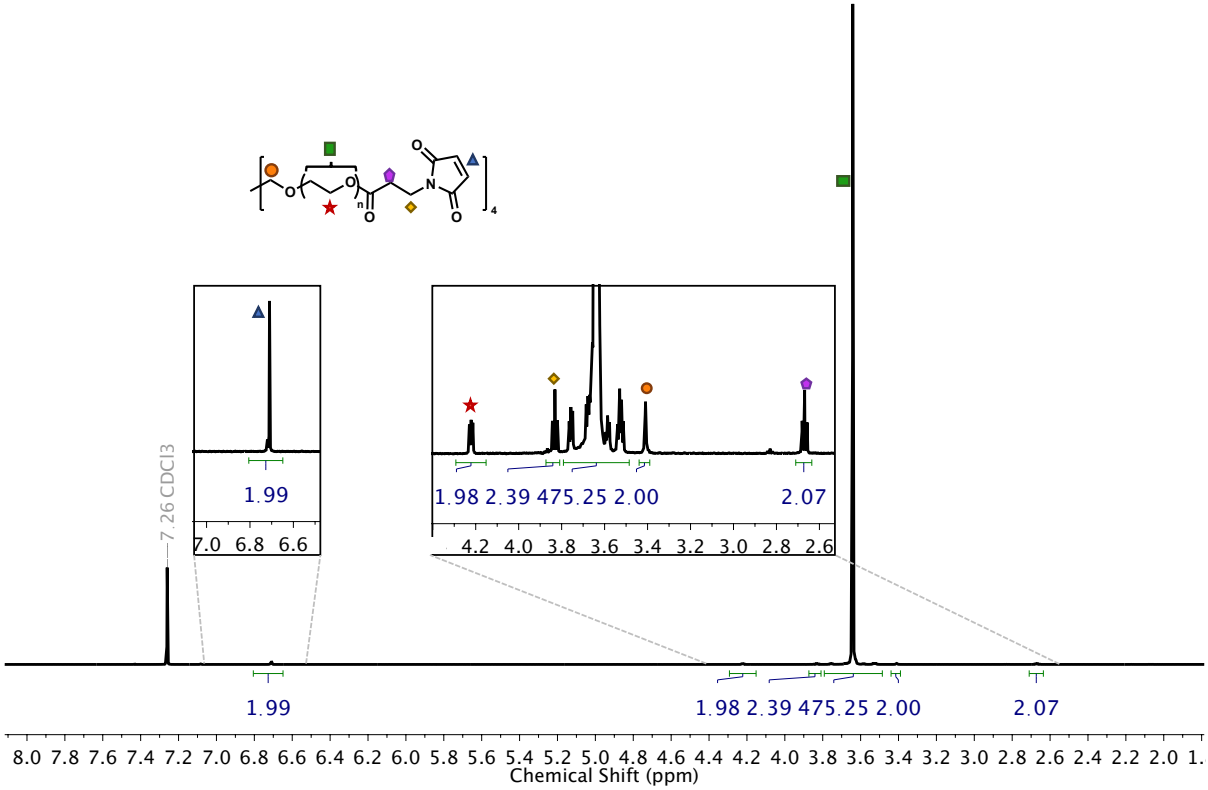

Figure S 3.21. ^{1}H NMR (600 MHz, $CDCl_3$) **PEG-mal$_4$**

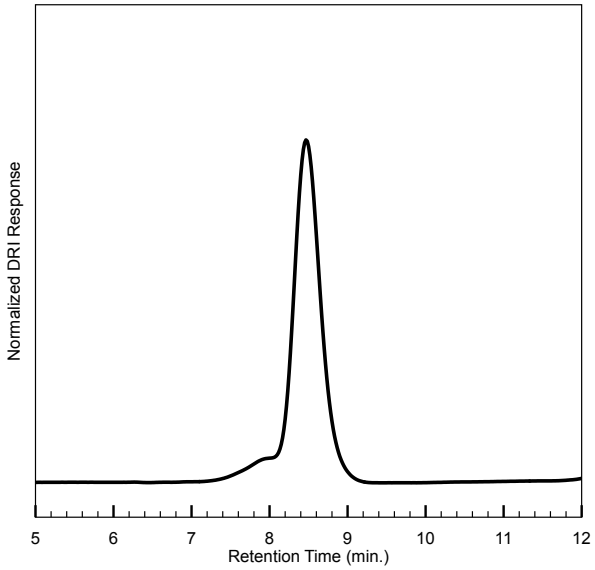

Figure S 3.22. SEC-RI trace of **PEG-mal$_4$**

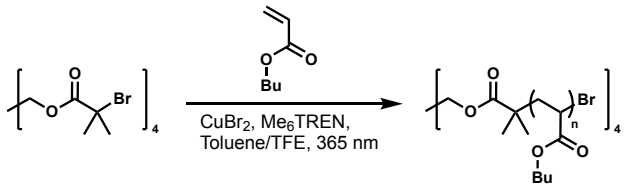

Preparation of tetra-poly(butyl acrylate):

Light induced ATRP polymerization conditions were adapted from literature.[78] A solution of copper(II) bromide (2.79 mg, 0.0125 mmol, 0.0800 eq) and tris[2-(dimethylamino)ethyl]amine (Me_6TREN, 20.1 μL, 0.0751 mmol, 0.480 eq) was prepared in 0.890 mL of trifluoroethanol. The mixture was allowed to sonicate for 30 min to completely dissolve the catalyst complex. In a 20 mL scintillation vial, butyl acrylate (5.00 mL, 34.9 mmol, 223 eq) was dissolved in 3.58 mL of toluene (inhibitor was removed from butyl acrylate by passing through a plug of basic alumina). The Cu(II)/trifluoroethanol solution was transferred into the acrylate solution, followed by 4f-BiB[71] (114 mg, 0.156 mmol, 1.00 eq). The vial was capped with a septum and the solution was degassed with nitrogen for 10 min. With stirring, the polymerization mixture was then irradiated ($\lambda \approx 365$ nm) in a commercial UV nail lamp system for 4.5 h. The resulting polymer was purified by passing the crude reaction solution through a column of basic alumina, concentrated, then precipitated into a mixture of H_2O:MeOH, 1:10 (100 mL) and cooled on ice. The supernatant was decanted, and the precipitation was repeated once more. The resulting polymer was dried under reduced pressure to afford **tetra-PBA** (2.15 g, 0.131 mmol, 84% recovered yield). Conversion = 60%. $M_{n(theor)}$ = 17,900 g/mol, $M_{n(NMR)}$ (DP = 122) = 16,400 g/mol, $M_{n(SEC)}$ = 14,400 g/mol, $Đ$ = 1.06.

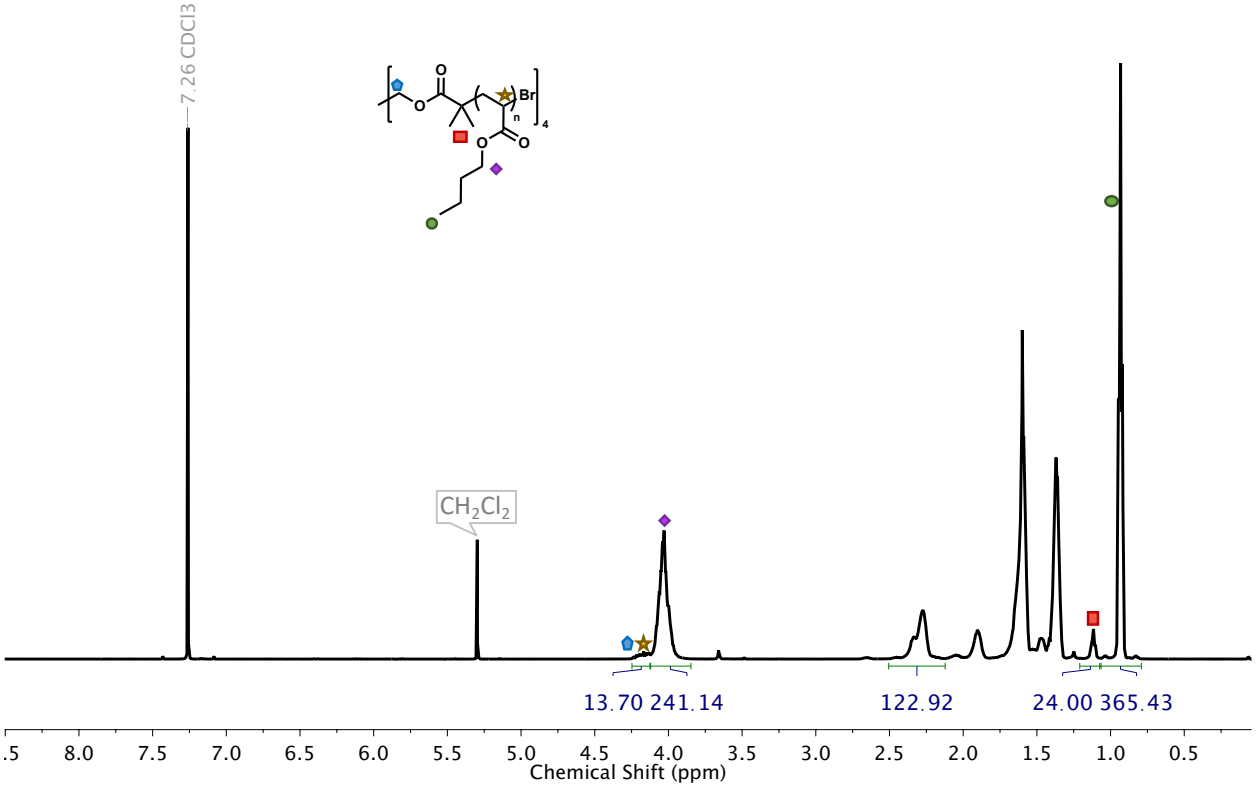

Figure S 3.23. ^{1}H NMR (600 MHz, $CDCl_3$) **tetra-PBA**

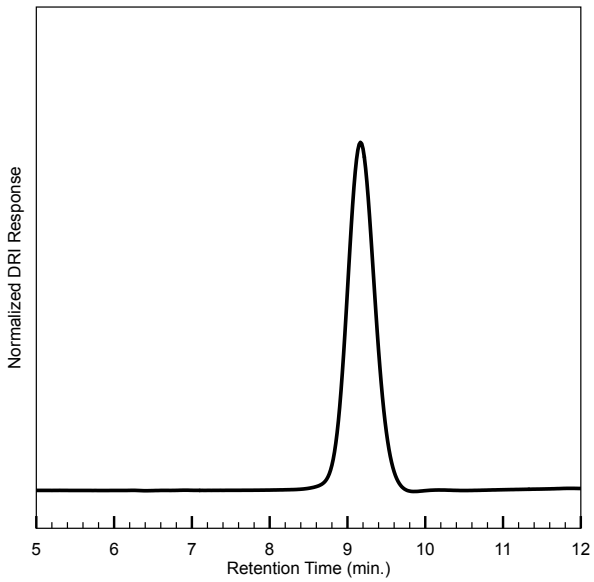

Figure S 3.24. SEC-RI trace of **tetra-PBA**

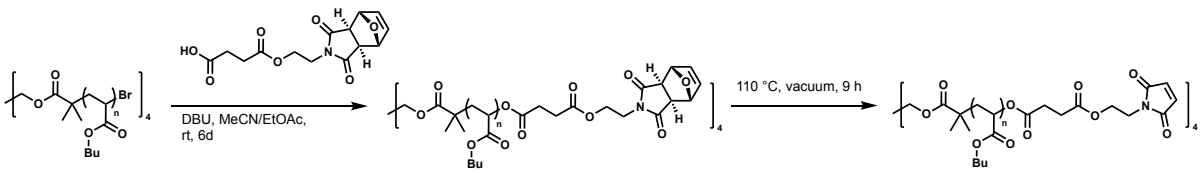

Maleimide functionalization of tetra-PBA:

In a 20 mL scintillation vial equipped with stir bar, **tetra-PBA** (2.00 g, 0.122 mmol, 1.00 mmol) was dissolved in EtOAc (3.40 mL). In a separate vial, 1,8-Diazabicyclo[5.4.0]undec-7-ene (DBU) (447 mL, 2.99 mmol, 24.5 eq) was added to a solution of exo-mal-COOH[75] (905 mg, 2.93 mmol, 24.0 eq) in acetonitrile (MeCN, 3.40 mL). Once dissolved, the acid-DBU solution was transferred to the polymer solution and the vial was capped under air. The solution was allowed to stir at rt for 6 d (at which complete formation of the ester was confirmed by crude ^{1}H NMR). The crude reaction mixture was precipitated into mixture of H_2O:MeOH, 1:10 (100 mL) and cooled on ice. The supernatant was discarded, and the resulting material was re-dissolved in minimal DCM. The precipitation process was repeated once more before drying the material under reduced pressure to afford the protected maleimide-polymer (1.56 g, 0.0902 mmol, 74% recovered yield $M_{n(SEC)}$ = 16,100 g/mol, $Đ$ = 1.12). The resulting residue was then heated at 110 °C under vacuum for 9 h to yield the corresponding maleimide functionalized tetra-PBA, **PBA-mal$_4$** $M_{n(NMR)}$ (DP = 126) = 17,500 g/mol, $M_{n(SEC)}$ = 16,900 g/mol, $Đ$ = 1.33.

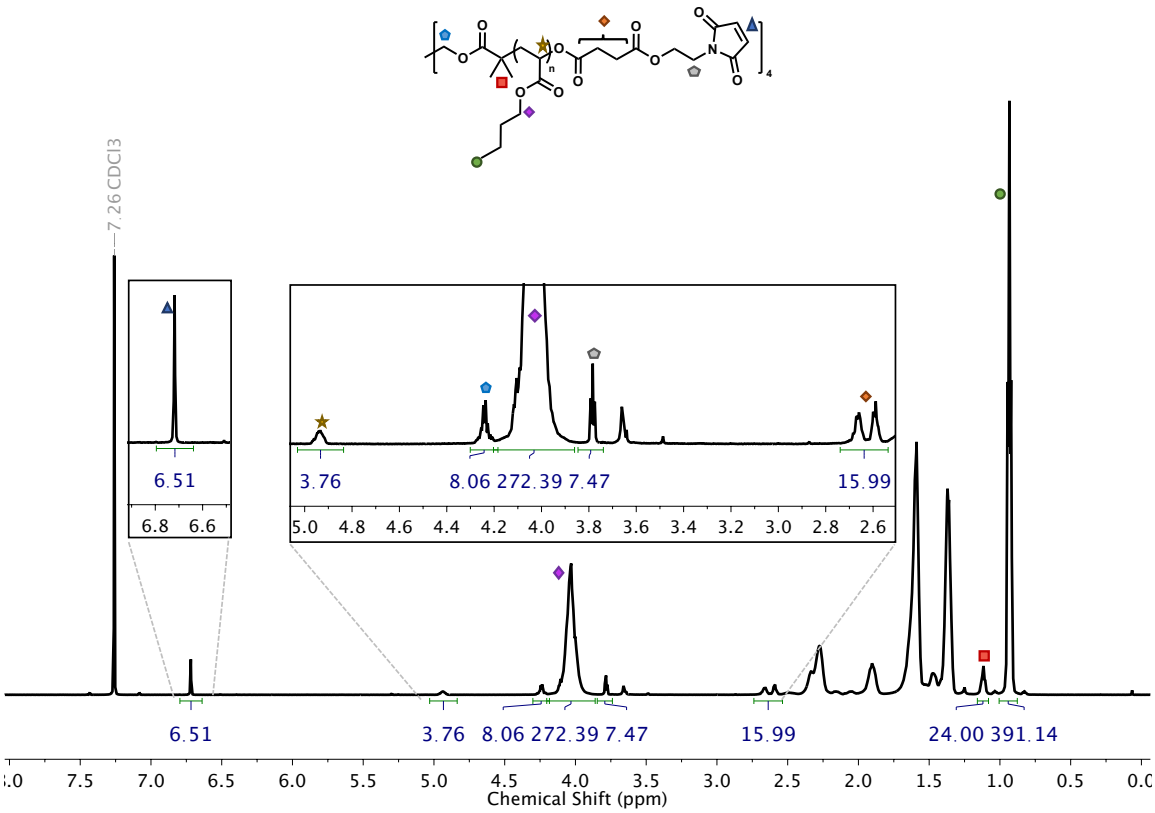

Figure S 3.25. ^{1}H NMR (600 MHz, $CDCl_3$) **PBA-mal$_4$**

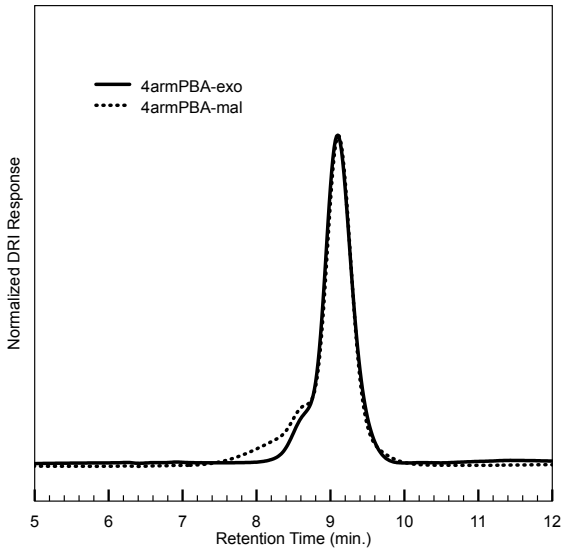

Figure S 3.26. Overlay of SEC-RI traces of protected **maleimide PBA** (solid black) and after heating under vacuum to deprotect **PBA-mal$_4$** (dotted black). Production of shoulder indicates unwanted polymer coupling occurs during deprotection step.

Comparative Study of Photo-Labile Adducts

TGA-MS

Thermo-gravimetric analysis (TGA) and Mass Spectra were collected on a TA Instruments Discovery Thermo-Gravimetric Analyzer with Mass Spectrometer Assembly. The measurements were taken under a nitrogen environment from room temperature ramping up to 300 °C at 20 °C per minute.

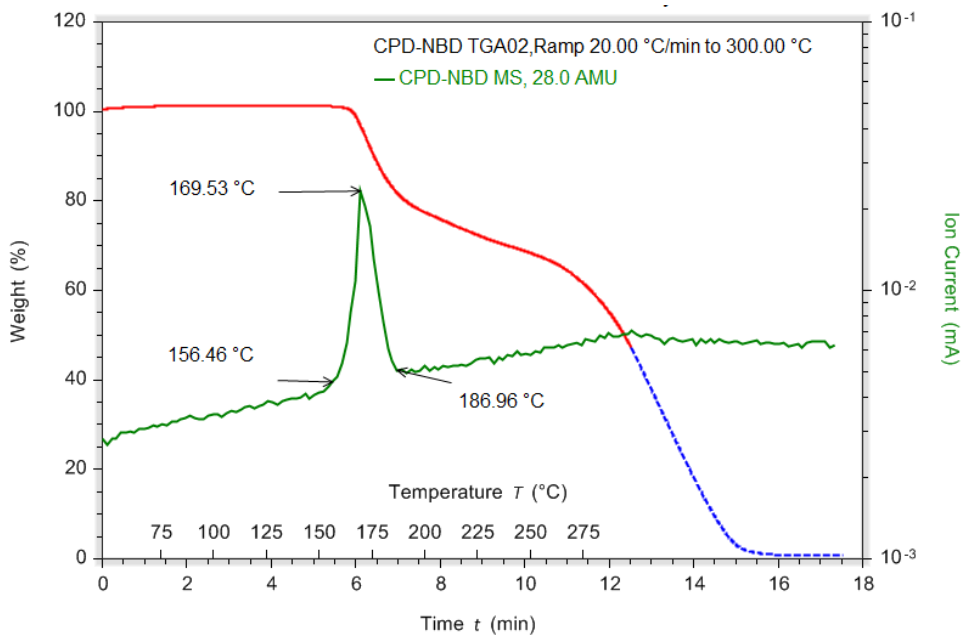

Figure S 3.27. Overlay of TGA Thermal Curve of Ph-CPD–NBD and ion current (28.0 AMU) corresponding to carbon monoxide, indicating weight loss event corresponds to the thermal de-carbonylation.

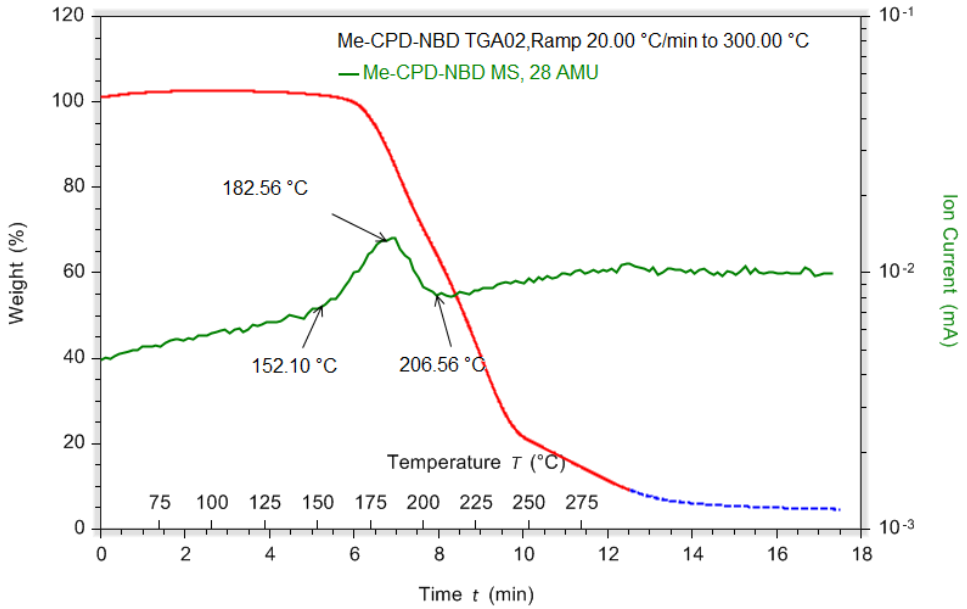

Figure S 3.28. Overlay of TGA Thermal Curve of Me-CPD–NBD and ion current (28.0 AMU) corresponding to carbon monoxide, indicating first weight lot event corresponds to the thermal de-carbonylation.

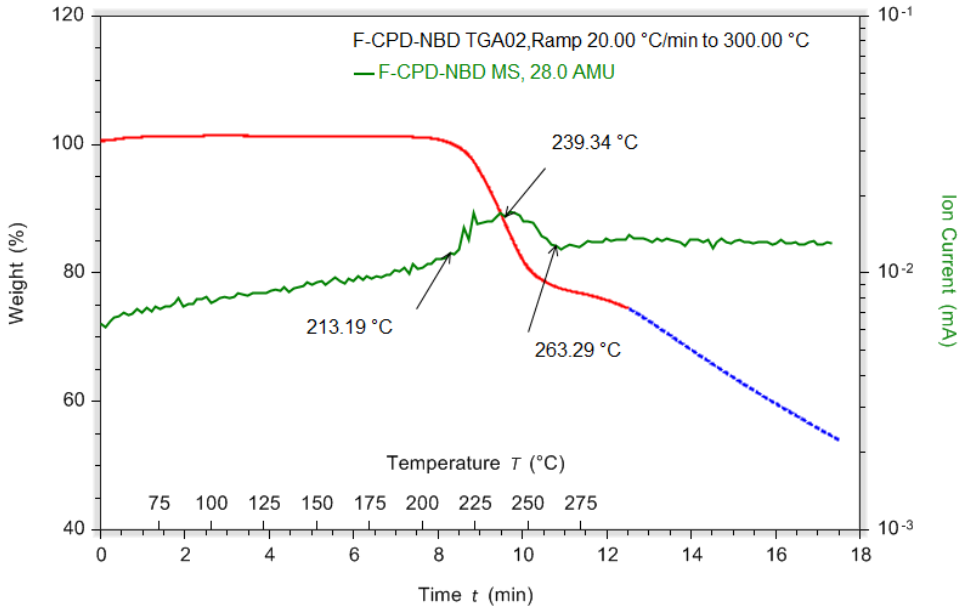

Figure S 3.29. Overlay of TGA Thermal Curve of B-CPD–NBD and ion current (28.0 AMU) corresponding to carbon monoxide, indicating first weight loss event corresponds to the thermal de-carbonylation.

Reaction Monitoring by ^{1}H NMR

25 mM solutions of each CPD–NBD adduct were prepared in toluene-d_8 then sparged with nitrogen for 5 min. The sparged solutions were transferred to sealed NMR tubes under nitrogen. The solutions were irradiated directly in NMR tubes within a Rayonet RPR-200 Chamber (300 nm) while monitored periodically by ^{1}H NMR over 240 min. ^{1}H NMR spectra were recorded on a Varian spectrometer (600 MHz) and are reported relative to the residual protio-signal in toluene-d_8. Conversion at each time point was determined by the ratio of integrals from the proton signals for the adduct and resulting cyclopentadiene (Figure 1c).

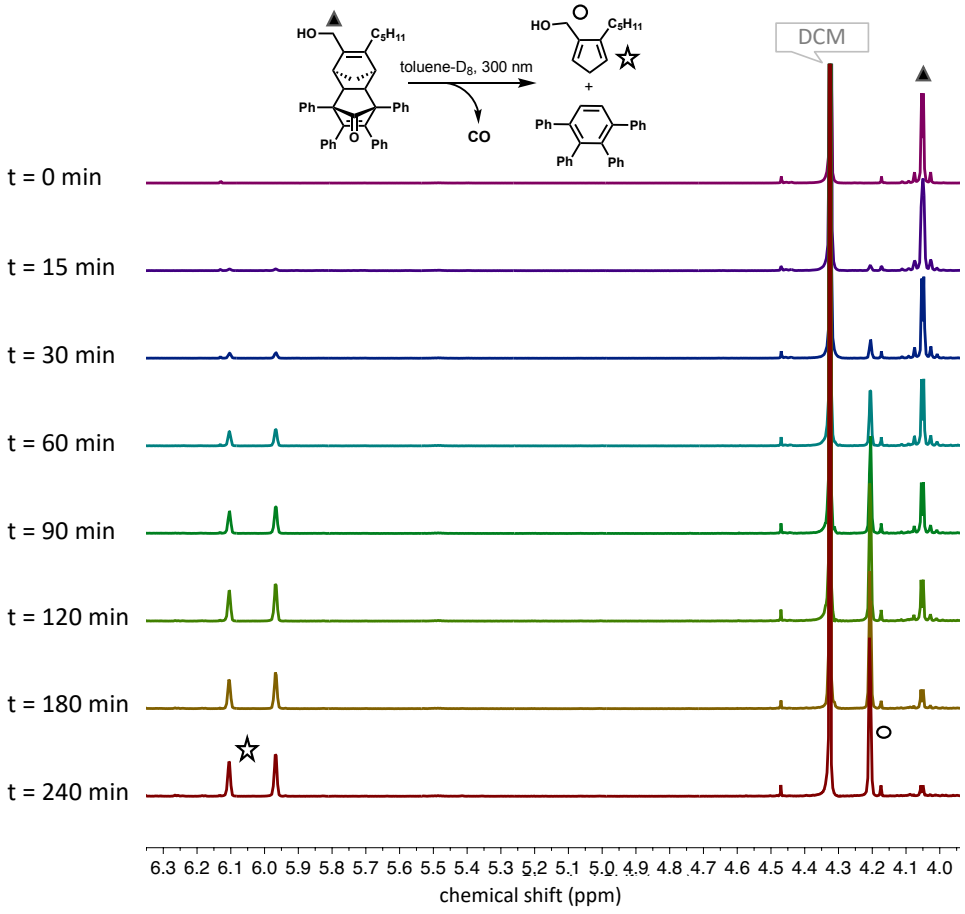

Figure S 3.30. Monitoring of photolysis of **Ph-CPD–NBD** by ^{1}H NMR in toluene-d_8. Appearance of diagnostic alkene peaks for Cp (star) confirm successful production of desired diene upon irradiation. Conversion determined by ratio of methylene protons indicated for **Ph-CPD–NBD** (triangle) and Cp (circle).

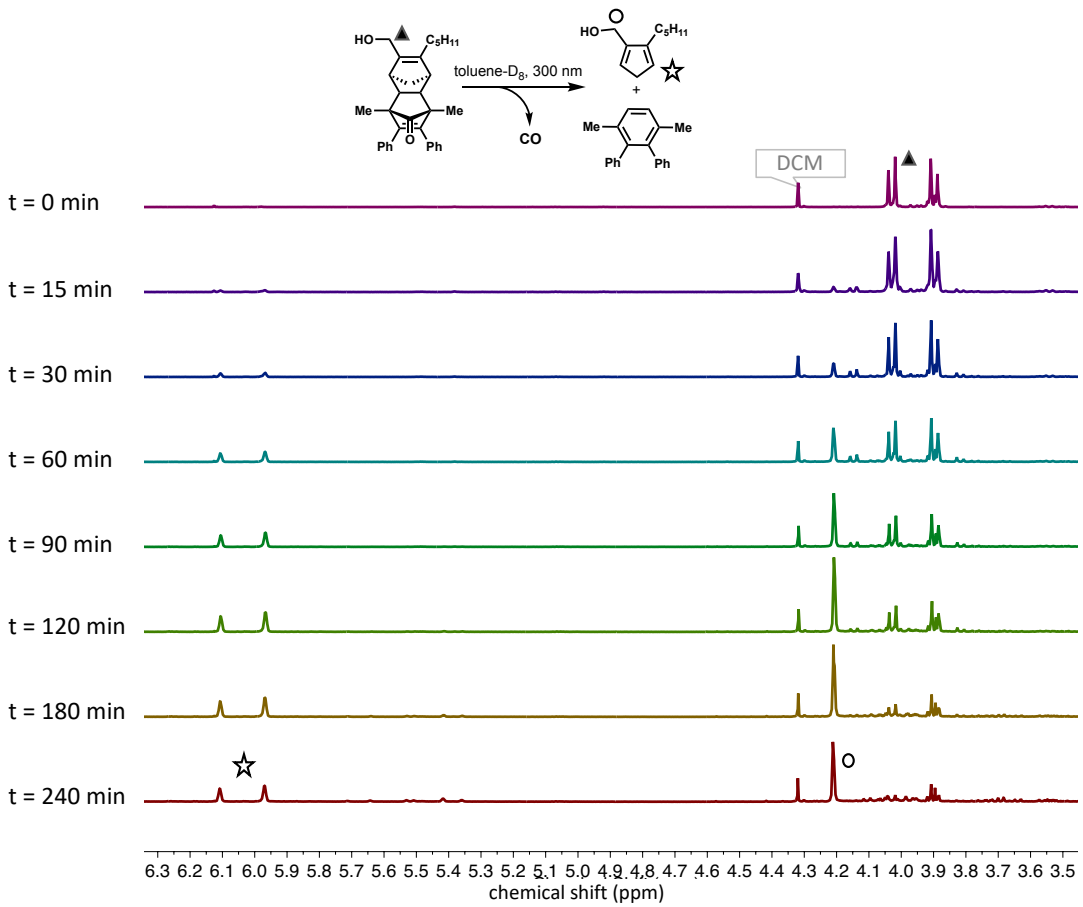

Figure S 3.31. Monitoring of photolysis of **Me-CPD–NBD** by ^{1}H NMR in toluene-d_8. Appearance of diagnostic alkene peaks for Cp (star) confirm successful production of desired diene upon irradiation. Conversion determined by ratio of methylene protons indicated for **Me-CPD–NBD** (triangle) and Cp (circle).

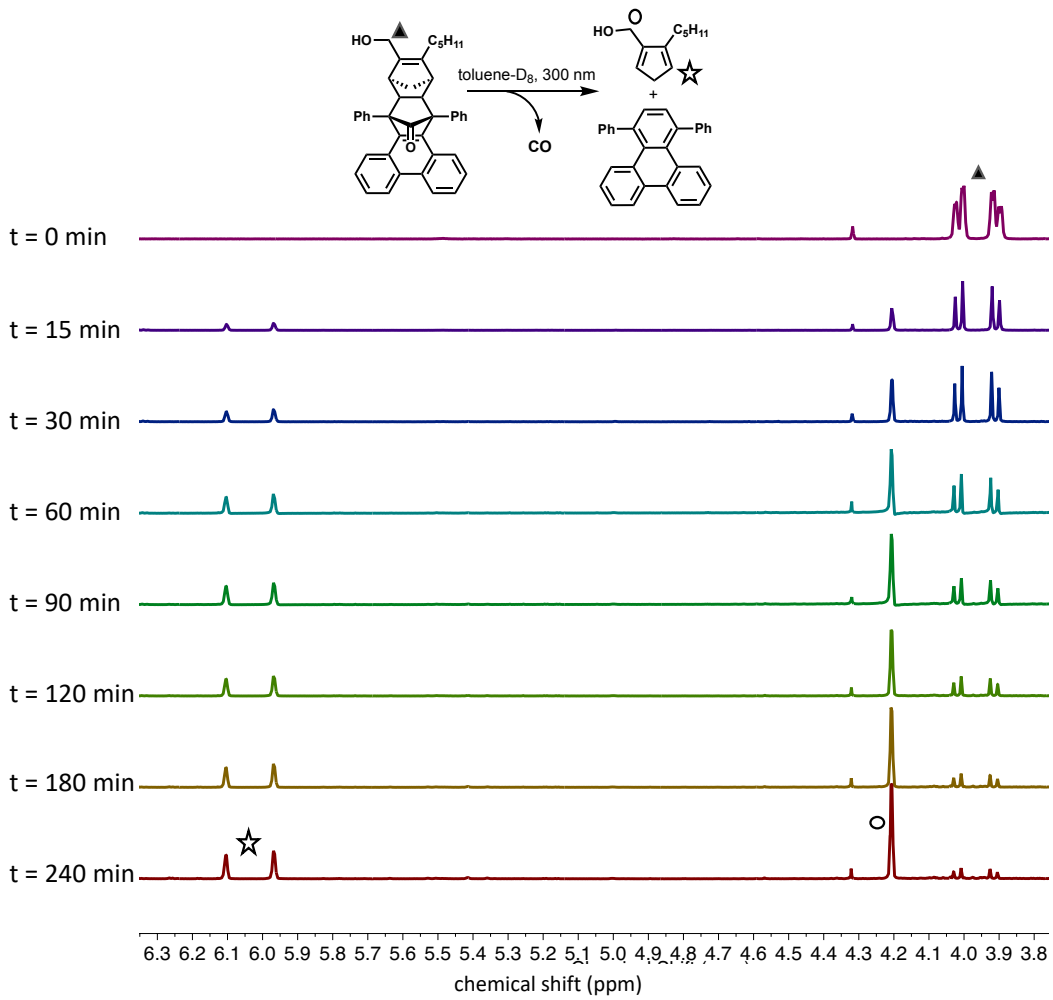

Figure S 3.32. Monitoring of photolysis of **B-CPD–NBD** by ^{1}H NMR in toluene-d_8. Appearance of diagnostic alkene peaks for Cp (star) confirm successful production of desired diene upon irradiation. Conversion determined by ratio of methylene protons indicated for **B-CPD–NBD** (triangle) and Cp (circle).

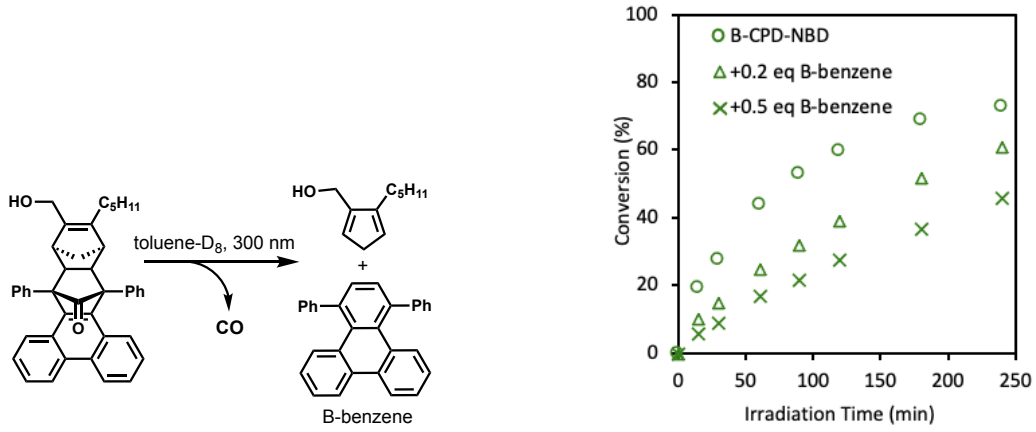

Figure S 3.33. Comparison of Cp production (determined by ^{1}H NMR in toluene-d_8) upon irradiation of 25 mM solutions of **B-CPD–NBD** initially (**Figure S32**, circles), and doped with 0.2 eq (triangles) and 0.5 eq (crosses) of **B-benzene**.

UV-Vis Spectroscopy

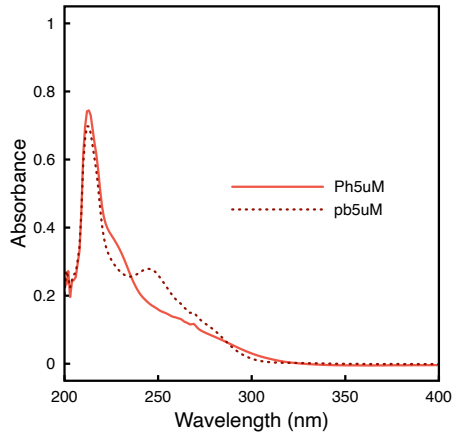

Figure S 3.34. UV-Vis at 5 μM in tetrahydrofuran for **Ph-CPD–NBD** (Ph) and **Ph-benzene** (pb).

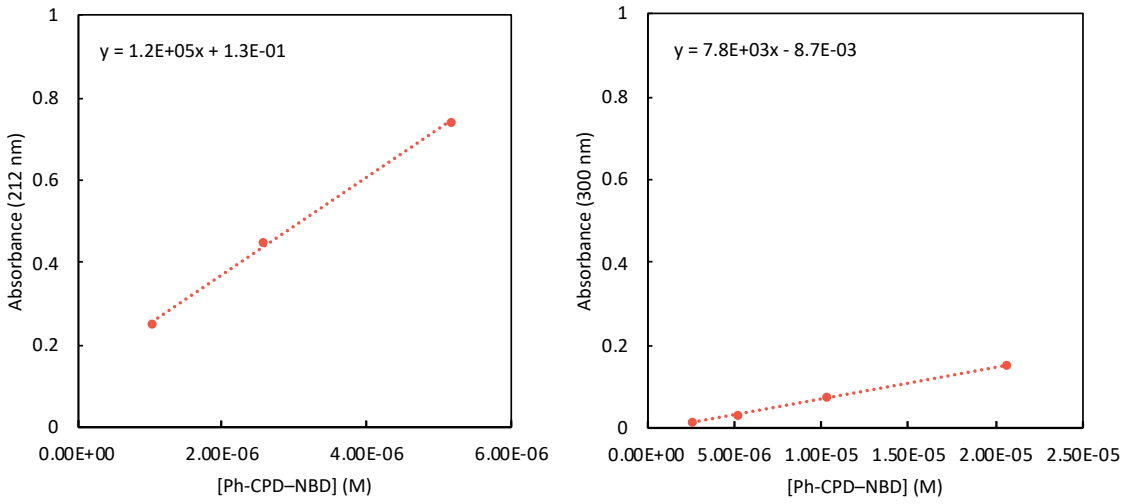

Figure S 3.35. Determination of molar extinction coefficient in tetrahydrofuran for **Ph-CPD–NBD** at l_{max} = 212 nm (left) and l_{irr} = 300 nm (right).

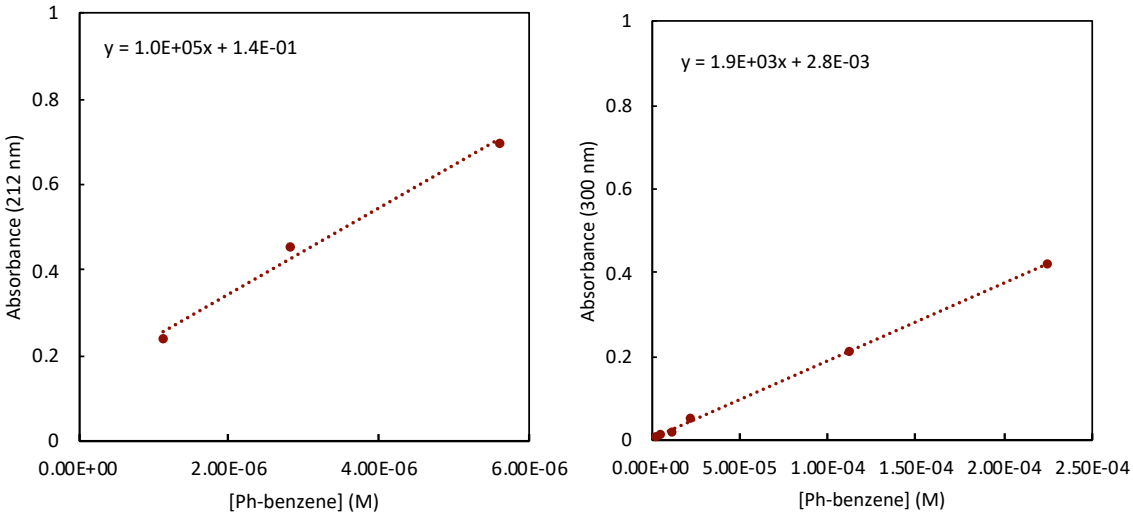

Figure S 3.36. Determination of molar extinction coefficient in tetrahydrofuran for **Ph-benzene** at l_{max} = 212 nm (left) and l_{irr} = 300 nm (right).

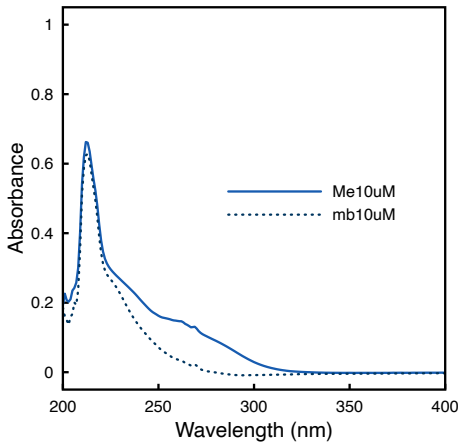

Figure S 3.37. UV-Vis at 10 μM in tetrahydrofuran for **Me-CPD–NBD** (Me) and **Me-benzene** (mb).

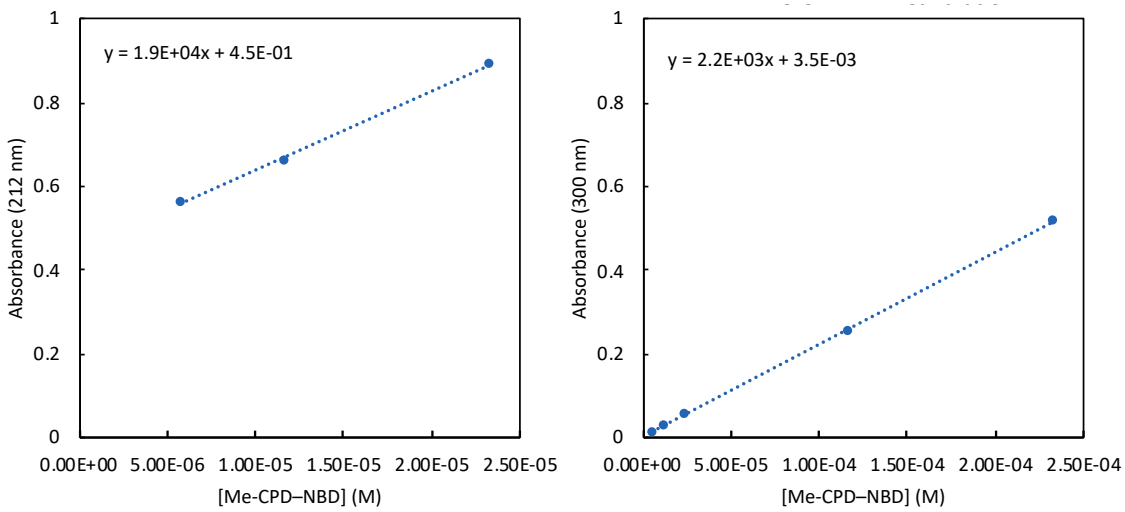

Figure S 3.38. Determination of molar extinction coefficient in tetrahydrofuran for **Me-CPD–NBD** at l_{max} = 212 nm (left) and l_{irr} = 300 nm (right).

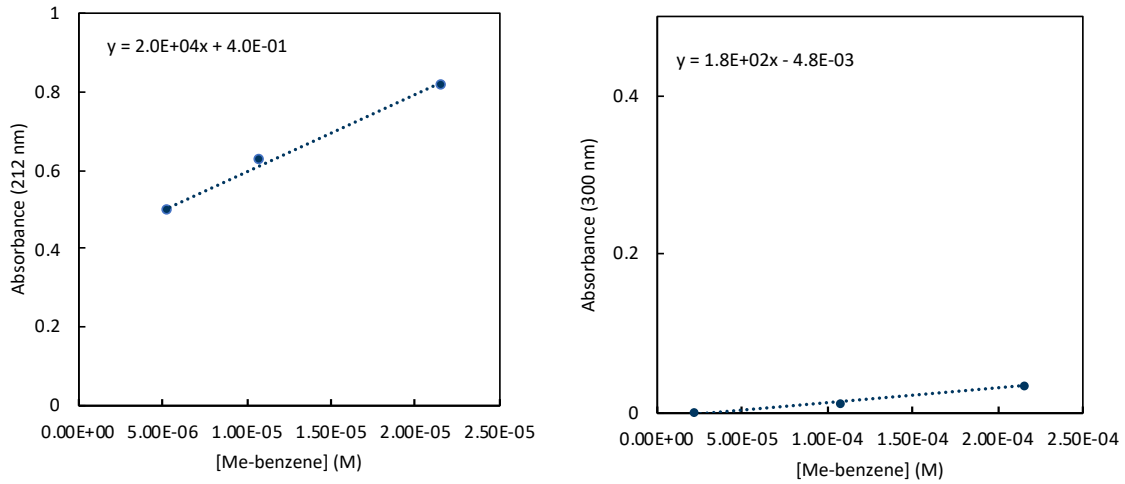

Figure S 3.39. Determination of molar extinction coefficient in tetrahydrofuran for **Me-benzene** at l_{max} = 212 nm (left) and l_{irr} = 300 nm (right).

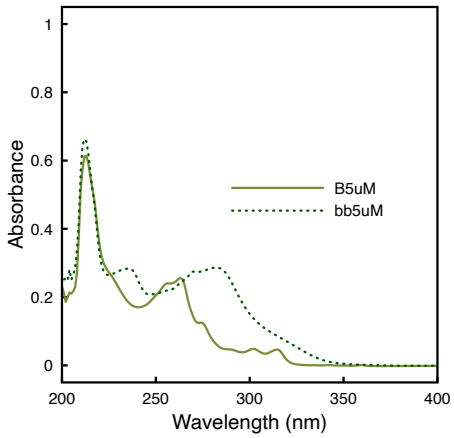

Figure S 3.40. UV-Vis at 10 μM in tetrahydrofuran for **B-CPD–NBD** (B) and **B-benzene** (bb).

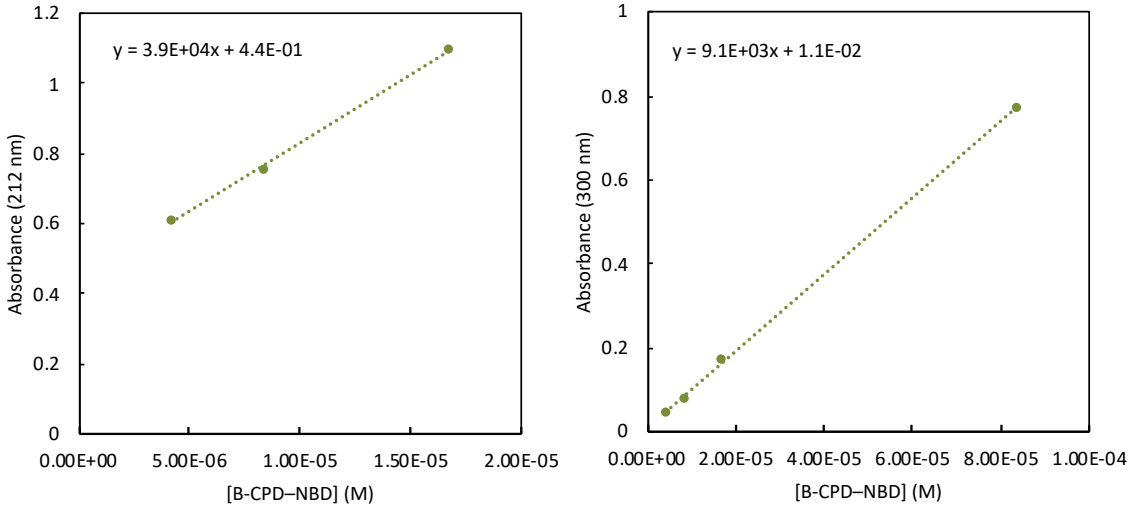

Figure S 3.41. Determination of molar extinction coefficient in tetrahydrofuran for **B-CPD–NBD** at l_{max} = 212 nm (left) and l_{irr} = 300 nm (right).

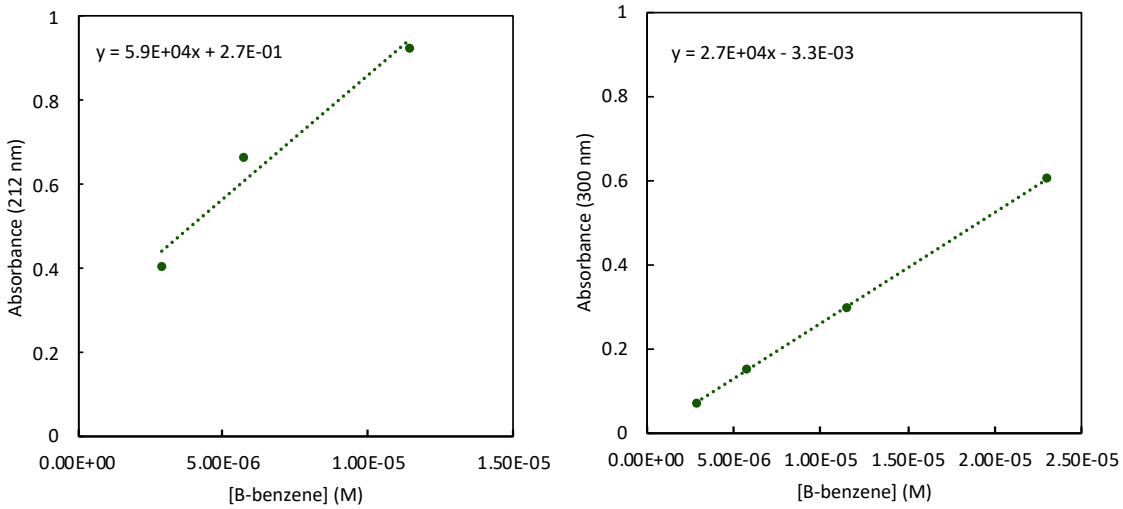

Figure S 3.42. Determination of molar extinction coefficient in tetrahydrofuran for **B-benzene** at l_{max} = 212 nm (left) and l_{irr} = 300 nm (right).

Emission Spectra of Light Sources

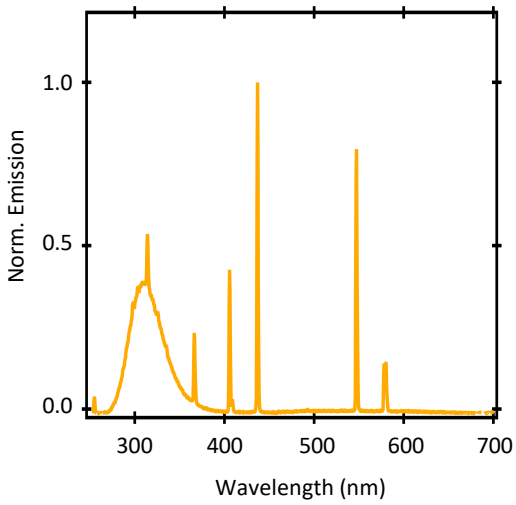

Figure S 3.43. Emission spectra of Rayonet RPR-200 (300 nm) used for ^{1}H NMR monitoring and quantum yield determinations.

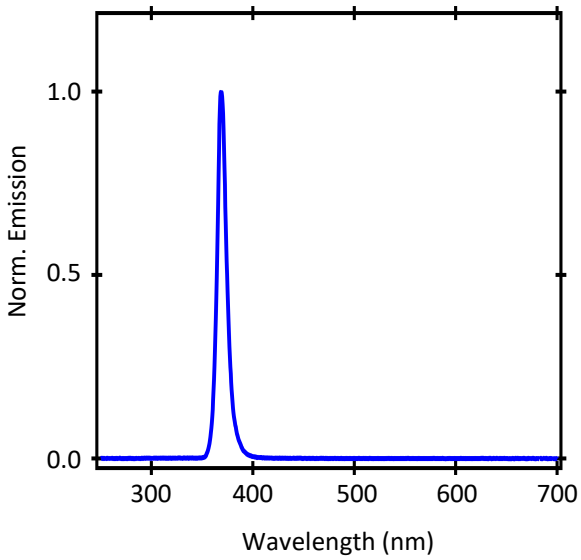

Figure S 3.44. Emission spectra of Thorlabs LED bulb (365 nm, 6.1 mW/cm^2) used for patterning polymer networks.

Quantum Yield Determination

Quantum yields were determined by potassium ferrioxalate actinometry. In a dark room, 6 mM potassium ferrioxalate solution was prepared as described.[79] 2 mL of aliquots were then irradiated while centered in the Rayonet RPR-200 equipped with 12 lamps (300 nm) for specified times in a quartz cuvette with 1 cm pathlength. After irradiation, 1 mL of the aliquots were transferred into 20 mL volumetric flasks and diluted with 1,10-phenanthroline developing solution as described.[82] The solutions were allowed to develop for 30 min before UV Vis measurements were taken.

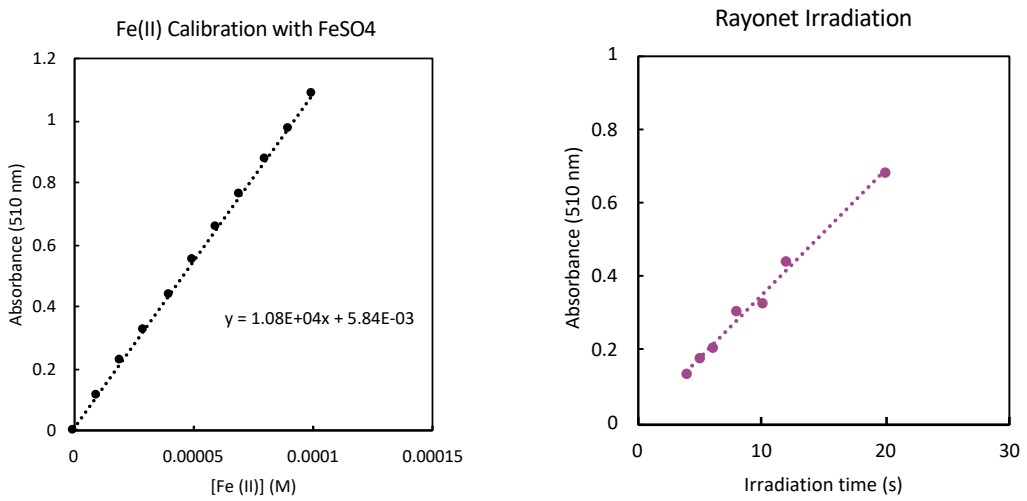

Figure S 3.45. Calibration curve obtained using known concentrations of $FeSO_4$ (left). Resulting absorbance of dilute developed solutions after irradiation for specified times (right).

The dilute concentrations of Fe(II) at each time point were determined using the $FeSO_4$ calibration curve and used to calculated the generated moles of Fe(II) (Δn) in the irradiated solution. The Rayonet flux (I) was calculated as follows:

$$I = \frac{\Delta n}{\Phi \mathrm{Vt}}$$

where Φ is the known quantum yield of potassium ferrioxalate, V is the volume irradiated (L) and t is the time irradiated (s). Using the time points obtained and Φ (300 nm) = 1.24, V = 0.002 L affords:

Rayonet Flux, $\boldsymbol{I}$ **= 0.000048 ± 0.000003 E/L/s**.

20 mM solutions of Me-CPD–NBD and Ph-CPD–NBD and a 10 mM solution of B-CPD–NBD were prepared by dissolving the appropriate compound and ethylene carbonate (2 – 10 mg) in 10 mL of nitrogen-sparged $CDCl_3$. For each compound, 2 mL aliquots were transferred into four nitrogen flushed quartz cuvettes (1 cm pathlength), which were capped and sealed with teflon tape. The cuvettes were then irradiated while centered in the Rayonet RPR-200 equipped with 12 lamps (300 nm) for specified times not exceeding 15% conversion. After irradiation, the solutions were left for at least 30 minutes to allow sufficient time for rDA to occur, then 0.6 mL were transferred into NMR tubes under air for quantitative ^{1}H NMR analysis. Spectra were recorded on a Varian spectrometer (600 MHz) with a relaxation delay of 20 s and a pulse width of 90°, chemical shifts are reported relative to the residual protio-signal in $CDCl_3$. Conversion was calculated from the ratio of integrals from the proton signals corresponding to the substituted benzene byproducts against the ethylene carbonate (EC) internal standard (4.5 ppm). The quantum yield (Φ) for each adduct was calculated as follows:

$$\Phi = \frac{\Delta n}{\mathrm{IVt}}$$

where Δn is the moles of substituted benzene generated, I is the calculated Rayonet Flux (E/L/s), V is the volume irradiated (L) and t is the time irradiated (s).

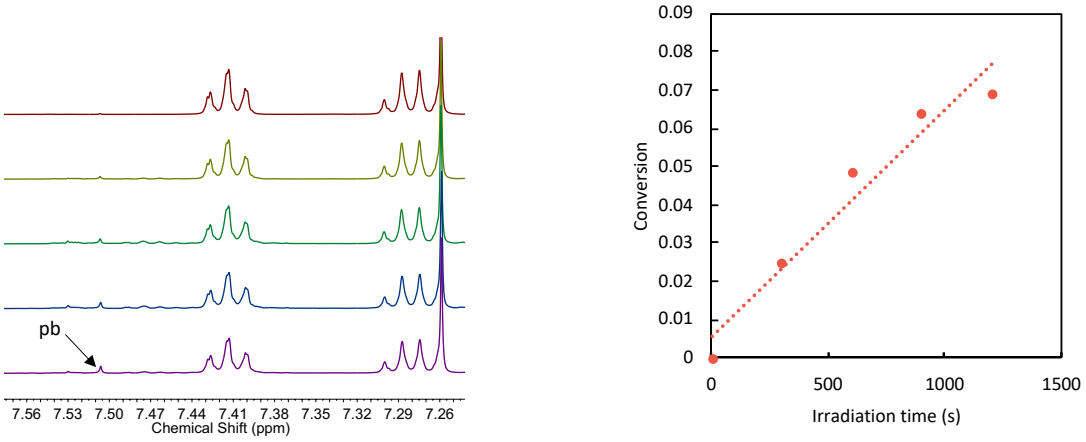

Figure S 3.46. q^{1}H NMR monitoring of **Ph-benzene** production (pb) upon irradiation of 20 mM **Ph-CPD–NBD** solution over 20 minutes in $CDCl_3$ (left). Plot of irradiation time against conversion determined by ratio of integrals of **Ph-benzene** and ethylene carbonate internal standard (right).

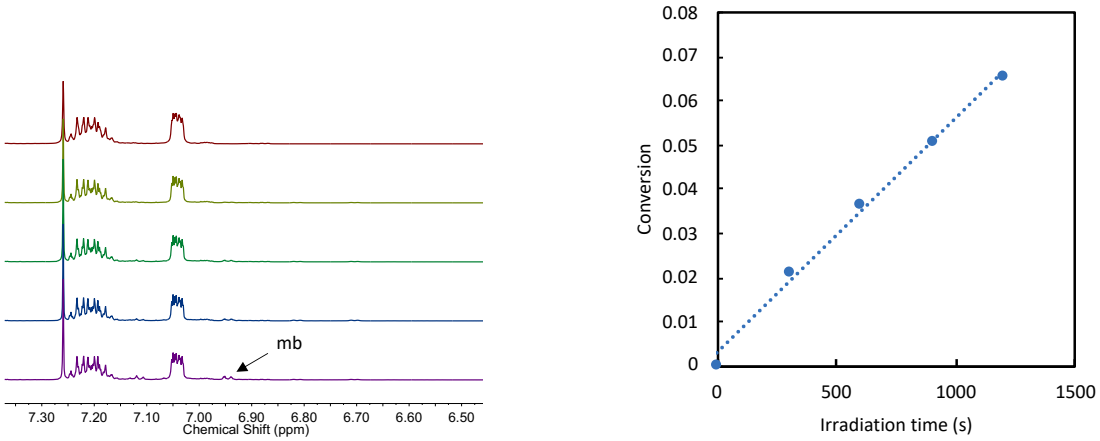

Figure S 3.47. q^{1}H NMR monitoring of **Me-benzene** production (mb) upon irradiation of 20 mM **Me-CPD–NBD** solution over 20 minutes in $CDCl_3$ (left). Plot of irradiation time against conversion determined by ratio of integrals of **Me-benzene** and ethylene carbonate internal standard (right).

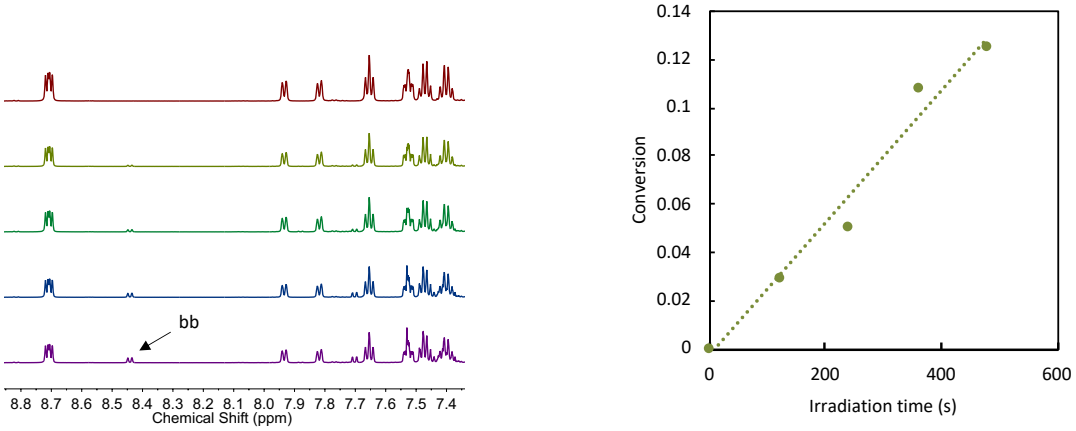

Figure S 3.48. q^{1}H NMR monitoring of **B-benzene** production (bb) upon irradiation of 10 mM **B-CPD–NBD** solution over 8 minutes in $CDCl_3$ (left). Plot of irradiation time against conversion determined by ratio of integrals of **B-benzene** and ethylene carbonate internal standard (right).

Photo-Deprotection and Patterning of Polymer Films

Additional PBA Network Example

A second PBA network was prepared by combining **PBA-mal$_4$** (20wt%) with B-CPD–NBD linker in DCM with 1:1 maleimide: spiro[2.4]hepta-4,6-diene stoichiometry. The mixture was then drop-casted onto a Teflon sheet in a small, closed vessel to slow solvent evaporation during network formation. After 1 h, evaporation of the remaining solvent provided a polymer network which was used for irradiation and dye patterning experiments. The material was irradiated under a quartz photomask (365 nm, 6.1 mW/cm^2, 2 h) before treatment with mal-Red (10 mM in DCM, 2 h). The material was rinsed with DCM to remove excess mal-Red then stored in DCM for 24 h to further remove residual mal-Red. A second pattern could be programmed into the films by irradiation followed by treatment with mal-Cy5 (10 mM in DCM, 2 h).

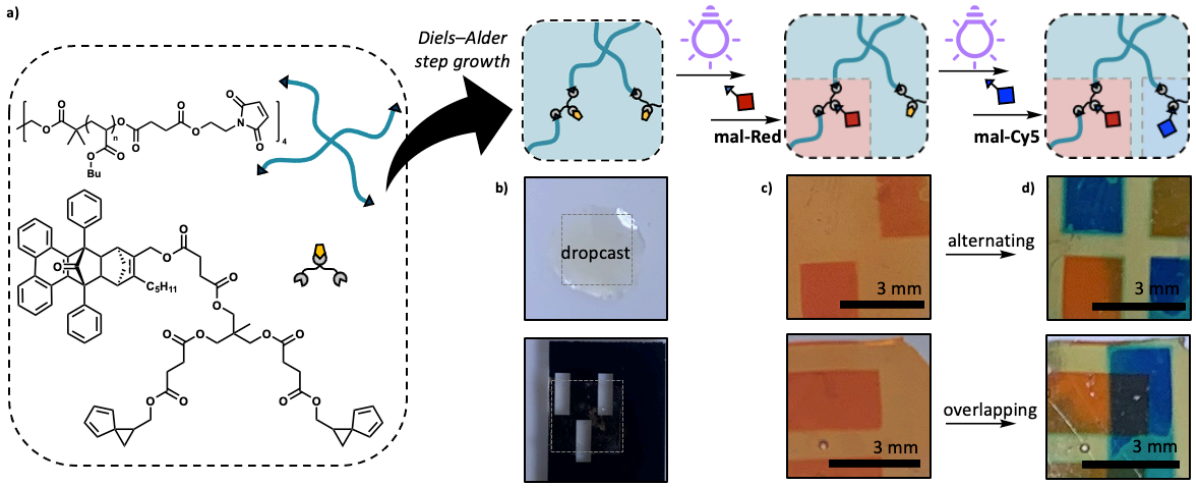

Figure S 3.49. a) Schematic of network formation and patterning. b) A photograph of the drop-cast network and quartz photomask before irradiation. c) Photographs after patterning with **mal-Red** d) Photographs after patterning with **mal-Cy5**. Interaction of dyes is also observed in these samples as seen in Figure 2.

Carbon Monoxide Detector

A carbon monoxide detection vessel was prepared using a CO sensor purchased from SPEC sensors (Product No. 110-102, sensitivity 4.75 ± 2.75 nA/ppm). A multimeter was used to read out and determine ppm CO according to the SPEC sensors website and the following web tutorial: https://www.digikey.com/en/maker/projects/create-your-own-co-detector/874229f4378346a7a0d86c28c5ca2850. The detector was calibrated by passing 200 ppm CO calibration gas (air balance) through the vessel for 10 min, affording the adjusted sensitivity of 0.017 mV/ppm CO. By sealing the system, the detected ppm CO produced upon irradiation could be used to estimate the moles of CO released (Δn_{CO}). The ideal gas law was used assuming pressure (P_{atm}) within the vessel remains at 1 atm. This estimate of moles of CO produced was used to determine conversion.

$$\Delta n_{CO} = \frac{ppm\ CO}{10^6}\frac{P_{atm}V}{RT}$$

where V is the vessel volume (0.616 L), R is the gas constant (L atm/mol/K), and T is temperature (K).

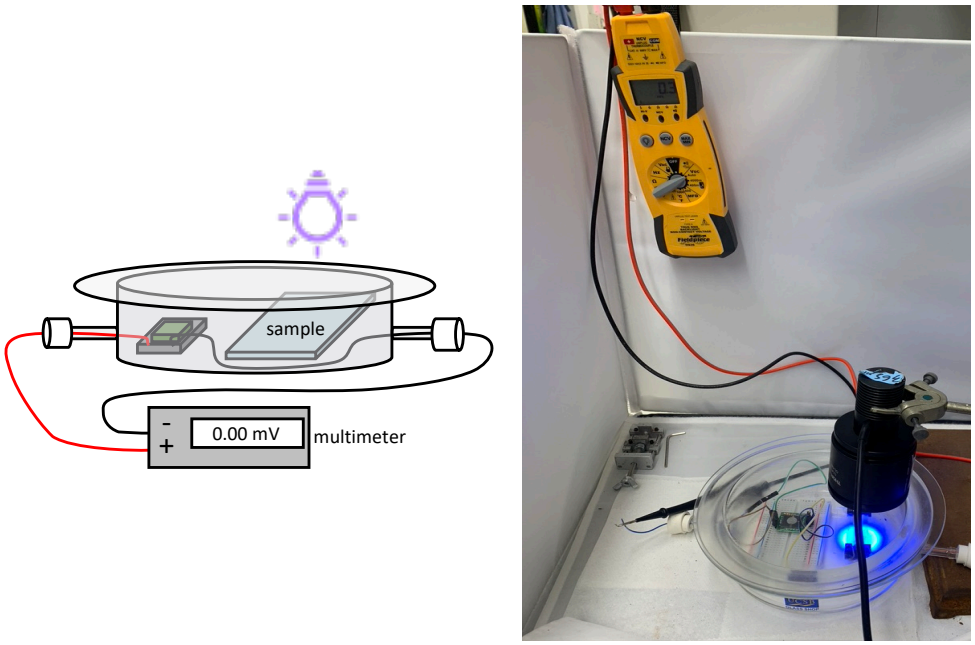

Figure S 3.50. Schematic representation and photograph of CO detection vessel.

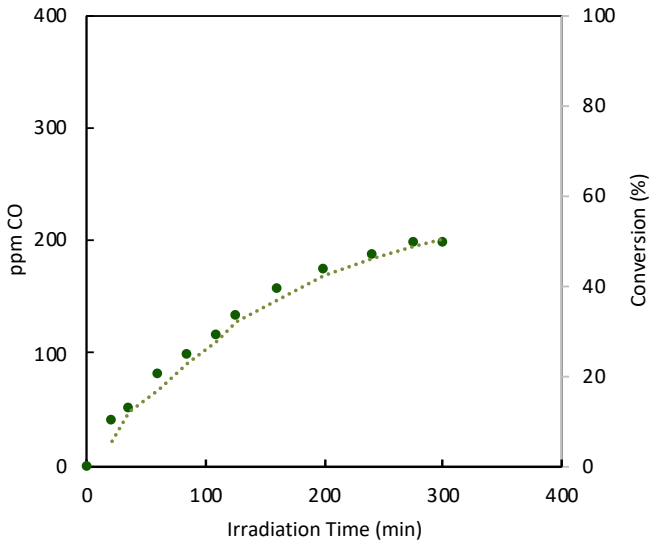

Figure S 3.51. Production of CO upon irradiation of neat, drop-casted sample of **B-CPD–NBD** (0.01 mmol, 365 nm, 6.1 mW/cm^2) was monitored in the detector over 300 min. Final conversion at 300 min was estimated to be 50% by ideal gas law.

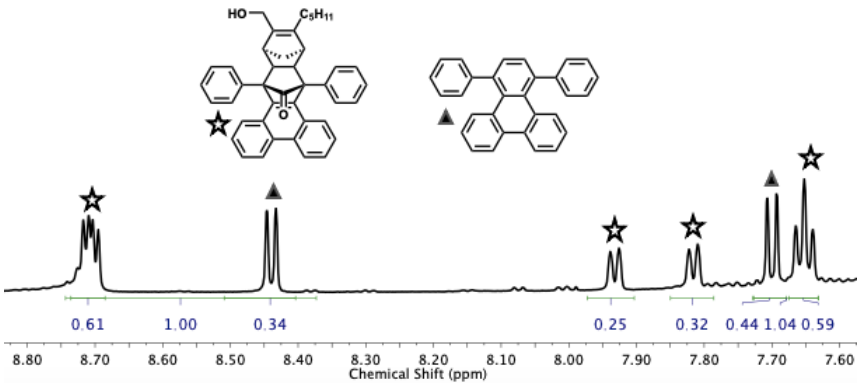

Figure S 3.52. Crude ^{1}H NMR of residue after irradiation in detector for 300 min indicates 40% conversion from **B-CPD–NBD** (star) to **B-benzene** (triangle). Indicating CO detection vessel provides a reasonable approximation of deprotection of materials.

Control Film Patterning

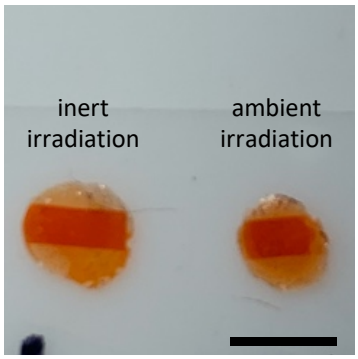

Figure S 3.53. Drop-casted polymer networks containing **B-CPD-NBD** irradiated in a vessel sparged with nitrogen (left) or in a vessel under an atmosphere of air for 2 h (365 nm, 6.1 mW/cm^2), then treated with a 10 mM solution of **mal-Red** in DCM for 1 h. Qualitative examination of films indicates photooxidation does not pose a major pathway during irradiation of thin films that affects preventing subsequent Diels–Alder clicking to dyes. Scale bar = 5 mm.

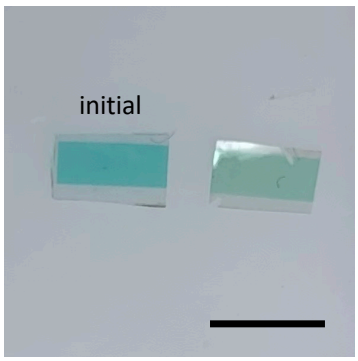

Figure S 3.54. 50 mm PBA film initially patterned with **Cy5-mal** (left) shows staining upon treatment with with non-functionalized Disperse Red 1 (10 mM, 2 h) and thorough rinsing (right). This indicates a dye interaction is responsible for green tint during second patterning steps in **Figure 2f.** Scale bar = 5 mm.

Fluorescence Microscopy

Patterned streptavidin immobilization was visualized with a spinning disk super resolution confocal microscope (Nikon) with a 4X lens. Images were captured with 100 ms exposure of 488 nm laser (75%).

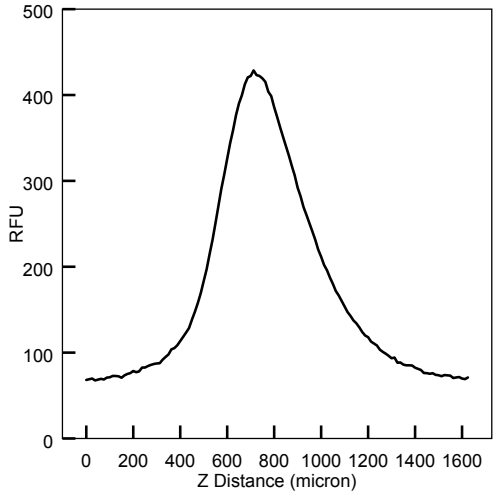

Figure S 3.55. Profile of Z-axis for one square of the pattern depicted in **Figure 3c**. Z-stacks, to measure pattern penetration, were taken every 12.5 µm for 1.6 mm with the same imaging settings and quantified with the *Plot Z axis Profile* function in FIJI.

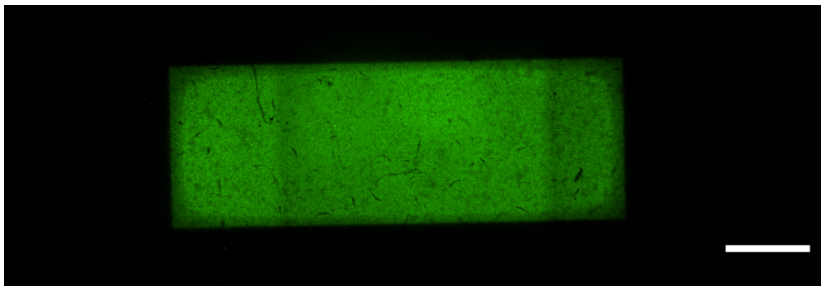

Figure S 3.56. Fluorescence image of hydrogel irradiated with alternative photomask as demonstrated in Figure 3. Multiple images were stitched due to the limited field of view. Scale bar = 1.0 mm.

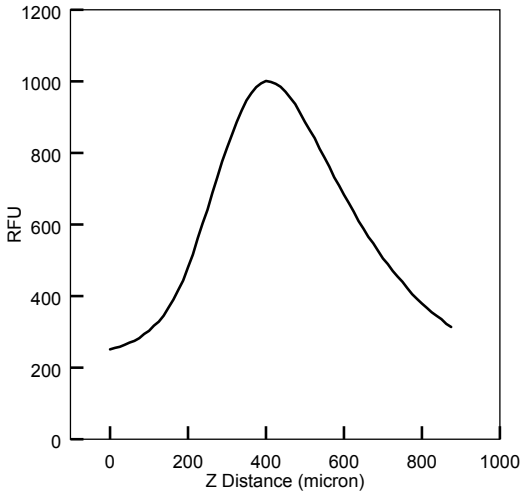

Figure S 3.57. Profile of Z-axis of pattern depicted in **Figure S56**. Z-stacks taken every 12.5 μm for 0.875 mm

3.7 References

(1) Zhang, W.; Wang, R.; Sun, Z.; Zhu, X.; Zhao, Q.; Zhang, T.; Cholewinski, A.; Yang, F. (Kuo); Zhao, B.; Pinnaratip, R.; Forooshani, P. K.; Lee, B. P. Catechol-Functionalized Hydrogels: Biomimetic Design, Adhesion Mechanism, and Biomedical Applications. *Chem. Soc. Rev.* **2020**, *49* (2), 433–464. DOI: 10.1039/C9CS00285E.

(2) Vermonden, T.; Censi, R.; Hennink, W. E. Hydrogels for Protein Delivery. *Chem. Rev.* **2012**, *112* (5), 2853–2888. DOI: 10.1021/cr200157d.

(3) Zhu, J. Bioactive Modification of Poly(Ethylene Glycol) Hydrogels for Tissue Engineering. *Biomaterials* **2010**, *31* (17), 4639–4656. DOI: 10.1016/j.biomaterials.2010.02.044.

(4) Küpfer, J.; Finkelmann, H. Nematic Liquid Single Crystal Elastomers. *Makromol. Chem., Rapid Commun.* **1991**, *12* (12), 717–726. DOI: 10.1002/marc.1991.030121211.

(5) Ge, F.; Yang, R.; Tong, X.; Camerel, F.; Zhao, Y. A Multifunctional Dye-Doped Liquid Crystal Polymer Actuator: Light-Guided Transportation, Turning in Locomotion, and Autonomous Motion. *Angew. Chem.* **2018**, *130* (36), 11932–11937. DOI: 10.1002/ange.201807495.

(6) Francis, W.; Dunne, A.; Delaney, C.; Florea, L.; Diamond, D. Spiropyran Based Hydrogels Actuators—Walking in the Light. *Sens. Actuators B Chem.* **2017**, *250*, 608–616. DOI: 10.1016/j.snb.2017.05.005.

(7) Lahikainen, M.; Kuntze, K.; Zeng, H.; Helanterä, S.; Hecht, S.; Priimagi, A. Tunable Photomechanics in Diarylethene-Driven Liquid Crystal Network Actuators. *ACS Appl. Mater. Interfaces* **2020**, *12* (42), 47393–47947. DOI: 10.1021/acsami.0c12735.

(8) Gelebart, A. H.; Mulder, D. J.; Vantomme, G.; Schenning, A. P. H. J.; Broer, D. J. A Rewritable, Reprogrammable, Dual Light-Responsive Polymer Actuator. *Angew. Chem. Int. Ed.* **2017**, *56* (43), 13436–13439. DOI: 10.1002/anie.201706793.

(9) Liu, Y.; Shaw, B.; Dickey, M. D.; Genzer, J. Sequential Self-Folding of Polymer Sheets. *Sci. Adv.* **2017**, *3* (3), e1602417. DOI: 10.1126/sciadv.1602417.

(10) Lahikainen, M.; Zeng, H.; Priimagi, A. Design Principles for Non-Reciprocal Photomechanical Actuation. *Soft Matter* **2020**, *16* (25), 5951–5958. DOI: 10.1039/D0SM00624F.

(11) DeForest, C. A.; Polizzotti, B. D.; Anseth, K. S. Sequential Click Reactions for Synthesizing and Patterning Three-Dimensional Cell Microenvironments. *Nat. Mater.* **2009**, *8* (8), 659–664. DOI: 10.1038/nmat2473.

(12) DeForest, C. A.; Tirrell, D. A. A Photoreversible Protein-Patterning Approach for Guiding Stem Cell Fate in Three-Dimensional Gels. *Nat. Mater.* **2015**, *14* (5), 523–531. DOI: 10.1038/nmat4219.

(13) Batalov, I.; Stevens, K. R.; DeForest, C. A. Photopatterned Biomolecule Immobilization to Guide Three-Dimensional Cell Fate in Natural Protein-Based Hydrogels. *Proc. Natl. Acad. Sci. USA.* **2021**, *118* (4), e2014194118. DOI: 10.1073/pnas.2014194118.

(14) Kolb, H. C.; Finn, M. G.; Sharpless, K. B. Click Chemistry: Diverse Chemical Function from a Few Good Reactions. *Angew. Chem. Int. Ed.* **2001**, *40* (11), 2004–2021. DOI: 10.1002/1521-3773(20010601)40:11<2004::AID-ANIE2004>3.0.CO;2-5.

(15) Rostovtsev, V. V.; Green, L. G.; Fokin, V. V.; Sharpless, K. B. A Stepwise Huisgen Cycloaddition Process: Copper(I)-Catalyzed Regioselective "Ligation" of Azides and Terminal Alkynes. *Angew. Chem. Int. Ed. Engl.* **2002**, *41* (14), 2596–2599. DOI: 10.1002/1521-3773(20020715)41:14<2596::AID-ANIE2596>3.0.CO;2-4

(16) Nair, D. P.; Podgórski, M.; Chatani, S.; Gong, T.; Xi, W.; Fenoli, C. R.; Bowman, C. N. The Thiol-Michael Addition Click Reaction: A Powerful and Widely Used Tool in Materials Chemistry. *Chem. Mater.* **2014**, *26* (1), 724–744. DOI: 10.1021/cm402180t.

(17) Hoyle, C. E.; Bowman, C. N. Thiol-Ene Click Chemistry. *Angew. Chem. Int. Ed.* **2010**, *49* (9), 1540–1573. DOI: 10.1002/anie.200903924.

(18) Kose, M. M.; Yesilbag, G.; Sanyal, A. Segment Block Dendrimers via Diels−Alder Cycloaddition. *Org. Lett.* **2008**, *10* (12), 2353–2356. DOI: 10.1021/ol800553t.

(19) Inglis, A. J.; Sinnwell, S.; Stenzel, M. H.; Barner-Kowollik, C. Ultrafast Click Conjugation of Macromolecular Building Blocks at Ambient Temperature. *Angew. Chem. Int. Ed.* **2009**, *48* (13), 2411–2414. DOI: 10.1002/anie.200805993.

(20) Billiet, S.; De Bruycker, K.; Driessen, F.; Goossens, H.; Van Speybroeck, V.; Winne, J. M.; Du Prez, F. E. Triazolinediones Enable Ultrafast and Reversible Click Chemistry for the Design of Dynamic Polymer Systems. *Nat. Chem.* **2014**, *6* (9), 815–821. DOI: 10.1038/nchem.2023.

(21) Hansell, C. F.; Espeel, P.; Stamenović, M. M.; Barker, I. A.; Dove, A. P.; Du Prez, F. E.; O'Reilly, R. K. Additive-Free Clicking for Polymer Functionalization and Coupling by Tetrazine–Norbornene Chemistry. *J. Am. Chem. Soc.* **2011**, *133* (35), 13828–13831. DOI: 10.1021/ja203957h.

(22) St. Amant, A. H.; Discekici, E. H.; Bailey, S. J.; Zayas, M. S.; Song, J.-A.; Shankel, S. L.; Nguyen, S. N.; Bates, M. W.; Anastasaki, A.; Hawker, C. J.; Read de Alaniz, J. Norbornadienes: Robust and Scalable Building Blocks for Cascade "Click" Coupling of High Molecular Weight Polymers. *J. Am. Chem. Soc.* **2019**, *141* (34), 13619–13624. DOI: 10.1021/jacs.9b06328.

(23) Samoshin, A. V.; Hawker, C. J.; Read de Alaniz, J. Nitrosocarbonyl Hetero-Diels–Alder Cycloaddition: A New Tool for Conjugation. *ACS Macro Lett.* **2014**, *3* (8), 753–757. DOI: 10.1021/mz500348y.

(24) Chen, X.; Wudl, F.; Mal, A. K.; Shen, H.; Nutt, S. R. New Thermally Remendable Highly Cross-Linked Polymeric Materials. *Macromolecules* **2003**, *36* (6), 1802–1807. DOI: 10.1021/ma0210675.

(25) Murphy, E. B.; Bolanos, E.; Schaffner-Hamann, C.; Wudl, F.; Nutt, S. R.; Auad, M. L. Synthesis and Characterization of a Single-Component Thermally Remendable Polymer Network: Staudinger and Stille Revisited. *Macromolecules* **2008**, *41* (14), 5203–5209. DOI: 10.1021/ma800432g.

(26) Liu, Y.-L.; Chuo, T.-W. Self-Healing Polymers Based on Thermally Reversible Diels–Alder Chemistry. *Polym. Chem.* **2013**, *4* (7), 2194. DOI: 10.1039/c2py20957h.

(27) Blackman, M. L.; Royzen, M.; Fox, J. M. Tetrazine Ligation: Fast Bioconjugation Based on Inverse-Electron-Demand Diels−Alder Reactivity. *J. Am. Chem. Soc.* **2008**, *130* (41), 13518–13519. DOI: 10.1021/ja8053805.

(28) Oliveira, B. L.; Guo, Z.; Bernardes, G. J. L. Inverse Electron Demand Diels–Alder Reactions in Chemical Biology. *Chem. Soc. Rev.* **2017**, *46* (16), 4895–4950. DOI: 10.1039/C7CS00184C.

(29) St. Amant, A. H.; Lemen, D.; Florinas, S.; Mao, S.; Fazenbaker, C.; Zhong, H.; Wu, H.; Gao, C.; Christie, R. J.; Read de Alaniz, J. Tuning the Diels–Alder Reaction for Bioconjugation to Maleimide Drug-Linkers. *Bioconjug. Chem.* **2018**, *29* (7), 2406–2414. DOI: 10.1021/acs.bioconjchem.8b00320.

(30) Kumar, A.; Mao, S.; Dimasi, N.; Gao, C. Design and Validation of Linkers for Site-Specific Preparation of Antibody–Drug Conjugates Carrying Multiple Drug Copies Per Cysteine Conjugation Site. *Int. J. Mol. Sci.* **2020**, *21* (18), 6882. DOI: 10.3390/ijms21186882.

(31) Smith, L. J.; Taimoory, S. M.; Tam, R. Y.; Baker, A. E. G.; Binth Mohammad, N.; Trant, J. F.; Shoichet, M. S. Diels–Alder Click-Cross-Linked Hydrogels with Increased Reactivity Enable 3D Cell Encapsulation. *Biomacromolecules* **2018**, *19* (3), 926–935. DOI: 10.1021/acs.biomac.7b01715.

(32) Yang, N. C.; Rivas, C. A New Photochemical Primary Process, the Photochemical Enolization of *o*-Substituted Benzophenones. *J. Am. Chem. Soc.* **1961**, *83* (9), 2213–2213. DOI: 10.1021/ja01470a053.

(33) Meador, M. A. B.; Meador, M. A.; Williams, L. L.; Scheiman, D. A. Diels−Alder Trapping of Photochemically Generated Dienes with a Bismaleimide: A New Approach to Polyimide Synthesis. *Macromolecules* **1996**, *29* (27), 8983–8986. DOI: 10.1021/ma960881n.

(34) Gruendling, T.; Oehlenschlaeger, K. K.; Frick, E.; Glassner, M.; Schmid, C.; Barner-Kowollik, C. Rapid UV Light-Triggered Macromolecular *Click* Conjugations via the Use of *o* -Quinodimethanes. *Macromol. Rapid Commun.* **2011**, *32* (11), 807–812. DOI: 10.1002/marc.201100159.

(35) Glassner, M.; Oehlenschlaeger, K. K.; Gruendling, T.; Barner-Kowollik, C. Ambient Temperature Synthesis of Triblock Copolymers via Orthogonal Photochemically and Thermally Induced Modular Conjugation. *Macromolecules* **2011**, *44* (12), 4681–4689. DOI: 10.1021/ma2010052.

(36) Pauloehrl, T.; Delaittre, G.; Winkler, V.; Welle, A.; Bruns, M.; Börner, H. G.; Greiner, A. M.; Bastmeyer, M.; Barner-Kowollik, C. Adding Spatial Control to Click Chemistry: Phototriggered Diels-Alder Surface (Bio)Functionalization at Ambient Temperature. *Angew. Chem. Int. Ed.* **2012**, *51* (4), 1071–1074. DOI: 10.1002/anie.201107095.

(37) Pauloehrl, T.; Welle, A.; Bruns, M.; Linkert, K.; Börner, H. G.; Bastmeyer, M.; Delaittre, G.; Barner-Kowollik, C. Spatially Controlled Surface Immobilization of Nonmodified Peptides. *Angew. Chem. Int. Ed.* **2013**, *52* (37), 9714–9718. DOI: 10.1002/anie.201302040.

(38) Tischer, T.; Claus, T. K.; Bruns, M.; Trouillet, V.; Linkert, K.; Rodriguez-Emmenegger, C.; Goldmann, A. S.; Perrier, S.; Börner, H. G.; Barner-Kowollik, C. Spatially Controlled Photochemical Peptide and Polymer Conjugation on Biosurfaces. *Biomacromolecules* **2013**, *14* (12), 4340–4350. DOI: 10.1021/bm401274v.

(39) Arumugam, S.; Popik, V. V. Light-Induced Hetero-Diels−Alder Cycloaddition: A Facile and Selective Photoclick Reaction. *J. Am. Chem. Soc.* **2011**, *133* (14), 5573–5579. DOI: 10.1021/ja200356f.

(40) Frazier, C. P.; Palmer, L. I.; Samoshin, A. V.; Read de Alaniz, J. Accessing Nitrosocarbonyl Compounds with Temporal and Spatial Control via the Photoredox Oxidation of N-Substituted Hydroxylamines. *Tetrahedron Lett.* **2015**, *56* (23), 3353–3357. DOI: 10.1016/j.tetlet.2015.01.024.

(41) Glassner, M.; Oehlenschlaeger, K. K.; Welle, A.; Bruns, M.; Barner-Kowollik, C. Polymer Surface Patterningvia Diels–Alder Trapping of Photo-Generated Thioaldehydes. *Chem. Commun.* **2013**, *49* (6), 633–635. DOI: 10.1039/C2CC37651B.

(42) Lemieux, V.; Gauthier, S.; Branda, N. R. Selective and Sequential Photorelease Using Molecular Switches. *Angew. Chem.* **2006**, *118* (41), 6974–6978. DOI: 10.1002/ange.200601584.

(43) Erno, Z.; Asadirad, A. M.; Lemieux, V.; Branda, N. R. Using Light and a Molecular Switch to 'Lock' and 'Unlock' the Diels–Alder Reaction. *Org. Biomol. Chem.* **2012**, *10* (14), 2787. DOI: 10.1039/c2ob06908c.

(44) Kumar, G. S.; Lin, Q. Light-Triggered Click Chemistry. *Chem. Rev.* **2020**, *121* (12), 6991–7031. DOI: 10.1021/acs.chemrev.0c00799.

(45) Sauer, J.; Lang, D.; Mielert, A. The Order of Reactivity of Dienes towards Maleic Anhydride in the Diels-Alder Reaction. *Angew. Chem. Int. Ed. Engl.* **1962**, *1* (5), 268–269. DOI: 10.1002/anie.196202683.

(46) Inglis, A. J.; Paulöhrl, T.; Barner-Kowollik, C. Ambient Temperature Synthesis of a Versatile Macromolecular Building Block: Cyclopentadienyl-Capped Polymers. *Macromolecules* **2010**, *43* (1), 33–36. DOI: 10.1021/ma902464a.

(47) Levandowski, B. J.; Raines, R. T. Click Chemistry with Cyclopentadiene. *Chem. Rev.* **2021**. DOI: 10.1021/acs.chemrev.0c01055.

(48) Bailey, S. J.; Discekici, E. H.; Barbon, S. M.; Nguyen, S. N.; Hawker, C. J.; Read de Alaniz, J. Norbornadiene Chain-End Functional Polymers as Stable, Readily Available Precursors to Cyclopentadiene Derivatives. *Macromolecules* **2020**, *53* (12), 4917–4924. DOI: 10.1021/acs.macromol.0c00967.

(49) Mackenzie, K. 98. Bicyclo[2,2,1]Heptadiene in the Diels–Alder Reaction. *J. Chem. Soc.* **1960**, 473–483. DOI: 10.1039/JR9600000473.

(50) Anderson, C. M.; Bremner, J. B.; Westberg, H. H.; Warrener, R. N. The Synthetic Potential of the 1,2-Photoaromatization (1) Reaction. *Tetrahedron Lett.* **1969**, *10* (20), 1585–1588. DOI: 10.1016/S0040-4039(01)87951-X.

(51) Wilson, W. S.; Warrener, R. N. Photodecarbonylation - a Gentle Route to Annelated Cyclohexadienes. *Tetrahedron Lett.* **1970**, *11* (60), 5203–5206. DOI: 10.1016/S0040-4039(00)99973-8.

(52) Findlay, D. M.; Roy, M. L.; McLean, S. Thermal Routes to Substituted Cyclopentadienes. *Can. J. Chem.* **1972**, *50* (19), 3186–3195. DOI: 10.1139/v72-508.

(53) Ogliaruso, M. A.; Romanelli, M. G.; Becker, E. I. Chemistry of Cyclopentadienones. *Chem. Rev.* **1965**, *65* (3), 261–367. DOI: 10.1021/cr60235a001.

(54) Fry, A. J.; Sherman, L. R.; Beaulieu, A. R.; Sherwin, C. The Reaction between 7-Oxanorbornadienes and Tetraarylcyclopentadienones: A Short Synthesis of 1,2,3,4-Tetraarylbenzenes. *J. Org. Chem.* **1990**, *55* (1), 389–391. DOI: 10.1021/jo00288a078.

(55) Ji, X.; Zhou, C.; Ji, K.; Aghoghovbia, R. E.; Pan, Z.; Chittavong, V.; Ke, B.; Wang, B. Click and Release: A Chemical Strategy toward Developing Gasotransmitter Prodrugs by Using an Intramolecular Diels-Alder Reaction. *Angew. Chem. Int. Ed.* **2016**, *55* (51), 15846–15851. DOI: 10.1002/anie.201608732.

(56) Ji, X.; Aghoghovbia, R. E.; De La Cruz, L. K. C.; Pan, Z.; Yang, X.; Yu, B.; Wang, B. Click and Release: A High-Content Bioorthogonal Prodrug with Multiple Outputs. *Org. Lett.* **2019**, *21* (10), 3649–3652. DOI: 10.1021/acs.orglett.9b01086.

(57) Dietrich, M.; Delaittre, G.; Blinco, J. P.; Inglis, A. J.; Bruns, M.; Barner-Kowollik, C. Photoclickable Surfaces for Profluorescent Covalent Polymer Coatings. *Adv. Funct. Mater.* **2012**, *22* (2), 304–312. DOI: 10.1002/adfm.201102068.

(58) Wang, Y.; Rivera Vera, C. I.; Lin, Q. Convenient Synthesis of Highly Functionalized Pyrazolines via Mild, Photoactivated 1,3-Dipolar Cycloaddition. *Org. Lett.* **2007**, *9* (21), 4155–4158. DOI: 10.1021/ol7017328.

(59) Michalek, L.; Krappitz, T.; Mundsinger, K.; Walden, S. L.; Barner, L.; Barner-Kowollik, C. Mapping Photochemical Reactivity Profiles on Surfaces. *J. Am. Chem. Soc.* **2020**, *142* (52), 21651–21655. DOI: 10.1021/jacs.0c11485.

(60) Wilson, P. J.; Wells, J. H. The Chemistry and Utilization of Cyclopentadiene. *Chem. Rev.* **1944**, *34* (1), 1–50. DOI: 10.1021/cr60107a001.

(61) Bertrand, G.; Wentrup, C. Nitrile Imines: From Matrix Characterization to Stable Compounds. *Angew. Chem. Int. Ed. Engl.* **1994**, *33* (5), 527–545. DOI: 10.1002/anie.199405271.

(62) Rickborn, B. The Retro-Diels-Alder Reaction Part I. C–C Dienophiles. In *Organic Reactions*; John Wiley & Sons, Inc., Ed.; John Wiley & Sons, Inc.: Hoboken, NJ, USA, 1998; pp 1–393. DOI: 10.1002/0471264180.or052.01.

(63) Motterlini, R.; Clark, J. E.; Foresti, R.; Sarathchandra, P.; Mann, B. E.; Green, C. J. Carbon Monoxide-Releasing Molecules: Characterization of Biochemical and Vascular Activities. *Circ. Res.* **2002**, *90* (2). DOI: 10.1161/hh0202.104530.

(64) Hasegawa, U.; van der Vlies, A. J.; Simeoni, E.; Wandrey, C.; Hubbell, J. A. Carbon Monoxide-Releasing Micelles for Immunotherapy. *J. Am. Chem. Soc.* **2010**, *132* (51), 18273–18280. DOI: 10.1021/ja1075025.

(65) Bohlender, C.; Gläser, S.; Klein, M.; Weisser, J.; Thein, S.; Neugebauer, U.; Popp, J.; Wyrwa, R.; Schiller, A. Light-Triggered CO Release from Nanoporous Non-Wovens. *J. Mater. Chem. B* **2014**, *2* (11), 1454–1463. DOI: 10.1039/C3TB21649G.

(66) Bryant, S. J.; Nuttelman, C. R.; Anseth, K. S. Cytocompatibility of UV and Visible Light Photoinitiating Systems on Cultured NIH/3T3 Fibroblasts in Vitro. *J. Biomater. Sci. Poly. Ed.* **2000**, *11* (5), 439–457. DOI: 10.1163/156856200743805.

(67) Froese, R. D. J.; Organ, M. G.; Goddard, J. D.; Stack, T. D. P.; Trost, B. M. Theoretical and Experimental Studies of the Diels-Alder Dimerizations of Substituted Cyclopentadienes. *J. Am. Chem. Soc.* **1995**, *117* (44), 10931–10938. DOI: 10.1021/ja00149a016.

(68) Byers, G. W.; Gross, S.; Henrichs, P. M. Direct and Sensitized Photooxidation of Cyanine Dyes. *Photochem. Photobiol.* **1976**, *23* (1), 37–43. DOI: 10.1111/j.1751-1097.1976.tb06768.x.

(69) Gorka, A. P.; Schnermann, M. J. Harnessing Cyanine Photooxidation: From Slowing Photobleaching to near-IR Uncaging. *Curr. Opin. Chem. Biol.* **2016**, *33*, 117–125. DOI: 10.1016/j.cbpa.2016.05.022.

(70) Forsyth, W. R.; Weisenburger, G. A.; Field, K. W. The Syntheses of Phencyclone and Dihydrophencyclone. Trans. Ill. State Acad. Science **1996**, *89*, 37–40. https://ilacadofsci.com/archives/2608, (accessed 30 March 2021).

(71) Fei, Y.; Liu, C.; Chen, G.; Hong, C. A Facile Approach for Preparing Multicyclic Polymers through Combining ATRP and a Photo-Induced Coupling Reaction. *Polym. Chem.* **2019**, *10* (28), 3895–3901. DOI: 10.1039/C9PY00472F.

(72) de Figueiredo, R.; Oczipka, P.; Fröhlich, R.; Christmann, M. Synthesis of 4-Maleimidobutyric Acid and Related Maleimides. *Synthesis* **2008**, *2008* (8), 1316–1318. DOI: 10.1055/s-2008-1032016.

(73) Kvach, M. V.; Ustinov, A. V.; Stepanova, I. A.; Malakhov, A. D.; Skorobogatyi, M. V.; Shmanai, V. V.; Korshun, V. A. A Convenient Synthesis of Cyanine Dyes: Reagents for the Labeling of Biomolecules. *Eur. J. Org. Chem.* **2008**, *2008* (12), 2107–2117. DOI: 10.1002/ejoc.200701190.

(74) Mantovani, G.; Lecolley, F.; Tao, L.; Haddleton, D. M.; Clerx, J.; Cornelissen, J. J. L. M.; Velonia, K. Design and Synthesis of *N* -Maleimido-Functionalized Hydrophilic Polymers via Copper-Mediated Living Radical Polymerization: A Suitable Alternative to PEGylation Chemistry. *J. Am. Chem. Soc.* **2005**, *127* (9), 2966–2973. DOI: 10.1021/ja0430999.

(75) Gacal, B.; Durmaz, H.; Tasdelen, M. A.; Hizal, G.; Tunca, U.; Yagci, Y.; Demirel, A. L. Anthracene−Maleimide-Based Diels−Alder "Click Chemistry" as a Novel Route to Graft Copolymers. *Macromolecules* **2006**, *39* (16), 5330–5336. DOI: 10.1021/ma060690c.

(76) Fry, A. J.; Sherman, L. R.; Beaulieu, A. R.; Sherwin, C. The Reaction between 7-Oxanorbornadienes and Tetraarylcyclopentadienones: A Short Synthesis of 1,2,3,4-Tetraarylbenzenes. *J. Org. Chem.* **1990**, *55* (1), 389–391. DOI: 10.1021/jo00288a078.

(77) Pan, Z.; Zhang, J.; Ji, K.; Chittavong, V.; Ji, X.; Wang, B. Organic CO Prodrugs Activated by Endogenous ROS. *Org. Lett.* **2018**, *20* (1), 8–11. DOI: 10.1021/acs.orglett.7b02775.

(78) Anastasaki, A.; Nikolaou, V.; Zhang, Q.; Burns, J.; Samanta, S. R.; Waldron, C.; Haddleton, A. J.; McHale, R.; Fox, D.; Percec, V.; Wilson, P.; Haddleton, D. M. Copper(II)/Tertiary Amine Synergy in Photoinduced Living Radical Polymerization: Accelerated Synthesis of ω-Functional and α,ω-Heterofunctional Poly(Acrylates). *J. Am. Chem. Soc.* **2014**, *136* (3), 1141–1149. DOI: 10.1021/ja411780m.

(79) Hatchard, C. G.; Parker, C. A.; Bowen, E. J. A New Sensitive Chemical Actinometer - II. Potassium Ferrioxalate as a Standard Chemical Actinometer. *Proc. R. Soc. Lond. Ser. Math. Phys. Sci.* **1956**, *235* (1203), 518–536. DOI: 10.1098/rspa.1956.0102.

4 Chapter 4: *Design, Synthesis, and Application of a Water-soluble Photocage for Aqueous Cyclopentadiene-based Diels–Alder Photoclick Chemistry in Hydrogels*

The establishment of phototriggered Cp precursors detailed in Chapter 3 provides numerous opportunities in photoinduced DA click chemistry. I was particularly excited about expanding the application of the platform into hydrogel materials, but the solubilities of the original CPD–NBD derivatives prohibited their direct use in aqueous systems. Thus, I worked to design new water-soluble CPD–NBD adducts for this purpose. This chapter presents the computational design, synthesis and application of a water soluble CPD–NBD derivative for facile incorporation into hydrogels for subsequent photopatterning. Portions of this chapter are included in a manuscript currently under peer review.

4.1 Abstract

Spatiotemporally functionalized hydrogels have exciting applications in tissue engineering, but routes to pattern these materials typically rely upon radical-based strategies that can be deleterious in biological settings. Herein, the computationally guided design, synthesis, and application of a water-soluble cyclopentadienone–norbornadiene (CPD–NBD) adduct is disclosed as a photocage for radical-free cyclopentadiene-based Diels–Alder click chemistry. We show that this scalable CPD–NBD derivative can be readily incorporated into hydrogel formulations and commercial 3D printing resins, providing hydrogels that can be patterned with dienophile-bearing species upon 365 nm uncaging of cyclopentadiene. The utility of this aqueous photoclick is demonstrated by the localized conjugation of maleimide dienophiles in both 2D hydrogel films and structurally complex 3D printed parts. This water-soluble photocaged cyclopentadiene adds an inexpensive, versatile, and radical-free photoclick reaction to the toolbox of strategies to pattern molecules of interest into hydrogel systems.

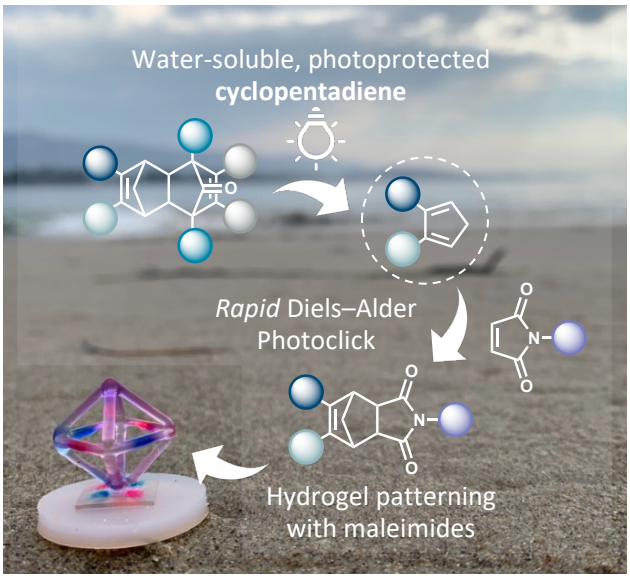

Figure 4.1. Graphical Abstract. A water-soluble cyclopentadienone–norbornadiene adduct as a biocompatible photocage for cyclopentadiene-based Diels–Alder photoclick chemistry.

4.2 Introduction

Synthetic and naturally derived hydrogels are an exciting class of soft materials that are noted by their high water content and tunable mechanicals which provide material properties akin to natural tissues.[1] Due to these desirable properties, hydrogels are regularly used in a variety of biomedical applications.[2,3] Notably, these hydrated polymer networks can provide an amenable cellular scaffold that make them great candidates for extracellular matrix (ECM) mimics.[4] Chemical modification of synthetic and biologically derived polymer networks can provide access to new materials that better recapitulate the structurally complex and dynamic biochemical and mechanical environment found in the natural ECM.[5] Notably, a number of technologies have been developed to control the spatial presentation of biochemical and biophysical signals within synthetic ECM mimics,[6–8] as the anisotropic environment of natural tissues is known to play a key role in dictating cell behavior.[9,10]

To achieve spatiotemporal functionalization of hydrogels, photoclick chemistry has emerged as a powerful tool which is controlled by the precise administration of light.[11,12] By incorporating "photoclickable" moieties within materials, spatially defined light irradiation can provide a route to the patterning of molecules via on-demand click reactions.[13] The thiol–ene photoclick reaction has found great utility in this space and has been employed extensively in the decoration hydrogels with biomolecules for cell culture.[6] Although this patterning strategy has been demonstrated in the presence of cells,[14,15] careful consideration of the photoinitating system is needed to avoid cytotoxicity,[16,17] and the reliance on a free-radical mechanism can have deleterious effects on protein structure.[18] Thus, recent reports[19–21] have highlighted the need for non-radical-propagating photo-click reactions to expand compatibility with sensitive cell lines and off-the-shelf protein-based hydrogels (e.g. collagen) commonly used for cell culture.[22]

Radical-free photoclick strategies typically rely upon installing a photoremovable protecting group, or photocage, on a clickable moiety.[23,24] A number of biologically relevant photoclick reactions have been demonstrated using photocages including strain promoted azide–alkyne cycloadditions,[25] Staudinger–Bertozzi ligations,[26] inverse electron demand Diels–Alder tetrazine ligations,[27–30] and oxime ligations.[31–34,19] Although this strategy has been employed to pattern hydrogels, these examples are largely limited to the photocaging of thiols[35–37] and amines.[38,20] The biological prevalence of thiol and amine functionalities makes them readily available for photocaging, but, consequently, can promote off-target clicking to native cysteine or lysine residues, or terminal amines. Thus, expanding the toolbox of photocaged click moieties to non-biologically relevant functional groups has the potential to

greatly advance tissue engineering technologies, as has been elegantly demonstrated with bioorthogonal photomediated oxime ligation.[19,21,34]

The development and uptake of new technologies, however, is largely dependent upon the cost and ease of use. Although many photoclick reactions have promise in improving bioorthogonality and expanding photopatterning technologies, their prohibitive cost and synthesis has likely prevented their adoption in hydrogel systems.[23] Instead, the scalable and well-established thiol–ene and photo-thiol Michael additions have prevailed in the patterning of hydrogel systems[6] to the detriment of advancing technologies that are bioorthogonal and radical-free. Therefore, the development of photocages for bioorthogonal click moieties that are scalable, affordable, and readily incorporated into currently available hydrogel technologies is needed to promote their uptake.

Our group recently reported a new photoclick strategy which exploits cyclopentadienone–norbornadiene (CPD–NBD) Diels–Alder adducts as photocages for cyclopentadiene.[39] Upon irradiation, CPD–NBD adducts undergo a decarbonylation followed by a rapid retro-Diels–Alder cleavage to yield cyclopentadiene and a substituted benzene byproduct. The incorporation of CPD–NBD adducts into polymer networks thus enabled the spatially controlled Cp-based click chemistry[40] with dienophiles (e.g. maleimide) in pre-determined locations. The Diels–Alder (DA) cycloaddition between Cp and maleimide provides rapid kinetics that are further accelerated in aqueous conditions due to the hydrophobic effect[41] resulting in a reported second order rate constant of 77 $M^{-1}s^{-1}$.[42] Thus, we anticipated the photouncaging of a cyclopentadiene moiety would provide spatial access to rapid click chemistry in hydrogels (**Figure 1**). Furthermore, because maleimide can be used as the coupling partner, this method also provides access to a wealth of commercially available dyes

and biomolecules for patterning due to the extensive use of maleimide in bioconjugation.[43] Therefore, we envisioned that CPD–NBD adducts could provide a facile route to the patterning of biocompatible hydrogels with the potential for widespread adoption.

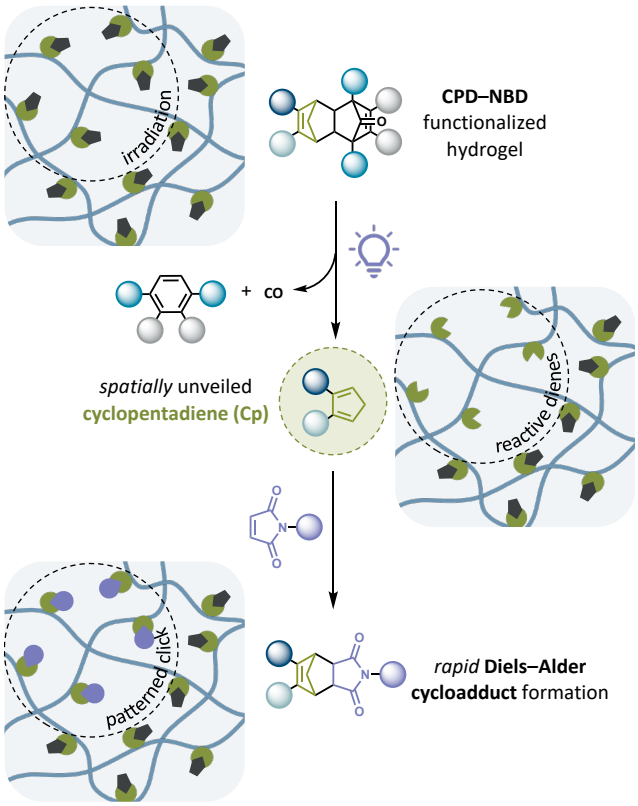

Figure 4.2. Schematic of hydrogel photopatterning from CPD–NBD adducts.

Previous work showed that PEG based hydrogels could be patterned with biotin–maleimide using CPD–NBD.[39] However, organic solvents were needed to incorporate the CPD–NBD into the PEG network with subsequent swelling into water to afford the desired hydrogel.[39] Although this was an encouraging proof-of-concept, the poor water solubility of the CPD–NBD adduct significantly limited the utility for the direct incorporation into commercial hydrogel systems. Given the promise of this platform as a new photo-patterning strategy for

hydrogel systems, we sought to improve the aqueous solubility of the CPD–NBD photopatterning platform to expand its utility. Herein, we present the computationally guided synthetic design of a water-soluble CPD–NBD derivative. We report the robust synthesis of an acrylamide bearing CPD–NBD monomer, which can be readily incorporated into aqueous PEGDA hydrogels under orthogonal photopolymerization conditions. These Diels–Alder "photoclickable" hydrogels can then be readily patterned by brief irradiation with 365 nm light (5 min, 6 mW/cm^2) followed by treatment with maleimide-bearing molecules such as water-soluble cyanine dyes. To highlight the user-friendly nature of our platform, we demonstrate the CPD–NBD monomer can be directly incorporated into commercially available PEGDA photoinks for the preparation and post-print patterning of structurally complex 3D hydrogel objects.

4.3 Results and Discussion

4.3.1 Computational Design

Previous work showed that some CPD–NBD adducts have a competing thermal decarbonylation process that poses a potential challenge.[39,44] Background thermal decarbonylation will prevent precise spatial control of unveiled Cp and result in non-selective patterning upon reaction with dienophiles. Therefore, understanding design principles to prevent thermal decarbonylation is vital in approaching the design of a new CPD–NBD derivative for photopatterning applications (**Figure 2a**). Our previously reported fused CPD–NBD derivative, **F1**, showed higher thermal stability over its "open" counter parts **O1** and **O2**.[39] We calculated the ΔG associated with the loss of carbon monoxide for these derivatives at the B3LYP/6-31+G(d,p) level of theory. The non-fused "open" CPD–NBD adducts had ΔG

of decarbonylation of -18 and -13 kcal/mol for **O1** and **O2**, respectively, in agreement with previously reported thermal instability (**Figure 2b**, Supplementary Information Section 5).[39] In contrast, the fused derivative, **F1**, had a ΔG of decarbonylation of +5 kcal/mol, in agreement with the thermal stability and photoselectivity shown previously.[39] This is likely due to a loss of aromaticity resulting from cheletropic extrusion of carbon monoxide from the system. The thermal stability of fused aromatic CPD–NBD systems was further corroborated by calculating the relative transition state energies of the extrusion of carbon monoxide from **F1** and **O1**, which revealed a 5 kcal/mol larger energy barrier for decarbonylation of the fused **F1** derivative in comparison to the open **O2** derivative (Supplementary Information, Section 5).

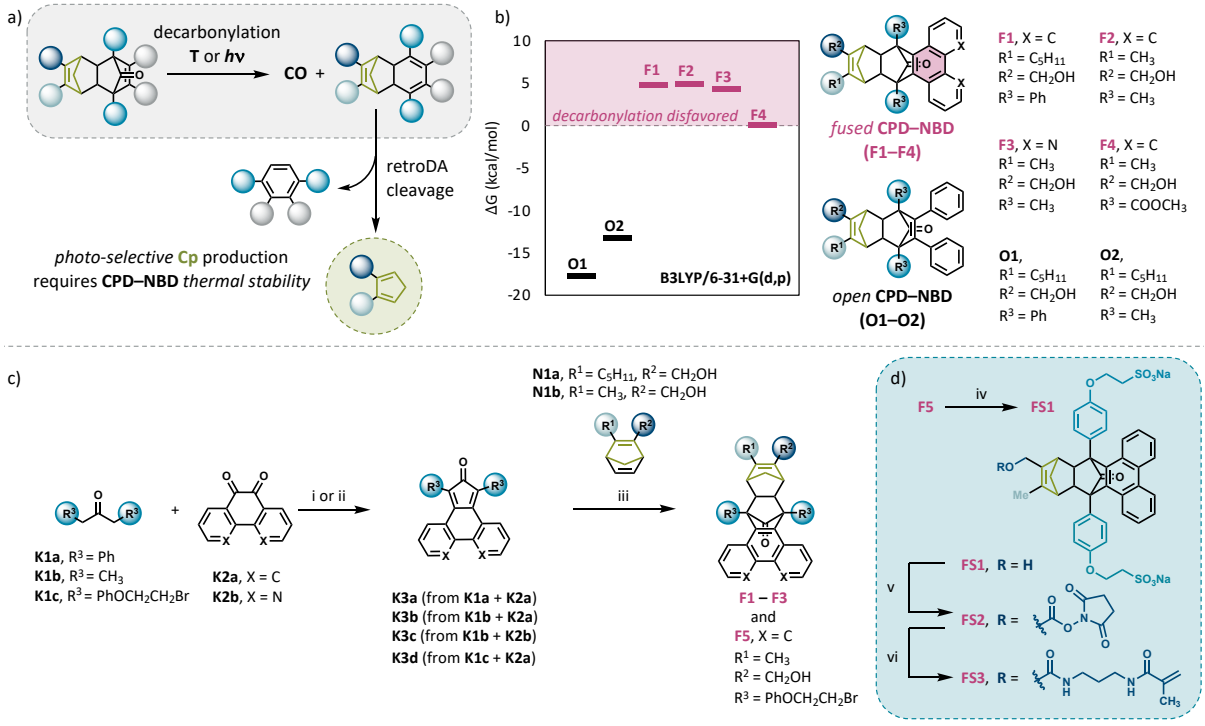

Figure 4.3. a) Schematic of photo- or thermal cascade to Cp from CPD–NBD adducts. b) Plot of ΔG values for the thermal decarbonylation of fused (pink) and open (black) CPD–NBD adducts. c) Synthesis of CPD–NBD scaffolds.[a] d) Introduction of water solubilizing sulfonate groups and polymerizable unit onto **F5**.[b]

[a]Conditions i) KOH, EtOH or MeOH, rt, 2 – 18 h. ii) 1. K_2CO_3, MeOH, rt, 12 h, 2. MsCl, DMAP, DCM, 0°C – rt, 16 h. iii) toluene, 60 or 110 °C, 12 – 18 h. [b] iv) Na_2SO_3, dioxane/EtOH/H2O, 80 °C, 72 h. v) N,N-Disuccinimidyl carbonate, Et_3N, DMSO, rt, 3 h. vi) N-(3-Aminopropyl)methacrylamide hydrochloride, Et_3N, DMSO, rt, 60 h.

The aromatic-to-non-aromatic destabilization seems critical for determining thermal stability, as minimal effect on the ΔG of decarbonylation was observed upon replacing substituents at R^1 and R^3 with methyl groups (**F2**, **Figure 2b**). Calculations were also conducted to investigate the electronic effects of the R^3 substituents, as well as aromatic, non-aromatic, anti-aromatic, hetero and strained ring systems (Supplementary Information, Section 5). It was found that highly electron withdrawing substituents in the R^3 position, like in the case of methyl esters on **F4**, had a destabilizing effect even on fused derivatives, reducing the calculated ΔG to 0 kcal/mol (**Figure 2b**). This computational study provided insights for the design of thermally stable CPD–NBD derivatives; thus, the identified design criteria for our water-soluble synthetic targets were as follows: 1) inclusion of water solubilizing moieties, 2) fusion of an aromatic ring system, and 3) avoidance of electron withdrawing substituents at the R^3 position. Thus, a phenanthroline derived CPD–NBD derivative, **F3**, was identified as a potential synthetic candidate as it had a calculated positive ΔG of decarbonylation and we envisioned that quaternization of the phenanthroline unit would provide a facile route to water solubility.

4.3.2 Synthetic Design

CPD–NBD species are readily prepared from the inverse electron demand DA (IEDDA) between cyclopentadienone (CPD) and norbornadiene (NBD).[39] To access improved solubility in aqueous systems, the NBD derivative **N1b** was chosen to avoid incorporation of the hydrophobic pentyl chain at the R^1 position of **O1**, **O2** and **F1** derivatives, while maintaining

a handle for polymer incorporation at R^2. Conveniently, **N1b** can be readily prepared on multi-gram scale following the robust synthesis previously established from **N1a** using inexpensive precursors.[45] Commercially available CPD derivatives were utilized to readily prepare **O1**, **O2** and **F1**;[39] however, commercial CPD derivatives were not expected to satisfy our outlined design criteria. Thus, we set out to design a scalable synthesis of a CPD which would incorporate water solubilizing moieties and bestow thermal stability on the final CPD–NBD adduct.

An initial synthetic target molecule **F3** was identified based on the promising thermal stability calculation and straightforward route to a water-soluble charged species via quaternization of the heterocyclic fused aromatic ring system. Additionally, through incorporation of the solubilizing moiety in the ring system, R^3 could be reduced from phenyl rings to less bulky methyl groups while shutting down potential pi-stacking interactions. The required CPD derivative, **K3c**, was readily prepared from a previously reported synthesis[46] and used in an IEDDA with **N1b** to afford the phenanthroline-based CPD–NBD derivative **F3** (**Figure 2c**). Attempts to quanternize this adduct provided water soluble material; however, initial ^{1}H NMR studies revealed that **F3** fails to unveil Cp under UV irradiation (Supplementary Information, Section 6).

A new strategy was adopted that relied on incorporation of sulfonate groups onto the original **F1** substructure. Direct sulfonation of the aromatic system of 9,10-phenanthrenequinone (**K2a**) has been reported;[47] however, we found this material was challenging to carry through a multi-step synthesis due to poor organic solubility. As an alternative strategy, a synthetic route was devised which relied on an early-stage incorporation of alkyl bromide substituents at the R^3 position. These bromides could then be displaced in a

late-stage reaction without facing the same challenges associated with sulfonate bearing substrates.

To access such material, the alkyl bromide containing bisbenzyl ketone derivative **K1b** was accessed in 20% yield over three steps (Supplementary information, Section 1) starting from an inexpensive precursor, methyl 4-hydroxyphenylacetate ($1.47/g).[48] Condensation with **K2a** afforded the desired CPD derivative, **K3b**, that underwent an IEDDA cycloaddition with **N1b** to afford an alkyl-bromide containing CPD–NBD derivative, **F5**. Upon treatment with sodium sulfite, the bromides were displaced to afford the sulfonated CPD–NBD derivative **FS1**. Due the incompatible solubilities of **F3**, sodium sulfite, the mono-substituted intermediate and the disubstituted **FS1**, an initial reaction solvent mixture of dioxane/ethanol/water (4:4:3) was found to be critical for efficient product formation, where **F5** was first dissolved in dioxane before ethanol was added, followed by the slow addition of water. Over the course of the 72-hour reaction additional water aliquots were added as the mono-substituted species with improved aqueous solubility was formed. This gradual increase in water content thus increased the concentration of dissolved sodium sulfite and enabled quantitative formation of the bis-substituted **FS1** to be achieved on multi-gram scale.

Upon accessing a sulfonated CPD–NBD derivative, initial investigations to test photo-induced Cp production and water solubility were performed. To confirm that photo-selective Cp production was conserved and compatible with aqueous systems, a 3.3 mM solution of **FS1** in a mixture of deuterated water and deuterated methanol was irradiated in the presence of 3-maleimidopropionic acid while monitored by ^{1}H NMR spectroscopy (Supplementary Information, Section 6). After 45 min irradiation at 365 nm, near complete disappearance of diagnostic CPD–NBD peaks was observed and quantitative formation of the Cp–maleimide

adduct was determined using ethylene carbonate as an internal standard. Although a mixture of deuterated water and deuterated methanol was required to observe formation of the Cp–maleimide adduct via ^{1}H NMR, we were pleased to find that **FS1** exhibited partial aqueous solubility without the need for methanol as a co-solvent. To quantify the absolute aqueous solubility a UV vis calibration curve was prepared by plotting the absorbance of aqueous solutions of **FS1** at 300 nm. This calibration was then used to determine the absolute aqueous solubility of **FS1** to be 13 mM (Supplementary Information, Section 7).

With a photolabile and water-soluble CPD–NBD derivative in hand, we next turned to the incorporation of a tunable handle at R^2 for incorporation into various hydrogel systems. We chose to prepare an amine reactive derivative, **FS2**, from activation of the alcohol at the R^2 position with *N,N*-disuccinimidyl carbonate (**Figure 2d**). We envisioned not only would **FS2** provide a utility in a variety of systems containing amine handles, but the resulting carbamate connection would also provide improved aqueous stability over the ester linkages previously utilized for polymer incorporation.[39,49] We were pleased to find that introduction of this reactive handle also increased the water solubility of the derivative to 90 mM. Subsequent reaction of this activated carbamate with N-(3-aminopropyl)methacrylamide (**Figure 2d**) provided the highly functional acrylamide monomer **FS3** with an absolute water solubility of 56 mM, enabling direct incorporation into aqueous hydrogel formulations. Complete synthetic details and characterization data for all adducts can be found in the Supplementary Information, Section 1.

4.3.3 Hydrogel Preparation and Patterning

To demonstrate the utility of this new CPD–NBD derivative and the ease of use of the patterning platform in hydrogel systems, **FS3** was directly incorporated into a common PEGDA hydrogel formulation. Orthogonal photopolymerization of CPD–NBD based monomers was anticipated to be achieved at 405 nm without deprotection of the CPD–NBD moiety,[39] enabling subsequent patterning of the hydrogels using 365 nm light. Copolymerization of the acrylamide-based **FS3** monomer (1 wt%) with PEGDA (8 kDa, 15 wt%) in DI water was achieved using the photoinitiator lithium phenyl-2,4,6-trimethylbenzoylphosphinate (LAP, 0.1 wt%) under 405 nm irradiation for 10 min to afford hydrogel **H1a** (**Figure 3a**). To access hydrogel geometries most amenable to subsequent patterning experiments, photopolymerization was conducted on a glass slide treated with 3-(trimethoxysilyl)propyl methacrylate (TMSPMA) to enable covalent attachment of the hydrogel to the glass. The pre-hydrogel solution containing 300 μm glass spacers was dropped onto a treated glass slide and topped with a RainX treated coverslip before polymerization (**Figure 3b**). Removal of the coverslip after irradiation afforded CPD–NBD functionalized PEGDA hydrogels (**H1a**) as thin square films (22 x 22 x 0.3 mm, **Figures 3b** and **4a**). Hydrogels were allowed to incubate overnight in DI water to remove any residual monomers and LAP before photopatterning.

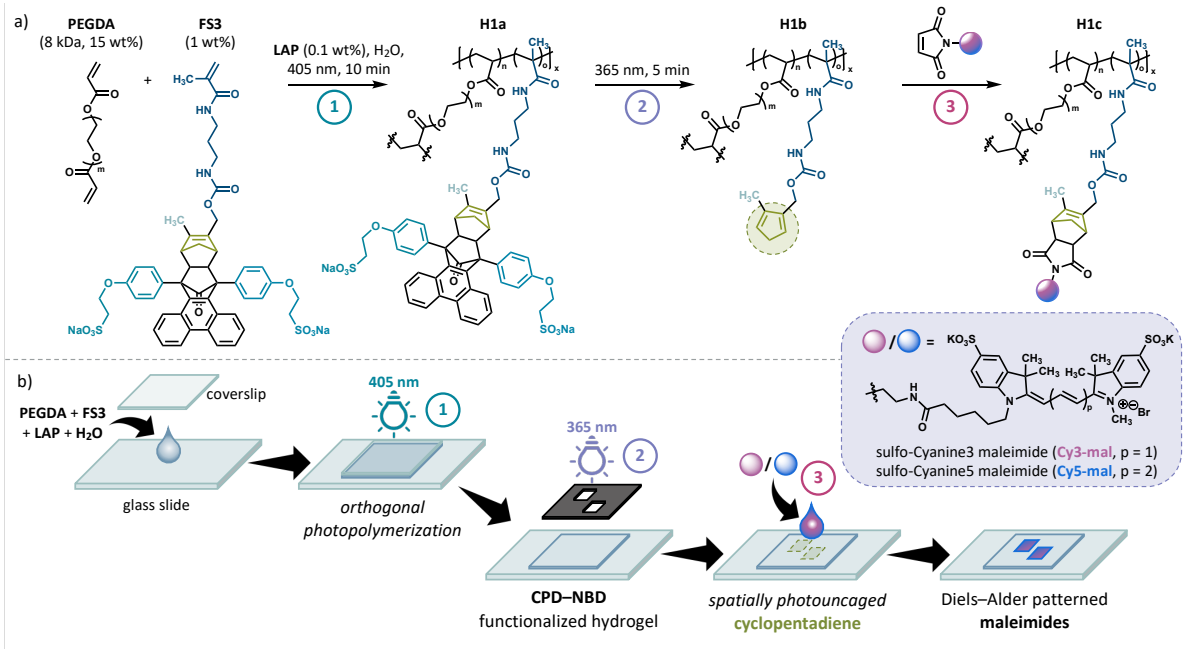

Figure 4.4. a) Synthetic scheme for the preparation and patterning of CPD–NBD containing hydrogels. b) Graphic depiction of hydrogel preparation.

These **H1a** hydrogels were readily patterned with maleimide functionalized cyanine dyes (**Cy3-mal** and **Cy5-mal**) following irradiation with 365 nm light to reveal reactive Cp units (**Figures 3a–b** and **4b–d**). Photopatterning of **FS3** containing hydrogels was conducted using a 365 nm LED (6 mW/cm^2). An initial irradiation time screen was completed to determine optimal patterning conditions by irradiation of various regions of a **H1a** hydrogel for 30 s – 10 min. After irradiation, the hydrogel was incubated in an aqueous solution of **mal-Cy5** (10 mM) for 3 hours. To remove non-conjugated dye, the hydrogel was rinsed with excess DI water and allowed to incubate overnight in a gently agitated 2 L beaker containing DI water.

The amount of dye covalently bound to the hydrogel after unveiling cyclopentadiene was qualitatively assessed by the color difference (ΔE*) between each dye patterned region following the International Commission on Illumination guidelines as previously reported (Supplementary Information, Section 2).[50–53] As revealed in **Figure 4b**, analysis of the change

in color corresponding to varied irradiation time shows a minimal increase in dye conjugation after 5 minutes irradiation, indicating that 5 minute irradiation of subsequent hydrogels would be sufficient for future patterning experiments. As depicted in **Figure 4c.i**, after masked irradiation (365 nm, 6 mW/cm^2) of **H1a** for 5 minutes followed by incubation in **Cy3-mal** (10 mM, 3 h) to afford a patterned hydrogel **H1c.i**. By repeating the patterning sequence with **Cy5-mal** the CPD–NBD functionalized hydrogel was patterned a second time to afford multiple patterns within one material (**H1C.ii**, **Figure 4c.ii–iii**). This procedure was used to prepare a variety of multi-patterned hydrogels (**Figure 4c–d**). Our patterned hydrogels could also be imaged by fluorescence microscopy (**Figure 4c.iii** and **4d.iii**) due to the incorporation of fluorescent cyanine dyes. Importantly, incorporation of these fluorescent dyes which are susceptible to photobleaching[54] was accomplished through a two-step patterning procedure which takes advantage of the uncaging of a stable diene that can be clicked to the maleimide-bearing dyes in a second step after irradiation.

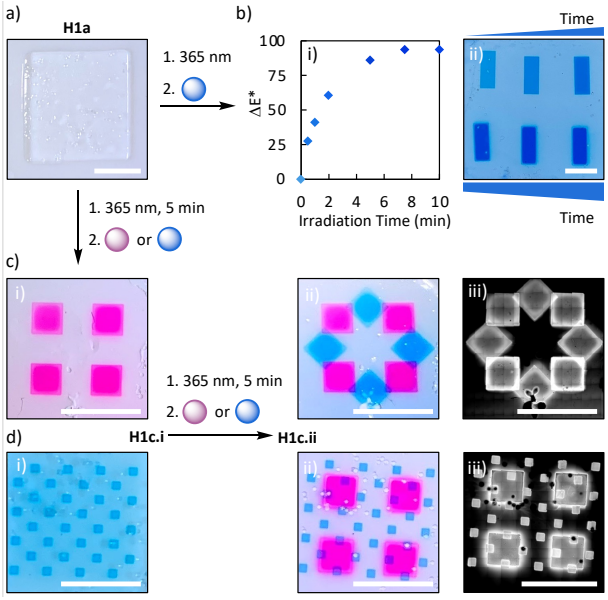

Figure 4.5. a) Photograph of **H1a** before patterning. b) Irradiation time screen i) Plot of change in color of Cy5 patterns (ΔE*) as a function of irradiation time of **H1a** with 365 nm LED (6 mW/cm^2). ii) Photograph of corresponding hydrogel used for color quantification. c) (i)

Photographs of hydrogels **H1c.i** after initial patterning with **Cy3-mal** followed by (ii) second patterning with **Cy5-mal** to afford **H1c.ii.** (iii) Overlay of fluorescence microscopy images of **H1c.ii** imaging Cy3 (550/605 nm) and Cy5 (640/690 nm). d) Photographs (i) and (ii) and fluorescence microscopy (iii) of hydrogel first patterned with **Cy5-mal** followed by **Cy3-mal**. Scale bars = 5 mm.

4.3.4 3D Hydrogel Printing and Post-Print Patterning

Given the growing interest in 3D printing complex hydrogel scaffolds for biomedical[55] and tissue engineering[56,57] applications, we sought to demonstrate the versatility of CPD–NBD derivatives to enable the post-print patterning of geometrically complex parts. Extrusion based 3D printing techniques provide one route to spatially vary hydrogel composition by using multiple print heads; however, these techniques are limited in resolution based on extrusion nozzle size (>100 μm) and require the design of high viscosity or shear thinning resins.[57] In vat polymerization printing techniques, like digital light processing (DLP), higher resolution can be accessed (>25 μm) and resins with low viscosity are preferred.[57] However, because these methods rely on a single composition provided by the vat-based resin, access to spatially controlled biochemical cues would be a challenge during the printing stage. To gain access to patterned DLP-based parts, we envisioned that the acrylamide-based monomer **FS3** could be incorporated into bulk commercial photoinks for use in printing structurally complex, photoclickable hydrogels.

As a proof-of-concept, a biocompatible PEGDA photoink was purchased from Cellink and mixed with **FS3** (1 wt%) directly before printing. Using a Mono3Z2 Panchromatic Printer, an **FS3** containing PEGDA octahedron was printed with 50 μm layer thickness, 2.2 s layer irradiation time, and 15 mW/cm^2 irradiance at 405 nm (**Figure 5a–c**). This 3D printed part was then patterned by masked irradiation (365 nm, 6 mW/cm^2, 5 min) in a similar fashion to the 2D hydrogel films. One alteration, however, was that before irradiation the part was first

swollen in a solution of commercially available, methyl orange dye (100 μM in DI water) to absorb light scattering throughout the part and prevent non-selective patterning. We were pleased to find that printed PEGDA parts could then be readily functionalized following the same cyanine dye incubations and rinsing procedure used for 2D hydrogel films. As depicted in **Figures 5c–e**, patterning can be accomplished on the base of the structure as well as mid-strut of the octahedron scaffold. Notably, this complex post-print functionalization could not be accomplished by simply dipping the structure in a dye post-print. Additionally, the mid-strut patterning highlights the benefit of using a photopatterning approach over multi-print head extrusion to modulate resin composition, as changing composition mid-strut would not be accessible through extrusion-based methods. This facile incorporation of **FS3** into off-the-shelf photoinks and subsequent post-print patterning with maleimide bearing molecules highlights the user-friendly nature of our CPD–NBD patterning platform for complex hydrogel applications.

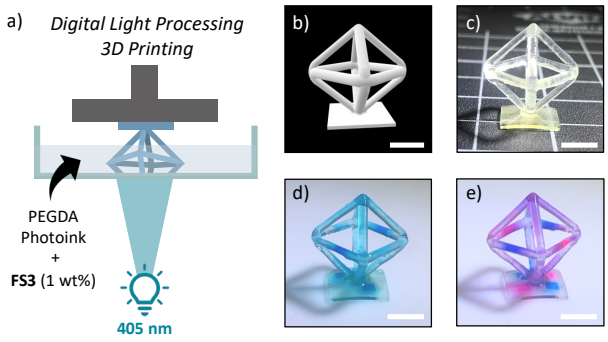

Figure 4.6. a) Graphic depiction of Digital Light Processing 3D printing b) Image of octahedron model used for 3D printing and photographs of resulting b) **FS3** functionalized octahedron print before patterning, c) print after patterning with **Cy5-mal** and d) print after patterning with **Cy3-mal**. Scale bars = 5 mm.

4.4 Conclusion

We have demonstrated that through thoughtful design, the scalable synthesis of a water-soluble acrylamide-based CPD–NBD monomer was achieved and employed in "photoclickable" 2D and 3D printed hydrogels. Here, we show patterning can be achieved through the photouncaging of cyclopentadiene followed by treatment with commercially available maleimide-bearing species in normal electron demand DA cycloadditions; however, the great utility of cyclopentadiene in numerous DA-based bioconjugation reactions, including completely bioorthogonal IEDDA reactions, has recently been reported and highlights the potential of this diene for bioconjugation.[58] Importantly, unlike thiol-ene chemistry which is traditionally used for preparing patterned hydrogels,[6] our DA patterning platform circumvents the use of a radical propagating click chemistry providing several advantages: 1) access to patterning photosensitive species (cyanine dyes) through a two-step patterning process 2) orthogonality with photoinduced and free radical polymerization conditions, and 3) future access to radical sensitive hydrogel scaffolds[21] and biomolecules. This new CPD–NBD patterning platform adds an affordable and readily synthesized photocleavable molecule to the toolbox of photopatterning strategies amenable to the patterning of radical and photo-sensitive biomolecules and matrices that we anticipate will provide exceptional utility in the advancement of biomimetic hydrogel scaffolds.

4.5 Acknowledgments

I would like to thank Kiara Rael and Arsalan Hashmi for their willingness to learn and assistance with material scale up, this project would not have gotten done without the extra synthetic hands! I would also like to sincerely thank Erik Hopkins for his efforts in attempting to culture cells on patterned 2D PEGDA hydrogels. I have been incredibly grateful to have a

cell biologist collaborator to turn to for insights, problem solving and new project ideas. I would also like to thank the UCSB Graduate Division for financial support through a Chancellor's Fellowship as well the Partnership for Research and Education in Materials (NSF DMR 2122108) for financially supporting Kiara's work on this project through a summer internship. I would also like to acknowledge the work here was partially supported by the National Science Foundation under award No. CHE-2204077 and partially supported by the BioPACIFIC Materials Innovation Platform (MIP) of the National Science Foundation under award No. DMR-1933487. Use was made of BioPACIFIC MIP instrumentation including the Mono3Z2 3D Printer and inverted optical microscope system (Zeiss Axio Observer), and I would like to thank Juan Manuel for his kindness and eagerness to help me use these resources. Use was also made of computational facilities purchased with funds from the National Science Foundation (CNS-1725797) and administered by the Center for Scientific Computing (CSC). The CSC is supported by the California NanoSystems Institute and the Materials Research Science and Engineering Center (MRSEC; NSF DMR 1720256) at UC Santa Barbara.

4.6 Supporting Information

Synthesis

Materials and Methods

All chemicals were obtained from Sigma Aldrich, TCI Europe or Fisher Scientific and used as received without further purification. Unless otherwise noted, reactions were performed under an atmosphere of nitrogen. Acetonitrile, tetrahydrofuran, dichloromethane and toluene were dispensed from a solvent purification system immediately before use or stored over 3Å molecular sieves. Ethanol and methanol were also stored over 3Å molecular sieves before use. **Compounds F1,**[39] **N1a,**[45] **K3a**,[59] **K3b**,[46] and **K3c**[46] were prepared following literature

procedures. **Mal-Cy3** and **mal-Cy5** were synthesized following literature procedures[60–62] or could be purchased from Lumiprobe. Thin-layer chromatography (TLC) was conducted with E. Merck silica gel 60 F254 pre-coated plates (0.25 mm) and visualized by exposure to UV light (254 nm) or stained with *p*-anisaldehyde. Flash column chromatography was performed using normal phase silica gel (60 Å, 0.040 – 0.063 mm, Geduran) with hexanes, ethyl acetate (EtOAc), DCM and/or MeOH as eluents. ^{1}H and ^{13}C NMR spectra were recorded on Varian spectrometers (100, 125, 500 or 600 MHz) and are reported relative to $CDCl_3$ (δ = 7.26 ppm for ^{1}H and 77.00 ppm for ^{13}C), DMSO-D6 (δ = 2.50 ppm for ^{1}H and 39.52 ppm for ^{13}C) or methanol-D_4 (δ = 3.31 ppm for ^{1}H). Data for ^{1}H NMR spectra are reported as follows: chemical shift (δ ppm), multiplicity, coupling constant (Hz) and integration. Data for ^{13}C NMR spectra are reported in terms of chemical shift (δ ppm). Mass spectra were obtained on a time-of-flight mass spectrometer with an ESI source. FTIR spectra were collected on a Thermo Nicolet iS10 FTIR Spectrometer equipped with a Smart Diamond attenuated total reflectance (ATR) accessory.

Small Molecule Building Blocks

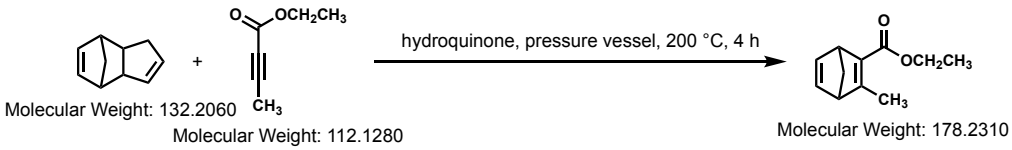

Ethyl 3-methylbicyclo[2.2.1]hepta-2,5-diene-2-carboxylate (Compound S1):

To a 100 mL pressure vessel was added ethyl 2-buytanoate (11.7 mL, 100 mmol, 1 eq), dicyclopentadiene (8.00 mL, 60 mmol, 0.6 eq) and hydroquinone (200 mg). The pressure vessel was sealed under an atmosphere of nitrogen then heated to 200 °C for 4 h, at which point conversion of ethyl 2-buytonoate was determined to be 82% by ^{1}H NMR of a crude aliquot of the reaction mixture. The crude reaction mixture was purified by fractional distillation where cyclopentadiene and ethyl 2-buytanoate were first removed (30–55 °C, ~200 mTorr) before **Compound S1** was isolated (55–60 °C, ~200 mTorr) as a clear oil (10.0 g, 56.1 mmol, 56%). Spectral data matched that of reported literature.[63]

Compound S1: ^{1}H NMR (500 MHz, $CDCl_3$) δ 6.89 (dd, J = 5.0, 3.1 Hz, 1H), 6.73 (dd, J = 4.6, 3.4 Hz, 1H), 4.22–4.12 (m, 2H), 3.88 (s, 1H), 3.39 (s, 1H), 2.22 (s, 3H), 2.05 (dt, J = 6.4, 1.4 Hz, 1H), 1.95 (dt, J = 6.4, 1.4 Hz, 1H), 1.29 (t, J = 6.3 Hz, 3H) ppm.

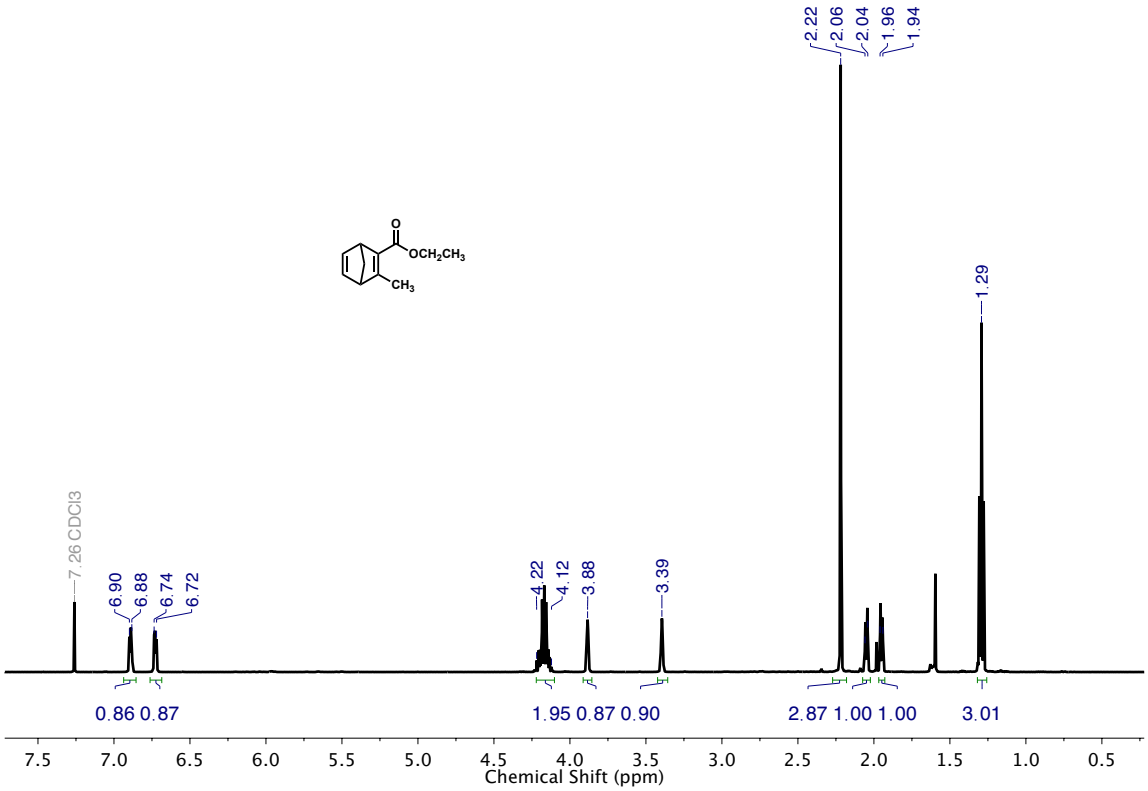

Figure S 4.1. ^{1}H NMR (500 MHz, $CDCl_3$) **Compound S1**

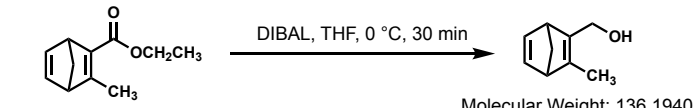

Molecular Weight: 178.2310

Molecular Weight: 136.1940

(3-methylbicyclo[2.2.1]hepta-2,5-dien-2-yl)methanol (Compound N1b)

To a 500 mL flame dried round bottom flask equipped with magnetic stir bar, Compound **N1b** (4.28 g, 24.0 mmol, 1 eq) was dissolved in tetrahydrofuran (130 mL) and the solution was cooled to 0 °C. A solution of diisobutylaluminium hydride (DIBAL) in hexanes (68.0 mL, 68.0 mmol, 2.8 eq) was added dropwise. The solution was stirred 30 min, at which point consumption of starting material was confirmed by TLC (hexanes:ethyl acetate, 4:1). The reaction was then quenched at 0 °C by dropwise addition of H_2O (2.5 mL) followed by 1 M NaOH (5 mL) then H_2O (2.5 mL) before being allowed to warm to room temperature. The reaction mixture was dried with magnesium sulfate then filtered and rinsed with diethyl ether (200 mL). The solvent was removed under reduced pressure, and the residue was subjected to column chromatography (hexanes:ethyl acetate, 4:1) to afford **Compound N1b** (2.33 g, 17.1 mmol, 71%) as a clear oil. Spectral data matched that of reported literature.[64]

Compound N1b: R_f (Hexanes:EtOAc, 4:1): 0.30; ^{1}H NMR (500 MHz, $CDCl_3$) δ 6.82 (dd, J = 4.9, 3.0 Hz, 1H), 6.76 (dd, J = 4.7, 3.1 Hz, 1H), 4.25 (d, J = 12.2 Hz, 1H), 4.14 (d, J = 12.2 Hz, 1H), 3.53 (s, 1H), 3.28 (s, 1H), 1.96 (dt, J = 5.9, 1.6 Hz, 1H), 1.89 (dt, J = 5.9, 1.4 Hz, 1H), 1.79 (s, 3H), 1.07 (br. s, 1H) ppm.

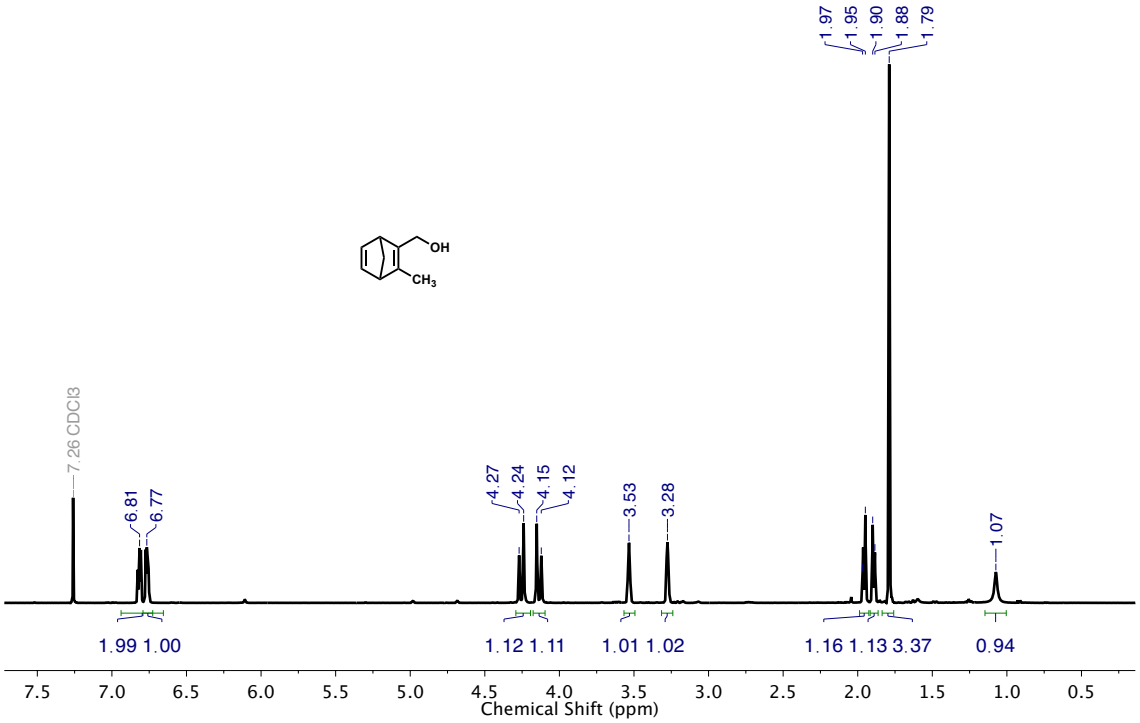

Figure S 4.2. ^{1}H NMR (500 MHz, $CDCl_3$) **Compound S1**

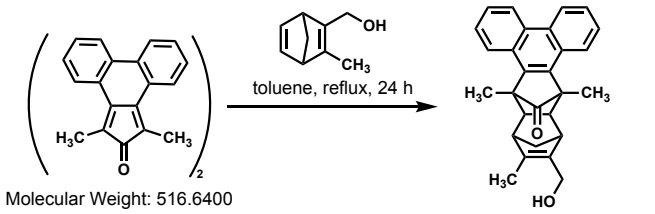

Molecular Weight: 516.6400

Molecular Weight: 394.5140

11-(hydroxymethyl)-9,12,14-trimethyl-9,9a,10,13,13a,14-hexahydro-9,14:10,13-dimethanobenzo[*f*]tetraphen-15-one (Compound F2):

To a 25 mL round bottom flask was added **Compound K3b** (dimer, 0.309 g, 1.20 mmol monomer, 1 eq), **Compound N1b** (0.195 g, 1.43 mmol, 1.19 eq) and toluene (7 mL). This solution was allowed to stir at reflux for 24 h, at which point consumption of starting material was confirmed by TLC (hexanes:ethyl acetate, 2:1). The solution was allowed to cool to room temperature and the solid was collected by vacuum filtration to afford **Compound F2** (0.252 g, 0.639 mmol, 53%) as a light pink powder.

Compound F2: R_f (Hexanes:EtOAc, 2:1): 0.38; ^{1}H NMR (500 MHz, $CDCl_3$) δ 8.77 (dt, *J* = 9.4, 1.9 Hz, 2H), 8.39–8.33 (m, 2H), 7.63 (pd, *J* = 6.9, 1.4 Hz, 4H), 4.18 (d, *J* = 12.6 Hz, 1H), 4.04 (d, *J* = 13.2 Hz, 1H), 2.82 (s, 1H), 2.49 (s, 1H), 2.10 (d, *J* = 8.3 Hz, 1H), 2.06 (s, 6H), 2.00 (d, *J* = 8.3 Hz, 1H), 1.66 (s, 3H), 0.28 (d, *J* = 9.7 Hz, 1H), -0.48 (d, *J* = 9.7 Hz, 1H) ppm; ^{13}C NMR (125 MHz, $CDCl_3$) δ 203.7, 145.7, 144.5, 134.9, 134.6, 130.3, 130.3, 128.9, 126.7, 126.7, 126.2, 126.1, 124.5, 124.4, 123.7, 123.6, 57.6, 54.8, 54.7, 50.1, 49.5, 49.0, 45.2, 38.9, 15.5, 15.5, 12.1 ppm; FTIR (ATR) 3730, 3263, 2940, 1980, 1764, 1614, 1517, 1466, 1438, 1186, 1158, 1034, 1001, 749 cm^{-1}; HRMS (ES+) Exact mass cald. for $C_{28}H_{26}O_2$ $[M+Na]^+$: 417.1830, found: 417.1814.

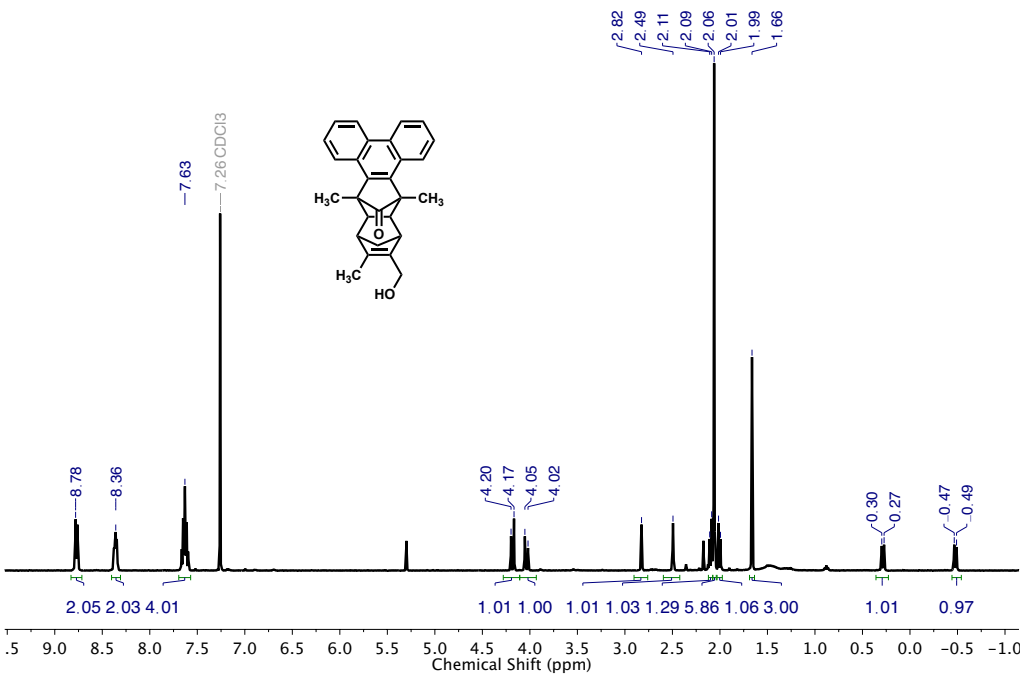

Figure S 4.3. ^{1}H NMR (500 MHz, $CDCl_3$) **Compound F2**

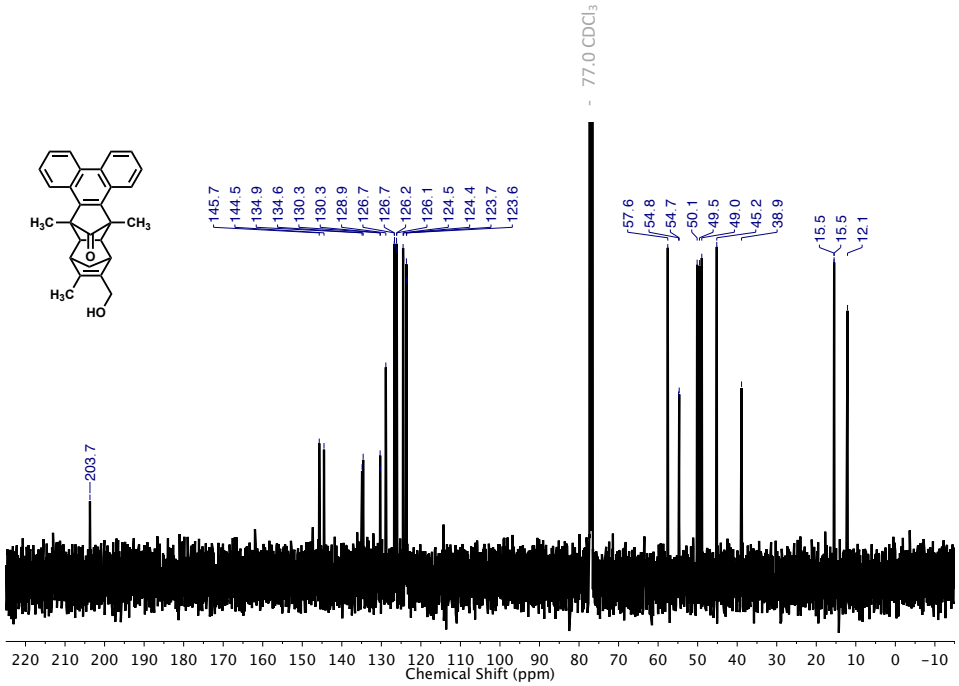

Figure S 4.4. ^{13}C NMR (125 MHz, $CDCl_3$) **Compound F2**

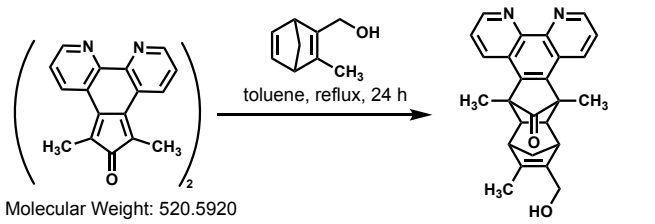

Molecular Weight: 520.5920

Molecular Weight: 396.4900

11-(hydroxymethyl)-9,12,14-trimethyl-9,9a,10,13,13a,14-hexahydro-9,14:10,13-dimethanonaphtho[2,3-*f*][1,10]phenanthrolin-15-one (Compound F3)

To a 25 mL round bottom flask was added **Compound K3c** (dimer, 0.228 g, 0.904 mmol monomer, 1 eq), **Compound N1b** (0.148 g, 1.09 mmol, 2.4 eq) and toluene (5 mL). This solution was allowed to stir at reflux for 24 h. The solution was allowed to cool to room temperature and the solid was collected by vacuum filtration to afford **Compound F3** (0.153 g, 0.386 mmol, 43%) as an ivory powder.

Compound F3: ^{1}H NMR (500 MHz, $CDCl_3$) δ 9.21 (d, *J* = 3.3 Hz, 2H), 8.71 (t, *J* = 7.2 Hz, 2H), 7.66 (dd, *J* = 8.3, 4.1 Hz, 2H), 4.18 (d, *J* = 12.6 Hz, 1H), 4.04 (d, *J* = 12.6 Hz, 1H), 2.80 (s, 1H), 2.46 (s, 1H), 2.16 (d, *J* = 8.3 Hz, 1H), 2.11–2.04 (m, 7H), 1.66 (s, 3H), 0.28 (d, *J* = 9.8 Hz, 1H), -0.67 (d, *J* = 9.7 Hz, 1H) ppm; ^{13}C NMR (100 MHz, $CDCl_3$) δ 202.5, 149.8, 149.8, 145.9, 145.9, 145.4, 144.4, 135.0, 134.7, 131.8, 131.7, 125.8, 125.8, 122.9, 122.9, 57.4, 55.3, 55.1, 50.0, 49.4, 48.8, 45.1, 38.7, 15.0, 15.0, 12.1 ppm. FT IR (ATR) 3730, 3300, 2930, 1988, 1764, 1613, 1516, 1503, 1449, 1185, 1160, 1037, 1001, 750 cm^{-1}; HRMS (ES+) Exact mass cald. for $C_{26}H_{24}N_2O_2Na$ $[M+Na]^+$: 419.1736, found: 419.1724.

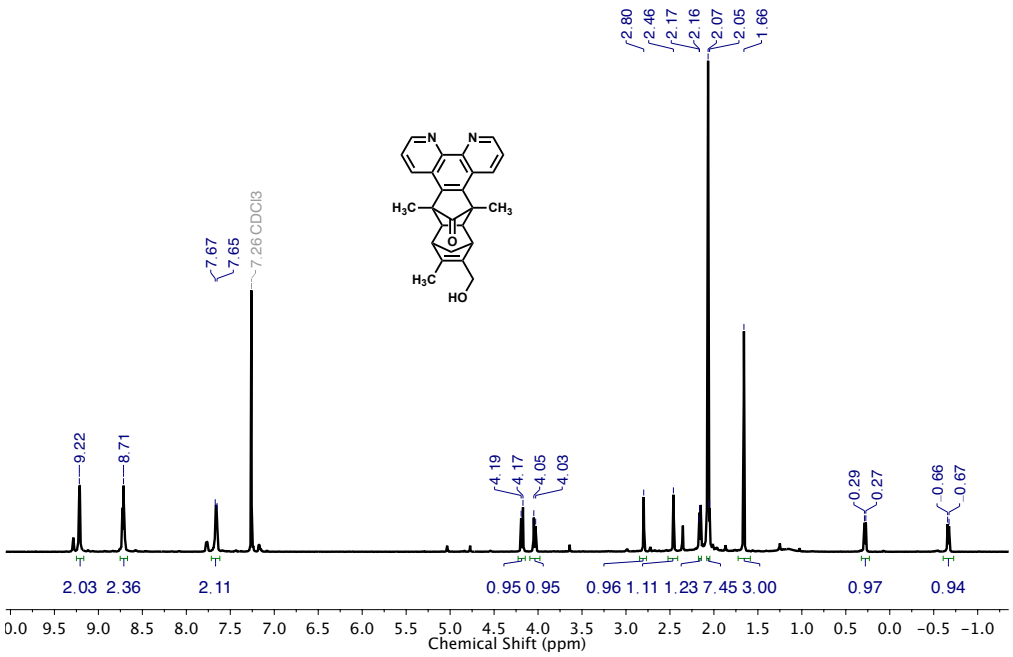

Figure S 4.5. ^{1}H NMR (600 MHz, $CDCl_3$) **Compound F3**

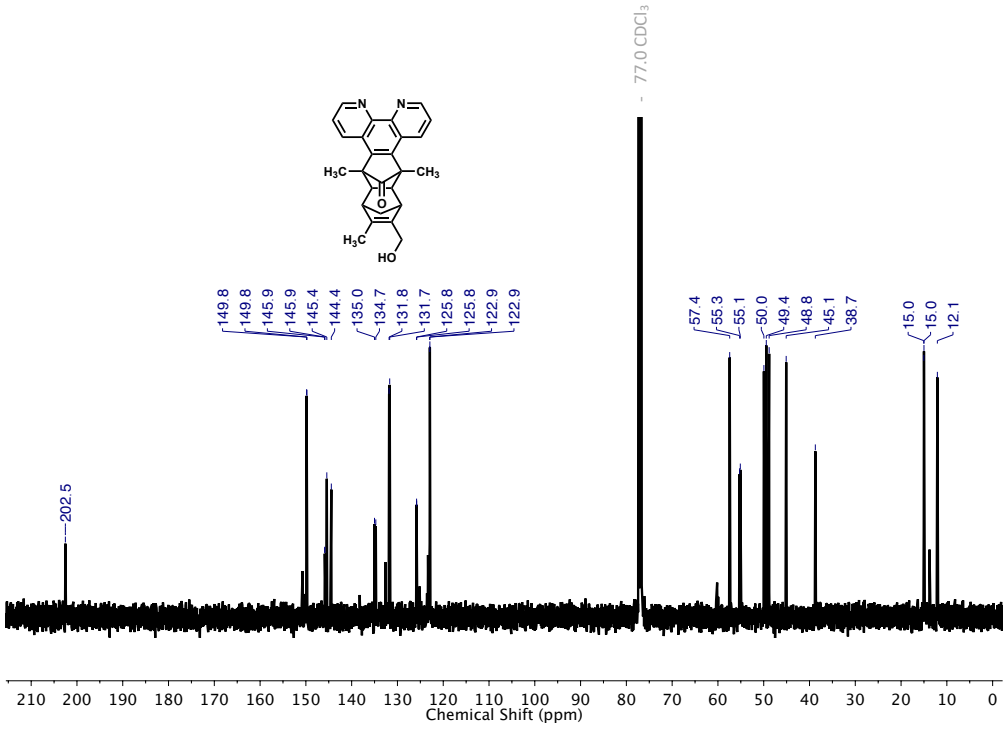

Figure S 4.6. ^{13}C NMR (100 MHz, $CDCl_3$) **Compound F3**

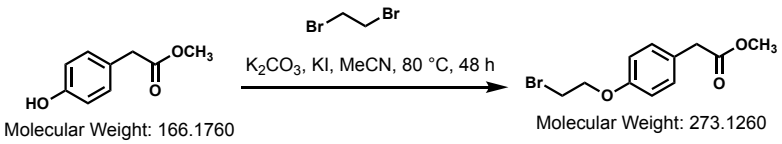

methyl 2-(4-(2-bromoethoxy)phenyl)acetate (Compound S2):

In a 500 mL flame dried round bottom flask equipped with magnetic stir bar and reflux condenser, methyl 4-hydroxy phenyl acetate (10.0 g, 60.2 mmol, 1 eq) was dissolved in acetonitrile (250 mL). To this solution was added potassium carbonate (25.0 g, 181 mmol, 3 eq), potassium iodide (0.500 g, 3.01 mmol, 0.05 eq), and dibromoethane (20.8 mL, 241 mmol, 4 eq). The heterogeneous solution was heated to reflux for 48 h then filtered through a plug of celite. The solvent was removed under reduced pressure, and the residue was subjected to column chromatography (hexanes:ethyl acetate, 9:1) to afford **Compound S2** (8.05 g, 29.5 mmol, 49%) as a clear oil.

Compound S2: R_f (Hexanes:EtOAc, 9:1): 0.30; ^{1}H NMR (600 MHz, $CDCl_3$) δ 7.20 (d, J = 8.6 Hz, 2H), 6.87 (d, J = 8.6 Hz, 2H), 4.27 (t, J = 6.3 Hz, 2H), 3.69 (s, 3H), 3.63 (t, J = 6.3 Hz, 2H), 3.57 (s, 2H) ppm; ^{13}C NMR (125 MHz, $CDCl_3$) δ 172.2, 157.2, 130.4, 126.9, 114.9, 67.9, 52.0, 40.2, 29.0 ppm; IR (ATR) 2971, 2930, 1987, 1735, 1610, 1513, 1210, 1196, 1161, 1014, 753 cm^{-1}; HRMS (ES+) Exact mass cald. for $C_{11}H_{13}BrO_3Na$ $[M+Na]^+$: 294.9946, found: 294.9947.

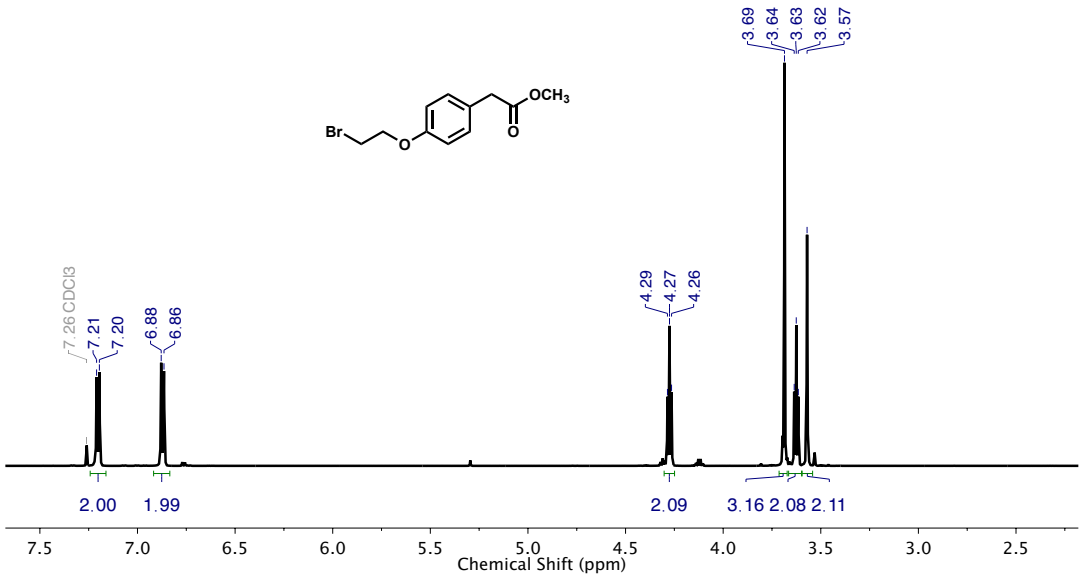

Figure S 4.7. ^{1}H NMR (600 MHz, $CDCl_3$) **Compound S2**

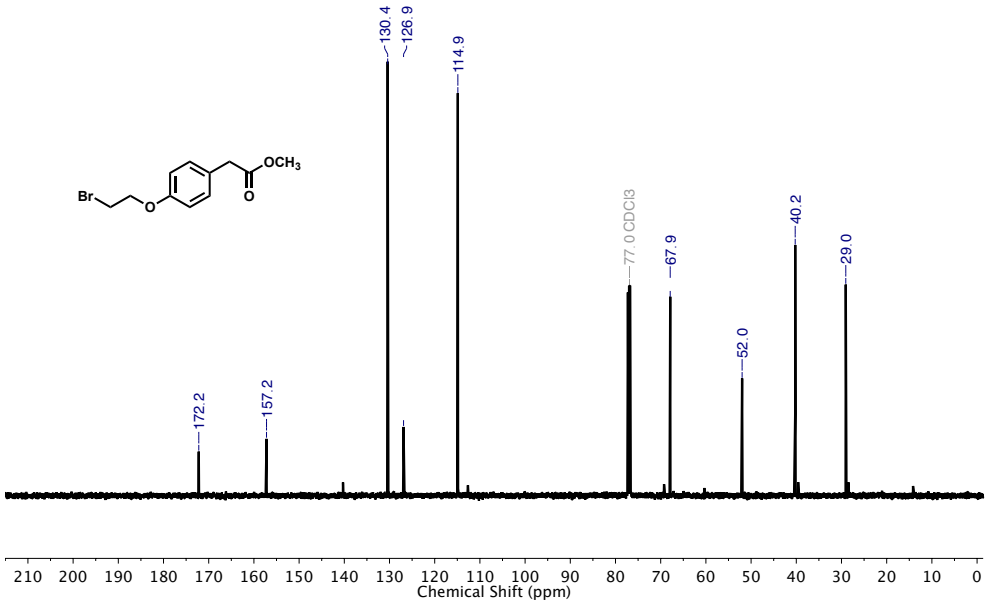

Figure S 4.8. ^{13}C NMR (125 MHz, $CDCl_3$) **Compound S2**

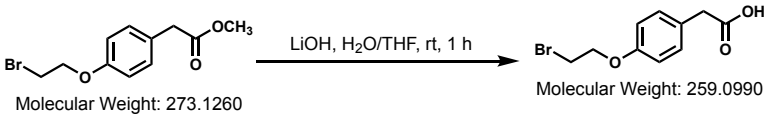

2-(4-(2-bromoethoxy)phenyl)acetic acid (Compound S3):

To a 500 mL round bottom flask equipped with stir bar, **Compound S2** (7.81 g, 28.6 mmol, 1 eq) was dissolved in tetrahydrofuran (170 mL). To this solution was added 1 M aqueous lithium hydroxide (86.0 mL, 86.0 mmol, 3 eq). The solution was stirred 1 h, at which point consumption of starting material was confirmed by TLC (hexanes:ethyl acetate, 4:1). The solution was acidified with 1 M aqueous hydrochloric acid (approximately 90 mL), then extracted with ethyl acetate (3 x 150 mL). The combined organic layers were then washed with brine (100 mL), dried with anhydrous magnesium sulfate and solvent removed under reduced pressure to afford **Compound S3** (7.13 g, 27.5 mmol, 96%) as white powder which was sufficiently pure to take forward without further purification.

Compound S3: ^{1}H NMR (500 MHz, $CDCl_3$) δ 7.19 (d, J = 7.9 Hz, 2H), 6.87 (d, J = 8.1 Hz, 2H), 4.27 (t, J = 6.2 Hz, 2H), 3.62 (t, J = 6.3 Hz, 2H), 3.58 (s, 2H) ppm; ^{13}C NMR (125 MHz, $CDCl_3$) δ 177.7, 157.4, 130.5, 126.2, 114.9, 67.9, 40.1, 29.0 ppm; IR (ATR) 2971, 2931, 2902, 1987, 1764, 1612, 1515, 1437, 1225, 1180, 1158, 1044, 751 cm^{-1}; HRMS (ES-) Exact mass cald. for $C_{10}H_{10}BrO_3$ $[M-H]^+$: 256.9813, found: 256.9810.

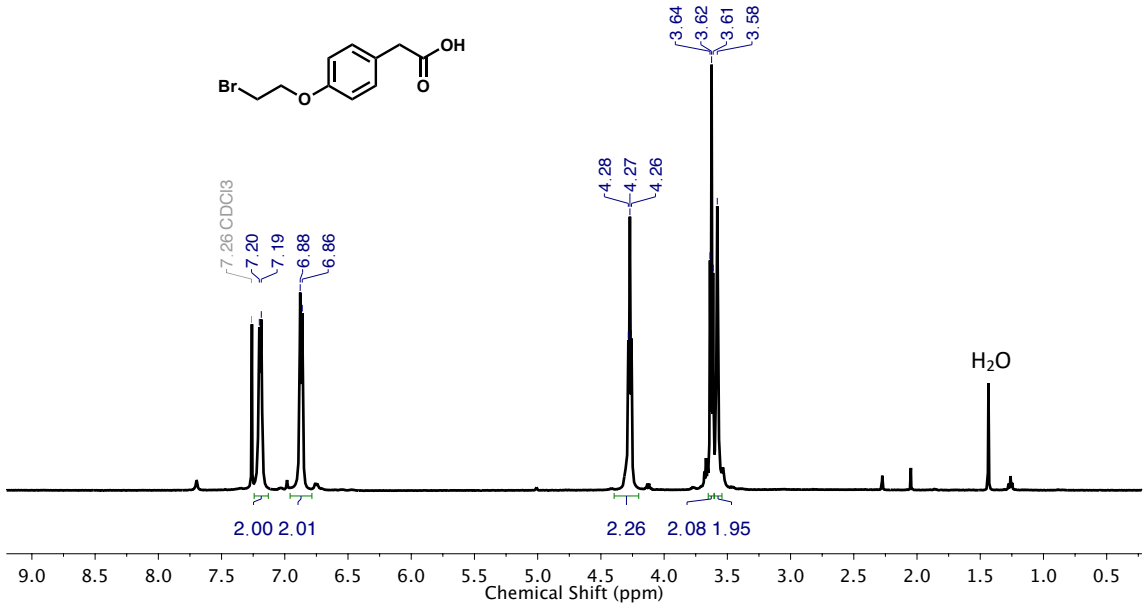

Figure S 4.9. ^{1}H NMR (500 MHz, $CDCl_3$) **Compound S3**

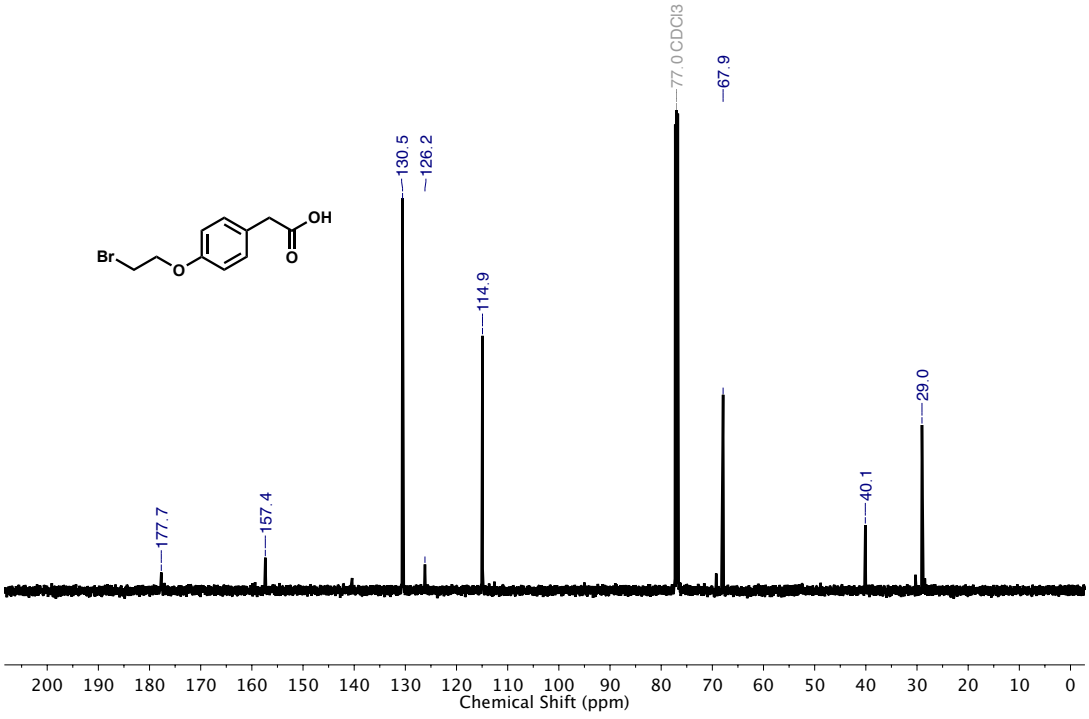

Figure S 4.10. ^{13}C NMR (125 MHz, $CDCl_3$) **Compound S3**

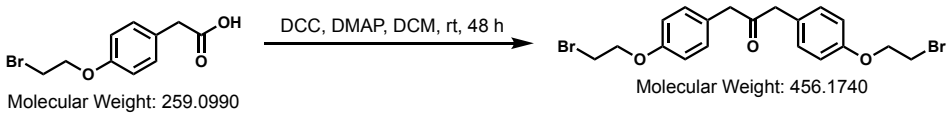

1,3-bis(4-(2-bromoethoxy)phenyl)propan-2-one (Compound K1c):

Prepared from a modified literature procedure.[65] To a 250 mL flame dried round bottom flask equipped with stir bar was added *N,N′*-Dicyclohexylcarbodiimide (DCC) (5.67 g, 27.5 mmol, 1.0 eq), 4-dimethylaminopyridine (DMAP) (0.840 g, 6.87 mmol, 0.25 eq) and dichloromethane (DCM) (50 mL). In a separate round bottom flask, **Compound S3** (7.13 g, 27.5 mmol, 1.0 eq) was dissolved in DCM and cannulated into the DCC/DMAP solution dropwise. The solution was stirred at room temperature under inert atmosphere for 48 h before filtering through a plug of celite to remove insoluble dicyclohexyl urea byproduct. The solvent was removed under reduced pressure, and the residue was triturated in methanol to afford **Compound K1c** (2.36 g, 5.17 mmol, 38%) as a white powder.

Compound K1c: R_f (Hexanes:EtOAc, 9:1): 0.26; ^{1}H NMR (600 MHz, $CDCl_3$) δ 7.06 (d, J = 8.5 Hz, 4H), 6.86 (d, J = 8.6 Hz, 4H), 4.28 (t, J = 6.3 Hz, 4H), 3.65 (s, 4H), 3.63 (t, J = 6.3 Hz, 4H) ppm; ^{13}C NMR (125 MHz, $CDCl_3$) δ 206.1, 157.2, 130.6, 126.9, 115.0, 67.9, 48.1, 29.1 ppm; IR (ATR) 2941, 1980, 1772, 1720, 1648, 1515, 1163, 1040, 761 cm^{-1}; HRMS (Cl+) Exact mass cald. for $C_{19}H_{20}Br_2O_3$ $[M+]^+$: 455.9760, found: 455.9759.

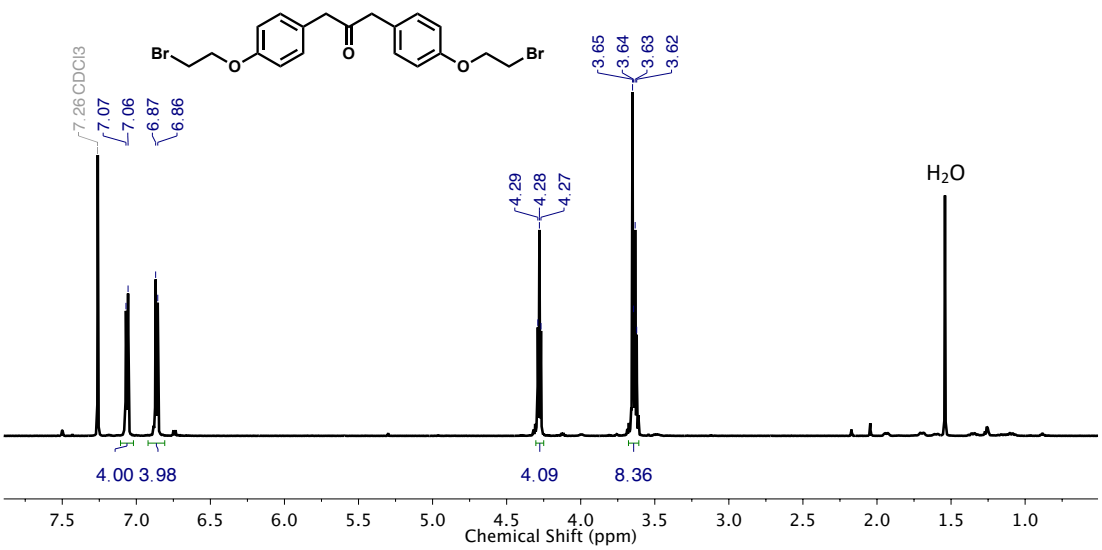

Figure S 4.11. ^{1}H NMR (600 MHz, $CDCl_3$) **Compound K1c**

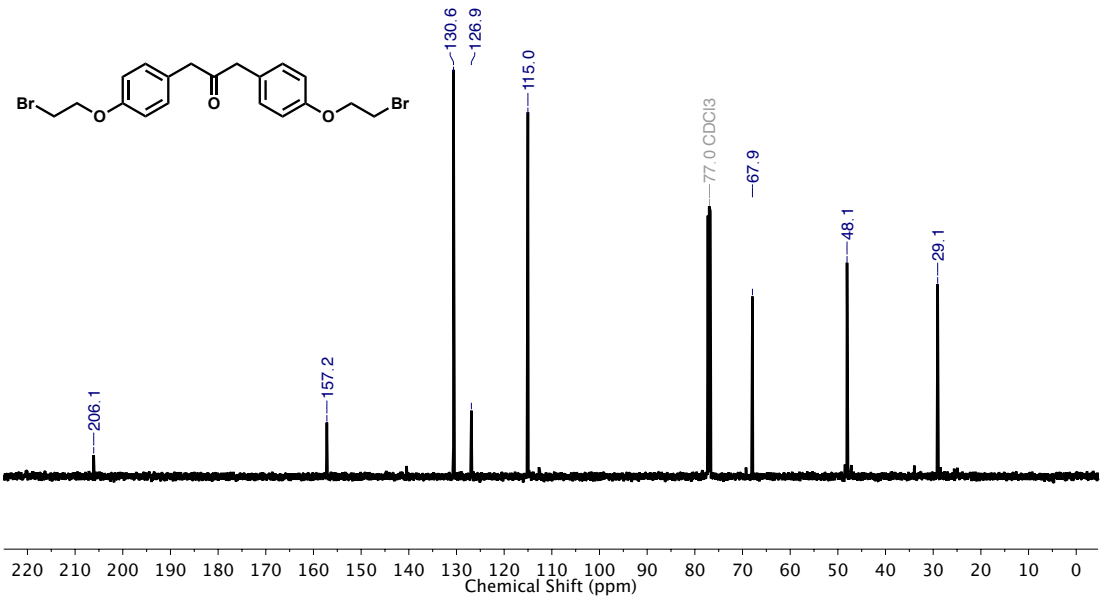

Figure S 4.12. ^{13}C NMR (125 MHz, $CDCl_3$) **Compound K1c**

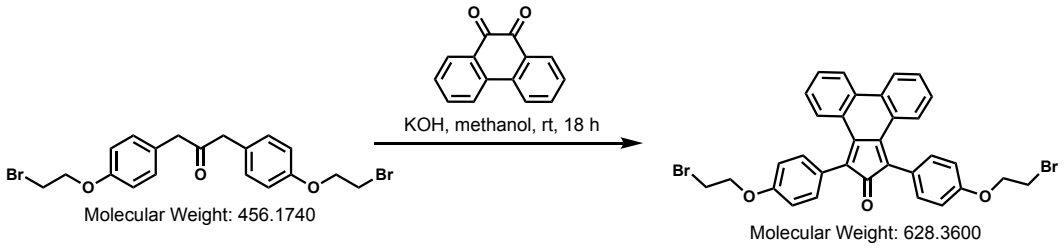

1,3-bis(4-(2-bromoethoxy)phenyl)-*2H*-cyclopenta[*l*]phenanthren-2-one (Compound K3d):

To a 100 mL round bottom flask was added **Compound K1c** (2.00 g, 4.38 mmol, 1 eq), 9,10-phenanthrenequinone (0.959 g, 4.60 mmol, 1.05 eq) and methanol (dried over sieves, 44 mL). To this heterogenous solution was then added potassium hydroxide (powder, 0.492 g, 8.77 mmol, 2 eq). The heterogenous solution was allowed to stir for 18 h, at which point complete consumption of **Compound K1c** was observed by ^{1}H NMR of a crude aliquot of the reaction mixture. The solution was filtered and the green solid rinsed with methanol and ethanol to afford Compound **K3d** (2.25 g, 3.58 mmol, 82%) as a green powder.

Compound K3d: ^{1}H NMR (500 MHz, $CDCl_3$) δ 7.79 (d, J = 7.9 Hz, 2H), 7.60 (d, J = 7.9 Hz, 2H), 7.34 (d, J = 8.5 Hz, 4H), 7.27 (t, J = 7.7 Hz, 2H), 7.01–6.95 (m, 6H), 4.35 (t, J = 6.1 Hz, 4H), 3.68 (t, J = 6.2 Hz, 4H) ppm; ^{13}C NMR (125 MHz, $CDCl_3$) δ 200.7, 158.1, 147.7, 133.6, 131.4, 131.2, 128.7, 128.7, 128.2, 125.1, 124.5, 122.3, 114.9, 67.8, 29.1 ppm; IR (ATR) 2932, 1980, 1686, 1629, 1599, 1508, 1241, 1163, 749 cm^{-1}; HRMS (ES+) Exact mass cald. for $C_{33}H_{24}Br_2O_3Na$ $[M+Na]^+$: 648.9990, found: 648.9995.

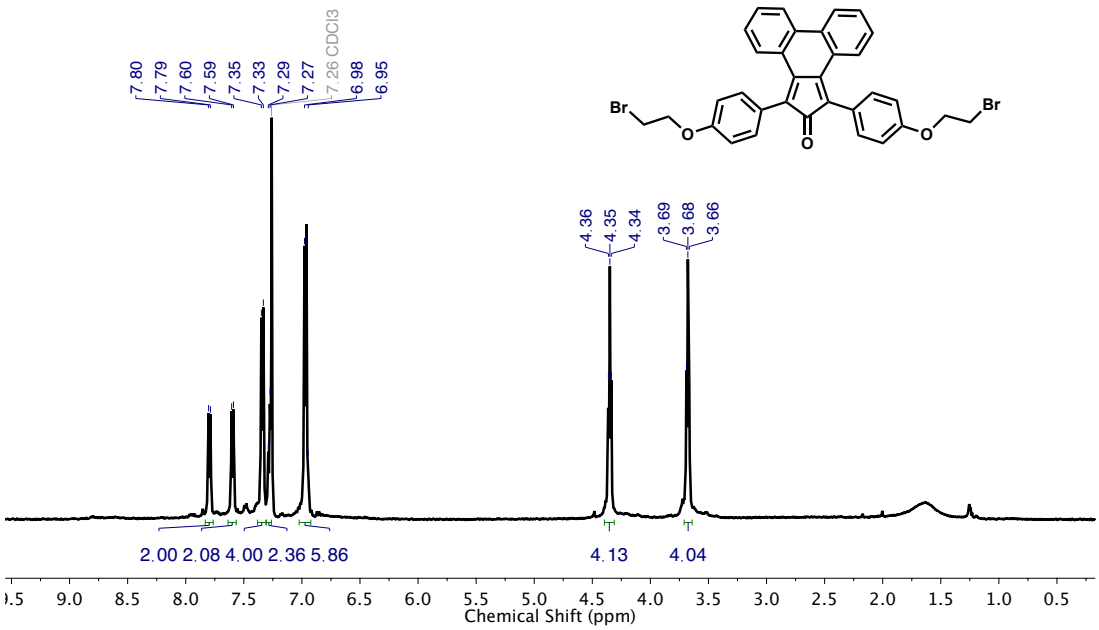

Figure S 4.13. ^{1}H NMR (500 MHz, $CDCl_3$) **Compound K3d**

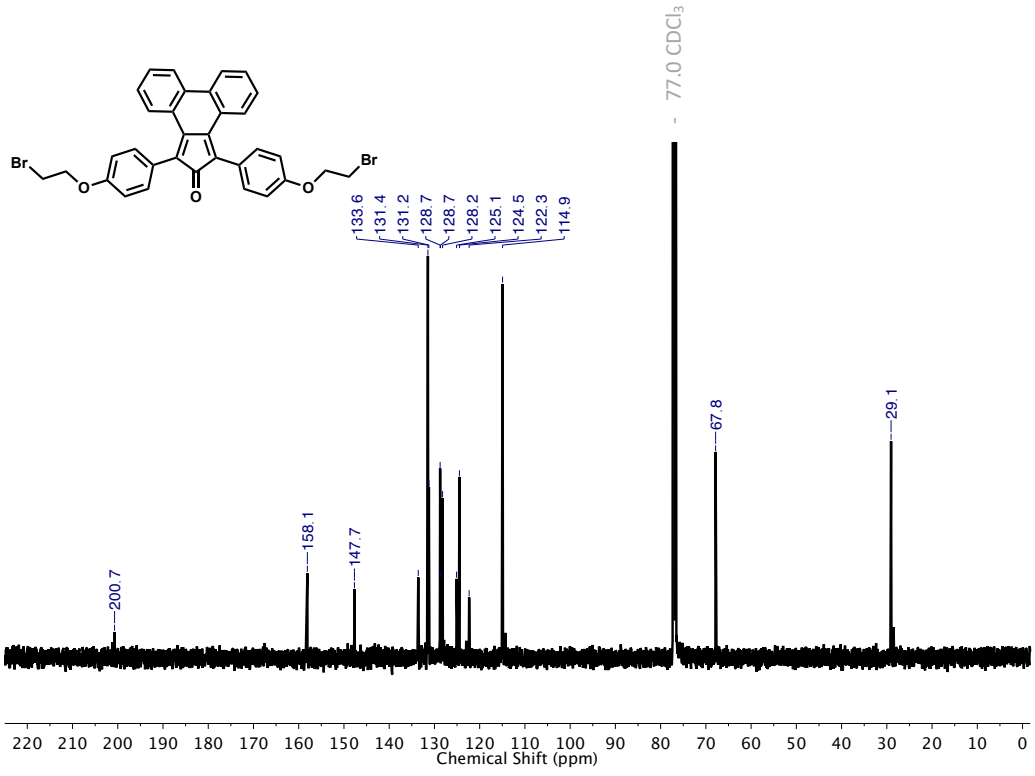

Figure S 4.14. ^{13}C NMR (125 MHz, $CDCl_3$) **Compound K3d**

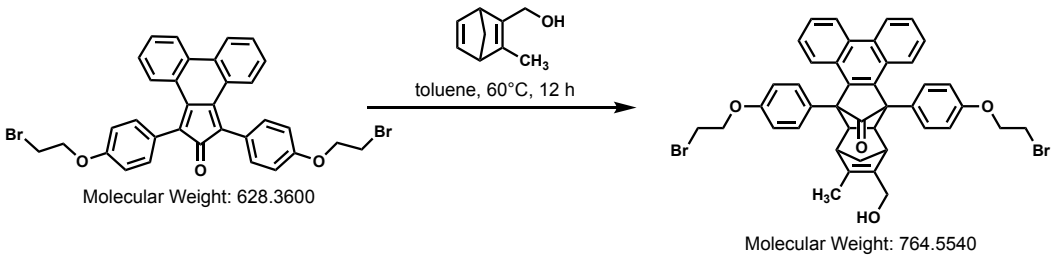

Molecular Weight: 628.3600

Molecular Weight: 764.5540

9,14-bis(4-(2-bromoethoxy)phenyl)-11-(hydroxymethyl)-12-methyl-9,9a,10,13,13a,14-hexahydro-9,14:10,13-dimethanobenzo[*f*]tetraphen-15-one (Compound F5):

To a 25 mL round bottom flask was added **Compound K3d** (2.25 g, 3.58 mmol, 1 eq), **Compound N1b** (0.536 g, 3.94 mmol, 1.1 eq) and toluene (8 mL). This heterogenous solution was allowed to stir vigorously at 60 °C for 12 h. The heterogenous solution was allowed to cool to room temperature before transferring to a centrifuge tube with an additional 2 mL toluene. After centrifugation, the supernatant was removed, and the pellet dissolved in minimal DCM before precipitating into 10 mL hexane. Centrifugation and isolation of the solid pellet afforded **Compound F5** (1.88 g, 2.46 mmol, 69%) as a light yellow powder.

Compound F5: ^{1}H NMR (600 MHz, $CDCl_3$) δ 8.71 (dd, *J* = 8.3, 3.0 Hz, 2H), 7.82 (dd, *J* = 8.5, 2.2 Hz, 1H), 7.71 (dd, *J* = 8.5, 2.2 Hz, 1H), 7.53 (t, *J* = 7.6 Hz, 2H), 7.24 (t, *J* = 7.7 Hz, 2H), 7.20–7.12 (m, 6H), 6.96 (ddd, *J* = 8.6, 6.9, 2.8 Hz, 2H), 4.42–4.28 (m, 6H), 3.71 (td, *J* = 6.3, 2.2 Hz, 4H), 3.10 (s, 1H), 3.07 (d, *J* = 8.3 Hz, 1H), 2.95 (d, *J* = 8.5 Hz, 1H), 2.79 (s, 1H), 1.87 (s, 3H), 0.43 (d, *J* = 9.6 Hz, 1H), -0.52 (d, *J* = 9.6 Hz, 1H) ppm; ^{13}C NMR (125 MHz, $CDCl_3$) δ 199.6, 157.6, 157.6, 145.5, 144.8, 134.9, 134.6, 132.7, 132.5, 130.9, 130.8, 130.2, 130.1, 129.1, 128.6, 128.0, 126.4, 126.3, 126.2, 125.3, 125.2, 123.4, 123.2, 115.5, 115.4, 115.1, 68.0, 68.0, 62.9, 62.6, 57.9, 50.6, 46.7, 46.4, 45.2, 39.4, 29.2, 12.6 ppm; IR (ATR) 3580, 3355,

2959, 1771, 1611, 1511, 1236, 1174, 1005, 757cm^{-1}; HRMS (ES+) Exact mass cald. for $C_{42}H_{36}Br_2O_4Na$ $[M+Na]^+$: 785.0878, found: 785.0899.

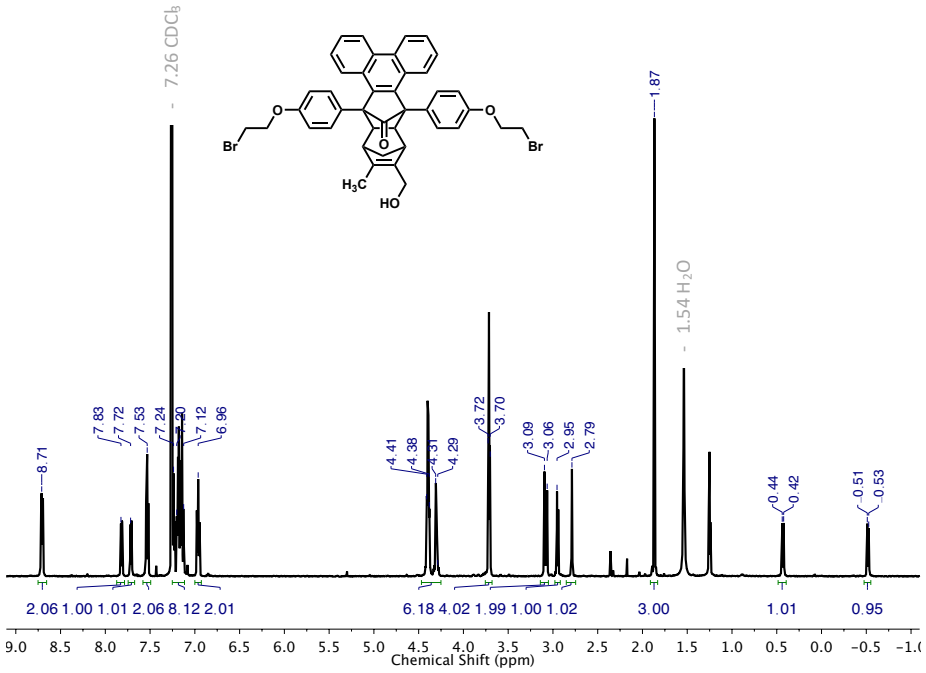

Figure S 4.15. ^{1}H NMR (600 MHz, $CDCl_3$) **Compound F5**

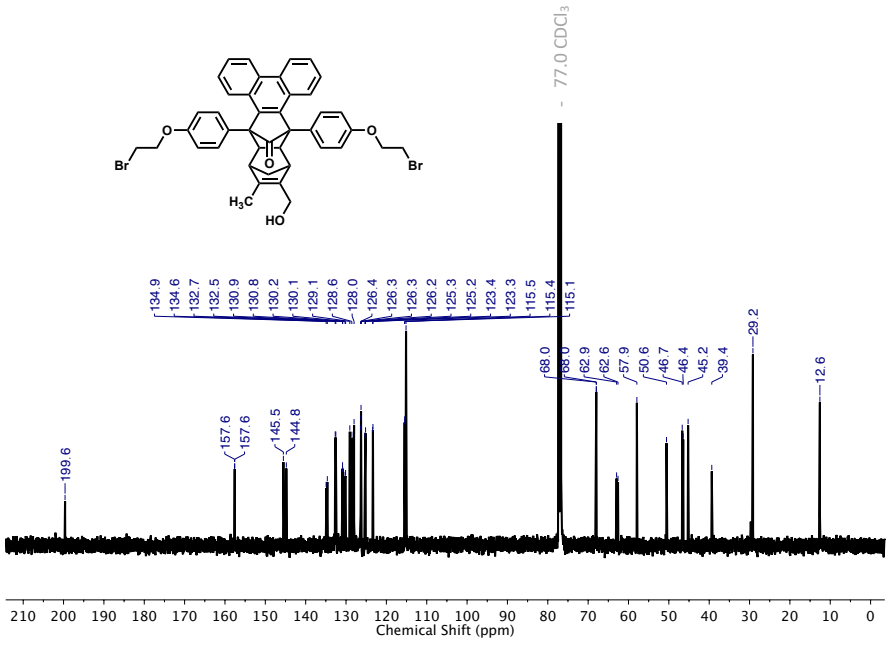

Figure S 4.16. ^{13}C NMR (125 MHz, $CDCl_3$) **Compound F5**

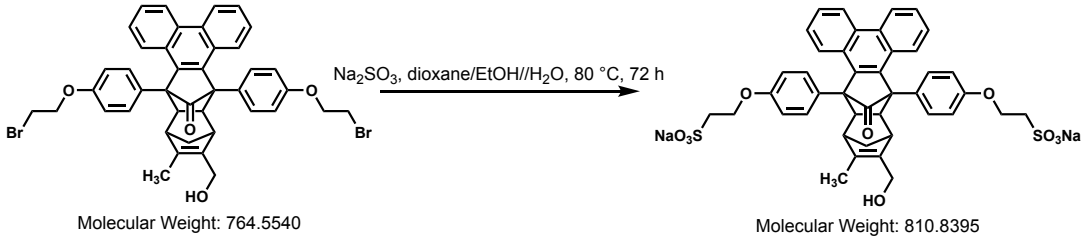

Sodium 2,2'-(((11-(hydroxymethyl)-12-methyl-15-oxo-9a,10,13,13a-tetrahydro-9,14:10,13-dimethanobenzo[*f*]tetraphene-9,14-diyl)bis(4,1-phenylene))bis(oxy))bis(ethane-1-sulfonate) (Compound FS1):

To a 1 L round bottom flask **Compound F5** (1.88 g, 2.46 mmol, 1 eq) was dissolved in dioxane (120 mL). To this solution was added ethanol (120 mL) followed by slow addition of deionized water (90 mL) to avoid precipitation of **Compound F5**. Sodium sulfite (6.20 g, 49.2 mmol, 20 eq) was then added before fitting the flask with a reflux condenser and the heterogenous solution was heated to 80 °C while stirring vigorously. Three additional portions of deionized water (30 mL) were added at 18 h, 42 h and 66 h, and complete consumption of alkyl bromide was confirmed by ^{1}H NMR of a crude reaction aliquot at 72 h before the reaction was cooled to room temperature and the reaction filtered. The solvents were removed under reduced pressure and the residue was triturated in dry methanol before filtering through celite to remove residual salts. Concentration of the filtrate afforded **Compound FS1** (1.98 g, 2.44 mmol, 99%) as a light yellow powder.

Compound FS1: ^{1}H NMR (600 MHz, Methanol-D$_4$) δ 8.78 (d, *J* = 8.4 Hz, 2H), 7.92 (dd, *J* = 8.6, 2.0 Hz, 1H), 7.80 (dd, *J* = 8.5, 2.0 Hz, 1H), 7.53 (t, *J* = 7.3 Hz, 2H), 7.27 (ddd, *J* = 17.0, 8.5, 2.7 Hz, 2H), 7.25–7.17 (m, 4H), 7.09 (ddd, *J* = 7.6, 5.2, 2.2 Hz, 2H), 7.01 (ddd, *J* = 8.4, 5.5, 2.7 Hz, 2H), 4.52–4.45 (m, 4H), 4.27 (d, *J* = 13.0 Hz, 1H), 4.20 (d, *J* = 12.9 Hz, 1H), 3.36 (t, *J* = 7.9 Hz, 4H), 3.12 (d, *J* = 8.4 Hz, 1H), 3.03 (s, 1H), 2.97 (d, *J* = 8.4 Hz, 1H), 2.76 (s,

1H), 1.88 (s, 3H), 0.38 (d, J = 9.3 Hz, 1H), -0.54 (d, J = 9.4 Hz, 1H) ppm; ^{13}C NMR (125 MHz, DMSO-D6) δ 199.9, 157.7, 157.7, 145.7, 142.5, 134.6, 134.4, 132.3, 132.3, 132.3, 130.3, 129.1, 129.1, 129.1, 129.1, 128.6, 128.6, 127.6, 126.5, 126.5, 124.5, 124.5, 123.9, 123.9, 115.2, 115.1, 114.7, 114.5, 64.5, 64.5, 62.5, 62.2, 55.8, 50.5, 50.5, 49.9, 48.6, 46.1, 45.8, 44.6, 12.2 ppm; IR (ATR) 3355, 2951, 1979, 1771, 1648, 1611, 1511, 1390, 1340, 1300, 1208, 1163, 1040, 757 cm^{-1}; HRMS (ES+) Exact mass cald. for $C_{42}H_{36}Na_3O_{10}S_2$ $[M+Na]^+$: 833.1443, found: 833.1422.

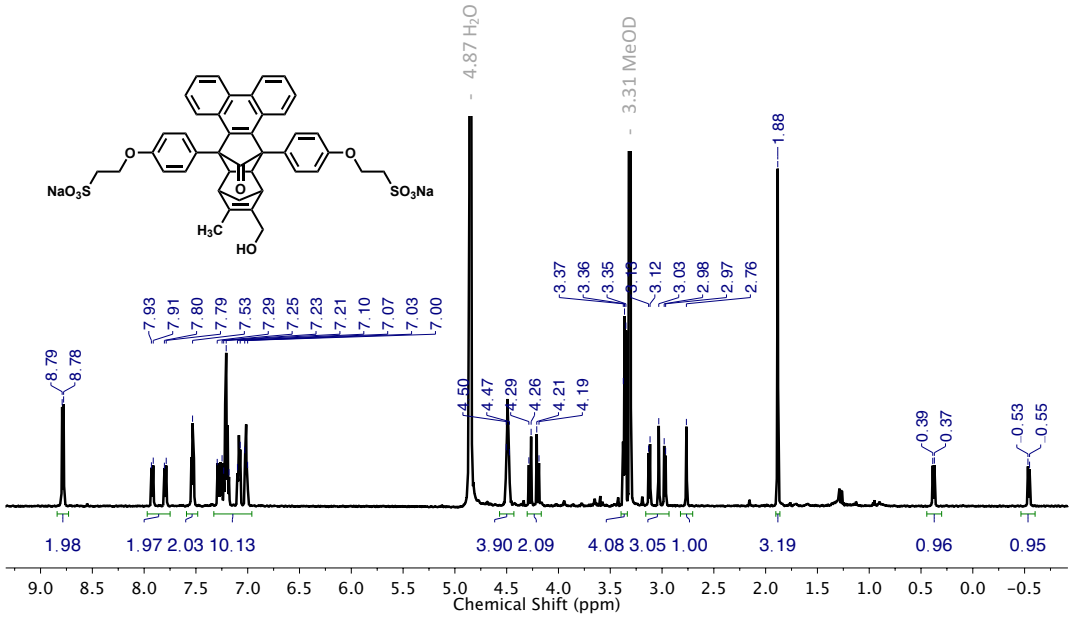

Figure S 4.17. ^{1}H NMR (600 MHz, Methanol-D$_4$) **Compound FS1**

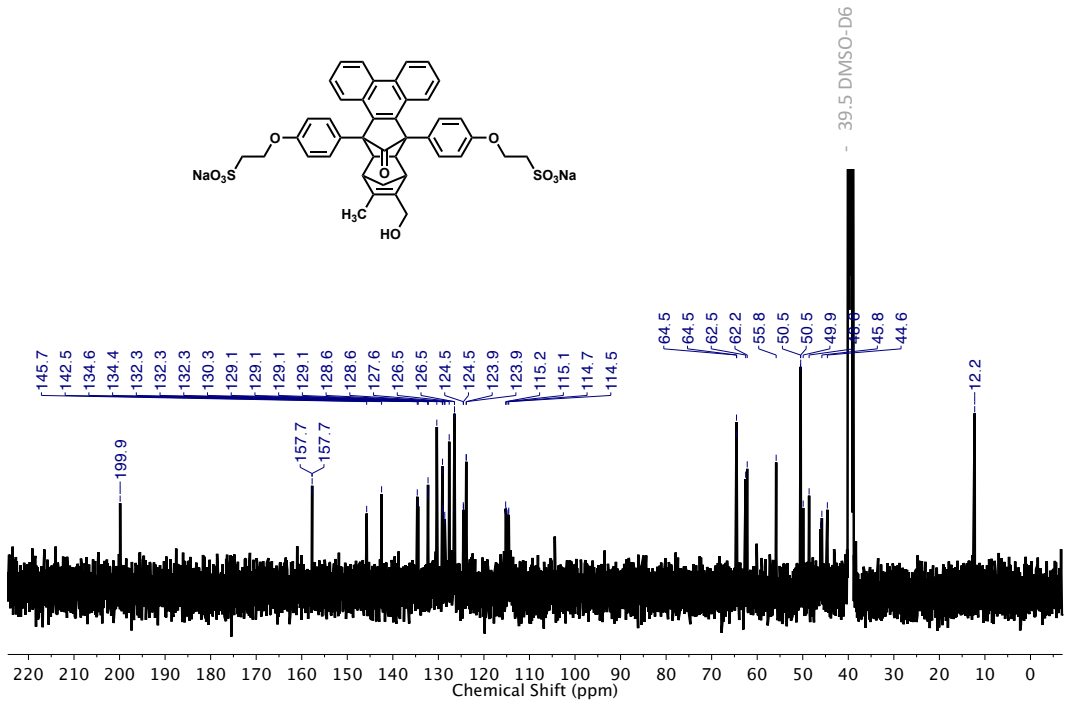

Figure S 4.18. ^{13}C NMR (125 MHz, DMSO-D_6) **Compound FS1**

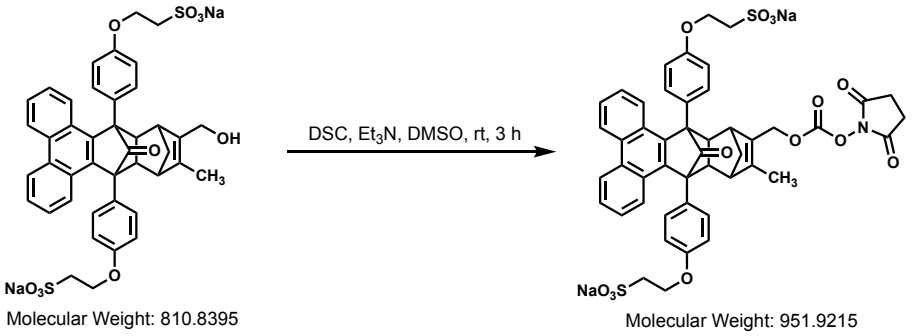

Sodium 2,2'-(((11-(((((2,5-dioxopyrrolidin-1-yl)oxy)carbonyl)oxy)methyl)-12-methyl-15-oxo-9a,10,13,13a-tetrahydro-9,14:10,13-dimethanobenzo[*f*]tetraphene-9,14-diyl)bis(4,1-phenylene))bis(oxy))bis(ethane-1-sulfonate) (Compound FS2):

To a 25 mL round bottom flask, **Compound FS1** (1.62 g, 2.00 mmol, 1 eq) was dissolved in anhydrous dimethyl sulfoxide (DMSO, 6 mL). To this solution was added triethylamine (1.12

mL, 8.00 mmol, 4 eq) followed by *N,N*-Disuccinimidyl carbonate (DSC, 2.05 g, 8.00 mmol, 4 eq). The solution was allowed to stir for 3 h, at which point complete consumption of **Compound FS1** was observed by ^{1}H NMR of a crude aliquot of the reaction mixture. The reaction solution was precipitated directly into ethyl acetate (150 mL) and filtered. The solid was re-dissolved in minimal methanol before repeating precipitation once more in ethyl acetate to afford **Compound FS2** (1.47 g, 1.54 mmol, 77%) as a light yellow powder.

Compound FS2: ^{1}H NMR (600 MHz, Methanol-D4) δ 8.79 (d, *J* = 8.4 Hz, 2H), 8.12 (dd, *J* = 8.5, 2.2 Hz, 1H), 7.78 (dd, *J* = 8.6, 2.2 Hz, 1H), 7.60–7.50 (m, 2H), 7.29 (dt, *J* = 8.5, 2.2 Hz, 2H), 7.27–7.16 (m, 4H), 7.08 (ddd, *J* = 8.5, 5.3, 2.3 Hz, 2H), 7.01 (ddd, *J* = 8.6, 6.9, 2.7 Hz, 2H), 4.80–4.73 (m, 2H), 4.55–4.46 (m, 4H), 3.36 (t, *J* = 6.5 Hz, 4H), 3.23 (s, 1H), 3.14 (d, *J* = 8.4 Hz, 1H), 2.96 (d, *J* = 8.5 Hz, 1H), 2.83 (s, 1H), 2.74–2.68 (m, 4H), 1.95 (s, 3H), 0.38 (d, *J* = 9.5 Hz, 1H), -0.50 (d, *J* = 9.7 Hz, 1H) ppm; ^{13}C NMR (125 MHz, DMSO-D6) δ 200.0, 175.2, 172.7, 158.0, 158.0, 151.7, 138.9, 134.8, 134.6, 132.5, 132.5, 132.4, 130.6, 130.6, 129.8, 129.2, 129.2, 129.0, 127.8, 127.8, 127.0, 126.9, 126.9, 126.9, 126.8, 124.8, 124.2, 115.6, 115.5, 114.9, 114.7, 71.00, 64.6, 62.6, 62.4, 50.8, 50.7, 50.2, 46.7, 46.0, 44.3, 40.4, 25.7, 25.3, 12.6 ppm; IR (ATR) 2989, 2941, 1980, 1764, 1713, 1633, 1514, 1427, 1295, 1166, 1041, 760 cm^{-1}; HRMS (ES+) Exact mass cald. for $C_{47}H_{41}NNaO_{14}S_2$ $[M\text{-}Na+2H]^+$: 930.1866, found: 930.1854.

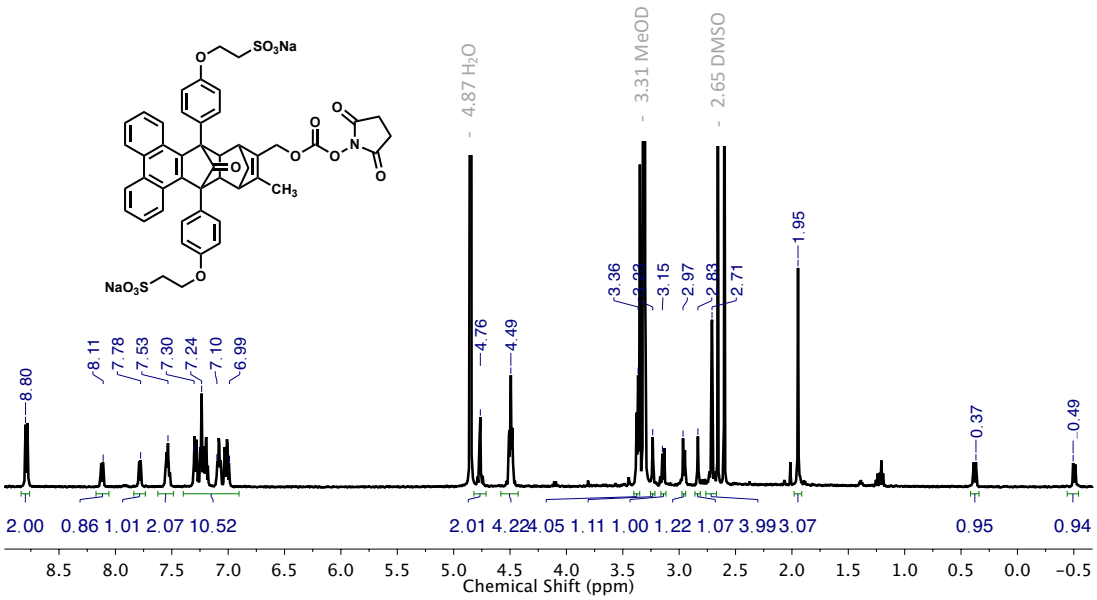

Figure S 4.19. H NMR (500 MHz, Methanol-D_4) **Compound FS2**

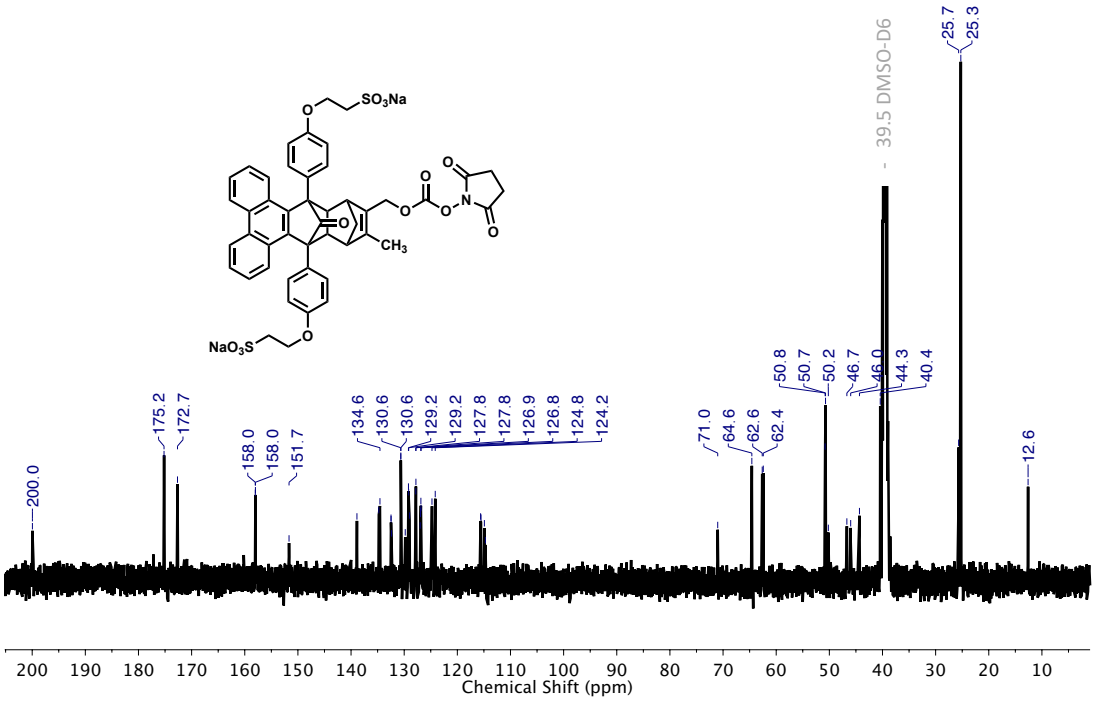

Figure S 4.20. ^{13}C NMR (125 MHz, DMSO-D_6) **Compound FS2**

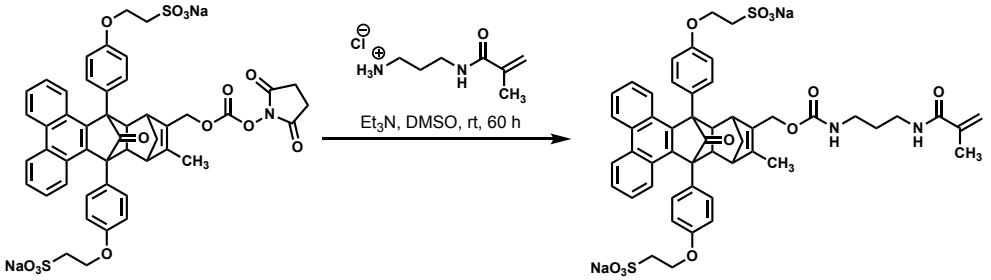

Sodium 2,2'-(((11-((((3-methacrylamidopropyl)carbamoyl)oxy)methyl)-12-methyl-15-oxo-9a,10,13,13a-tetrahydro-9,14:10,13-dimethanobenzo[*f*]tetraphene-9,14-diyl)bis(4,1-phenylene))bis(oxy))bis(ethane-1-sulfonate) (Compound FS3):

To a 25 mL round bottom flask, *N*-(3-Aminopropyl)methacrylamide hydrochloride (0.930 g, 5.20 mmol, 4 eq) was dissolved in DMSO (6.5 mL). To this solution was added triethylamine (1.09 mL, 7.80 mmol, 6 eq) followed by **Compound FS2** (1.24 g, 1.30 mmol, 1 eq). The solution was allowed to stir for 60 h, at which quantitative transformation of **Compound FS2** to **Compound FS3** was observed by ^{1}H NMR of a crude aliquot of the reaction mixture. The reaction solution was precipitated directly into ethyl acetate (100 mL) and filtered. The pellet was dissolved in minimal methanol before repeating precipitation one more in ethyl acetate (100 mL), followed by a third precipitation into isopropyl alcohol (50 mL) to afford **Compound FS3** (0.634 g, 0.648 mmol, 50%) as a white powder.

Compound FS3: ^{1}H NMR (600 MHz, Methanol-D$_4$) δ 8.78 (d, *J* = 8.3 Hz, 2H), 8.00 (d, *J* = 9.3 Hz, 1H), 7.78 (d, *J* = 9.4 Hz, 1H), 7.58–7.48 (m, 2H), 7.32–7.16 (m, 6H), 7.12–6.97 (m, 4H), 5.69 (s, 1H), 5.33 (s, 1H), 4.58–4.45 (m, 6H), 3.37 (t, *J* = 7.0 Hz, 4H), 3.24 (t, *J* = 6.7 Hz, 2H), 3.21–3.09 (m, 4H), 2.96 (d, *J* = 8.2 Hz, 1H), 2.79 (s, 1H), 1.91 (s, 6H), 1.67 (p, *J* = 6.5 Hz, 2H), 0.39 (d, *J* = 9.2 Hz, 1H), -0.54 (d, *J* = 9.0 Hz, 1H) ppm; ^{13}C NMR (125 MHz, DMSO-D6) δ 199.6, 171.1, 167.3, 157.8, 157.7, 148.6, 140.3, 140.0, 140.0, 134.6, 134.4, 132.3, 132.3,

132.1, 130.3, 129.0, 128.7, 128.6, 127.6, 126.6, 126.6, 126.6, 126.5, 126.5, 124.6, 124.5, 123.9, 118.9, 118.9, 115.4, 115.3, 114.6, 114.6, 64.6, 64.5, 62.4, 62.2, 50.5, 50.4, 36.4, 36.3, 36.2, 29.2, 29.1, 27.8, 24.5, 18.6, 18.6, 12.4, 7.7 ppm; IR (ATR) 3085, 2950, 1980, 1771, 1651, 1611, 1537, 1513, 1436, 1212, 1168, 1040, 757 cm^{-1}; HRMS (ES-) Exact mass cald. for $C_{50}H_{49}N_2O_{14}S_2$ $[M-2Na+H]^-$: 933.2727, found: 933.2602.

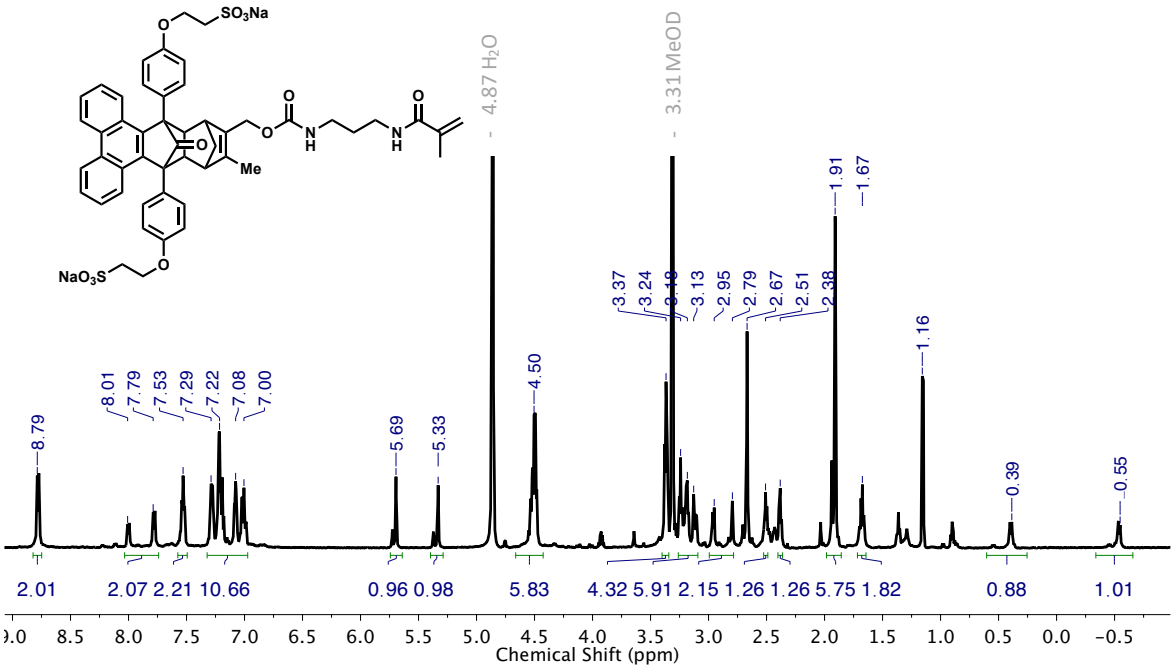

Figure S 4.21. ^1H NMR (600 MHz, $CDCl_3$) **Compound FS3**

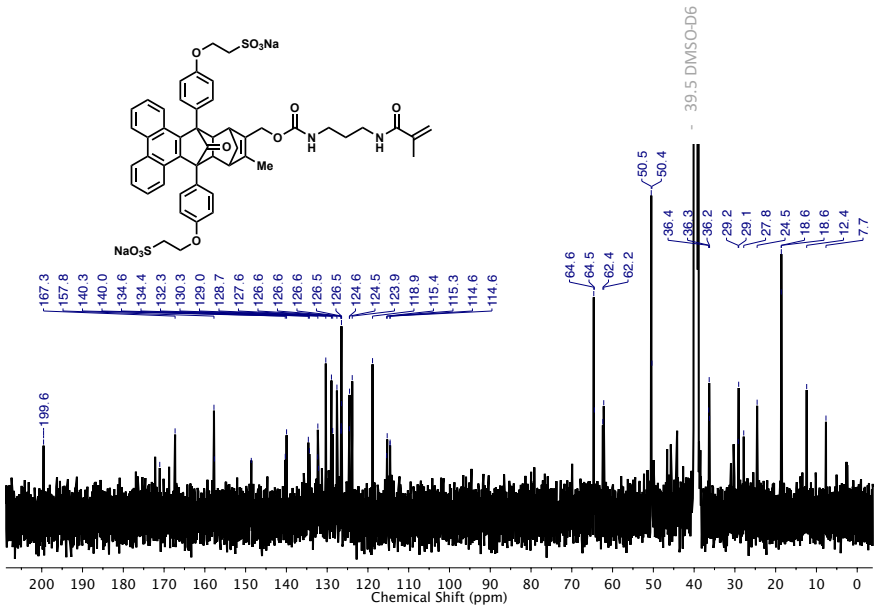

Figure S 4.22. ^{13}C NMR (125 MHz, DMSO-D6) **Compound FS3**

Synthesis of PEGDA

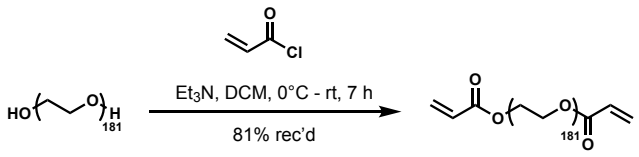

Poly(ethylene glycol) diacrylate (PEGDA):

In a 25 mL round bottomed flask, poly(ethylene glycol) (purchased from Sigma Aldrich, M_n = 8,000 g/mol, 4.0 g, 0.50 mmol, 1.0 eq) was dissolved in anhydrous DCM (5 mL) and cooled to 0 °C under inert atmosphere. To this solution was added triethylamine (0.42 mL, 3.0 mmol, 6.0 eq) followed by acryloyl chloride (0.24 mL, 3.0 mmol, 6.0 eq). The solution was allowed to stir and warm to rt over 7 h (at which complete formation of the ester was confirmed by ^{1}H NMR of an aliquot of the crude reaction solution). After completion of the reaction the solution was transferred directly into 50 mL ethanol, cooled to 0 °C and left unagitated for 30 minutes to allow precipitation. The white solid was filtered and rinsed with cold EtOH and diethyl ether. The collected solid was dissolved in minimal DCM and the precipitation was repeated once more in 50 mL diethyl ether. Filtration and removal of residual solvent under reduced pressure afforded **PEGDA** (3.25 g, 0.40 mmol, 81% recovered yield).

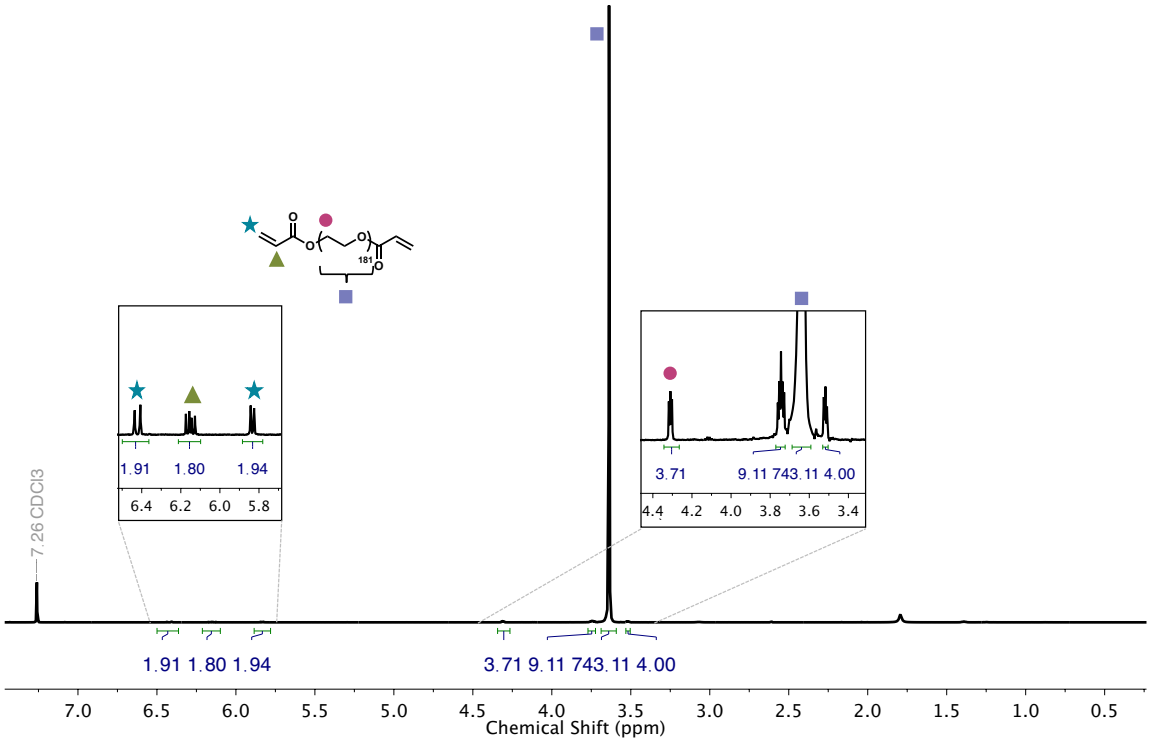

Figure S 4.23. ^{1}H NMR (600 MHz, $CDCl_3$) **PEGDA**

2D PEGDA Hydrogels

Hydrogel Preparation

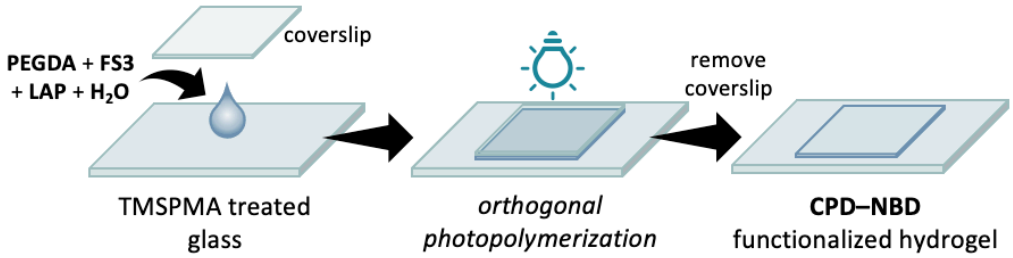

Figure S 4.24. Depiction of hydrogel preparation.

Glass slides (25 x 75 x 1 mm) were functionalized with 3-(trimethoxysilyl)propyl methacrylate (TMSPMA) by coating them in a solution of 5 vol% TMSPMA in ethanol and incubating at room temperature for 2–3 h. The slides were then rinsed with ethanol, followed by DI water and allowed to air dry before use. Glass coverslips (22 x 22 x 0.2 mm) were treated with RainX water repellent to aid in their removal after photopolymerization.

In a dram vial, **FS3** (10 mg, 1 wt%, 10 mM) and **PEGDA** (150 mg, 15 wt%) were dissolved in DI water (820 uL). Once ready to use, lithium phenyl-2,4,6-trimethylbenzoylphosphinate (LAP) photoinitator was added (20 mL of freshly prepared 5 wt% stock solution in DI water, 0.1 wt%). The pre-hydrogel solution was thoroughly mixed via pipette tip before a 100 mL aliquot was transferred to a TMSPMA glass slide. Using the tip of a glass pipette, 300 µm glass spacer particles (approximately 20–50 particles per sample) were added to the droplet before a RainX-treated coverslip was placed on top to ensure even gel thickness. Photopolymerization was completed by irradiating the sample through the coverslip side with a Thorlabs LED (405 nm, 26.0 mW/cm^2, 10 min). After irradiation, the coverslip was removed from the top of the hydrogel, **H1a**, and the glass slide was placed in a petri dish containing DI water overnight

allowing the hydrogel to swell to equilibrium and any residual monomers and photoinitiator to be removed before patterning experiments.

Hydrogel Patterning

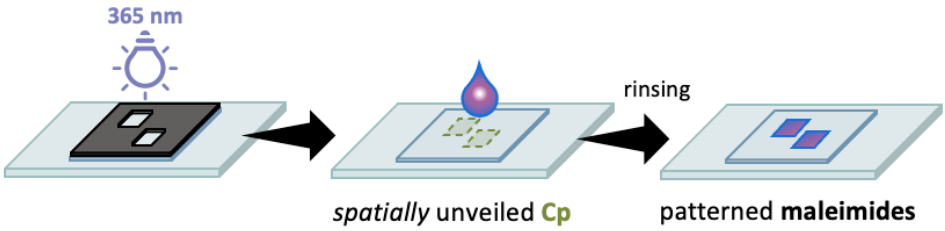

Figure S 4.25. Depiction of hydrogel patterning.

Hydrogels are irradiated through quartz photomasks with rectangles/squares ranging in size from 0.5 mm to 3 mm with a Thorlabs LED (365 nm, 6 mW/cm^2). Top-down irradiation was required with only a coverslip (0.2 mm) and the quartz photomask between the light source and hydrogel. Bottom-up irradiation through the glass slide resulted in significant light absorption/scattering and poor patterning results. After irradiation H1b hydrogels are immediately covered in 10 mM aqueous solutions (approximately 200 µL) of mal-Cy3 or mal-Cy5 and incubated at room temperature for 3 h before rinsing thoroughly. To removed residual non-conjugated dyes, the hydrogels were placed in a 2 L beaker containing stirred DI water for 18 h.

Quantification of patterning with Cyanine Dyes

To quantify the dye pattern efficiency of hydrogels after varied irradiation times (30 s – 10 min) the color differences between background and patterned regions were evaluated. Δ*E** values were determined following International Commission on Illumination guidelines as previously reported.[50–53] The software GNU Image Manipulation Platform (GIMP) was used to quantify chromic values L* (lightness), a* (red/green), and b* (yellow/blue) of an image of **H1a** hydrogel after varied masked irradiation times and treatment with **mal-Cy5**, and Δ*E** was determined within each box as:

$$\Delta E^* = [(L_{t=x} - L_{t=0})^2 + (a_{t=x} - a_{t=0})^2 + (b_{t=x} - b_{t=0})^2]^{1/2}$$

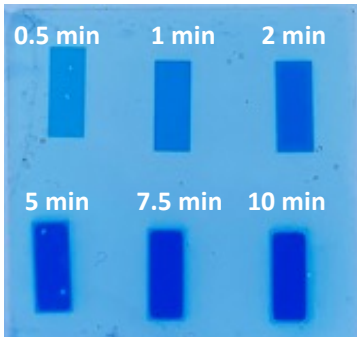

Figure S 4.26. Photograph of hydrogel analyzed by GIMP

Table S 4.1. Table of L*, a* and b* and ΔE* values determined from **Figure S4.26.**

Irradiation Time, t (min)	L*	a*	b*	ΔE*
0	141	120	101	0
0.5	118	118	86	27.5317998
1	107	125	79	40.8044115
2	91	136	71	60.4648658
5	72	151	60	86.040688
7.5	67	157	57	93.7069901
10	67	156	57	93.3166652

3D printed PEGDA Hydrogels

Digital light processing 3D printing was conducted on a Mono3Z2 Panchromatic Printer with a 405 nm light source. Fusion 360 software was used to design the desired octahedron prints as STL files which were sliced with MonoWare software and saved with desired print parameters before uploading to the Mono3Z2 printer. To prepare photo-patternable 3D printed parts, PEGDA Start Photoink™ was purchased from Cellink and mixed with **FS3** (1 wt%). Once **FS3** fully dissolved in the resin, 4 mL was transferred into the vat of the Mono3Z2 printer. All prints were conducted with a layer thickness of 50 μm, irradiance of 15 mW/cm2, and irradiation time of each layer of 2.2 s (the first two base layers were irradiated for 30 s to promote adhesion to the build stage). Printed parts were allowed to incubate overnight in DI water to remove any residual monomers, dye and photoinitiator before photopatterning. Photopatterning of printed parts was conducted similarly to 2D hydrogels. To prevent light scattering in 3D geometries printed parts were first incubated in a 100 μm aqueous solution of methyl orange before parts were irradiated for 5 minutes (365 nm, 6.1 mW/cm^2). After irradiation, gels were incubated in maleimide dyes and thoroughly rinsed as described for 2D hydrogels.

Computational Investigation of Thermal CPD–NBD Decarbonylation

DFT calculations were performed following previously established methods using Gaussian16 at the B3LYP/6-31+G(d,p) level of theory in the gas phase.[66,67] The optimized geometries and frequencies were calculated for "A" and the decarbonylated product "B" for each for each CPD–NBD derivative. The ΔG of decarbonylation was determined by subtracting the free energy of "A" from the sum of the energies of "B" and carbon monoxide. Transition states of **O1** and **F1** were found by conducting redundant coordinate scans, breaking the bond between the bridge CO system and the adduct. The highest energy geometry from those scans were further optimized using Berny transition state optimization.

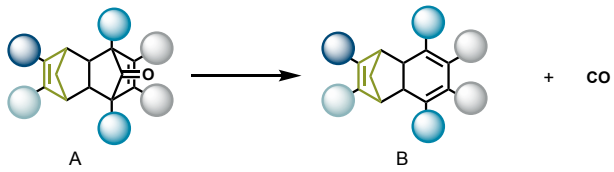

Thus, ΔG for each derivative was determined as:

$$\Delta G = (G_B + G_{CO}) - G_A$$

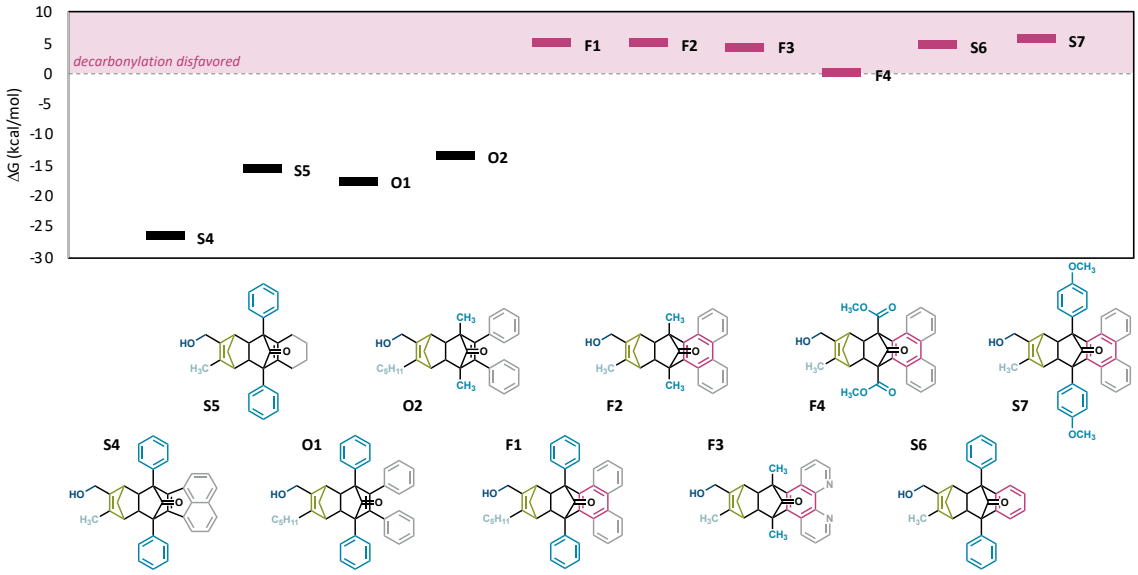

Figure S 4.27. Plot of ΔG values for a series of CPD–NBD structures

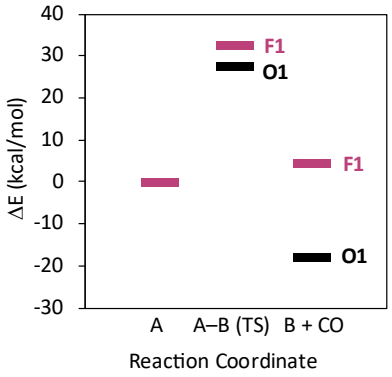

Figure S 4.28. Comparison of transition states of **O1** to **F1** indicates in addition to destabilization of the decarbonylated product, the activation barrier from the fused system **F1** is also higher.

The cartesian coordinates for the optimized ground state and transition state geometries are listed below:

CO equilibrium geometry

O	0.0000000000	0.0000000000	0.4873960000
C	0.0000000000	0.0000000000	-0.6498620000

Electronic energy = -113.312304 Hartree
Electronic energy + thermal free energy correction = -113.331441 Hartree

O1 equilibrium geometry (A)

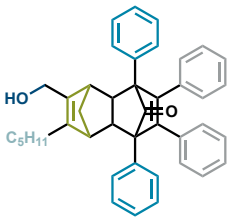

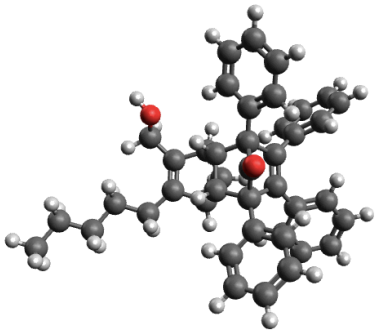

O	-2.5474950000	-3.7325470000	0.0558020000
O	0.9537690000	0.1058640000	-3.0543320000
C	-3.0251930000	-2.9685300000	1.1818890000
C	-9.2846080000	-0.0298630000	0.2009900000
C	-7.9894420000	-0.8160030000	0.4346700000
C	-6.7449800000	0.0777090000	0.5184810000
C	-5.4436330000	-0.7031890000	0.7506240000
C	-4.2203350000	0.2179670000	0.8372480000
C	-0.3899070000	5.0199340000	-2.7529020000
C	0.8683440000	4.4112900000	-2.7887960000
C	-1.4413470000	4.3771510000	-2.0985930000
C	1.0684020000	3.1765030000	-2.1735430000
C	-1.2363000000	3.1371200000	-1.4850940000
C	0.0213070000	2.5181550000	-1.5073190000
C	2.9039820000	4.3645670000	2.4631410000

C	3.8115810000	3.4706490000	1.8889530000
C	1.5359520000	4.1836160000	2.2459380000
C	3.3573040000	2.4033810000	1.1135930000
C	1.0824010000	3.1195650000	1.4659820000
C	1.9818090000	2.2000250000	0.8930070000
C	5.1377450000	-1.9851020000	2.3807270000
C	5.3754190000	-1.4711130000	1.1034460000
C	3.8497890000	-1.9222600000	2.9161060000
C	4.3336900000	-0.8974550000	0.3725270000
C	2.8077710000	-1.3507180000	2.1813350000
C	3.0335430000	-0.8211500000	0.9005450000
C	2.7076360000	-4.7471390000	-2.3968440000
C	1.6160090000	-4.7929130000	-1.5284310000
C	3.2417430000	-3.5077630000	-2.7600260000
C	1.0648520000	-3.6117850000	-1.0223370000
C	2.6934900000	-2.3307270000	-2.2501130000
C	1.6008350000	-2.3621900000	-1.3673350000
C	0.7950040000	0.0704510000	-1.8642110000
C	1.4792250000	1.0618030000	0.0918690000
C	1.9221040000	-0.2276120000	0.1026970000
C	0.2783440000	1.1691960000	-0.8764340000
C	1.0288490000	-1.0720580000	-0.8282190000
C	-0.9726020000	0.3491150000	-0.3824250000
C	-0.4523850000	-1.1315140000	-0.2903710000
C	-0.6940750000	-0.1948750000	1.9750840000
C	-2.8510190000	-0.3736840000	1.0330390000
C	-1.6337750000	0.5698010000	1.0223320000
C	-0.8283570000	-1.5197920000	1.1890020000
C	-2.3608050000	-1.6288450000	1.1545260000
H	-2.8829860000	-4.6355160000	0.1285120000
H	-4.1142310000	-2.8849010000	1.1527360000
H	-2.7484440000	-3.4861590000	2.1149160000
H	-9.4654540000	0.6859970000	1.0116710000
H	-10.1522690000	-0.6960760000	0.1460440000
H	-9.2402780000	0.5366210000	-0.7367280000
H	-8.0784900000	-1.3993290000	1.3617910000
H	-7.8548150000	-1.5472220000	-0.3743670000
H	-6.6572640000	0.6619020000	-0.4091840000
H	-6.8798130000	0.8097060000	1.3283580000
H	-5.5376590000	-1.2839920000	1.6777880000
H	-5.3069850000	-1.4248020000	-0.0650070000
H	-4.1801730000	0.8275990000	-0.0802790000
H	-4.3847370000	0.9494970000	1.6448010000
H	-0.5475660000	5.9823650000	-3.2311050000
H	1.6949380000	4.8974660000	-3.2990660000
H	-2.4251070000	4.8370320000	-2.0630700000

H	2.0503040000	2.7149680000	-2.2125680000
H	-2.0699680000	2.6596470000	-0.9815570000
H	3.2588250000	5.1962260000	3.0649440000
H	4.8790330000	3.6054760000	2.0392290000
H	0.8181960000	4.8750310000	2.6782420000
H	4.0766620000	1.7278660000	0.6675460000
H	0.0177370000	3.0041490000	1.2991590000
H	5.9472340000	-2.4313230000	2.9510560000
H	6.3717430000	-1.5172150000	0.6728900000
H	3.6514190000	-2.3182930000	3.9081200000
H	4.5297410000	-0.5013100000	-0.6190100000
H	1.8135390000	-1.3123360000	2.6124870000
H	3.1335890000	-5.6648710000	-2.7924470000
H	1.1845710000	-5.7489210000	-1.2446570000
H	4.0821470000	-3.4557540000	-3.4466520000
H	0.2026360000	-3.6749650000	-0.3676110000
H	3.1064370000	-1.3761600000	-2.5586130000
H	-1.8616520000	1.6099170000	1.2695690000
H	-0.3110770000	-2.3971980000	1.5830410000
H	-1.7322630000	0.4463250000	-1.1645570000
H	-0.9994530000	-1.7861080000	-0.9715430000
H	-1.1180030000	-0.2787880000	2.9806750000
H	0.3095440000	0.2166130000	2.0441250000

Electronic energy = -1774.347300 Hartree
Electronic energy + thermal free energy correction = -1774.421761 Hartree

Decarbonylated O1 equilibrium geometry (B)

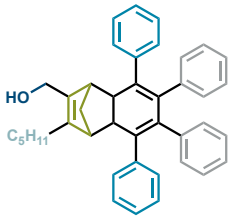

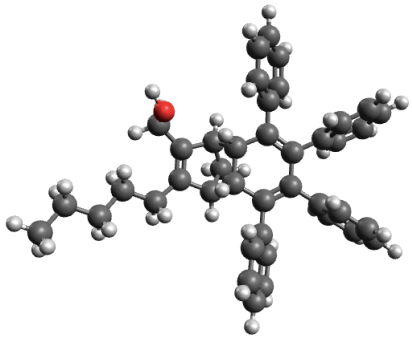

O	3.1854010000	-3.2486980000	0.8712710000
C	3.4450510000	-2.9601930000	-0.5220910000
C	9.2321440000	0.5752790000	0.8396930000
C	8.0524130000	-0.3414420000	0.4959390000

C	6.7800620000	0.4252720000	0.1116820000
C	5.5939490000	-0.4871630000	-0.2309860000
C	4.3422590000	0.3080800000	-0.6228210000
C	1.2549850000	5.4102590000	0.4000270000
C	1.4039940000	4.5119580000	1.4603930000
C	0.6244110000	4.9878920000	-0.7726070000
C	0.9288700000	3.2042130000	1.3442800000
C	0.1439450000	3.6807290000	-0.8831800000
C	0.2810510000	2.7676320000	0.1748090000
C	-4.5497050000	4.0697870000	0.1092160000
C	-4.0884670000	3.5806640000	-1.1157190000
C	-4.0211090000	3.5576350000	1.2965690000
C	-3.1070990000	2.5876190000	-1.1492940000
C	-3.0392570000	2.5646680000	1.2576220000
C	-2.5652580000	2.0673110000	0.0350430000
C	-6.1623590000	-1.2829400000	0.2272930000
C	-5.3616840000	-1.4018580000	1.3657150000
C	-5.5851850000	-0.8773340000	-0.9792510000
C	-3.9954630000	-1.1195980000	1.2955790000
C	-4.2197850000	-0.5924800000	-1.0435650000
C	-3.4024510000	-0.7139550000	0.0904770000
C	-2.0616440000	-5.6158250000	0.3732460000
C	-1.2902950000	-5.0118510000	1.3699580000
C	-2.4978200000	-4.8513650000	-0.7119380000
C	-0.9577900000	-3.6588830000	1.2796140000
C	-2.1727330000	-3.4960330000	-0.7949770000
C	-1.4040930000	-2.8716970000	0.2025710000
C	-1.4998940000	1.0071210000	0.0080820000
C	-1.9296430000	-0.4236730000	0.0327350000
C	-0.1891040000	1.3508070000	0.0710280000
C	-1.0197260000	-1.4295370000	0.1118910000
C	0.9204560000	0.3215660000	0.0829020000
C	0.4735780000	-1.1772630000	0.1183020000
C	1.0332910000	-0.5863540000	-2.1506080000
C	3.0683950000	-0.4265880000	-0.9377330000
C	1.8076760000	0.3819320000	-1.2375060000
C	1.1885570000	-1.7662300000	-1.1735210000
C	2.6903730000	-1.7259050000	-0.9046770000
H	3.4820050000	-4.1490900000	1.0593490000
H	4.5201790000	-2.8424000000	-0.6860090000
H	3.0976690000	-3.8018560000	-1.1389700000
H	9.4956820000	1.2170720000	-0.0094950000
H	10.1230820000	-0.0024470000	1.1089330000
H	8.9915640000	1.2296540000	1.6860390000
H	8.3365080000	-1.0073720000	-0.3309040000
H	7.8352150000	-0.9945570000	1.3524870000

H	6.4973690000	1.0926890000	0.9389650000
H	6.9976980000	1.0790520000	-0.7457850000
H	5.8837920000	-1.1507420000	-1.0565550000
H	5.3694950000	-1.1295160000	0.6298410000
H	4.1105690000	1.0200960000	0.1862300000
H	4.5822790000	0.9477820000	-1.4869830000
H	1.6258430000	6.4274410000	0.4873400000
H	1.8878870000	4.8290470000	2.3801390000
H	0.5045710000	5.6756270000	-1.6051680000
H	1.0446140000	2.5176800000	2.1789880000
H	-0.3432490000	3.3634610000	-1.7992870000
H	-5.3127710000	4.8423440000	0.1377640000
H	-4.4912380000	3.9722480000	-2.0458830000
H	-4.3707580000	3.9312280000	2.2549990000
H	-2.7531370000	2.2144660000	-2.1066670000
H	-2.6306370000	2.1726710000	2.1846820000
H	-7.2248090000	-1.5031670000	0.2790140000
H	-5.7983420000	-1.7169760000	2.3093900000
H	-6.1977290000	-0.7816250000	-1.8716080000
H	-3.3768660000	-1.2201230000	2.1827220000
H	-3.7813920000	-0.2807430000	-1.9872670000
H	-2.3181430000	-6.6692150000	0.4408170000
H	-0.9456520000	-5.5935620000	2.2205990000
H	-3.0935430000	-5.3088070000	-1.4970540000
H	-0.3552490000	-3.2072500000	2.0622870000
H	-2.5181780000	-2.9127740000	-1.6419490000
H	1.9797960000	1.3982660000	-1.5985500000
H	0.7960420000	-2.7379490000	-1.4803150000
H	1.5692050000	0.5483370000	0.9366210000
H	0.8975310000	-1.6842690000	0.9894100000
H	1.5365230000	-0.7591650000	-3.1068490000
H	-0.0060250000	-0.2894990000	-2.3266470000

Electronic energy = -1661.043427 Hartree
Electronic energy + thermal free energy correction = -1661.118560 Hartree

O1 transition state geometry (A–B)

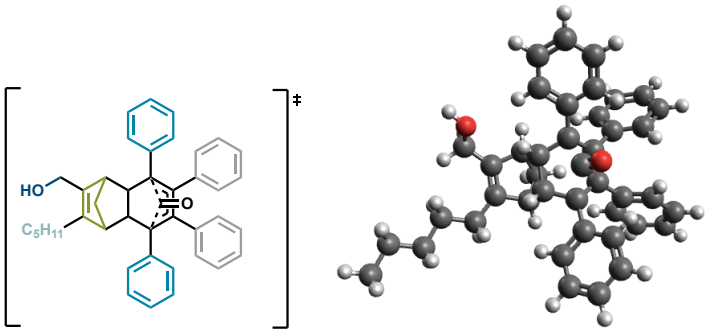

O	2.8356600000	-3.6655820000	0.2298090000
O	-1.4627130000	0.1915010000	3.1641450000
C	3.2641640000	-2.9846970000	-0.9687550000
C	9.3110000000	0.4158990000	-0.1968900000
C	8.0711920000	-0.4672800000	-0.3784990000
C	6.7740990000	0.3355920000	-0.5440120000
C	5.5278130000	-0.5428100000	-0.7239810000
C	4.2497100000	0.2882900000	-0.8923650000
C	0.8556430000	5.1422410000	2.2259720000
C	-0.3972600000	4.5732670000	2.4725410000
C	1.7783410000	4.4417020000	1.4474510000
C	-0.7233950000	3.3288240000	1.9372760000
C	1.4492590000	3.1937460000	0.9136730000
C	0.1837910000	2.6132340000	1.1301660000
C	-3.6699170000	4.2455860000	-1.8257240000
C	-4.0569870000	3.7393160000	-0.5826450000
C	-2.5614610000	3.6967070000	-2.4738370000
C	-3.3459170000	2.6891020000	0.0013180000
C	-1.8487510000	2.6517540000	-1.8810700000
C	-2.2317970000	2.1235720000	-0.6371520000
C	-5.4458670000	-1.6704870000	-2.0847840000
C	-5.5444990000	-0.7983070000	-0.9980250000
C	-4.1856500000	-2.1069480000	-2.4998070000
C	-4.3942750000	-0.3588810000	-0.3398240000
C	-3.0389610000	-1.6711900000	-1.8336960000
C	-3.1189380000	-0.7819530000	-0.7471040000
C	-2.4439700000	-5.0847650000	2.0678210000
C	-1.1801680000	-5.0017180000	1.4813320000
C	-3.2261490000	-3.9295780000	2.1655840000
C	-0.7050810000	-3.7855890000	0.9838880000
C	-2.7540630000	-2.7169620000	1.6693570000
C	-1.4919000000	-2.6174990000	1.0481250000

C	-0.8341360000	0.0167470000	2.2046150000
C	-1.4184110000	1.0011360000	-0.0569430000
C	-1.8416590000	-0.3473220000	-0.0950590000
C	-0.1685530000	1.2634330000	0.6049560000
C	-0.9850650000	-1.3026130000	0.5644460000
C	0.9807120000	0.3103630000	0.2988130000
C	0.5077160000	-1.1869160000	0.2923740000
C	0.7625460000	-0.4424930000	-2.0198590000
C	2.9238990000	-0.4037870000	-1.0575550000
C	1.6508750000	0.4504330000	-1.1345680000
C	0.9865170000	-1.6834930000	-1.1372360000
C	2.5156100000	-1.6940220000	-1.0704970000
H	3.2384220000	-4.5435880000	0.2468960000
H	4.3454930000	-2.8296300000	-0.9522450000
H	3.0227640000	-3.6092440000	-1.8442180000
H	9.4574800000	1.0757340000	-1.0603330000
H	10.2181150000	-0.1870930000	-0.0816140000
H	9.2182020000	1.0506010000	0.6923530000
H	8.2095570000	-1.1151330000	-1.2553700000
H	7.9718330000	-1.1394650000	0.4850370000
H	6.6371860000	0.9846510000	0.3332180000
H	6.8735250000	1.0082480000	-1.4086170000
H	5.6703510000	-1.1872590000	-1.6016060000
H	5.4269420000	-1.2055190000	0.1450980000
H	4.1572210000	0.9596960000	-0.0230540000
H	4.3797810000	0.9669580000	-1.7506790000
H	1.1115060000	6.1116480000	2.6435930000
H	-1.1196040000	5.0936760000	3.0951040000
H	2.7597580000	4.8647730000	1.2514100000
H	-1.6845480000	2.8895070000	2.1739280000
H	2.1870200000	2.6789160000	0.3105990000
H	-4.2238830000	5.0610520000	-2.2816670000
H	-4.9127900000	4.1623190000	-0.0638540000
H	-2.2461890000	4.0828200000	-3.4391260000
H	-3.6547920000	2.3162830000	0.9727800000
H	-0.9838080000	2.2373980000	-2.3906300000
H	-6.3409120000	-2.0104210000	-2.5977600000
H	-6.5191120000	-0.4603790000	-0.6569470000
H	-4.0928620000	-2.7906320000	-3.3389940000
H	-4.4939750000	0.3001410000	0.5141640000
H	-2.0650200000	-2.0238230000	-2.1593480000
H	-2.8103110000	-6.0310680000	2.4554590000
H	-0.5530630000	-5.8864190000	1.4112100000
H	-4.2025280000	-3.9698100000	2.6402780000
H	0.2886010000	-3.7580710000	0.5517550000
H	-3.3648400000	-1.8292350000	1.7822760000

H	1.8046750000	1.4800450000	-1.4655130000
H	0.5302780000	-2.6213460000	-1.4612960000
H	1.7496600000	0.4609800000	1.0620860000
H	1.0411670000	-1.7563060000	1.0549640000
H	1.1798770000	-0.5699830000	-3.0239260000
H	-0.2750980000	-0.1181700000	-2.0959640000

Electronic energy = -1774.303705 Hartree
Electronic energy + thermal free energy correction = -1774.377842 Hartree

O2 equilibrium geometry (A)

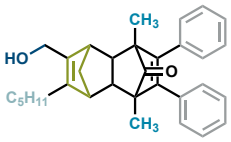

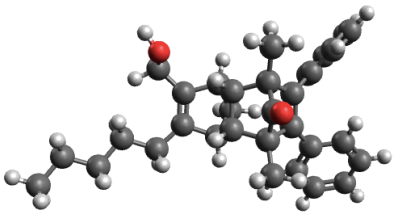

O	3.0638660000	-3.2443450000	0.1326360000
O	-0.9259520000	-0.4337230000	3.6212350000
C	-1.3014810000	-2.8014670000	1.7365780000
C	-1.0087360000	-1.3758670000	1.2964720000
C	-0.4052860000	2.2340360000	2.2852080000
C	-0.5698780000	0.9205970000	1.5369960000
C	3.1536200000	-2.4561710000	-1.0733710000
C	8.9231480000	1.3096070000	-0.0961110000
C	7.7510560000	0.3613360000	-0.3737850000
C	6.3835410000	1.0549980000	-0.3173750000
C	5.2048560000	0.1099270000	-0.5904880000
C	3.8542750000	0.8353900000	-0.5408700000
C	-4.1053980000	4.0369350000	-0.9049590000
C	-4.7411110000	2.9911690000	-0.2289230000
C	-2.7182000000	4.0057620000	-1.0686940000
C	-3.9981380000	1.9230180000	0.2739670000
C	-1.9744990000	2.9387300000	-0.5610220000
C	-2.6006370000	1.8736460000	0.1127750000
C	-5.2803690000	-2.3876270000	-1.7477110000
C	-5.1459180000	-2.6555690000	-0.3829370000
C	-4.3698650000	-1.5294620000	-2.3688190000
C	-4.1070320000	-2.0785880000	0.3497760000
C	-3.3345190000	-0.9489080000	-1.6341110000
C	-3.1785220000	-1.2144270000	-0.2610410000
C	-0.8541280000	-0.3244270000	2.4223600000

C	-1.8134310000	0.7424280000	0.6510360000
C	-2.0787200000	-0.5899540000	0.5196960000
C	0.7393280000	0.3495920000	0.8740810000
C	0.4282850000	-1.1769660000	0.6724820000
C	0.3574640000	-0.0404470000	-1.5022730000
C	2.5809670000	0.0550250000	-0.7197420000
C	1.2386940000	0.7885930000	-0.5454190000
C	0.7526070000	-1.3848890000	-0.8501620000
C	2.2823570000	-1.2500690000	-0.9199640000
H	-0.4300890000	-3.2148500000	2.2530820000
H	-1.5283180000	-3.4477310000	0.8833100000
H	-2.1420360000	-2.8445140000	2.4347790000
H	-0.0885940000	3.0455930000	1.6237800000
H	0.3492070000	2.1201010000	3.0701640000
H	-1.3406400000	2.5374740000	2.7646920000
H	3.4806520000	-4.1014520000	-0.0262570000
H	4.1933260000	-2.1822940000	-1.2709570000
H	2.7918460000	-3.0523180000	-1.9257580000
H	8.9542530000	2.1261120000	-0.8274100000
H	9.8829420000	0.7839290000	-0.1437600000
H	8.8400690000	1.7607720000	0.8997810000
H	7.8813580000	-0.1006170000	-1.3624180000
H	7.7676800000	-0.4628410000	0.3526920000
H	6.2550460000	1.5190360000	0.6714590000
H	6.3665850000	1.8794080000	-1.0454840000
H	5.3418230000	-0.3522870000	-1.5770260000
H	5.2150740000	-0.7032960000	0.1463560000
H	3.7753360000	1.3575470000	0.4268620000
H	3.8582590000	1.6450430000	-1.2883660000
H	-4.6842260000	4.8690610000	-1.2951160000
H	-5.8181830000	3.0085940000	-0.0883150000
H	-2.2124560000	4.8126870000	-1.5916560000
H	-4.4991200000	1.1199760000	0.8044430000
H	-0.8982920000	2.9256130000	-0.7011370000
H	-6.0871810000	-2.8382470000	-2.3183980000
H	-5.8534710000	-3.3114080000	0.1166150000
H	-4.4648860000	-1.3066110000	-3.4278850000
H	-4.0320140000	-2.2821460000	1.4122310000
H	-2.6435990000	-0.2777000000	-2.1322630000
H	1.2857580000	1.8699580000	-0.7055430000
H	0.3465880000	-2.3003350000	-1.2881300000
H	1.5412550000	0.5077130000	1.6047850000
H	1.1007550000	-1.8089880000	1.2575950000
H	0.7063970000	0.0256690000	-2.5375800000
H	-0.7004020000	0.2021800000	-1.4620330000

Electronic energy = -1390.969334 Hartree
Electronic energy + thermal free energy correction = -1391.034200 Hartree

Decarbonylated O2 equilibrium geometry (B)

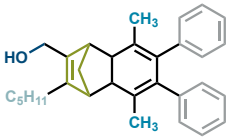

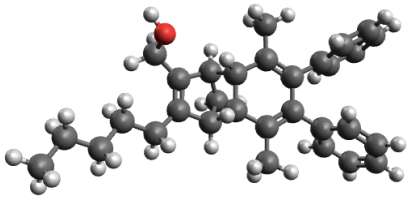

O	-3.3480610000	-3.0212840000	-0.8315720000
C	1.1284580000	-3.0868790000	-0.3212370000
C	0.2072890000	2.7646340000	-0.3070910000
C	-3.6744070000	-2.5298790000	0.4874480000
C	-8.9561070000	1.7171490000	-1.0351360000
C	-7.9070130000	0.6602710000	-0.6709630000
C	-6.5483770000	1.2611930000	-0.2869570000
C	-5.4919230000	0.2076840000	0.0749440000
C	-4.1499320000	0.8390020000	0.4662430000
C	5.1480520000	3.4199290000	-0.0202890000
C	4.3812370000	3.1915140000	1.1249430000
C	4.8081480000	2.7777850000	-1.2144150000
C	3.2842050000	2.3272750000	1.0732730000
C	3.7130110000	1.9120540000	-1.2603140000
C	2.9322880000	1.6743280000	-0.1182320000
C	6.0631660000	-2.1196260000	-0.2325810000
C	5.3229240000	-2.0708540000	-1.4167490000
C	5.4724210000	-1.7058830000	0.9644300000
C	4.0039170000	-1.6100950000	-1.4009740000
C	4.1530690000	-1.2465830000	0.9752340000
C	3.3970650000	-1.1931850000	-0.2057350000
C	1.7388470000	0.7639660000	-0.1626680000
C	1.9745710000	-0.7104890000	-0.1899590000
C	0.4879530000	1.2829910000	-0.2109980000
C	0.9443820000	-1.5904210000	-0.2337410000
C	-0.7442340000	0.4074600000	-0.2148270000
C	-0.4997540000	-1.1410130000	-0.2203040000

C	-0.9855000000	-0.4296050000	2.0344840000
C	-2.9809580000	-0.0459320000	0.8026210000
C	-1.6294310000	0.6044560000	1.0932310000
C	-1.2852800000	-1.6028010000	1.0839750000
C	-2.7698450000	-1.3824180000	0.8079050000
H	0.7504890000	-3.5886710000	0.5786780000
H	2.1713280000	-3.3774210000	-0.4472450000
H	0.5503170000	-3.4913230000	-1.1628580000
H	-0.1879280000	3.1697630000	0.6339030000
H	-0.5587140000	2.9532140000	-1.0713020000
H	1.0963420000	3.3421540000	-0.5635300000
H	-3.8134020000	-3.8563290000	-0.9730260000
H	-4.7274650000	-2.2391910000	0.5323790000
H	-3.5125260000	-3.3322060000	1.2239440000
H	-9.1393920000	2.3990990000	-0.1962040000
H	-9.9126600000	1.2557940000	-1.3036080000
H	-8.6280600000	2.3232210000	-1.8880090000
H	-8.2795270000	0.0478900000	0.1621050000
H	-7.7712110000	-0.0268250000	-1.5176390000
H	-6.1774670000	1.8759170000	-1.1202230000
H	-6.6843770000	1.9481770000	0.5613540000
H	-5.8698760000	-0.4031670000	0.9054990000
H	-5.3482930000	-0.4681980000	-0.7776020000
H	-3.8244590000	1.5015000000	-0.3528670000
H	-4.3122300000	1.5182250000	1.3184920000
H	6.0013540000	4.0911640000	0.0166840000
H	4.6350920000	3.6856970000	2.0588600000
H	5.3963850000	2.9497090000	-2.1116610000
H	2.6890900000	2.1550750000	1.9662520000
H	3.4559430000	1.4177820000	-2.1926000000
H	7.0893140000	-2.4759470000	-0.2423350000
H	5.7712300000	-2.3905480000	-2.3536150000
H	6.0382930000	-1.7402720000	1.8914040000
H	3.4322250000	-1.5753950000	-2.3247320000
H	3.7012720000	-0.9271970000	1.9101790000
H	-1.6826810000	1.6391760000	1.4393080000
H	-1.0277820000	-2.6076890000	1.4243380000
H	-1.3483090000	0.7026820000	-1.0829670000
H	-0.9913650000	-1.6059030000	-1.0814990000
H	-1.5086200000	-0.5144210000	2.9922170000
H	0.0826930000	-0.2614280000	2.2071180000

Electronic energy = -1277.658319 Hartree
Electronic energy + thermal free energy correction = -1277.724055 Hartree

F1 equilibrium geometry (A)

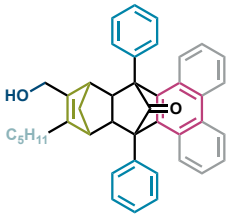

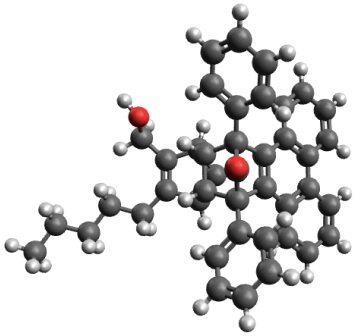

O	2.6210450000	-3.6979240000	-0.1085340000
O	-0.8710260000	-0.0683040000	3.1016660000
C	3.0260700000	-2.9321840000	-1.2634520000
C	9.2069450000	0.2490160000	-0.6033310000
C	7.9326880000	-0.5870820000	-0.7685550000
C	6.6532140000	0.2590960000	-0.8056180000
C	5.3727320000	-0.5721260000	-0.9687080000
C	4.1130110000	0.3018930000	-1.0101900000
C	0.5451710000	4.7915610000	3.0932150000
C	-0.6932280000	4.1531970000	3.2147210000
C	1.5250170000	4.2324380000	2.2717440000
C	-0.9460880000	2.9718420000	2.5189090000
C	1.2683160000	3.0458540000	1.5769210000
C	0.0279790000	2.4006130000	1.6824370000
C	-3.3067600000	4.0682240000	-2.3685560000
C	-3.7905750000	2.7726880000	-2.3838990000
C	-2.1757190000	4.3846430000	-1.5950620000
C	-3.1854100000	1.7392760000	-1.6267970000
C	-1.5705590000	3.4063280000	-0.8290120000
C	-2.0638060000	2.0756550000	-0.8023310000
C	-5.0892100000	-1.3531810000	-2.6970500000
C	-4.7111550000	-0.0303460000	-2.5558510000
C	-4.3964940000	-2.3588250000	-1.9993260000
C	-3.6419470000	0.3551660000	-1.7098730000
C	-3.3603960000	-2.0182700000	-1.1505040000
C	-2.9716000000	-0.6660680000	-0.9630130000
C	-2.6528490000	-4.7740440000	2.5586630000
C	-1.4735060000	-4.8254080000	1.8142890000
C	-3.2965120000	-3.5455410000	2.7396100000
C	-0.9404980000	-3.6612150000	1.2497600000
C	-2.7661000000	-2.3867840000	2.1746100000
C	-1.5856990000	-2.4265890000	1.4132470000

C	-0.7682770000	-0.0373700000	1.9056110000
C	-1.4745200000	1.0367450000	0.0021290000
C	-1.9114510000	-0.2731520000	-0.0715350000
C	-0.2791950000	1.1078750000	0.9613230000
C	-1.0333700000	-1.1425970000	0.8365310000
C	0.9443550000	0.3062380000	0.3686180000
C	0.4410710000	-1.1845360000	0.2833560000
C	0.5599000000	-0.2566710000	-1.9873690000
C	2.7598290000	-0.3428270000	-1.1392840000
C	1.5080210000	0.5537630000	-1.0767470000
C	0.7789630000	-1.5688320000	-1.2022750000
C	2.3139520000	-1.6177240000	-1.2262350000
H	2.9872760000	-4.5885840000	-0.1848160000
H	4.1116870000	-2.8100900000	-1.2774220000
H	2.7317220000	-3.4736390000	-2.1771330000
H	9.3240330000	0.9604490000	-1.4294740000
H	10.1004460000	-0.3841160000	-0.5806580000
H	9.1841110000	0.8256370000	0.3289780000
H	8.0013470000	-1.1788280000	-1.6920550000
H	7.8621960000	-1.3121070000	0.0540930000
H	6.5860040000	0.8520210000	0.1182390000
H	6.7237060000	0.9846640000	-1.6292970000
H	5.4462430000	-1.1615840000	-1.8922520000
H	5.3003830000	-1.2872530000	-0.1391890000
H	4.0908560000	0.9207330000	-0.0982460000
H	4.2135230000	1.0290540000	-1.8319720000
H	0.7432640000	5.7118330000	3.6350850000
H	-1.4627390000	4.5738370000	3.8557080000
H	2.4923630000	4.7161360000	2.1682910000
H	-1.9117080000	2.4874520000	2.6237660000
H	2.0427500000	2.6345620000	0.9385300000
H	-3.7952380000	4.8344890000	-2.9634730000
H	-4.6509000000	2.5543420000	-3.0047230000
H	-1.7776830000	5.3951080000	-1.5942500000
H	-0.7058060000	3.6631270000	-0.2335150000
H	-5.9123920000	-1.6121750000	-3.3566240000
H	-5.2490370000	0.7196260000	-3.1228490000
H	-4.6739290000	-3.4015700000	-2.1224230000
H	-2.8382040000	-2.7987110000	-0.6148910000
H	-3.0645550000	-5.6782550000	2.9979230000
H	-0.9595350000	-5.7720480000	1.6717260000
H	-4.2103130000	-3.4890100000	3.3243000000
H	-0.0182530000	-3.7280620000	0.6819120000
H	-3.2760040000	-1.4396470000	2.3224640000
H	1.6762870000	1.6024710000	-1.3354560000
H	0.2785510000	-2.4673670000	-1.5700830000

H	1.7543870000	0.3977980000	1.0985030000
H	1.0131170000	-1.8254800000	0.9563400000
H	0.9528790000	-0.3308990000	-3.0059500000
H	-0.4648390000	0.1014710000	-2.0308820000

Electronic energy = -1773.198178 Hartree
Electronic energy + thermal free energy correction = -1773.268173 Hartree

Decarbonylated F1 equilibrium geometry (B)

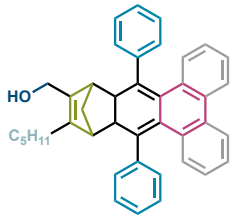

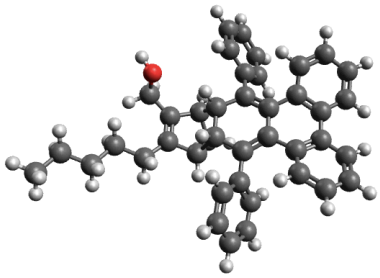

O	-3.0261860000	-3.3062530000	-1.0380240000
C	-3.3993110000	-2.9604600000	0.3162850000
C	-9.1545990000	0.5840640000	-1.2346210000
C	-7.9843670000	-0.3338540000	-0.8627860000
C	-6.7280140000	0.4312530000	-0.4262190000
C	-5.5509790000	-0.4821820000	-0.0558400000
C	-4.3159230000	0.3110490000	0.3891040000
C	-1.3447170000	5.2559910000	0.8537210000
C	-1.7339010000	4.6238670000	-0.3303220000
C	-0.4180950000	4.6291970000	1.6928780000
C	-1.2022850000	3.3770860000	-0.6695880000
C	0.1189670000	3.3885550000	1.3472020000
C	-0.2554090000	2.7444730000	0.1548030000
C	4.6078560000	4.0929240000	-0.2607830000
C	3.3384320000	4.4035140000	-0.7552370000
C	4.9232040000	2.7661720000	0.0079280000
C	2.3771310000	3.4033780000	-0.8535700000
C	3.9783870000	1.7324430000	-0.1479230000
C	2.6368110000	2.0735200000	-0.4647080000
C	6.1969140000	-1.3002460000	-0.5881850000
C	5.2697610000	-2.2129320000	-1.0988020000
C	5.7612980000	-0.0422960000	-0.1882240000
C	3.9172200000	-1.8909580000	-1.0937620000
C	4.3991810000	0.3176050000	-0.2268390000
C	3.4422400000	-0.6680760000	-0.5785830000
C	1.9581680000	-5.5213080000	0.7175910000

C	1.1884770000	-5.2013260000	-0.4042500000
C	2.4525370000	-4.4923830000	1.5253740000
C	0.9163790000	-3.8670390000	-0.7155640000
C	2.1907090000	-3.1597060000	1.2061280000
C	1.4287440000	-2.8217830000	0.0732810000
C	1.5616310000	1.0456320000	-0.3840080000
C	1.9890030000	-0.3938660000	-0.4192670000
C	0.2525560000	1.3743200000	-0.1653740000
C	1.0817180000	-1.3953820000	-0.2109810000
C	-0.8629850000	0.3439780000	-0.1904590000
C	-0.4154390000	-1.1527490000	-0.2198440000
C	-1.0605980000	-0.5789810000	2.0259720000
C	-3.0494280000	-0.4221860000	0.7361400000
C	-1.8037010000	0.3904300000	1.0888190000
C	-1.1738520000	-1.7529260000	1.0366500000
C	-2.6652650000	-1.7186530000	0.7120750000
H	-3.3542650000	-4.1951280000	-1.2284970000
H	-4.4827240000	-2.8287750000	0.3845820000
H	-3.1126720000	-3.7801590000	0.9919230000
H	-9.4484360000	1.2145310000	-0.3869080000
H	-10.0342240000	0.0074160000	-1.5407330000
H	-8.8877800000	1.2494430000	-2.0643680000
H	-8.2941020000	-1.0108500000	-0.0543800000
H	-7.7365320000	-0.9755160000	-1.7196900000
H	-6.4200700000	1.1101830000	-1.2349900000
H	-6.9761370000	1.0730760000	0.4319670000
H	-5.8664080000	-1.1583910000	0.7498150000
H	-5.2961150000	-1.1116280000	-0.9178890000
H	-4.0611970000	1.0357640000	-0.4015390000
H	-4.5872170000	0.9377710000	1.2534810000
H	-1.7605790000	6.2230190000	1.1212110000
H	-2.4526970000	5.0999200000	-0.9917100000
H	-0.1127410000	5.1067450000	2.6198120000
H	-1.5102350000	2.8999490000	-1.5962070000
H	0.8419060000	2.9102160000	2.0012090000
H	5.3601790000	4.8663720000	-0.1360980000
H	3.0933650000	5.4178410000	-1.0558890000
H	5.9380440000	2.5293730000	0.3043020000
H	1.4025310000	3.6648280000	-1.2387430000
H	7.2545010000	-1.5451580000	-0.5519140000
H	5.5952070000	-3.1700950000	-1.4953420000
H	6.5046410000	0.6848300000	0.1156560000
H	3.2142370000	-2.6069150000	-1.4953660000
H	2.1655570000	-6.5589490000	0.9628440000
H	0.7947900000	-5.9911680000	-1.0383070000
H	3.0433910000	-4.7272410000	2.4064410000

H	0.3065360000	-3.6361160000	-1.5840710000
H	2.5823650000	-2.3660610000	1.8352530000
H	-2.0012400000	1.3976160000	1.4563890000
H	-0.7958150000	-2.7234990000	1.3581660000
H	-1.4747940000	0.5689330000	-1.0735120000
H	-0.8089130000	-1.6463480000	-1.1148660000
H	-1.5955540000	-0.7581390000	2.9635350000
H	-0.0280500000	-0.2785870000	2.2393590000

Electronic energy = -1659.858472 Hartree
Electronic energy + thermal free energy correction = -1659.929245 Hartree

F1 transition state geometry (A–B)

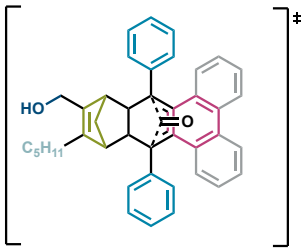

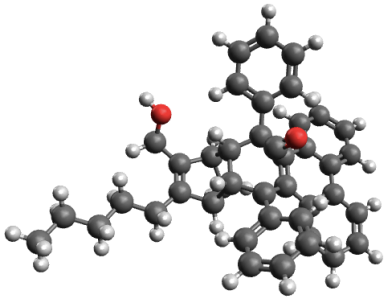

O	2.9124940000	-3.6103270000	0.0276680000
O	-1.4849120000	0.1578640000	3.0723660000
C	3.3370860000	-2.8844620000	-1.1458300000
C	9.3176640000	0.5979720000	-0.2415880000
C	8.0944700000	-0.3011140000	-0.4549930000
C	6.7847370000	0.4835030000	-0.6081380000
C	5.5551060000	-0.4111460000	-0.8198080000
C	4.2637390000	0.4017300000	-0.9754330000
C	0.7149460000	4.9735300000	2.5197610000
C	-0.5532310000	4.3889900000	2.6255250000
C	1.6858490000	4.3520560000	1.7342840000
C	-0.8437880000	3.2082100000	1.9498250000
C	1.3940400000	3.1635110000	1.0582280000
C	0.1194140000	2.5693310000	1.1387760000
C	-4.1255400000	3.9885930000	-1.6060400000
C	-4.5577920000	2.6830650000	-1.4404340000
C	-2.7700710000	4.2971810000	-1.4156520000
C	-3.6764340000	1.6509570000	-1.0423810000
C	-1.8969480000	3.3114700000	-0.9880340000

C	-2.3316530000	1.9899430000	-0.7236740000
C	-5.6584860000	-1.4813770000	-1.8015720000
C	-5.3518630000	-0.1542820000	-1.5496680000
C	-4.6687200000	-2.4628390000	-1.6390940000
C	-4.0734200000	0.2408170000	-1.0910910000
C	-3.4217730000	-2.1044790000	-1.1563240000
C	-3.1112100000	-0.7676680000	-0.8072450000
C	-2.1630030000	-5.0401790000	2.2874230000
C	-0.9656380000	-4.9767190000	1.5743720000
C	-2.9606560000	-3.8932500000	2.3846740000
C	-0.5683590000	-3.7877520000	0.9545220000
C	-2.5697220000	-2.7106650000	1.7654100000
C	-1.3723470000	-2.6324890000	1.0211070000
C	-0.8338500000	-0.0047720000	2.1304190000
C	-1.4133400000	0.9719650000	-0.2027430000
C	-1.8084390000	-0.4108460000	-0.2378990000
C	-0.1845030000	1.2717780000	0.4763220000
C	-0.9350880000	-1.3437480000	0.4182020000
C	0.9810370000	0.3464850000	0.1856450000
C	0.5450370000	-1.1682340000	0.1497600000
C	0.7959310000	-0.3609940000	-2.1470550000
C	2.9511460000	-0.3085790000	-1.1676870000
C	1.6654430000	0.5252710000	-1.2368440000
C	1.0378920000	-1.6192940000	-1.2933880000
C	2.5655400000	-1.6052520000	-1.2161900000
H	3.3366640000	-4.4783460000	0.0230180000
H	4.4150820000	-2.7097800000	-1.1152940000
H	3.1146060000	-3.4864450000	-2.0418530000
H	9.4582270000	1.2829410000	-1.0862300000
H	10.2342970000	0.0077090000	-0.1361510000
H	9.2082920000	1.2071070000	0.6635210000
H	8.2495990000	-0.9229440000	-1.3477430000
H	8.0012260000	-0.9976480000	0.3897290000
H	6.6310000000	1.1066110000	0.2850120000
H	6.8779880000	1.1804550000	-1.4539660000
H	5.7146190000	-1.0295750000	-1.7130750000
H	5.4601740000	-1.0982640000	0.0308050000
H	4.1540900000	1.0485720000	-0.0895800000
H	4.3873930000	1.1047170000	-1.8148450000
H	0.9416600000	5.8943170000	3.0491410000
H	-1.3158140000	4.8509230000	3.2462100000
H	2.6764470000	4.7891270000	1.6431110000
H	-1.8270160000	2.7629810000	2.0568110000
H	2.1659740000	2.7101640000	0.4471000000
H	-4.8273530000	4.7568660000	-1.9172820000
H	-5.5957320000	2.4553310000	-1.6503700000

H	-2.4022670000	5.3018520000	-1.6019390000
H	-0.8539310000	3.5625720000	-0.8513240000
H	-6.6484380000	-1.7508000000	-2.1580390000
H	-6.1121030000	0.5932930000	-1.7404630000
H	-4.8740810000	-3.4991870000	-1.8903910000
H	-2.6662630000	-2.8699450000	-1.0409770000
H	-2.4672320000	-5.9633120000	2.7722930000
H	-0.3283290000	-5.8537350000	1.5003010000
H	-3.8852460000	-3.9185790000	2.9545390000
H	0.3763510000	-3.7701500000	0.4224360000
H	-3.1925920000	-1.8282370000	1.8657450000
H	1.8048550000	1.5661500000	-1.5395930000
H	0.5977490000	-2.5564400000	-1.6413140000
H	1.7344450000	0.4963490000	0.9638890000
H	1.1013320000	-1.7328740000	0.8989270000
H	1.2205320000	-0.4584590000	-3.1511630000
H	-0.2460780000	-0.0509140000	-2.2239540000

Electronic energy = -1773.145765 Hartree
Electronic energy + thermal free energy correction = -1773.215977 Hartree

F2 equilibrium geometry (A)

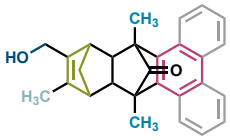

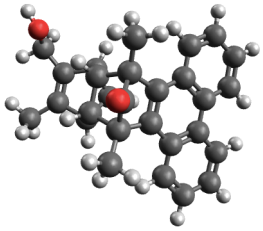

O	-4.9105080000	1.7118410000	-0.2690540000
O	-0.7854900000	-0.2203940000	3.5693630000
C	-0.3072180000	-2.7122400000	2.0186960000
C	-0.8534910000	2.3573060000	2.0813080000
C	-4.2422630000	-2.1954820000	-1.5222360000
C	-4.6139280000	1.0459330000	-1.5123210000
C	4.3062890000	-2.4891150000	-1.0638520000
C	4.1848930000	-1.1135820000	-0.9906370000
C	3.2704800000	-3.3097140000	-0.5823340000
C	3.0423020000	-0.4910210000	-0.4296490000
C	2.1476890000	-2.7366980000	-0.0161680000

C	2.0060210000	-1.3284900000	0.0961490000
C	3.6962590000	3.1961250000	-0.9877250000
C	3.8701190000	1.8247840000	-0.9506650000
C	2.5105750000	3.7652630000	-0.4892410000
C	2.8867190000	0.9594510000	-0.4103560000
C	1.5361600000	2.9524700000	0.0578680000
C	1.6975570000	1.5439940000	0.1335040000
C	-0.5995360000	-0.1833870000	2.3784050000
C	0.8606080000	-0.7029370000	0.7010660000
C	0.7121860000	0.6746390000	0.7188850000
C	-0.3621740000	-1.3346690000	1.3703020000
C	-0.6154530000	1.0154790000	1.3998640000
C	-1.6656740000	-1.0667620000	0.5203470000
C	-1.8375620000	0.4986110000	0.5432220000
C	-1.0945350000	-0.1791230000	-1.6932480000
C	-3.2268740000	-1.1097080000	-1.3512880000
C	-1.7582450000	-1.3998780000	-1.0120560000
C	-2.0122950000	0.8417510000	-0.9794530000
C	-3.3741710000	0.2334450000	-1.3369140000
H	-1.1037100000	-2.7799860000	2.7669950000
H	0.6407110000	-2.8828240000	2.5363800000
H	-0.4628940000	-3.5193700000	1.2966840000
H	-1.6468120000	2.2362200000	2.8257810000
H	-1.1801320000	3.1283180000	1.3776970000
H	0.0373010000	2.7127520000	2.6066960000
H	-3.9886280000	-2.8414830000	-2.3729310000
H	-5.2515040000	-1.8058930000	-1.6815040000
H	-4.2697840000	-2.8427990000	-0.6351490000
H	-5.6185050000	2.3514460000	-0.4204010000
H	-5.4554960000	0.4091850000	-1.8160740000
H	-4.4565400000	1.7973780000	-2.3021490000
H	5.1963250000	-2.9310340000	-1.5020360000
H	4.9911560000	-0.5071750000	-1.3849350000
H	3.3502160000	-4.3905430000	-0.6535710000
H	1.3591950000	-3.3800100000	0.3460520000
H	4.4714300000	3.8282850000	-1.4107810000
H	4.7862840000	1.4140630000	-1.3571450000
H	2.3587650000	4.8398300000	-0.5324670000
H	0.6293540000	3.4032860000	0.4335480000
H	-1.3977810000	-2.3933250000	-1.2930560000
H	-1.8883840000	1.8979940000	-1.2311860000
H	-2.4821340000	-1.5688690000	1.0514220000
H	-2.7406190000	0.8020910000	1.0793620000
H	-1.2657340000	-0.1841040000	-2.7741110000
H	-0.0307220000	-0.0636730000	-1.5044250000

Electronic energy = -1232.663814 Hartree
Electronic energy + thermal free energy correction = -1232.716392 Hartree

Decarbonylated F2 equilibrium geometry (B)

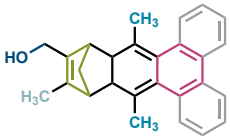

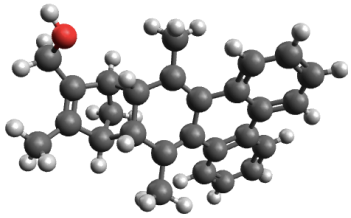

O	4.7554460000	2.3661260000	0.1498490000
C	5.0796040000	-1.5527610000	-1.1349990000
C	0.2409850000	-2.5685730000	-1.7384930000
C	0.6189750000	2.7821120000	0.7878300000
C	5.1617750000	1.1152780000	0.7419440000
C	-4.3245760000	-2.7253630000	0.9779710000
C	-3.1365080000	-3.4306360000	0.7723940000
C	-4.3588580000	-1.3580420000	0.7199040000
C	-2.0082580000	-2.7612470000	0.3050500000
C	-3.2343610000	-0.6737740000	0.2263960000
C	-2.0317260000	-1.3868990000	-0.0060290000
C	-4.5332360000	2.8042370000	-0.5558230000
C	-3.3360170000	3.5098800000	-0.6925810000
C	-4.4902990000	1.4458320000	-0.2568760000
C	-2.1210070000	2.8548300000	-0.5065780000
C	-3.2720680000	0.7747300000	-0.0516490000
C	-2.0531310000	1.4933830000	-0.1476310000
C	-0.7939850000	-0.6649340000	-0.3997600000
C	-0.7509190000	0.7821670000	-0.0275490000
C	0.2824210000	-1.2578020000	-0.9862480000
C	0.4378290000	1.3843000000	0.2433030000
C	1.6528830000	-0.6183460000	-0.9198150000
C	1.7464790000	0.7041880000	-0.0855350000
C	2.2660640000	-1.1876860000	1.3406350000
C	4.0420490000	-0.9881000000	-0.2154940000
C	2.6402350000	-1.5761620000	-0.1048390000
C	2.6684210000	0.2866480000	1.1413370000
C	4.0665390000	0.1181020000	0.5583030000
H	5.3257050000	-2.5884210000	-0.8661840000

H	6.0061220000	-0.9719300000	-1.1288840000
H	4.7080980000	-1.5776600000	-2.1685380000
H	0.8541390000	-2.4705980000	-2.6446150000
H	-0.7723550000	-2.8352400000	-2.0445300000
H	0.6560220000	-3.4192510000	-1.1817590000
H	1.4497910000	2.7901750000	1.5016490000
H	-0.2688810000	3.1569710000	1.2996800000
H	0.8953330000	3.5008790000	0.0027730000
H	5.3948050000	3.0472440000	0.3960400000
H	6.0924320000	0.7588090000	0.2806310000
H	5.3526960000	1.2647530000	1.8163050000
H	-5.2069200000	-3.2285180000	1.3626220000
H	-3.0777880000	-4.4904400000	1.0033400000
H	-5.2698470000	-0.8087740000	0.9315520000
H	-1.0805790000	-3.3115620000	0.2196650000
H	-5.4880400000	3.2971530000	-0.7139760000
H	-3.3439150000	4.5596060000	-0.9719520000
H	-5.4209500000	0.8905240000	-0.2142200000
H	-1.2092070000	3.4066460000	-0.6870130000
H	2.5636920000	-2.6291890000	-0.3817510000
H	2.5916590000	0.9514380000	2.0041730000
H	2.0460370000	-0.4812540000	-1.9360930000
H	2.3110080000	1.4528020000	-0.6525330000
H	2.8845390000	-1.6962540000	2.0867910000
H	1.2069760000	-1.3290920000	1.5770040000

Electronic energy = -1119.325841 Hartree
Electronic energy + thermal free energy correction = -1119.377233Hartree

F3 (Py) equilibrium geometry (A)

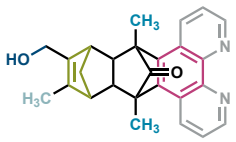

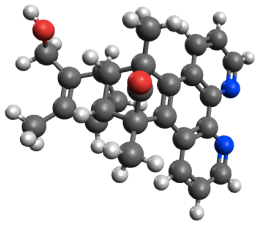

O	-4.8963990000	1.7325540000	-0.2583250000
O	-0.7885700000	-0.2220920000	3.5718530000

N	3.8722150000	1.6985700000	-0.9679580000
N	4.1570310000	-1.0054370000	-1.0054250000
C	-0.3019060000	-2.7176120000	2.0077450000
C	-0.8394400000	2.3635090000	2.0736830000
C	-4.2531430000	-2.1860800000	-1.5137660000
C	-4.6153170000	1.0578760000	-1.5002070000
C	4.2951620000	-2.3184400000	-1.0768810000
C	3.3260140000	-3.2290330000	-0.6114930000
C	3.0354740000	-0.4983230000	-0.4435080000
C	2.1814270000	-2.7288710000	-0.0252710000
C	2.0027440000	-1.3281350000	0.0963540000
C	3.7330980000	3.0129660000	-1.0031240000
C	2.5964800000	3.6884510000	-0.5164190000
C	2.8824280000	0.9537440000	-0.4235160000
C	1.5827180000	2.9449820000	0.0522330000
C	1.7009290000	1.5350810000	0.1354100000
C	-0.6008620000	-0.1844780000	2.3818890000
C	0.8575590000	-0.7058610000	0.7023230000
C	0.7119350000	0.6720120000	0.7211610000
C	-0.3641380000	-1.3357530000	1.3708290000
C	-0.6127380000	1.0156070000	1.4019790000
C	-1.6688730000	-1.0644870000	0.5232720000
C	-1.8371300000	0.5011540000	0.5466980000
C	-1.1004610000	-0.1784210000	-1.6917530000
C	-3.2347060000	-1.1029840000	-1.3444530000
C	-1.7658610000	-1.3972390000	-1.0089370000
C	-2.0135360000	0.8449370000	-0.9756260000
C	-3.3780140000	0.2404770000	-1.3296280000
H	-1.1041010000	-2.8022490000	2.7479550000
H	0.6430510000	-2.8830710000	2.5329360000
H	-0.4426030000	-3.5189110000	1.2759670000
H	-1.6424820000	2.2601280000	2.8101230000
H	-1.1471450000	3.1343030000	1.3610690000
H	0.0508240000	2.7090620000	2.6069670000
H	-4.0039200000	-2.8309480000	-2.3665440000
H	-5.2617940000	-1.7936480000	-1.6691840000
H	-4.2795110000	-2.8349650000	-0.6278290000
H	-5.6062880000	2.3711520000	-0.4050770000
H	-5.4624880000	0.4233940000	-1.7925320000
H	-4.4610680000	1.8034440000	-2.2961440000
H	5.2156670000	-2.6819610000	-1.5311820000
H	3.4826440000	-4.2984480000	-0.7142630000
H	1.4226400000	-3.4078020000	0.3380250000
H	4.5564280000	3.5727490000	-1.4443320000
H	2.5263800000	4.7693900000	-0.5898170000
H	0.6995300000	3.4399170000	0.4311900000

H	-1.4096020000	-2.3919220000	-1.2910460000
H	-1.8880590000	1.9009390000	-1.2275990000
H	-2.4846590000	-1.5650450000	1.0566150000
H	-2.7382450000	0.8071280000	1.0845200000
H	-1.2736420000	-0.1827730000	-2.7720950000
H	-0.0355710000	-0.0659690000	-1.5062180000

Electronic energy = -1264.758476 Hartree
Electronic energy + thermal free energy correction = -1264.810874 Hartree

Decarbonylated F3 equilibrium geometry (B)

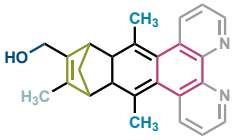

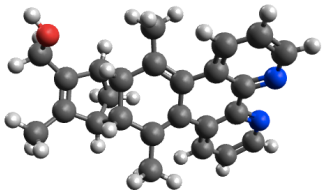

O	-4.7580340000	2.3611280000	-0.0482000000
N	4.3862830000	-1.2493310000	-0.6197390000
N	4.4745000000	1.3724950000	0.1537690000
C	-5.0824140000	-1.6276830000	1.0442480000
C	-0.2482620000	-2.6391850000	1.6355480000
C	-0.6361480000	2.8161670000	-0.6479310000
C	-5.1692640000	1.1370350000	-0.6901530000
C	4.3856810000	-2.5581880000	-0.8659120000
C	3.2427960000	-3.3534390000	-0.7491920000
C	2.0627930000	-2.7510650000	-0.3284200000
C	3.2467040000	-0.6708610000	-0.2077550000
C	2.0386030000	-1.3823420000	-0.0024970000
C	4.5309010000	2.6733290000	0.4324280000
C	3.3919050000	3.4503140000	0.6554480000
C	2.1464460000	2.8449740000	0.5318360000
C	3.2706860000	0.7890280000	0.0381030000
C	2.0443110000	1.4894330000	0.1661890000
C	0.7891580000	-0.6791810000	0.3805000000
C	0.7419030000	0.7803490000	0.0601070000
C	-0.2889900000	-1.2999110000	0.9353410000
C	-0.4497560000	1.3941320000	-0.1719220000
C	-1.6612090000	-0.6646090000	0.8903400000
C	-1.7565270000	0.6976040000	0.1250210000

C	-2.2625320000	-1.1204570000	-1.3989030000
C	-4.0446820000	-1.0106830000	0.1593240000
C	-2.6395720000	-1.5854080000	0.0227440000
C	-2.6732380000	0.3393900000	-1.1252520000
C	-4.0717330000	0.1344040000	-0.5555360000
H	-5.3240940000	-2.6480850000	0.7192140000
H	-6.0110150000	-1.0507270000	1.0664240000
H	-4.7138840000	-1.7068610000	2.0760910000
H	-0.8848390000	-2.5856870000	2.5286010000
H	0.7598320000	-2.9067740000	1.9581570000
H	-0.6390150000	-3.4706990000	1.0341840000
H	-1.4967460000	2.8650790000	-1.3228720000
H	0.2327130000	3.2042390000	-1.1825560000
H	-0.8686350000	3.5025260000	0.1790940000
H	-5.4028110000	3.0505700000	-0.2537960000
H	-6.0966240000	0.7607340000	-0.2383270000
H	-5.3671450000	1.3317840000	-1.7559400000
H	5.3318260000	-2.9865020000	-1.1920150000
H	3.2720710000	-4.4083900000	-1.0045020000
H	1.1542850000	-3.3374670000	-0.2879580000
H	5.5265840000	3.1068840000	0.5072640000
H	3.4788120000	4.4946640000	0.9397020000
H	1.2588230000	3.4195000000	0.7565360000
H	-2.5575270000	-2.6508210000	0.2455350000
H	-2.5973990000	1.0481000000	-1.9523440000
H	-2.0600010000	-0.5817350000	1.9100460000
H	-2.3240070000	1.4163370000	0.7264430000
H	-2.8757570000	-1.5925440000	-2.1726240000
H	-1.2020010000	-1.2441750000	-1.6391790000

Electronic energy = -1151.421262 Hartree
Electronic energy + thermal free energy correction = -1151.472689 Hartree

F4 equilibrium geometry (A)

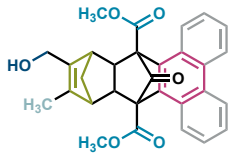

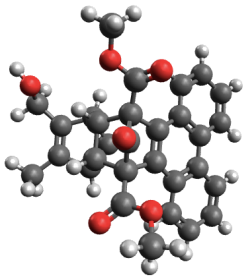

O	-0.7452170000	2.5129920000	2.6204140000
O	0.2270570000	-3.7865380000	1.0605730000
O	1.6123780000	-2.4978400000	2.2969010000
O	-2.6874270000	2.1436230000	1.5282550000
O	-5.1155940000	0.0124040000	-0.8615510000
O	-0.7663770000	-0.6793100000	3.0607360000
C	2.1169930000	-3.6766530000	2.9538070000
C	-3.3132970000	3.1574530000	2.3401990000
C	-1.3876980000	1.9011950000	1.7930700000
C	0.6546940000	-2.6923170000	1.3759730000
C	-3.0908780000	-3.2263850000	-2.3369740000
C	-4.5352660000	-0.3135260000	-2.1396400000
C	4.9414760000	-0.8649220000	-1.5359250000
C	4.4092060000	0.4003620000	-1.3647630000
C	4.2024550000	-1.9982970000	-1.1501440000
C	3.1297030000	0.6004010000	-0.7907040000
C	2.9598890000	-1.8397620000	-0.5669110000
C	2.4073080000	-0.5525120000	-0.3480790000
C	2.5605900000	4.3257150000	-1.1561640000
C	3.1744510000	3.0864370000	-1.1706180000
C	1.2474080000	4.4545690000	-0.6688620000
C	2.5209790000	1.9244110000	-0.6920960000
C	0.5874360000	3.3458410000	-0.1754510000
C	1.2040500000	2.0699680000	-0.1493340000
C	-0.4978570000	-0.4672960000	1.9131540000
C	1.1338560000	-0.3488330000	0.2818920000
C	0.5567880000	0.8999840000	0.3765590000
C	0.1505720000	-1.3766090000	0.8262600000
C	-0.8326140000	0.7451140000	0.9879000000
C	-1.1308200000	-1.4841560000	-0.0778510000
C	-1.8071770000	-0.0598440000	0.0393200000
C	-0.8025720000	-0.2712900000	-2.1883230000
C	-2.5082230000	-1.8815380000	-2.0378010000
C	-1.0413110000	-1.6950620000	-1.6307680000

C	-2.0331810000	0.3264170000	-1.4657450000
C	-3.0990240000	-0.6697180000	-1.9426420000
H	2.8567160000	-3.3140490000	3.6662460000
H	2.5775470000	-4.3500790000	2.2265420000
H	1.3060400000	-4.1972940000	3.4678320000
H	-2.8247910000	4.1231590000	2.1885170000
H	-3.2513870000	2.8859910000	3.3963270000
H	-4.3501860000	3.1913750000	2.0078370000
H	-2.6035790000	-3.6796560000	-3.2099720000
H	-4.1663610000	-3.1849520000	-2.5293580000
H	-2.9242510000	-3.9120650000	-1.4957910000
H	-5.9984150000	0.3770760000	-1.0066350000
H	-5.0773650000	-1.1483030000	-2.6035840000
H	-4.6133610000	0.5554650000	-2.8115630000
H	5.9244150000	-0.9808250000	-1.9828740000
H	4.9932860000	1.2514050000	-1.6932810000
H	4.6040630000	-2.9943630000	-1.3106880000
H	2.3961620000	-2.7216700000	-0.2882760000
H	3.0908020000	5.1952670000	-1.5331690000
H	4.1779710000	3.0153890000	-1.5721610000
H	0.7539560000	5.4217940000	-0.6747860000
H	-0.4201540000	3.4621860000	0.2007500000
H	-0.3597200000	-2.4890190000	-1.9437830000
H	-2.2635400000	1.3805840000	-1.6349030000
H	-1.7499340000	-2.2692390000	0.3621920000
H	-2.7720740000	-0.1068960000	0.5445520000
H	-0.9264760000	-0.2446730000	-3.2749920000
H	0.1544470000	0.1758640000	-1.9336250000

Electronic energy = -1609.759557 Hartree
Electronic energy + thermal free energy correction = -1609.822009 Hartree

Decarbonylated F4 equilibrium geometry (B)

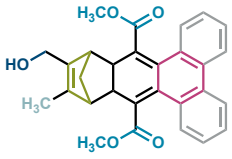

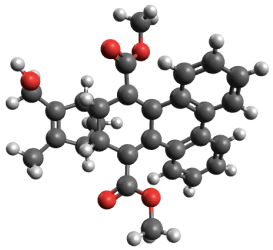

O	-1.1597590000	-3.1410050000	-1.5467880000
O	0.1824630000	3.3885260000	0.9624350000
O	1.5083990000	3.4266920000	-0.8687200000
O	0.9125670000	-3.7514800000	-0.8960090000
O	5.0796640000	1.5210120000	-0.8902530000
C	-1.3709130000	-4.4832610000	-2.0151380000
C	0.3658230000	4.8101620000	1.0979630000
C	0.7846080000	2.8149420000	-0.1039690000
C	0.0322910000	-2.9047200000	-0.9486160000
C	4.8260040000	-2.3686180000	-0.0973910000
C	5.2771910000	0.8204000000	0.3531830000
C	-4.3897230000	-2.0495550000	1.9084050000
C	-3.2479620000	-2.8566320000	1.8768310000
C	-4.3755160000	-0.8112840000	1.2732760000
C	-2.1145420000	-2.4166940000	1.2024850000
C	-3.2440330000	-0.3617220000	0.5705860000
C	-2.0973330000	-1.1894420000	0.5117080000
C	-4.3696820000	2.8519170000	-1.1062940000
C	-3.1414420000	3.3975210000	-1.4881830000
C	-4.3983150000	1.6315870000	-0.4380840000
C	-1.9615790000	2.7275660000	-1.1779590000
C	-3.2152010000	0.9495120000	-0.1054640000
C	-1.9664220000	1.5214470000	-0.4520090000
C	-0.8489810000	-0.6937330000	-0.1082590000
C	-0.7068020000	0.7821040000	-0.1776320000
C	0.1881800000	-1.4908080000	-0.5092700000
C	0.5330200000	1.3406330000	-0.1645290000
C	1.6150150000	-0.9945730000	-0.5284500000
C	1.8060740000	0.5402570000	-0.2816600000
C	2.1123360000	-0.5979070000	1.8159890000
C	3.8863940000	-1.3320390000	0.4321030000
C	2.4201620000	-1.6262550000	0.7114360000
C	2.7141420000	0.5769140000	1.0220720000
C	4.0646370000	-0.0069990000	0.6276720000
H	-0.6146380000	-4.7549220000	-2.7556410000
H	-2.3648070000	-4.4788540000	-2.4621910000
H	-1.3263980000	-5.1923760000	-1.1837800000
H	-0.1515040000	5.0812960000	2.0177990000
H	-0.0722410000	5.3325870000	0.2431740000
H	1.4284110000	5.0560670000	1.1618310000
H	4.9285150000	-3.2028600000	0.6083110000
H	5.8215190000	-1.9652930000	-0.3017460000
H	4.4359930000	-2.7979520000	-1.0294480000
H	5.7205370000	2.2410020000	-0.9536330000
H	6.1719680000	0.1858480000	0.2946410000
H	5.4293180000	1.5445160000	1.1678000000

H	-5.2739000000	-2.3690170000	2.4521640000
H	-3.2302940000	-3.8062960000	2.4031830000
H	-5.2494990000	-0.1738390000	1.3493820000
H	-1.2127500000	-3.0174560000	1.2440950000
H	-5.2987670000	3.3541010000	-1.3592510000
H	-3.1022080000	4.3225190000	-2.0557770000
H	-5.3585980000	1.1875240000	-0.2001610000
H	-1.0282400000	3.1291490000	-1.5538900000
H	2.1727510000	-2.6714220000	0.8888100000
H	2.7453130000	1.5571490000	1.5043750000
H	2.1026290000	-1.3099500000	-1.4548680000
H	2.3722450000	1.0046170000	-1.0943900000
H	2.6574030000	-0.8051630000	2.7417950000
H	1.0459690000	-0.4852440000	2.0372920000

Electronic energy = -1496.429230 Hartree
Electronic energy + thermal free energy correction = -1496.490633 Hartree

S4 equilibrium geometry (A)

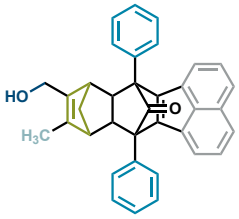

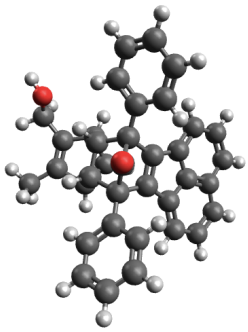

O	-4.2389180000	-2.6648340000	-0.9771710000
O	-0.1571450000	-0.5710770000	2.9533360000
C	1.1866550000	4.6232440000	-1.9334660000
C	-0.1412330000	4.6013090000	-1.5376540000
C	0.0852370000	2.4085800000	-0.5462250000
C	-0.7145690000	3.4981710000	-0.8387550000
C	3.4156070000	3.3634560000	-1.9867270000
C	2.0367210000	3.5123380000	-1.6463600000
C	4.0951930000	2.2069250000	-1.6389420000
C	1.4490380000	2.4439060000	-0.9614780000
C	3.4706780000	1.1321410000	-0.9396040000
C	2.1361630000	1.2488300000	-0.5965550000

C	1.1261700000	0.4324750000	0.0840210000
C	-0.0695730000	1.1084850000	0.1145460000
C	-0.6647520000	-4.5425500000	-2.2181550000
C	-3.4975560000	-2.9112770000	-2.1890120000
C	4.5338360000	-2.7519880000	2.3465070000
C	4.1205370000	-1.4811130000	2.7589300000
C	3.7801310000	-3.4419090000	1.3960120000
C	2.9675510000	-0.9091870000	2.2219240000
C	2.6221640000	-2.8668880000	0.8621520000
C	2.1992520000	-1.5916730000	1.2629660000
C	-4.4808910000	2.3085060000	2.5703230000
C	-4.7119930000	1.2680240000	1.6693210000
C	-3.1654080000	2.6688300000	2.8795730000
C	-3.6399260000	0.5910720000	1.0779040000
C	-2.0973120000	1.9960560000	2.2867480000
C	-2.3165720000	0.9496080000	1.3745220000
C	-0.1201750000	-0.4490780000	1.7617070000
C	0.9615380000	-0.9324550000	0.7056670000
C	-1.1295710000	0.2492610000	0.7593000000
C	-0.0336180000	-1.8158970000	-0.1403640000
C	-1.4055430000	-1.0377170000	-0.1047190000
C	-0.4240390000	-0.8084950000	-2.3402860000
C	-0.9367550000	-3.0833040000	-2.0270400000
C	0.1681220000	-2.0746540000	-1.6782610000
C	-1.7884750000	-0.9550200000	-1.6269240000
C	-2.1053620000	-2.4064030000	-2.0041530000
H	1.5815720000	5.4850970000	-2.4650530000
H	-0.7745520000	5.4542190000	-1.7643650000
H	-1.7589770000	3.5334220000	-0.5441590000
H	3.9310420000	4.1573580000	-2.5209240000
H	5.1437310000	2.1094540000	-1.9054320000
H	4.0494180000	0.2495870000	-0.6843980000
H	0.0048430000	-4.7103380000	-3.0718540000
H	-1.5772850000	-5.1213450000	-2.3859290000
H	-0.1606570000	-4.9624990000	-1.3371140000
H	-5.1664490000	-2.8874400000	-1.1299560000
H	-3.4963710000	-3.9830700000	-2.4272510000
H	-3.9785700000	-2.3788650000	-3.0250340000
H	5.4315490000	-3.1987280000	2.7640860000
H	4.6941040000	-0.9361190000	3.5033320000
H	4.0893950000	-4.4299390000	1.0664730000
H	2.6542050000	0.0759730000	2.5539770000
H	2.0539290000	-3.4204950000	0.1226130000
H	-5.3145920000	2.8310640000	3.0307310000
H	-5.7292800000	0.9757940000	1.4236960000
H	-2.9707270000	3.4707640000	3.5861780000

H	-3.8470680000	-0.2189230000	0.3863390000
H	-1.0797850000	2.2810830000	2.5380350000
H	1.1804860000	-2.3657390000	-1.9699450000
H	-2.5642070000	-0.2241230000	-1.8655530000
H	-0.1195550000	-2.7724850000	0.3849180000
H	-2.1647480000	-1.6167960000	0.4248630000
H	-0.5233070000	-0.9340620000	-3.4229060000
H	0.1127410000	0.1147670000	-2.1393450000

Electronic energy = -1538.631335 Hartree
Electronic energy + thermal free energy correction = -1538.691472 Hartree

Decarbonylated S4 equilibrium geometry (B)

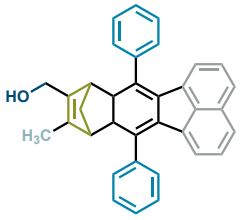

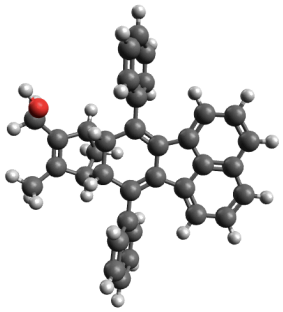

O	4.4732230000	-2.2357870000	-1.2474180000
C	-2.3620740000	4.8381080000	0.0356980000
C	-0.9836030000	4.9703200000	0.0111370000
C	-0.6478150000	2.5743330000	-0.0115140000
C	-0.1083180000	3.8516740000	-0.0164390000
C	-4.3406970000	3.2372070000	0.0162290000
C	-2.9513790000	3.5433160000	0.0253330000
C	-4.7585040000	1.9172980000	-0.0261130000
C	-2.0627400000	2.4451380000	0.0062810000
C	-3.8471760000	0.8279850000	-0.0554360000
C	-2.4857510000	1.0896530000	-0.0332170000
C	-1.2603580000	0.2600980000	-0.0781850000
C	-0.0926760000	1.2021300000	-0.0631560000
C	1.7094230000	-4.9073380000	0.0558720000
C	4.2766410000	-2.9015690000	0.0176650000
C	-4.3459170000	-3.9221480000	-0.2883640000
C	-3.6011470000	-3.6573050000	-1.4410120000
C	-4.0391260000	-3.2510370000	0.8989070000

C	-2.5554190000	-2.7314500000	-1.4045880000
C	-2.9977480000	-2.3204920000	0.9314120000
C	-2.2428580000	-2.0421970000	-0.2205550000
C	4.6485250000	3.3334720000	-0.1198590000
C	3.8681350000	3.1890950000	1.0309390000
C	4.2934260000	2.6445950000	-1.2829800000
C	2.7388290000	2.3672310000	1.0149510000
C	3.1690160000	1.8158630000	-1.2943780000
C	2.3675290000	1.6732200000	-0.1492310000
C	-1.1038120000	-1.0784760000	-0.1834050000
C	1.1837460000	0.7648700000	-0.1574470000
C	0.2759440000	-1.6993640000	-0.2984240000
C	1.5008790000	-0.7126220000	-0.3027080000
C	1.2704230000	-1.6570750000	1.9008410000
C	1.8237790000	-3.4816240000	0.4958780000
C	0.6161710000	-2.6572760000	0.9261830000
C	2.3775070000	-1.2671070000	0.9003350000
C	2.8820320000	-2.6433280000	0.4828450000
H	-2.9967240000	5.7202950000	0.0542840000
H	-0.5476500000	5.9657550000	0.0099600000
H	0.9609630000	4.0196950000	-0.0433840000
H	-5.0708990000	4.0421300000	0.0341870000
H	-5.8230750000	1.6996190000	-0.0411230000
H	-4.2339240000	-0.1825710000	-0.0974920000
H	1.3274210000	-5.5408560000	0.8668730000
H	2.6649960000	-5.3203810000	-0.2787560000
H	0.9953450000	-4.9993850000	-0.7736870000
H	5.4186150000	-2.2191160000	-1.4456270000
H	4.4564250000	-3.9797610000	-0.0892590000
H	4.9947750000	-2.5095600000	0.7538790000
H	-5.1570200000	-4.6440660000	-0.3149930000
H	-3.8346420000	-4.1693170000	-2.3703910000
H	-4.6100710000	-3.4510450000	1.8014410000
H	-1.9864690000	-2.5264540000	-2.3075680000
H	-2.7671880000	-1.7970270000	1.8549940000
H	5.5250400000	3.9749940000	-0.1097360000
H	4.1372590000	3.7159570000	1.9423220000
H	4.8919310000	2.7508920000	-2.1834890000
H	2.1324630000	2.2621760000	1.9101790000
H	2.9034840000	1.2827670000	-2.2028130000
H	-0.2418970000	-3.2299880000	1.2834360000
H	3.1449120000	-0.5675430000	1.2363600000
H	0.2780470000	-2.3053320000	-1.2129830000
H	2.0850820000	-0.8319290000	-1.2209850000
H	1.6623450000	-2.1397430000	2.8013650000
H	0.6153680000	-0.8251160000	2.1813670000

Electronic energy = -1425.342193 Hartree
Electronic energy + thermal free energy correction = -1425.402380 Hartree

S5 equilibrium geometry (A)

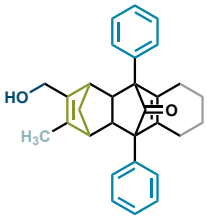

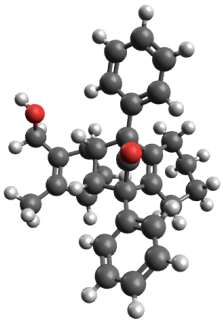

O	-3.0427680000	3.3503130000	-1.0078870000
O	0.3394040000	-1.5176490000	-2.1988140000
C	1.9493320000	-1.4523720000	2.1030010000
C	1.3047330000	-2.5128320000	3.0145520000
C	-0.1311350000	-2.1238210000	3.4035230000
C	-1.0456000000	-1.9806270000	2.1696810000
C	-2.3383650000	4.0424620000	0.0415690000
C	0.8742480000	4.6394850000	-0.0667520000
C	5.4269970000	-0.6068930000	-1.6657870000
C	4.6031510000	-1.7324960000	-1.5692220000
C	4.9212220000	0.6431850000	-1.3065250000
C	3.2900800000	-1.6054070000	-1.1157390000
C	3.6034280000	0.7667520000	-0.8547010000
C	2.7663740000	-0.3533550000	-0.7481420000
C	-4.7081780000	-2.5185830000	-1.4683460000
C	-4.6540810000	-1.1455710000	-1.2243600000
C	-3.5515970000	-3.2886010000	-1.3111590000
C	-3.4568400000	-0.5440880000	-0.8220660000
C	-2.3596310000	-2.6876410000	-0.9072060000
C	-2.2922250000	-1.3071680000	-0.6500970000
C	0.2517970000	-0.9543210000	-1.1410130000
C	0.9987920000	-1.0479750000	1.0124970000
C	-0.3304970000	-1.2910820000	1.0396250000
C	1.3434530000	-0.2589780000	-0.2543810000
C	-0.9820860000	-0.6988720000	-0.2116440000
C	0.6699100000	1.1653390000	-0.2416050000

C	-0.8779420000	0.8705930000	-0.2145470000
C	-0.1947040000	1.7009620000	1.9901870000
C	0.1301320000	3.4486480000	0.4510080000
C	0.8416280000	2.1811470000	0.9477240000
C	-1.3718070000	1.7546410000	0.9892510000
C	-1.1954050000	3.1919700000	0.4866630000
H	2.2303710000	-0.5660200000	2.6953160000
H	2.8863320000	-1.8283820000	1.6764060000
H	1.9158430000	-2.6539410000	3.9135270000
H	1.2890080000	-3.4765990000	2.4877240000
H	-0.1041990000	-1.1704180000	3.9486950000
H	-0.5535380000	-2.8633580000	4.0934690000
H	-1.3965980000	-2.9684110000	1.8402760000
H	-1.9560590000	-1.4251950000	2.4320000000
H	0.2076270000	5.4172520000	-0.4495390000
H	-3.8432000000	3.8458200000	-1.2246090000
H	-1.9835290000	5.0194580000	-0.3122190000
H	-3.0231170000	4.2171680000	0.8869970000
H	1.5512680000	4.3494990000	-0.8817030000
H	1.5001090000	5.0854250000	0.7173240000
H	6.4493190000	-0.7041530000	-2.0196930000
H	4.9810210000	-2.7104830000	-1.8539020000
H	5.5493100000	1.5269480000	-1.3773740000
H	2.6576010000	-2.4859700000	-1.0588280000
H	3.2329720000	1.7485810000	-0.5807540000
H	-5.6378270000	-2.9840980000	-1.7832210000
H	-5.5436510000	-0.5343460000	-1.3498590000
H	-3.5757740000	-4.3564370000	-1.5100610000
H	-3.4387760000	0.5273740000	-0.6527470000
H	-1.4647110000	-3.2943370000	-0.8036400000
H	1.8686760000	2.3250990000	1.2930320000
H	-2.3664340000	1.5065630000	1.3663820000
H	0.9573960000	1.6533150000	-1.1786070000
H	-1.3593920000	1.2201390000	-1.1304210000
H	-0.3190950000	2.4297200000	2.7973530000
H	0.0048720000	0.7214690000	2.4163660000

Electronic energy = -1311.203603 Hartree
Electronic energy + thermal free energy correction = -1311.259967 Hartree

Decarbonylated S5 equilibrium geometry (B)

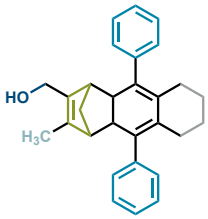

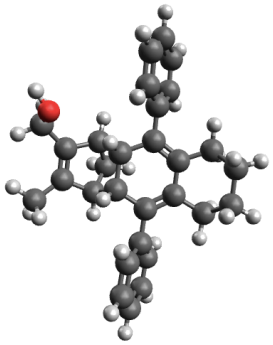

O	-2.3652660000	3.5367240000	-1.3877710000
C	1.7092650000	-3.0026660000	0.2825580000
C	1.1974370000	-4.0531190000	-0.7256310000
C	-0.3511560000	-4.1765150000	-0.7199300000
C	-1.0160110000	-3.2349910000	0.3064940000
C	0.9680040000	-1.6874130000	0.1373220000
C	-0.5118940000	-1.8117560000	0.1558770000
C	-1.8399350000	4.0377390000	-0.1398160000
C	1.4077850000	4.2614890000	-0.1116830000
C	5.8697230000	0.0184700000	-0.2264810000
C	5.0789760000	0.2999860000	-1.3443890000
C	5.2615090000	-0.4379940000	0.9456660000
C	3.6941690000	0.1288460000	-1.2877280000
C	3.8761940000	-0.6125680000	0.9973940000
C	3.0663330000	-0.3398750000	-0.1192960000
C	-5.6359440000	-0.9517580000	-0.0340460000
C	-4.9137850000	-1.3533230000	1.0926770000
C	-4.9482440000	-0.4823270000	-1.1569880000
C	-3.5181460000	-1.2908790000	1.0918180000
C	-3.5537200000	-0.4147830000	-1.1524590000
C	-2.8100060000	-0.8301560000	-0.0328450000
C	1.5813020000	-0.4964140000	-0.0659760000
C	-1.3190840000	-0.7384520000	-0.0308510000
C	0.7979890000	0.7865400000	-0.2669570000
C	-0.7660790000	0.6551290000	-0.2659100000
C	-0.0512600000	1.4341600000	1.8976680000
C	0.5148100000	3.1713760000	0.3923600000
C	1.0525700000	1.8391380000	0.8996660000
C	-1.1851050000	1.6725610000	0.8797130000
C	-0.8318590000	3.0690360000	0.3828610000
H	2.7836910000	-2.8629730000	0.1529330000
H	1.5683770000	-3.3891410000	1.3027380000

H	1.5458950000	-3.7707770000	-1.7257340000
H	1.6634810000	-5.0188690000	-0.4981530000
H	-0.7484090000	-3.9375760000	-1.7131310000
H	-0.6561250000	-5.2074160000	-0.5058530000
H	-0.7952010000	-3.5986260000	1.3209660000
H	-2.1001780000	-3.2799490000	0.1934420000
H	0.8473750000	5.1193250000	-0.4937230000
H	-3.1570600000	4.0416850000	-1.6145780000
H	-1.3856200000	5.0262850000	-0.2907910000
H	-2.6612870000	4.1491490000	0.5843050000
H	2.0485300000	3.8914060000	-0.9235200000
H	2.0815940000	4.6166660000	0.6788330000
H	6.9465540000	0.1543230000	-0.2685680000
H	5.5405420000	0.6504360000	-2.2635600000
H	5.8639980000	-0.6553040000	1.8234740000
H	3.0932040000	0.3429080000	-2.1674970000
H	3.4103080000	-0.9592520000	1.9155490000
H	-6.7211020000	-1.0008290000	-0.0362840000
H	-5.4355560000	-1.7120010000	1.9758310000
H	-5.4979470000	-0.1675340000	-2.0398700000
H	-2.9652870000	-1.5942520000	1.9763580000
H	-3.0355520000	-0.0445670000	-2.0321190000
H	2.0840110000	1.8517220000	1.2581900000
H	-2.2133120000	1.5407570000	1.2222580000
H	1.1374290000	1.2362150000	-1.2074600000
H	-1.1809400000	1.0271110000	-1.2073250000
H	-0.1071900000	2.1045520000	2.7610070000
H	0.0248780000	0.3958390000	2.2379200000

Electronic energy = -1197.895821 Hartree
Electronic energy + thermal free energy correction = -1197.953127 Hartree

S6 equilibrium geometry (A)

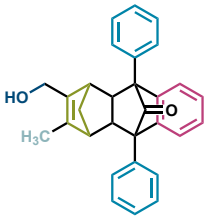

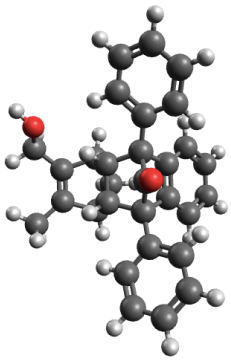

O	-2.9683590000	3.3085780000	-1.0696050000
O	0.3133670000	-1.6030650000	-2.1051890000
C	-0.1440760000	-2.2926160000	3.3154160000
C	1.2361240000	-2.0604300000	3.2799870000
C	-0.9629020000	-1.9068970000	2.2452640000
C	1.8280960000	-1.4357670000	2.1737890000
C	0.9668020000	4.5673980000	-0.1714760000
C	-2.2548520000	4.0269650000	-0.0435890000
C	5.4308330000	-0.8043850000	-1.5830080000
C	4.6049820000	-1.9168050000	-1.3934190000
C	4.9312150000	0.4715490000	-1.3196390000
C	3.2954800000	-1.7509370000	-0.9432320000
C	3.6162110000	0.6345010000	-0.8717510000
C	2.7778810000	-0.4719060000	-0.6741390000
C	-4.7546600000	-2.5051720000	-1.3504570000
C	-4.6582490000	-1.1220250000	-1.1926680000
C	-3.6303940000	-3.3024020000	-1.1141400000
C	-3.4500620000	-0.5360360000	-0.8001460000
C	-2.4275030000	-2.7176800000	-0.7190990000
C	-2.3176550000	-1.3261680000	-0.5527710000
C	0.2419850000	-1.0358660000	-1.0496070000
C	1.0129860000	-1.0405880000	1.1174060000
C	-0.3772630000	-1.2762150000	1.1515830000
C	1.3564770000	-0.3355250000	-0.1865620000
C	-0.9954610000	-0.7343120000	-0.1290430000
C	0.7026740000	1.0967680000	-0.2257920000
C	-0.8525080000	0.8309450000	-0.1870800000
C	-0.1476830000	1.7190110000	1.9884480000
C	0.2039140000	3.4072420000	0.3872170000
C	0.8943720000	2.1471490000	0.9292430000
C	-1.3265900000	1.7607120000	0.9886950000
C	-1.1261470000	3.1747020000	0.4333750000
H	-0.5848470000	-2.7825630000	4.1789390000
H	1.8557720000	-2.3724610000	4.1158280000
H	-2.0316160000	-2.0976250000	2.2686180000
H	2.8999770000	-1.2646960000	2.1416230000
H	1.6000300000	5.0295690000	0.5970920000
H	0.3125310000	5.3422810000	-0.5804780000
H	1.6389480000	4.2394940000	-0.9760000000
H	-3.7614350000	3.8076700000	-1.3044230000
H	-1.8844150000	4.9848940000	-0.4316600000
H	-2.9382070000	4.2420730000	0.7934120000
H	6.4508090000	-0.9323980000	-1.9338160000
H	4.9789840000	-2.9152980000	-1.6012830000
H	5.5615070000	1.3449430000	-1.4621110000
H	2.6638600000	-2.6231100000	-0.8062620000

H	3.2506250000	1.6359390000	-0.6726820000
H	-5.6927380000	-2.9584550000	-1.6580290000
H	-5.5230020000	-0.4907090000	-1.3775350000
H	-3.6882650000	-4.3796480000	-1.2422750000
H	-3.3999760000	0.5427010000	-0.6959470000
H	-1.5604990000	-3.3476540000	-0.5439380000
H	1.9248420000	2.2824720000	1.2671690000
H	-2.3239600000	1.5401350000	1.3750260000
H	0.9956470000	1.5441420000	-1.1805970000
H	-1.3258040000	1.1578580000	-1.1148000000
H	-0.2582080000	2.4791100000	2.7679690000
H	0.0352270000	0.7559700000	2.4576790000

Electronic energy = -1308.848593 Hartree
Electronic energy + thermal free energy correction = -1308.903937 Hartree

Decarbonylated S6 equilibrium geometry (B)

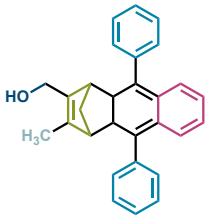

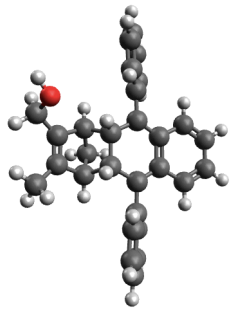

O	-2.3406370000	3.5635580000	-1.2056990000
C	1.4329420000	4.1785840000	0.1071840000
C	0.5387220000	3.0564260000	0.5322850000
C	1.7389910000	-3.0260620000	-0.1103640000
C	1.1464260000	-4.2445060000	-0.0644410000
C	-0.2948220000	-4.3605530000	-0.0566430000
C	-1.0750270000	-3.2521720000	-0.0902850000
C	-1.8150560000	3.9691300000	0.0761830000
C	5.8706970000	-0.0222360000	-0.2478330000
C	5.0986870000	0.3727170000	-1.3441650000
C	5.2445200000	-0.6051270000	0.8571480000
C	3.7144420000	0.1897510000	-1.3327130000
C	3.8604840000	-0.7930740000	0.8638250000
C	3.0687730000	-0.4045410000	-0.2326400000

C	-5.6333110000	-0.9468200000	-0.0798350000
C	-4.9716030000	-0.3788420000	-1.1723310000
C	-4.8848620000	-1.4701220000	0.9779260000
C	-3.5768070000	-0.3332560000	-1.2063830000
C	-3.4894350000	-1.4319380000	0.9383040000
C	-2.8072490000	-0.8708390000	-0.1578310000
C	0.9709330000	-1.7845610000	-0.1324190000
C	-0.5169150000	-1.9034670000	-0.1174460000
C	1.5860390000	-0.5641810000	-0.2193230000
C	-1.3189270000	-0.7944950000	-0.1899640000
C	0.8071340000	0.7278200000	-0.3172260000
C	-0.7571420000	0.6041000000	-0.3183490000
C	-0.0275490000	1.2069230000	1.8968250000
C	1.0729590000	1.6879390000	0.9302690000
C	-1.1662040000	1.5328490000	0.9096820000
C	-0.8089490000	2.9606220000	0.5223870000
H	-2.1523620000	-3.3584620000	-0.1261720000
H	-0.7501750000	-5.3468360000	-0.0525100000
H	1.7537500000	-5.1452790000	-0.0619180000
H	2.8192120000	-2.9574990000	-0.1562620000
H	2.1159620000	4.4670220000	0.9165830000
H	0.8737090000	5.0663600000	-0.2007770000
H	2.0639830000	3.8704660000	-0.7374920000
H	-3.1255620000	4.0924290000	-1.3995920000
H	-1.3583440000	4.9650290000	0.0000840000
H	-2.6359660000	4.0271620000	0.8068610000
H	6.9470170000	0.1232180000	-0.2546480000
H	5.5744640000	0.8207620000	-2.2122060000
H	5.8322000000	-0.9112780000	1.7182650000
H	3.1290940000	0.4916050000	-2.1969380000
H	3.3805720000	-1.2390270000	1.7302690000
H	-6.7187030000	-0.9782280000	-0.0519250000
H	-5.5418410000	0.0301000000	-2.0019070000
H	-5.3860160000	-1.9057270000	1.8380230000
H	-3.0794880000	0.1138750000	-2.0617930000
H	-2.9158400000	-1.8308730000	1.7699010000
H	2.1062360000	1.6661440000	1.2818180000
H	-2.1928570000	1.3771650000	1.2454820000
H	1.1470570000	1.2504620000	-1.2190860000
H	-1.1783230000	1.0533300000	-1.2226700000
H	-0.0759260000	1.8053480000	2.8118270000
H	0.0459020000	0.1438720000	2.1514270000

Electronic energy = -1195.509961 Hartree
Electronic energy + thermal free energy correction = -1195.565562 Hartree

S7 equilibrium geometry (A)

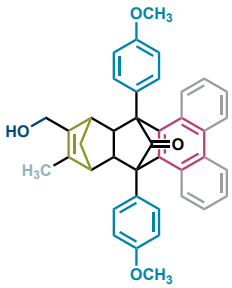

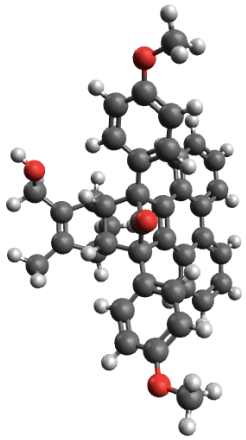

O	-6.3866430000	-1.1524360000	-2.6353060000
O	6.2099790000	-0.4953620000	-2.9169100000
O	2.6473270000	-4.1148080000	1.8439170000
O	-0.0726580000	-0.9264630000	-2.4413330000
C	6.4850100000	0.3181250000	-4.0499400000
C	-6.7731670000	-0.4181250000	-3.7903050000
C	1.8535380000	-3.9006850000	3.0280000000
C	-1.4089130000	-4.1149070000	3.0503440000
C	-5.1396550000	-0.9400230000	-2.1143610000
C	-4.2053070000	-0.0321890000	-2.6293860000
C	-4.8069480000	-1.7020540000	-0.9869280000
C	-2.9590950000	0.1009930000	-2.0129740000
C	-3.5581390000	-1.5561400000	-0.3883720000
C	-2.6082920000	-0.6460400000	-0.8809660000
C	-3.1070570000	4.1394010000	1.7979330000
C	-1.7309660000	4.2370580000	1.6999510000
C	-3.7530480000	2.9474030000	1.4242490000
C	-0.9374970000	3.1667020000	1.2179970000
C	-3.0132340000	1.8889790000	0.9316020000
C	-1.6029070000	1.9719590000	0.7925320000
C	2.6022050000	4.4135170000	1.7183650000
C	1.2207400000	4.3781600000	1.6624560000
C	3.3491550000	3.2913870000	1.3169830000
C	0.5204170000	3.2381040000	1.1960500000
C	2.7007490000	2.1684290000	0.8388620000
C	1.2854200000	2.1160030000	0.7423880000
C	4.9727190000	-0.4098710000	-2.3374050000

C	4.7493800000	-1.2491050000	-1.2384040000
C	3.9485730000	0.4418800000	-2.7709950000
C	3.5210790000	-1.2355170000	-0.5817100000
C	2.7241720000	0.4443190000	-2.0990620000
C	2.4849410000	-0.3791530000	-0.9915440000
C	-0.0615680000	-0.6364570000	-1.2755020000
C	-0.8026560000	0.8987270000	0.2614990000
C	0.5781770000	0.9699480000	0.2328300000
C	-1.2403580000	-0.4760290000	-0.2625630000
C	1.1342560000	-0.3506960000	-0.3148120000
C	-0.7553690000	-1.6127390000	0.7190160000
C	0.8180360000	-1.5254830000	0.6857630000
C	0.0215220000	-0.6618940000	2.8420640000
C	-0.5199850000	-2.9489610000	2.7496180000
C	-1.0638420000	-1.5980840000	2.2612620000
C	1.1870940000	-1.4608170000	2.2133020000
C	0.8277530000	-2.8586080000	2.7287480000
H	-0.8461050000	-5.0158560000	3.3099230000
H	5.8066100000	0.0892970000	-4.8815080000
H	7.5089430000	0.0830750000	-4.3436120000
H	6.4134160000	1.3854310000	-3.8044330000
H	-6.1124940000	-0.6317840000	-4.6398580000
H	-6.7792220000	0.6617630000	-3.5951990000
H	-7.7854550000	-0.7480790000	-4.0272210000
H	3.3835100000	-4.6999980000	2.0647700000
H	1.3780230000	-4.8376480000	3.3465900000
H	2.5054600000	-3.5562650000	3.8466590000
H	-2.0417390000	-4.3545660000	2.1850610000
H	-2.0885120000	-3.8882580000	3.8822590000
H	-4.4280690000	0.5673180000	-3.5039650000
H	-5.5366430000	-2.4040990000	-0.5963280000
H	-2.2489320000	0.8084650000	-2.4291560000
H	-3.3341650000	-2.1569010000	0.4865730000
H	-3.6829560000	4.9797670000	2.1746470000
H	-1.2591530000	5.1601730000	2.0139500000
H	-4.8311470000	2.8556890000	1.5185030000
H	-3.5209180000	0.9802150000	0.6405920000
H	3.1053050000	5.3037400000	2.0847310000
H	0.6718420000	5.2490830000	1.9994190000
H	4.4333550000	3.3040100000	1.3795200000
H	3.2835930000	1.3128460000	0.5275550000
H	5.5471520000	-1.9106030000	-0.9159530000
H	4.0849680000	1.0969080000	-3.6232430000
H	3.3798570000	-1.9057380000	0.2599110000
H	1.9422980000	1.1108030000	-2.4504340000
H	-2.1026860000	-1.3848010000	2.5255830000

H	2.2034320000	-1.1239510000	2.4284450000
H	-1.0978080000	-2.5577570000	0.2866140000
H	1.2470330000	-2.4313350000	0.2536780000
H	0.0472380000	-0.7121060000	3.9348650000
H	-0.0516610000	0.3786010000	2.5386320000

Electronic energy = -1845.040391 Hartree
Electronic energy + thermal free energy correction = -1845.108955 Hartree

Decarbonylated S7 equilibrium geometry (B)

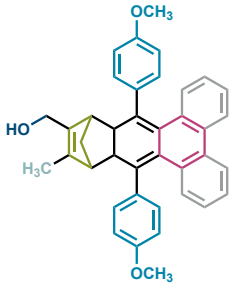

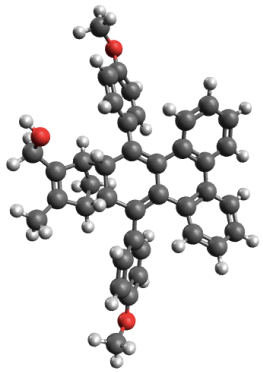

O	-6.9864600000	-0.9310970000	0.9227490000
O	6.8823480000	-0.3802250000	1.1003210000
O	2.2587270000	-4.3746400000	-1.6105560000
C	7.8361930000	-1.0532750000	0.2898810000
C	-7.8821350000	-1.5879990000	0.0356000000
C	1.6741640000	-4.8500750000	-0.3779660000
C	-1.5827740000	-4.9064680000	-0.3643090000
C	-5.6866780000	-0.7611500000	0.5305480000
C	-5.1598280000	-1.1947310000	-0.6913710000
C	-4.8501790000	-0.1053780000	1.4475430000
C	-3.8079750000	-0.9689480000	-0.9800320000
C	-3.5149440000	0.1196070000	1.1387600000
C	-2.9616160000	-0.2976860000	-0.0883480000
C	-3.0004350000	4.7668590000	0.0331880000
C	-3.6208550000	3.6803890000	-0.5892370000
C	-1.6415440000	4.6977100000	0.3160710000
C	-2.9024220000	2.5086740000	-0.8006520000
C	-0.8850290000	3.5394820000	0.0471720000
C	-1.5564230000	2.3719080000	-0.4032810000

C	2.6217390000	4.9346540000	-0.2124490000
C	3.2714820000	3.8579370000	-0.8227490000
C	1.2891300000	4.8003830000	0.1586740000
C	2.6122800000	2.6402620000	-0.9458700000
C	0.5912220000	3.5870270000	-0.0082810000
C	1.3012480000	2.4476830000	-0.4645200000
C	5.5821400000	-0.3325000000	0.6751190000
C	5.1086930000	-0.9123600000	-0.5074360000
C	4.6869360000	0.3476250000	1.5153770000
C	3.7524200000	-0.8039590000	-0.8374400000
C	3.3477700000	0.4575270000	1.1650660000
C	2.8479530000	-0.1040870000	-0.0274790000
C	-0.8427490000	1.0645670000	-0.4502080000
C	0.6584040000	1.1061570000	-0.4519980000
C	-1.5033910000	-0.1308670000	-0.3715280000
C	1.3905130000	-0.0453280000	-0.3485930000
C	-0.7930130000	-1.4632840000	-0.5334760000
C	0.7703100000	-1.4178790000	-0.5296980000
C	0.0121300000	-2.1464330000	1.6325030000
C	-0.6358300000	-3.8586280000	0.1308460000
C	-1.1066150000	-2.4984000000	0.6320340000
C	1.1353270000	-2.4472240000	0.6205550000
C	0.7134340000	-3.8260300000	0.1271260000
H	7.9183850000	-0.5896310000	-0.7014870000
H	7.5864480000	-2.1159130000	0.1750020000
H	8.7893470000	-0.9608350000	0.8121950000
H	-7.9835360000	-1.0399530000	-0.9098150000
H	-8.8456630000	-1.6085320000	0.5463730000
H	-7.5587790000	-2.6160730000	-0.1719080000
H	-1.0666500000	-5.7960530000	-0.7361550000
H	2.9854560000	-4.9636080000	-1.8523880000
H	1.1654300000	-5.8086510000	-0.5464660000
H	2.4709090000	-5.0138150000	0.3636850000
H	-2.2026220000	-4.5128940000	-1.1813560000
H	-2.2749990000	-5.2183050000	0.4285230000
H	-5.7784810000	-1.7041310000	-1.4209520000
H	-5.2681810000	0.2180380000	2.3955870000
H	-3.4197720000	-1.3095130000	-1.9363230000
H	-2.8827010000	0.6332590000	1.8566990000
H	-3.5551560000	5.6756700000	0.2480010000
H	-4.6596080000	3.7391790000	-0.9006120000
H	-1.1545320000	5.5790310000	0.7160270000
H	-3.4016050000	1.6797830000	-1.2804360000
H	3.1303940000	5.8845600000	-0.0754530000
H	4.2856010000	3.9630860000	-1.1968330000
H	0.7736800000	5.6725290000	0.5424680000

H	3.1284880000	1.8176950000	-1.4203500000
H	5.7722180000	-1.4509100000	-1.1739340000
H	5.0626850000	0.7813990000	2.4366430000
H	3.4048610000	-1.2743750000	-1.7524660000
H	2.6693350000	0.9916260000	1.8232760000
H	-2.1351940000	-2.4634370000	0.9908120000
H	2.1645160000	-2.3715690000	0.9704650000
H	-1.1503240000	-1.8935020000	-1.4779340000
H	1.1597950000	-1.8164820000	-1.4727940000
H	0.0302920000	-2.8121120000	2.5008690000
H	-0.0112840000	-1.1024360000	1.9660710000

Electronic energy = -1731.699789 Hartree
Electronic energy + thermal free energy correction = -1731.768882 Hartree

Photo-decarbonylation Monitoring by ^{1}H NMR

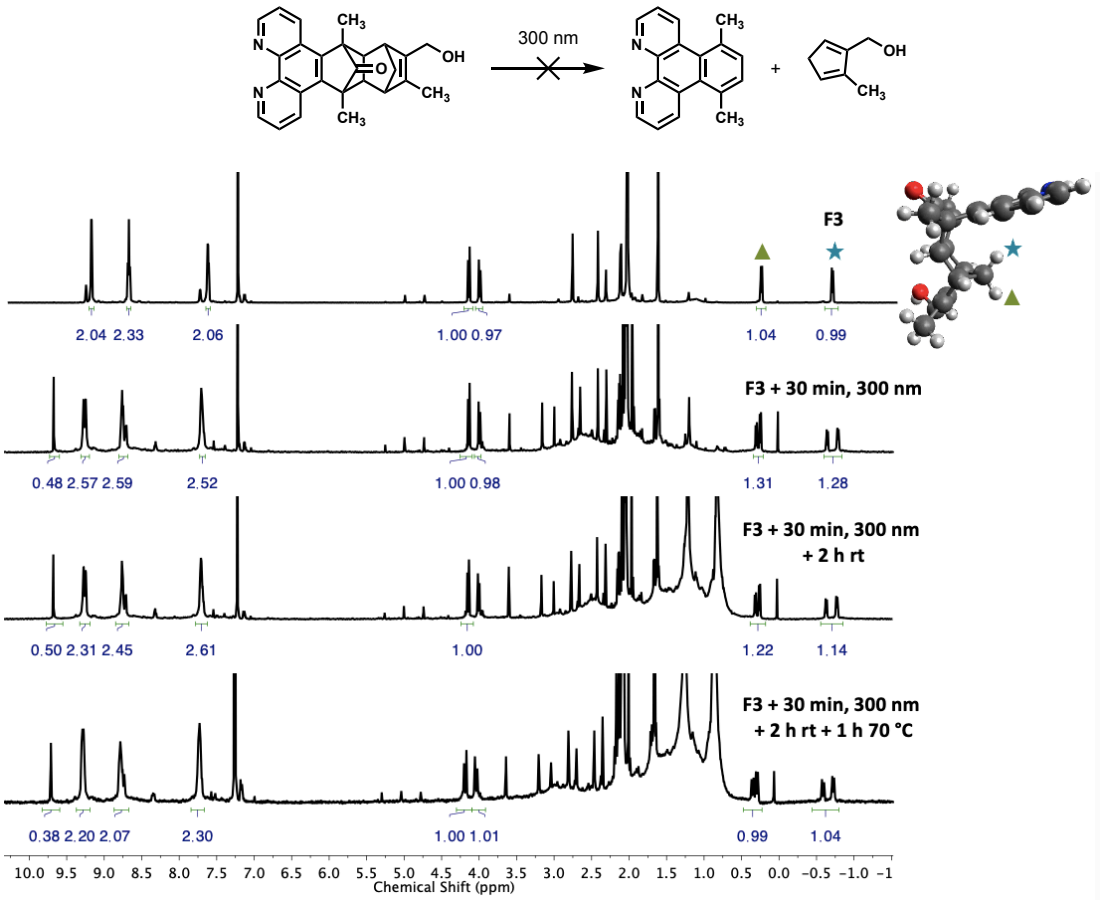

Figure S 4.29. Overlay of ^{1}H NMR spectra upon irradiation of a solution of **F3** prepared in $CDCl_3$ (top) for 30 min in a Rayonet RPR-200 chamber (300 nm). Some decomposition is observed as an increase in broad aliphatic peaks (0.5–3 ppm). Diagnostic alkene Cp peaks are not observed, and more notably, the slight shift and persistence of upfield protons (labeled with star and square symbols at -0.67 and 0.28 ppm, respectively) which are indicative of the proximity of the bridged carbon to the phenanthroline ring[68] suggests that the adduct does not cleave upon irradiation, though decarbonylation might be occurring. Prolonged time to allow for thermal cleavage (2 h) or heating the solution (70 °C, 1 h) after irradiation also do not appear to promote a thermal cleavage event.

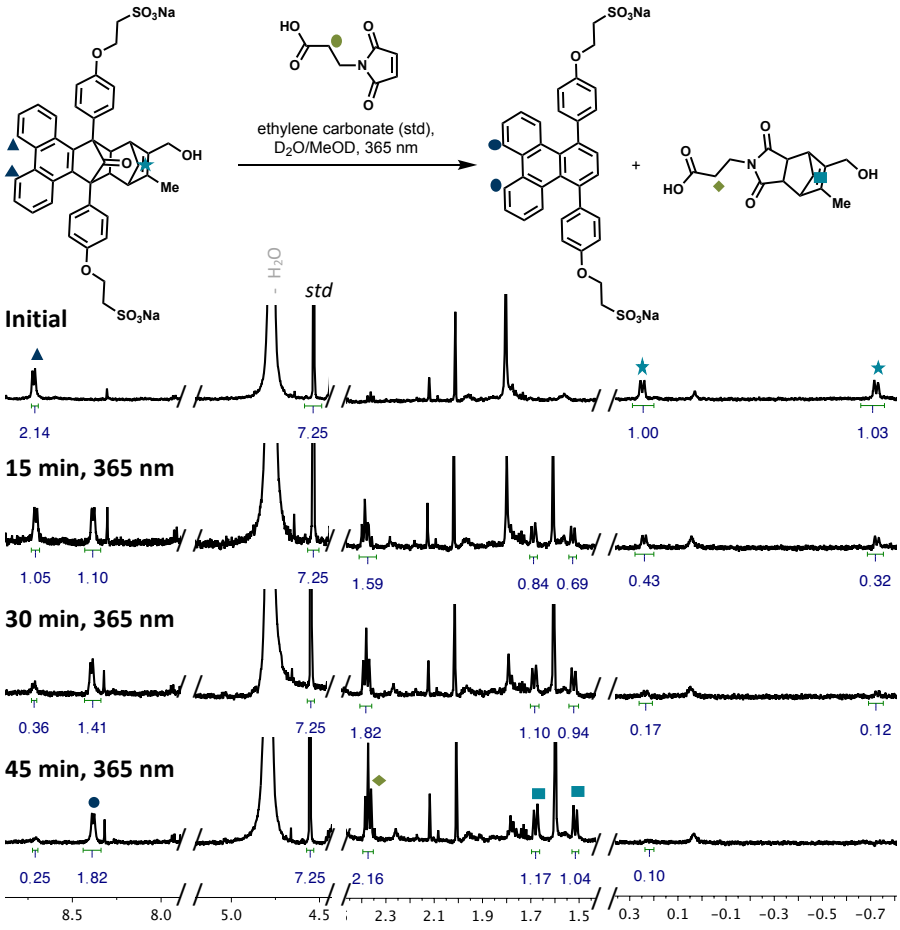

Figure S 4.30. Overlay of ^{1}H NMR spectra upon irradiation of a 3.3 mM solution of **FS1** prepared in a mixture of methanol-D_4 and D_2O (1:2) containing 3-maleimidopropionic acid (2 eq) and spiked with ethylene carbonate as an internal standard (top). The solution was irradiated inside of the NMR tube with a 365 nm light and monitored periodically over 45 min. Near complete cleavage of the adduct (approx. 90% consumption of **FS1** relative to integration of ethylene carbonate internal standard at 4.55 ppm) is confirmed by disappearance of upfield protons (-0.74 and 0.23 ppm) indicated with stars. Appearance of diagnostic peaks corresponding to the substituted benzene byproduct (circle) and maleimide–cyclopentadiene adduct (diamond and square) are also observed. Integration against the ethylene carbonate internal standard indicates quantitative formation of the maleimide–cyclopentadiene species from the cleaved **FS1** adduct.

UV Vis Spectroscopy and Solubility Determination

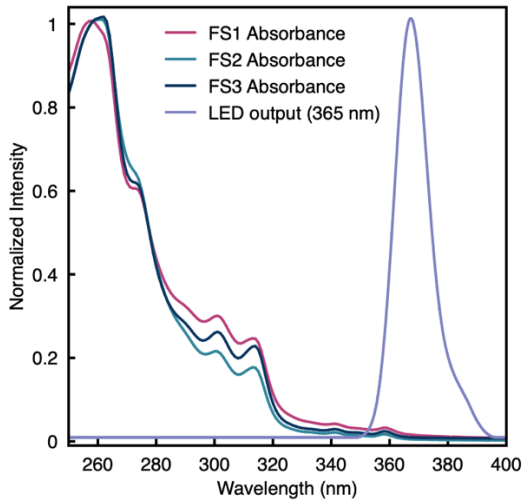

Figure S 4.31. Normalized plots of UV vis absorbance of **FS1**, **FS2**, and **FS3** dissolved in DI water and output spectra of light source used for patterning (collimated 365 nm LED purchased from Thorlabs Product No. M365L2-C1, 6 mW/cm^2).

Stock solutions (1 mM) of each compound were prepared in triplicate by dissolving approximately 0.005 mmol of **FS1**, **FS2**, or **FS3** in 5 mL DI water. To obtain concentration calibrations curves, solutions of known concentration were prepared by diluting each stock solution by 50x, 100x, 200x and 500x. The UV vis spectra of these solutions were collected and absorbance at 300 nm was plotted against concentration (**Figure S32**). To determine the absolute water solubility for each compound, triplicate saturated solutions were prepared in DI water and passed through a 0.2 μm syringe filter before diluting 500x (for **FS1**) or 2500x (for **FS2** and **FS3**) with DI water. The absorbance spectra of these diluted solutions were measured, and the concentration of dissolved compound in each saturated solution was determined using the prepared calibration curves and Beer-Lambert Law.

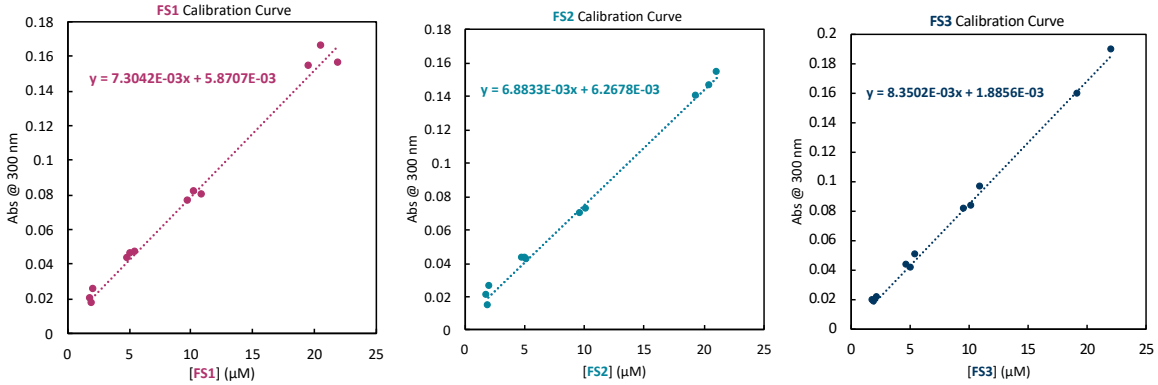

Figure S 4.32. Calibration curves of **FS1**, FS2 and **FS3** dissolved in DI water at known concentrations (2–20 μM).

Table S 4.2. Table of ε, b and A values at 300 nm determined from **Figure S4.32** and calculated concentrations of unknown solutions.

Compound	$\varepsilon_{300\ nm}$	$b_{300\ nm}$	Average Unknown Abs @ 300 nm (n=3)	Unknown Concentration (μM)	Saturated Concentration (mM)
FS1	7300	0.006	0.20 ± 0.06	27 (500x dilution)	**13**
FS2	6900	0.006	0.25 ± 0.04	35 (2500x dilution)	**90**
FS3	8400	0.002	0.19 ± 0.02	22 (2500x dilution)	**56**

4.7 References

(1) Drury, J. L.; Mooney, D. J. Hydrogels for Tissue Engineering: Scaffold Design Variables and Applications. *Biomaterials* **2003**, *24* (24), 4337–4351. DOI: 10.1016/S0142-9612(03)00340-5.

(2) Hoffman, A. S. Hydrogels for Biomedical Applications. *Adv. Drug Deliv. Rev.* **2012**, *64*, 18–23. DOI: 10.1016/j.addr.2012.09.010.

(3) Slaughter, B. V.; Khurshid, S. S.; Fisher, O. Z.; Khademhosseini, A.; Peppas, N. A. Hydrogels in Regenerative Medicine. *Adv. Mater.* **2009**, *21* (32–33), 3307–3329. DOI: 10.1002/adma.200802106.

(4) Tibbitt, M. W.; Anseth, K. S. Hydrogels as Extracellular Matrix Mimics for 3D Cell Culture. *Biotechnol. Bioeng.* **2009**, *103* (4), 655–663. DOI: 10.1002/bit.22361.

(5) Lutolf, M. P.; Hubbell, J. A. Synthetic Biomaterials as Instructive Extracellular Microenvironments for Morphogenesis in Tissue Engineering. *Nat. Biotechnol.* **2005**, *23* (1), 47–55. DOI: 10.1038/nbt1055.

(6) Grim, J. C.; Marozas, I. A.; Anseth, K. S. Thiol-Ene and Photo-Cleavage Chemistry for Controlled Presentation of Biomolecules in Hydrogels. *J. Control. Release* **2015**, *219*, 95–106. DOI: 10.1016/j.jconrel.2015.08.040.

(7) Brown, T. E.; Anseth, K. S. Spatiotemporal Hydrogel Biomaterials for Regenerative Medicine. *Chem. Soc. Rev.* **2017**, *46* (21), 6532–6552. DOI: 10.1039/C7CS00445A.

(8) Munoz-Robles, B. G.; Kopyeva, I.; DeForest, C. A. Surface Patterning of Hydrogel Biomaterials to Probe and Direct Cell–Matrix Interactions. *Advanced Materials Interfaces* **2020**, *7* (21), 2001198. DOI: 10.1002/admi.202001198.

(9) Murry, C. E.; Keller, G. Differentiation of Embryonic Stem Cells to Clinically Relevant Populations: Lessons from Embryonic Development. *Cell* **2008**, *132* (4), 661–680. DOI: 10.1016/j.cell.2008.02.008.

(10) Keung, A. J.; Kumar, S.; Schaffer, D. V. Presentation Counts: Microenvironmental Regulation of Stem Cells by Biophysical and Material Cues. *Annu. Rev. Cell Dev. Biol.* **2010**, *26* (1), 533–556. DOI: 10.1146/annurev-cellbio-100109-104042.

(11) Fairbanks, B. D.; Macdougall, L. J.; Mavila, S.; Sinha, J.; Kirkpatrick, B. E.; Anseth, K. S.; Bowman, C. N. Photoclick Chemistry: A Bright Idea. *Chem. Rev.* **2021**, *121* (12), 6915–6990. DOI: 10.1021/acs.chemrev.0c01212.

(12) Kumar, G. S.; Lin, Q. Light-Triggered Click Chemistry. *Chem. Rev.* **2020**, *121* (12), 6991–7031. DOI: 10.1021/acs.chemrev.0c00799.

(13) Kolb, H. C.; Finn, M. G.; Sharpless, K. B. Click Chemistry: Diverse Chemical Function from a Few Good Reactions. *Angew. Chem. Int. Ed.* **2001**, *40* (11), 2004–2021. DOI: 10.1002/1521-3773(20010601)40:11<2004::AID-ANIE2004>3.0.CO;2-5.

(14) DeForest, C. A.; Polizzotti, B. D.; Anseth, K. S. Sequential Click Reactions for Synthesizing and Patterning Three-Dimensional Cell Microenvironments. *Nat. Mater.* **2009**, *8* (8), 659–664. DOI: 10.1038/nmat2473.

(15) DeForest, C. A.; Anseth, K. S. Cytocompatible Click-Based Hydrogels with Dynamically Tunable Properties through Orthogonal Photoconjugation and Photocleavage Reactions. *Nat. Chem.* **2011**, *3* (12), 925–931. DOI: 10.1038/nchem.1174.

(16) Bryant, S. J.; Nuttelman, C. R.; Anseth, K. S. Cytocompatibility of UV and Visible Light Photoinitiating Systems on Cultured NIH/3T3 Fibroblasts in Vitro. *J. Biomater. Sci., Polym. Ed.* **2000**, *11* (5), 439–457. DOI: 10.1163/156856200743805.

(17) Williams, C. G.; Malik, A. N.; Kim, T. K.; Manson, P. N.; Elisseeff, J. H. Variable Cytocompatibility of Six Cell Lines with Photoinitiators Used for Polymerizing Hydrogels and Cell Encapsulation. *Biomaterials* **2005**, *26* (11), 1211–1218. DOI: 10.1016/j.biomaterials.2004.04.024.

(18) Dean, R. T.; Fu, S.; Stocker, R.; Davies, M. J. Biochemistry and Pathology of Radical-Mediated Protein Oxidation. *Biochem. J.* **1997**, *324* (1), 1–18. DOI: 10.1042/bj3240001.

(19) Farahani, P. E.; Adelmund, S. M.; Shadish, J. A.; DeForest, C. A. Photomediated Oxime Ligation as a Bioorthogonal Tool for Spatiotemporally-Controlled Hydrogel Formation and Modification. *J. Mater. Chem. B* **2017**, *5* (23), 4435–4442. DOI: 10.1039/C6TB03400D.

(20) Broguiere, N.; Lüchtefeld, I.; Trachsel, L.; Mazunin, D.; Rizzo, R.; Bode, J. W.; Lutolf, M. P.; Zenobi-Wong, M. Morphogenesis Guided by 3D Patterning of Growth Factors in Biological Matrices. *Adv. Mater.* **2020**, *32* (25), 1908299. DOI: 10.1002/adma.201908299.

(21) Batalov, I.; Stevens, K. R.; DeForest, C. A. Photopatterned Biomolecule Immobilization to Guide Three-Dimensional Cell Fate in Natural Protein-Based Hydrogels. *Proc. Natl. Acad. Sci. USA* **2021**, *118* (4), e2014194118. DOI: 10.1073/pnas.2014194118.

(22) Caliari, S. R.; Burdick, J. A. A Practical Guide to Hydrogels for Cell Culture. *Nat. Methods* **2016**, *13* (5), 405–414. DOI: 10.1038/nmeth.3839.

(23) Truong, V. X. Break Up to Make Up: Utilization of Photocleavable Groups in Biolabeling of Hydrogel Scaffolds. *ChemPhotoChem* **2020**, *4* (8), 564–570. DOI: 10.1002/cptc.202000072.

(24) Bao, C.; Zhu, L.; Lin, Q.; Tian, H. Building Biomedical Materials Using Photochemical Bond Cleavage. *Adv. Mater.* **2015**, *27* (10), 1647–1662. DOI: 10.1002/adma.201403783.

(25) Poloukhtine, A. A.; Mbua, N. E.; Wolfert, M. A.; Boons, G.-J.; Popik, V. V. Selective Labeling of Living Cells by a Photo-Triggered Click Reaction. *J. Am. Chem. Soc.* **2009**, *131* (43), 15769–15776. DOI: 10.1021/ja9054096.

(26) Shah, L.; Laughlin, S. T.; Carrico, I. S. Light-Activated Staudinger–Bertozzi Ligation within Living Animals. *J. Am. Chem. Soc.* **2016**, *138* (16), 5186–5189. DOI: 10.1021/jacs.5b13401.

(27) Liu, L.; Zhang, D.; Johnson, M.; Devaraj, N. K. Light-Activated Tetrazines Enable Precision Live-Cell Bioorthogonal Chemistry. *Nat. Chem.* **2022**, *14* (9), 1078–1085. DOI: 10.1038/s41557-022-00963-8.

(28) Mayer, S. V.; Murnauer, A.; Wrisberg, M.; Jokisch, M.; Lang, K. Photo-induced and Rapid Labeling of Tetrazine-Bearing Proteins via Cyclopropenone-Caged Bicyclononynes. *Angew. Chem. Int. Ed.* **2019**, *58* (44), 15876–15882. DOI: 10.1002/anie.201908209.

(29) Kumar, P.; Jiang, T.; Li, S.; Zainul, O.; Laughlin, S. T. Caged Cyclopropenes for Controlling Bioorthogonal Reactivity. *Org. Biomol. Chem.* **2018**, *16* (22), 4081–4085. DOI: 10.1039/C8OB01076E.

(30) Jiang, T.; Kumar, P.; Huang, W.; Kao, W.; Thompson, A. O.; Camarda, F. M.; Laughlin, S. T. Modular Enzyme- and Light-Based Activation of Cyclopropene–Tetrazine Ligation. *ChemBioChem* **2019**, *20* (17), 2222–2226. DOI: 10.1002/cbic.201900137.

(31) Christman, K. L.; Broyer, R. M.; Tolstyka, Z. P.; Maynard, H. D. Site-Specific Protein Immobilization through N-Terminal Oxime Linkages. *J. Mater. Chem.* **2007**, *17* (19), 2021. DOI: 10.1039/b618002g.

(32) Pauloehrl, T.; Delaittre, G.; Bruns, M.; Meißler, M.; Börner, H. G.; Bastmeyer, M.; Barner-Kowollik, C. (Bio)Molecular Surface Patterning by Phototriggered Oxime Ligation. *Angew. Chem. Int. Ed.* **2012**, *51* (36), 9181–9184. DOI: 10.1002/anie.201202684.

(33) Park, S.; Yousaf, M. N. An Interfacial Oxime Reaction To Immobilize Ligands and Cells in Patterns and Gradients to Photoactive Surfaces. *Langmuir* **2008**, *24* (12), 6201–6207. DOI: 10.1021/la8005663.

(34) DeForest, C. A.; Tirrell, D. A. A Photoreversible Protein-Patterning Approach for Guiding Stem Cell Fate in Three-Dimensional Gels. *Nat. Mater.* **2015**, *14* (5), 523–531. DOI: 10.1038/nmat4219.

(35) Luo, Y.; Shoichet, M. S. A Photolabile Hydrogel for Guided Three-Dimensional Cell Growth and Migration. *Nat. Mater.* **2004**, *3* (4), 249–253. DOI: 10.1038/nmat1092.

(36) Aizawa, Y.; Wylie, R.; Shoichet, M. Endothelial Cell Guidance in 3D Patterned Scaffolds. *Adv. Mater.* **2010**, *22* (43), 4831–4835. DOI: 10.1002/adma.201001855.

(37) Wylie, R. G.; Ahsan, S.; Aizawa, Y.; Maxwell, K. L.; Morshead, C. M.; Shoichet, M. S. Spatially Controlled Simultaneous Patterning of Multiple Growth Factors in Three-Dimensional Hydrogels. *Nat. Mater.* **2011**, *10* (10), 799–806. DOI: 10.1038/nmat3101.

(38) Mosiewicz, K. A.; Kolb, L.; van der Vlies, A. J.; Martino, M. M.; Lienemann, P. S.; Hubbell, J. A.; Ehrbar, M.; Lutolf, M. P. In Situ Cell Manipulation through Enzymatic

Hydrogel Photopatterning. *Nat. Mater.* **2013**, *12* (11), 1072–1078. DOI: 10.1038/nmat3766.

(39) Bailey, S. J.; Stricker, F.; Hopkins, E.; Wilson, M. Z.; Read de Alaniz, J. Shining Light on Cyclopentadienone–Norbornadiene Diels–Alder Adducts to Enable Photoinduced Click Chemistry with Cyclopentadiene. *ACS Appl. Mater. Interfaces* **2021**, *13* (30), 35422–35430. DOI: 10.1021/acsami.1c08670.

(40) Levandowski, B. J.; Raines, R. T. Click Chemistry with Cyclopentadiene. *Chem. Rev.* **2021**, *121* (12), 6777–6801. DOI: 10.1021/acs.chemrev.0c01055.

(41) Rideout, D. C.; Breslow, R. Hydrophobic Acceleration of Diels-Alder Reactions. *J. Am. Chem. Soc.* **1980**, *102* (26), 7816–7817. DOI: 10.1021/ja00546a048.

(42) St. Amant, A. H.; Lemen, D.; Florinas, S.; Mao, S.; Fazenbaker, C.; Zhong, H.; Wu, H.; Gao, C.; Christie, R. J.; Read de Alaniz, J. Tuning the Diels–Alder Reaction for Bioconjugation to Maleimide Drug-Linkers. *Bioconjugate Chem.* **2018**, *29* (7), 2406–2414. DOI: 10.1021/acs.bioconjchem.8b00320.

(43) Renault, K.; Fredy, J. W.; Renard, P.-Y.; Sabot, C. Covalent Modification of Biomolecules through Maleimide-Based Labeling Strategies. *Bioconjugate Chem.* **2018**, *29* (8), 2497–2513. DOI: 10.1021/acs.bioconjchem.8b00252.

(44) Findlay, D. M.; Roy, M. L.; McLean, S. Thermal Routes to Substituted Cyclopentadienes. *Can. J. Chem.* **1972**, *50* (19), 3186–3195. DOI: 10.1139/v72-508.

(45) St. Amant, A. H.; Discekici, E. H.; Bailey, S. J.; Zayas, M. S.; Song, J.-A.; Shankel, S. L.; Nguyen, S. N.; Bates, M. W.; Anastasaki, A.; Hawker, C. J.; Read de Alaniz, J. Norbornadienes: Robust and Scalable Building Blocks for Cascade "Click" Coupling of High Molecular Weight Polymers. *J. Am. Chem. Soc.* **2019**, *141* (34), 13619–13624. DOI: 10.1021/jacs.9b06328.

(46) Li, P.; Parker, T. M.; Hwang, J.; Deng, F.; Smith, M. D.; Pellechia, P. J.; Sherrill, C. D.; Shimizu, K. D. The CH−π Interactions of Methyl Ethers as a Model for Carbohydrate–*N* -Heteroarene Interactions. *Org. Lett.* **2014**, *16* (19), 5064–5067. DOI: 10.1021/ol502418k.

(47) Guédouar, H.; Aloui, F.; Beltifa, A.; Ben Mansour, H.; Ben Hassine, B. Synthesis and Characterization of Phenanthrene Derivatives with Anticancer Property against Human Colon and Epithelial Cancer Cell Lines. *C. R. Chim.* **2017**, *20* (8), 841–849. DOI: 10.1016/j.crci.2017.03.008.

(48) Based on MilliporeSigma price on September 9, 2022.

(49) Ghosh, A. K.; Brindisi, M. Organic Carbamates in Drug Design and Medicinal Chemistry. *J. Med. Chem.* **2015**, *58* (7), 2895–2940. DOI: 10.1021/jm501371s.

(50) Chen, Q.; Diaz, Y. J.; Hawker, M. C.; Martinez, M. R.; Page, Z. A.; Xiao-An Zhang, S.; Hawker, C. J.; Read de Alaniz, J. Stable Activated Furan and Donor–Acceptor Stenhouse

Adduct Polymer Conjugates as Chemical and Thermal Sensors. *Macromolecules* **2019**, *52* (11), 4370–4375. DOI: 10.1021/acs.macromol.9b00533.

(51) Diaz, Y. J.; Page, Z. A.; Knight, A. S.; Treat, N. J.; Hemmer, J. R.; Hawker, C. J.; Read de Alaniz, J. A Versatile and Highly Selective Colorimetric Sensor for the Detection of Amines. *Chem. Eur. J.* **2017**, *23* (15), 3562–3566. DOI: 10.1002/chem.201700368.

(52) Yam, K. L.; Papadakis, S. E. A Simple Digital Imaging Method for Measuring and Analyzing Color of Food Surfaces. *J. Food Eng.* **2004**, *61* (1), 137–142. DOI: 10.1016/S0260-8774(03)00195-X.

(53) Pedreschi, F.; León, J.; Mery, D.; Moyano, P. Development of a Computer Vision System to Measure the Color of Potato Chips. *Food Res. Int.* **2006**, *39* (10), 1092–1098. DOI: 10.1016/j.foodres.2006.03.009.

(54) Gorka, A. P.; Schnermann, M. J. Harnessing Cyanine Photooxidation: From Slowing Photobleaching to near-IR Uncaging. *Curr. Opin. Chem. Biol.* **2016**, *33*, 117–125. DOI: 10.1016/j.cbpa.2016.05.022.

(55) Li, J.; Wu, C.; Chu, P. K.; Gelinsky, M. 3D Printing of Hydrogels: Rational Design Strategies and Emerging Biomedical Applications. *Mater. Sci. Eng.: R: Rep.* **2020**, *140*, 100543. DOI: 10.1016/j.mser.2020.100543.

(56) Zhu, W.; Ma, X.; Gou, M.; Mei, D.; Zhang, K.; Chen, S. 3D Printing of Functional Biomaterials for Tissue Engineering. *Curr. Opin. Biotechnol.* **2016**, *40*, 103–112. DOI: 10.1016/j.copbio.2016.03.014.

(57) Lee, M.; Rizzo, R.; Surman, F.; Zenobi-Wong, M. Guiding Lights: Tissue Bioprinting Using Photoactivated Materials. *Chem. Rev.* **2020**, *120* (19), 10950–11027. DOI: 10.1021/acs.chemrev.0c00077.

(58) Ting, C.-Y.; Kolbeck, P. T.; Colombo, R.; Chakiath, C.; Rice, M.; Marelli, M.; Christie, R. J. Cyclopentadiene as a Multifunctional Reagent for Normal- and Inverse-Electron Demand Diels–Alder Bioconjugation. *Bioconjugate Chem.* **2022**, *33* (9), 1609–1619. DOI: 10.1021/acs.bioconjchem.2c00222.

(59) Forsyth, W. R.; Weisenburger, G. A.; Field, K. W. The Syntheses of Phencyclone and Dihydrophencyclone. Trans. Ill. State Acad. Science **1996**, *89*, 37–40. https://ilacadofsci.com/archives/2608, (accessed 26 September 2022).

(60) Kvach, M. V.; Ustinov, A. V.; Stepanova, I. A.; Malakhov, A. D.; Skorobogatyi, M. V.; Shmanai, V. V.; Korshun, V. A. A Convenient Synthesis of Cyanine Dyes: Reagents for the Labeling of Biomolecules. *Eur. J. Org. Chem.* **2008**, *2008* (12), 2107–2117. DOI: 10.1002/ejoc.200701190.

(61) Park, J. W.; Kim, Y.; Lee, K.-J.; Kim, D. J. Novel Cyanine Dyes with Vinylsulfone Group for Labeling Biomolecules. *Bioconjugate Chem.* **2012**, *23* (3), 350–362. DOI: 10.1021/bc200232d.

(62) Sasmal, R.; Das Saha, N.; Pahwa, M.; Rao, S.; Joshi, D.; Inamdar, M. S.; Sheeba, V.; Agasti, S. S. Synthetic Host–Guest Assembly in Cells and Tissues: Fast, Stable, and Selective Bioorthogonal Imaging via Molecular Recognition. *Anal. Chem.* **2018**, *90* (19), 11305–11314. DOI: 10.1021/acs.analchem.8b01851.

(63) Tranmer, G. K.; Yip, C.; Handerson, S.; Jordan, R. W.; Tam, W. Synthesis of 2,3-Disubstituted Norbornadienes. *Can. J. Chem.* **2000**, *78* (5), 527–535. DOI: 10.1139/v00-047.

(64) Tranmer, G. K.; Tam, W. Intramolecular 1,3-Dipolar Cycloadditions of Norbornadiene-Tethered Nitrones. *J. Org. Chem.* **2001**, *66* (15), 5113–5123. DOI: 10.1021/jo015610b.

(65) Bhandari, S.; Ray, S. A Novel Synthesis of Bisbenzyl Ketones by DCC Induced Condensation of Phenylacetic Acid. *Syn. Commun.* **1998**, *28* (5), 765–771. DOI: 10.1080/00032719808006472.

(66) Beyer, M. K. The Mechanical Strength of a Covalent Bond Calculated by Density Functional Theory. *J. Chem. Phys.* **2000**, *112* (17), 7307–7312. DOI: 10.1063/1.481330.

(67) Gaussian 16, Revision C.01, Frisch, M. J.; Trucks, G. W.; Schlegel, H. B.; Scuseria, G. E.; Robb, M. A.; Cheeseman, J. R.; Scalmani, G.; Barone, V.; Petersson, G. A.; Nakatsuji, H.; Li, X.; Caricato, M.; Marenich, A. V.; Bloino, J.; Janesko, B. G.; Gomperts, R.; Mennucci, B.; Hratchian, H. P.; Ortiz, J. V.; Izmaylov, A. F.; Sonnenberg, J. L.; Williams-Young, D.; Ding, F.; Lipparini, F.; Egidi, F.; Goings, J.; Peng, B.; Petrone, A.; Henderson, T.; Ranasinghe, D.; Zakrzewski, V. G.; Gao, J.; Rega, N.; Zheng, G.; Liang, W.; Hada, M.; Ehara, M.; Toyota, K.; Fukuda, R.; Hasegawa, J.; Ishida, M.; Nakajima, T.; Honda, Y.; Kitao, O.; Nakai, H.; Vreven, T.; Throssell, K.; Montgomery, J. A., Jr.; Peralta, J. E.; Ogliaro, F.; Bearpark, M. J.; Heyd, J. J.; Brothers, E. N.; Kudin, K. N.; Staroverov, V. N.; Keith, T. A.; Kobayashi, R.; Normand, J.; Raghavachari, K.; Rendell, A. P.; Burant, J. C.; Iyengar, S. S.; Tomasi, J.; Cossi, M.; Millam, J. M.; Klene, M.; Adamo, C.; Cammi, R.; Ochterski, J. W.; Martin, R. L.; Morokuma, K.; Farkas, O.; Foresman, J. B.; Fox, D. J. Gaussian, Inc., Wallingford CT, **2016**.

(68) Warrener, R. N.; Schultz, A. C.; Houghton, M. A.; Butler, D. N. Rigid Molecular Racks Featuring the 1,10-Phenanthroline Ligand Especially Those Co-Functionalised with Redox-Active Groups or Other Bidentate Ligands. *Tetrahedron* **1997**, *53* (11), 3991–4012. DOI: 10.1016/S0040-4020(97)00014-8.

5 Chapter 5: *Diels–Alder-based Patterning of Natural Hydrogels for Cell Culture*

The exciting potential application of CPD–NBD photoclick chemistry for the advancement of tissue engineering technologies was alluded to throughout Chapter 4 and is the area of exploration in this next chapter. Given the radical-free nature of our CPD–NBD photoclick platform, we anticipated our patterning technology could be applied to protein-based matrices, which are ubiquitously used in tissue culture but are incompatible with traditional radical-based photopatterning techniques. By patterning biomolecules within these hydrogels, we demonstrate the use of CPD–NBD photoclick chemistry to fabricate spatially patterned microenvironments for cell culture and highlight their promise in spatially controlling cell fate decisions. This project began much before the work presented in Chapter 4 and instead uses a modestly soluble CPD–NBD derivative that, in fact, motivated the design of the water-soluble CPD–NBD adduct. Given the success of the less soluble CPD–NBD presented here, we anticipate the application of the water-soluble CPD–NBD derivative outlined in Chapter 4 will also provide great utility in the patterning of cellular microenvironments.

5.1 Abstract

Strategies that mimic the spatial complexity of natural tissues can provide cellular scaffolds to probe fundamental questions in cell biology and offer new therapeutics for regenerative medicine. Here, we demonstrate a next-generation patterning strategy that enables use in protein-based hydrogels which are most amenable to facilitating native cellular behaviors. This strategy utilizes a photocaged diene, which undergoes Diels–Alder based click chemistry upon uncaging with 365 nm light. By interfacing with commercially available maleimide dienophiles, facile patterning of off-the-shelf protein matrices (collagen, fibronectin Matrigel,

laminin) is demonstrated with readily purchased functional fluorophores, proteins, and growth factors. Finally, we highlight the compatibility of our materials with HeLa, HEK, 3T3 and human embryonic stem cell lines and demonstrate spatially controlled kinase activation by the patterning of epidermal growth factor on protein-based surfaces.

5.2 Introduction

The spatial organization of cell types and complex orchestration of cellular behaviors are essential features of tissue growth from individual cell fate decisions[1] to embryonic development.[2] Within the field of tissue engineering, the development of extracellular matrix (ECM) mimics which control the spatial presentation of biochemical and biophysical cues is an exciting route to access these dynamic cellular processes.[3] Synthetic and naturally derived hydrogels provide amenable scaffolds for cell culture, due to their tissue-like properties arising from high water content and tunable mechanics, making them a go-to choice for preparing ECM mimics.[4] A number of photopatterning technologies have been developed to enable the spatially controlled immobilization of biomolecules within hydrogel matrices,[5,6] enabling the preparation of anisotropic microenvironments to control a number of cellular processes including: cell spreading[7–9] proliferation,[10] differentiation,[11] and morphogenesis.[12]

Patterning of biochemical cues within hydrogels has largely been demonstrated in synthetic hydrophilic polymer networks (i.e. poly(ethylene glycol)) due to the superior chemical tunability of these systems; however, these inert matrices do not facilitate native cellular behaviors without considerable modification.[13] Thus, the need for additional processing steps has limited the widespread use of these synthetic materials by biologists interested in understanding and controlling cellular processes. Instead, protein-based matrices such as collagen, laminin, fibronectin, and Matrigel which possess inherent bioactivity are often

selected for their ease-of-use and compatibility with numerous cell lines.[13] Implementing photopatterning strategies within these protein-based matrices would promote the uptake of these technologies by the cell biology community; however, the technologies currently available often rely upon radical-based chemistry (i.e., thiol–ene) that is incompatible with these materials.[5] Recent work has highlighted the need for non-radical propagating photopatterning strategies in protein-based hydrogels to investigate spatially controlled cell behaviors which are not readily observed in synthetic hydrogel environments like axon outgrowth[12] and hepatocyte proliferation.[10] Thus, next-generation photopatterning strategies for tissue engineering must avoid radicals to enable use in protein-based hydrogels; furthermore, these strategies should also strive to be low cost and easy to use to promote their uptake by biological communities.

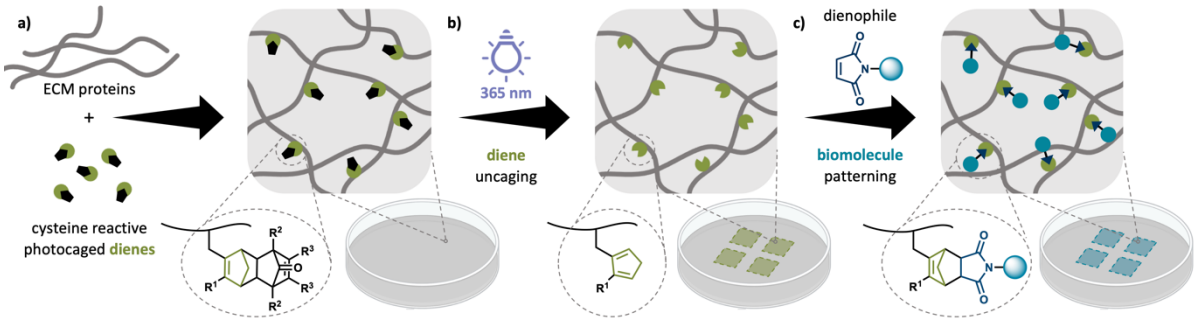

Figure 5.1. Graphic depiction of protein-based hydrogel patterning platform using CPD–NBD as a photocaged diene for patterning biomolecules via Diels–Alder cycloadditions.

As highlighted in Chapters 3–4, our group has recently reported the use of cyclopentadienone–norbornadiene (CPD–NBD) as photocaged cyclopentadiene (Cp) which enables rapid, photo-triggered Diels–Alder click chemistry with dienophiles.[14] Previous work demonstrated the utility of this photoclick platform for patterning biomolecules within hydrogels and highlighted the potential of this strategy for preparing patterned surfaces for cell culture. Because the photouncaging of Cp proceeds without the production of free radicals, we

envisioned this strategy would be amenable to patterning off-the-shelf protein-based matrices. Additionally, the use of maleimide as the dienophile partner enables our strategy to interface with a number of commercially available maleimide-bearing species labeling agents, growth factors, peptides and proteins, which we anticipate will enable uptake by the bioengineering, biology and material science communities (**Figure 5.1**).

In this chapter, we present the facile functionalization of protein-based matrices with a cysteine-reactive CPD–NBD derivative and subsequent patterning for cell culture. We highlight the compatibility of our platform with commercial systems by patterning maleimide–streptavidin within hydrogels that provides a mix-and-match approach with a variety of biotinylated growth factors to enable spatially defined cellular responses. Finally, we demonstrate that human embryonic stem cells (hESCs) can be cultured and differentiated on CPD–NBD functionalized laminin hydrogels, a notorious challenge in synthetic materials. This preliminary work highlights the great promise of this platform in the preparation of patterned surfaces to control stem cell fate decisions.

5.3 Results and Discussion

5.3.1 Functionalization of Matrices with CPD–NBD

To introduce CPD–NBD functionality into hydrogel systems for subsequent patterning, a CPD–NBD derivative to enable facile protein conjugation was designed. To encourage ease-of-use, we sought to develop a strategy that would seamlessly integrate into protocols for cell culture matrix preparation. Importantly, because the maleimide agents intended for use in patterning steps can also react with thiols, we anticipated that conjugation of our CPD–NBD unit via cysteine residues would prevent off-target conjugation during subsequent patterning

steps. Thus, a CPD–NBD derivative, **10**, bearing a cysteine reactive handle was synthesized in five steps from inexpensive precursors **1**, **2**, **5** and **6** ($0.05 – $5.00 /g) (**Figure 5.2a**).[15] With this maleimide-bearing CPD–NBD in hand, we anticipated cysteine functionalization would be easily achieved as previously demonstrated with maleimide-benzylguanine in collagen hydrogels.[16]

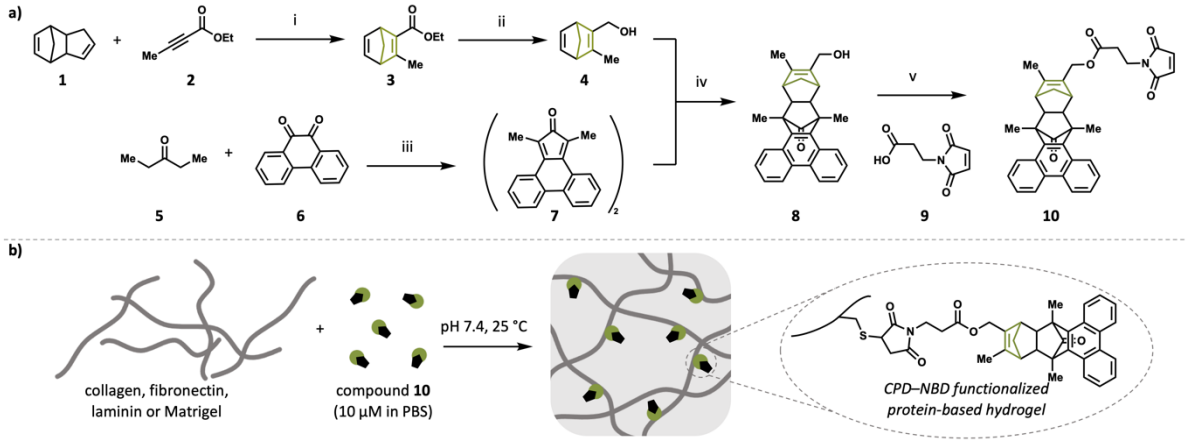

Figure 5.2. a) Synthesis of CPD–NBD adduct (10) for protein functionalization i) hydroquinone, 200 °C, pressure vessel, 4 h, 56%, ii) DIBAL, THF, 0 °C, 30 min, 71%, iii) 1. K2CO3, MeOH, rt, 16 h, 2. MsCl, DMAP, 0 °C – rt, 16 h, 64%, iv) toluene, 100 °C, 24 h, 53% v) 9, EDC, DMAP, DCM, rt, 1 h, 66% b) Schematic of protein hydrogel preparation.

Notably, by altering substituents on CPD–NBD adduct **10** from originally reported pentyl and phenyl groups[14] to methyl groups provided improved solubility in phosphate buffered saline with dimethyl sulfoxide (DMSO) as a co-solvent, enabling the facile functionalization of off-the-shelf protein-based matrices. Manufacturer protocols for 2D surface preparation of Collagen Type 1, fibronectin, laminin and Matrigel were slightly modified by dilution in phosphate buffered saline solutions containing CPD–NBD **10** (0.1–100 µM), followed by gelation at room temperature. Rinsing surfaces to remove residual non-conjugated **10** provided CPD–NBD functionalized surfaces for patterning experiments (**Figure 2b**). Full details of hydrogel surface preparation protocols can be found in the Supporting Information.

5.3.2 Tunable Fluorescent Dye Patterning

Initial investigations focused on validating the use of our protein-conjugated CPD–NBD moieties to pattern maleimide bearing species within matrices. Fluorescent dyes are commonly employed as labeling agents in a number of biological applications and can be purchased with a large range of excitation wavelengths (350–900 nm) and functionalities, including maleimide reactive handles. Thus, we chose to visualize our CPD–NBD uncaging and maleimide click with a commercially available maleimide bearing Alexa Fluor 555 dye. Following masked irradiation (LED, 365 nm, 6 mW/cm^2) of CPD–NBD functionalized surfaces, gels were incubated in Alexa Fluor solutions before thorough rinsing and imaging by microscopy. To probe the required CPD–NBD irradiation dose to obtain visible patterns, we initially screened patterning in each polymer matrix prepared at 20 μM **Compound 10** with irradiation times ranging from 2 – 15 minutes. We were pleased to find high resolution patterns were readily achieved in all four matrices within 5 minutes irradiation time (LED, 365 nm, 6 mW/cm^2), and maximal patterning intensities were obtained around 10 minutes irradiation (Supplementary Information, **Figure S5.5**). Notably, the two-step procedure used by our platform enables the patterning of fluorescent species that are susceptible to bleaching under prolonged light irradiation.

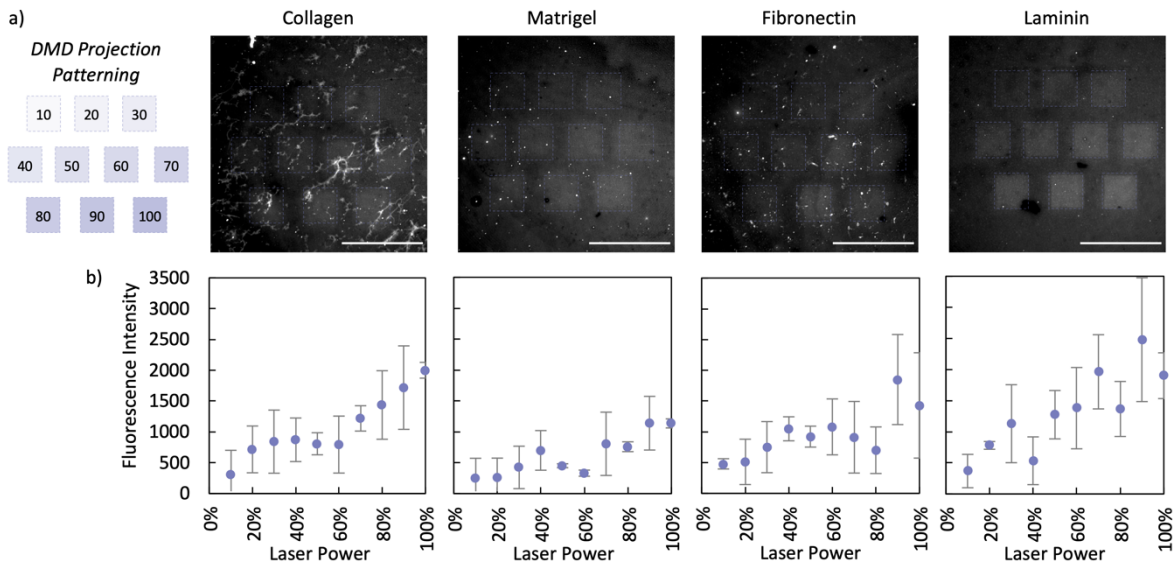

Figure 5.3. a) Representative images of patterned maleimide–Alexa Fluor 555 after irradiation with digital micromirror devices (DMDs, 365 nm, 10 min) in each protein-based matrix. b) Quantification of background corrected fluorescence as a function of laser intensity for each matrix (n = 3). Scale bars = 500 μm.

To further highlight the tunability of this platform and investigate the feasibility of patterning with typical light projection setups used by cellular biologists we turned to patterning surfaces with digital micromirror devices (DMDs) on a confocal microscope. As illustrated in **Figure 5.3a–b** tunable Alexa Fluor patterning in protein matrices functionalized with CPD–NBD (100 μM) was easily achieved by varying the laser power within a projected DMD pattern (365 nm, 10 min). Additionally, the efficiency of protein functionalization and subsequent patterning was assessed by comparing the fluorescence intensity of resulting patterns to that of wild type protein gels treated with maleimide–Alexa. As expected, nonfunctionalized wild type protein gels result in high fluorescence signal corresponding to maleimide–cysteine conjugation (Supplementary Information, **Figure S5.6**). The fluorescence from these wild type surfaces also reflects the maximum intensity accessible by CPD–NBD patterning as our functionalization strategy utilizes these same residues. After functionalization

with Compound 10, a decrease in Alexa fluorescence signal in non-irradiated regions is observed corresponding to saturation of cysteine residues by CPD–NBD units. Some residual fluorescence from the AlexaFluor is noted in non-irradiated regions and is attributed to nonspecific interactions of the dye with matrices due to the high concentration (10 μM) and long incubation time (3 hours) employed; although, background conjugation to unreacted cysteine residues from the initial functionalization step is also possible. Efficient uncaging and Cp–maleimide cycloaddition are reflected by the fluorescence of patterns approaching the maximum values expected from wild type surfaces (Supplementary Information, **Figure S5.6**). With confirmation that the CPD–NBD photopatterning platform can be easily translated from the synthetic polymer networks highlighted in previous chapters to protein-based matrices, we directed our efforts to the development of a method for preparing patterned surfaces for cell culture.

5.3.3 "Mix-and-Match" Patterning Approach with Biotinylated Species

To establish a readily interchangeable platform, we envisioned that the wealth of commercially available biotinylated biomolecules could be leveraged in conjunction with commercially available maleimide–streptavidin to decorate our surfaces with a variety of proteins and growth factors for use in cell culture (**Figure 5.4a**). This strategy also circumvents the need to incorporate maleimide moieties onto protein-based patterning agents, which could pose challenges due to maleimide–cysteine reactivity. To optimize patterning with biotinylated species, a two-step incubation was invoked where after irradiation (365 nm LED, 10 min, 6 mW/cm^2), surfaces were first incubated with maleimide–streptavidin solutions (1 μM), then thoroughly rinsed before treatment with biotin solutions (0.1–1 μM). By removing excess non-conjugated maleimide–streptavidin before biotin treatment, the amount of immobilized

biotinylated species could be maximized (up to 4/streptavidin) by exclusive interaction with covalently bound streptavidin units. However, before attempting to pattern biotinylated-biomolecules for cell culture, we first explored the viability of this system to immobilize biotin–fluorescein in pre-patterned locations. A CPD–NBD functionalized fibronectin surface (10 μM) was prepared and irradiated through a quartz photomask possessing a diamond pattern (500 μm). To our delight, after successive incubations with maleimide–streptavidin (1 μM) then biotin–fluorescein (0.5 μM), distinct diamonds could be visualized by fluorescence microscopy (**Figure 5.4b**). With this successful demonstration of the streptavidin–biotin immobilization strategy, we were encouraged to turn to patterning bioactive species for cell culture.

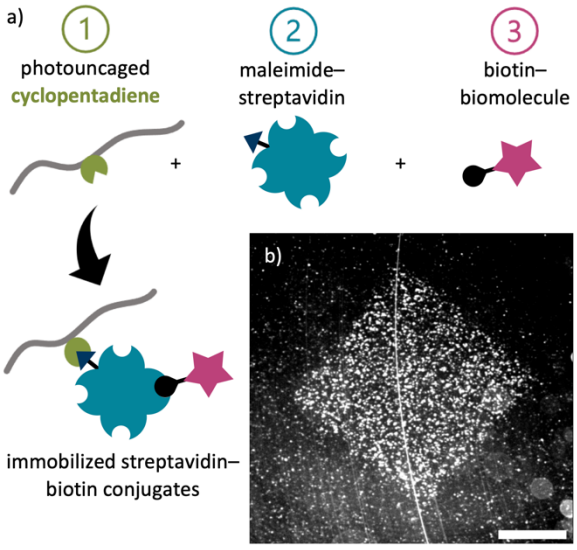

Figure 5.4. a) Schematic depiction of "mix-and-match" strategy by patterning maleimide–streptavidin and immobilizing biotinylated biomolecules. b) Image of immobilized biotin-fluorescein on fibronectin gel. Scale bar = 100 μm.

5.3.4 Cellular Responses to CPD–NBD Patterned Surfaces

To investigate the feasibility of the CPD–NBD photoclick platform to spatially pattern biochemical cues on surfaces for 2D cell culture, we envisioned the immobilization of growth

factors would provide control over a variety of cellular processes including cell growth, signaling and differentiation. Additionally, numerous growth factors can be purchased commercially or directly functionalized with amine-reactive *N*-hydroxysuccinimidyl (NHS) activated biotin; this accessibility provides potential for controlling numerous cellular processes and investigating the combinatorial effects of multiple patterned growth factors. To determine a concentration regime for patterning that would not negatively impact cell culture, a viability screen of CPD–NBD functionalized surfaces was first completed. We were pleased to find for HeLa, 3T3 and HEK cell lines, metabolic activity was unaltered on protein-based surfaces prepared with up to 10 μM CPD–NBD. Notably, HeLa and HEK cell lines remained largely unaffected on collagen surfaces prepared with 100 μM CPD–NBD; however, some change in cell density and morphology was observed with 3T3 cell lines (Supporting Information, **Figure S5.7**).

With tissue culture compatibility confirmed, fibronectin surfaces were prepared under sterile conditions containing 10 μM CPD–NBD, and wells were flood-irradiated and incubated in maleimide–streptavidin as described in **Section 5.3.3**. After rinsing, surfaces were incubated in solutions of biotinylated epidermal growth factor (EGF, ThermoFisher, E3477, 1 μM) for 2 hours then thoroughly rinsed before seeding HeLa cells expressing the ERK kinase translocation reporter (KTR)[17] to visualize ERK activation by patterned EGF. Cells were allowed to adhere overnight then switched into serum depleted media the following day. Once in serum depleted media, KTR localization was monitored for 6 hours to track ERK activity. Over the course of live cell imaging, an increase in cytoplasmic KTR signal correlating to increased phosphorylated ERK[17] was observed in cells cultured on EFG functionalized surfaces (**Figure 5.5a–e**). Additionally, a significant increase in cell movement was noted on

EGF functionalized surfaces, as illustrated by plotting the total cell displacement over the 6 hour experiment (**Figure 5.5f**). These results corroborate ERK activation by photoimmoblized EGF, which enables KTR signaling and increased movement to be maintained over the course of the experiment as surface immobilized EGF cannot be metabolized by the cells.

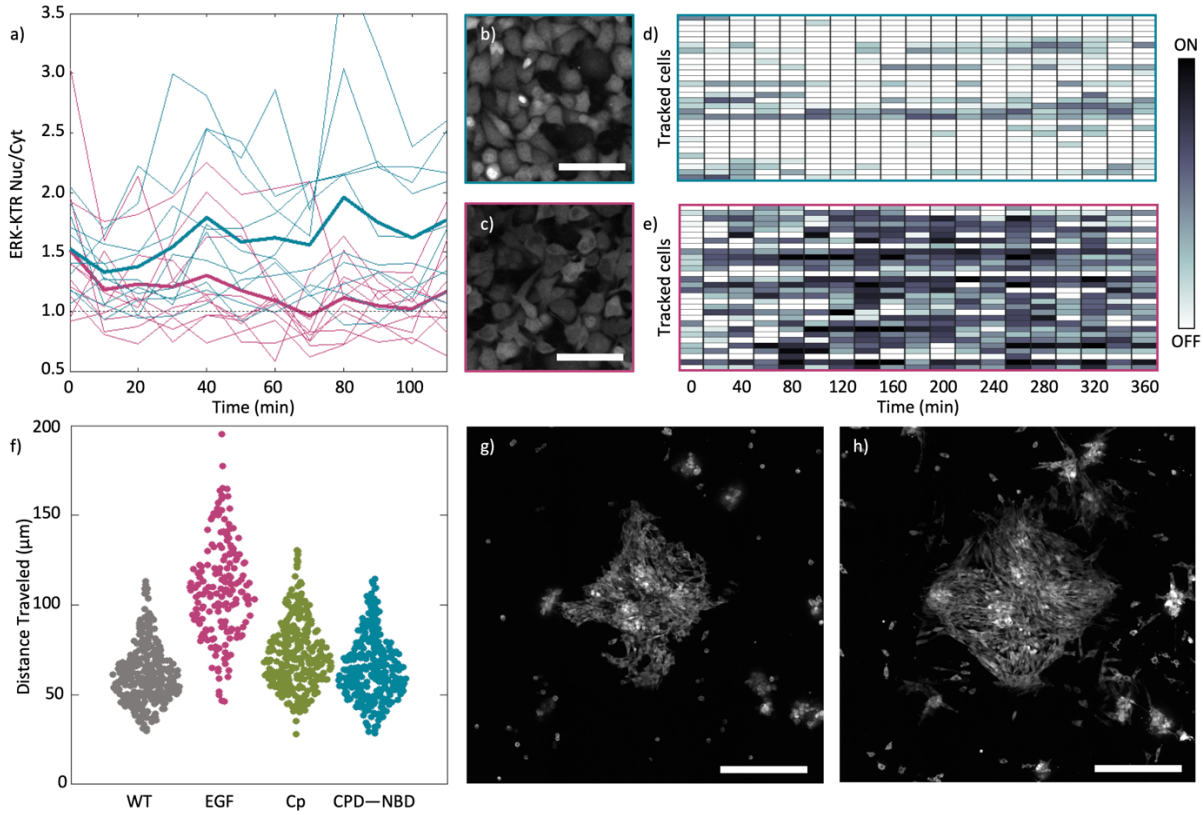

Figure 5.5. a) Overlay of nuc/cyt ratios of individually tracked cells (averages displayed as bold lines) cultured on CPD–NBD functionalized fibronectin surfaces with photoimmoblized EGF (pink) or nonirradiated, nontreated controls (blue) in serum depleted media. Representative images of cells cultured on b) nonpatterned control surfaces and c) EGF patterned surfaces. Scale bars = 100 µm. KTR signal (ON = nuc/cyt < 1, OFF = nuc/cyt > 1) of individual cells plotted over 6 hours of tracking on d) nonpatterned control surfaces and e) EGF patterned surfaces. f) Plots of cell displacement over 6 hours for wild type fibronectin surfaces (gray), compared to EGF patterned (pink), photouncaged cyclopentadiene (green), or nonirradiated CPD–NBD functionalized. Images of 3T3 cells cultured on CPD–NBD functionalized collagen patterned with diamonds and treated with 1 µM EGF at g) initial timepoint after serum depletion and h) final timepoint after 10 hours. Scale bars = 200 µm.

With success in flood illumination, new surfaces were prepared by masked irradiation to investigate the effects of spatially controlled EGF presentation. CPD–NBD (10 μM) functionalized collagen surfaces were patterned with 500 μm diamonds of EGF (0.1–1 μM) and seeded with 3T3 cells. Within hours, the 3T3 cells displayed complete preference for both concentrations of the EGF functionalized diamonds. After culturing for one day, full media was removed, wells were exposed to serum depleted media and live cell monitoring was conducted over the course of 10 hours. Imaging revealed that the cells grew distinctly in patterned diamonds while maintaining high cytoplasmic KTR signals over 10 hours (**Figure 5.5g-h**); however, cell death was observed outside of the immobilized patterns. This striking result highlights the efficiency of our patterning strategy to immobilize growth factors while maintaining bioactivity. However, work remains in optimizing concentration regimes of this system for culturing more sensitive cell lines while maintaining desired responses of patterned biomolecules.

5.3.5 Viability of Human Pluripotent Stem Cells on CPD–NBD Surfaces

Embryonic development depends upon the precise orchestration of cell fate decisions of differentiating cells to form structured tissues within an organism. This coordinated behavior is guided by gradients of extracellular signals, known as morphogens, within the cellular microenvironment.[18] However, the ability to recreate these signals in vitro has been prohibited by the incompatibility of current radical-based photopatterning technologies with the matrices needed for the culturing of human embryonic stem cells (hESCs). Thus, we envisioned our platform could unlock access to patterning synthetic morphogen gradients to enable control over tissue morphogenesis.[12] To investigate the compatibility of our CPD–NBD surfaces for the normal culture and differentiation of hESCs, we prepared laminin surfaces functionalized

with 10 μM CPD–NBD and seeded hESCs in the presence of ROCK inhibitor Y-27632. The following day, ROCK inhibitor was removed, and differentiation was induced with BMP-4. After 48 hours, expression of markers for pluripotency (SOX2) and mesoderm (brachyury) were assessed for each surface. Excitingly, we observed that CPD–NBD functionalized laminin surfaces supported the culture and differentiation of hESCs similarly to wild type laminin surfaces (**Figure 5.6a–b**). Inspired by these results, we have begun the preparation of surfaces with photoimmobilized biotin–BMP-4 to spatially trigger differentiation, the next step in using the CPD–NBD photopatterning platform to control stem cell fate.

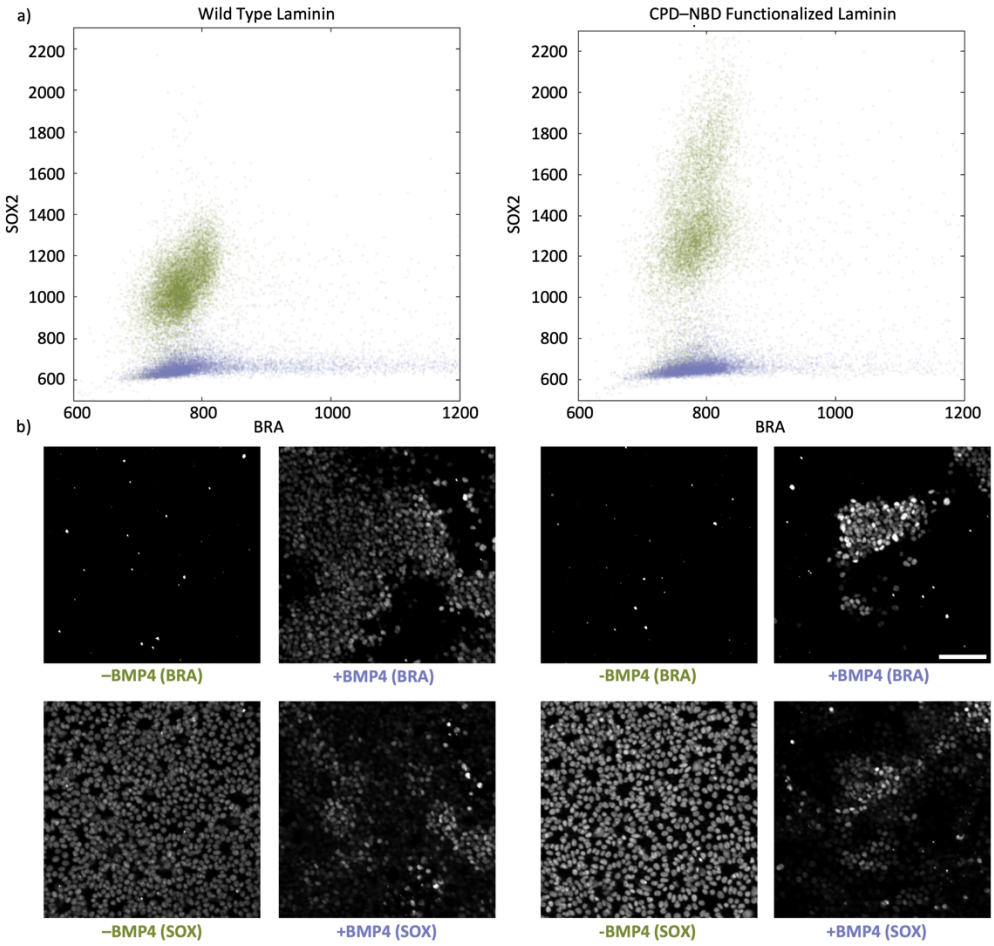

Figure 5.6. a) Plots of brachyury (BRA) and SOX2 expression for hESCs in nondifferentiated wells (–BMP4) and differentiated wells (+BMP4) cultured on wild type laminin surfaces (left)

and CPD–NBD functionalized (10 μM) laminin surfaces (right). b) Representative images of brachyury and SOX2 expression. Scale bar = 100 μm.

5.4 Conclusion

The radical-based mechanisms of many current hydrogel patterning technologies preclude their application in the most common used cell culture matrices: proteins. To address this shortcoming, we present a next-generation photopatterning strategy that avoid radicals to enable use in protein-based hydrogels. By employing CPD–NBD adducts as photocaged cyclopentadiene units, rapid, photoinduced Diels–Alder chemistry enables radical-free photopatterning of hydrogels with commercially available patterning agents (maleimide and biotin functionalized species). We have highlighted that this platform enables the facile patterning of biotinylated growth factors in protein-based materials to control cell movement, growth and signaling. Furthermore, we have demonstrated the compatibility of our CPD–NBD functionalized surfaces with human embryonic stem cells, a cell line typically incompatible with synthetic hydrogels. This preliminary work illustrating the importance of expanding photopatterning technologies to protein-based matrices and provides a foundation for work currently underway in the patterning of growth factors to control stem cell fates. We envision morphogen gradients will be readily recreated by varying light dose across a surface before growth factor immobilization, unlocking the ability to harness the natural self-assembly mechanisms stem cells utilize during the formation of organs. Altogether, the CPD–NBD platform enables the facile preparation of patterned hydrogels for cell culture by interfacing with of-the-shelf protein matrices and commercial patterning agents and provides great promise in the preparation of synthetic morphogen gradients to enable “user-defined’ tissue morphogenesis.

5.5 Acknowledgments

I would also like to sincerely thank Erik Hopkins and Prof. Maxwell Z. Wilson for their eagerness to collaborate in the development of a CPD–NBD photopatterning platform for cell culture. They have been wonderful collaborators who have made a dream application become a reality. I would like to thank Erik for his contributions to this work, including all cell culture experiments and image acquisition. This project would be absolutely nothing without his unfaltering dedication and perseverance on this project – I am so grateful for his enthusiasm, insights, and friendship. I would also like to thank the UCSB Graduate Division for financial support through a Chancellor's Fellowship. I would also like to acknowledge the work here was partially supported by the National Science Foundation under award No. CHE-2204077 and partially supported by the BioPACIFIC Materials Innovation Platform (MIP) of the National Science Foundation under award No. DMR-1933487.

5.6 Supporting Information

Synthesis

Synthetic Scheme

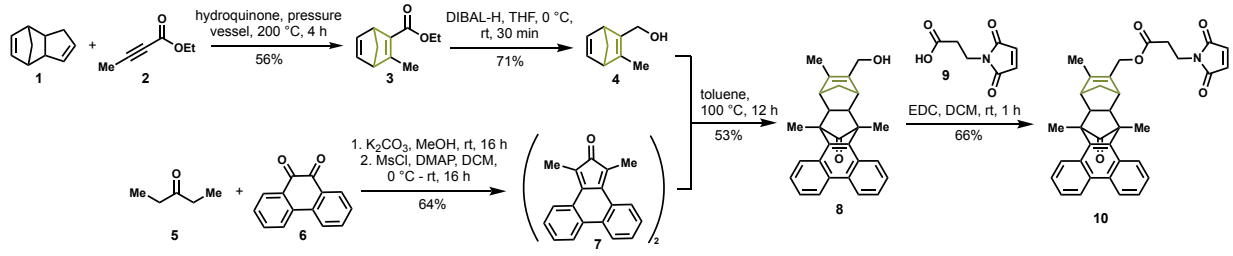

Materials and Methods

All chemicals including Compounds **1**, **2**, **5**, **6** and **9** were obtained from Sigma Aldrich, Oakwood Chemical or Fisher Scientific and used as received without further purification. Unless

otherwise noted, reactions were performed under an atmosphere of nitrogen. Tetrahydrofuran, dichloromethane and toluene were dispensed from a solvent purification system immediately before use or stored over 3Å molecular sieves. Ethanol and methanol were also stored over 3Å molecular sieves before use. Thin-layer chromatography (TLC) was conducted with E. Merck silica gel 60 F254 pre-coated plates (0.25 mm) and visualized by exposure to UV light (254 nm) or stained with *p*-anisaldehyde. Flash column chromatography was performed using normal phase silica gel (60 Å, 0.040 – 0.063 mm, Geduran) with hexanes and ethyl acetate (EtOAc) as eluents. ^{1}H and ^{13}C NMR spectra were recorded on Varian spectrometers (100, 125, 500 or 600 MHz) and are reported relative to $CDCl_3$ (δ = 7.26 ppm for ^{1}H and 77.00 ppm for ^{13}C), DMSO-D6 (δ = 2.50 ppm for ^{1}H and 39.52 ppm for ^{13}C) or methanol-D_4 (δ = 3.31 ppm for ^{1}H). Data for ^{1}H NMR spectra are reported as follows: chemical shift (δ ppm), multiplicity, coupling constant (Hz) and integration. Data for ^{13}C NMR spectra are reported in terms of chemical shift (δ ppm). Mass spectra were obtained from the UC Irvine Mass Spectrometry Facility on a time-of-flight mass spectrometer with an ESI source. FTIR spectra were collected on a Thermo Nicolet iS10 FTIR Spectrometer equipped with a Smart Diamond attenuated total reflectance (ATR) accessory.

Synthesis of Small Molecules

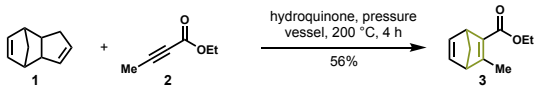

ethyl 3-methylbicyclo[2.2.1]hepta-2,5-diene-2-carboxylate (Compound 3):

Compound 3 was prepared as previously reported in Chapter 4. To a 100 mL pressure vessel was added dicyclopentadiene (**Compound 1**, 8.00 mL, 60 mmol, 0.6 eq), ethyl 2-buytanoate (**Compound 2**, 11.7 mL, 100 mmol, 1 eq), and hydroquinone (200 mg). The pressure vessel

was sealed under an atmosphere of nitrogen then heated to 200 °C for 4 h, at which point conversion of ethyl 2-buytonoate was determined to be 82% by ^{1}H NMR of a crude aliquot of the reaction mixture. The crude reaction mixture was purified by fractional distillation where cyclopentadiene and ethyl 2-buytanoate were first removed (30–55 °C, ~200 mTorr) before **Compound 3** was isolated (55–60 °C, ~200 mTorr) as a clear oil (10.0 g, 56.1 mmol, 56%). Spectral data matched that of reported literature.[19]

Compound 3: ^{1}H NMR (500 MHz, $CDCl_3$) δ 6.89 (dd, *J* = 5.0, 3.1 Hz, 1H), 6.73 (dd, *J* = 4.6, 3.4 Hz, 1H), 4.22–4.12 (m, 2H), 3.88 (s, 1H), 3.39 (s, 1H), 2.22 (s, 3H), 2.05 (dt, *J* = 6.4, 1.4 Hz, 1H), 1.95 (dt, *J* = 6.4, 1.4 Hz, 1H), 1.29 (t, *J* = 6.3 Hz, 3H) ppm.

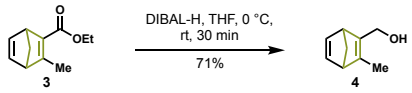

(3-methylbicyclo[2.2.1]hepta-2,5-dien-2-yl)methanol (Compound 4)

Compound 4 was prepared as previously reported in Chapter 4. To a 500 mL flame dried round bottom flask equipped with magnetic stir bar, **Compound 3** (4.28 g, 24.0 mmol, 1 eq) was dissolved in tetrahydrofuran (130 mL) and the solution was cooled to 0 °C. A solution of diisobutylaluminium hydride (DIBAL) in hexanes (68.0 mL, 68.0 mmol, 2.8 eq) was added dropwise. The solution was stirred 30 min, at which point consumption of starting material was confirmed by TLC (hexanes:ethyl acetate, 4:1). The reaction was then quenched at 0 °C by dropwise addition of H_2O (2.5 mL) followed by 1 M NaOH (5 mL) then H_2O (2.5 mL) before being allowed to warm to room temperature. The reaction mixture was dried over magnesium sulfate then filtered and rinsed with diethyl ether (200 mL). The solvent was removed under reduced pressure, and the residue was subjected to column chromatography

(hexanes:ethyl acetate, 4:1) to afford **Compound 4** (2.33 g, 17.1 mmol, 71%) as a clear oil. Spectral data matched that of reported literature.[20]

Compound 4: R_f (Hexanes:EtOAc, 4:1): 0.30; ^{1}H NMR (500 MHz, $CDCl_3$) δ 6.82 (dd, *J* = 4.9, 3.0 Hz, 1H), 6.76 (dd, *J* = 4.7, 3.1 Hz, 1H), 4.25 (d, *J* = 12.2 Hz, 1H), 4.14 (d, *J* = 12.2 Hz, 1H), 3.53 (s, 1H), 3.28 (s, 1H), 1.96 (dt, *J* = 5.9, 1.6 Hz, 1H), 1.89 (dt, *J* = 5.9, 1.4 Hz, 1H), 1.79 (s, 3H) 1.07 (br. s, 1H) ppm.

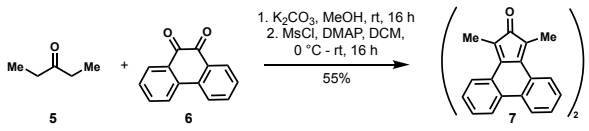

1,3-dimethyl-2H-cyclopenta[l]phenanthren-2-one, dimer (Compound 7):

Compound 7 was prepared as previously reported.[21] To a 1 L round bottom equipped with magnetic stir bar was added K_2CO_3 (13.0 g, 96.0 mmol, 1.99 eq) and MeOH (dried over sieves, 500 mL). To this stirred heterogenous solution was added 3-pentanone (10.0 mL, 95 mmol, 1.98 eq) followed by phenanthroquinone (10.0 g, 48.0 mmol, 1 eq). The reaction was allowed to stir for 16 h, then the reaction mixture was concentrated under reduced pressure. The residue was taken up in DCM and transferred to a separatory funnel containing 500 mL water. The material was extracted with DCM (3 x 300 mL) then the combined organic layers were dried over magnesium sulfate and the solvent was removed under reduced pressure. The crude material was then taken forward without further purification. The β-hydroxyketone crude intermediate was dissolved in dry dichloromethane (500 mL) then 4-dimethylaminopyridine (DMAP, 16.6 g, 136 mmol, 2.83 mmol). The reaction mixture was cooled to 0 ºC before

methanesulfonyl chloride (MsCl, 9.30 mL, 120 mmol, 2.50 eq) was added and the reaction was left to stir for 16 h while warming to room temperature under an atmosphere of nitrogen. The reaction mixture was then transferred to a separatory funnel and washed with water (3 x 50 mL) then brine (1 x 50 mL). The solvent was removed under reduced pressure, and the residue was triturated in cold MeOH then filtered to afford **Compound 7** (7.73 g, 15.4 mmol, 64%) as a pink-white solid. Spectral data matched that of reported literature.[21]

Compound 10: ^{1}H NMR (500 MHz, $CDCl_3$) δ 8.56–8.21 (m, 2H), 7.84 (br. s, 1H), 7.56–7.52 (m, 3H), 7.18 (t, *J* = 7.5 Hz, 1H), 6.93 (br. s, 1H), 1.88 (br. s, 3H), 1.22 (s, 3H) ppm.

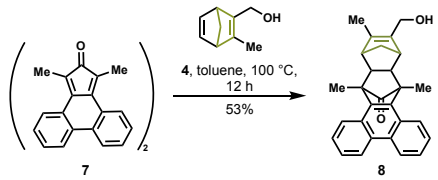

11-(hydroxymethyl)-9,12,14-trimethyl-9,9a,10,13,13a,14-hexahydro-9,14:10,13-dimethanobenzo[*f*]tetraphen-15-one (Compound 8):

Compound 4 was prepared as previously reported in Chapter 4. To a 25 mL round bottom flask was added **Compound K3b** (dimer, 0.309 g, 1.20 mmol monomer, 1 eq), **Compound N1b** (0.195 g, 1.43 mmol, 1.19 eq) and toluene (7 mL). This solution was allowed to stir at 100 °C for 24 h, at which point consumption of starting material was confirmed by TLC (hexanes:ethyl acetate, 2:1). The solution was allowed to cool to room temperature and the solid was collected by vacuum filtration to afford **Compound F2** (0.252 g, 0.639 mmol, 53%) as a light pink powder.

Compound 8: R_f (Hexanes:EtOAc, 2:1): 0.38; ^{1}H NMR (500 MHz, $CDCl_3$) δ 8.77 (dt, *J* = 9.4, 1.9 Hz, 2H), 8.39–8.33 (m, 2H), 7.63 (pd, *J* = 6.9, 1.4 Hz, 4H), 4.18 (d, *J* = 12.6 Hz, 1H), 4.04 (d, *J* = 13.2 Hz, 1H), 2.82 (s, 1H), 2.49 (s, 1H), 2.10 (d, *J* = 8.3 Hz, 1H), 2.06 (s, 6H), 2.00 (d, *J* = 8.3 Hz, 1H), 1.66 (s, 3H), 0.28 (d, *J* = 9.7 Hz, 1H), -0.48 (d, *J* = 9.7 Hz, 1H) ppm.

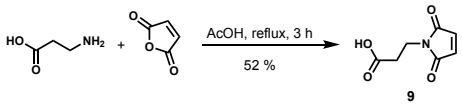

9

3-maleimidopropionic acid (Compound 9):

3-maleimidopropionic acid is *commercially available* (CAS 7423-55-4), but was prepared according to a literature procedure.[21] In a 100 mL round bottom flask, maleic anhydride (6.00 g, 61.2 mmol, 1 eq) and beta-alanine (5.50 g, 61.7 mmol, 1.01 eq) were dissolved in acetic acid (45 mL) and the solution was brought to reflux. After 3 h the solution was cooled to room temperature and the acetic acid was removed under reduced pressure. The residue was subjected to flash column chromatography (2.5% methanol in dichloromethane) to afford **Compound 9** (5.38 g, 31.8 mmol, 52 %) as a white powder. Spectral data matches reported literature.[22] The compound was further purified by recrystallization from hot water to afford colorless crystals.

^{1}H NMR (400 MHz, $CDCl_3$) δ 10.87 (br. s, 1H), 6.72 (s, 2H), 3.84 (t, *J* = 7.2 Hz, 2H), 2.71 (t, *J* = 7.2 Hz, 2H) ppm.

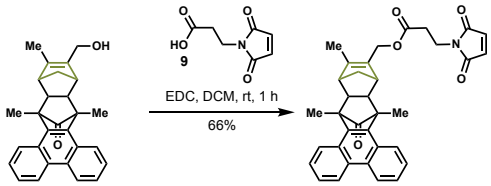

(9,12,14-trimethyl-15-oxo-9,9a,10,13,13a,14-hexahydro-9,14:10,13-dimethanobenzo[*f*]tetraphen-11-yl)methyl 3-(2,5-dioxo-2,5-dihydro-1*H*-pyrrol-1-yl)propanoate (Compound 10):

To a scintillation vial was added 1-ethyl-3-(3-dimethylaminopropyl)carbodiimide (EDC, 182 mg, 0.950 mmol, 1.5 eq), DMAP (7.7 mg, 0.063 mmol, 0.1 eq) and 2.5 mL DCM. To this solution was added **Compound 9** (0.161 g, 0.950 mmol, 1.5 eq) followed by **Compound 8** (0.250 g, 0.634 mmol, 1 eq). This solution was allowed to stir at room temperature for 1 h, at which point consumption of starting material was confirmed by TLC (hexanes:ethyl acetate, 4:1). The solution was transferred to a separatory funnel with an additional 10 mL DCM and washed with water (3 x 10 mL) then brine (1 x 10 mL). The organic layer is dried with magnesium sulfate and solvent was removed under reduced pressure. The afforded residue was subjected to column chromatography (hexanes:ethyl acetate, 4:1) to afford **Compound 10** (0.227 g, 0.416 mmol, 66%) as a light pink foam.

Compound 10: R_f (Hexanes:EtOAc, 4:1): 0.20; ^{1}H NMR (500 MHz, $CDCl_3$) δ 8.77 (d, J = 8.1 Hz, 2H), 8.37 (dd, J = 15.1, 8.6 Hz, 2H), 7.68 – 7.59 (m, 4H), 6.64 (s, 2H), 4.57 (d, J = 12.5 Hz, 1H), 4.51 (d, J = 12.5 Hz, 1H), 3.82 (t, J = 7.1 Hz, 2H), 2.68 (s, 1H), 2.62 (t, J = 7.1 Hz, 2H), 2.51 (s, 1H), 2.08 (m, 2H), 2.06 (s, 6H), 2.00 (d, J = 8.3 Hz, 1H), 1.69 (s, 3H), 0.29 (d, J = 9.6 Hz, 1H), -0.49 (d, J = 9.6 Hz, 1H) ppm.. ^{13}C NMR (125 MHz, $CDCl_3$) δ 203.5, 170.7, 170.2, 148.8, 139.6, 134.8, 134.6, 134.2, 130.3, 130.3, 128.8, 126.8, 126.7, 126.2, 126.1, 124.5,

124.4, 123.7, 123.6, 59.8, 54.8, 54.6, 50.1, 49.6, 48.7, 45.9, 38.9, 33.6, 32.9, 15.5, 15.4, 12.2 ppm; FTIR (ATR) 3096, 2957, 2903, 2166, 2031, 1768, 1731, 1704, 1438, 1405, 1380, 1178, 824, 754, 722, 695 cm^{-1}; HRMS (ES+) Exact mass cald. for $C_{35}H_{32}NO_5Na$ [M+Na]+: 568.2100, found: 568.2115.

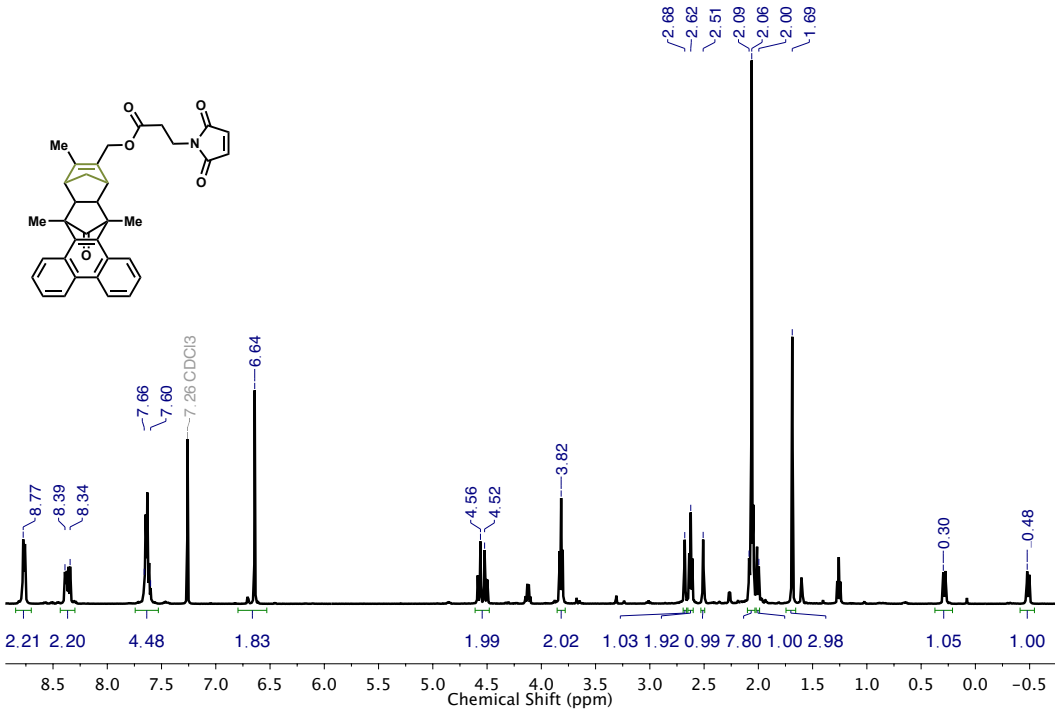

Figure S 5.1. ^{1}H NMR (500 MHz, $CDCl_3$) **Compound 10**

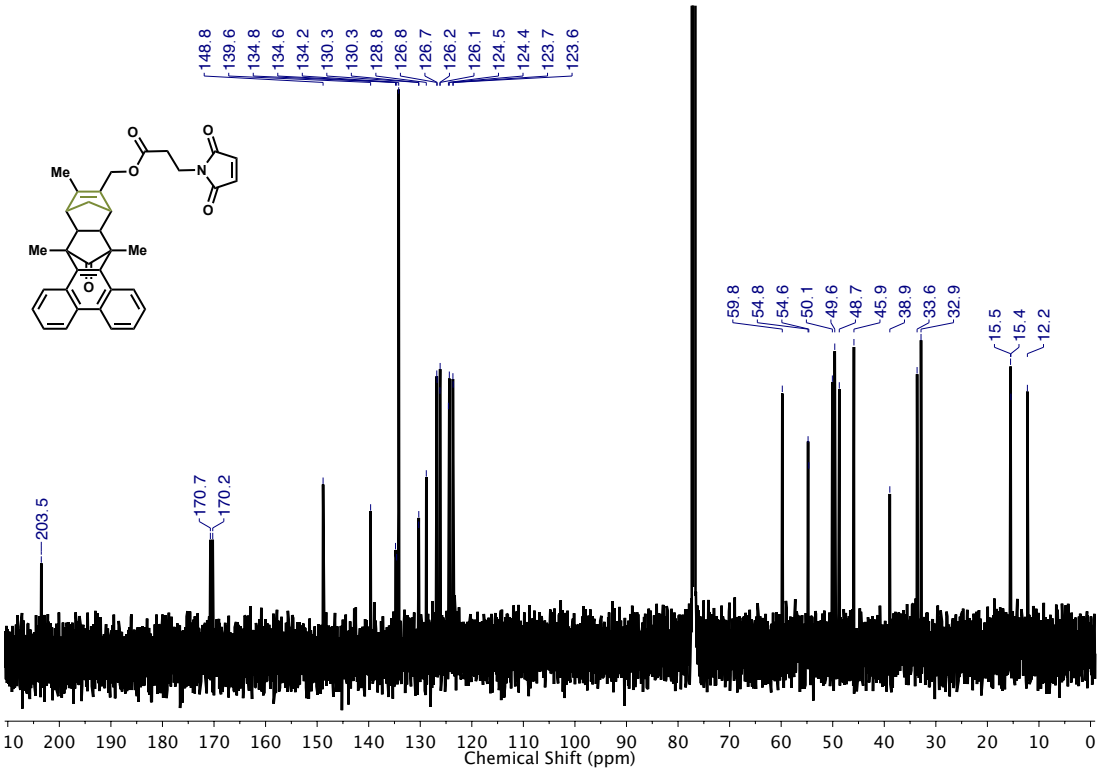

Figure S 5.2. ^{13}C NMR (125 MHz, $CDCl_3$) **Compound 10**

Decarbonylation and Click Monitoring by ^{1}H NMR

A 2.5 mM solution of **Compound 8** was prepared in acetone-d_6 and spiked with ethylene carbonate (EC) as an internal standard and hydroquinone (HQ) to prevent radical degradation of Cp over prolonged irradiation. The solution was sparged with nitrogen (2 min) in a sealed vial then irradiated (365 nm LED, 6 mW/cm^2) for 2 hours. Aliquots were removed periodically to determine conversion by ^{1}H NMR spectroscopy.

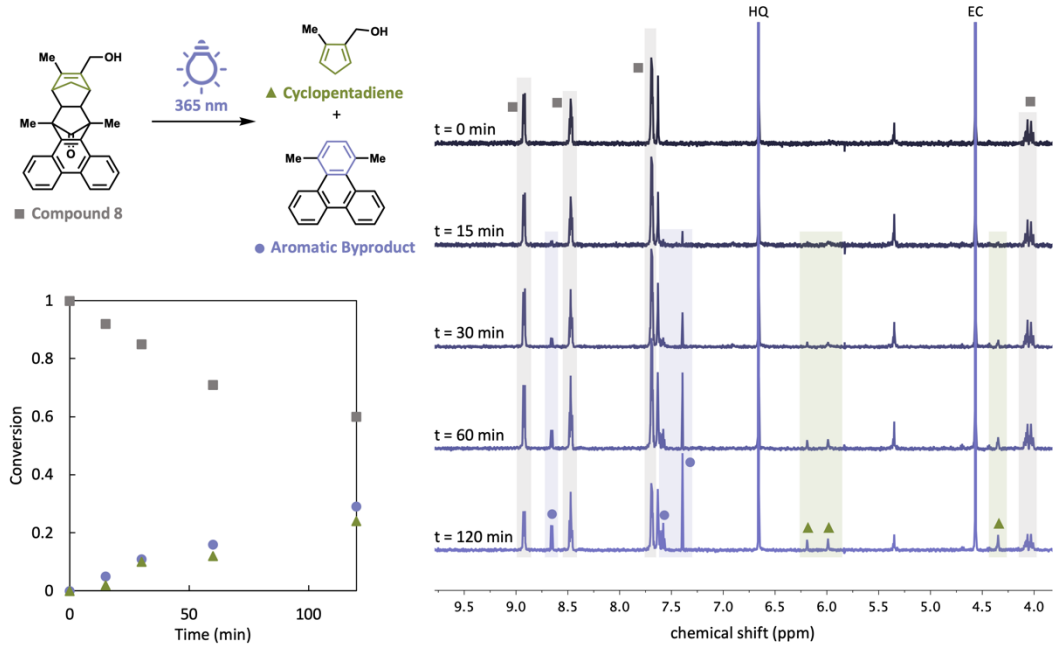

Figure S 5.3. Overlay of the ^{1}H NMR spectra of reaction aliquots taken over the course of solution irradiation. Photocleavage is observed by the reduction of CPD–NBD peaks (gray squares) and appearance of diagnostic peaks corresponding to the substituted aromatic byproduct (purple circles) and cyclopentadiene (green diamonds). Conversion determined by integrating resonance signals relative to the ethylene carbonate internal standard at 4.6 ppm.

UV-vis Spectroscopy

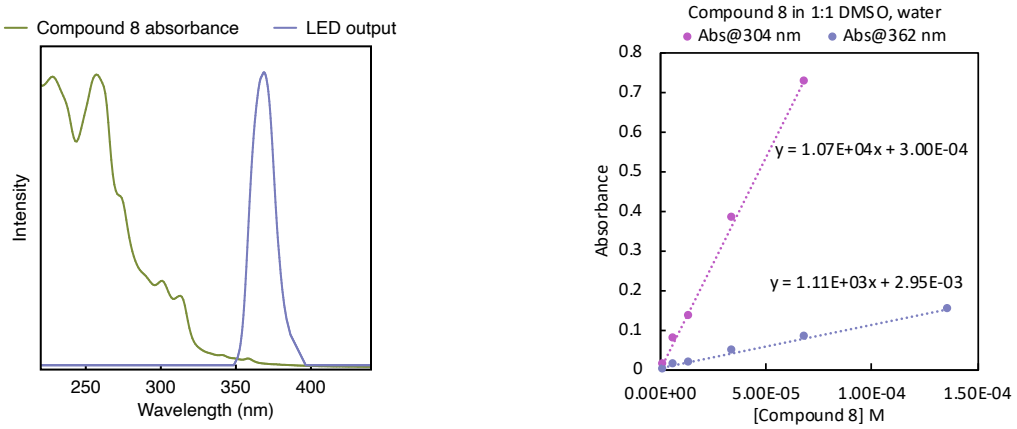

Figure S 5.4. UV vis spectra of obtained of **Compound 8** (20 μM) in a 1:1 mixture of DMSO and water overlayed with the output of 365 nm LED used for patterning experiments. Calibration curves prepared from absorbance values at λ_{max} of peaks at 304 and 362 nm for **Compound 8** in a 1:1 mixture of DMSO and water.

From the calibration curve in **Figure S5.4,** extinction coefficients and solubility of saturated solutions in 1:1 DMSO, water were determined. The saturated solution was passed through a 0.2 μm syringe filter before diluting 10x in 1:1 DMSO, water. The absorbance spectra was measured, and the concentration of dissolved compound in the saturated solution was determined using the prepared calibration curves and Beer-Lambert Law.

Peak	ε (M^{-1} cm^{-1})	Absorbance Unknown Solution	Unknown Concentration (μM)	Saturated Concentration (μM)
304 nm	11000	0.635	59 (10x dilution)	590
362 nm	1100	0.059	51 (10x dilution)	510

ECM Surface Preparation and Patterning

To promote ECM gel attachment, 96-well glass bottom plates (Cellvis, P96-1.5H-N) were first functionalized with (3-aminopropyl)triethoxysilane (APTS) and glutaraldehyde. Under sterile conditions, each well was treated with 70 μL of APTS (2 vol%) in ethanol for 2 hours at room temperature then rinsed with ethanol followed by deionized water. Each well is then treated with 70 μL of glutaraldehyde (2 vol%) in deionized water for 2 hours at room temperature. The wells are then thoroughly rinsed with deionized water and allowed to dry before hydrogels are deposited in wells.

A 1 mM stock solution of CPD–NBD (**Compound 10**) was prepared in anhydrous dimethyl sulfoxide and was stored at 4 °C. This stock solution can be stored for months without any observable degradation. At the time of gel preparation, working solutions of CPD–NBD (1-100 μM) were prepared by diluting the stock (1 mM) CPD–NBD into the working solutions of respective polymers.

Matrix polymers* were diluted per manufacturers recommendations with the addition of CPD-NBD to desired concentrations (0– 100 μM). Immediately after mixing polymer solutions, 50 μL aliquots were transferred into the bottom of a functionalized 96-well plate. The plate was immediately centrifuged (1000 rpm) to promote even distribution of the thin protein gel on the bottom of the well plate. The distributed solutions were protected from light and incubated at room temperature for 3 hours. Excess polymer and CPD-NBD were rinsed from the wells with PBS and surfaces were patterned as indicated.

*Matrix polymers used:

- Collagen Type I, Corning, PN 354249
- Matrigel Basement Membrane Matrix, Corning, PN 354234

- Laminin-521, Stem Cell Technologies, PN 200-0117
- Fibronectin Bovine Protein, Gibco, PN 33010018

Hydrogels were patterned by irradiating in a bottom-up fashion through the 1.5H glass bottom well plate with a collimated LED (Thorlabs, M365L2-C1, 365 nm, 6 mW/cm^2), or digital micromirror device equipped with the Nikon W2 SoRa spinning-disk confocal microscope (365 nm). After irradiation, PBS was removed from each well then maleimide containing solutions were deposited on the top of each gel and gently agitated to ensure complete well coverage. Surfaces were incubated with 0.1–10 μM AlexaFluor-maleimide (Invitrogen™, A20346) or 1 μM maleimide-streptavidin (CellMosaic®, CM52401) for 1.5–3 hours at room temperature. Surfaces treated with maleimide-streptavidin were thoroughly rinsed (> 10 well volumes) with PBS before incubating with the appropriate biotin-bearing proteins at indicated concentrations for an additional 1.5 hours at room temperature. Surfaces were thoroughly rinsed before imaging or seeding cells.

Quantification of Patterning with Alexa Fluor

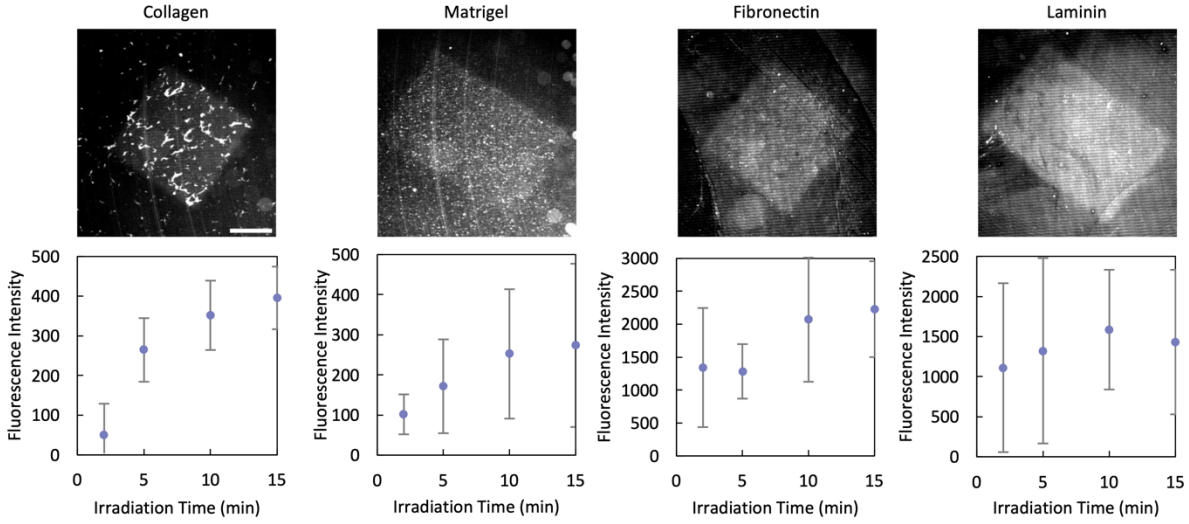

Figure S 5.5. a) Representative images of patterned maleimide–Alexa Fluor 555 after irradiation (LED, 365 nm, 10 min, 6 mW/cm^2) in each protein-based matrix. b) Quantification of fluorescence as a function of irradiation time for each matrix. Scale bar = 100 µm.

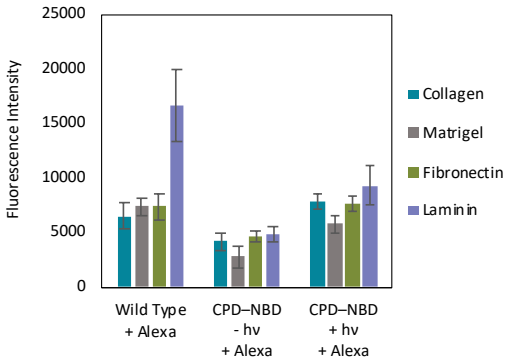

Figure S 5.6. Fluorescence values of wild type surfaces treated with maleimide–Alexa reflecting cysteine–maleimide conjugation (Wild Type + Alexa) compared to CPD–NBD functionalized surfaces from **Figure 5.3** of nonirradiated background (CPD–NBD – *hν* + Alexa) and "100% Power" irradiated patterns (CPD–NBD + *hν* + Alexa). All fluorescence values are corrected to nontreated wild type surfaces.

Non-stem cell tissue culture and cell viability

HeLa, HEK, and 3T3 cells were cultured at 37°C with 5% CO_2 in Dulbecco's Modified Eagle Medium (DMEM) containing 10% fetal bovine serum and 1% antibiotic (25units/mL penicillin, 25μ g/mL streptomycin, Invitrogen). Serum-depleted media was made by adding fetal bovine serum to 0.5%. Cells were seeded on functionalized surfaces at 20,000-40,000 cells/well and allowed to adhere overnight before being placed in serum-depleted media for indicated times. Cell viability on CPD-NBD functionalized matrices was assessed with AlamarBlue (Invitrogen, DAL1025). Briefly, cells growing on functionalized matrices were incubated in media supplemented with 10% AlamarBlue solution. After an hour, 100 μL samples of media were taken and fluorescence signal (Ex/Em 560 nm/590 nm) was quantified with a plate reader (Biotek).

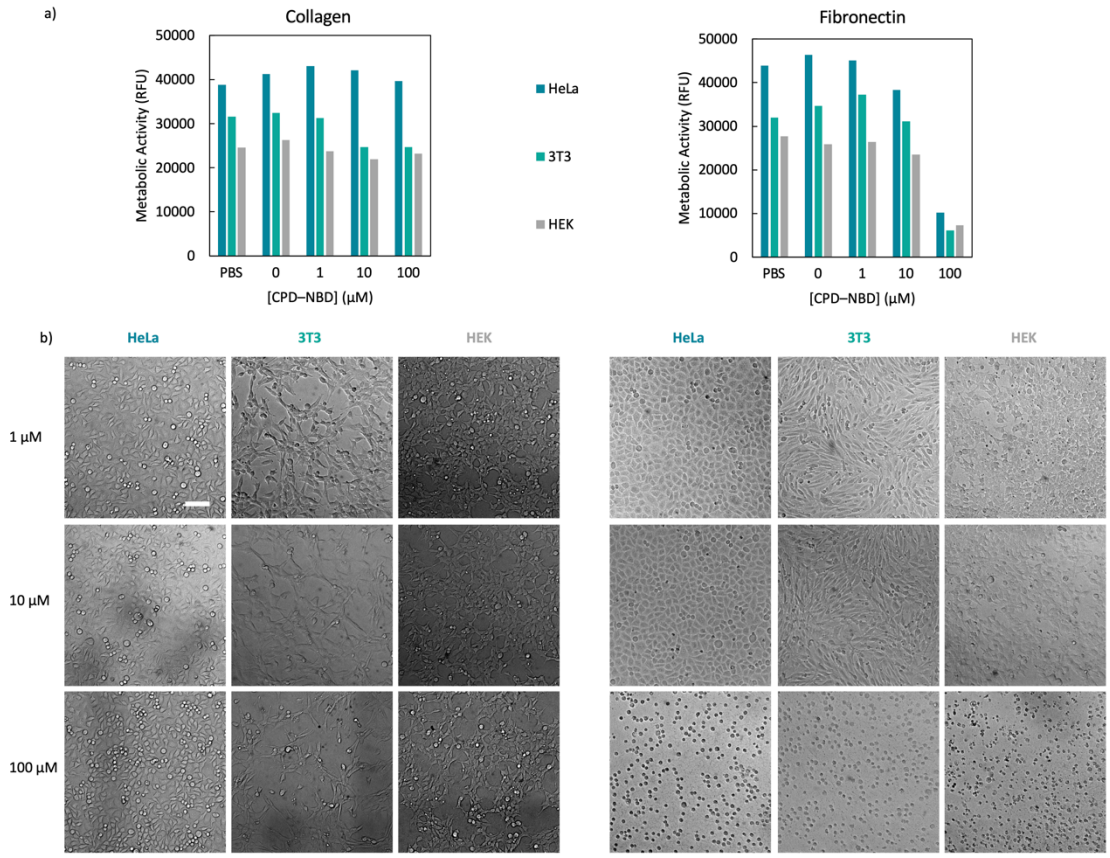

Figure S 5.7. a) Plots of metabolic activity of HeLa, 3T3 and HEK cells cultured in PBS or on CPD–NBD functionalized surfaces (0–100 μM). b) Representative images of cell morphologies of HeLa, 3T3 and HEK cells on each surface.

Human embryonic stem cell (hESC) culture and differentiation

Experiments in hESC lines were done using the H9 hESC line purchased from the William K. Bowes Center for Stem Cell Biology and Engineering at University of California, Santa Barbara. hESCs were propagated on Matrigel-coated (Corning) tissue culture dishes in mTeSR Plus medium (Stem Cell Technologies). For experiments, hESCs were seeded on to laminin-coated (Stem Cell Technologies) wells of a 96-well plate at 40,000-50,000 cells per well in the presence of ROCK inhibitor Y-27632. The following day ROCK inhibitor was removed, and differentiation was induced with BMP-4 (50 ng/mL) for 48 hours.

Immunofluorescence

Cells were fixed with 4% PFA for 25 minutes followed by permeabilization with ice cold methanol for 10 minutes. Samples were blocked with a 1% BSA solution and incubated overnight in the appropriate primary antibody (1:200). The following day samples were rinsed and incubated with Alexa-conjugated secondary antibodies (1:1000).

Image Collection and Processing

All live- and fixed-cell imaging was done with a Nikon W2 SoRa spinning-disk confocal microscope. When necessary, an incubation chamber was used to maintain 37 °C and 5% CO_2. Migration distance was tracked using the FIJI plugin TrackMate[23] and further analyzed using custom MatLab (R2022a) scripts. KTR nuclear to cytoplasmic ratios and fluorescence intensity of patterns was carried out with hand-picked ROIs and processed with custom FIJI and MatLab scripts.

5.7 References

(1) Rompolas, P.; Mesa, K. R.; Greco, V. Spatial Organization within a Niche as a Determinant of Stem-Cell Fate. *Nature* **2013**, *502* (7472), 513–518. DOI: 10.1038/nature12602.

(2) Murry, C. E.; Keller, G. Differentiation of Embryonic Stem Cells to Clinically Relevant Populations: Lessons from Embryonic Development. *Cell* **2008**, *132* (4), 661–680. DOI: 10.1016/j.cell.2008.02.008.

(3) Brown, T. E.; Anseth, K. S. Spatiotemporal Hydrogel Biomaterials for Regenerative Medicine. *Chem. Soc. Rev.* **2017**, *46* (21), 6532–6552. DOI: 10.1039/C7CS00445A.

(4) Drury, J. L.; Mooney, D. J. Hydrogels for Tissue Engineering: Scaffold Design Variables and Applications. *Biomaterials* **2003**, *24* (24), 4337–4351. DOI: 10.1016/S0142-9612(03)00340-5.

(5) Grim, J. C.; Marozas, I. A.; Anseth, K. S. Thiol-Ene and Photo-Cleavage Chemistry for Controlled Presentation of Biomolecules in Hydrogels. *J. Control. Release* **2015**, *219*, 95–106. DOI: 10.1016/j.jconrel.2015.08.040.

(6) Munoz-Robles, B. G.; Kopyeva, I.; DeForest, C. A. Surface Patterning of Hydrogel Biomaterials to Probe and Direct Cell–Matrix Interactions. *Adv. Mater. Interfaces* **2020**, *7* (21), 2001198. DOI: 10.1002/admi.202001198.

(7) Luo, Y.; Shoichet, M. S. A Photolabile Hydrogel for Guided Three-Dimensional Cell Growth and Migration. *Nature Mater* **2004**, *3* (4), 249–253. DOI: 10.1038/nmat1092.

(8) DeForest, C. A.; Polizzotti, B. D.; Anseth, K. S. Sequential Click Reactions for Synthesizing and Patterning Three-Dimensional Cell Microenvironments. *Nat. Materials* **2009**, *8* (8), 659–664. DOI: 10.1038/nmat2473.

(9) Wade, R. J.; Bassin, E. J.; Gramlich, W. M.; Burdick, J. A. Nanofibrous Hydrogels with Spatially Patterned Biochemical Signals to Control Cell Behavior. *Adv. Mater.* **2015**, *27* (8), 1356–1362. DOI: 10.1002/adma.201404993.

(10) Batalov, I.; Stevens, K. R.; DeForest, C. A. Photopatterned Biomolecule Immobilization to Guide Three-Dimensional Cell Fate in Natural Protein-Based Hydrogels. *Proc. Natl. Acad. Sci. U.S.A.* **2021**, *118* (4), e2014194118. DOI: 10.1073/pnas.2014194118.

(11) DeForest, C. A.; Tirrell, D. A. A Photoreversible Protein-Patterning Approach for Guiding Stem Cell Fate in Three-Dimensional Gels. *Nat. Materials* **2015**, *14* (5), 523–531. DOI: 10.1038/nmat4219.

(12) Broguiere, N.; Lüchtefeld, I.; Trachsel, L.; Mazunin, D.; Rizzo, R.; Bode, J. W.; Lutolf, M. P.; Zenobi-Wong, M. Morphogenesis Guided by 3D Patterning of Growth Factors in Biological Matrices. *Adv. Mater.* **2020**, *32* (25), 1908299. DOI: 10.1002/adma.201908299.

(13) Caliari, S. R.; Burdick, J. A. A Practical Guide to Hydrogels for Cell Culture. *Nat. Methods* **2016**, *13* (5), 405–414. DOI: 10.1038/nmeth.3839.

(14) Bailey, S. J.; Stricker, F.; Hopkins, E.; Wilson, M. Z.; Read de Alaniz, J. Shining Light on Cyclopentadienone–Norbornadiene Diels–Alder Adducts to Enable Photoinduced Click Chemistry with Cyclopentadiene. *ACS Appl. Mater. Interfaces* **2021**, *13* (30), 35422–35430. DOI: 10.1021/acsami.1c08670.

(15) Based on Oakwood Chemical Prices November 14, 2022.

(16) Hopkins, E.; Valois, E.; Stull, A.; Le, K.; Pitenis, A. A.; Wilson, M. Z. An Optogenetic Platform to Dynamically Control the Stiffness of Collagen Hydrogels. *ACS Biomater. Sci. Eng.* **2021**, *7* (2), 408–414. DOI: 10.1021/acsbiomaterials.0c01488.

(17) Kudo, T.; Jeknić, S.; Macklin, D. N.; Akhter, S.; Hughey, J. J.; Regot, S.; Covert, M. W. Live-Cell Measurements of Kinase Activity in Single Cells Using Translocation Reporters. *Nat. Protoc.* **2018**, *13* (1), 155–169. DOI: 10.1038/nprot.2017.128.

(18) Rogers, K. W.; Schier, A. F. Morphogen Gradients: From Generation to Interpretation. *Annu. Rev. Cell Dev. Biol.* **2011**, *27* (1), 377–407. DOI: 10.1146/annurev-cellbio-092910-154148.

(19) Tranmer, G. K.; Yip, C.; Handerson, S.; Jordan, R. W.; Tam, W. Synthesis of 2,3-Disubstituted Norbornadienes. *Can. J. Chem.* **2000**, *78* (5), 527–535. DOI: 10.1139/v00-047.

(20) Tranmer, G. K.; Tam, W. Intramolecular 1,3-Dipolar Cycloadditions of Norbornadiene-Tethered Nitrones. *J. Org. Chem.* **2001**, *66* (15), 5113–5123. DOI: 10.1021/jo015610b.

(21) Li, P.; Parker, T. M.; Hwang, J.; Deng, F.; Smith, M. D.; Pellechia, P. J.; Sherrill, C. D.; Shimizu, K. D. The CH−π Interactions of Methyl Ethers as a Model for Carbohydrate–*N* -Heteroarene Interactions. *Org. Lett.* **2014**, *16* (19), 5064–5067. DOI: 10.1021/ol502418k.

(22) de Figueiredo, R.; Oczipka, P.; Fröhlich, R.; Christmann, M. Synthesis of 4-Maleimidobutyric Acid and Related Maleimides. *Synthesis* **2008**, *2008* (8), 1316–1318. DOI: 10.1055/s-2008-1032016.

(23) Ershov, D.; Phan, M.-S.; Pylvänäinen, J. W.; Rigaud, S. U.; Le Blanc, L.; Charles-Orszag, A.; Conway, J. R. W.; Laine, R. F.; Roy, N. H.; Bonazzi, D.; Duménil, G.; Jacquemet, G.; Tinevez, J.-Y. TrackMate 7: Integrating State-of-the-Art Segmentation Algorithms into Tracking Pipelines. *Nat. Methods* **2022**, *19* (7), 829–832. DOI: 10.1038/s41592-022-01507-1.

6 Chapter 6: *Rational Mechanochemical Design of Diels–Alder Crosslinked Biocompatible Hydrogels with Enhanced Properties*

This chapter takes a step back from asking the question "What materials can be made from Diels–Alder cycloadditions?" And, instead, asks "What are the effects of Diels–Alder cycloadducts on resulting material properties?" Initially, we were interested in how the rapid kinetics of DA cycloadditions with cyclopentadiene could affect bulk materials, but I became more intrigued by how the propensity of certain Diels–Alder cycloadducts to undergo mechanochemical scission would affect material failure. In particular, I was interested in investigating the effects of Diels–Alder cycloadducts within the types of hydrogel materials I had begun synthesizing alongside materials discussed in Chapters 3 and 4. This chapter presents a new concept in the rational design of hydrogels constructed from Diels–Alder cycloadditions and highlights the use of a sterically "tamed" cyclopentadiene derivative which provides rapid hydrogel formation and enhanced properties. Portions of this chapter were originally published in *Material Horizons.* Reproduced from *Mater. Horiz.* **2022**, *9*, 1947–1953, DOI: 10.1039/D2MH00338D, with permission from the Royal Society of Chemistry.

6.1 Abstract

An important but often overlooked feature of Diels–Alder (DA) cycloadditions is the ability for DA adducts to undergo mechanically induced cycloreversion when placed under force. Herein, we demonstrate that the commonly employed DA cycloaddition between furan and maleimide to crosslink hydrogels results in slow gelation kinetics and "mechanolabile" crosslinks that relate to reduced material strength. Through rational computational design, "mechanoresistant" DA adducts were identified by constrained geometries simulate external force models and employed to enhance failure strength of crosslinked hydrogels. Additionally,

utilization of a cyclopentadiene derivative, spiro[2.4]hepta-4,6-diene, provided mechanoresistant DA adducts and rapid gelation in minutes at room temperature. This study illustrates that strategic molecular-level design of DA crosslinks can provide biocompatible materials with improved processing, mechanical durability, lifetime, and utility.

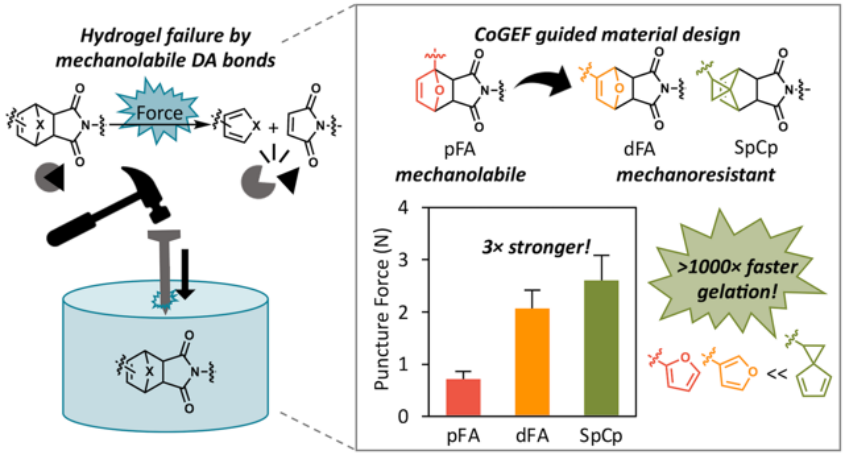

Figure 6.1. Graphical Abstract. Through combined mechanochemical and kinetic design principles we present a new diene that imparts rapid gelation and improved material toughness.

6.2 Introduction

Diels–Alder (DA) cycloadditions have found extensive use in drug delivery, biomedical device fabrication and tissue engineering due to their cytocompatible, additive free and efficient click nature.[1,2] In addition to the advantages that DA cycloadditions offer in the construction of materials, the thermal reversibility has also provided numerous advances in the design of remendable materials,[3] on-demand reactivity,[4,5] and drug delivery systems.[6] While thermal retro-DA (rDA) reactions are well-known and exploited, the *mechanically* induced cycloreversion has only recently been explored.[7–11] Interestingly, mechanochemical reactivity is particularly sensitive to the geometry of a molecule relative to the forces applied; thus, regio- and stereo-isomers of DA adducts have been shown to exhibit notable differences in their ability to undergo mechanically induced cycloreversion.[10,11] Furthermore, the effect of mechanically labile (or mechanolabile) bonds on macroscopic material properties was recently highlighted by Craig and coworkers, who showed that the macroscopic fracture properties of poly(ethylene glycol) (PEG) gels can be directly related to the presence and reactivity of cyclobutane mechanophores as "weak links."[12] However, the direct use of mechanochemical reactivity to improve material properties has yet to be addressed.

In designing biocompatible materials, one inherent drawback of synthetic hydrogels is that they often do not possess the same strength of the natural soft tissues they are designed to interface with or replace. Given that extensive work has been conducted improve the mechanical properties of biocompatible hydrogels,[13–15] we envision that the rational design of DA cycloadducts could provide a facile route to improved strength of materials by structurally modifying the diene–dienophile pairs invoked to prevent mechanically induced rDA reactions

(**Figure 6.2a–b**). This hypothesis is predicated on the striking difference in threshold forces reported for the mechanically induced rDA between furan regioisomers[10] and the recently reported effect of mechanical bond strength on macroscopic fracture properties.[12,16] In reviewing the multitude of elegant and exciting DA-based biomaterials reported in literature[1,2,17–19] we recognized a striking commonality: furan–maleimide crosslinked biomaterials have exclusively used *proximal* furans. However, this regioisomer is known to provide facile and selective polymer mechanoscission by rDA with maximum force values (F_{max}) of 3.6 and 3.8 nN for *endo* and *exo* isomers, respectively, determined by constrained geometries simulate external force (CoGEF) computational methods.[10] In contrast, the *distal* furan–maleimide regioisomer was reported to possess increased mechanical resistance (or mechanoresistance), with the F_{max} of the *endo* isomer increasing to 4.3 nN to induce rDA and the *exo* isomer becoming mechanically inert; thus, applied forces resulted in non-selective bond rupture instead of rDA with F_{max} = 5.8 nN.[10] Given the significant difference in mechanolability of these DA adducts, we hypothesized that the failure strength of biocompatible materials could be increased through strategic employment of mechanoresistant DA linkages.

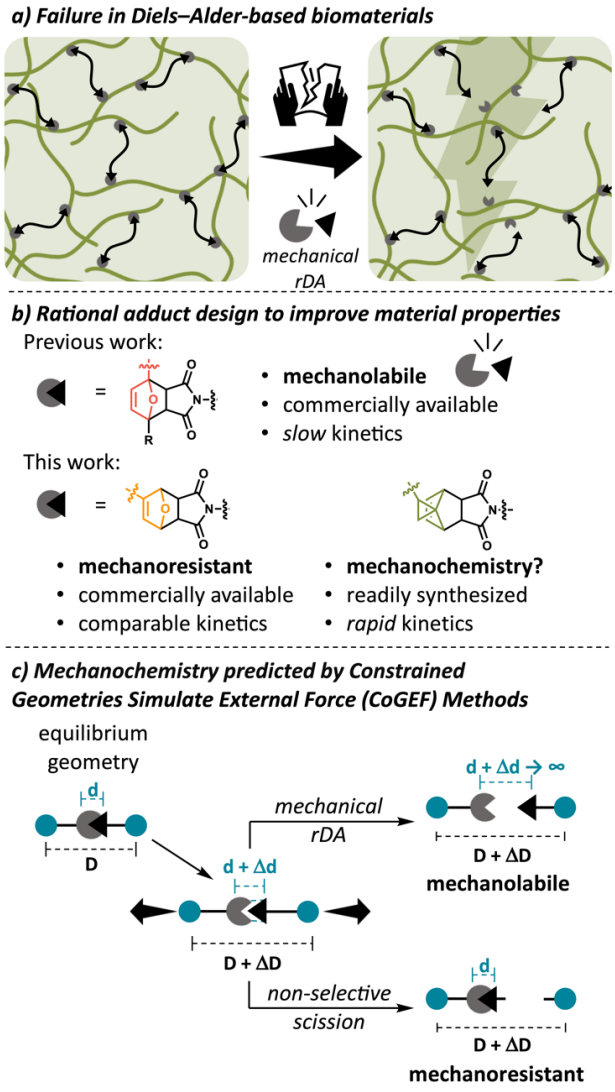

Figure 6.2. a) Graphical depiction of force-induced material fracture. b) Structures of DA cycloadducts investigated. c) Schematic representation of the CoGEF method.

6.3 Results and Discussion

To elucidate the impact of DA adduct mechanolability on the strength of materials, three dienes were chosen for investigation: *proximal* furan (pFA), mechanoresistant *distal* furan (dFA), and a new cyclopentadiene derivative, spiro[2.4]hepta-4,6-diene (SpCp) with unknown mechanochemical reactivity (**Figure 6.2b**). We were particularly interested in the employment

of SpCp–maleimide crosslinking as the cycloaddition has a reported second-order rate constant of 2.6 $M^{-1}s^{-1}$ in water,[20] providing promise in rapid gelation applications such as 3D printing[21] and cell encapsulation[19, 22] which are traditionally incompatible with the slow cycloaddition between furan and maleimide. In comparison to cyclopentadiene, attachment of a bulky cyclopropane ring prevents unwanted dimerization of SpCp[23] which provides improved control and long-term storage of functionalized building blocks. Though cyclopentadiene–maleimide adducts require high temperatures (>200 °C) to induce thermal cycloreversion,[24] *proximal* cyclopentadiene–maleimide adducts are reported to undergo mechanical rDA reactions.[25,26] However, we hypothesized that the non-traditional connectivity of the SpCp–maleimide adduct might reduce the ability to transduce forces to the DA bond. Additionally, *gem*-dihalocyclopropane (gDHC) units are known to act as nonscissile mechanophores such that mechanical ring opening dissipates stress in gDHC containing polymers without scission of the main chain.[27] Thus, we envisioned that the cyclopropane unit might also affect the overall mechanolability of SpCp–maleimide.

6.3.1 Computational Investigation of Mechanochemical Reactivity

To assess the mechanochemical reactivity of SpCp–maleimide we completed a comparative CoGEF investigation on truncated structures of the three adducts we intend to employ within hydrogels following reported methods (**Figure 6.2c**).[28] Plotting the relative energy of each optimized constrained geometry against the displacement (ΔD) from equilibrium afforded the maximum energy before scission (U_{max}) and the slope of CoGEF curves preceding U_{max} provided a measure of the maximum force imparted on the system (F_{max}) (see Supplementary

Information).[28] The calculated U_{max} and F_{max} values for pFA and dFA adducts were in good agreement with previous CoGEF analyses (**Table 6.1**, **Figures S6.18–6.20**).[10,11,28]

Table 6.1. Summary of mechanochemical reactivity of DA adducts determined by CoGEF

	U_{max} (kJ/mol)	F_{max} (nN)	Mechanolabile?
***endo* pFA**	231	3.9	**Yes**
***exo* pFA**	295	4.0	**Yes**
***endo* dFA**	493	4.8	**Yes**
***exo* dFA**	553	5.7	**No**
***endo* SpCp**	492	5.7	**No**
***exo* SpCp**	517	5.7	**No**

As previously reported and depicted in **Figure 6.3a**, the stepwise elongation of pFA and dFA–maleimide adducts reveals an exponential increase in the change in bond length (Δd) between furan and maleimide (bond indicated in blue, **Figure 6.3b**) for both *endo* and *exo* pFA–maleimide and *endo* dFA–maleimide, indicating preferential cycloreversion to furan and maleimide. In contrast, elongation of *exo* dFA–maleimide results in a plateau and eventual relaxation to initial DA bond length, indicative of non-selective bond rupture (**Figure 6.3a**). Notably, elongation of both *endo* and *exo* SpCp–maleimide adducts resulted in the same behavior, again indicating non-selective bond rupture. The implications of these plots are corroborated by each optimized geometry after the simulated scission event by CoGEF. For "mechanolabile" adducts – *endo* pFA, *exo* pFA and *endo* dFA – the scission event results in reformation of furan and maleimide, whereas "mechanoresistant" adducts, *exo* dFA, *endo* SpCp and *exo* SpCp, prompt terminal bond rupture of the truncated structure, indicative of

non-selective polymer scission (**Figure 6.3b**, **S6.18–6.20**). These results suggest that employment of SpCp–maleimide adducts would provide mechanically robust crosslinks, similar to *distal* furan–maleimide adducts, and in contrast to the pFA–maleimide counterparts.

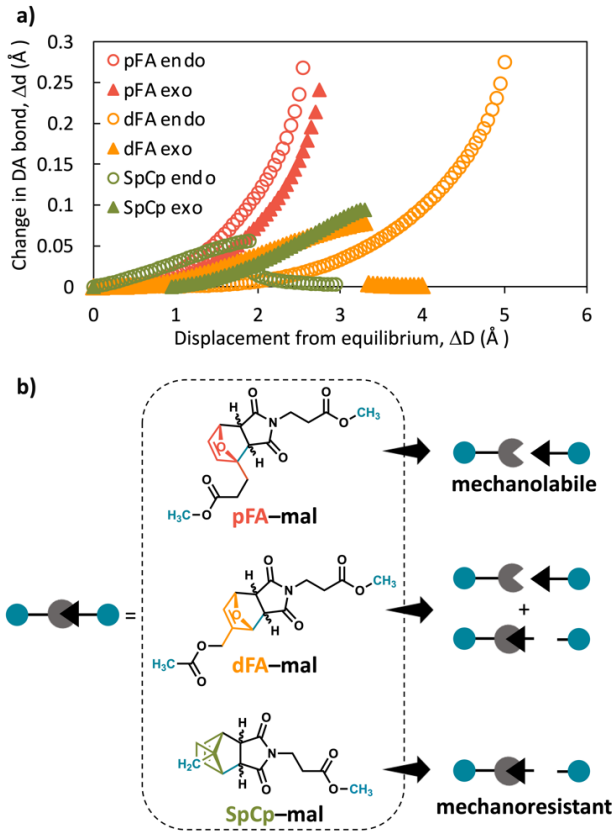

Figure 6.3. a) Change in DA bond length (Δd) plotted against displacement from equilibrium (ΔD) for each adduct. b) Truncated structures used for CoGEF and graphical depiction of scission route for each adduct.

6.3.2 DA Hydrogel Preparation and Characterization

To validate the computational studies and probe the effect of DA mechanochemical reactivity on failure strength in biologically relevant materials, we prepared PEG hydrogels from DA-based crosslinking of maleimide with pFA, dFA or SpCp. Hydrogels were prepared

from crosslinking four armed telechelic maleimide poly(ethylene glycol) (tetramalPEG) (20 kDa) to provide precise control over network structure[29–31] and enable a straightforward comparison of adduct molecular structure on resulting material mechanics. Diene containing crosslinkers were prepared by functionalizing 2 kDa PEG with carboxylic acid containing pFA, dFA and SpCp derivatives (see Supplementary Information). TetraPEG hydrogels were then prepared by combining these diene crosslinkers and tetramalPEG at 8 wt% polymer in water with diene and maleimide groups in stoichiometric balance and allowing to cure at room temperature over 10 days (**Figure 6.4a**, Supplementary Information).

Small angle neutron scattering (SANS) measurements on fully cured 8 wt% gels in deuterium oxide (D, 99.9%) were conducted to compare the resulting nanostructures from each diene type. As presented in **Figure 6.4b**, SANS curves of the hydrogels indicate signatures consistent with previously reported scattering from tetraPEG networks,[32,33] but with indistinguishably different structural features for networks prepared with SpCp, pFA or dFA. Notably, the mesh size l was determined to be approximately 60 nm, where $l=2\pi/q^*$ and $q^* \sim 0.01\ Å^{-1}$ is the critical scattering vector below which scattering intensity shows a featureless upturn. The 12 kDa PEG chains have a contour length of approximately 90 nm, so the measured mesh size is consistent with expectations for hydrogels constructed of 12 kDa PEG chains between crosslinks. This similarity of the underlying nanostructure is further corroborated by similarities in the swelling behavior of each hydrogel (**Figure 6.4c**, **Table S6.2**). Some variance in the measured Young's modulus (E) of fully cured hydrogels was observed and attributed to the more efficient crosslinking obtained through SpCp–maleimide which occurs rapidly within minutes, resulting in a final modulus value of 14.5 kPa; by contrast, pFA and

dFA networks required 7–10 days to reach comparable modulus values of 10.3 and 11.9 kPa, respectively (**Figure 6.4d**). Taken together, these results support that SpCp, pFA and dFA can be used interchangeably without greatly affecting the final morphology of the network, although variance in final modulus values should be considered in the assessment of material failure strength.

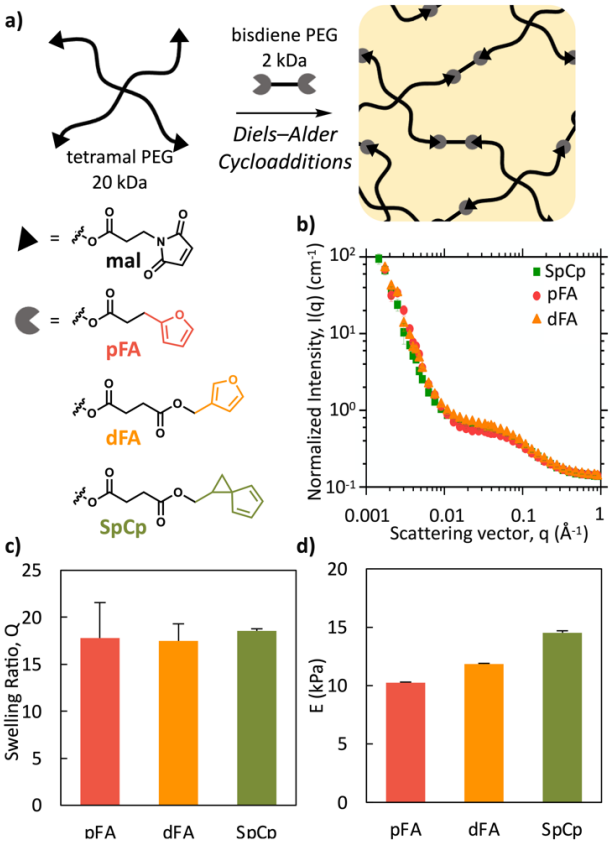

Figure 6.4. a) Schematic representation of tetraPEG hydrogel formation from crosslinking maleimide-functionalized tetraPEG (20 kDa) with diene functionalized PEG linkers (2 kDa). b) Overlay of SANS plots of fully cured hydrogels prepared at 8 wt% in deuterium oxide. The critical scattering vector q^* is approximately 0.01 $Å^{-1}$ for the three hydrogels, wherein scattering from individual PEG chains between crosslinks dominate for $q>q^*$. c) Equilibrium swelling ratio, Q, for each hydrogel (n = 3). d) Modulus determined by indentation for each hydrogel (n = 6 pFA, n = 4 dFA/SpCp).

The contrasting curing times for furan (pFA/dFA) and cyclopentadiene (SpCp) derived hydrogels were in agreement with reported kinetics of hydrophobic accelerated DA cycloadditions.[20,34] As anticipated, the SpCp containing linker provided rapid gelation, passing a flip-test within 2 minutes (**Figure 6.5a**). However, pFA and dFA based hydrogels, which undergo a much slower cycloaddition required 20 h and 42 h to gel, respectively, and multiple days to reach full cure at room temperature as determined by *in situ* indentation measurements (**Figure 6.5a**, **Table S6.3**). To further compare the efficiency of these cycloadditions, a kinetics study was completed by monitoring the reaction of each diene crosslinker (prepared at 2.5 mM in D_2O) with two equivalents of 3-maleimidopropionic acid by ^1H NMR spectroscopy (Supplementary Information). Strikingly, the SpCp–maleimide system reached 85% conversion within 5 minutes, and quantitative conversion was confirmed after 30 minutes (**Figure 6.5b**). In contrast, the two furan-based crosslinkers exhibit considerably slowed kinetics in agreement with gelation times (**Figure 6.5a**) and previous reports.[19,20] Given that SpCp network morphology is comparable to classically employed pFA, the enhanced kinetics and crosslinking efficiency offers a significant advantage for material throughput and for applications such as 3D printing where rapid gelation is desired. Additionally, this study provided insights into the anticipated *endo:exo* ratio of FA-mal cycloadducts within each hydrogel (**Figure 6.5b**, **S6.15–6.16**). This ratio is most important in the case of dFA where the *endo* and *exo* isomers have strikingly different mechanochemical behavior. After 120 h, the *endo*:*exo* ratio for dFA–mal was determined to be 1:0.8, indicating that under room temperature curing conditions nearly half of the formed linkages in our hydrogel will be mechanoresistant *exo* dFA–mal.

6.3.3 Comparison of Failure Properties of DA hydrogels

Initial investigations into the fracture properties of the tetra-PEG hydrogels were attempted via notch tests; however, multi-day curing was incompatible with preparing the thin film (1 mm) geometries required for this method due to solvent evaporation from molds. Additionally, the low working time of the SpCp samples (less than 2 minutes) prohibited the creation of films with uniform thickness. As an alternative, we identified puncture as a preferable technique that involved facile sample preparation within sealed glass vials, did not require the manipulation of fragile gels, and provided high throughput and repeatable measurements.[35–37] Puncture of samples was accomplished by inserting a blunt needle (359 μm outer radius) into samples with constant displacement rate (1 mm/s) until puncture was achieved (see Supplementary Information). Here puncture force is used as a relative indicator of the strength of the different samples, as has been done previously.[36] Note that while the puncture force is representative of a material strength, a positive relationship between this quantity and fracture toughness has been previously observed in experiment[38] and modeling.[39] Further, recent work has suggested a link between bond strength and puncture force.[16] As presented in **Figure 6.5c**, significantly different puncture forces were required for dFA and SpCp-based hydrogels compared to pFA, although scattering measurements, Young's moduli and swelling behaviors indicate similar nanostructures. Hydrogels containing mechanolabile pFA–maleimide crosslinks punctured most readily with a required puncture force (F_c) nearly 3 times lower than that required of the dFA and SpCp analogs (**Figure 6.5c**). This observation is in agreement with the trends in mechanochemical reactivity predicted from CoGEF calculations. Some difference in F_c can be attributed to the variance of Young's modulus values presented in

Figure 6.5d in addition to the displacement distance of the needle before puncture (d_c). If the weakest bond strengths in the materials were equal, a molecular argument (Supplementary Information) predicts that having a reduced crosslinking density in the pFA samples relative to the SpCp samples should result in a 22% increase in F_c in the pFA samples, in contrast to the to the observed 72% decrease in F_c. This indicates that the changes in crosslinking density are not sufficiently large to overcome the changes induced by weakening the bonds in the material. Further, from the continuum perspective, deconvoluting the effect of d_c and E on F_c (**Figure S6.12**, **Table S6.4**) indicates that the observed increases in puncture force can be primarily attributed to changes in d_c. This finding suggests that F_c can be used in this case as a relative indicator of the mechanoresistance of DA adducts. The increase in F_c observed in the dFA and SpCp relative to the pFA samples indicates an increase in the molecular strength, or conversely a decrease in the mechanochemical reactivity.

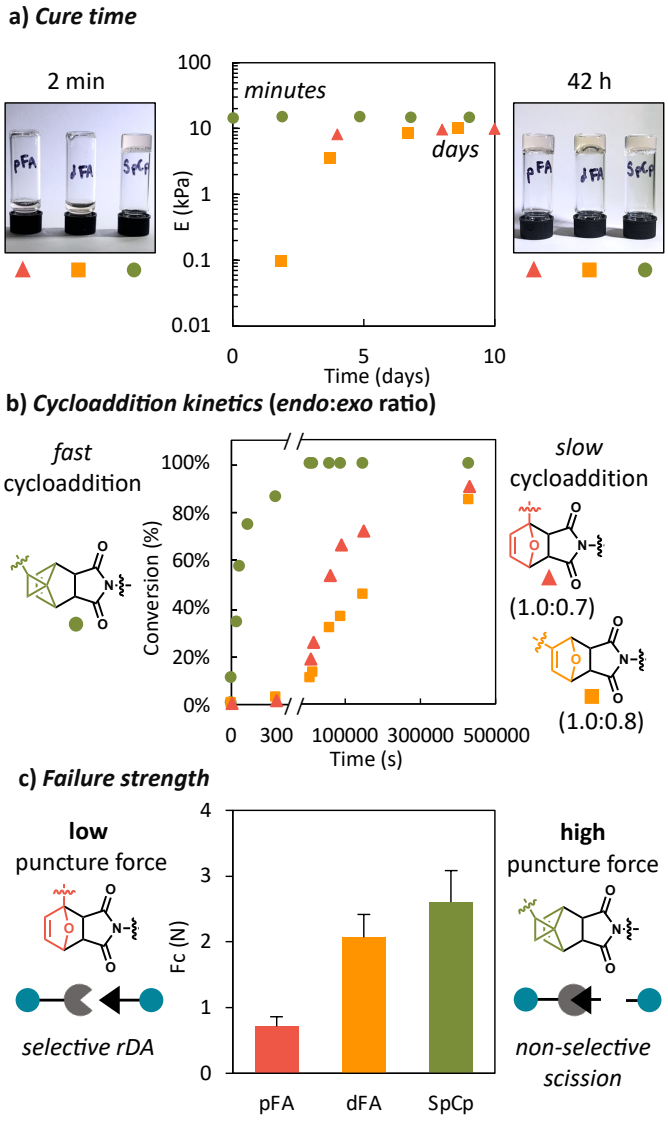

Figure 6.5. a) Plot of Young's modulus (E) measured via indentation as samples cured over multiple days. b) Cycloaddition kinetics of diene crosslinkers determined by ^{1}H NMR and final *endo*:*exo* ratio of FA–mal adducts. Conversion and ratio of isomers determined by integration of diene signals against ethylene carbonate internal standard. c) The required puncture force (F_c) for pFA (n = 6), dFA (n = 4) and SpCp hydrogels (n = 3).

6.4 Conclusion

In conclusion, we have demonstrated that rational consideration of the mechanolability of DA cycloadducts plays a critical role in the resulting macroscopic properties of networks

prepared from them. Specifically, we find a direct relationship between the presence of mechanolabile DA linkages and the resulting puncture force of the network. As such, by employing mechanoresistant DA adducts in place of traditional *proximal* furan–maleimide, the puncture resistance of networks was increased 3-fold. Based on the reported results of this study, we suggest that the simple substitution of traditional *proximal* furans for the *distal* regioisomer, which is commercially available, will provide a facile route to improved lifetime, utility, and mechanical durability in furan-based biomaterials while maintaining potential for thermal reversibility and dynamic behavior. Alternatively, we present a second thermally stable and mechanoresistant diene, spiro[2.4]hepta-4,6-diene, with significantly improved gelation kinetics that we anticipate will have great utility in bioprinting and cell encapsulation applications. This study highlights how mechanochemical reactivity can optimize for mechanical robustness. Conversely, we also envision that the purposeful design and use of DA mechanophores could provide unique advantages in the preparation of dynamic self-healing or stress relaxing materials that could mimic the viscoelasticity of natural tissues. Thus, the combinatorial mechanical and thermal rDA for improved dissociative stress relaxing biomimetic materials is an exciting future direction. Given the ubiquity of DA cycloadditions in the preparation of hydrogels for a variety of biomedical applications, this work demonstrates that DA cycloadduct mechanochemistry should be an important consideration in the synthetic design of devices and therapeutics.

6.5 Acknowledgments

I would like to thank Dr. Christopher Barney for his insights and expertise in the acquisition and analysis of puncture measurements presented in this chapter. I would also like to thank Dr.

Nairiti Sinha and Dr. Sai Venkatesh Pangali for their assistance in acquiring and analyzing scattering measurements. I would also like to thank the UCSB Graduate Division for financial support through a Chancellor's Fellowship and acknowledge the research reported here was partially supported by and made use of equipment provided by the BioPACIFIC Materials Innovation Platform of the National Science Foundation under award No. DMR-1933487. Use was also made of computational facilities purchased with funds from the National Science Foundation (CNS-1725797) and administered by the Center for Scientific Computing (CSC). The CSC is supported by the California NanoSystems Institute and the Materials Research Science and Engineering Center (MRSEC; NSF DMR 1720256) at UC Santa Barbara. Neutron scattering research was conducted at the Bio-SANS instrument, a DOE Office of Science, Office of Biological and Environmental Research resource, and used resources at the High Flux Isotope Reactor, a DOE Office of Science, Scientific User Facility operated by the Oak Ridge National Laboratory.

6.6 Supporting Information

Synthesis of Network Building Blocks

Materials and Methods

Unless otherwise noted, all chemicals were obtained from Sigma Aldrich, Fisher Scientific or Oakwood Chemical and used as received without further purification and all reactions were performed under an atmosphere of nitrogen. Acetonitrile, tetrahydrofuran, dichloromethane and toluene were dispensed from a solvent purification system immediately before use or stored over 3Å molecular sieves. Ethanol and methanol were also stored over 3Å molecular sieves before use. Thin-layer chromatography (TLC) was conducted with E. Merck silica gel

60 F254 pre-coated plates (0.25 mm) and visualized by exposure to UV light (254 nm) or stained with *p*-anisaldehyde. Flash column chromatography was performed using normal phase silica gel (60 Å, 0.040 – 0.063 mm, Geduran) with hexanes, ethyl acetate (EtOAc), DCM and/or MeOH as eluents. ^{1}H and ^{13}C NMR spectra were recorded on Varian spectrometers (100, 400 or 600 MHz) and are reported relative to $CDCl_3$ (δ = 7.26 ppm for ^{1}H and 77.00 ppm for ^{13}C). Data for ^{1}H NMR spectra are reported as follows: chemical shift (δ ppm), multiplicity, coupling constant (Hz) and integration. Data for ^{13}C NMR spectra are reported in terms of chemical shift (δ ppm). Mass spectra were obtained from the UC Irvine Mass Spectrometry Facility on a time-of-flight mass spectrometer with an ESI source. Size exclusion chromatography (SEC) eluting with chloroform ($CHCl_3$) and calibrated relative to poly(ethylene glycol) standards was performed on a Waters Alliance HPLC System, 2695 separation module equipped with a Waters 2410 differential refractometer and Waters 2998 photodiode array detector.

Synthesis of Small Molecules

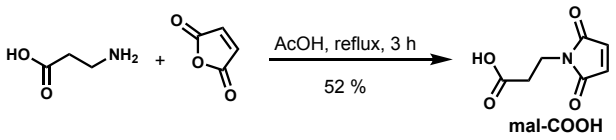

mal-COOH

3-maleimidopropionic acid (mal-COOH):

3-maleimidopropionic acid is *commercially available* (CAS 7423-55-4), but was prepared according to a literature procedure.[40] In a 100 mL round bottom flask, maleic anhydride (6.00 g, 61.2 mmol, 1 eq) and beta-alanine (5.50 g, 61.7 mmol, 1.01 eq) were dissolved in acetic acid (45 mL) and the solution was brought to reflux. After 3 h the solution was cooled to room

temperature and the acetic acid was removed under reduced pressure. The residue was subjected to flash column chromatography (2.5% methanol in dichloromethane) to afford **mal-COOH** (5.38 g, 31.8 mmol, 52 %) as a white powder. Spectral data matches reported literature.[40] The compound was further purified by recrystallization from hot water to afford colorless crystals before being used to functionalize **tetraPEG**.

^{1}H NMR (400 MHz, $CDCl_3$) δ 10.87 (brs, 1H), 6.72 (s, 2H), 3.84 (t, J = 7.2 Hz, 2H), 2.71 (t, J = 7.2 Hz, 2H) ppm.

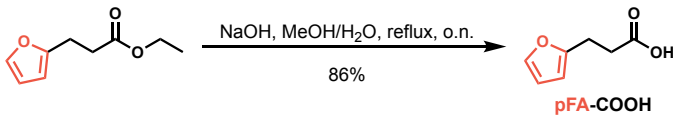

2-furanpropionic acid (pFA-COOH):

2-furanpropionic acid is *commercially available* (CAS 935-13-7) but was prepared from the more affordable ester precursor (CAS 10031-90-0). In a 500 mL round bottom flask ethyl 3-(furan-2-yl)propionate (7.20 g, 42.8 mmol, 1 eq) was dissolved in in methanol (MeOH, 75 mL) before 2.5 M NaOH (200 mL) was slowly added. The solution was refluxed overnight (15.5 h) before cooling to rt. The solution was neutralized with 3 M HCl and extracted with dichloromethane (3 X 200 mL). The combined organic layers were washed with brine (100 mL), dried over magnesium sulfate, and concentrated under reduced pressure to afford **pFA-COOH** (5.13 g, 36.6 mmol, 86 %) as an off-white solid. Spectral data matches reported literature.[41]

^{1}H NMR (600 MHz, $CDCl_3$) δ 10.67 (brs, 1H), 7.32 – 7.30 (m, 1H), 6.29 – 6.27 (m, 1H), 6.05 – 6.04 (m, 1H), 2.98 (t, J = 7.5 Hz, 2H), 2.72 (t, J = 7.6 Hz, 2H) ppm.

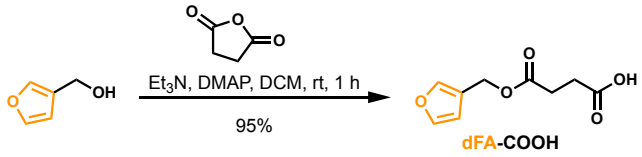

4-(furan-3-ylmethoxy)-4-oxobutanoic acid (dFA-COOH):

In a scintillation vial equipped with stir bar furan-3-methanol (CAS 4412-91-3) (1.72 mL, 200 mmol, 1 eq) was dissolved in dichloromethane (DCM) (7.5 mL), then triethyl amine (2.79 mL, 20.0 mmol, 1 eq), 4-dimethylaminopyridine (DMAP, 244 mg, 2.00 mmol, 0.1 eq), and succinic anhydride (2.60 g, 26.0 mmol, 1.3 eq) were added. The reaction was stirred at rt until complete consumption of the starting material (TLC, 1 h). The solution was transferred to a separatory funnel along with additional DCM (50 mL). The organic layer was washed with 1 M HCl (2 X 50 mL) then water (1 X 50 mL) and dried over magnesium sulfate. The solvent removed to afford **dFA-COOH** (3.76 g, 19.0 mmol, 95%) as an off-white solid.

dFA-COOH: ^{1}H NMR (600 MHz, $CDCl_3$) δ 7.47 (m, 1H), 7.40 (m, 1H), 6.42 (m, 1H), 5.02 (s, 2H), 2.71 – 2.64 (m, 4H) ppm; ^{13}C NMR (125 MHz, $CDCl_3$) δ 177.56, 171.99, 143.44,

141.61, 120.14, 110.49, 58.11, 28.82, 28.77 ppm; HRMS (ES+) Exact mass cald. for $C_9H_{10}O_5Na$ $[M+Na]^+$: 221.0426, found: 221.0426.

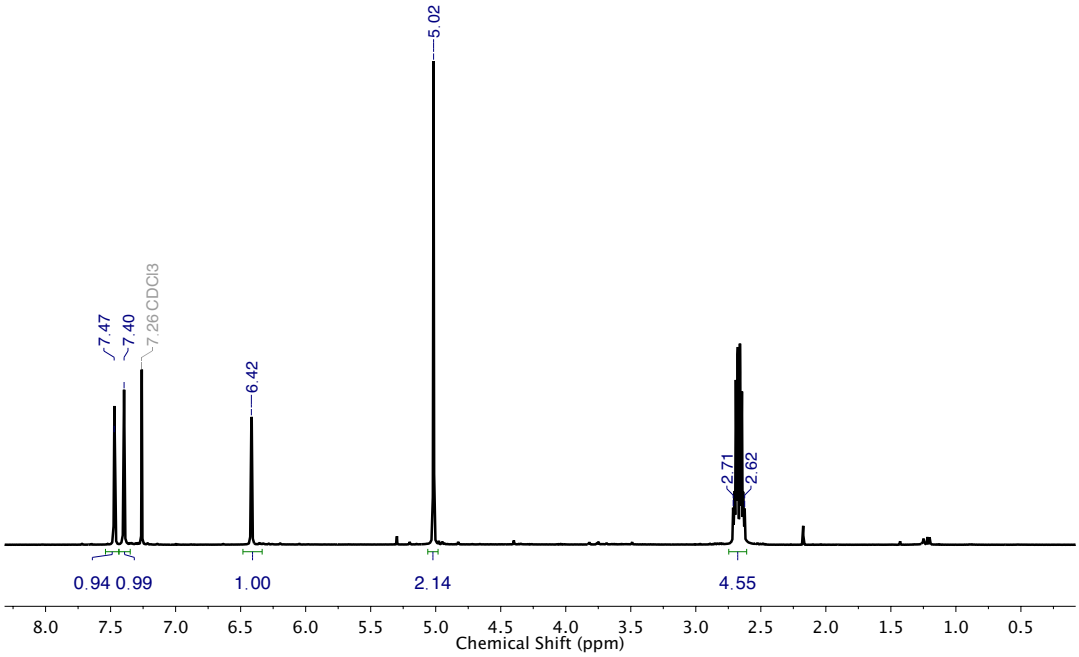

Figure S 6.1. ^1H NMR (400 MHz, $CDCl_3$) **dFA-COOH**

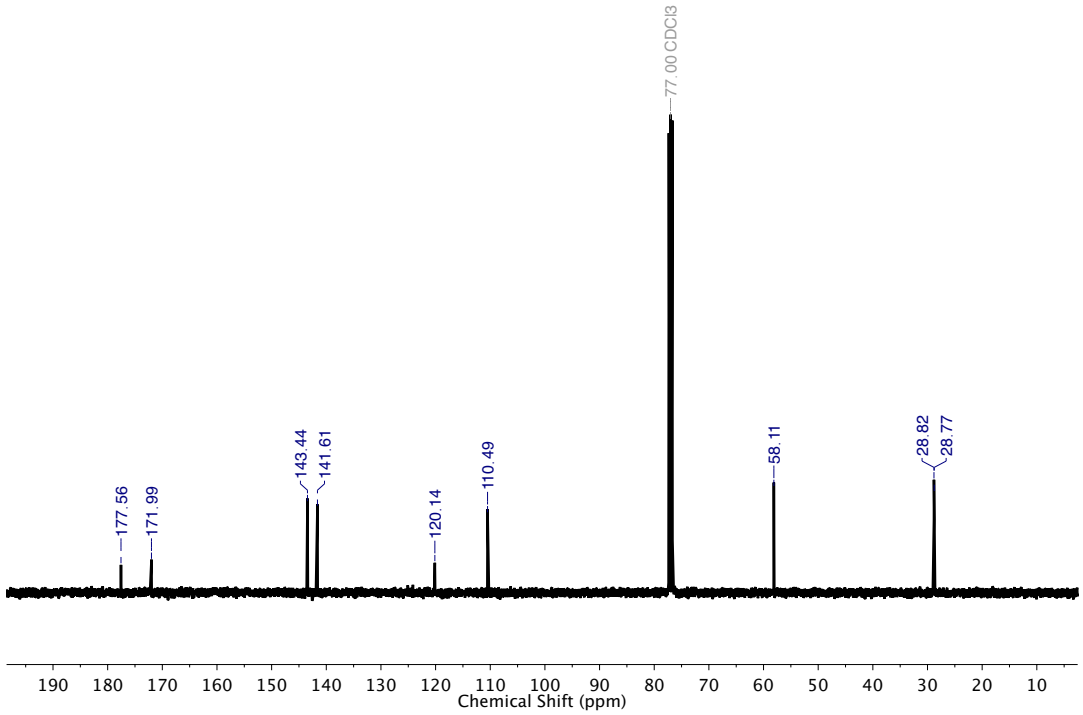

Figure S 6.2. ^{13}C NMR (125 MHz, $CDCl_3$) **dFA-COOH**

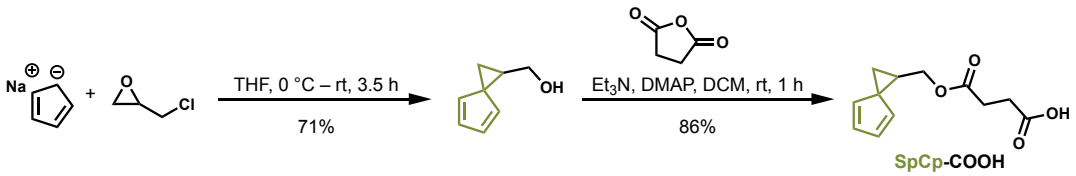

4-oxo-4-(spiro[2.4]hepta-4,6-dien-1-ylmethoxy)butanoic acid (SpCp-COOH):

SpCp-COOH was prepared according to a literature procedure.[20]

Step 1: Epichlorohydrin (4.05 mL, 51.7 mmol, 1 eq) was dissolved in tetrahydrofuran (200 mL) in a flame dried, 1 L round bottom flask equipped with dropping funnel. The solution was cooled to 0 °C before sodium cyclopentadienylide (100 mL, 2-3 M solution purchased from Strem Chemical) was added dropwise and allowed to stir for 3.5 h (at which point complete consumption of epichlorohydrin was confirmed by ^{1}H NMR). To the solution was added H_2O (200 mL) followed by saturated sodium bicarbonate (200 mL) before extracting with diethyl

ether (3 X 200 mL). The combined organic layers were washed with brine (200 mL), dried over magnesium sulfate, and concentrated under reduced pressure. The residue was subjected to flash column chromatography (hexanes:ethyl acetate, 2:1) to afford **SpCp-OH** (4.36 g, 35.7 mmol, 71 %).

Step 2: In a scintillation vial equipped with stir bar **SpCp-OH** (1.28 g, 10.4 mmol, 1 eq) was dissolved in DCM (3 mL), then triethyl amine (1.45 mL, 10.4 mmol, 1 eq), DMAP (127 mg, 1.04 mmol, 0.1 eq), and succinic anhydride (1.36 g, 13.6 mmol, 1.3 eq) were added. The reaction was stirred at rt until complete consumption of the starting material (TLC, 1 h). The solution was transferred to a separatory funnel along with additional DCM (100 mL). The organic layer was washed with 1 M HCl (2 X 75 mL) then water (1 X 75 mL) and dried over magnesium sulfate. The solvent removed to afford **SpCp-COOH** (1.99 g, 8.95 mmol, 86 %) as a yellow-white solid. Spectral data matches reported literature.[20]

^{1}H NMR (400 MHz, $CDCl_3$) δ 9.85 (brs, 1H) 6.57 (dt, *J* = 5.2, 1.9 Hz, 1H), 6.48 (dt, *J* = 5.1, 1.5 Hz, 1H), 6.20 (dt, *J* = 5.2, 1.7 Hz, 1H), 6.06 (dt, *J* = 5.1, 1.7 Hz, 1H), 4.35 (dd, *J* = 11.7, 7.5 Hz, 1H), 4.18 (dd, *J* = 11.6, 7.3 Hz, 1H), 2.69 – 2.60 (m, 4H), 2.41 (quin, *J* = 7.3 Hz, 1H), 1.83 (dd, *J* = 8.6, 4.5 Hz, 1H), 1.67 (dd, *J* = 7.0, 4.5 Hz, 1H) ppm.

Chain-end Functionalization of Poly(ethylene glycol)

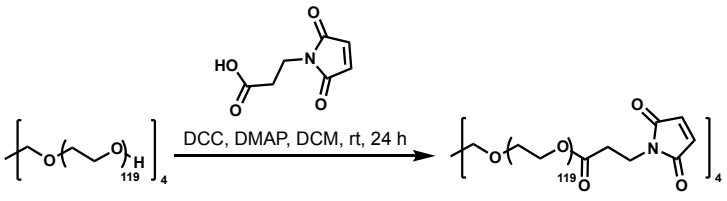

Poly(ethylene glycol)-tetra-maleimide:

In a 200 mL round bottom flask equipped with stir bar **tetraPEG** (purchased from JenKem Technology, M_n = 20,000 g/mol, 40.0 g, 2.00 mmol, 1 eq) was dissolved in dichloromethane 80 mL. To this solution was added **mal-COOH** (3.38 g, 20.0 mmol, 10 eq), *N,N′*-Dicyclohexylcarbodiimide (DCC, 4.54 g, 22.0 mmol, 11 eq), and 4-dimethylaminopyridine (DMAP, 24.4 mg, 0.200 mmol, 0.1 eq). The solution was allowed to stir at rt for 24 h (at which point complete formation of the ester was confirmed by ^{1}H NMR). The reaction solution then was passed through a plug of celite before the solvent was removed under reduced pressure. The residue was taken up in ethanol (EtOH, 800 mL), cooled to 0 °C and left unagitated for 30 minutes to allow **tetramalPEG** to precipitate. The solid was filtered and rinsed with cold EtOH then diethyl ether. The precipitate was thoroughly dried under reduced pressure to afford **tetramalPEG** (27.7 g, 1.32 mmol, 66% recovered yield) as a pink-white solid. $M_{n(NMR)}$ (DP = 119/arm) = 21,500 g/mol, $M_{n(SEC)}$ = 17,000 g/mol, $Đ$ = 1.14.

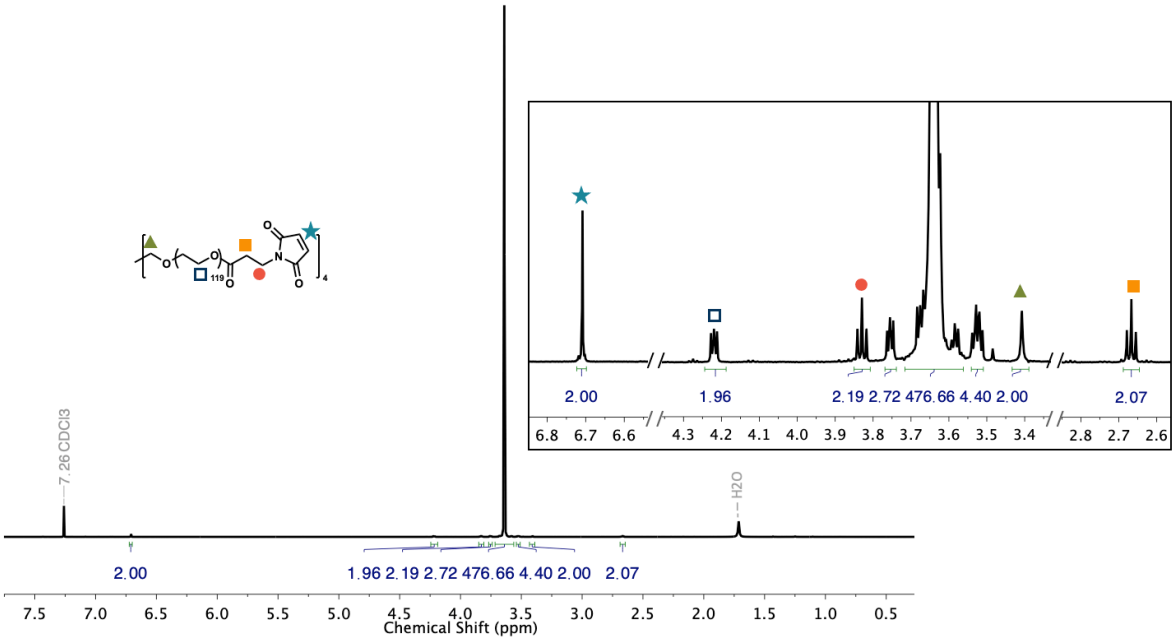

Figure S 6.3. ^{1}H NMR (600 MHz, $CDCl_3$) **tetramalPEG** indicates quantitative chain-end functionalization with maleimide.

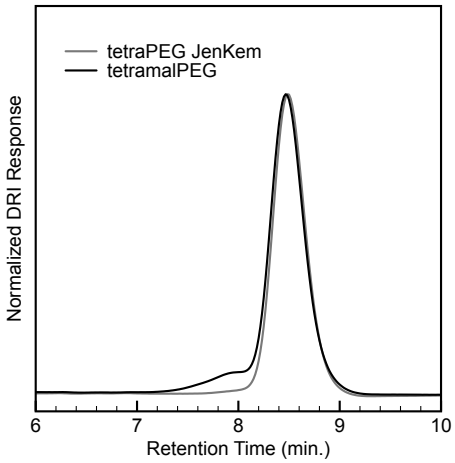

Figure S 6.4. Overlay of size exclusion chromatography (SEC) trace of starting tetraPEG and product **tetramalPEG**

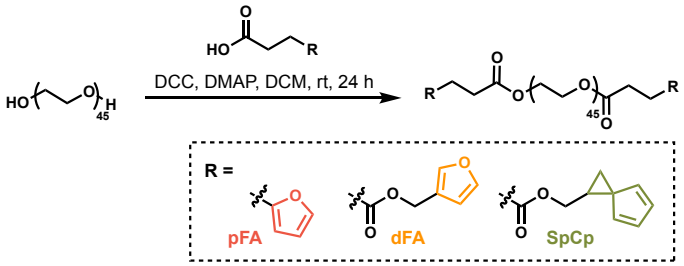

General Procedure for bisdiene-PEG functionalization:

Poly(ethylene glycol) (purchased from Sigma Aldrich, M_n = 2,000 g/mol, 1 eq) was dissolved in DCM to afford a 0.125 M solution of polymer. To this solution was then added the diene carboxylic acid (SpCp-COOH, pFA-COOH or dFA-COOH, 4 eq), DCC) (3 eq), and DMAP (0.2 eq). The solution was allowed to stir at rt for 24 h (at which complete formation of the ester was confirmed by crude ^{1}H NMR). The reaction solution then was passed through a plug of celite before the solvent was removed under reduced pressure. The residue was taken up in ethanol (EtOH, 100 mL/g PEG), cooled to 0 °C and left unagitated for 30 minutes to allow the polymer to precipitate. The solid was filtered and rinsed with cold EtOH then diethyl ether before being thoroughly dried under reduced pressure to afford the diene functionalized polymers as waxy solids.

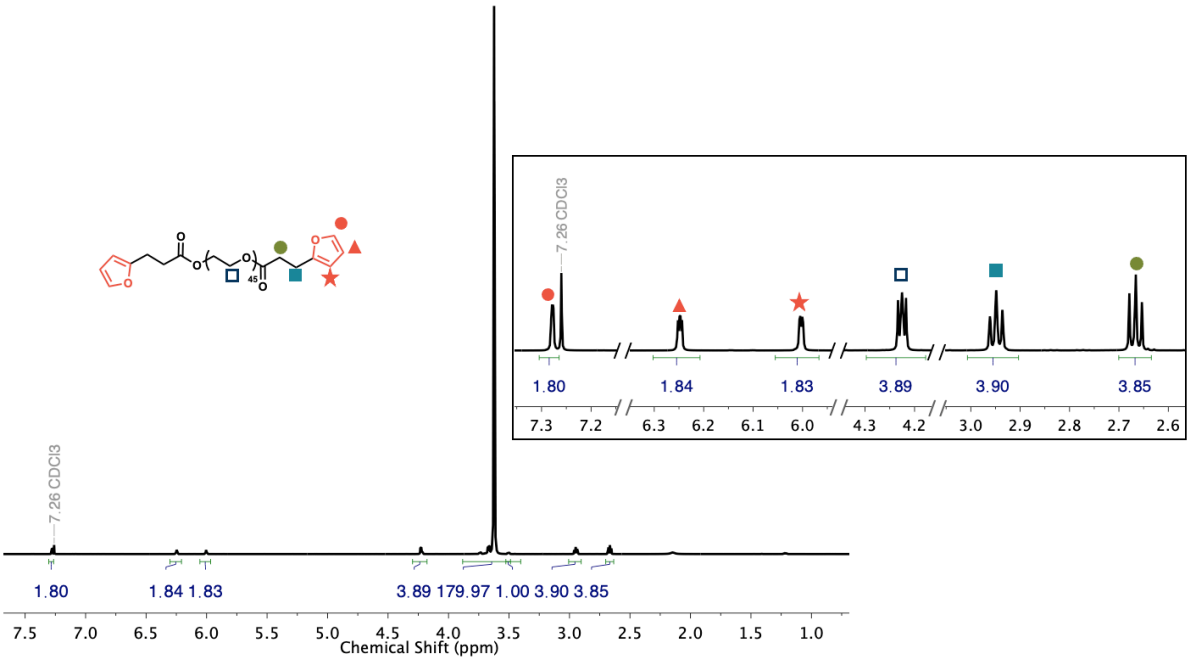

Figure S 6.5. ^{1}H NMR (600 MHz, $CDCl_3$) **bispFAPEG** ($M_{n(NMR)}$ = 2,300 g/mol) indicates quantitative chain-end functionalization with *proximal* furan (**pFA**).

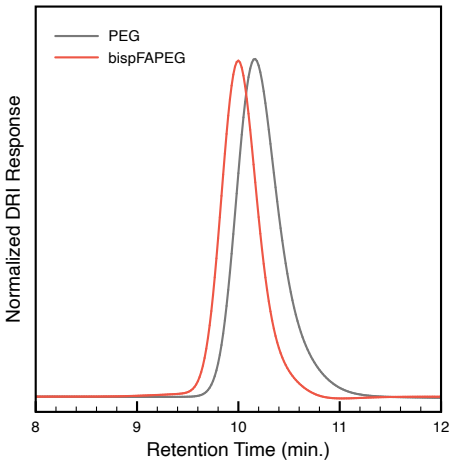

Figure S 6.6. Overlay of SEC trace of starting PEG and product **bispFAPEG**, $M_{n(SEC)}$ = 3,100 g/mol, $Đ$ = 1.05.

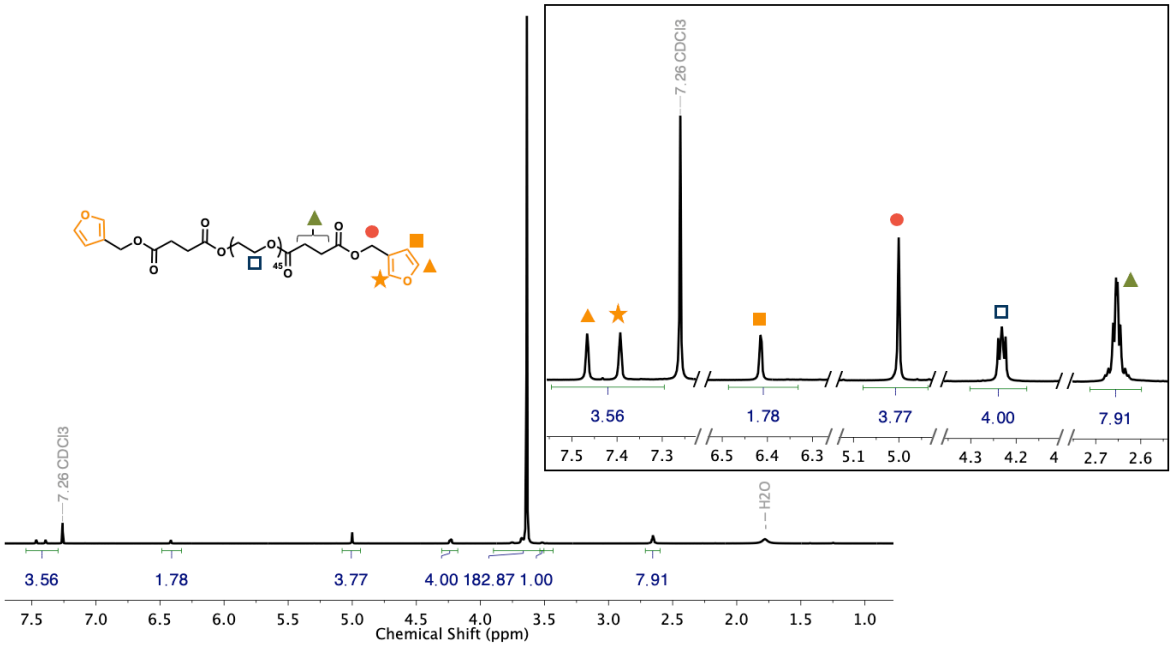

Figure S 6.7. ^{1}H NMR (600 MHz, $CDCl_3$) **bisdFAPEG** ($M_{n(NMR)}$ = 2,400 g/mol) indicates quantitative chain-end functionalization with *distal* furan (**dFA**).

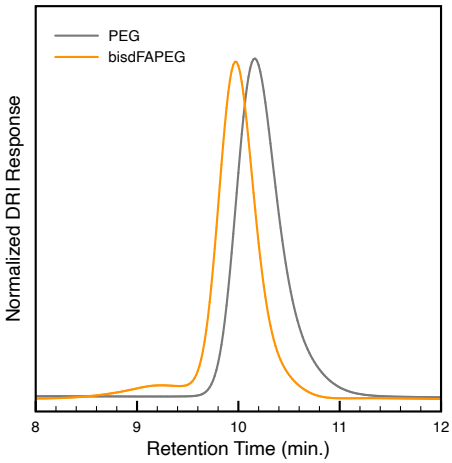

Figure S 6.8. Overlay of SEC trace of starting PEG and product **bisdFAPEG**, $M_{n(SEC)}$ = 3,300 g/mol, $Đ$ = 1.09.

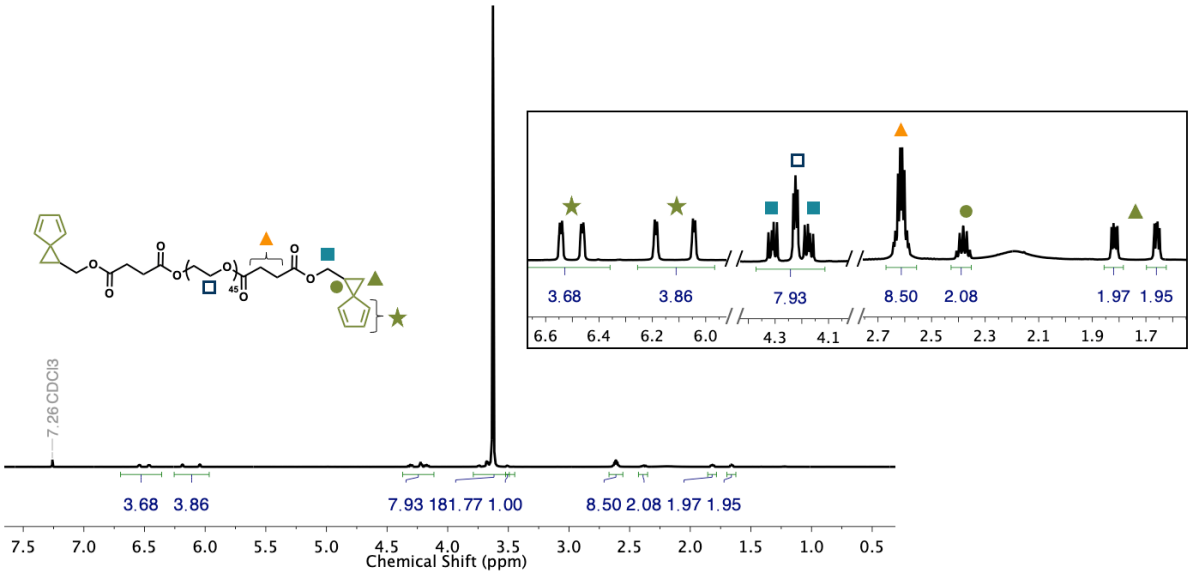

Figure S 6.9. ^{1}H NMR (600 MHz, $CDCl_3$) **bisSpCpPEG** ($M_{n(NMR)}$ = 2,400 g/mol) indicates quantitative chain-end functionalization with spiro[2.4]hepta-4,6-diene (**SpCp**).

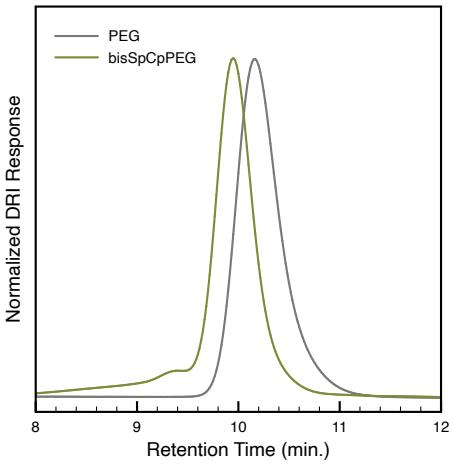

Figure S 6.10. Overlay of SEC-RI trace of starting PEG and product **bisdFAPEG**, $M_{n(SEC)}$ = 3,400 g/mol, $Đ$ = 1.15.

Hydrogel Preparation

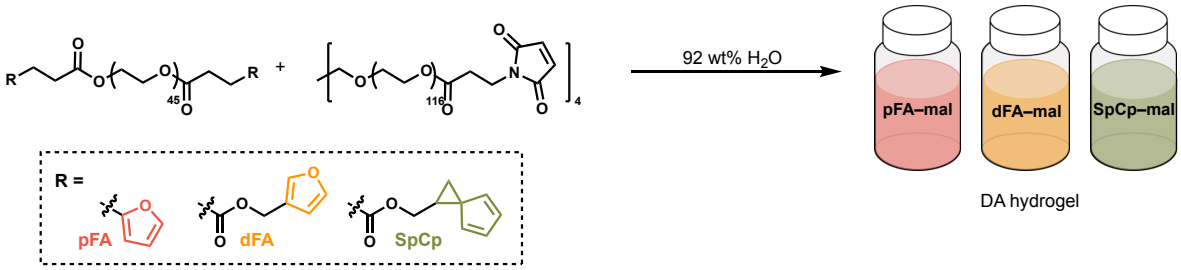

General Procedure for Hydrogel Preparation:

To prepare multiple samples (15 – 17 mL/sample) for indentation and puncture experiments, large batches of pre-hydrogel solutions were prepared and transferred into scintillation vials, capped, and sealed with parafilm for 10 days before puncture experiments. To prepare pre-hydrogel solutions, **tetramalPEG** and each **bisdiene PEG** were dissolved at 8 wt% polymer in deionized water. The solutions were then combined to achieve stoichiometric balance between maleimide, and diene chain ends as indicated in **Table S6.1**.

Table S 6.1. Hydrogel formulations

Linker Type	mmol tetramal PEG	mass 8 wt% solution tetramalPEG (g)	MW bisdiene PEG (g/mol)	mmol bisdienePEG	mass 8wt% solution tetramalPEG (g)
pFA	0.214	**56.25**	2300	0.428	**12.32**
dFA	0.214	**56.25**	2400	0.428	**12.86**
SpCp	0.214	**56.25**	2400	0.428	**12.86**

For SpCp, gelling is rapid (<2 min), thus upon combining the two solutions, care was taken to avoid the introduction of bubbles while mixing solutions, then the viscous pre-hydrogel was

quickly distributed between scintillation vials. For pFA and dFA, gelling was much slower and solution preparation was completed without issue.

Gel Fraction and Swelling Ratios

For determination of gel fraction and swelling ratio, small hydrogels (approx. 100 mg polymer) were prepared in dram vials from the solutions described in Section 1.4. After 10 days the gels were removed from the vials and dried under reduced pressure for 24 h to measure the initial sol + gel mass (W_i). Each gel was then allowed to swell in 150 mL of water for 36 h (exchanging the solvent once) before the equilibrium swelling mass (W_s) was measured. The gels were again dried under reduced pressure for 24 h to afford dry gel mass (W_d). Each hydrogel type was prepared and investigated in triplicate and results of these studies are summarized in **Table S6.2**.

$$\text{gel fraction} = \frac{Wd}{Wi} \times 100$$

$$Q = \frac{Ws - Wd}{Wd}$$

Table S 6.2. Summary of gel fraction and swelling behavior for each hydrogel.

Hydrogel Type	Gel Fraction	Eq. Swelling Ratio, Q
pFA	96 ± 4 %	18 ± 4
dFA	98 ± 3%	17 ± 2
SpCp	94 ± 4%	18.6 ± 0.2

Indentation and Puncture Measurements

Indentation measurements were used to monitor the curing process while puncture measurements were used to quantify the failure strength. Both measurements were performed on a TA.XT Plus Connect Texture Analyzer. The instrument has a load cell with a force capacity of 49 N and a displacement resolution of 1 μm. Indentation was performed with a 2 mm diameter flat steel cylinder moving at a displacement rate of 0.1 mm/s to a max turnaround force of 20 mN. The observed stiffness κ can be used in conjunction with the contact radius a and sample height h ($\approx 30\,mm$) to extract Young's modulus E (Equation 6.1).[42]

$$E = \frac{3}{8a}\kappa\left[1 + 1.33\frac{a}{h} + 1.33\left(\frac{a}{h}\right)^3\right]^{-1} \qquad \text{(Equation 6.1)}$$

Migration of solvent is known to cause shifts in observed the stiffness for gels.[43] This poroelastic effect is typically quantified by comparing the poroelastic relaxation time $\tau_{poro} = \frac{a^2}{D}$, where D is the diffusion coefficient of solvent in the network, to the time scale of the test. Estimating $D = 4.4 \times 10^{-10}\ m^2/s$, measured from the diffusion of water through a PEG methacrylate gel,[44] gives a value of $\tau_{poro} \approx 2200\ s$ which is much longer than the test time of approximately 60 s. Due to this difference in time scales, it is not likely that poroelastic relaxation is significantly altering the stiffness observed with this measurement. E values for each gel were monitored over several days to let the gels cure to completion. A summary of this data is available in **Table S6.3**.

Table S 6.3. Table showing the curing data collected at different times.

Cure Time (Days)	**pFA** E (kPa)	Cure Time (Days)	**dFA** E (kPa)	Cure Time (Days)	**SpCp** E (kPa)
4	8.3±0.6	1.85	0.101±0.004	0.02083	14.83±0.05
8	9.7±0.2	3.725	3.63±0.01	1.89583	15.5±0.2
10	9.9±0.1	6.6833	8.72±0.02	4.8542	15.3±0.1
23	10.1±0.1	8.6208	10.66±0.02	6.7917	15.1±0.1
38	10.3±0.1	10.85	11.83±0.05	9.0209	15.0±0.1
		14.642	12.18±0.06	12.8126	14.6±0.1
		16.767	11.85±0.02	14.9376	14.5±0.2

Puncture measurements were used to quantify the failure strength of the gels once curing had occurred. Puncture measurements were performed with a 22 gauge (207 μm inner radius and 359 μm outer radius) blunt-tipped steel needle sourced from Hamilton Company. A similar calculation to that performed for indentation above gives $\tau_{poro} \approx 293\ s$ while the testing time is kept at approximately 60 s by increasing the displacement rate to 1 mm/s. Puncture tests are performed by inserting a needle into a gel at a constant displacement rate to a displacement beyond the puncture point.[35] An example plot of the force displacement curve observed during puncture of a gel with dFA linkers is shown in **Figure S6.11a**. The initial elastic loading curve is nonlinear in nature and has been shown to be well modeled with an empirically derived force-displacement relationship,[35]

$$F = k'Ed^2 + k''ERd, \quad \text{(Equation 6.2)}$$

where F is force, d is displacement, R is indenter radius, and both k' and k'' are fitting constants that appear to be characteristic for different materials.[35,36,38,45] The elastic loading phase terminates in puncture of the gel. Puncture of the gel displays a characteristic drop in the force-displacement curve giving a critical puncture force F_c and displacement d_c. Here displacement is normalized to the initial contact point between the needle and the gel surface. This point is defined by convention here as occurring once the measured force value reaches 10 mN which is well above the 1 mN noise threshold of the load cell. This results in a small yet consistent underestimation error in the values reported here for d_c. Assuming Hertzian contact holds in this low strain regime then the samples with pFA, dFA, and SpCp linkers are expected to overestimate the initial contact displacement by 1.0, 0.9, and 0.7 mm, respectively, which translates to an approximate underestimation of d_c by 7.4%, 4.6%, and 3.5% respectively.

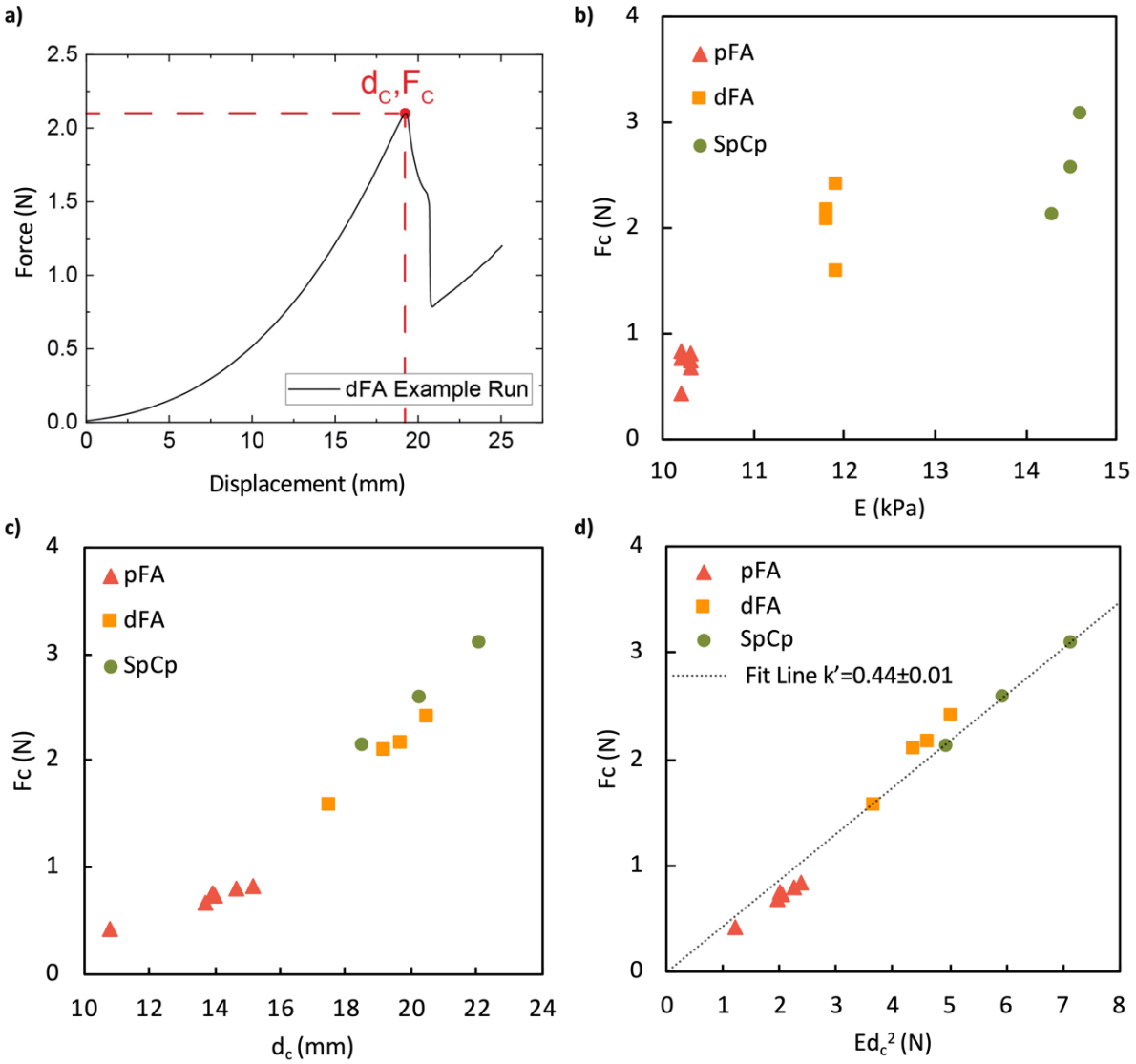

Figure S 6.11. a) A plot showing an example force-displacement curve for a dFA sample. b-c) Plots of $\boldsymbol{F_c}$ against $\boldsymbol{E}$ and $\boldsymbol{d_c}$ showing that $\boldsymbol{F_c}$ is a function of both variables. d) Plot of $\boldsymbol{F_c}$ against $\boldsymbol{Ed_c^2}$ where the observed linear collapse justifies the treatment of $\boldsymbol{k'}$ as a constant value.

A comparison of F_c against E is shown in **Figure S6.11b.** This comparison shows there is a systematic increase in F_c as E increases between the samples. A similar comparison between F_c and d_c in **Figure S6.11c** shows that there is also a systematic increase in F_c as d_c increases.

The systematic variation of F_c with both E and d_c is of concern as this suggests that the changes observed in F_c may be conflated by changes in E. From the molecular perspective, it is true that both modulus and fracture toughness have an explicit dependence on the crosslinking density. According to Lake-Thomas theory,[46] $G_c \sim \sqrt{N}$ where G_c is the fracture toughness and N represents the number of Kuhn segments between crosslinks. According to statistical theory,[47] $E \sim N^{-1}$ where E is Young's modulus giving that $G_c \sim E^{-1/2}$ when altering the number of elastically effective crosslinks at constant network concentration. If the weakest bond strengths in our networks were equal, this would predict that G_c should increase by a factor of approximately 1.22 when going from SpCp samples to pFA samples. If this translated directly to a change in F_c (past measurements[49] have observed that $\frac{F_c}{R} \sim \sqrt{G_c}$ which would predict an increase of 10%), this would predict a 22% increase in the puncture force of the pFA samples relative to the SpCp samples instead of the 72% decrease observed experimentally. This decrease is most likely associated with the fact that we are altering the weakest bond in our system and $G_c \sim U$ where U is related to the strength of the weakest bond in the system. Our results here suggest that the crosslinking density is not altered enough to overcome the changes induced by weakening the bonds in the system and that these changes are better quantified using our understanding of the mechanics at the continuum level.

The impact of E and d_c on F_c can be estimated by substituting into Equation 6.2 and ignoring the lower order term ($k'' = 0$) to get Equation 6.3.

$$F_c = k' E {d_c}^2 \qquad \text{(Equation 6.3)}$$

The plot of F_c against $E{d_c}^2$ in **Figure S6.11d** confirms that k' is reasonably well approximated with a constant value of 0.44 ± 0.01 for the gels used in this study. This agreement suggests that this relationship is valid for these gels and can be used to deconvolute the impact that changes in E and d_c have on F_c. Taking the pFA samples as a reference point, the values of F_c predicted from the observed changes in E and d_c are shown in **Figure S6.12**. These calculations are performed by taking the changes in E and d_c in combination with the above equation to estimate the change in F_c relative to the pFA samples used here as a reference point. This can be expressed as follows:

$$F_{c,pred} = F_{c,ref}\left(\frac{E_{obs}}{E_{ref}}\right)\left(\frac{d_{c,obs}^2}{d_{c,ref}^2}\right) \quad \text{(Equation 6.4)}$$

where $F_{c,pred}$ is the predicted value of the critical puncture force, E_{obs} and $d_{c,obs}$ are the observed values of the Young's modulus and critical puncture displacement, respectively, and $F_{c,ref}$, E_{ref} and $d_{c,ref}$ refer to reference values of the same. For example, the average values of E and d_c for the pFA and dFA samples are 10.3 kPa and 11.85 kPa, respectively, and 13.73 mm and 19.3 mm, respectively. Using the ratio approach described in Equation 6.4, we find a predicted multipliers of $\left(\frac{E_{obs}}{E_{ref}}\right)$ =1.15 and $\left(\frac{d_{c,obs}^2}{d_{c,ref}^2}\right)$ =1.98 resulting in a total predicted multiplier of 2.28. However, the linear relationship that we observed between both E and F_c and d_c^2 and F_c suggests that the 15% increase that is expected from the change in E, will influence the 1.98 multiplier value. Assuming a linear relationship between E_c and d_c^2 we estimate the amplitude of this effect to be 0.15*1.98, which gives a value of 0.297 and a total multiplier value of 1.98+0.297=2.277. Normalizing this value by the total predicted multiplier

suggests that the predicted shift in F_c that is attributable to changes in E is $\frac{0.297}{2.277} \times 100 = 13.04\%$. Similar calculations comparing SpCp samples to the pFA samples suggest that 29.1% of the observed change in F_c is attributable to changes in E, as summarized in **Table S6.4**.

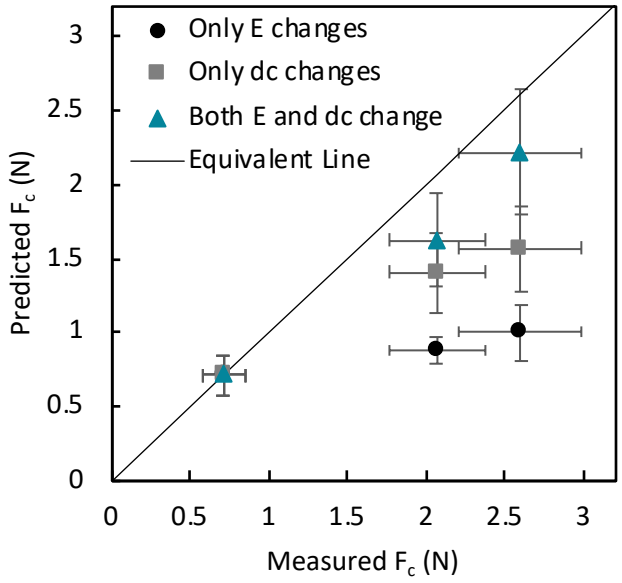

Figure S 6.12. Plot showing predicted changes in F_c due to changes in E and d_c predicted using pFA gels as a reference point in conjunction with Equation 3.

Table S 6.4. Summary of predicted values of $\boldsymbol{F_c}$ plotted in **Figure S6.12.**

Sample	Measured Fc (N)	Predicted Fc (N)		
		Only E Changes	Only dc Changes	Both E and dc change
pFA	0.7135±0.1340	Ref. Point	Ref. Point	Ref. Point
dFA	2.0674±0.3025	0.887±0.088	1.41±0.27	1.63±0.31
SpCp	2.6044±0.3914	1.006±0.189	1.57±0.29	2.21±0.42

Puncture of the gel occurs due to the nucleation of a crack near the needle. Past observations have shown that this crack morphology can be quite complex and likely relates to tip geometry,

materials properties, and materials defects.[48–50] Two different crack morphologies were observed during the puncture measurements performed for this study. The first is the cone-like crack morphology that has been observed and reported previously.[50] Example images and schematic representations of this morphology at different points during the puncture process are shown in **Figure S6.13**. Notably, propagation of a conical crack fails to release strain energy from a large volume of material below the indenter and can both support post-puncture forces that are significantly higher than the puncture force and display a nonlinear force-displacement relationship in the post-puncture regime. The second crack morphology observed during puncture measurements is a combination of those previously reported in the literature. This crack morphology starts as a conical crack and then transitions into a tube-like crack morphology. Example images and schematic representations of this morphology at different points during the puncture process are shown in **Figure S6.14**. The transition between crack morphologies appears to be associated with an abrupt deflection of the needle tip in the radial plane. This deflection is associated with the drop in force observed at approximately 26 s in **Figure S6.14**. Together these observations suggest that the crack morphology may shift because the bending stiffness of the indenter is low enough to enable the tip to deflect and follow the path of least resistance. A summary of the puncture data gathered in this study, including the crack morphology observed, is contained in **Table S6.5**.

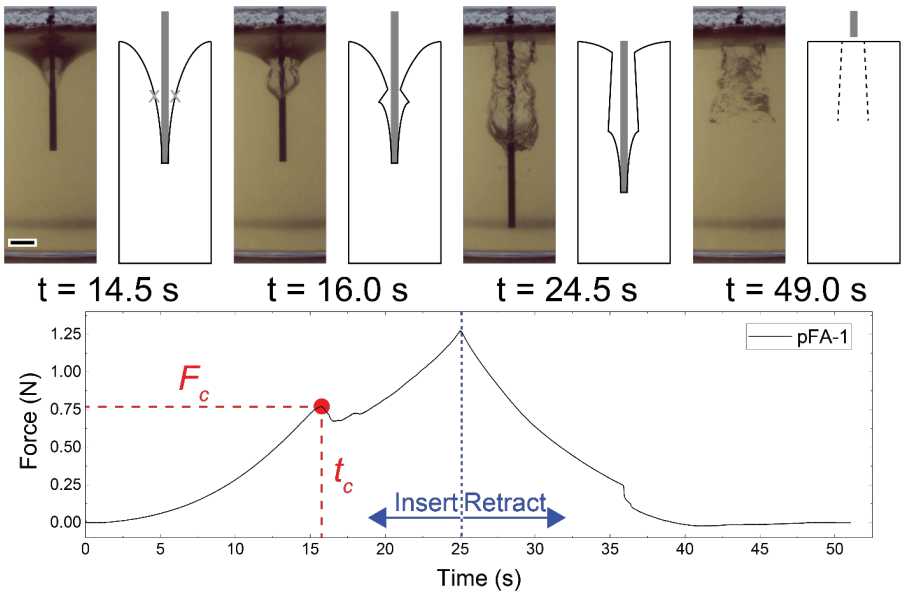

Figure S 6.13. Images and schematic representations of the nucleation and propagation of a conical crack during puncture at different points during the puncture process. From the left, there is deep indentation before puncture, post-puncture, post-propagation near the turnaround point, and the leftover morphology once the needle in fully retracted. The scale bar on the first image represents 2.5 mm.

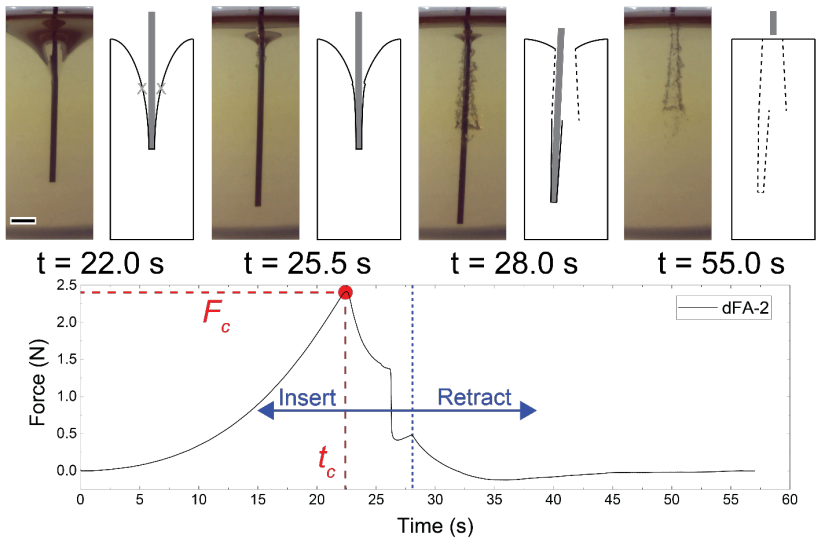

Figure S 6.14. Images and schematic representations of the nucleation and propagation of a cone and tube type crack during puncture at different points during the puncture process. From the left, there is deep indentation before puncture, post-puncture, post-propagation near the turnaround point, and the leftover morphology once the needle in fully retracted. The scale bar on the first image represents 2.5 mm.

Table S 6.5. Summary of the puncture data taken for the samples in this study. Sample denotes the material used for that specific run. Needle radius shows the outer radius of the needle used during puncture. E reports the values of Young's modulus measured via indentation. d_c and F_c stand for the critical puncture displacement and force. Crack morphology reports the type of crack observed during the puncture process. C denotes conical cracks and C+T denotes cone and tube cracks.

Sample	Needle Radius (mm)	E (kPa)	d_c (mm)	F_c (N)	Crack Morphology
pFA-1	0.359	10.2	13.95	0.769	C
pFA-2	0.359	10.3	13.72	0.683	C+T
pFA-3	0.359	10.3	14	0.745	C+T
pFA-4	0.359	10.3	14.67	0.809	C+T
pFA-5	0.359	10.2	10.82	0.435	C+T
pFA-6	0.359	10.2	15.22	0.84	C+T
dFA-1	0.359	11.9	17.529	1.5851	C+T
dFA-2	0.359	11.8	19.19	2.0949	C
dFA-3	0.359	11.9	20.553	2.41557	C+T
dFA-4	0.359	11.8	19.735	2.17404	C+T
SpCp-1	0.359	14.7	--	--	C+T
SpCp-2	0.359	14.6	22.087	3.09405	C+T
SpCp-3	0.359	14.5	20.267	2.58316	C+T
SpCp-4	0.359	14.3	18.546	2.13612	C+T

Scattering Measurements

Small-angle neutron scattering measurements were performed using the Bio-SANS instrument located at the High Flux Isotope Reactor in Oak Ridge National Laboratory.[51,52] A single standard configuration of the dual detector system was set with the Panel Scan feature of the instrument with the small-angle detector at 7 m and the wide-angle detector at 1.3 m and 3.2° to the sample position.[53] Using this configuration, the Q range spanning $0.007 < Q$ (Å-1) < 1 was obtained using 6 Å wavelength neutrons with a relative wavelength spread ($\Delta\lambda/\lambda$) of 15%, ($Q = 4\pi \sin(\theta) / \lambda$, with scattering angle as 2θ and wavelength, λ). The data were corrected for instrument background, detector sensitivity, and instrument geometry using facility data reduction software, drt-SANS. All SANS measurements were performed in 1 mm path length glass cell. To prepare samples for scattering, 8 wt% solutions of **tetramalPEG** and each **bisdiene PEG** were prepared by dissolving each polymer in deuterium oxide (D, 99.9% Cambridge Isotope Laboratories) and small-scale pre-hydrogel solutions (100 mg PEG) were prepared in stoichiometric ratio as described in Section 1.4. Once mixed, the pre-hydrogel solutions were quickly transferred into glass cells of dimensions 1 X 20 X 20 mm which were sealed with parafilm and allowed to cure for 10 days at rt before storing at 5 °C until scattering data was obtained. Scattering data for each cell was obtained at 20 °C and scattering signal was recorded in the entire accessible q-range of 0.0009 $Å^{-1}$ to 1 $Å^{-1}$ and the background intensity of an empty glass cell was subtracted.

Kinetic and Stereochemical Model Study by ^{1}H NMR Monitoring

For assessment of pFA, dFA and SpCp cycloaddition kinetics with maleimide and subsequent *endo/exo* ratio determination for pFA and dFA, a model study was completed by combining each diene crosslinker – **bispFAPEG**, **bisdFAPEG**, or **bisSpCpPEG** – with a small molecule maleimide: 3-maleimideopropionic acid (**mal-COOH**). Solutions of each diene crosslinker were prepared in D_2O at a concentration of 2.5 mM and spiked with ethylene carbonate as an internal standard for determination of reaction conversion. Initial ^{1}H NMR spectra were recorded (t = 0) before **mal-COOH** (2 eq from 250 mM stock solution) was added to each solution. ^{1}H NMR spectra were collected periodically to determine conversion. *Endo/exo* ratios were determined by relative integrations of resonances corresponding to each stereoisomer.

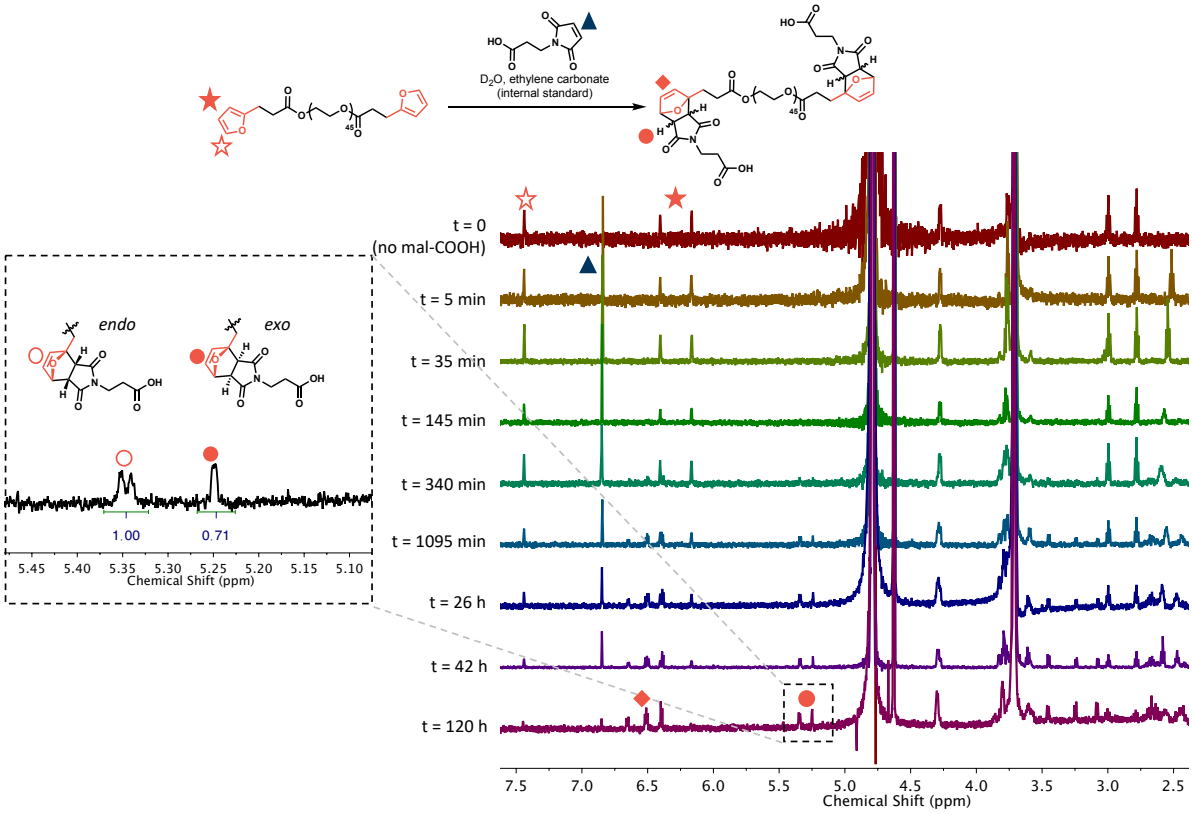

Figure S 6.15. Monitoring of cycloaddition between **bispFAPEG** with **mal-COOH** over 120 h in D_2O. Near-complete disappearance of furan resonances (red stars) is observed after 120 h and appearance of diagnostic **pFA–mal** cycloadduct peaks are observed at 5.3 (red circle) and 6.4 ppm (red diamond). Integration of *endo* and *exo* resonances indicate a final *endo*:*exo* ratio of 1:0.7 is obtained.

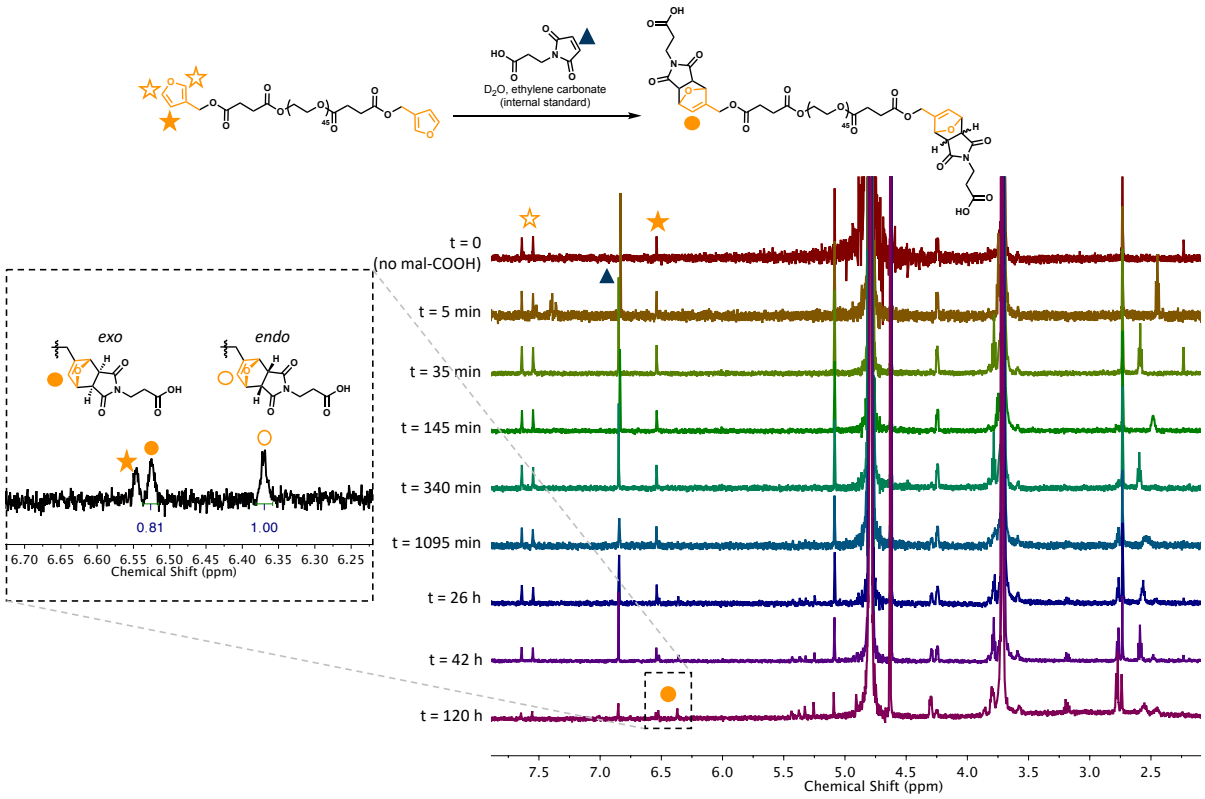

Figure S 6.16. Monitoring of cycloaddition between **bisdFAPEG** with **mal-COOH** over 120 h in D_2O. Near-complete disappearance of furan resonances (orange stars) is observed after 120 h and appearance of diagnostic **dFA–mal** cycloadduct peaks are observed at 6.4 ppm (orange circle). Integration of *endo* and *exo* resonances indicate a final *endo*:*exo* ratio of 1:0.8 is obtained.

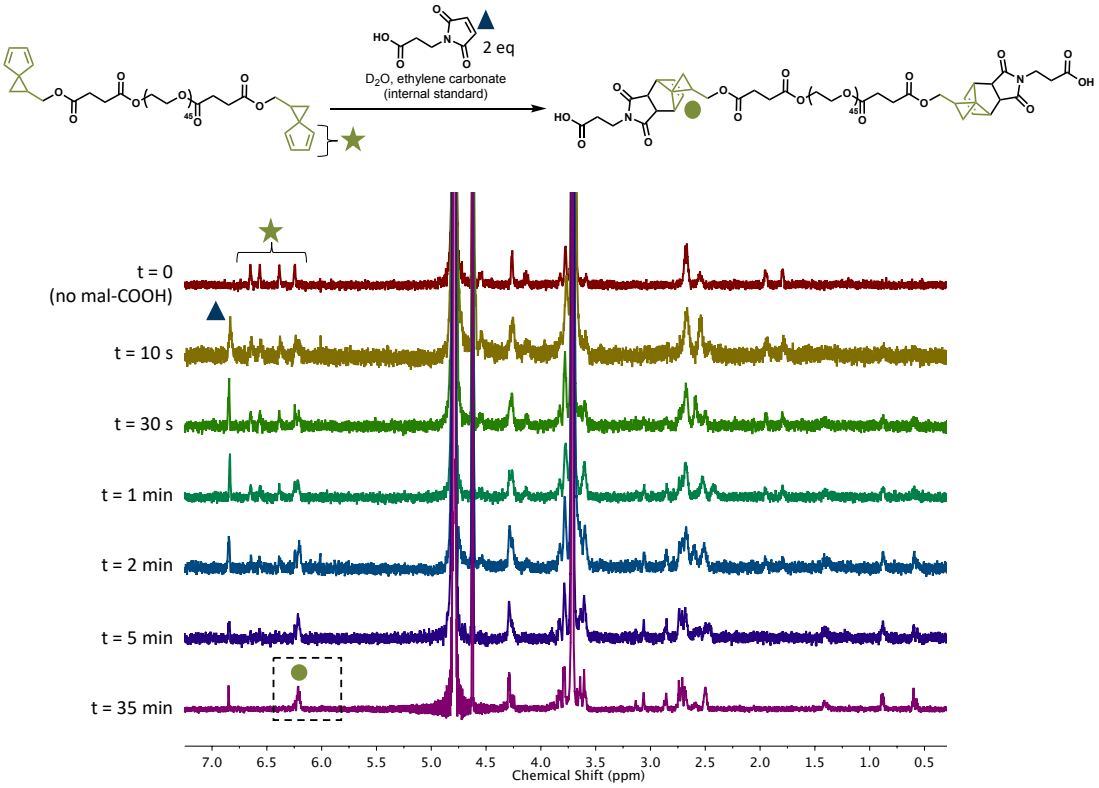

Figure S 6.17. Monitoring of cycloaddition between **bisSpCpPEG** with **mal-COOH** over 35 min in D_2O. Complete disappearance of SpCp resonances (green stars) is observed after 35 min and appearance of diagnostic **SpCp–mal** cycloadduct peaks are observed at 6.2 ppm (green circle).

Constrained Geometries Simulate External Force Calculations

DFT calculations were performed following previously established methods[28,54] using Gaussian16 at the B3LYP/6-31+G(d,p) level of theory in the gas phase.[55] Starting from each ground state optimized geometry for each DA adduct a redundant coordinate scan was run while displacing the indicated atoms by 0.05 Å for 100 steps and/or until a bond was broken. The energy relative to the ground state equilibrium geometry (i) is plotted against the displacement to afford CoGEF curves which provide bond dissociation energy as the maximum energy before scission (E_{max}). Additionally, the slope of these curves ($\Delta E/\Delta\Delta D$) provides a measure of the force imparted on the system. Maximum force (F_{max}) values are reported as the slope between the two points before bond scission (ii). CoGEF curves for each adduct are provided with the structures corresponding to the initial optimized geometry and the computed structure immediately after bond scission are provided below.

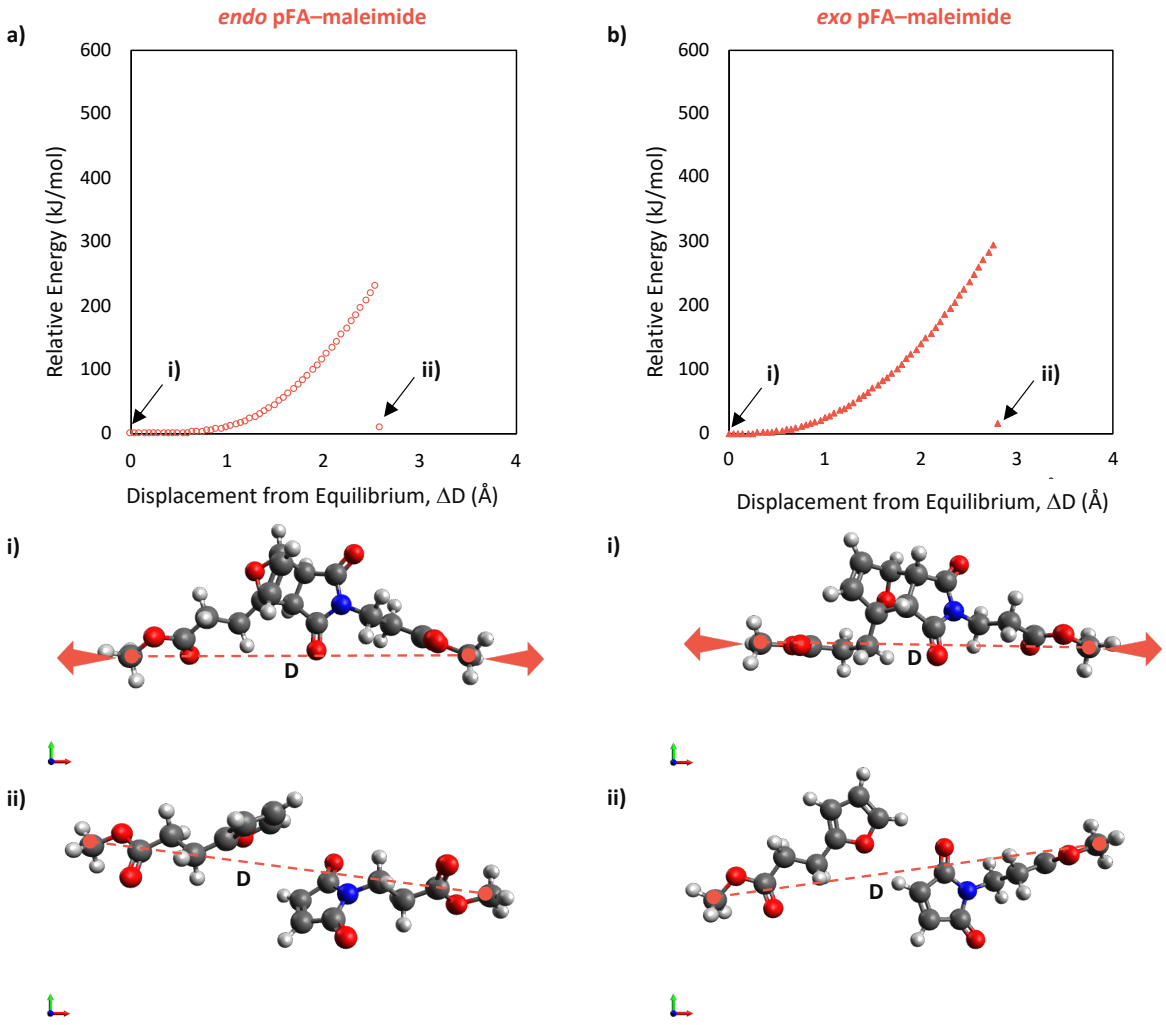

Figure S 6.18. CoGEF results for pFA–maleimide adducts. a) Plot of relative energies versus displacement starting from optimized equilibrium geometry (i) of *endo* stereoisomer upon stepwise elongation. Computed structure upon scission (ii) indicates selective cycloreversion of the DA bond. b) Plot of relative energies versus displacement starting from optimized equilibrium geometry (i) of *exo* stereoisomer upon stepwise elongation. Computed structure upon bond scission (ii) indicates selective cycloreversion of the DA bond.

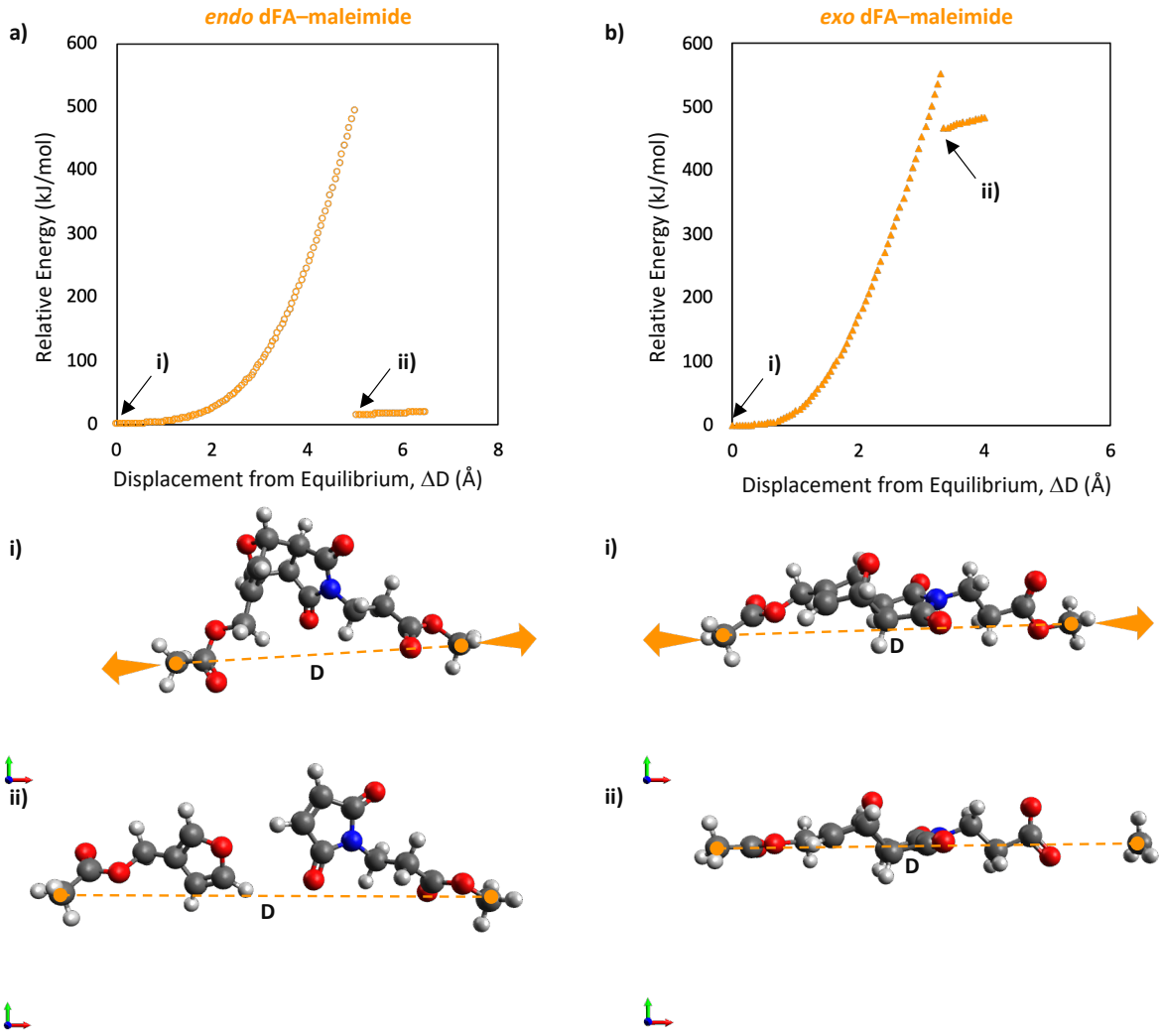

Figure S 6.19. CoGEF results for dFA–maleimide adducts. a) Plot of relative energies versus displacement starting from optimized equilibrium geometry (i) of *endo* stereoisomer upon stepwise elongation. Computed structure upon scission (ii) indicates selective cycloreversion of the DA bond. b) Plot of relative energies versus displacement starting from optimized equilibrium geometry (i) of *exo* stereoisomer upon stepwise elongation. Computed structure upon bond scission (ii) indicates rupture of terminal non-DA bond.

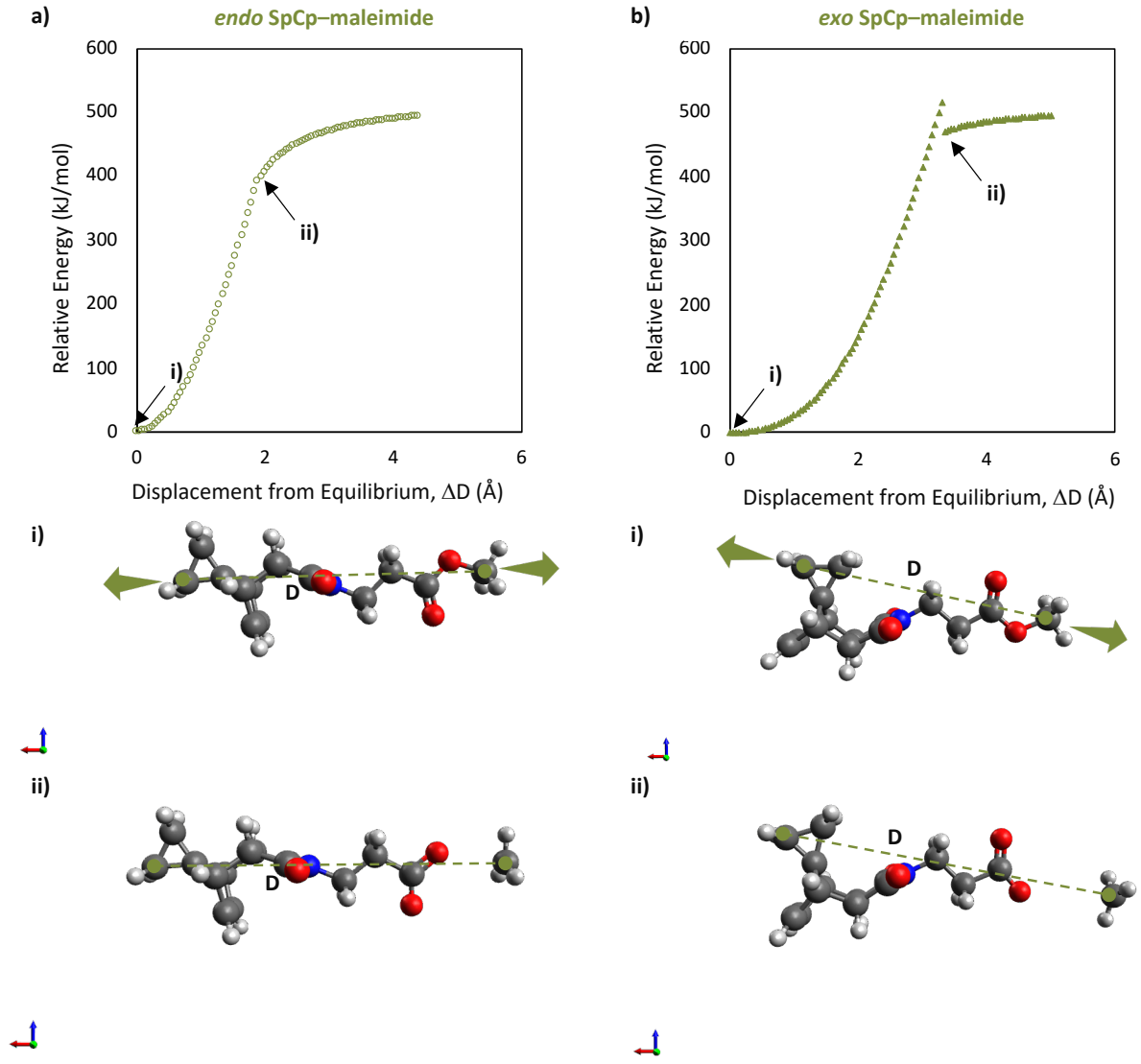

Figure S 6.20. CoGEF results for SpCp–maleimide adducts. a) Plot of relative energies versus displacement starting from optimized equilibrium geometry (i) of *endo* stereoisomer upon stepwise elongation. Computed structure upon scission (ii) indicates rupture of terminal non-DA bond. b) Plot of relative energies versus displacement starting from optimized equilibrium geometry (i) of *exo* stereoisomer upon stepwise elongation. Computed structure upon bond scission (ii) indicates rupture of terminal non-DA bond.

The cartesian coordinates for the optimized ground state geometries and post-scission geometries are listed below.

endo pFA–maleimide equilibrium geometry (i)

C	0.67830500	-0.39357500	-0.38580000
C	-0.41511100	0.47399200	-0.98507800
C	0.14109900	1.91117600	-0.93928700
C	1.52608300	1.78449400	-0.32874500
N	1.75413300	0.43391400	-0.04975100
O	2.32253700	2.67691800	-0.10251200
O	0.65810200	-1.59785200	-0.20843100
C	2.96584900	-0.05534800	0.60537500
H	2.68512000	-0.90989700	1.22312500
H	3.33607300	0.74214200	1.25156200
C	-1.75396600	0.61472200	-0.14024900
C	-1.33667600	0.85358900	1.31243900
C	-0.85118800	2.09943200	1.36096700
C	-0.95931500	2.63123900	-0.06064000
O	-2.13013400	1.95495900	-0.54619700
H	-1.34706200	0.10318700	2.09414100
H	-0.37541800	2.61041300	2.18907300
C	-2.83291700	-0.40275000	-0.44871600
H	-2.45039100	-1.39775100	-0.19500900
H	-3.01623100	-0.40912400	-1.52772700
H	-1.03552800	3.70703700	-0.20507500
C	4.03414700	-0.45920400	-0.41583100
H	4.30456100	0.39141100	-1.05170200
H	3.65788000	-1.24489400	-1.08072700
C	-5.24439600	-1.09349700	-0.09881200
O	-5.20046300	-1.88452500	-1.01950100
C	7.46691600	-1.82109600	-0.12160300
H	7.94661400	-1.06419100	0.50322100
H	7.29083600	-2.72071500	0.47260600
H	8.08028000	-2.04781500	-0.99287200
H	-0.66088300	0.12073500	-1.98967700
H	0.20658000	2.39795600	-1.91491700
C	5.29050400	-0.96791200	0.25921700
O	6.22269400	-1.31878000	-0.65123300
O	5.45566000	-1.05584500	1.45941900
C	-7.44543700	-1.80542700	0.41467500

H	-8.19884000	-1.55702500	1.16155400
H	-7.81842600	-1.60369100	-0.59231600
H	-7.16050600	-2.85761800	0.48788700
C	-4.14504300	-0.12803600	0.29108300
H	-4.49998900	0.88639500	0.07329900
H	-4.01872000	-0.17140800	1.37847200
O	-6.31814600	-0.95779400	0.71212700

Electronic Energy: -1202.546165 Hartree

endo pFA–maleimide post-scission geometry (ii)

C	2.05092000	-1.72249100	0.56242400
C	0.80967000	-2.13340400	-0.17680700
C	0.61236300	-1.27929000	-1.18701800
C	1.71469900	-0.25867800	-1.17398000
N	2.54085000	-0.58805500	-0.09400200
O	1.88249500	0.67556500	-1.93541200
O	2.55469200	-2.24859900	1.53661500
C	3.73139100	0.15457800	0.30384600
H	3.79393900	0.12705500	1.39345100
H	3.59146100	1.19133400	-0.00646900
C	-2.92979400	0.80798000	0.61537200
C	-2.20817600	1.47549700	1.56354200
C	-1.15750000	2.17258500	0.87346000
C	-1.31242800	1.88183600	-0.44723400
O	-2.38722800	1.04993700	-0.62343000
H	-2.39932600	1.46966100	2.62748100
H	-0.39345100	2.80333100	1.30526600
C	-4.13536400	-0.07009300	0.66458300
H	-4.35668400	-0.29200200	1.71245900
H	-3.92470100	-1.03223700	0.18347800
H	-0.77602600	2.15885600	-1.34137400
C	5.00434200	-0.42892000	-0.32019600
H	4.94600800	-0.40305400	-1.41466500
H	5.12764500	-1.48011500	-0.03678600
C	-6.58480900	-0.33029000	0.03623200
O	-6.61762700	-1.46213400	0.47606200
C	8.60631900	0.40507200	-0.05674600

H	8.61678700	1.43705700	-0.41489100
H	8.74861800	0.39720500	1.02627200
H	9.37722500	-0.18385200	-0.55222700
H	0.21824200	-2.98704200	0.12693200
H	-0.18172500	-1.25395300	-1.92125300
C	6.24305100	0.32944200	0.10839900
O	7.35865000	-0.23299500	-0.40214000
O	6.25118900	1.31543900	0.81815300
C	-8.88806600	-0.46585000	-0.51336300
H	-9.63353400	0.20074100	-0.94582000
H	-8.77037100	-1.36233600	-1.12703000
H	-9.17239400	-0.75916400	0.49987000
C	-5.36576800	0.56796600	-0.00278200
H	-5.15711200	0.80979000	-1.05141200
H	-5.62372000	1.51860200	0.47807900
O	-7.66241300	0.29289700	-0.49256400

Electronic Energy: -1202.542218 Hartree

exo pFA–maleimide equilibrium geometry (i)

C	0.71507300	-0.33722900	0.71959500
C	-0.44484100	0.58428600	1.07643100
C	-0.03876200	1.96160200	0.49452900
C	1.29106600	1.72061300	-0.20442800
N	1.64197200	0.38303600	-0.03406100
O	1.95583300	2.53687800	-0.81513100
O	0.84933400	-1.50757700	1.02799700
C	2.84827200	-0.21187700	-0.60628600
H	2.62487700	-1.25487200	-0.83545800
H	3.06432000	0.31570900	-1.53660500
C	-1.78455100	0.28667500	0.26776500
C	-2.79678800	1.29822200	0.81674800
C	-2.44668200	2.48682900	0.31405000
C	-1.20553900	2.22138500	-0.52532900
O	-1.44070500	0.88763600	-1.00448200
H	-3.57203200	1.05408200	1.53149900
H	-2.86428800	3.46370400	0.52651400
C	-2.19965300	-1.16651500	0.11223400

H	-2.37662400	-1.58726900	1.10703000
H	-1.36135600	-1.71961000	-0.31803700
C	-4.76159600	-1.18952600	-0.05802400
O	-4.91677600	-1.07062100	1.14272600
H	-0.61127000	0.55279500	2.15502800
H	0.07076800	2.77094000	1.21970500
C	-3.43711100	-1.37577300	-0.77105100
H	-3.44236800	-2.40219200	-1.15916900
H	-3.41378400	-0.72485000	-1.65041800
C	-7.10882700	-1.08687500	-0.37170700
H	-7.79009400	-1.13377800	-1.22063600
H	-7.30136600	-1.90640400	0.32469600
H	-7.21382300	-0.13524000	0.15469300
O	-5.78763600	-1.20563300	-0.93536300
C	4.03581500	-0.11559300	0.35697000
H	4.25297900	0.93011000	0.60240600
H	3.80993100	-0.62320600	1.30163200
O	5.36299600	-1.26416100	-1.32053100
C	5.28589300	-0.73706900	-0.22901100
C	7.57456100	-1.19553600	0.17253500
H	8.28087500	-1.01936200	0.98303500
H	7.46279600	-2.26546300	-0.01780200
H	7.90435100	-0.69905200	-0.74300600
O	6.32581200	-0.63374000	0.62565000
H	-0.96653700	2.89873100	-1.34374500

Electronic Energy: -1202.548898 Hartree

exo pFA–maleimide post-scission geometry (ii)

C	-2.49743900	-2.35054900	0.17681000
C	-1.03258600	-2.32651500	-0.15246400
C	-0.60339600	-1.05979100	-0.11078700
C	-1.76607300	-0.17875000	0.25112500
N	-2.86826300	-1.02013600	0.40917000
O	-1.77760600	1.03141800	0.38744700
O	-3.23812900	-3.30972200	0.23830900
C	-4.20810800	-0.57964400	0.78098600
H	-4.68281500	-1.39534300	1.32913400
H	-4.10494000	0.27292000	1.45478800
C	3.34427400	1.42838300	0.09328800

C	3.55982000	2.77630900	0.05630700
C	2.27055000	3.40633700	0.16026200
C	1.35850900	2.40221100	0.25397100
O	1.99767000	1.18757400	0.21239900
H	4.51666200	3.27061400	-0.03250400
H	2.05857500	4.46599600	0.16529800
C	4.21563000	0.21667400	0.03106400
H	3.92323700	-0.40784700	-0.82223400
H	4.05032600	-0.40375700	0.92051300
C	6.57844500	-0.66724800	-0.16085300
O	6.19008900	-1.81228900	-0.16696000
H	-0.48289300	-3.23130500	-0.37632300
H	0.38608500	-0.65355500	-0.27738700
C	5.70035200	0.56405700	-0.08052100
H	6.03457300	1.16265700	0.77516900
H	5.89903200	1.17459000	-0.96978900
C	8.81833400	-1.41977800	-0.31566900
H	9.80267800	-0.95524100	-0.36325300
H	8.73561100	-2.06098200	0.56500400
H	8.62751000	-2.01411700	-1.21230700
O	7.88310900	-0.32589700	-0.22985100
C	-5.04210900	-0.19662500	-0.44634800
H	-4.54912900	0.59873700	-1.01679000
H	-5.14832200	-1.05059300	-1.12518100
O	-6.85705300	0.35706200	1.08677500
C	-6.42645100	0.28177900	-0.06083600
C	-8.48331700	1.09687400	-0.91143200
H	-8.89391800	1.31941600	-1.89560900
H	-9.07375600	0.32577200	-0.41114200
H	-8.46142200	1.99454100	-0.28916900
O	-7.14325800	0.62299400	-1.15525000
H	0.28354800	2.35699000	0.34521600

Electronic Energy: -1202.543109 Hartree

endo dFA–maleimide equilibrium geometry (i)

C	-0.18937100	0.34516700	1.10251100

C	0.75028100	1.52269700	1.29922900
C	0.29373800	2.57760200	0.26870800
C	-0.88617600	1.94813600	-0.45055200
N	-1.09709900	0.67650900	0.09325100
O	-1.55289200	2.43023800	-1.34696400
O	-0.17895100	-0.71884000	1.69470000
C	-2.12490700	-0.24221300	-0.39512300
H	-1.74224700	-1.25766100	-0.28066700
H	-2.27274200	-0.03754500	-1.45657300
C	2.26048100	1.31456100	0.87480500
C	2.28810100	0.58698600	-0.47098200
C	1.88568800	1.50223900	-1.36482500
C	1.61944300	2.77058800	-0.57006600
O	2.58783900	2.66124800	0.49185900
H	1.70166400	1.37301800	-2.42488100
H	1.70610100	3.72459900	-1.08583200
C	-3.43983500	-0.07366300	0.37285500
H	-3.81347800	0.95253800	0.28039500
H	-3.29290800	-0.26275000	1.44212900
C	-6.75002900	-1.72434200	0.16359400
H	-7.02339400	-1.52593800	-0.87528300
H	-6.47379200	-2.77589700	0.26956700
H	-7.57048300	-1.47105500	0.83395400
H	0.70598300	1.86332200	2.33612500
H	-0.00401100	3.53261600	0.70714700
C	-4.51006400	-1.01619200	-0.13687200
O	-5.65421000	-0.87563000	0.56426700
O	-4.37439400	-1.79993200	-1.05467500
H	2.92208500	0.95281500	1.65820900
C	2.58721400	-0.85946600	-0.66645500
H	1.84772600	-1.50059900	-0.17332000
H	2.61231900	-1.12178000	-1.72720600
O	3.88464400	-1.12424300	-0.07114200
O	3.73192200	-3.26483800	-0.78296400
C	4.34251200	-2.39606500	-0.19649000
C	5.67683200	-2.56385300	0.48583300
H	6.07257300	-3.55502600	0.26562600
H	6.37637400	-1.79235800	0.15241100
H	5.55280200	-2.45097800	1.56777500

Electronic Energy: -1163.229085 Hartree

endo dFA–maleimide post-scission geometry (ii)

C	-3.04876900	-2.13567000	-0.08908100
C	-1.67405900	-2.55487700	0.34392700
C	-0.90759000	-1.46339100	0.44917100
C	-1.73826700	-0.26206100	0.09278800
N	-3.01852900	-0.74098800	-0.20553300
O	-1.38591600	0.90293900	0.05819900
O	-4.01616600	-2.84015400	-0.30838300
C	-4.13861400	0.06851300	-0.67778800
H	-4.55913900	-0.41069800	-1.56512000
H	-3.73194400	1.03663900	-0.97424300
C	3.68241600	-0.95620500	0.43742900
C	4.47707400	-0.05041900	-0.20233000
C	3.64179900	1.10028300	-0.44081500
C	2.41615200	0.80294300	0.06776100
O	2.42387600	-0.45760900	0.60868100
H	3.92776200	2.02257900	-0.92647300
H	1.47321200	1.32652900	0.11876400
C	-5.22186300	0.23139900	0.39494600
H	-4.82964900	0.76578900	1.26847400
H	-5.56220700	-0.74681700	0.75015300
C	-8.61827500	1.71965000	0.39029800
H	-8.40098300	2.76515000	0.15977500
H	-9.05700400	1.24003400	-0.48764800
H	-9.28707800	1.64365900	1.24677600
H	-1.42157600	-3.59270400	0.51735300
H	0.13580200	-1.37243500	0.72367800
C	-6.42297600	0.99047000	-0.13074100
O	-7.41269000	1.03151600	0.78609900
O	-6.50399100	1.49938200	-1.23088800
H	3.85474400	-1.95408700	0.81130800
C	5.89743300	-0.25797900	-0.60710600
H	6.20414200	-1.29777500	-0.46556400
H	6.06169500	-0.00261100	-1.65825500
O	6.75474300	0.59558000	0.20394700
O	8.54676300	-0.23755800	-0.89619500
C	8.08230600	0.50135500	-0.05123200
C	8.88251000	1.41465800	0.84522500
H	8.73794800	1.12896100	1.89179700
H	9.93790900	1.34267000	0.58373800
H	8.53744400	2.44726100	0.73783300

Electronic Energy: -1163.224005 Hartree

exo dFA–maleimide equilibrium geometry (i)

C	0.80475500	0.79856900	0.41782300
C	-0.57994800	0.38094100	-0.06016400
C	-0.39330600	-1.05304600	-0.61400600
C	1.08500900	-1.35898200	-0.41382100
N	1.68968200	-0.25210400	0.18236000
O	1.66524400	-2.38661200	-0.70900600
O	1.11104400	1.85995500	0.92770800
C	3.09595800	-0.22220800	0.58183300
H	3.16985300	0.39195900	1.48063100
H	3.38886300	-1.24407000	0.82749900
C	-1.56195900	0.11350100	1.14011000
C	-2.91356700	-0.25302800	0.52085300
C	-2.75087100	-1.49240700	0.03959000
C	-1.31318300	-1.87255600	0.36564200
O	-1.08517800	-1.16005600	1.59789300
H	-3.44777700	-2.08231300	-0.54099800
H	-0.96505200	1.12151600	-0.76464200
H	-0.66306800	-1.20063600	-1.66156700
C	3.98481200	0.34175800	-0.53122800
H	3.89668600	-0.26186700	-1.44170300
H	3.67725500	1.36007900	-0.79477900
O	5.88008500	0.00811400	0.94883700
C	5.44245300	0.37611000	-0.12256600
C	7.62532500	0.95628100	-0.83519600
H	8.07237600	1.37581200	-1.73570800
H	7.80658900	1.60464500	0.02514900
H	8.02942100	-0.03754700	-0.62919700
O	6.21213400	0.87518700	-1.11288200
H	-1.06234100	-2.92683700	0.46979600
H	-1.53685100	0.85572400	1.93761500
C	-4.06014700	0.69265400	0.44705900
H	-3.76044800	1.65233500	0.00610500
H	-4.45460000	0.91767300	1.44591800
O	-5.10281700	0.10441000	-0.35330400

O	-6.35540000	1.95741100	-0.02292000
C	-6.22618200	0.85340700	-0.50781200
C	-7.25233400	0.12921100	-1.34115800
H	-6.82622300	-0.14712500	-2.31012400
H	-7.55395800	-0.79537800	-0.83913300
H	-8.12029800	0.77225900	-1.48373600

Electronic Energy: -1163.232665 Hartree

exo dFA–maleimide post-scission geometry (ii)

C	-0.68131200	-1.00431900	-0.04869900
C	0.67994400	-0.44671100	-0.47612100
C	0.44023900	1.07041400	-0.65937000
C	-1.03766200	1.27818800	-0.33184600
N	-1.61266000	0.04234000	-0.01967600
O	-1.63536600	2.33713300	-0.32534900
O	-0.93016700	-2.16038600	0.23127100
C	-2.98186600	-0.09574200	0.51295300
H	-2.99798300	-1.01328700	1.10145700
H	-3.16308100	0.75238300	1.17448300
C	1.72231500	-0.44838300	0.70734600
C	3.06095500	0.11533300	0.18639500
C	2.83083000	1.42484000	0.01929100
C	1.38575000	1.65562900	0.45396800
O	1.22598500	0.65575700	1.48210600
H	3.50455400	2.18169000	-0.36149700
H	1.03445300	-0.98608500	-1.35746400
H	0.65838400	1.47432800	-1.65008100
C	-4.05459000	-0.13854100	-0.58679300
H	-4.05269000	0.77109900	-1.19233600
H	-3.93928500	-1.00317600	-1.24469100
O	-5.61724200	-0.18219600	1.26787300
C	-5.56069900	-0.23596200	0.03368000
C	-10.38186800	-0.49817500	-0.34595900
H	-10.35018800	-1.45783300	-0.84658100
H	-10.35137800	-0.45009400	0.73555800
H	-10.42767500	0.41404300	-0.92761000
O	-6.41554900	-0.34234700	-0.87785100

H	1.11295100	2.64344200	0.82202900
H	1.74856500	-1.36391100	1.29822000
C	4.28013500	-0.72804100	-0.02802800
H	4.17733400	-1.37361800	-0.90967100
H	4.43487400	-1.39405500	0.82861200
O	5.46217000	0.09842100	-0.18939400
O	6.68824000	-1.80032600	-0.26671100
C	6.63999500	-0.58801800	-0.26917400
C	7.85916700	0.31622500	-0.32491100
H	7.67302200	1.19784300	-0.94282200
H	8.09239500	0.65881000	0.68897000
H	8.70179400	-0.25682400	-0.71078400

Electronic Energy: -1163.055075 Hartree

endo SpCp–maleimide equilibrium geometry (i)

C	-0.27582100	-1.16973800	-0.20203700
C	-1.64767600	-0.77522300	-0.72151000
C	-1.64775900	0.77579600	-0.72102700
C	-0.27595500	1.17014100	-0.20127400
N	0.44255700	0.00015400	0.06187700
O	0.16133900	2.29398400	-0.03152200
O	0.16162400	-2.29363600	-0.03302300
C	1.79124600	0.00003700	0.62378500
H	1.88743500	-0.88797500	1.25052500
H	1.88759800	0.88820200	1.25028800
C	-2.87145900	-1.13454100	0.21048900
C	-2.52246700	-0.67216300	1.61898500
C	-2.52252500	0.67119400	1.61939700
C	-2.87158400	1.13440700	0.21118800
H	-2.23564800	-1.33004700	2.43180800
H	-2.23577600	1.32861000	2.43262200
H	-3.22274500	2.16132300	0.10262200
C	2.85875000	-0.00024400	-0.47526800
H	2.75140000	0.87948600	-1.11994800
H	2.75118900	-0.88028800	-1.11951300
C	6.56300500	0.00066700	-0.45015700
H	6.77417200	0.89080200	0.14700800

H	6.77446500	-0.89083400	0.14486500
H	7.15254000	0.00186600	-1.36631700
H	-1.79358500	-1.21302800	-1.71312000
H	-1.79369400	1.21420300	-1.71236800
C	4.25918800	-0.00040900	0.09960900
O	5.18697500	0.00096100	-0.88163700
O	4.53374700	-0.00168800	1.28279100
H	-3.22251900	-2.16142400	0.10128700
C	-3.81949000	0.00001100	-0.21330400
C	-4.68573000	0.00024800	-1.43819400
C	-5.30468400	-0.00007800	-0.04439100
H	-4.75713900	-0.91279200	-2.02483100
H	-4.75733400	0.91341100	-2.02459800
H	-5.78492600	0.91259900	0.29810000
H	-5.78505200	-0.91279000	0.29781500

Electronic Energy: -937.5138132 Hartree

endo SpCp–maleimide post-scission geometry (ii)

C	-0.39793900	-1.16558700	-0.23393700
C	-1.82067400	-0.77114600	-0.68496700
C	-1.82068800	0.77118500	-0.68492400
C	-0.39795100	1.16563300	-0.23389600
N	0.40000300	0.00003200	-0.13595900
O	0.01417100	2.29066200	-0.02884500
O	0.01420200	-2.29060900	-0.02890300
C	1.80414300	0.00001800	0.41861300
H	1.87140500	-0.88636500	1.05036300
H	1.87142800	0.88638800	1.05038100
C	-3.07775100	-1.13393000	0.22957000
C	-2.73384900	-0.67167500	1.63780500
C	-2.73386200	0.67153600	1.63785400
C	-3.07777600	1.13388800	0.22965000
H	-2.44566000	-1.33035200	2.44947800
H	-2.44568900	1.33015800	2.44957600
H	-3.41257300	2.16641900	0.12016100
C	3.00845500	0.00001500	-0.59268600
H	2.98644000	0.88417300	-1.23571800

H	2.98643000	-0.88414000	-1.23572400
C	8.20301900	-0.00002900	-0.34818100
H	8.24556100	0.93276700	0.20020500
H	8.24558100	-0.94085300	0.18629900
H	8.19603100	0.00797200	-1.43049500
H	-1.96803800	-1.19911200	-1.68224900
H	-1.96807400	1.19920500	-1.68218100
C	4.47228400	0.00000000	0.14648400
O	5.46009800	0.00001900	-0.69686100
O	4.47992500	-0.00001400	1.37260400
H	-3.41254100	-2.16645600	0.12001000
C	-4.06404800	-0.00000800	-0.19604100
C	-4.93402400	0.00003100	-1.41844400
C	-5.61852400	-0.00001900	-0.05637000
H	-4.99286600	-0.91041800	-2.01215500
H	-4.99286900	0.91051700	-2.01209900
H	-6.08832900	0.91751700	0.28439100
H	-6.08831500	-0.91758900	0.28432100

Electronic Energy: -937.361956 Hartree

exo SpCp–maleimide equilibrium geometry (i)

C	-0.40672900	-0.47067500	-1.16019000
C	-1.73455300	-1.10166600	-0.76472700
C	-1.73534900	-1.08491800	0.78850700
C	-0.40790400	-0.44561700	1.17168400
N	0.29932600	-0.15549800	0.00283000
O	0.00171100	-0.21273000	2.29457900
O	0.00406700	-0.26192100	-2.28740500
C	1.59789700	0.51380000	-0.00374000
H	1.64334600	1.13820400	-0.89756800
H	1.64403100	1.15384600	0.87890300
C	-2.99402000	-0.22717500	-1.13107000
C	-4.19411600	-1.04506500	-0.66145200
C	-4.19480800	-1.03059100	0.68142200
C	-2.99520500	-0.20271500	1.13455400
H	-4.85842400	-1.60016100	-1.31491500
H	-4.85979400	-1.57148700	1.34600700

H	-1.79432400	-2.09615000	-1.21429400
H	-1.79568800	-2.06945600	1.25937700
C	2.75116200	-0.49473900	0.00463700
H	2.69692600	-1.13825800	0.89009300
H	2.69622100	-1.15368600	-0.86934100
O	4.27587600	1.39480700	-0.01247400
C	4.09989100	0.19302600	-0.00189700
C	6.44105300	-0.16573500	0.00041900
H	7.10358100	-1.03051800	0.00778100
H	6.60241400	0.43778800	-0.89580800
H	6.60300600	0.45341000	0.88581900
O	5.10486500	-0.70853800	0.00562300
H	-3.00504200	0.17387100	2.15852400
H	-3.00276100	0.12722700	-2.16293800
C	-2.94266000	0.82131000	-0.00940800
C	-2.15120600	2.10004700	-0.02281700
C	-3.67220500	2.12668600	-0.02386200
H	-1.63895400	2.38292900	-0.93906800
H	-1.63980200	2.40267200	0.88758000
H	-4.17530300	2.44459300	0.88542200
H	-4.17435200	2.42488000	-0.94032400

Electronic Energy: -937.5149912 Hartree

exo SpCp–maleimide post-scission geometry (ii)

C	-0.48850400	0.15871200	1.16652900
C	-1.71318300	0.98096500	0.77465300
C	-1.71328500	0.98007600	-0.77597300
C	-0.48842600	0.15773500	-1.16712000
N	0.22065500	-0.16571200	-0.00014400
O	-0.12839300	-0.13733800	-2.29095500
O	-0.12860000	-0.13555900	2.29061800
C	1.54384700	-0.80796300	0.00027900
H	1.61158900	-1.43432400	0.88992800
H	1.61181200	-1.43530500	-0.88865400
C	-3.14052400	0.42072400	1.13337200
C	-4.09593500	1.52354700	0.67053400
C	-4.09603100	1.52258300	-0.67238600

C	-3.14066300	0.41909400	-1.13374300
H	-4.59999500	2.22260900	1.32920800
H	-4.60018100	2.22070000	-1.33199200
H	-1.57302700	1.97131200	1.21873700
H	-1.57356500	1.96992800	-1.22128200
C	2.65102700	0.26165800	-0.00019900
H	2.59860000	0.89531200	-0.88913500
H	2.59825100	0.89655200	0.88780700
O	4.20583600	-1.59728200	-0.00105200
C	4.15561700	-0.36290200	0.00019300
C	9.02472500	0.73573600	0.00018000
H	8.80142700	1.76911100	0.23384300
H	9.15542600	0.01588100	0.79848100
H	9.10006200	0.41811500	-1.03225300
O	5.00968600	0.55666100	0.00157200
H	-3.24263000	0.06870100	-2.16201700
H	-3.24243400	0.07171300	2.16212100
C	-3.37993400	-0.59160500	0.00052800
C	-3.03316800	-2.05101800	0.00155700
C	-4.49440700	-1.60249600	0.00128300
H	-2.63697700	-2.48862000	0.91467400
H	-2.63690800	-2.48998200	-0.91087200
H	-5.06565000	-1.73694500	-0.91306500
H	-5.06554000	-1.73569800	0.91588400

Electronic Energy: -937.3355523 Hartree

6.7 References

(24) Gevrek, T. N.; Sanyal, A., Furan-Containing Polymeric Materials: Harnessing the Diels-Alder Chemistry for Biomedical Applications. *Eur. Polym. J.* **2021**, *153*, 110514. DOI: 10.1016/j.eurpolymj.2021.110514.

(25) Cadamuro, F.; Russo, L.; Nicotra, F., Biomedical Hydrogels Fabricated Using Diels–Alder Crosslinking. *Eur. J. Org. Chem.* **2021**, *2021*, 374–382. DOI: 10.1002/ejoc.202001042.

(26) Chen, X.; Dam, M. A.; Ono, K.; Mal, A.; Shen, H.; Nutt, S. R.; Sheran, K.; Wudl, F., A Thermally Re-Mendable Cross-Linked Polymeric Material. *Science* **2002**, *295*, 1698–1702. DOI: 10.1126/science.1065879.

(27) Gandini, A., The Furan/Maleimide Diels–Alder Reaction: A Versatile Click–Unclick Tool in Macromolecular Synthesis. *Prog. Polym. Sci.* **2013**, *38*, 1–29. DOI: 10.1016/j.progpolymsci.2012.04.002.

(28) Discekici, E. H.; St. Amant, A. H.; Nguyen, S. N.; Lee, I.-H.; Hawker, C. J.; Read de Alaniz, J., *Endo* and *Exo* Diels–Alder Adducts: Temperature-Tunable Building Blocks for Selective Chemical Functionalization. *J. Am. Chem. Soc.* **2018**, *140*, 5009–5013. DOI: 10.1021/jacs.8b01544.

(29) Gregoritza, M.; Brandl, F. P., The Diels–Alder Reaction: A Powerful Tool for the Design of Drug Delivery Systems and Biomaterials. *Eur. J. Pharm. Biopharm.* **2015**, *97*, 438–453. DOI: 10.1016/j.ejpb.2015.06.007.

(30) Konda, S. S. M.; Brantley, J. N.; Varghese, B. T.; Wiggins, K. M.; Bielawski, C. W.; Makarov, D. E., Molecular Catch Bonds and the Anti-Hammond Effect in Polymer Mechanochemistry. *J. Am. Chem. Soc.* **2013**, *135*, 12722–12729. DOI: 10.1021/ja4051108.

(31) Min, Y.; Huang, S.; Wang, Y.; Zhang, Z.; Du, B.; Zhang, X.; Fan, Z., Sonochemical Transformation of Epoxy–Amine Thermoset into Soluble and Reusable Polymers. *Macromolecules* **2015**, *48*, 316–322. DOI: 10.1021/ma501934p.

(32) Duan, H.-Y.; Wang, Y.-X.; Wang, L.-J.; Min, Y.-Q.; Zhang, X.-H.; Du, B.-Y., An Investigation of the Selective Chain Scission at Centered Diels–Alder Mechanophore under Ultrasonication. *Macromolecules* **2017**, *50*, 1353–1361. DOI: 10.1021/acs.macromol.6b02370.

(33) Stevenson, R.; De Bo, G., Controlling Reactivity by Geometry in Retro-Diels–Alder Reactions under Tension. *J. Am. Chem. Soc.* **2017**, *139*, 16768–16771. DOI: 10.1021/jacs.7b08895.

(34) Wang, Z.; Craig, S. L., Stereochemical Effects on the Mechanochemical Scission of Furan–Maleimide Diels–Alder Adducts. *Chem. Commun.* **2019**, *55*, 12263–12266. DOI: 10.1039/C9CC06361G.

(35) Wang, S.; Beech, H. K.; Bowser, B. H.; Kouznetsova, T. B.; Olsen, B. D.; Rubinstein, M.; Craig, S. L., Mechanism Dictates Mechanics: A Molecular Substituent Effect in the Macroscopic Fracture of a Covalent Polymer Network. *J. Am. Chem. Soc.* **2021**, *143*, 3714–3718. DOI: 10.1021/jacs.1c00265.

(36) Sun, J.-Y.; Zhao, X.; Illeperuma, W. R. K.; Chaudhuri, O.; Oh, K. H.; Mooney, D. J.; Vlassak, J. J.; Suo, Z., Highly Stretchable and Tough Hydrogels. *Nature* **2012**, *489*, 133–136. DOI: 10.1038/nature11409.

(37) Truong, V. X.; Ablett, M. P.; Richardson, S. M.; Hoyland, J. A.; Dove, A. P., Simultaneous Orthogonal Dual-Click Approach to Tough, *in-Situ*-Forming Hydrogels

for Cell Encapsulation. *J. Am. Chem. Soc.* **2015**, *137*, 1618–1622. DOI: 10.1021/ja511681s.

(38) Deng, Y.; Huang, M.; Sun, D.; Hou, Y.; Li, Y.; Dong, T.; Wang, X.; Zhang, L.; Yang, W., Dual Physically Cross-Linked κ-Carrageenan-Based Double Network Hydrogels with Superior Self-Healing Performance for Biomedical Application. *ACS Appl. Mater. Interfaces* **2018**, *10*, 37544–37554. DOI: 10.1021/acsami.8b15385.

(39) Boots, J. N. M.; te Brake, D. W.; Clough, J. M.; Tauber, J.; Ruiz-Franco, J.; Kodger, T. E.; van der Gucht, J., Quantifying Bond Rupture during Indentation Fracture of Soft Polymer Networks Using Molecular Mechanophores. *Phys. Rev. Materials* **2022**, *6*, 025605. DOI: 10.1103/PhysRevMaterials.6.025605.

(40) Nimmo, C. M.; Owen, S. C.; Shoichet, M. S., Diels–Alder Click Cross-Linked Hyaluronic Acid Hydrogels for Tissue Engineering. *Biomacromolecules* **2011**, *12*, 824–830. DOI: 10.1021/bm101446k.

(41) Owen, S. C.; Fisher, S. A.; Tam, R. Y.; Nimmo, C. M.; Shoichet, M. S., Hyaluronic Acid Click Hydrogels Emulate the Extracellular Matrix. *Langmuir* **2013**, *29*, 7393–7400. DOI: 10.1021/la305000w.

(42) Smith, L. J.; Taimoory, S. M.; Tam, R. Y.; Baker, A. E. G.; Binth Mohammad, N.; Trant, J. F.; Shoichet, M. S., Diels–Alder Click-Cross-Linked Hydrogels with Increased Reactivity Enable 3D Cell Encapsulation. *Biomacromolecules* **2018**, *19*, 926–935. DOI: 10.1021/acs.biomac.7b01715.

(43) St. Amant, A. H.; Lemen, D.; Florinas, S.; Mao, S.; Fazenbaker, C.; Zhong, H.; Wu, H.; Gao, C.; Christie, R. J.; Read de Alaniz, J., Tuning the Diels–Alder Reaction for Bioconjugation to Maleimide Drug-Linkers. *Bioconjugate Chem.* **2018**, *29*, 2406–2414. DOI: 10.1021/acs.bioconjchem.8b00320.

(44) Mueller, E.; Poulin, I.; Bodnaryk, W. J.; Hoare, T., Click Chemistry Hydrogels for Extrusion Bioprinting: Progress, Challenges, and Opportunities. *Biomacromolecules* **2022**, *23*, 619–640. DOI: 10.1021/acs.biomac.1c01105.

(45) Madl, C. M.; Heilshorn, S. C., Rapid Diels–Alder Cross-Linking of Cell Encapsulating Hydrogels. *Chem. Mater.* **2019**, *31*, 8035–8043. DOI: 10.1021/acs.chemmater.9b02485.

(46) Froese, R. D. J.; Organ, M. G.; Goddard, J. D.; Stack, T. D. P.; Trost, B. M., Theoretical and Experimental Studies of the Diels-Alder Dimerizations of Substituted Cyclopentadienes. *J. Am. Chem. Soc.* **1995**, *117*, 10931–10938. DOI: 10.1021/ja00149a016.

(47) Rickborn, B. The Retro-Diels-Alder Reaction Part I. C–C Dienophiles. In *Organic Reactions*; John Wiley & Sons, Inc., Ed.; John Wiley & Sons, Inc.: Hoboken, NJ, USA, 1998; pp 1–393. DOI: 10.1002/0471264180.or052.01.

(48) Hu, X.; McFadden, M. E.; Barber, R. W.; Robb, M. J., Mechanochemical Regulation of a Photochemical Reaction. *J. Am. Chem. Soc.* **2018**, *140*, 14073–14077. DOI: 10.1021/jacs.8b09628.

(49) Barber, R. W.; Robb, M. J., A Modular Approach to Mechanically Gated Photoswitching with Color-Tunable Molecular Force Probes. *Chem. Sci.* **2021**, *12*, 11703–11709. DOI: 10.1039/D1SC02890A.

(50) Lenhardt, J. M.; Black, A. L.; Craig, S. L., *gem* -Dichlorocyclopropanes as Abundant and Efficient Mechanophores in Polybutadiene Copolymers under Mechanical Stress. *J. Am. Chem. Soc.* **2009**, *131*, 10818–10819. DOI: 10.1021/ja9036548.

(51) Klein, I. M.; Husic, C. C.; Kovács, D. P.; Choquette, N. J.; Robb, M. J., Validation of the CoGEF Method as a Predictive Tool for Polymer Mechanochemistry. *J. Am. Chem. Soc.* **2020**, *142*, 16364–16381. DOI: 10.1021/jacs.0c06868.

(52) Sakai, T.; Matsunaga, T.; Yamamoto, Y.; Ito, C.; Yoshida, R.; Suzuki, S.; Sasaki, N.; Shibayama, M.; Chung, U., Design and Fabrication of a High-Strength Hydrogel with Ideally Homogeneous Network Structure from Tetrahedron-like Macromonomers. *Macromolecules* **2008**, *41*, 5379–5384. DOI: 10.1021/ma800476x.

(53) Akagi, Y.; Katashima, T.; Katsumoto, Y.; Fujii, K.; Matsunaga, T.; Chung, U.; Shibayama, M.; Sakai, T., Examination of the Theories of Rubber Elasticity Using an Ideal Polymer Network. *Macromolecules* **2011**, *44*, 5817–5821. DOI: 10.1021/ma201088r.

(54) Sakai, T.; Akagi, Y.; Kondo, S.; Chung, U., Experimental Verification of Fracture Mechanism for Polymer Gels with Controlled Network Structure. *Soft Matter* **2014**, *10*, 6658–6665. DOI: 10.1039/C4SM00709C.

(55) Matsunaga, T.; Sakai, T.; Akagi, Y.; Chung, U.; Shibayama, M., Structure Characterization of Tetra-PEG Gel by Small-Angle Neutron Scattering. *Macromolecules* 2009, **42**, 1344–1351. DOI: 10.1021/ma802280n.

(56) Malo de Molina, P.; Lad, S.; Helgeson, M. E., Heterogeneity and Its Influence on the Properties of Difunctional Poly(Ethylene Glycol) Hydrogels: Structure and Mechanics. *Macromolecules* **2015**, *48*, 5402–5411. DOI: 10.1021/acs.macromol.5b01115.

(57) Rideout, D. C.; Breslow, R., Hydrophobic Acceleration of Diels-Alder Reactions. *J. Am. Chem. Soc.* **1980**, *102*, 7816–7817. DOI: 10.1021/ja00546a048.

(58) Fakhouri, S.; Hutchens, S. B.; Crosby, A. J., Puncture Mechanics of Soft Solids. *Soft Matter* **2015**, *11*, 4723–4730. DOI: 10.1039/c5sm00230c.

(59) Rattan, S.; Li, L.; Lau, H. K.; Crosby, A. J.; Kiick, K. L., Micromechanical Characterization of Soft, Biopolymeric Hydrogels: Stiffness, Resilience, and Failure. *Soft Matter* **2018**, *14*, 3478–3489. DOI: 10.1039/c8sm00501j.

(60) Barney, C.W.; Chen, C.; Crosby, A. J., Deep Indentation and Puncture of a Rigid Cylinder Inserted into a Soft Solid. *Soft Matter* **2021**, *17*, 5574–5580. DOI: 10.1039/d0sm01775b.

(61) Rattan, S.; Crosby, A. J., Effect of Polymer Volume Fraction on Fracture Initiation in Soft Gels at Small Length Scales, *ACS Macro Lett.*, **2019**, *8*, 492–498. DOI: 10.1021/acsmacrolett.9b00086.

(62) Fregonese, S.; Bacca, M., Piercing soft solids: A mechanical theory for needle insertion, *J. Mech. Phys. Solids* **2021**, *154*, 104497. DOI: 10.1016/j.jmps.2021.104497.

(63) de Figueiredo, R.; Oczipka, P.; Fröhlich, R.; Christmann, M. Synthesis of 4-Maleimidobutyric Acid and Related Maleimides. *Synthesis* **2008**, *2008* (8), 1316–1318. DOI: 10.1055/s-2008-1032016.

(64) Kassianidis, E.; Pearson, R. J.; Philp, D. Probing Structural Effects on Replication Efficiency through Comparative Analyses of Families of Potential Self-Replicators. *Chem. - Eur. J.* **2006**, *12* (34), 8798–8812. DOI: 10.1002/chem.200600460.

(65) Shull, K. R.; Ahn, D.; Chen, W.-L.; Flanigan, C. M.; Crosby, A. J. Axisymmetric Adhesion Tests of Soft Materials. *Macromol. Chem. Phys.* **1998**, *199* (4), 489–511. DOI: 10.1002/(SICI)1521-3935(19980401)199:4<489::AID-MACP489>3.0.CO;2-A.

(66) Hu, Y.; Zhao, X.; Vlassak, J. J.; Suo, Z. Using Indentation to Characterize the Poroelasticity of Gels. *Appl. Phys. Lett.* **2010**, *96* (12), 2008–2011. DOI: 10.1063/1.3370354.

(67) Chan, E. P.; Hu, Y.; Johnson, P. M.; Suo, Z.; Stafford, C. M. Spherical Indentation Testing of Poroelastic Relaxations in Thin Hydrogel Layers. *Soft Matter* **2012**, *8* (5), 1492–1498. DOI: 10.1039/c1sm06514a.

(68) Rattan, S.; Crosby, A. J. Effect of Far-Field Compliance on Local Failure Dynamics of Soft Solids. *Extreme Mech. Lett.* **2018**, *24*, 14–20. DOI: 10.1016/j.eml.2018.08.003.

(69) Lake, G. J.; Thomas, A. G. The Strength of Highly Elastic Materials. *Proc. R. Soc. Lond. Ser. Math. Phys. Sci.* **1967**, *300* (1460), 108–119.

(70) Flory, P. J. Network Structure and the Elastic Properties of Vulcanized Rubber. *Chem. Rev.* **1944**, *35* (1), 51–75. DOI: 10.1021/cr60110a002.

(71) Stevenson, A.; Ab Malek, K. On The Puncture Mechanics of Rubber. *Rubber Chem. Technol.* **1994**, *67* (5), 743–760.

(72) Shergold, O. A.; Fleck, N. A. Experimental Investigation Into the Deep Penetration of Soft Solids by Sharp and Blunt Punches, With Application to the Piercing of Skin. DOI: 10.1115/1.1992528.

(73) Lin, W.; Otim, K. J.; Lenhart, J. L.; Cole, P. J.; Shull, K. R. Indentation Fracture of Silicone Gels. *J. Mater. Res.* **2009**, *24* (03), 957–965. DOI: 10.1557/jmr.2009.0128.

(74) Heller, W. T. Small-Angle Neutron Scattering and Contrast Variation: A Powerful Combination for Studying Biological Structures. *Acta Crystallogr. D Biol. Crystallogr.* **2010**, *66* (11), 1213–1217. DOI: 10.1107/S0907444910017658.

(75) Heller, W. T.; Urban, V. S.; Lynn, G. W.; Weiss, K. L.; O'Neill, H. M.; Pingali, S. V.; Qian, S.; Littrell, K. C.; Melnichenko, Y. B.; Buchanan, M. V.; Selby, D. L.; Wignall, G. D.; Butler, P. D.; Myles, D. A. The Bio-SANS Instrument at the High Flux Isotope Reactor of Oak Ridge National Laboratory. *J. Appl. Crystallogr.* **2014**, *47* (4), 1238–1246. DOI: 10.1107/S1600576714011285.

(76) Yao, X.; Avery, B.; Bobrek, M.; Debeer-Schmitt, L.; Geng, X.; Gregory, R.; Guyotte, G.; Harrington, M.; Hartman, S.; He, L.; Heroux, L.; Kasemir, K.; Knudson, R.; Kohl, J.; Lionberger, C.; Littrell, K.; Pearson, M.; Pingali, S. V.; Pratt, C.; Qian, S.; Ruiz-Rodriguez, M.; Sedov, V.; Taufer, G.; Urban, V.; Vodopivec, K. A Unified User-Friendly Instrument Control and Data Acquisition System for the ORNL SANS Instrument Suite. *Appl. Sci.* **2021**, *11* (3), 1216. DOI: 10.3390/app11031216.

(77) Beyer, M. K. The Mechanical Strength of a Covalent Bond Calculated by Density Functional Theory. *J. Chem. Phys.* **2000**, *112* (17), 7307–7312. DOI: 10.1063/1.481330.

(78) Gaussian 16, Revision C.01, Frisch, M. J.; Trucks, G. W.; Schlegel, H. B.; Scuseria, G. E.; Robb, M. A.; Cheeseman, J. R.; Scalmani, G.; Barone, V.; Petersson, G. A.; Nakatsuji, H.; Li, X.; Caricato, M.; Marenich, A. V.; Bloino, J.; Janesko, B. G.; Gomperts, R.; Mennucci, B.; Hratchian, H. P.; Ortiz, J. V.; Izmaylov, A. F.; Sonnenberg, J. L.; Williams-Young, D.; Ding, F.; Lipparini, F.; Egidi, F.; Goings, J.; Peng, B.; Petrone, A.; Henderson, T.; Ranasinghe, D.; Zakrzewski, V. G.; Gao, J.; Rega, N.; Zheng, G.; Liang, W.; Hada, M.; Ehara, M.; Toyota, K.; Fukuda, R.; Hasegawa, J.; Ishida, M.; Nakajima, T.; Honda, Y.; Kitao, O.; Nakai, H.; Vreven, T.; Throssell, K.; Montgomery, J. A., Jr.; Peralta, J. E.; Ogliaro, F.; Bearpark, M. J.; Heyd, J. J.; Brothers, E. N.; Kudin, K. N.; Staroverov, V. N.; Keith, T. A.; Kobayashi, R.; Normand, J.; Raghavachari, K.; Rendell, A. P.; Burant, J. C.; Iyengar, S. S.; Tomasi, J.; Cossi, M.; Millam, J. M.; Klene, M.; Adamo, C.; Cammi, R.; Ochterski, J. W.; Martin, R. L.; Morokuma, K.; Farkas, O.; Foresman, J. B.; Fox, D. J. Gaussian, Inc., Wallingford CT, **2016**.

7 Chapter 7: Future Directions and Outlook

As made evident by previous chapters, taming the reactivity of cyclopentadiene derivatives has enabled Diels–Alder-based materials with improved synthesis, functionality, properties, and applications. NBD-based precursors introduced in Chapter 2 provided straightforward access to cyclopentadiene-functionalized materials with improved stability for long term storage of building blocks. This enabled rapid click chemistry compatible with the demands of polymer–polymer conjugation and provided access to numerous architectures using a "mix-and-match" approach with NBD and maleimide bearing building blocks. Alternatively, by utilizing the inherent dimerization of cyclopentadiene units, this platform also provides promise in the preparation of cyclopentadiene-based building blocks for high-performance, single component remendable materials.[1]

The development of a novel cyclopentadiene photocage described in Chapters 3–5 illuminates numerous opportunities for photoinduced DA chemistry. For example, Chapter 5 highlights the ability of CPD–NBD adducts to spatially pattern growth factors in off-the-shelf protein-based matrices (collagen, fibronectin, laminin) commonly used for cell culture,[2] where radical sensitivity typically prohibits the implementation of thiol–ene based patterning strategies. We were particularly excited to demonstrate the compatibility of our functionalized materials with human pluripotent stem cells and envision the utilization of CPD–NBD photoclick chemistry as a protocol to photopattern synthetic morphogen gradients could provide a route to "user-defined' tissue morphogenesis.[3] In addition, we speculate that the extended and planar π system – which is an essential feature of molecules with high two-photon absorption cross sections[4] – might permit photouncaging by multiphoton absorption. Two

photon absorbance techniques are particularly advantageous as the use of highly focused laser beams enables precise uncaging within matrices with resolutions approaching 1 μm.[5,6] The use of this technology in 3D encapsulated cell cultures would therefore enable the fabrication of high resolution biomolecule patterns and morphogen gradients that better mimic the multidimensional microenvironment of natural tissues.

Not explored in this dissertation, but an equally interesting application of this photoclick reaction is in photoinduced DA step growth polymerization. As highlighted in Chapter 6, the step growth polymerization of maleimide and cyclopentadiene functionalized PEG macromonomers enabled the rapid gelation of hydrogels within minutes.[7] Thus, we envision the rapid aqueous cycloaddition kinetics ($k \approx 10^2$ $M^{-1}s^{-1}$)[8] between photoliberated Cp and maleimide will enable rapid and light-induced hydrogel formation. In combination with commercial digital light processing printing techniques, we anticipate this photoinduced step growth platform could provide a route to radical-free vat-based printing with applications in the 3D printing of radical sensitive matrices and cell lines with improved feature resolution over extrusion based bioprinting.[6,9] Moreover, we speculate the application of CPD–NBD photoclick chemistries to biological systems can be made entirely orthogonal by pairing CPD–NBD photoclick with tetrazine derivatives in IEDDA cycloadditions.[10] Thus, we anticipate that the work outlined in this dissertation will serve as the foundation for a bright future of CPD–NBD-based photoclick chemistry that can provide novel biomaterials to probe fundamental questions in cell biology, advance tissue engineering scaffolds and offer new therapeutics for regenerative medicine.

Finally, the establishment of mechanochemical design principles in Chapter 6 highlights the mechanical robustness of cyclopentadiene–maleimide cycloadducts afforded through the unique geometry of the cyclopentadiene derivative spiro[2.4]hepta-4,6-diene. Conversely, the reported mechanochemical lability of cyclopentadiene derivatives with *proximal* geometries[11,12] conjures new questions as to the bulk properties of materials comprised of cycloadducts which are mechanically labile yet rapidly remendable - might this afford mechanically induced dynamic behavior? Diels–Alder cycloadditions are typically precluded from consideration in the development of dynamic covalent hydrogels to mimic the viscoelasticity of natural tissues due to the high thermal cycloreversion temperature;[13] however, the possibility of mechanically induced, dynamic DA behavior presents an intriguing route to on-demand viscoelasticity.

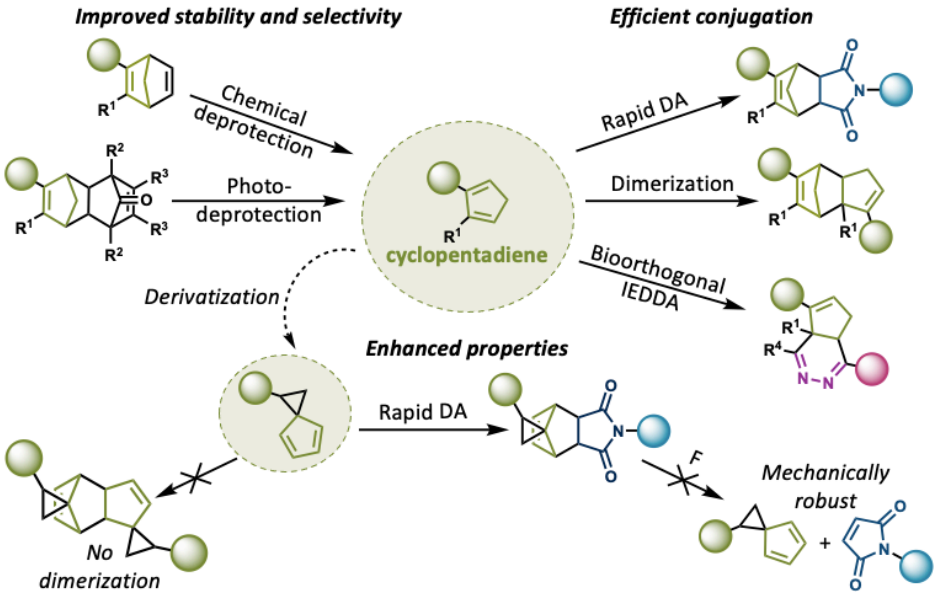

Figure 7.1. Summary of strategies outlined in this dissertation and future directions to utilize tamed cyclopentadiene precursors and derivatives for DA click chemistry.

7.1 Concluding remarks

The establishment of strategies outlined in this thesis to harness cyclopentadiene and unlock its practical use in rapid DA cycloadditions has enabled the facile synthesis of polymer architectures, selective modification of matrices and rational design of soft materials with enhanced properties. As highlighted throughout this thesis, the key improvements of these strategies provided 1) inexpensive and scalable syntheses, 2) radical free conditions, 3) computationally guided design for optimized properties, 4) thermally stable material building blocks, 5) orthogonality with free-radical polymerizations and sensitive functional groups and 6) reactivity with commercially available reagents (e.g. maleimides). We anticipate that the establishment of such accessible, orthogonal, and robust conjugation strategies will enable their adoption by chemists, materials scientists, engineers, and biologists alike. Such widespread uptake by these interdisciplinary communities is essential to promote the advancement of fabrication technologies and inspiration for novel material designs and applications.

7.2 References

(1) Murphy, E. B.; Bolanos, E.; Schaffner-Hamann, C.; Wudl, F.; Nutt, S. R.; Auad, M. L. Synthesis and Characterization of a Single-Component Thermally Remendable Polymer Network: Staudinger and Stille Revisited. *Macromolecules* **2008**, *41* (14), 5203–5209. DOI: 10.1021/ma800432g.

(2) Caliari, S. R.; Burdick, J. A. A Practical Guide to Hydrogels for Cell Culture. *Nat. Methods* **2016**, *13* (5), 405–414. DOI: 10.1038/nmeth.3839.

(3) Broguiere, N.; Lüchtefeld, I.; Trachsel, L.; Mazunin, D.; Rizzo, R.; Bode, J. W.; Lutolf, M. P.; Zenobi-Wong, M. Morphogenesis Guided by 3D Patterning of Growth Factors in Biological Matrices. *Adv. Mater.* **2020**, *32* (25), 1908299. DOI: 10.1002/adma.201908299.

(4) Reinhardt, B. A.; Brott, L. L.; Clarson, S. J.; Dillard, A. G.; Bhatt, J. C.; Kannan, R.; Yuan, L.; He, G. S.; Prasad, P. N. Highly Active Two-Photon Dyes: Design, Synthesis, and Characterization toward Application. *Chem. Mater.* **1998**, *10* (7), 1863–1874. DOI: 10.1021/cm980036e.

(5) Ovsianikov, A.; Mironov, V.; Stampfl, J.; Liska, R. Engineering 3D Cell-Culture Matrices: Multiphoton Processing Technologies for Biological and Tissue Engineering Applications. *Expert Rev. Med. Devices* **2012**, *9* (6), 613–633. DOI: 10.1586/erd.12.48.

(6) Lee, M.; Rizzo, R.; Surman, F.; Zenobi-Wong, M. Guiding Lights: Tissue Bioprinting Using Photoactivated Materials. *Chem. Rev.* **2020**, *120* (19), 10950–11027. DOI: 10.1021/acs.chemrev.0c00077.

(7) Bailey, S. J.; Barney, C. W.; Sinha, N. J.; Pangali, S. V.; Hawker, C. J.; Helgeson, M. E.; Valentine, M. T.; Read de Alaniz, J. Rational Mechanochemical Design of Diels–Alder Crosslinked Biocompatible Hydrogels with Enhanced Properties. *Mater. Horiz.* **2022**, *9* (7), 1947–1953. DOI: 10.1039/D2MH00338D.

(8) St. Amant, A. H.; Lemen, D.; Florinas, S.; Mao, S.; Fazenbaker, C.; Zhong, H.; Wu, H.; Gao, C.; Christie, R. J.; Read de Alaniz, J. Tuning the Diels–Alder Reaction for Bioconjugation to Maleimide Drug-Linkers. *Bioconjugate Chem.* **2018**, *29* (7), 2406–2414. DOI: 10.1021/acs.bioconjchem.8b00320.

(9) Ozbolat, I. T.; Hospodiuk, M. Current Advances and Future Perspectives in Extrusion-Based Bioprinting. *Biomaterials* **2016**, *76*, 321–343. DOI: 10.1016/j.biomaterials.2015.10.076.

(10) Ting, C.-Y.; Kolbeck, P. T.; Colombo, R.; Chakiath, C.; Rice, M.; Marelli, M.; Christie, R. J. Cyclopentadiene as a Multifunctional Reagent for Normal- and Inverse-Electron Demand Diels–Alder Bioconjugation. *Bioconjugate Chem.* **2022**, acs.bioconjchem.2c00222. DOI: 10.1021/acs.bioconjchem.2c00222.

(11) Hu, X.; McFadden, M. E.; Barber, R. W.; Robb, M. J. Mechanochemical Regulation of a Photochemical Reaction. *J. Am. Chem. Soc.* **2018**, *140* (43), 14073–14077. DOI: 10.1021/jacs.8b09628.

(12) Barber, R. W.; Robb, M. J. A Modular Approach to Mechanically Gated Photoswitching with Color-Tunable Molecular Force Probes. *Chem. Sci.* **2021**, *12* (35), 11703–11709. DOI: 10.1039/D1SC02890A.

(13) Tang, S.; Richardson, B. M.; Anseth, K. S. Dynamic Covalent Hydrogels as Biomaterials to Mimic the Viscoelasticity of Soft Tissues. *Prog. Mater. Sci.* **2021**, *120*, 100738. DOI: 10.1016/j.pmatsci.2020.100738.